# Study of Alfalfa and Flaxseed Gums as Co-structurants in Probiotic Cryogel Scaffolds

Thierry Hellebois

# Study of Alfalfa and Flaxseed Gums as Co-Structurants in Probiotic Cryogel Scaffolds

## THESIS

Presented and publicly defended on November 24th 2023

in order to get the degree of

**Doctor of Biotechnology and Food Engineering**

of the

**Université de Lorraine**

By

**Thierry Hellebois**

Jury composition:

| | | |
|---|---|---|
| Pr. Serafim Bakalis | University of Copenhagen, Copenhagen, Denmark | Referee |
| Dr. Denis Renard | Institut National de Recherche pour l'Agriculture, l'Alimentation et l'Environnement, Nantes, France | Referee |
| Pr. Tatiana Budtova | Centre for Material Forming, Mines Paris, PSL University, Sophia Antipolis, France | President |
| Pr. Fang Zhong | Jiangnan University, Wuxi, China | Examiner |
| Pr. Claire Gaiani | Laboratoire d'ingénierie des Biomolécules, Université de Lorraine, Nancy, France | Co-director |
| Dr. Christos Soukoulis | Luxembourg Institute of Science and Technology, Esch-sur-Alzette, Luxembourg | Co-director |

*“I have not failed. I’ve just found 10,000 ways that won’t work.”*

*–Thomas Edison*

# ACKNOWLEDGEMENTS

I would like to express my gratitude to the Luxembourg Institute of Science and Technology (LIST) and the Laboratoire d'Ingénierie des Biomolécules (LIBio) for providing a favourable environment to conduct my research activities, and to the Luxembourgish National Research Fund (FNR) for their financial support which made this work possible.

I would like to extend my deepest gratitude to my thesis supervisors, Dr. Christos Soukoulis and Pr. Claire Gaiani, for their constant guidance, feedback, support and the trust placed in me throughout this research journey.

My sincere thanks go to Jennyfer Fortuin and Romain Canuel for their invaluable assistance in the labs. Collaborating with you and sharing knowledge has been a truly enriching experience.

Thanks goes also to Silas Villas-Boas for his positive and enriching discussions.

A heartfelt thank you to all the collaborators from LIST who played pivotal roles in this research project: Alexander Shaplov for his counsel and assistance in the characterisation of the polymers; Sébastien Cambier and Servane Contal for aiding in the setup of the mucoadhesion experiments; Frédéric Addiego for the x-ray microtomography experiments; Jean Nicolas Audinot for the HIM microscopy; and Xuan Xu for her expertise with the sugar analysis. I'm also grateful to the dedicated personnel who make daily experiments seamless, notably Anaïs Noo, Aude Corvisy, Delphine Collard, Denis Pittois, François Barnich, Cécile Walzack, and Laurent Solinhac.

Special recognition goes to the members of LIBio, Carole Jeandel and Carole Perroud, for their technical expertise on the experimental analyses.

Lastly, my deepest gratitude goes to my family and my friends for their unwavering support and encouragement throughout this academic journey.

# RÉSUMÉ

Dans l'univers en constante expansion des compléments alimentaires, l'incorporation de cellules probiotiques vivantes présente divers défis principalement en ce qui concerne leur stabilité tout au long du cycle de vie du produit, c'est-à-dire lors de la production, du stockage et pendant leur digestion. Cette étude doctorale a utilisé des fibres alimentaires solubles isolées de la luzerne et du lin pour renforcer les compléments alimentaires formulés à base de protéines de lait enrichis en probiotiques utilisant la souche *Lacticaseibacillus rhamnosus* GG (LGG).

L'étude présente une méthode innovante d'extraction de gommes, utilisant une déprotéinisation induite par précipitation isoélectrique combinée à une précipitation des gommes induites par solvant. Une caractérisation approfondie des gommes extraites a révélé leurs propriétés moléculaires et techno-fonctionnelles. En particulier, un nouveau type de galactomannane de luzerne a montré des similitudes avec la gomme de fenugrec, suggérant son potentiel d'interchangeabilité. L'interaction entre les gommes et les protéines a été évaluée lors de la digestion simulée *in vitro*, révélant que des interactions complexes influençaient les vitesses de digestion des protéines. Bien que l'ajout de gomme ait augmenté la viscosité des mélanges digestifs, cela a également impacté l'agrégation des protéines induite par l'acidité, accélérant leur protéolyse. Enfin, les cryogels ont été explorés comme méthode alternative pour l'encapsulation de probiotiques. Lors de la production et du stockage, il a été montré que la composition protéique était le facteur principal pour la préservation de la viabilité bactérienne. Lors de l'exposition aux fluides digestifs gastriques, les probiotiques ont montré une stabilité accrue grâce à leurs encapsulations au sein de la structure des cryogels. Leur libération contrôlée dans les fluides intestinaux a été observée à la suite de l'hydrolyse complète des protéines. De plus, l'inclusion de gommes, en particulier la gomme de lin, a amélioré l'adhésion bactérienne sur un épithélium intestinal simulé *in vitro*, suggérant leur potentiel pour promouvoir des bienfaits pour la santé.

Dans l'ensemble, cette recherche a démontré les divers avantages des gommes issues de graines et l'importance du choix des protéines dans la conception de compléments alimentaires probiotiques, de leur extraction et caractérisation à leurs interactions avec les protéines et leur rôle dans les systèmes d'encapsulation de probiotiques.

# ABSTRACT

In the ever-growing realm of health-promoting food supplements, incorporating living probiotic cells presents various challenges, predominantly concerning their stability throughout the product lifecycle, i.e. production, storage, and digestion. This PhD research employed soluble dietary fibres isolated from alfalfa (*Medicago sativa* L.) and flax (*Linum usitatissimum* L.) seeds to fortify milk-protein (sodium caseinate and whey proteins) xero-scaffolds embedding *Lacticaseibacillus rhamnosus* GG (LGG) probiotic cells.

The research details an innovative gum extraction method for isolating dietary fibres, using isoelectric combined with solvent-induced precipitation. Extensive characterisation of the extracted gums revealed significant insights into their molecular and techno-functional properties. In particular, a novel galactomannan from alfalfa seeds showcased similarities with fenugreek gum, hinting at its potential interchangeability. The interplay between gums and proteins was evaluated during *in vitro* digestion, revealing complex interactions that influenced protein digestion rates. While the addition of gum increased the viscosity of digestive mixtures, it also impacted the acid-induced aggregation of proteins, accelerating the proteolysis. Lastly, cryogels were explored as an alternative method for delivering probiotics. During cryogels' production and storage, it was observed that the viability of LGG was predominantly dictated by the protein composition, rather than the presence of gum. Upon exposure to gastric digestive fluids, the probiotics exhibited enhanced stability as the LGG cells remained largely shielded within the cryogel structures, followed by a controlled bacterial release in the intestine fluids. Notably, the inclusion of gums, especially flaxseed gum, improved bacterial adhesion on an *in vitro* gut epithelium, suggesting their potential in promoting sustained health benefits.

Overall, this research demonstrated the multifaceted benefits of plant seed gums and the importance of the protein selection in designing of probiotic food supplements, from extraction and characterisation to their interplay with proteins and their role in probiotic delivery systems.

# CONTENTS

# LIST OF TABLES

# LIST OF FIGURES

# LIST OF ABBREVIATIONS AND ACRONYMS

| | |
|---|---|
| AAG | Alfalfa gum |
| $a_c$ | Frequency shift factor |
| ACE | Angiotensin-converting enzyme |
| $A_{H_2O}$ | Area of a single water molecule |
| AOAC | Association of official agricultural chemists |
| ATP | Adenosine triphosphate |
| ATR | Attenuated total reflectance |
| $a_w$ | Water activity |
| AX | Arabinoxylan |
| $b_c$ | Viscoelastic shift factor |
| BET | Brunauer–Emmett–Teller |
| BF | Brown flaxseed gum |
| BFAC | Brown flaxseed gum extracted in acid conditions |
| BFAL | Brown flaxseed gum extracted in alkaline conditions |
| c* | Critical coil overlap concentration |
| c | Concentration |
| CCG | Critical concentration of gelation |
| CCP | Colloidal calcium phosphate |
| CFU | Colony forming units |
| CLSM | Confocal laser scanning microscope |
| CMC | Carboxymethyl cellulose |
| $D_{[4,3]}$ | Volume-weighted mean particle size |
| $D_f$ | Feret's diameter |
| DH | Degree of hydrolysis |
| $d_H$ | Hydrodynamic diameter |
| DLS | Dynamic light scattering |
| $DP_n$ | Degree of polymerisation |
| DPP-IV | Dipeptidyl peptidase-4 |
| DSC | Dynamic scanning calorimetry |
| DTG | First derivative of thermogravimetric curve |
| DTT | Dithiothreitol |
| DVS | Dynamic vapour sorption |

| | |
|---|---|
| DW | Distal primary cell wall |
| $E_a$ | Activation energy |
| EFSA | European food safety authority |
| EtOH | Ethanol |
| EPS | Exopolysaccharide |
| f | Frequency |
| FA | Formic acid |
| FAA | Free amino acid |
| FAO | Food and agriculture organisation |
| FDA | Food and drug administration |
| FG | Flaxseed gum |
| FM | Food matrix |
| FTIR | Fourier-transform infrared spectroscopy |
| G' | Storage modulus |
| $G'_f$ | Storage modulus at flow point |
| $G'_{LVE}$ | Storage modulus within the linear viscoelastic region |
| G" | Loss modulus |
| $G"_{LVE}$ | Loss modulus within the linear viscoelastic region |
| GAB | Guggenheim-Anderson-De Boer |
| GF | Golden flaxseed gum |
| GFAC | Golden flaxseed gum extracted in acid conditions |
| GFAL | Golden flaxseed gum extracted in alkaline conditions |
| GG | Guar gum |
| GIT | Grastrointestinal tract |
| GIP | Glucose-dependent insulinotropic polypeptide |
| GLP-1 | Glucagon-like peptide 1 |
| GPC/SEC | Gel permeation size-exclusion chromatography |
| GRAS | Generally recognised as safe |
| HIM | Helium ion microscopy |
| $IC_{50}$ | Half maximal inhibitory concentration |
| II | Instability Index |
| IPDT | Integral procedure decomposition temperature |
| $k_H$ | Huggins constant |
| $k_K$ | Kraemer constant |

| | |
|---|---|
| LC | Liquid chromatography |
| LBG | Locust bean gum |
| LGG | *Lacticaseibacillus rhamnosus* GG |
| LVE | Linear viscoelastic |
| LVR | Linear viscoelastic range |
| M/G | Mannose to galactose ratio |
| M | Molar |
| $M_0$ | Molecular weight of the repeating unit |
| MFGM | Milk fat globule membrane |
| MKHS | Mark–Kun–Houwink–Sakurada |
| $M_n$ | Number average molecular weight |
| $m_{NaCN/WPI}$ | Sodium caseinate to whey protein mass fraction |
| MPC | Milk protein concentrate |
| MRS | De Man, Rogosa and Sharpe |
| MS | Mass spectrometry |
| MSC | Mucilage secretory cell |
| $M_w$ | Weight-average molecular weight |
| $M_z$ | Size-average molecular weight |
| N1:3W | Cryogel with a protein content of 25% NaCN and 75%WPI |
| N1:1W | Cryogel with a protein content of 50% NaCN and 50%WPI |
| N3:1W | Cryogel with a protein content of 75% NaCN and 25%WPI |
| $N_0$ | Number of viable bacteria after 0 day |
| $N_A$ | Avogadro number |
| NaCN | Sodium caseinate |
| NEM | N-ethylmaleimide |
| NMR | Nuclear magnetic resonance |
| $N_t$ | Number of viable bacteria after t days of storage |
| OPA | O-phthaldialdehyde |
| OTR | Oscillatory thermo-rheology |
| PBS | Phosphate-buffered saline |
| $R_g$ | Radius of gyration |
| RG-I | Rhamnogalacturonan I |
| RH | Relative humidity |
| RW | Radial cell wall |

| | |
|---|---|
| SAOS | Small amplitude oscillatory shear |
| SDS | Sodium dodecyl sulfate |
| SDS-PAGE | Sodium dodecyl sulfate-polyacrylamide gel electrophoresis |
| SEM | Scanning electron microscopy |
| SGF | Simulated gastric fluids |
| SIF | Simulated intestinal fluids |
| SLS | Static light scattering |
| $S_m$ | Surface of the monolayer |
| SSF | Simulated saliva fluids |
| T | Temperature |
| t | Time |
| Tanδ | Loss factor |
| TCS | Time concentration superimposition |
| $T_g$ | Glass transition |
| TGA | Thermogravimetric analysis |
| $t_{gel}$ | Gelation time |
| $T_m$ | Melting temperature |
| TMA | Thermo-mechanical analysis |
| $T_{ref}$ | Reference temperature |
| TVC | Total viable counts |
| $t_\theta$ | Gelation inflection time |
| vt | Vessel thickness |
| WHC | Water holding capacity |
| WHO | World health organisation |
| WPI | Whey protein isolate |
| wt. | Weight |
| $X_m$ | Monolayer water content |
| ρ | Bulk density |
| φ | Porosity |
| τ | Shear stress |
| $\tau_{1/2}$ | Half life |
| $\tau_{99\%}$ | Time to achieve a 99% reduction |
| $\tau_f$ | Flow point |
| $\tau_y$ | Yield stress |

| | |
|---|---|
| $[\eta]$ | Intrinsic viscosity |
| µCT | Micro-computed X-ray tomography |
| Đ | Polydispersity index |
| α-La | α-lactalbumin |
| β-Lg | β-lactoglobulin |
| $\dot{\gamma}$ | Shear Rate |
| $\Delta T$ | Temperature difference |
| $\eta_\infty$ | Infinite shear viscosity |
| $\eta^*$ | Complex viscosity |
| $\eta$ | Viscosity |
| $\eta_0$ | Zero shear viscosity |
| $\eta_{rel}$ | Relative viscosity |
| $\eta_{sp}$ | Specific viscosity |
| $\omega$ | Angular frequency |

# INTRODUCTION

## OUTLINE

In today's modern society, the significance of a healthy diet is paramount, especially given medical advancements that have extended human lifespan. Alongside longevity, there's a pressing need to enhance life quality. Thus, a balanced diet, combined with other preventive measures like regular exercise and mental well-being practices, can elevate the quality for extended years. Adopting these holistic health measures ensures individuals optimal well-being during their lifespan.

One such pathway to achieve this balance is through regulating our gut microbiota, the community of microorganisms living in our digestive tract. Current research points to the crucial role of a balanced microbiota in promoting overall health. Dietary fibre and probiotics − beneficial bacteria that help digestion − have been found to be excellent candidates for maintaining this balance. They promote a healthy gut environment, thereby indirectly influencing various facets of our health, including immunity, mental well-being, and even cardiovascular health.

However, considering our fast-paced lifestyles, maintaining a consistent intake of these health beneficial foods nutrients can sometimes be challenging. To overcome this need, the consumption of food supplements has seen a growing trend. These supplements, often designed with concentrated levels of vital nutrients, probiotics, and fibres, are intended to enhance the daily intake of these beneficial elements, filling in the gaps left by our regular diet. As it stands, dietary food supplements have been instrumentalised in supporting a healthier lifestyle, but improvements are still needed to ensure maximised health outcomes.

## POLYSACCHARIDES

### OVERVIEW

Polysaccharides are complex biopolymers formed by long chains of monosaccharidic units (i.e. > 40) naturally occurring across all kingdoms of life (Aspinall, 1983). They play a crucial role in a plethora of biological functions spanning from energy storage reserve (e.g. starch, glycogen, etc.) (Dawes & Senior, 1973; Schneider & Gear, 2008;

Sturm, 1999), structural support (e.g. cellulose, chitin, etc.) (Guérin et al., 2022; Martínez et al., 2014; Whitney et al., 1999), to cell communication and signalisation (e.g. glycated proteins) (Chang et al., 2023; Dennis et al., 1999; Haltiwanger & Lowe, 2004). Structural conformation, physicochemical, thermophysical and rheological properties of polysaccharides are inextricably associated with the type of monosaccharide subunits, the nature of their glycosidic linkages, their molecular weight and their degree of branching, which leads to a broad spectrum of techno-functional properties (i.e. water solubility, viscosity, gelation capacity, and film-forming ability) (Hosseini et al., 2023; Li et al., 2023; Maier et al., 1993; Najafian et al., 2022) while also modulating their resistance against thermal, physical, mechanical and enzymatic degradation (Sengupta & Datta, 2021). For instance, the linear structure of cellulose (β-(1 → 4) D-glucose repeating units) makes it water-insoluble, indigestible by human digestive enzymes and remarkably resistant to degradation rendering it valuable to industries such as textiles and paper manufacturing. However, by modifying the type of linkage of cellulose structure, from β- to α-, and increasing the extent of branching, one can transform – in theory – the cellulose into starch. This seemingly subtle change in structure has critical effects on the resultant material's characteristics. Unlike cellulose, starch can be solubilised in water upon heating, undergoes a solution-gel phase transition during cooling and is readily digestible by human gastrointestinal enzymes (Hermiati et al., 2023). These unique properties have positioned starch as a first choice as texturising agent in the food industry. Thus, it becomes evident that the exploration and understanding of the structure-property relationships of polysaccharides hold a crucial role in the identification of new industrially-relevant polysaccharides offering diverse applications and functionality.

## GUMS

Gums are a family of polysaccharides belonging to the group of hydrocolloids. They consist of either homo- or heteropolymers of high molecular weight, typically in the range of $10^5$ to $10^7$ Da, having moderate to high solubility in water and often exhibit a broad range of industrially-relevant techno-functional properties. These complex biopolymers have found applications in the food industry due to their excellent texturising, viscosifying, and gelling abilities even when used in low concentrations. They are also extensively used in the stabilisation of foams and emulsions and the controlled release of flavours, among others. (Williams & Phillips, 2021). Besides their diverse functional properties, gums are typically indigestible, and thus, can promote gut health by

stimulating the growth and biological activity of beneficial gut microbes, contributing to overall digestive wellness (Williams & Phillips, 2021; Kang et al., 2022). However, it is important to note that some gums may negatively impact human health by causing gut inflammation and herniation (Williams & Phillips, 2021; Yang et al., 2022). Gums originate from a diverse range of sources, including plants, microorganisms, and animals (Aspinall, 1983; Tudu & Samanta, 2023). Gums can also be synthesised for instance, through chemical or enzymatic modification of existing polysaccharides. A schematic representation of the origin of gums is shown in Figure 1.

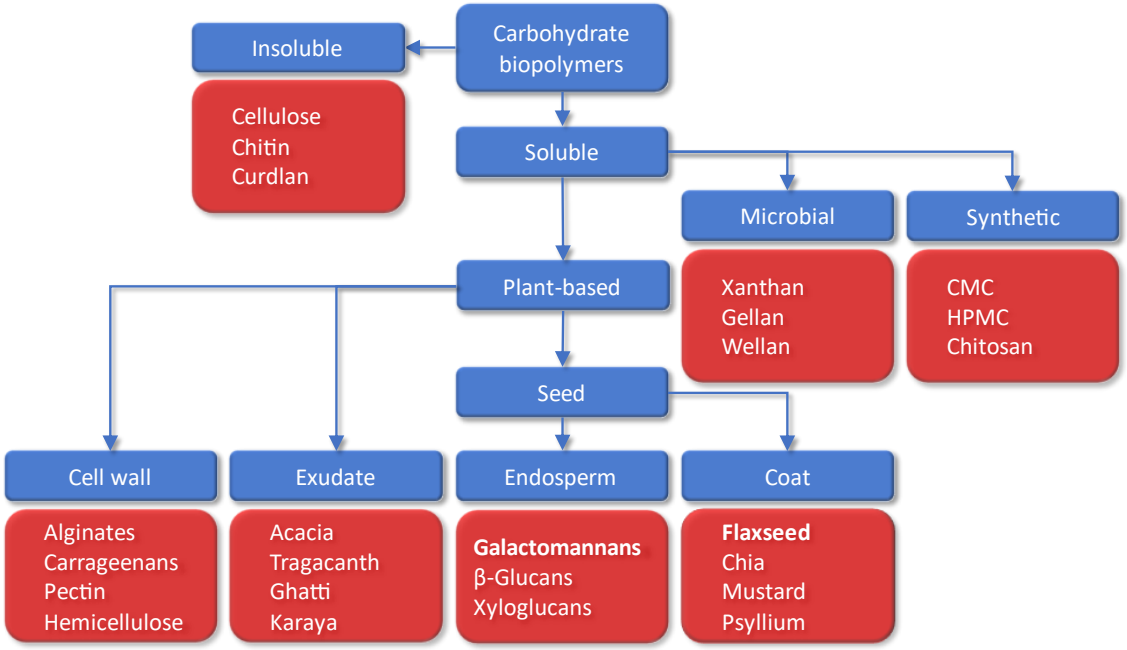


*Figure 1: Schematic representation of the origin of soluble polysaccharides relevant for the food industry.*

Plant-based gums are derived from various parts of plants such as the exudates, roots, corms, seeds, and more (Williams & Phillips, 2021; Eghbaljoo et al., 2022; Ali et al., 2023). Exudate gums are secreted by the plant, often in response to mechanical damage or environmental stress. Examples of exudates include arabic gum and tragacanth gum. Plant seed gums (PSGs) can be divided into two main categories: endosperm-originating gums, like galactomannans (e.g. isolated from guar, locust beans, etc.) (Kontogiorgos, 2019; Prajapati et al., 2013), and seed coat-isolated gums (e.g. chia, psyllium, mustard, quince, flaxseed, etc.) (Soukoulis et al., 2018; Western, 2012). Furthermore, plant-based gums can also be obtained from the cell wall material of seaweed (alginates, carrageenans), fruits (pectins, hemicellulose), etc. (Williams & Phillips, 2021; Aspinall, 1983). Microbial gums are exopolysaccharides (EPS) produced by certain bacterial species during fermentation, such as xanthan and gellan gum produced by *Xanthomonas*

*campestris* and *Sphingomonas elodea*, respectively. Fungal species can also produce EPS such as pullulan and scleroglucan produced by *Aureobasidium pullulans* and *Sclerotium rolfsii*, respectively (Singh et al., 2019). Animal-based gums are less common, with notable examples being chondroitin sulphate and hyaluronic acid, primarily used in the pharmaceutical and cosmetic industries (Muzzarelli et al., 2012). Synthetic gums are artificially created by modification of insoluble polysaccharides, which improves their techno-functional properties. For example, chitin (typically sourced from the exoskeletons of crustaceans) can be transformed into chitosan through a deacetylation process. In a similar manner, cellulose can be modified by chloroacetic acid to graft carboxylic groups, leading to an increase in solubility (Golbaghi et al., 2017; Issahaku et al., 2023). These synthetic gums are widely used because of their versatility and the tremendous biomass available as raw material. Therefore, a gum's origin greatly influences its characteristics and applications, underscoring the vast potential of this category of polysaccharides in various industrial sectors.

# PLANT SEED GUMS

## Galactomannans

Acting as a food reserve in the endosperm for germinating seeds, galactomannans also retain water, thereby preventing the seeds of plants from the *Fabaceae*, *Mimosaceae*, and *Caesalpiniaceae* subfamilies from drying out (Cerqueira et al., 2011) (Figure 2). Reports also indicate the presence of galactomannans in other species beyond the *Leguminosae* family, including *Palmae*, *Loganiaceae*, *Annonaceae*, among others (Prajapati et al., 2013). Galactomannans are non-ionic heteropolysaccharides composed of D-mannose residues linked together by β-(1 → 4) osidic linkages, forming the linear backbone chain of the molecule on which branching of single D-galactose monomeric residues are attached by a α-(1 → 6) osidic linkages (Kontogiorgos, 2019).

The extraction of a clarified gum requires several pre-treatments, which includes a) the dehusking and splitting to remove the husk and the germ from the seed, b) milling of the seed and the solubilisation of the gum into water c) a centrifugation step to remove the insoluble part, d) precipitation of the gum with an organic solvent and e) drying of the clarified gum (Nwokocha, 2021).

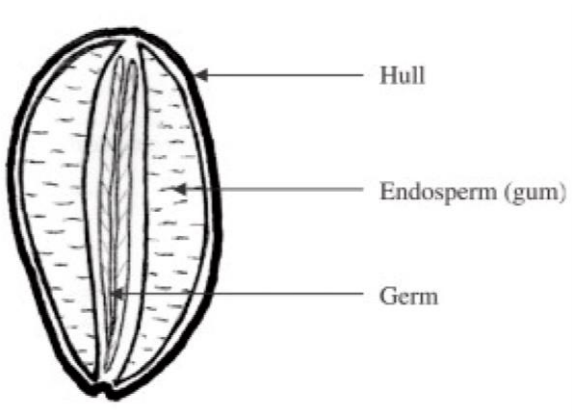


*Figure 2: Representation of a galactomannan-containing seed, illustrating the structural organisation and distribution of galactomannan polysaccharides within the seed. Adapted from Petitjean & Isasi, (2022)*

Galactomannans are highly desirable for the food and cosmetic industry due to their diverse techno-functional properties, including thickening, gelling, cryogelling, emulsifying and stabilising characteristics. Even though the molecular weight of galactomannans ranges from $10^5$ to $10^6$ Da, their physicochemical and techno-functional properties are essentially driven by the mannose-to-galactose ratio (M/G), which typically range from 1:1 to 4:1 (Figure 3). In galactomannans with M/G ratio >1:1, it was previously found that the D-galactose branching pattern along the mannose backbone does not follow a homogeneous probabilistic distribution. Instead, they are organised into areas rich in D-galactose (hairy) and long regions that are depleted of D-galactose (smooth) (Dea et al., 1977; Dea & Morrison, 1975; Doublier & Launay, 1981; O'Connell et al., 2023; Wu et al., 2012). Variation in the M/G ratio is known to be mainly influenced by the botanical origin of the plant (Figure 3) and the extraction procedure (Kontogiorgos, 2019; Nwokocha, 2021).

An increase in D-galactose substitution on the mannan backbone directly correlates with the improved solubility of these biopolymers. This can be explained by the steric hindrance obstructing intra- and interchain associations between the hydroxyl groups in carbons 2 and 3 of the mannose residues, preventing the extensive development of crystalline regions (Nwokocha, 2021; Rinaudo, 2008). Thus, fenugreek (*Trigonella foenum-graecum*) gum (M/G ~ 1:1) is cold water-swelling while locust bean (*Ceratonia siliqua*) gum (M/G ~ 4:1) required a heat treatment (about 85 °C) – weakening the intra- and interchain hydrogen bonds – to be solubilised (Maier et al., 1993). Yet, even upon heat treatment, a minimal degree of galactosyl substitution of at least 12% is required to solubilise galactomannans (Nwokocha, 2021).

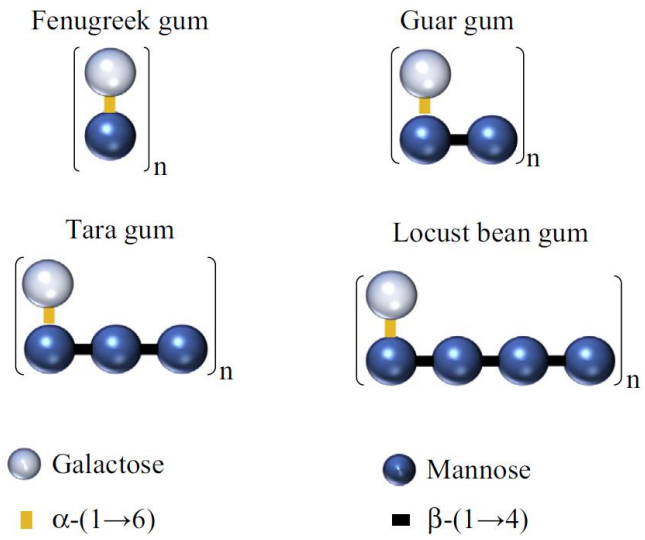


*Figure 3: Idealised structures of repeating units of the four major galactomannans. Mannose residues are linked with β-(1 → 4) whereas galactose via α-(1 → 6) glycosidic bonds (Kontogiorgos, 2019).*

Concerning their techno-functional properties, it is well established that even modest quantities of galactomannans can significantly increase the viscosimetric and viscoelastic response of aqueous systems. Generally, one can observe a pseudoplastic shear-thinning behaviour starting at around 0.5% wt. or lower, depending on the structure conformational properties of the gum (Kontogiorgos, 2019; Nwokocha, 2021). Indeed, the transition from the dilute state to semi-dilute state of galactomannan solutions is delimited by the critical coil overlap concentrations (c*) and can be observed in the range of 0.1 to 0.31% wt. (Table 1). In addition, galactomannans are less influenced by variation of pH, ionic strength, or heat treatment when compared to other hydrocolloids such as pectins or alginates, primarily due to their composition, the lack of surface charge and their structure conformational properties (Prajapati et al., 2013). In their study, Doyle et al., (2009) demonstrated that the dissolution of fenugreek gum in concentrated (5 M) sodium hydroxide (NaOH) resulted in a decrease in the measured intrinsic viscosity from 16 $dL.g^{-1}$ to 11.5 $dL.g^{-1}$. It should be noted that a marginal decline in the intrinsic viscosity values was observed even at lower NaOH content, i.e. 1 mM. This observation is primarily attributed to the ionisation of the hydroxyl groups, which generates repulsive electrostatic forces that prevent the hyperentanglement of the galactomannan polymer chains. In the concentrated regime, generally above a critical concentration (c**), typically 1–2% wt., galactomannan polymer chains possess the ability to undergo self-association by hydrogen bonding. This process occurs between the hydroxyl groups of the galactose residues, predominantly in a low M/G ratio, and the hydrophobic interaction between the smooth regions, typically in high M/G ratio galactomannans. A combination

of these factors contributes to the formation of weak gels, dependent on the concentration. Furthermore, high M/G ratio galactomannans, such as locust bean gum, exhibit the unique capability to form three-dimensional gel networks during freezing and thawing cycles (Patmore et al., 2003). The freeze-concentration of the polymer chains in the unfrozen phase allows an exacerbated interaction between the smooth regions of the biopolymers. Noteworthy, it was previously reported that the absence of extended smooth regions – e.g. guar and fenugreek – hamper the formation of a cryogel (Doyle et al., 2009; Prajapati et al., 2013). This notable characteristic is extensively used in the contemporary frozen food industry, specifically in the production of ice cream. As an ice recrystallisation inhibiting agent, locust bean gum enhances both the texture and overall quality of the products (Patmore et al., 2003). Besides, fenugreek gum has been identified to possess a superior emulsification capacity in comparison to other galactomannans. In a comprehensive study, Youssef et al., (2009) demonstrated that the emulsifying activity of galactomannans does not primarily derive from the gum itself. Rather, it appears to originate from the residual impurities having amphiphilic properties that remain following the extraction process, such as saponins and proteins. The deproteinisation achieved by Youssef et al., (2009) from the fenugreek gum from 3.7 to 0.2% increase the surface tension of the solutions (0.4% gum extract content) from 62 to 72 dyn.cm$^{-1}$.

Numerous instances of synergistic interactions between galactomannans and other biomacromolecules have been documented in the literature, including interactions with xanthan, κ-carrageenan, agar and various types of starches (Table 1). While there have been reports indicating a synergistic relationship between fenugreek-derived galactomannan and xanthan, the level of synergy observed remains modest, particularly when compared to gums characterised by a high M/G ratio, such as locust bean gum. A partial explanation for this phenomenon may lie in the specific interaction mechanism, referred to as the "junction zone". This mechanism elucidates the relationship through hydrophobic interactions between the smooth regions of galactomannan molecules and the hydrophobic patches of the synergistic polymer (Wu et al., 2009b). A secondary mechanism predominantly found in highly substituted galactomannans involves the segregative association of polymer chains in a single phase (Grisel et al., 2015).

*Table 1: Molecular properties of the four main commercially available galactomannans*

| Gum source | M/G ratio | Molecular weight ($10^6$ Da) | Intrinsic viscosity ($dL.g^{-1}$) | Critical concentration ($g.dL^{-1}$) | Techno-functionnal properties | Synergism | References |
|---|---|---|---|---|---|---|---|
| Fenugreek | 1:1 | 1.4–3.1 | 6.6–16.1 | 0.18–0.31 | Stabiliser, Thickener, Emulsifier | Starches, Xanthan | (Brennan et al., 2006; Gadkari et al., 2018; Niknam et al., 2020; Pollard et al., 2010; Prado et al., 2005; Youssef et al., 2009) |
| Guar | 2:1 | 1.3–2.9 | 9.3-16.9 | 0.10–0.13 | Stabiliser, Thickener | Xanthan, Starches, Cellulose, Agar, κ-carrageenan | (Doublier & Launay, 1981; Gadkari et al., 2018; Prado et al., 2005; Prajapati et al., 2013; Richardson et al., 1998; Wientjes et al., 2000) |
| Tara | 3:1 | 1.5–2.5 | 12.4–16.5 | 0.11–0.18 | Stabiliser, Thickener, Gelling,Cryogelling, Emulsifier | Xanthan, κ-carrageenan, Agar | (Huamaní-Meléndez et al., 2021; Oliveira et al., 2013; Pollard et al., 2010; Prado et al., 2005; Prajapati et al., 2013) |
| Locust | 4:1 | 1.2–2.2 | 11.0–15.2 | 0.10–0.22 | Stabiliser, Thickener, Gelling, Cryogelling | Agar,κ-carrageenan, xanthan | (Andrade et al., 1999; Gadkari et al., 2018; Nwokocha, 2021; Patmore et al., 2003; Prado et al., 2005; Richardson et al., 1998; Sittikijyothin et al., 2005) |

Galactomannans aqueous solution mixed with proteins (e.g. whey protein, caseins, etc.) can be observed either in a single phase − under conditions of low protein and/or galactomannan concentrations − or in a biphasic state consisting of protein-rich and gum-rich microdomains (Doublier et al., 2000; Schorsch et al., 1999). The predisposition for such phase separation to occur is influenced by a multitude of factors, including the molecular weight, composition (presence of *co*-solutes such as sugars and salt), surface charge density and conformational structure of the biopolymers. These parameters can significantly impact the nature of the biopolymer interactions and thus, the colloidal conformation (Liu & Foster, 2022). A comprehensive understanding of these complex interactions between biopolymers is therefore crucial in the design of food products with specific functionalities. This can be achieved through the prediction of their microstructural features based on these interactions, thereby enabling the creation of products with desired physical and sensory attributes (Doublier et al., 2000).

Beyond the complex interactions of galactomannans with other biomolecules and their

behaviour in different solutions, their impact on human health is well-documented. The incorporation of galactomannans in a healthy diet can offer significant health benefits. Firstly, acting as a dietary fibre, they can be used in maintaining gastrointestinal tract (GIT) health, as they promote the growth of commensal gut bacteria, thereby aiding digestion and nutrient absorption (Mary & Kapoor, 2022; Zemzmi et al., 2020). The intake of galactomannans has also been associated with improved blood sugar regulation, which is particularly beneficial for individuals with type-II diabetes (Juhász et al., 2023). By slowing the rate of sugar absorption into the bloodstream, they help to maintain stable blood glucose levels. Furthermore, galactomannans have been linked to better cardiovascular health. They can lower LDL cholesterol levels and increase HDL cholesterol levels, reducing the risk of heart disease (Juhász et al., 2023). Lastly, their high fibre content can help induce a sense of satiety, aiding in weight management. Recently, partially hydrolysed galactomannans have emerged – predominantly hydrolysed guar gum – as a promising source of prebiotic fibre. By decreasing their molecular weight, these fibres become more accessible to the gut microbiota enzymes, simultaneously reducing their viscosifying properties, which makes them usable at higher concentrations (Kapoor et al., 2017, 2023; Miao et al., 202; Pi et al., 2024).

From a regulatory perspective, guar, tara and locust bean gum are the only galactomannan approved by the european food safety authority (EFSA) as food additive. Following their re-evaluation in 2016, no safety concerns or maximal acceptable daily intake was established (Nwokocha, 2021). Future trend for the use of new galactomannans will depend on the availability in established sources of galactomannans such as LBG and guar in the next years. Indeed, the global market in 2020 was of 9 MT, USD 116 M for LBG and 414 MT, USD 993 M for guar gum and forecasted to grow to 13MT, USD 213 M for LBG and 606 MT, USD 1775 M for guar gum by 2023 (Frost & Sulivan, 2023).

Galactomannans are not only beneficial for health as dietary fibres but also possess significant techno-functional properties. These attributes make them essential for texturing, stabilising, and viscosity in the food, cosmetic, and pharmaceutical sectors. Their versatility highlights their dual importance in both health and functional applications.

## Mucilages

Mucilages are soluble polysaccharides commonly found in the seed coats of numerous plant species. They are characterised by complex, high molecular weight heteropolymeric

polysaccharides that possess various compositions, structure conformational and techno-functional properties. Notable examples include seeds from species like flaxseed (*Linum usitatissimum*), psyllium (*Plantago ovata*), chia (*Salvia hispanica*), and yellow mustard (*Sinapis alba*) (Cakmak et al., 2023; Lira et al., 2023; Qian et al., 2012; Soukoulis et al., 2018; Wu et al., 2009a). In their natural context, mucilages were reported as germination aid through several mechanisms including: the retention of water by forming a gel-like coating in the vicinity of the seed acting as a water reservoir for the early stages of germination, the reduction of oxidative stress (reduced oxygen diffusion into the embryo), and the adhesion to soil and animals for improved dispersion and germination (Western, 2012). Mucilages are typically composed of a complex blend of pectinaceous, notably rhamnogalacturonan-I (RG-I), and hemicellulosic polysaccharides like arabinoxylans (AX), as illustrated in Figure 4 (Soukoulis et al., 2018). Previous research demonstrated that the techno-functional characteristics of mucilages are directly associated with their osidic composition (including the AX/RG-I ratio), degree of side branching, molecular weight, and overall composition and are primarily determined by the botanical origin of the seeds. (Beikzadeh et al., 2020; Kassem et al., 2021; Soukoulis et al., 2018; Western, 2012).

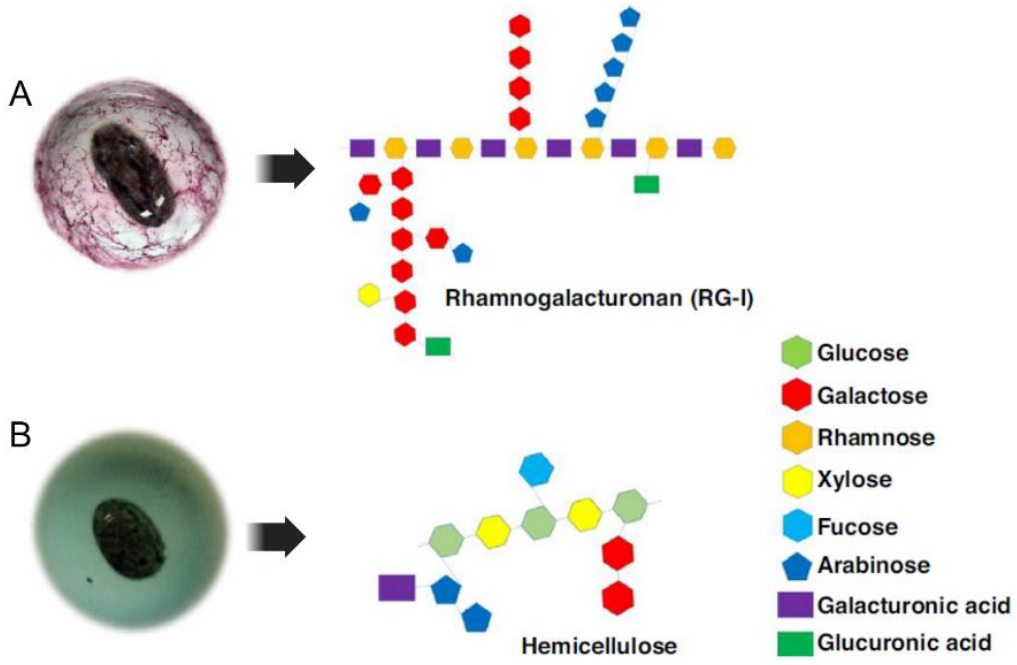


*Figure 4: Illustration of the chemical structure of major polysaccharide fractions of crude chia seed mucilage (A). Pectic polysaccharide fraction mucilage stained with ruthenium red and (B) hemicellulose stained with methylene blue, from Soukoulis et al., (2018).*

Unlike their galactomannan counterparts, seed mucilage can be extracted from intact seeds by a sufficient soaking time in water, allowing the swelling and hydration of the

mucilage (Figure 5). In most cases, the extraction comprises – after the soaking of the seeds – a solid-liquid separation, a precipitation of the gum with an organic solvent – generally ethanol – and drying (Cakmak et al., 2023). Several factors may influence the composition and increase impurity of mucilages, such as protein contaminations, which can alter or improve the techno-functional properties of the gum extract. The first determinant in this regard is the botanical origin of the seed (i.e. total protein content, degree of glycation, protein solubility). A second factor that can modulate the gum's characteristics, including its purity and extraction yield, are the extraction conditions. These conditions encompass various parameters such as time, temperature, pH, mechanical stirring, ultrasonic pre-treatment, ionic strength, seed to water ratio, etc. (Hedayati et al., 2021; Kaushik et al., 2017; Ziolkovska, 2012). For example, Kaushik et al., (2017) demonstrated the influence of the extraction conditions flaxseed mucilage compositional and physicochemical properties. Increasing the extraction temperature from 30 to 90 °C significantly increased the yield of the gum extract from 2 to 8% at the cost of a concomitant increase from 4.4 to 15.1% in proteinaceous matter contaminants, in keeping with other studies (Cui et al., 1994, 1996; Fedeniuk & Biliaderis, 1994; Qian et al., 2012).

Another contrast to galactomannans are the high residual impurities following the wet extraction of the gum. The increased contamination can be closely linked to the mechanism of mucilage release upon water contact with the seed coat, as depicted in Figure 5 (Miart et al., 2019). The intricate entanglement of RG-I and AX within the coat, coupled with the mucilage's discharge through membrane rupture, suggests that its strong anchorage to the seed wall – glycation of the cell wall protein, mainly by the hemicellulosic fraction – is the primary reason behind higher contaminant levels in mucilage extraction (Ray et al., 2013; Western et al., 2000).

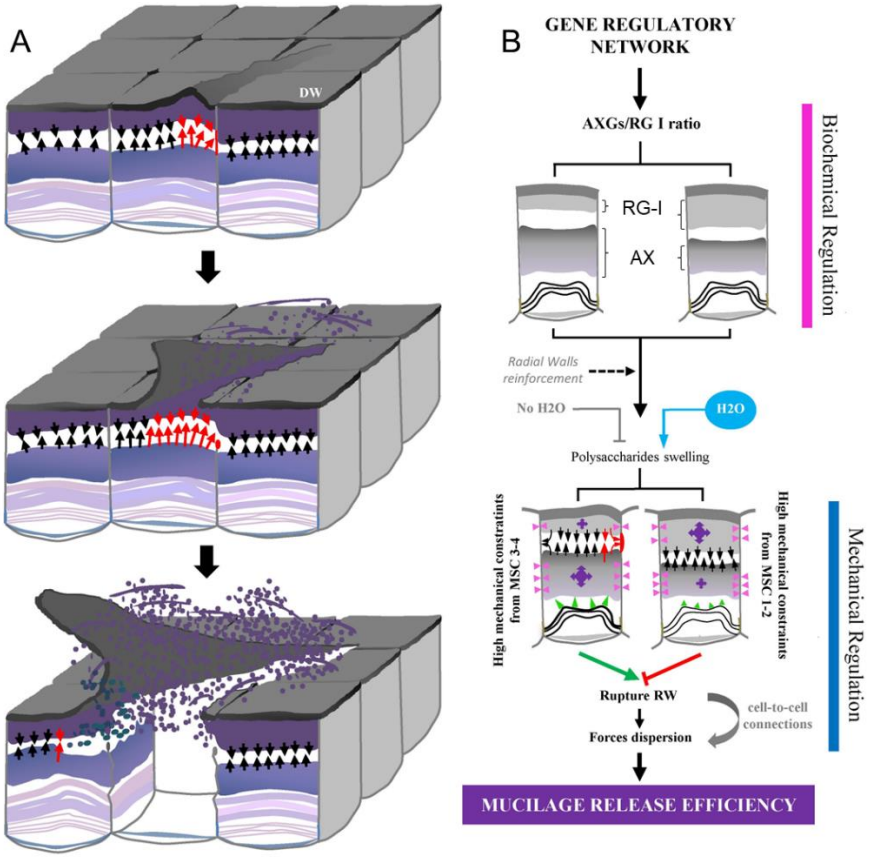


*Figure 5: Flax seed coat mucilage release mechanism: an overview of the release process when seeds are soaked in water (A) and a proposed model detailing the relationship between the polysaccharide composition and its release (B) according to (Miart et al., 2019). Arrows indicate high (red) and medium (black) putative mechanical pressures which induces one of the RW to break and the DW to peel off. Pink arrowheads also indicate putative mechanical forces from swelling polysaccharides on RW. Purple arrows indicate the importance of the mechanical constraints. Abbreviations: distal primary cell wall (DW), radial cell wall (RW), mucilage secretory cell (MSC).*

Purification steps can be implemented during the extraction of the gum to improve the quality of the gum extract. In general, the proteinaceous impurities are associated with the sterical hindrance between the mucilage side chain groups. Deproteinisation is thus essential as it favours the homopolymeric interactions, resulting in improved techno-functional properties (i.e. gelling, thickening) (Razmkhah, Razavi, Mohammadifar, et al., 2016). Several attempts, via the use enzymatic treatments to hydrolyse protein, clay adsorption and chromatographic filtration improved the purity of the gum extract (Elboutachfaiti et al., 2017; Fedeniuk & Biliaderis, 1994; Kaewmanee et al., 2014; Liu, Shim, et al., 2016; Qian et al., 2012). However, it should be noted that the deproteinisation step may also cause undesirable hydrolysis of the mucilage (Safdar et al., 2020).

Given the broad range of structure conformational properties of mucilages, dependent on the botanical origin and extraction methods, mucilages exhibit an outstanding variation

in their techno-functional properties (Lira et al., 2023; Soukoulis et al., 2018). Studies have identified a marked disparity in its intrinsic viscosity based on the source of the mucilage. For instance, the mucilage from *Plantago ovata* has been reported to have an intrinsic viscosity of approximately 3 $dL.g^{-1}$, whereas basil seed gum can exhibit viscosities as high as 42 $dL.g^{-1}$ (Naji-Tabasi et al., 2016; Yu et al., 2017). Concerning flaxseed mucilage, most of the studies revealed intermediate intrinsic viscosities ranging from 4.3 to 6.6 $dL.g^{-1}$ (Cui et al., 1996; Qian et al., 2012). Furthermore, it has been established that factors such as temperature, pH, and the concentration-dependent presence of salts and sugars significantly influence the viscosimetric response (Chen et al., 2006; Hesarinejad et al., 2018). In opposition to galactomannans, the anionic character of mucilage renders their viscoelastic response more susceptible to changes in ionic strength. When present in specific concentrations, sugar or salt *co*-solutes can change the structural conformation of mucilages, promoting the formation of a random coil structure, enhancing the solvent affinity of the mucilage. In some cases, adverse effects have been reported when solutes were added in low concentrations, resulting in the reduction of hydrodynamic diameter of the polymer and a consequent reduction in the viscosimetric response (Behrouzian et al., 2013; Capitani et al., 2015). Beyond the spectrum of rheological properties exhibited by mucilages, they have been associated with decent interfacial activities. This association is contingent upon the quantity of residual protein, whether free or glycosylated, and the presence of hydrophobic side chain groups. Notably, the surface tension values observed for mucilages align with those reported for galactomannan gum extracts, showcasing values (at a concentration of 0.4% wt.) of 63 $dyn.cm^{-1}$ for cress seed mucilage, 57 $dyn.cm^{-1}$ for yellow mustard gum, and 55 $dyn.cm^{-1}$ for flaxseed gum (Behrouzian et al., 2014; Qian et al., 2012; Wu et al., 2015). Elevated concentrations of mucilages have been observed to aid in emulsion stabilisation, a mechanism that operates not solely due to the stabilisation of the interface attributed to their amphiphilic nature, but also through the enhancement of the system's viscosity and by forming a steric barrier against the coalescence of the lipid droplets (Avila-de la Rosa et al., 2015; Soukoulis et al., 2018).

Mucilages have been extensively incorporated in designing various experimental food and pharmaceutical products. Their inclusion not only enhances the physical properties but also the nutritional value. Both in combination with *co*-solutes and proteins, as well as independently, mucilages have been successfully employed in the production of low-density aerogels (i.e. 0.05−0.16 $g.cm^{-3}$) (Comin et al., 2015; Falahati & Ghoreishi, 2019; Ubeyitogullari & Ciftci, 2020). Furthermore, they have been utilised in the fabrication of

edible films designed to deliver probiotic bacteria (Semwal et al., 2022), as well as in the development of edible films for food packaging applications (Jouki, Yazdi, et al., 2014; Nazir & Wani, 2022) and coatings (Rodrigues et al., 2018). Additionally, mucilages have been incorporated in food powders enriched with probiotics and oil (Bustamante et al., 2015, 2017; de Campo et al., 2017), hydrogels (Soukoulis et al., 2019; Yu et al., 2021), and emulsions (Fernandes et al., 2023; Wu et al., 2015). Efforts to integrate mucilage into bakery and dairy products have been documented in the literature. Korus et al., (2015) explored the potential of flaxseed mucilage as a structure-forming agent in gluten-free bread (at $c_{mucilage}$ = 1.8−2.4% wt. starch content). Their findings revealed that the gum extract enhanced the sensory acceptance of the bread amongst consumers. However, this inclusion had a negligible effect on the bread's texture and staling. Similarly, Campos et al., (2016) incorporated 1−2% wt. of chia seed mucilage into ice cream formulations. In this context, the mucilage served effectively as both a stabiliser and an emulsifier, without adversely impacting the texture and overrun properties of the ice cream. Nonetheless, the inclusion of the gum notably diminished consumer acceptability, primarily due to a significant alteration in the product's colour.

Like their galactomannan counterparts, plant seed mucilages are considered as dietary fibres. They can positively influence the gut microbiota balance, aiding in digestion and offering protection against gastrointestinal diseases including inflammatory bowel disease, colorectal cancer and type II diabetes (Soukoulis et al., 2018). Their gut health promoting and disease prevention abilities was previously associated with the presence of soluble AX polysaccharides (Bernstein et al., 2013; Ricklefs-Johnson et al., 2017). Besides, plant seed gums (i.e. okra, quince, cress, and basil) demonstrated antimicrobial activities suggesting that their addition in wound dressing may be beneficial (Jouki, Mortazavi, et al., 2014; S. Kang et al., 2020; Sangeethapriya & Siddhuraju, 2014; Tantiwatcharothai & Prachayawarakorn, 2020; Tosif et al., 2021). Recent studies revealed the potential of chia seed mucilage as an aid in the regulation of the digestion. Chia mucilage demonstrated resistance to digestive breakdown, retaining its structure despite the acidic conditions and the presence of digestive enzymes of gastrointestinal digestion. This resilience contributed to increased stomach viscosity, moderating digestion rates and enhancing overall food functionality (Cakmak et al., 2023; Câmara et al., 2020; Vera C. et al., 2019).

In the context of the regulation concerning the application of mucilages in food and pharmaceutical products, the geographic factor is a critical determinant. The USA FDA has designated mucilages with the GRAS status. Notably, mucilages derived from cress

and psyllium are presently employed in drug delivery systems, serving as disintegration aids (Alam et al., 2014). In China, flaxseed gum can be found in a purified form for use in pharmaceutical and food industry (*Flaxseed Gum*, 2022; *Soluble Linseed Gum Powder*, 2021). In Europe, the EFSA has not explicitly defined the status of purified mucilages for industrial applications. At present, the use of mucilages in Europe predominantly rotates around the incorporation of the whole seed or its powdered form in the formulation of novel products. Companies keen on integrating mucilages into their products must take initiatives to exchange with European regulatory agencies for a thorough assessment of their utilisation.

# PROBIOTICS

## OVERVIEW

The use of microorganisms for human needs has a long and fascinating history that dates back thousands of years, even before people even knew what microorganisms are. The earliest recorded utilisation of microorganisms dates between 10,000 and 5,000 BC, evidenced by the production of fermented foods. This led to the creation of new products including bread, yoghurt, natto, kefir, sauerkraut, cider, wine, and beer among others (Campbell-Platt, 1994). Despite the lack of understanding about the underlying mechanisms, fermented food products – either ethanolic or lactic acid-mediated – gained popularity due to the prolongation of shelf-life, consequently yielding safer food and beverage resources. Centuries of optimisation have maintained fermentation as a prevalent practice for food design and preservation, contributing to 20–40% of our current food supply and remaining as one of the most natural methods of microorganism intake (Campbell-Platt, 1994). It was only a few centuries ago that scientific evidence of microorganisms' existence began to emerge, followed by an understanding of their implications on human health, firstly in inducing or combating diseases and then in fermentation. By the end of the 19$^{th}$ century, the first studied on the idea of a microbiota-gut-brain axis – a two-way biochemical signalling occurring between the brain and the GIT – was established (Cryan et al., 2019). This imply that the gut microbiota can modulate the level of dopamine, norepinephrine and serotonin through its exchanges with the brain via systemic circulation and by affecting neural communications. In turn, this modulates the level of anxiety and depression of the host, affecting the cognitive behaviour and the host general well-being (Figure 6) (Gareau, 2014; Oriach et al., 2016).

Over the past decades, the importance of commensal organisms, especially bacteria and yeasts residing on the skin's surface or adhered to mucosal tissues (e.g. lungs, gut, etc.) in human physiology has been established (Torres-Fuentes et al., 2017). Alteration of the gut microbiome – e.g. via the diet or antibiotic intake – known as dysbiosis have been associated with several diseases such as irritable bowel syndrome, cancers, liver diseases and obesity, among others (Bull-Otterson et al., 2013; Moayyedi et al., 2010; Sivamaruthi et al., 2020; Turnbaugh et al., 2009).

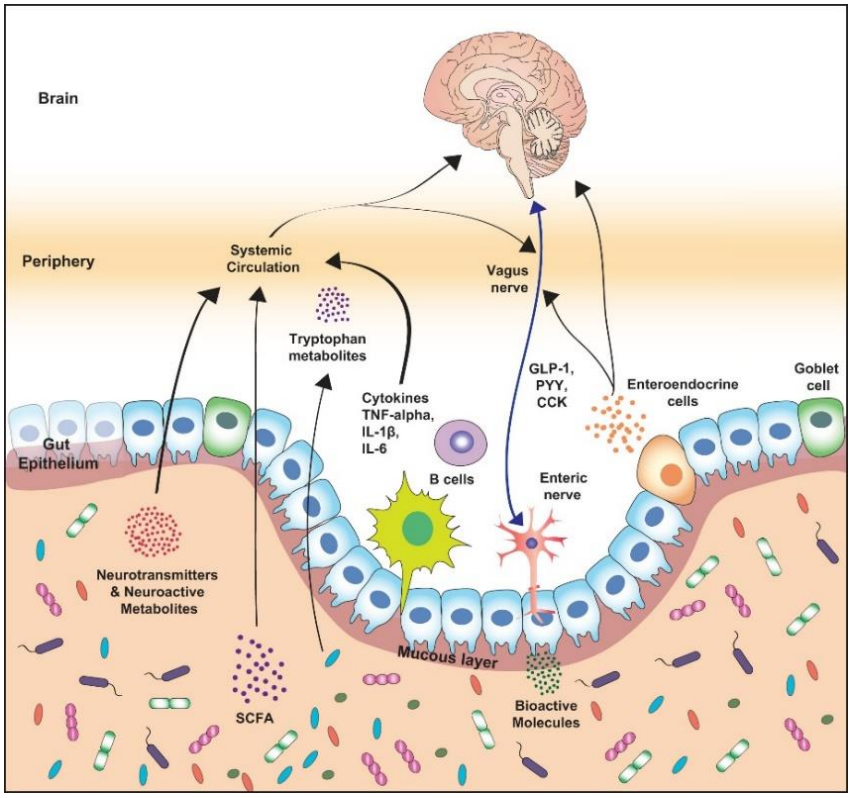


*Figure 6: Schematic outlining the various known bidirectional pathways of communication between the gut-microbiota and the brain. Adapted from Cryan et al., (2019).*

Nowadays, the term "probiotic," as defined by the World Health Organisation (WHO) and the Food and Agriculture Organisation (FAO), refers to “live microorganisms that, when administered in adequate amounts, confer a health benefit on the host” (Hill et al., 2014). The definition encompasses a wide variety of microbes and uses, emphasising the core qualities of probiotics i.e. being microbial, alive, and health beneficial. It distinguishes between microbes used for processing or as compound sources and those taken primarily for their health advantages. Whilst gut commensals can lead to probiotic strains, they aren't termed "probiotics" until isolated, identified, and proven beneficial for health.

There has been a steep increase in probiotic-focused publications over the past few

decades. As depicted in Figure 7, the annual number of records increased from 348 documents in 2000 to 6772 documents, two decades later, indicating significant interest in the prospection of new probiotic strains and the discovery of new beneficial health facets (de Melo Pereira et al., 2018). Probiotics are primarily isolated form human samples (faeces, skin, etc.) but also from many biological sources like fruits, grains, dairy products and even waste (de Melo Pereira et al., 2018). The most extensively studied probiotics are lactic-acid producing bacteria (LAB), notably *Lactobacilli* (*L. rhamnosus, L. acidophilus, L. casei, L. plantarum*, etc.) (Divyashree et al., 2021; Ghorbani et al., 2022; Venema & Meijerink, 2015).

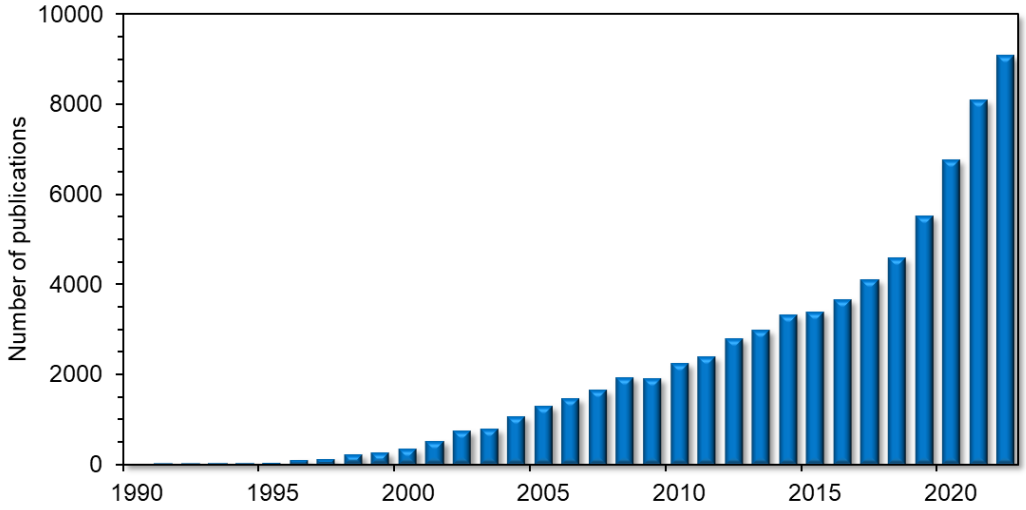


*Figure 7: Annual papers published using the term "probiotic" from 1990 to 2022. The obtained results are based of Scopus research engine using the term "probiotic*" on the 14th of July 2023.*

In addition, probiotic commensals from other families have been reported, including non-lactic acid producing bacteria such as *Bifidobacteria* (*B. bifidum, B infantis, B. animalis* subsp. *lactis, etc*.) (Bergmann et al., 2013; Guglielmetti et al., 2011; Martín et al., 2016) and *Bacillus* (*B. subtilis, B. coagulans*, etc.) (Baccigalupi et al., 2015), other organisms like yeasts (*S. boulardii, S. cerevisiae, etc.*) (Sadeghi et al., 2022; Shruthi et al., 2022), among others. It is noteworthy that new probiotic candidates derived from potentially harmful bacterial strains such as *B. cereus* or *E. coli* have been recently reported (Cutting, 2011; Yu et al., 2023). However, their industrial relevance remains limited – at least at European level – due to the difficulties to control the absence of pathogens from the same subspecies with the current detection methods and the risk of horizontal gene transfers.

Although the terms "probiotic" is widely accepted in scientific society, it is not recognised by EFSA. Instead, microorganisms identified as probiotics are granted a "qualified presumption of safety" (QPS) status, allowing their use in the European market (Hazards (BIOHAZ) et al., 2023). Similar classification i.e. "generally recognised as safe" (GRAS)

status is given to probiotics in the USA by the Food and Drug Administration (FDA). It is important to note that despite the widespread research and use of probiotics, the EFSA and FDA has not yet granted any specific health claims for these microorganisms (Saldanha, 2008). Consequently, while the historical significance and modern implications of probiotics are undeniable, the regulatory landscape underscores the need for continued research and validation to establish definitive health benefits.

## BIOLOGICAL ACTIVITY OF PROBIOTICS

Despite extensive research over the past decades unveiling numerous pathways on the governing mechanisms of the biological activity and interactions if probiotics, it is likely that we have only begun to discover the tip of the iceberg. Countless investigations of the biological functions of probiotics have affirmed their significant role in human health. These functions include influencing the equilibrium and diversity of gut microbiota (commensals vs. pathogens), modulating the immune system (particularly inflammation), and potentially playing a role in the management of various health conditions such as obesity, diabetes, cardiovascular diseases, cancers, among others (Torres-Fuentes et al., 2017; Venema & Carmo, 2015). Nonetheless, to ensure optimal effectiveness, several factors surrounding the usage of probiotics need careful consideration. Firstly, the dosage of intake is a critical determinant. Larsen et al., (2006) associated the daily intake of probiotics (specifically *B. animalis* and *L. paracasei*) with health metrics like stool consistency, blood lipid composition, and the presence of the probiotic cells in the stool. Their research demonstrated a dose-dependent response for *B. animalis*, revealing that as the daily intake increased from $10^8$ to $10^{11}$ *B. animalis* cells, the percentage of patients with the strain detected in their faeces rose from 21.4% to 86.7%. Additionally, the study underscored the importance of strain dependency, as *L. paracasei* was absent from patient faeces even at the highest uptake levels. In case of oral delivery, the ability of probiotics to adhere to the intestinal mucosa (mucoadhesion) should be rigorously evaluated. This evaluation is crucial to prevent the washout effect – the decline in probiotic counts in the gut over time – and to select probiotic strains that can effectively colonise gastrointestinal tract over an extended duration (from few days to several weeks), thereby providing sustained health benefits (de Melo Pereira et al., 2018; Kearney & Gibbons, 2018). Yet, to maintain the health benefits derived from probiotics, continuous supplementation is typically required.

As depicted in Figure 8, the selection process of probiotic strains for oral delivery should

consider various intrinsic (such as stress tolerance, antipathogenic activity, safety) and extrinsic factors (host microbiota, mucosa and tissue physicochemical properties like pH, enzymes, contact with oxygen etc.). Another parameter required in the selection of new probiotic strain is the antibiotic resistance. Antibiotic resistant probiotic intake during treatment with antibiotic may help in the recovery of a balanced gut microbiota. However, it should be ensured that no horizontal gene transfers occur between the probiotics and other microorganisms residing in the gastrointestinal tract, and thus limiting the propagation of antibiotic resistances (Moubareck et al., 2005).

The production process of probiotic supplements, specifically the growth media, can significantly influence the activity of the probiotics. For instance, *Lactobacilli* are typically grown in an optimal culture medium such as de Man, Rogosa and Sharpe (MRS) broth in the vast majority of research studies. However, due to its high cost, cheaper alternatives are often employed in industrial-scale production, potentially altering the physiology of the strains via changes in gene expression. This, in turn, could account for variations seen in the outcomes observed in the different studies (Venema & Carmo, 2015). The complexity of probiotic modulation demands a holistic approach, aligning production, selection, and administration with health outcomes.

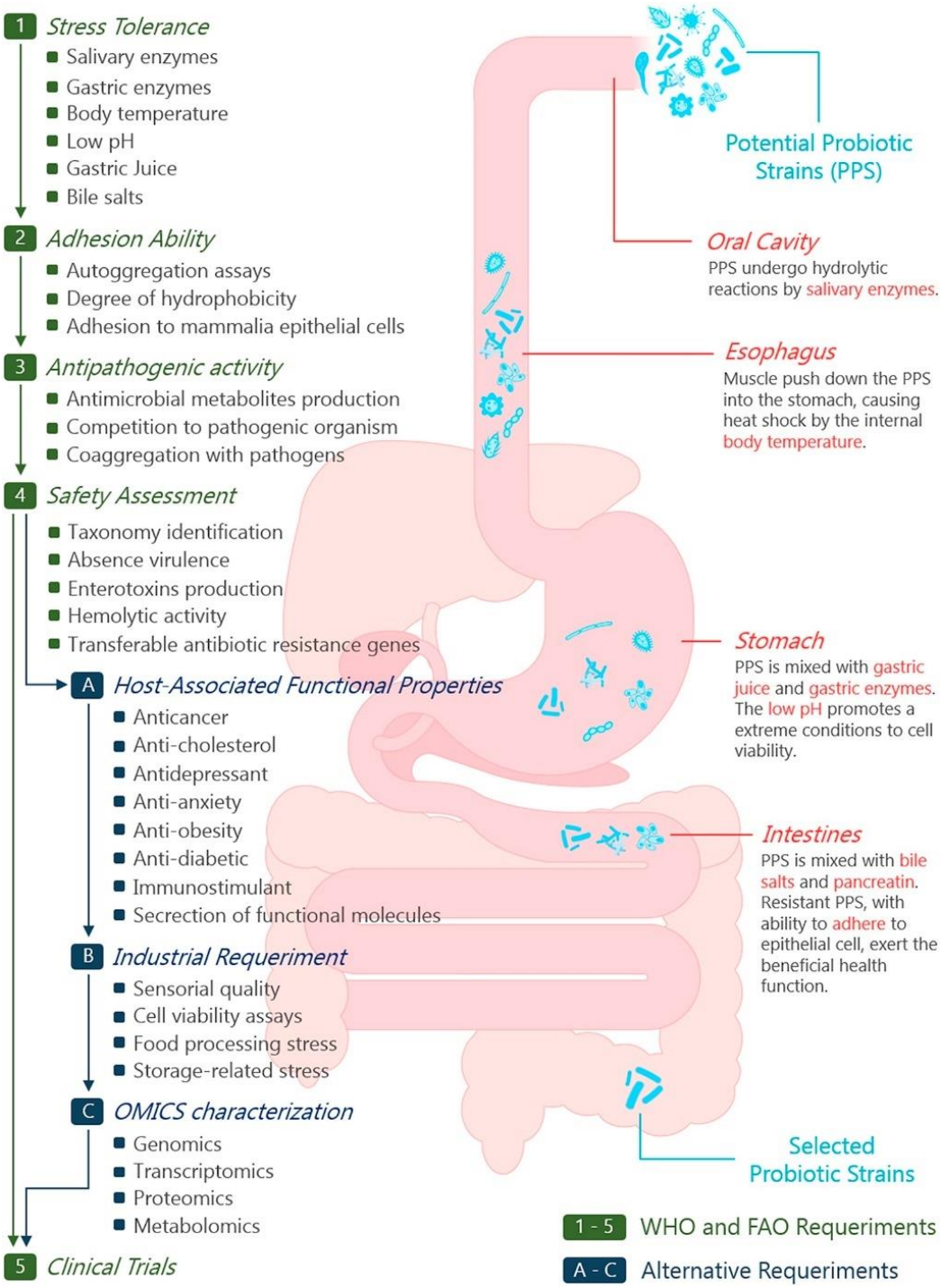


*Figure 8: Screening approaches used for characterisation of probiotic strains intended for the gastrointestinal tract according to de Melo Pereira et al., (2018)*

The biological activity of probiotics is exceptionally complex. Gaining a profound understanding of the molecular interactions between the probiotic cells, the food matrix, and the host conditions is crucial for advancing in this field of research (Venema & Carmo, 2015).

# *LACTICASEIBACILLUS RHAMNOSUS* GG: A PROBIOTIC MODEL

*Lactobacillus rhamnosus* GG (ATCC 53103), now known as *Lacticaseibacillus rhamnosus* GG (LGG) is a gram-positive, non-sporulating, anaerobic facultative bacterium, isolated in 1985 by Sherwood Gorbach & Barry Goldin from a human gut microbiota (Zheng et al., 2020). Nowadays, this strain is regarded as a model for probiotic strains and it is one of the most extensively studied and commercialised probiotic strains in the market (Gorbach et al., 2017; Segers & Lebeer, 2014). Indeed, using the research terms "LGG" or "rhamnosus GG" in Scopus search engine revealed a total of 5387 papers (researched on September 14$^{th}$ 2023) growing steadily from the date of its discovery. Several characteristics established LGG as a promising probiotic candidate. Clinical studies have explored its effects on various aspects of human health. Nermes et al., (2011) demonstrated that LGG intake (9 logCFU.d$^{-1}$ for 3 months) may enhance the gut barrier function and aid in the development of immune responses. In another clinical trial oral intake of LGG cells showed that the skin condition of infants displaying atopic eczema was alleviated after a probiotic treatment of 2 months (Isolauri et al., 2000). The efficiency of LGG intake against acute diarrhoea seems however moderate (Szajewska et al., 2007). In addition, LGG has demonstrated stability and robustness throughout production, storage, and digestion (Goldin et al., 1992). LGG has the ability to produce heat stable bacteriocins (antimicrobial substances) – others than lactic acid and acetic acid – effective against different *E. coli, Pseudomonas* sp., *Staphylococcus* sp., *Streptococcus* sp., and *Salmonella* sp. strains (Silva et al., 1987). However, several studies have been unable to conclusively demonstrate LGG's prevalence in reducing antimicrobial-resistant pathogen strains within the human gut (Rauseo et al., 2022). LGG resilience enables its incorporation into a variety of product formats, such as capsule and powder supplements, along with fermented dairy products (de Melo Pereira et al., 2018; Romero-Chapol et al., 2022). It is also able to withstand the harsh conditions of the gastrointestinal tract reasonably well, including low pH, bile salts, enzymes and osmotic pressure. As compared to other Lactobacilli (i.e. *L. gasseri*, *L. salivarius*, *L. rhamnosus* E800, *L. paracasei*) LGG demonstrated an increased stability in gastric conditions (Corcoran et al., 2005). However, *L. acidophilus* strains show greater stability in intestinal chyme compared to *L. rhamnosus* strains (Moser & Savage, 2001; Tanaka et al., 1999). In addition, the oxygen tolerance of LGG compared to other probiotic strain such as *Bifidobacterium* sp. makes is easier to handle from the production to the customer (Leser

et al., 2015).

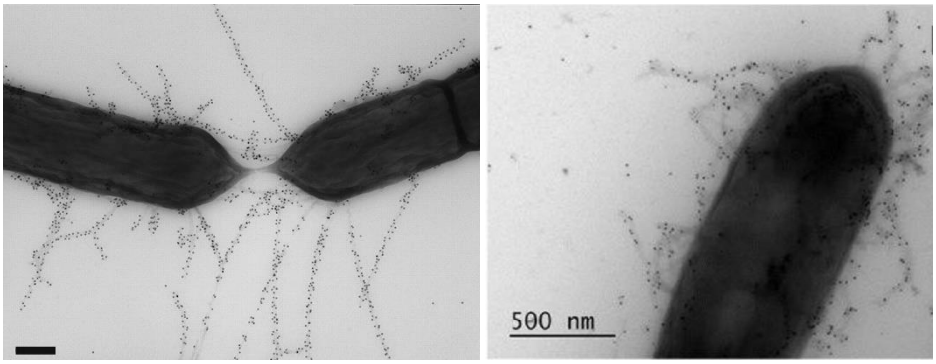


*Figure 9: Transmission electron microscopy (TEM) image of Lacticaseibacillus rhamnosus GG cells tagged with SpaA antiserum and 10-nm protein A gold particles. Scale bar represents 200 nm. Adapted from Reunanen et al., (2012, left image) and Tytgat et al., (2021, right image).*

One of the most important parameters that make LGG such a desirable probiotic strain is its ability to competitively adhere to the human intestinal mucosa – among the best lactobacilli (Gorbach, 2000) – resulting in an exclusion of pathogens (Segers & Lebeer, 2014). The adhesive characteristics of LGG was shown to depend on the molecular structure of its pili, specifically spaCBA encoded pili (Figure 9). These pili have specific properties including a deformable molecular structure capable the withstand high shear deformation, the ability to undergo molecular bridging via homophilic (pili-pili) and heterophilic (pili-mucin) bonds organised in a multiple zipper-like or single nanospring-like structures. However, the exact sites of adhesion are still unknown (Segers & Lebeer, 2014; Tripathi & Giri, 2014). Guerin et al., (2018) have showcased that LGG spaCBA pili interact with milk fat globule membrane (MFGM) inducing a significant reduction in the number of adhered bacteria to Caco-2 cells. These studies evaluated the adhesion of LGG cells *in vitro* conditions highlighting the mechanism of adhesion of LGG. In *in vivo* conditions, several potential complex interactions with the host microbiome and food digestive chymes may improve or alter the sustainable colonisation by LGG cells. Few studies revealed the *in vivo* colonisation of LGG cells. In their study Meurman et al., (1994) tested the adhesion of LGG in the oral cavity. The patients ingested yoghurt produced with the strain twice daily for 7 days. Two weeks after the discontinuation of the treatment, LGG cells (> 5 logCFU.mL$^{-1}$) were found in approx. 90% of the patients. Alander et al., (1999) have confirmed that LGG possesses the ability to adhere to the colonic mucosa *in vivo* and can persist there for extended periods (28 days in biopsy specimens), even after the administration of strain GG has been discontinued. It is also worth noting that several mechanisms may contribute to the health benefits of LGG. For example, Lam et al., (2007) reported that the intake of LGG cells (9 logCFU.d$^{-1}$) for 3

days upregulated mucin 6 mRNA expression and/or through prostaglandin $E_2$ activation led to the increase the mucus layer thickness. The increased mucosa thickness improves the resilience of the epithelium against lesions from extrinsic stressors by reducing its permeability.

LGG stands as an excellent candidate within the realm of probiotic studies, largely due to its extensive research coverage. This abundant knowledge not only facilitates a clearer and more precise understanding when conducting experimental assessments, but also has highlighted detailed mechanistic pathways in relation to storage and digestive survivability as well as its interactions with a plethora of molecules and organisms. Furthermore, LGG garners scientific interest thanks to its inherent qualities of a potent probiotic contender, attributed to its robustness and probiotic activity.

# ENCAPSULATION

## OVERVIEW

Microencapsulation became a pivotal technique not only for bioactive molecules but also for probiotics delivery thanks to several key factors. The main reason is that it offers an enhanced degree of protection to these sensitive molecules or microorganisms during manufacturing, storage, and transit; reducing the risk of deterioration or loss of viability/bioactivity (Jayaprakash, Maudhuit, et al., 2023; Manojlović et al., 2010). Microencapsulation can offer significantly improved stability of these sensitive substances against environmental stressors such as heat, light, and oxygen (Alves et al., 2021; Manojlović et al., 2010). Thus, it can significantly enhance the effectiveness and longevity of both probiotics and bioactive molecules. The encapsulation also allows the compound of interest to remain functional following the harsh environmental conditions of, for example, the stomach, ensuring they reach the intestines where they are absorbed or exert their beneficial effects. Microencapsulation also allows – by modulating the matrix composition, physical state, etc. – the precise controlled release of the compound of interest over time. Moreover, microencapsulation has the added advantage of masking the unpleasant tastes or odours of some bioactive compounds, improving the consumer acceptance (Di Giorgio et al., 2021; Manojlović et al., 2010). Lastly, the encapsulation aids in efficiently delivering beneficial substances, like probiotics and bioactives, in a highly concentrated, with improved shelf-life and stability, making them more market

and consumer-friendly (Manojlović et al., 2010).

When designing the carrier for probiotic microencapsulation, it is crucial to take four principal parameters into account: the product properties, the target host, the production process, and the probiotic strain used (Sanders & Marco, 2010). An illustration of the principal branches is displayed in Figure 10. The product properties refer to the encapsulation material used, including its biocompatibility, and ability to protect the probiotics effectively while releasing them at the right location. The target host concerns the specific characteristics of the human host receiving the probiotics, such as its physiology, dietary habits, and health status. The production process denotes the ability of the designed process in maximising the probiotic survival. Lastly, the characteristics of the probiotic strain itself must be considered, including its tolerance to encapsulation and storage conditions, survivability in the gastrointestinal tract, and its ability to colonise the gut and confer health benefits to the host.

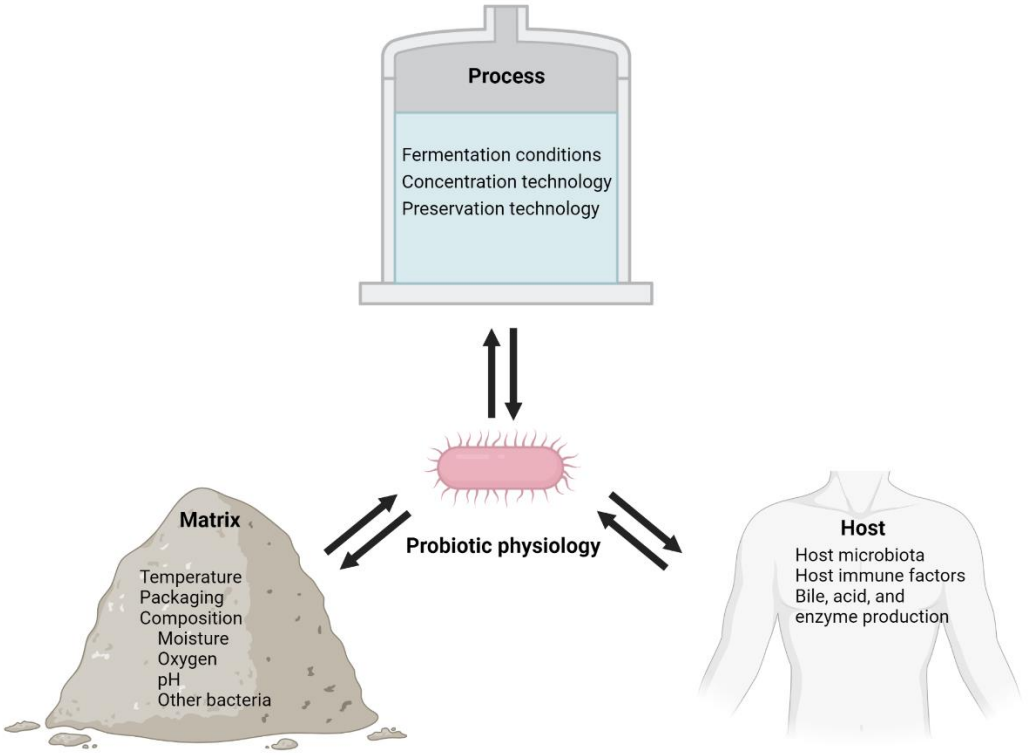


*Figure 10: illustration of the potential factors influencing probiotic physiology, in vivo functionality and stability (Sanders & Marco, 2010).*

# CURRENT METHODS OF PROBIOTIC ENCAPSULATION

## Wet-scaffolds encapsulation

One of the primary challenges linked to the encapsulation of probiotic cells in aqueous systems is their limited shelf-life. To maintain the biological activity of the bacteria, storage under refrigerated conditions is frequently chosen. Encapsulation of probiotics within wet scaffolds can be accomplished using various methods. Among these, fermentation emerges as the predominant approach for encapsulating probiotics in semi-solid aqueous scaffolds like yogurt or cheese. (Doherty et al., 2010; Vasiljevic, 2022). However, the organoleptic quality of fermented products is significantly influenced by both the specific probiotic strain utilised and the nature of the food matrix (Vasiljevic, 2022). The integration of probiotics into food systems has been limited due to challenges such as consumer acceptance. As a result, the range of foods that naturally incorporate probiotics is limited. To address the demand for innovative probiotic products, researchers have developed immobilisation techniques using wet-based carriers for higher cell loadings, greater strain diversity, and enhanced stability during storage (Vivek et al., 2023).

Extruded microbeads and microbeads from water-in-oil (w/o) emulsions (Figure 11) relying on the formation of microgelled particles (0.3–3 mm) by ionotropic, cold, acid or rennet gelation of a polysaccharide (e.g. sodium alginate, κ-carrageenan) or proteins (e.g. whey protein, egg white) were evaluated as a potential encapsulation technique (Heidebach et al., 2009b, 2009a; Vivek et al., 2023).

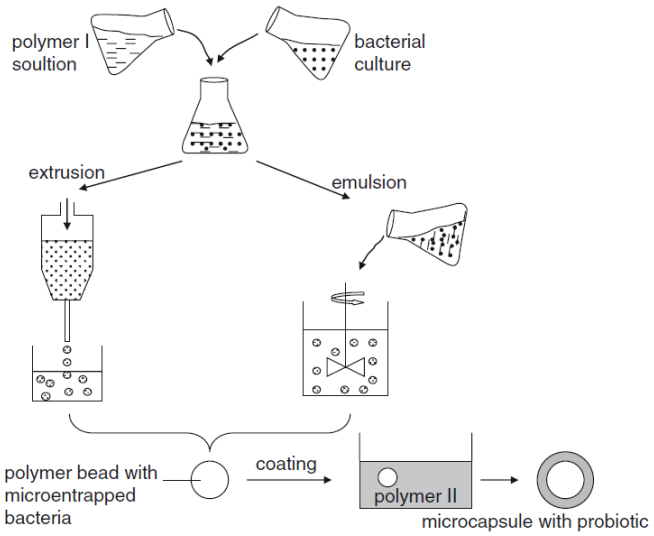


*Figure 11: Gel particle technologies for encapsulation of probiotic in microbeads. Adapted from Manojlović et al., (2010).*

Modifying the microbeads' composition enables the controlled release of entrapped bacteria throughout gastrointestinal digestion. Typically, encapsulation within sodium alginate microbeads is the most prevalent method to ensure optimal cell encapsulation while preserving their structural integrity during gastric digestion followed by bacterial release in the intestinal tract (Ding & Shah, 2007; Gómez-Mascaraque et al., 2019). Moreover, the incorporation of sodium alginate enhances mucoadhesive properties, optimising the delivery of bioactive molecules and probiotics (El-Kamel et al., 2002; Solanki & Shah, 2016). Coatings of these microcapsules with digestive enzyme-resistant biopolymers, like chitosan, has shown increased cell survivability. However, this can slow down the release of the cells (Manojlović et al., 2010; Qi et al., 2020; Sohail et al., 2011).

Both hydrogels, 3D-printed scaffolds, and fibres produced by electrospinning have garnered scientific attention for the delivery of probiotic cells. The significance of these structures extends beyond the realm of food, where they present opportunities to develop food products with complex shapes, precise internal architectures, customised compositions, and personalised nutritional values (Divyashree et al., 2021; Duman & Karadag, 2021; Ma et al., 2021; Xu et al., 2023). In the biomedical domain, several studies on 3D-printed structures and hydrogels embedding probiotic demonstrated a fair antibacterial activity that booted the tissue healing process (Mei et al., 2022; Yang et al., 2020).

Bigels are innovative semi-solid materials created by merging hydrogels with organogels under high shear conditions (Zhuang et al., 2021). Such delivery systems have the advantage of being able to carry and deliver both hydrophilic and lipophilic compounds. They have demonstrated potential in drug delivery for both pharmaceutical and cosmetic uses (Mao et al., 2020). Recently, Zhuang et al., (2021) demonstrated the feasibility of bigels for the encapsulation of probiotics, reducing the probiotic inactivation and encapsulated in bigels compared to non-encapsulated *B. lactis* and *L. acidophilus*. However, it was reported that the industrial relevance of bigels is still limited due to their high temperature sensitivity and product composition (Mao et al., 2020)

Emulsion and liposomes found their market in delivery systems for probiotic in liquid-based products. In standard emulsions, bacteria act as solid Pickering particles that adhere to the oil-water interface, acting as a physical barrier preventing the oil droplets from coalescing with each other and thus stabilises the emulsion. In the case of liposome structures (water-in-oil-in-water, w/o/w), the probiotic bacteria are entrapped within the liposome with the oil phase ensuring reducing impact of environmental stressors such as

oxygen (Haji et al., 2022; Xu et al., 2022).

## Anhydrobiotics

In wet matrices, bacteria demonstrate elevated vulnerability to environmental stressors such as pH and oxygen, frequently resulting in diminished viability. The preservation of these matrices in a wet-state demands energy-intensive refrigeration, thereby introducing substantial logistical hurdles, notably during transportation. Conversely, dry carriers for probiotics, referred to as anhydrobiotic, present a more robust storage alternative. Encapsulation within these desiccated matrices minimises the metabolic activity of the bacteria while also hampering the development of competitive microorganisms, thereby extending shelf-life and securing adequate viable counts until ingestion (Capozzi et al., 2016; Ventura et al., 2011).

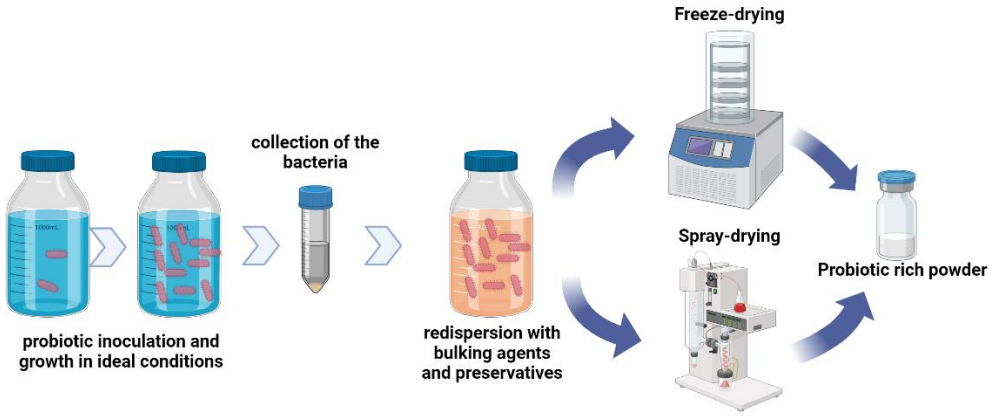


*Figure 12: Schematic representation of the methodologies utilised in the production of powders containing probiotic cells.*

The two predominant methods for embedding probiotics within these dry matrices are spray-drying and freeze-drying (Figure 12) (Cook et al., 2012; Rahman, 2007; Yao et al., 2020). In the food industry, spray drying – i.e. atomisation of a solution/emulsion containing a suspension of probiotics – is typically considered the golden standard, as it is easily scalable, flexible in terms of feed matrix, and cost-efficient. However, the high temperatures required for this method have been associated with a significant loss in probiotic viability during the process (Burgain et al., 2015; Cook et al., 2012). Depending on the composition of the precursors, the viability may vary. Ying et al., (2010) observed that emulsions stabilised by corn starch and whey protein, when spray dried, allowed a LGG cells survivability of approximately 3%. This result aligns with most of the literature, which typically reports 1–2 $\log CFU.g^{-1}$ reduction. However, a limited number of studies have demonstrated stable probiotic counts throughout the drying process (Cook et al., 2012; Huang et al., 2017). Spray-drying is primarily suitable for water-soluble

components, which often leads to inadequate protection of probiotics during digestion owing to matrix disintegration. Conversely, freeze-drying provides enhanced preservation of the probiotics' structural integrity throughout the drying process, albeit at the expense of extended processing durations and increased operational costs (Cook et al., 2012; Yao et al., 2020). Freeze-dried systems can be produced utilising partially water-soluble precursors, which facilitate improved preservation of probiotics under unfavourable conditions, such as in gastric fluids (Burgain et al., 2015). Short-chain carbohydrates like trehalose, lactose, and glucose frequently serve as cryoprotectants, facilitating the vitrification of the serum phase and simultaneously preserving membrane integrity against potential damage from intracellular ice formation (Aschenbrenner et al., 2012; Aschenbrenner, Först, et al., 2015; Sun et al., 2021). Rapid cooling, as achieved through techniques such as quench freezing in liquid nitrogen ($LN_2$), minimises cryo- and osmo-injuries attributed to the formation of fine ice crystals, which in turn, prevents the lysis of bacterial cells (Aschenbrenner, Först, et al., 2015). In a recent study, Sun et al., (2021) investigated the role of trehalose in the preservation of *L. plantarum* probiotic cells within milk protein/pullulan-based hydrogels during freeze-drying and subsequent storage. Their findings revealed that trehalose markedly enhanced survival rates during freeze-drying, an effect attributed to the elevation of the glass transition temperature, which facilitates the formation of a stable glassy state throughout the drying phase allowing the preservation of the cell membrane's structural integrity and mitigated unfavourable chemical reactions (Aschenbrenner, Först, et al., 2015; Carpenter et al., 1987). Furthermore, the enhanced storage stability can be ascribed to trehalose's ability to retain the minimal moisture content required by the *L. plantarum* probiotic cells. The cooling rate of the precursors plays a pivotal role in preserving bacteria during the freezing process. Proteins, specifically milk proteins, and polysaccharides such as alginates and pullulan, or their combinations, can be employed to modulate the dissolution properties and digestibility of probiotic carriers. This allows an enhanced preservation of probiotic bacteria during storage and in the adverse conditions present in the stomach by impeding the diffusion of environmental stressors (e.g. oxygen, acid) (Burgain et al., 2013; Guerin, Burgain, et al., 2017; Guerin, Petit, et al., 2017; Sun et al., 2021; Xie et al., 2023; Xie et al., 2022). However, previous studies have showcased that the use of polysaccharides alone does not provide a matrix that satisfactorily preserve probiotics (Shah et al., 2016).

In both scenarios, it is crucial to judiciously select the encapsulating matrix – whether

proteins, mono-, di-, oligo- or polysaccharides, polyols, lipids or a combination thereof – to mitigate the effects of environmental stressors and minimise cell lethality (Agudelo et al., 2017; Ahlawat et al., 2023; Aschenbrenner et al., 2012; Sun et al., 2021; Ying et al., 2010).

Several alternative encapsulation techniques have been showcased in the literature but remain relatively underexploited. These techniques include the formation of edible films (Pavli et al., 2018; Soukoulis et al., 2017; Soukoulis, Yonekura, et al., 2014), electrostatic spray-drying (Jayaprakash, Gaiani, et al., 2023), spray-freeze-drying (Her et al., 2015; Semyonov et al., 2010), vacuum-drying (Foerst et al., 2012; Santivarangkna et al., 2006), fluidised-bed drying (Schell & Beermann, 2014; Stummer et al., 2012), refractance window drying (Aragón-Rojas et al., 2019; Yoha et al., 2020). Recently, cryogel monoliths based on freeze-dried 3D printed structures made of agar and gelatin (Kuo et al., 2022) and freeze-dried hydrogels made of whey proteins and pullulan (Sun et al., 2021) showed promising results for the bacteria preservation during storage at chilling conditions under a dry atmosphere. However, their performance under various atmosphere-controlled conditions, *in vitro* digestion and the probiotic mucoadhesion remain unexplored.

Worth to note that in several case studies, combination of the above-mentioned techniques was reported to improve the performance of the delivery systems. For instance, the production of cryogel monoliths required the production of a hydrogel precursor followed by a dehydration step.

# PROJECT OBJECTIVES

The central aims of this thesis are multi-dimensional, rotating around the exploration and understanding of industrially significant gums extracted from underexploited resources and their use in the development in food supplements combining probiotic cells and milk proteins. The fundamental concept of this project is rooted in the utilisation of ingestible dietary fibres to mitigate probiotics' exposure to environmental stressors during storage and restrain protein digestibility during the gastric phases achieved by impeding the diffusion of enzymes through the matrix, concurrently providing protection to bacteria against the harsh conditions of the gastrointestinal tract. Furthermore, the hypothesis posits that the inclusion of dietary fibres may also enhance the bioadhesion of bacteria to the gut mucosa favouring the GIT colonisation. To access the hypothesis, objectives were strategically divided into five key points:

i. To develop an optimised gum extraction method from underexploited plant seeds – alfalfa and flaxseed – ensuring high gum purity.

ii. To characterise the compositional, physicochemical and techno-functional profile of the purified gums.

iii. To understand the interactions between these gums and milk proteins in aqueous systems, thereby exploring how the gums may modulate protein colloidal changes and digestibility.

iv. To formulate innovative anhydrobiotic structures containing *Lacticaseibacillus rhamnosus* GG in the form of self-standing cryogel monoliths using milk protein as matrix skeleton.

v. To enhance bacteria viability under various conditions such as storage and digestion, and to improve the adhesion to the gut epithelium by the incorporation of the gums in the cryogels monoliths.

The following chapters outline the effects of meeting these objectives and presenting innovative opportunities for the design of novel food products with enhanced functionality. The initial chapter focuses on addressing the first two objectives, the second delves into an in-depth analysis of the third point, and the third chapter discusses the final two objectives (Figure 13).

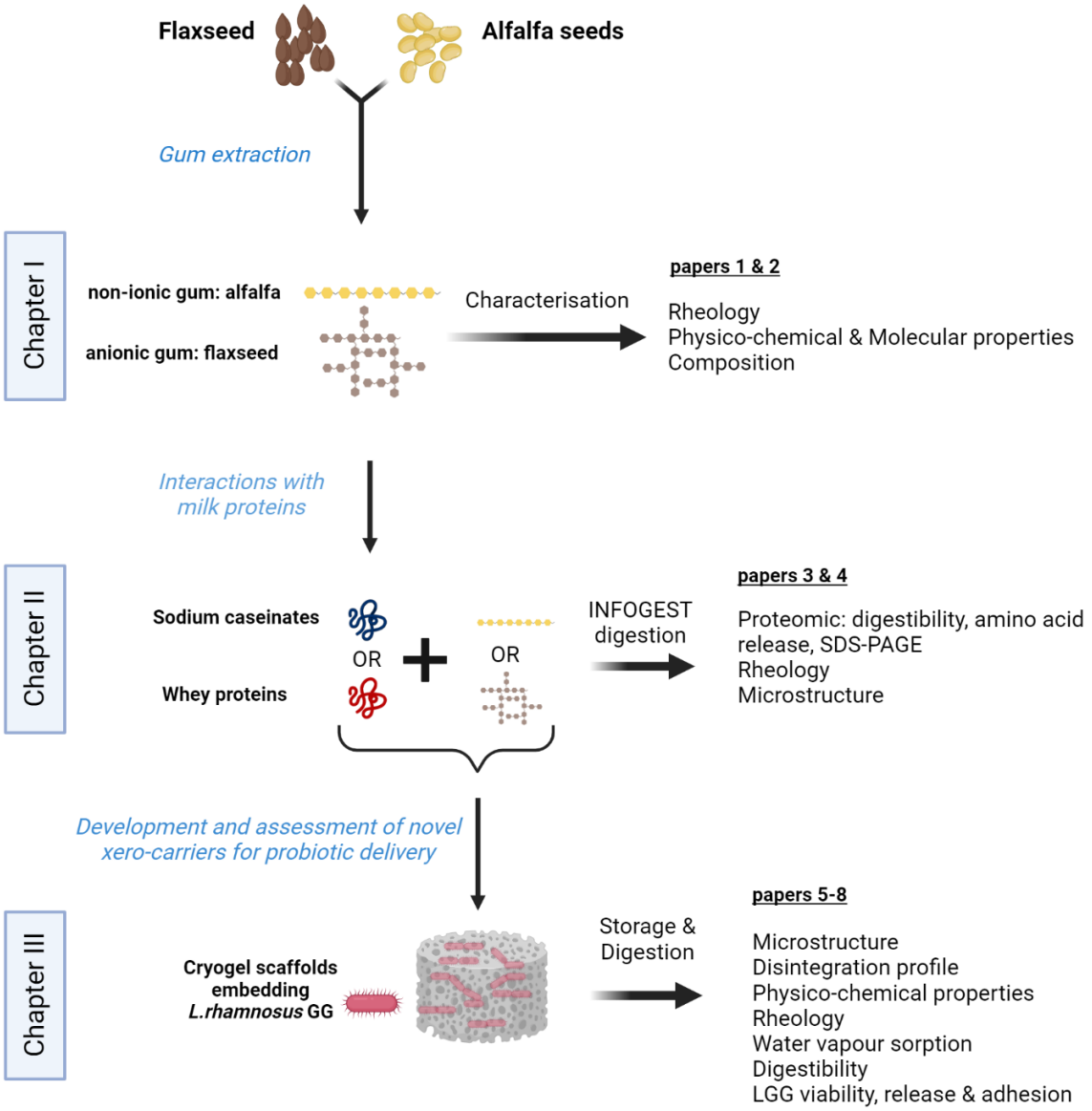


*Figure 13: Graphical abstract illustrating the structural organisation and key themes of the PhD thesis.*

# CHAPTER I: ISOLATION AND CHARACTERISATION OF PLANT SEED GUMS

## PREAMBLE

This chapter is dedicated to the comprehensive understanding of food relevant gum extracted from underexploited resources, specifically those derived from the endosperm of alfalfa seed and the seed coat of flaxseed. It is well established that the composition and the molecular conformation of gums dictates their techno-functional properties, including thickening, gelling, emulsifying and foaming capacity. The feasibility of a food grade extraction and purification method combining different crops and extraction procedures was assessed. Our investigations comprised the proximate composition and osidic composition, key parameters in determining the polysaccharide subcategories and their potential functional properties. The chapter further investigates the molecular structure conformational properties of the extracted gums such as the molecular weight, intrinsic viscosities, hydrodynamic radii etc., elucidating their three-dimensional arrangement and their polymer-polymer interaction in aqueous solutions. Alongside, this chapter provide deep insights into the rheological properties of the mucilages, namely flow behaviour, viscosity, viscoelasticity and gelling property. This meticulous examination of alfalfa and flaxseed gums creates a holistic understanding of their unique characteristics, thereby paving the way for further studies on the multifaceted roles these mucilages can play in improving food quality, nutrition, and sustainability in the food industry.

# STRUCTURE CONFORMATIONAL AND RHEOLOGICAL CHARACTERISATION OF ALFALFA SEED (*Medicago sativa* L.*)* GALACTOMANNAN

Thierry HELLEBOIS[1,2], Christos SOUKOULIS[1], Xuan XU[1], Jean-Francois HAUSMAN[1], Alexander SHAPLOV[4], Petros S. TAOUKIS[3], and Claire GAIANI[2]

[1]Environmental Research and Innovation (ERIN) Department, Luxembourg Institute of Science and Technology (LIST), Esch-sur-Alzette, Luxembourg
[2]Université de Lorraine, LIBio, Nancy, France
[3]Laboratory of Food Chemistry and Technology, School of Chemical Engineering, National Technical University of Athens, Athens, Greece
[4]Materials Research and Technology (MRT) Department, Luxembourg Institute of Science and Technology (LIST), Esch-sur-Alzette, Luxembourg

Carbohydrate Polymers
Volume 256, 15 March 2021, 117394
doi.org/10.1016/j.carbpol.2020.117394

# ABSTRACT

In the present work a galactomannan extract of low protein residue (< 1.3% wt dry basis) was isolated from alfalfa (*Medicago sativa* L.) seed endosperm meal. The alfalfa gum (AAG) comprised primarily mannose and galactose at a ratio of 1.18:1, had a molecular weight of $2 \times 10^6$ Da and a radius of gyration of 48.7 nm. The average intrinsic viscosity of the dilute AAG dispersions calculated using the modified Mark-Houwink, Huggins and Kraemer equations was 9.33 $dL.g^{-1}$ at 25 °C. The critical overlap concentration was estimated at 0.306% whereas the concentration dependence of specific viscosity for the dilute and semi-dilute regimes was $\propto c^{2.3}$ and $c^{4.2}$, respectively. The compliance to the Cox-Merz rule was satisfied at 1% of AAG, whereas a departure from superimposition was observed at higher concentrations. Viscoelasticity measurements demonstrated that AAG dispersions exhibit a predominant viscous character at 1% wt., whereas a weak gel-like behaviour was reached at AAG concentrations ≥ 3% wt.

# INTRODUCTION

Market globalisation, emerging issues associated with food security and sustainable management of food biomass and natural resources concern a major challenge for food ingredient manufacturers. Carbohydrate food biopolymers i.e. polysaccharides and oligosaccharides constitute a major group of food ingredients due to their multifaceted techno-functionality and important role as dietary and biologically active macromolecules (Williams & Phillips, 2009). In the last decade, the attempts to valorise food industry side-streams or underexploited food biomass as alternative sources of food and nutraceutical relevant carbohydrate polymers are steadily gaining popularity. In this context, different food industry side-streams including cereals, legumes, oilseed crops, vegetable and fruit residues, plant cladodes etc. have been evaluated for their potential to provide marketable solutions in the domain of food biomacromolecules (Ben-Othman et al., 2020; Soukoulis et al., 2018).

Galactomannans are heterogeneous polysaccharides comprising a β-(1→4) D-mannose backbone branched with α-(1→6) linked D-galactose monomeric units. It is well established that the mannose to galactose (M/G) ratio varies with their botanical origin and modulates their techno-functional properties i.e. cold-water swelling ability, thickening, gelling, film forming and cryogelation properties commercially available galactomannans (on approximate increasing M/G ratio) include fenugreek (1:1, *Trigonella foenum-graecum* L.), guar (2:1, *Cyamopsis tetragonoloba*), tara gum (3:1, *Caesalpinia spinosa*), locust bean gum (4:1, *Ceratonia siliqua*) and cassia gum (5:1, *Cassia tora*) (Prajapati et al., 2013). In addition, galactomannans from underexploited plant seed sources such as honey locust (*Gleditsia triacanthos*), Chinese locust (*Gleditsia sinensis*), clover (*Melilotus albus* and *Melilotus officinalis*), flame tree (*Delonix regia*), yellow flame tree (*Peltophorum pterocarpum),* creamy peacock flower (*Delonix elata*), mesquite (*Prosopsis juliflora*), henna (*Cassia fistula*), and malu creeper (*Bauhinia vahlii*) *have been successfully isolated and characterised* (Jamir et al., 2019; Liu et al., 2019; López-Franco et al., 2013; Rodriguez-Canto et al., 2019; Sciarini et al., 2009). Recently, spent coffee grounds have been reported as a promising bioresource for exploiting galactomannan and arabinogalactan rich fractions (Moreira et al., 2015).

Alfalfa (*Medicago sativa* L.) is a perennial herbaceous forage legume cultivated world-wide due to its high nutritional value as fodder and feed for livestock. Alfalfa is also recognised for its sustainable character, excellent adaptability to extreme climate conditions, and ecological resilience e.g. alfalfa assists in soil protection, nitrogen

fixation, mitigation of soil contaminants, lowering of air contaminants, carbon dioxide sequestration etc (Bacenetti et al., 2018). From an economical viewpoint, combined alfalfa exploitation (forage and seeds) can significantly improve several economic indices including gross margin, cost effectiveness quotient, and profit rate (Boelt et al., 2015; Pajić & Marković, 2016). In the framework of actions for counteracting food security issues, alfalfa leaf meal has received much attention in the last years. It has been previously reported that alfalfa leaf meal contains at least 20% proteinaceous matter of similar essential amino acid composition to that of soybean protein concentrate, and 17 to 27% of soluble and insoluble dietary fibres (Hojilla-Evangelista et al., 2017; Mielmann, 2013). In addition, a plethora of micronutrients including carotenoids, tocopherol, polyphenols, saponins and vitamins of the B-complex have been identified (Cornara et al., 2016; Mielmann, 2013). Regarding the polysaccharides profile of alfalfa forage, it has been shown that total the polysaccharides content and the sugar monomers composition are dependent on the extraction and fractionation conditions (Wang et al., 2013, 2014). Wang et al. (2014) demonstrated that polysaccharide fractions of 20– 60 kDa containing ca. 37–52% of uronic acids could be obtained via ion-exchange and size-exclusion chromatography. All polysaccharide fractions exerted a dose dependant (up to 1000 $\mu g.mL^{-1}$) protective effect against hydrogen peroxide induced oxidative stress, whereas the hepatotoxicity levels were minimised when fractions of high uronic content and molecular weight were administered to the hepatocytes *in vitro* model. In two consecutive studies Chen, Liu, Zhang, Dai, et al. (2015) and Chen, Liu, Zhang, Niu, et al. (2015) investigated the techno-functionality and bioactivity of the hemicellulosic and pectic polysaccharide fractions isolated from hot alkali extracts of alfalfa stems. Despite the differences in their structure conformational profile, both polysaccharide fractions exerted good thermal stability and significant suppression effects on pro-inflammatory cytokine genes such as IL-1β, IL-6 and COX-2.

Rudimentary studies of alfalfa seed compositions reported that the major polysaccharide component of alfalfa seeds belongs in the galactomannan class (Dobrenz et al., 1993; Grasdalen & Painter, 1980; McCleary & Matheson, 1975). Nonetheless, the structure conformational and technological aspects of the alfalfa galactomannans remain poorly studied. This study aimed at the extraction, purification and assessment of the structure conformational, steady, dynamic and thermo-rheological properties of galactomannan from the endosperm of alfalfa seeds.

# MATERIALS & METHODS

## Materials

Organic alfalfa seeds (Food to Live, New York, NY, United States) were purchased from the local market. All organic solvents and chemicals used for the extraction and the analysis of the alfalfa gum were of analytical grade and obtained from Sigma-Aldrich (Leuven, Belgium).

## Extraction and isolation of the alfalfa gum

A schematic representation of the method used for the extraction and isolation of alfalfa gum is given in Figure 14. In specific, alfalfa seeds were soaked in Milli-Q water (pH = 4 using 0.5% wt. citric acid), Millipore Inc., Burlington, MA, United States) at 50 °C for 2 h under mild magnetic stirring (IKA GmbH, Staufen, Germany). To facilitate the hydration of the seeds, the alfalfa seed to water ratio was maintained at 1:10 (wt.). The alfalfa seed suspension was vacuum filtered using a Buchner funnel with fritted disc and the obtained seed solids were freeze-dried at –80 °C for 72 h (Alpha 2-4 LSCplus, Christ, Osterode am Harz, Germany). The lyophilised seeds were ground (8,000 rpm for 5 min) using a knife mill (Grindomix GM300, Retsch, Haan, Germany) and the obtained alfalfa meal was mixed with Milli-Q water at a 1:50 (wt.) ratio and kept at 50 °C under mechanical stirring for 2 h to allow sufficient extraction of the water-soluble biopolymers. Then, the alfalfa meal suspension was centrifuged at 18,000*g* for 15 min and the supernatants obtained after two consecutive washings of the alfalfa solids (with Milli-Q water at 1:10 ratio) were pooled and mixed (1:2) with anhydrous ethanol to promote aggregation and precipitation of the polysaccharides. The ethanolic suspension was centrifuged at 4,800*g* for 10 min and the obtained gum pellets were flashed with nitrogen to evaporate the ethanol excess and reconstituted in Milli-Q water adjusted with sodium carbonate at pH = 10 and kept under stirring at 50 °C until complete dissolution of the gum solids. To remove the protein impurities, the pH of the biopolymer solution was adjusted at the isoelectric point of alfalfa proteins (i.e. pI ≈ 4–4.25) using citric acid. The resulting suspension was centrifuged at 18,000*g* for 15 min and the supernatant was neutralised (pH = 7) using sodium carbonate. For removing the residual sodium citrate, the polysaccharide solution was dialysed (cut-off 12.4 kDa) against Milli-Q water for 72 h. Finally, the dialysed polysaccharide aliquots were freeze-dried at −80 °C for 5 days (Alpha 2–4 LSCplus, Christ, Haan, Germany), and the obtained gum lyophilisates were stored under controlled temperature and relative humidity conditions ($a_w$ = 0.11, 25 °C).

For comparison purposes, galactomannans were also extracted from defatted fenugreek seed meal (*Trigonella foenum-graecum*, Arkopharma, Carros, France) following the aforementioned procedure.

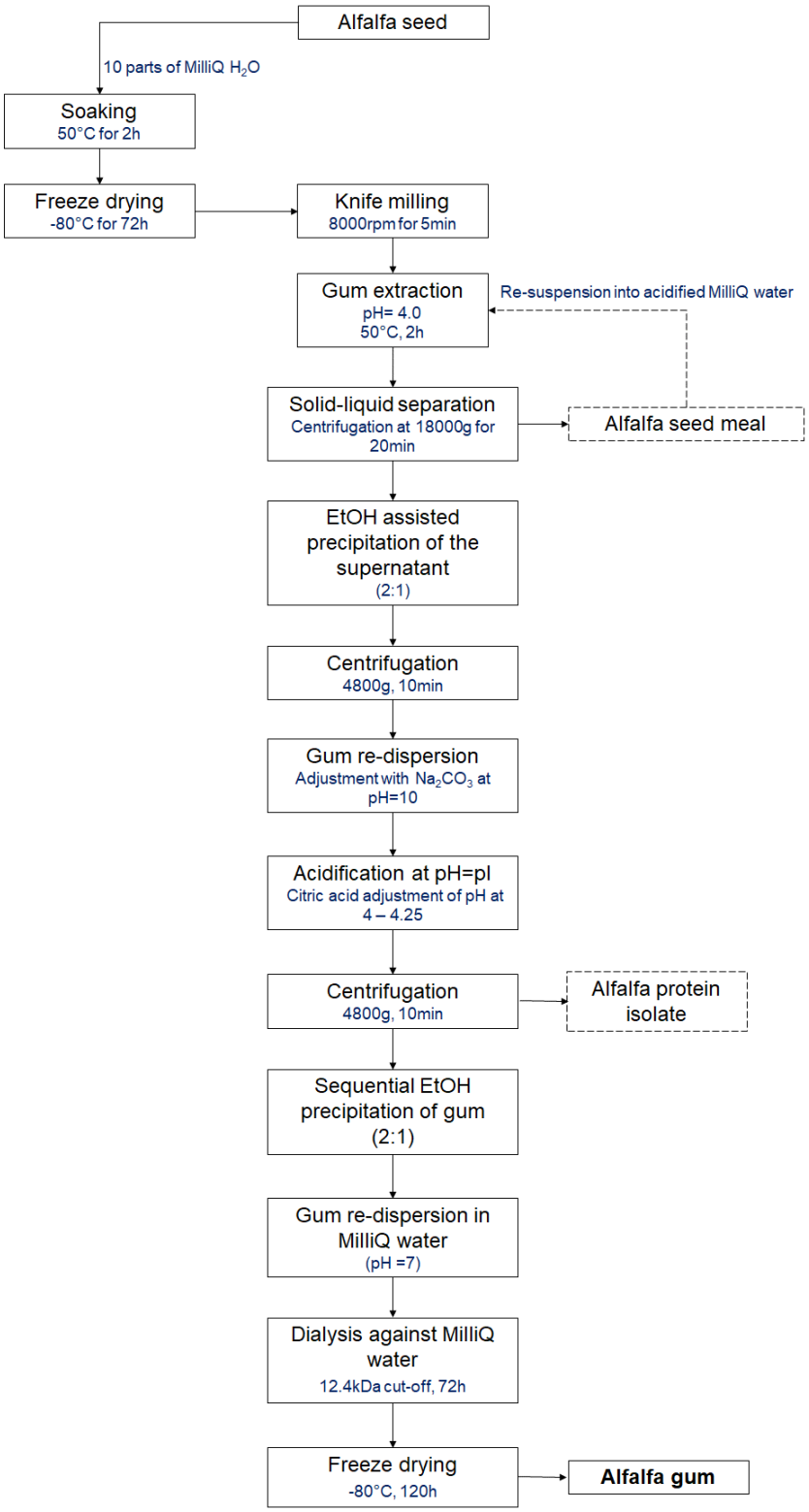


*Figure 14: Illustration of the clean label methodology adopted for extracting and purifying the galactomannan from the endosperm of alfalfa seeds.*

## Compositional and structure conformational properties determination

### i. Proximate composition analysis

Moisture and ash content of the galactomannan gum extracts were gravimetrically determined according to the AOAC standard methods. The protein content was determined according to the Dumas method using a CHNS analyser (Elementar Vario Cube, Langensenbold, Germany). Total carbohydrate content was determined using an enzymatic assay kit (Megazyme, K-ACHDF 08/16). Total lipid content was determined by difference.

### ii. Sugar monomer and uronic acid composition analysis

The sugar monomer composition of the galactomannan gum extracts was determined according to the method of Qian et al., (2012) with minor modifications. In brief, 20 mg of the galactomannan were transferred into an Eppendorf tube with screw cap, mixed with 1 mL of sulphuric acid 2 M and incubated at 99 °C with intermittent stirring for 4 h using a Thermomixer (Thermomixer R, Eppendorf, Hamburg, Germany). On completion of incubation, the tubes were cooled down in an ice bath, centrifuged at 10,000*g* for 5 min and the supernatants were carefully collected using a syringe. The sample preparation was carried out in four replicates.

The hydrolysate was diluted 1:300 and 1:500 with Milli-Q water and analysed using a Dionex ICS-5000+ Capillary HPIC System coupled with a pulsed electrochemical detector (Thermo Scientific Dionex, Waltham, MA, United States). The separation of monosaccharides was performed with a CarboPac SA10 analytic column (2 × 250 mm, Thermo Scientific Dionex) and a CarboPac PA20 analytic column (3 × 150 mm, Thermo Scientific Dionex, Waltham, MA, United States). For SA10 column, 100% 1 mM NaOH was used as an eluent to separate the monosaccharide at a constant flow rate of 0.38 $ml.min^{-1}$ at 45 °C. For the PA20 column, the separation of monosaccharides was performed using 4% 1 mM NaOH at a flow rate of 0.5 $ml.min^{-1}$ at 30 °C. The retention time obtained with a single injection of each standard was used to identify each monosaccharide. The quantification of monosaccharides was performed using a calibration curve generated with varying standard concentrations (1, 2.5, 5, 7.5, 10, 25, 50, 75 and 100 $\mu mol.L^{-1}$). Data acquisition and analysis were carried out using Chromeleon Chromatography Data System Software (Thermo Scientific, Waltham, MA, United States).

### iii. Gel permeation size-exclusion chromatography (GPC/SEC)

A 1200 Infinity gel permeation chromatograph (GPC, Agilent Technologies, Santa Clara, CA, United States) was used to determine $M_n$, $M_w$, $M_z$ and $M_w/M_n$ of the polymers. The chromatograph was equipped with an integrated IR detector, two columns (PL aquagel-OH MIXED-H and PL aquagel-OH MIXED-M) and a PL aquagel-OH guard column (Agilent Technologies, Santa Clara, CA, United States). 0.1 M NaNO3 aqueous solution containing 0.02% (w/v) of NaN3 was used as an eluent, the flow rate was maintained at 1.0 $mL.min^{-1}$and the measurements were performed at 50 °C. Pullulan standards (ReadyCal-Kit Pullulan high, PSS Polymer Standards Service GmbH, Mp = 180–1,530 × $10^3$) were used to perform calibration. All the samples were filtered through a 0.2 µm Teflon filter prior injection.

The Flory-Fox model (Equation 1) was used to calculate the radius of gyration ($R_g$) as follows:

Equation 1 $$R_g = \left[\frac{[\eta]\overline{M_w}}{\Phi_0}\right]^{1/3}$$

where $\Phi_0$ is a proportionality constant equal to 2.86 × $10^{23}$ $mol^{-1}$ for random coil and linear polysaccharides (Gillet et al., 2017).

The number-average degree of polymerisation of the gum ($DP_n$) was calculated (Equation 2) as follows:

Equation 2 $$DP_n = \frac{M_n}{M_0}$$

where $M_n$ is the number-average molecular weight of the polymer and $M_0$ the molecular weight of the repeating unit.

iv. Intrinsic viscosity measurements

The intrinsic viscosity [η] of dilute alfalfa gum dispersions (0.01–0.1% wt.) in Milli-Q water was measured using 0C Ubbelohde capillary viscometer (Paragon Scientific, Birkenhead, United Kingdom) at 25 ± 0.1 °C. The intrinsic viscosity was determined as the intercepts of the Huggins (Equation 3) and Kraemer (Equation 4) equations by extrapolating to an infinite dilute system:

Equation 3 $$\frac{\eta_{sp}}{c} = [\eta] + k_H[\eta]^2 c$$

Equation 4 $$\frac{\ln \eta_{rel}}{c} = [\eta] + k_K[\eta]^2 c$$

where: $\eta_{sp}$ and $\eta_{rel}$ denote the specific and relative viscosity, respectively, c is the alfalfa gum concentration, and $k_H$ and $k_K$ are the Huggins and Kraemer coefficients.

## Steady state and dynamic rheological measurements

Aqueous dispersions (0.1, 0.25, 0.5, 0.75, 1, 2, 3, and 4% wt.) of alfalfa gum in Milli-Q water (adjusted at pH = 7 using NaOH 0.1 M) were prepared for conducting the rheological measurements. All rheological measurements were performed in an Anton-Paar oscillatory rheometer (MCR 302, Graz, Austria) equipped with either a concentric cylinder (steady state rheological measurements) or cone plate geometry (dynamic rheological measurements).

### i. Flow behaviour

Aliquots of the galactomannan dispersions (ca. 15 mL) were transferred to the measuring geometry and tempered at ambient temperature (25 ± 0.05 °C) for 20 min prior to the analyses. Due to the time-dependent flow behaviour of the solutions, a pre-shearing (at 200 $s^{-1}$ for 5 min) of the gum dispersions was applied until a steady state to be achieved. Upward shear rate sweeps in the range of 1 to 1,000 $s^{-1}$ were performed. The obtained shear stress $\tau$ (Pa) – shear rate $\dot{\gamma}$ ($s^{-1}$) data were fitted into the Ostwald-de Waele (Power) model (Equation 5) as follows:

Equation 5 $$\tau = K\,\dot{\gamma}^{n}$$

where K ($Pa.s^{-n}$), n, $\tau_0$ (Pa) and $\eta_\infty$ (Pa.s) denote the consistency coefficient, rheological behaviour index, yield stress and limiting viscosity at infinite shear rate, respectively.

### ii. Zero shear viscosity measurements

To determine the critical concentration of alfalfa gum, the limiting viscosity at zero shear rate ($\eta_0$) was determined for galactomannan gum aqueous dispersions in the concentration range of 0.1–2% wt. For this purpose, the Williamson-Cross model (Equation 6), was fitted into the obtained viscosity – shear rate (0.01 to 1,000 $s^{-1}$) data:

Equation 6 $$\eta = \eta_\infty + \frac{\eta_0 - \eta_\infty}{1 + C\cdot\dot{\gamma}^{m}}$$

where $\eta_0$ and $\eta_\infty$ represent the zero and infinite shear viscosity, and C, m are the Cross time and rate constants, respectively.

### iii. Amplitude and frequency sweep measurements

For the dynamic rheological measurements, alfalfa gum dispersions in the concentration range of 1–4% wt. were prepared. Amplitude sweeps were conducted to determine the linear viscoelastic region (LVR) under controlled shear stress conditions, at 1 Hz and 25 °C. From the obtained amplitude sweep rheological spectra, the viscoelastic moduli and stiffness ($G'_{LVR}$ and $G''_{LVR}$, $\tan\delta_{LVR}$) in the LVR regime, the yield stress at the limit of

LVR regime (τy) and the strain and stress flow-point (G′ = G″) were calculated using the RheoCompass analysis software (Anton-Paar, Graz, Austria)

Frequency sweeps (0.1 to 100 Hz) within the LVR regime (strain = 0.5%) were performed at 25 °C to evaluate the viscoelastic profile of the alfalfa gum dispersions. The slope of the double logarithmic storage modulus (G′) – angular frequency (ω) curves was calculated. In addition, the frequency (f) at the which the crossover of the viscoelastic moduli (G′ = G″) takes place was calculated using Solver (Excel, Microsoft Inc, Redmond, WA, United States).

iv. Oscillatory thermo-rheology (OTR) and determination of non-isothermal kinetic parameters

For the OTR measurements, the alfalfa gum dispersions were heated from 25 to 70 °C at the rate of 5 °C.min$^{-1}$ and kept isothermally for 10 min. A small amount of silicon oil had been carefully applied on the cone-plate edge surface to prevent water evaporation. Monitoring of storage (G′) and loss moduli (G″) as well as complex viscosity ($\eta^*$) was conducted within the LVE regime (strain: 1%, frequency: 1 Hz). The following temperature ramp protocol was implemented: a) cooling from 70 to 5 °C at the rate of 2 °C.min$^{-1}$, b) isothermal holding at 5°C for 10 min and c) heating from 5 to 70 °C at the rate of 2 °C.min$^{-1}$. The temperature point where the viscoelastic crossover (G′ = G″) occurs were recorded.

It was previously shown (Razavi et al., 2018) that the temperature dependence of rheological parameters on heating or cooling cycles can be described by three main equations: the rate of reaction (Equation 7), the Arrhenius equation (Equation 8) and the time-temperature relationship (Equation 9)

Equation 7 $$\frac{d\eta^*}{dt} = k \cdot \eta^{*n}$$

where $\eta^*$ is the complex viscosity (in Pa.s), and n is the order of the viscosity change kinetics.

Equation 8 $$k = k_0(T_{ref}) \cdot \exp\left(-\frac{E_a}{R(T-T_{ref})}\right)$$

where $k_0$ is the pre-exponential factor, R the universal gas constant (R = 8.314 J.mol$^{-1}$.K$^{-1}$), T the temperature (°K) and $E_a$ the activation energy (J.mol$^{-1}$)

Equation 9 $$T = T_0 + \lambda \cdot t$$

where, $T_0$ is the initial temperature (i.e. 70 or 5 °C for cooling and heating profiles) and λ the cooling or heating rate (i.e. 2 °C.min$^{-1}$).

Using the Arrhenius equation, the Equation 7 can be re-written as follows:

Equation 10 $$\frac{d\eta^*}{dt} = k_0(T_{ref}) \cdot \exp\left(-\frac{E_a}{R(T-T_{ref})}\right) \cdot \eta^{*n}$$

which by logarithmic transformation yields:

Equation 11 $$\ln\left(\frac{d\eta^*}{dt}\right) - \ln(\eta^{*n}) = \ln k_0(T_{ref}) - \frac{E_a}{R(T-T_{ref})}$$

Derivation of Equation 9 gives:

Equation 12 $$dT = \lambda \cdot dt$$

Considering that the data were best fitting to second-order kinetics i.e. $n = 2$ and taking into account the Equation 10 and Equation 11, it is obtained:

Equation 13 $$\ln\left(\lambda \frac{d\eta^*}{dT} \times \frac{1}{\eta^{*2}}\right) = \ln k_0(T_{ref}) - \frac{E_a}{R(T-T_{ref})}$$

For the calculation of the kinetic parameters i.e. $k_0$ and $E_a$, the $\frac{d\eta^*}{dT}$ parameter was determined by deriving a low order polynomial model fitting the elastic modulus – temperature data:

Equation 14 $$\frac{d\eta^*(T)}{dT} = \frac{d\,(a_m T^m + a_{m-1} T^{m-1} + \ldots + a_1 T^1 + a_0)}{dT}, \text{ with } m \leq 3$$

The adopted approach for calculating the $\frac{d\eta^*}{dT}$ was also pre-validated numerically to ensure sufficient accuracy in the estimation of the kinetic parameters.

### Statistical analyses

The normal distribution of the data was verified by means of the Shapiro-Wilk test and Q-Q plot representation. In addition, the equality of variance among the variables was verified using the Levene's test. To determine the significance of the alfalfa gum concentration on the physicochemical and rheological properties, one-way ANOVA was performed using SPSS software (IBM, Armonk, NY, United States). Tukey's multiple range test was used to separate means of data when significant differences ($p < 0.05$) were detected.

## RESULTS & DISCUSSION

### Proximate and sugar monomers composition

For comparison purposes, the compositional profile of alfalfa gum was contrasted to that of in-house extracted fenugreek gum as well as commercially available guar and locust bean gums. It is well established that the yield and compositional profile of plant seed

extracts are influenced by several parameters including the botanical origin and cultivar type of the plant seed, the extraction conditions (temperature, seed to solvent mass ratio, pH and ionic strength) as well as the gum purification treatments (Soukoulis et al., 2018). The yield of the extraction for the alfalfa gum was estimated at 20.53 ± 0.22%, whereas following the same extraction protocol, the yield for fenugreek gum was determined at 27.0 ± 2.1%. As seen in Table 2, alfalfa gum was composed of 96.7% total carbohydrates, 1.3% protein, 2.0% ash and < 0.1% lipids residual matter (on dry basis). Interestingly, both alfalfa and fenugreek gum extracts were characterised by a notably low protein residue (protein content in the commercial galactomannans was 3.9 and 6.0% wt. for guar and locust bean gum, respectively), suggesting that the acid-assisted extraction and the isoelectric protein precipitation steps concomitantly resulted in a significantly lower amount of protein impurities in the purified gum extract. Galactomannans can be further stripped of their protein impurities via either enzymatic (proteases) or organic-solvent (e.g. isopropanol or biphasic phenol-water system) assisted deproteinisation treatments.
In terms of sugar monomers composition (Table 2), alfalfa gum was primarily composed of mannose (M) and galactose (G) sugar moieties at a M/G ratio of 1.18, whilst substantially lower amounts of other sugars such as arabinose and glucose were also detected. As expected, alfalfa gum exhibited an almost identical sugar composition profile to that of fenugreek gum obtained following the same extraction procedure (M/G = 1.24), whilst significantly higher M/G ratios were observed in the case of guar and locust bean gums i.e. 2.00 and 2.74, respectively. Our observations corroborate the literature data for alfalfa (M/G 1.09–1.28), fenugreek (M/G 1.05–1.26), guar gum i.e. M/G 1.65–2.00 and locust bean gum i.e. M/G 3.00–3.70 (Bourbon et al., 2010; Dhull et al., 2020; Grasdalen & Painter, 1980; Liu et al., 2020; Wu et al., 2009a).

## Structure conformation molecular properties

The GPC/SEC chromatographs of alfalfa, fenugreek, guar and locust bean gum are shown in Figure 15 Contrary to locust bean gum, alfalfa, fenugreek and guar gum exhibited a monomodal (less pronounced for guar gum) size distribution with a long tail towards the lower molecular weight. The molecular weight of alfalfa gum was calculated as $2.00 \times 10^6$ Da, which was almost identical to that fenugreek gum extracted with the same procedure ($2.02 \times 10^6$ Da) and lower than the $M_w$ of the commercial guar gum ($2.31 \times 10^6$ Da).

*Table 2: Proximate and sugar monomer compositional properties of the alfalfa, fenugreek, guar and locust bean gums*

| | Alfalfa gum | Fenugreek gum | Guar gum | Locust bean gum |
|---|---|---|---|---|
| Proximate composition[1] | | | | |
| Total carbohydrates (%) | 96.7 ± 1.2$^{bc}$ | 97.1 ± 0.4$^{c}$ | 95.2 ± 0.1$^{b}$ | 92.9 ± 0.2$^{a}$ |
| Protein (%) | 1.3 ± 0.1$^{a}$ | 1.3 ± 0.3$^{a}$ | 3.9 ± 0.1$^{b}$ | 6.0 ± 0.3$^{c}$ |
| Ash (%) | 2.0 ± 0.2$^{c}$ | 1.6 ± 0.4$^{c}$ | 0.9 ± 0.01a | 1.1 ± 0.01$^{b}$ |
| Sugar monomers composition (g.100g$^{-1}$ of total carbohydrate matter) | | | | |
| Arabinose | 0.20 ± 0.0$^{a}$ | 0.7 ± 0.0$^{b}$ | 1.4 ± 0.1$^{c}$ | 1.2 ±0.1$^{c}$ |
| Galactose | 46.0 ± 2.8$^{c}$ | 44.1 ± 0.9$^{c}$ | 33.0 ± 2.1$^{b}$ | 25.2 ±1.5$^{a}$ |
| Glucose | 0.30 ± 0.0$^{b}$ | 0.2 ± 0.0$^{a}$ | 1.2 ± 0.1$^{c}$ | 2.0 ±0.1$^{d}$ |
| Mannose | 53.8 ± 3.0$^{a}$ | 55.1± 0.2$^{a}$ | 64.3 ± 3.9$^{b}$ | 71.6 ±2.1$^{c}$ |
| Fucose | Nd | Nd | Nd | Nd |
| Rhamnose | Nd | Nd | 0.1 ± 0.0 | Nd |
| Uronic acids | Nd | Nd | Nd | Nd |
| M/G | 1.18 ± 0.14$^{a}$ | 1.24 ± 0.08$^{a}$ | 2.00 ± 0.24$^{b}$ | 2.74 ± 0.09$^{c}$ |

*[1] calculated on dry basis; lipid matter was detected in traces. [a-d] Different letters between the rows indicate significant difference ($p < 0.05$) according to Tukey's post hoc means comparison test. Nd: not detected.*

It is well established that the Mw of galactomannans can be highly diversified by parameters such as their botanical and geographical origin, the extraction and fractionation conditions (e.g. pH, temperature, type of organic solvents used for aggregation), the extent of the galactosyl substitution or depolymerisation etc. (Mathur, 2016). It is also worth noting that the presence of protein impurities in the gum extract could modify significantly the average molecular weight of the gum. Youssef et al. (2009) reported an increase in fenugreek gum molecular weight from $1.46 \times 10^6$ to $2.28 \times 10^6$ Da by reducing the protein content from 3.7% to 1.1%, respectively. In this context, $M_W$ of alfalfa gum was found to be in range with other galactomannans having a M/G ratio of ~ 1.0, such as fenugreek (from $0.56 \times 10^6$ to $2.35 \times 10^6$ Da) (Brummer et al., 2003; Wei et al., 2015; Youssef et al., 2009).

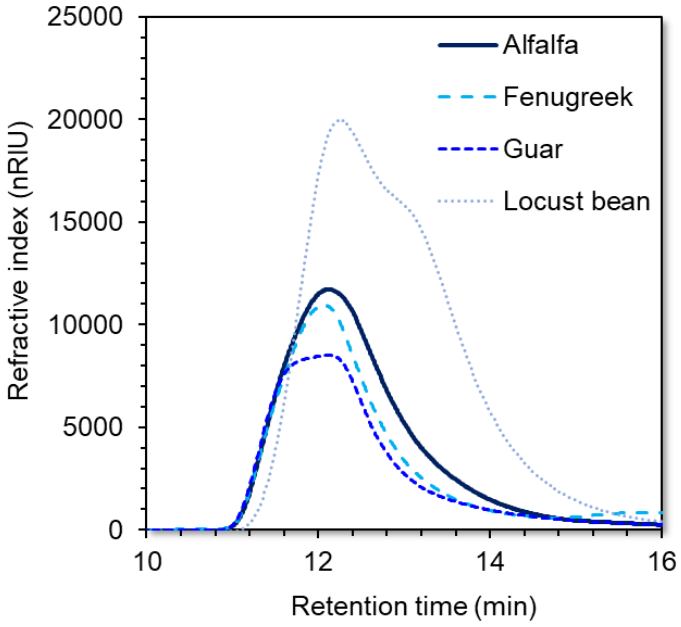


*Figure 15: Gel permeation size-exclusion chromatogram (GPC/SEC) of commercial (dotted lines) and in-house extracted (straight lines) galactomannan gums.*

The intrinsic viscosity [η] of the alfalfa gum dispersions was experimentally determined in the dilute regime i.e. $1.2 < \eta_{rel} < 2.0$ and $c < 0.1\%$ wt. using the Huggins and Kraemer equations (Figure 16). For comparison purposes, the [η] of all galactomannans was also determined using the Mark-Houwink equation as modified by Doublier & Launay (1981) for aqueous galactomannan dispersions (Equation 15):

Equation 15
$$[\eta] = 11.55 \cdot 10^{-6} \left( \left( 1 - \frac{G}{(G+M)} \right) \cdot \overline{M_w} \right)^{0.98}$$

where G and M denote the mass fractions for galactose and mannose sugar monomers and $\overline{M_w}$ is the polymer weight average molecular weight obtained from GPC/SEC analysis. As illustrated in Figure 16, the [η] of alfalfa gum was determined at 9.16 and 9.45 $dL.g^{-1}$ according to Huggins and Kraemer equations, respectively, whilst it was estimated at 9.40 $dL.g^{-1}$using the modified Mark-Houwink equation (Table 3). Thus, there is practically no discrepancy between the value of [η] obtained from GPC experiments carried out at 50 °C and the intrinsic viscosity calculated using the MKHS coefficients obtained at a different temperature (25 °C). In turn, this suggests that the volume occupied by macromolecules in solution was not strongly dependent on temperature. The [η] values for the rest galactomannans were estimated at 9.04, 12.87 and 7.86 $dL.g^{-1}$ for fenugreek, guar, and locust bean gum, respectively. Therefore, it can be deduced that the Huggins-derived [η] of alfalfa gum is in range with that reported for other galactomannans of ~ 1.0 M/G ratio, such as fenugreek gum (9.1–13.6 $dL\ g^{-1}$) and

*Mimosa scabrella* (9.0.dL.g$^{-1}$), and lower than guar gum (9.1–17.2 dL.g$^{-1}$) (Cheng et al., 2002; Doublier & Launay, 1981; Gadkari et al., 2018; Ganter et al., 1992; Gillet et al., 2017; Liu et al., 2020).

The [η] provides a proximate estimation of the size and structure molecular conformation of the polymer chains in a given solvent. The Huggins and Kraemer constants $k_H$ and $k_K$ for alfalfa gum were 0.85 and 0.02, respectively, indicating a rather poor solvent (deionised water) affinity that favours the self-association (aggregation) of the polymer chains. In general, a good polymer solvation is achieved when $0.25 < k_H < 0.5$ and $k_K < 0$ (Marani et al., 2013). The obtained $k_H$ and $k_K$ values for alfalfa gum, are higher than the literature reported for fenugreek gum ($k_K$ = -0.07) albeit their $M_W$ and M/G ratio similarities (Gadkari et al., 2018). Nonetheless, the $k_H$ and $k_K$ values for alfalfa gum remain significantly lower than those reported for galactomannans of remarkably different chemical structure conformation such as guar, locust bean and tara gum. Gillet et al. (2017) ascribed the disparities in the $k_H$ and $k_K$ values to differences in the polymer chains length and distribution of galactosyl groups (resulting in localised hydrophobic patches) which are induced by the gum extraction and/or fractionation conditions.

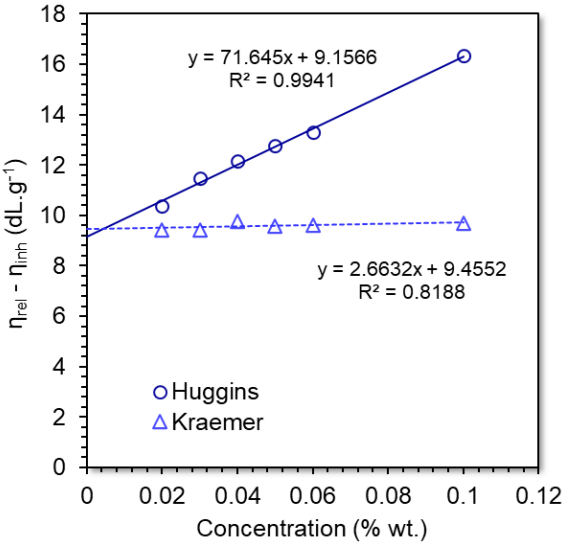


*Figure 16: Inherent (Kraemer) and relative (Huggins) viscosity as a function of alfalfa gum concentration at 25 °C.*

Comparing the radii of gyration ($R_g$) data obtained using either the Fox-Flory equation (Equation 1) or experimentally by means of dynamic light scattering (Table 3), discrepancies between the measured and predicted values were found. The Flory Fox equation resulted in underestimated $R_g$ values for all galactomannans, most probably due to the occurrence of associative aggregation. Interestingly, galactomannans having identical M/G ratio and $M_W$, did not exhibit the same hydrodynamic volume occupancy (

〈Rg〉z was larger in the case of alfalfa gum), which supports the hypothesis that the polymer – solvent and polymer – polymer interactions in the dilute state were governed not only by the $M_W$ and galactosyl substitution level but also by the chemical structure conformation of the polymer chains.

*Table 3: Comparison of structure conformational characteristics of different galactomannans. Alfalfa and fenugreek gums were extracted adopting the herein reported method whilst guar and locust bean gums were of commercial grade.*

| | Alfalfa gum | Fenugreek gum | Guar gum | Locust bean gum |
|---|---|---|---|---|
| $\overline{Mn}$ ($\times 10^5$ Da) | 10.21 ± 0.75$^{b}$ | 12.85 ± 0.98$^{c}$ | 12.86 ± 1.5$^{c}$ | 5.5 ± 0.55$^{a}$ |
| $\overline{Mw}$ ($\times 10^5$ Da) | 19.96 ± 1.92$^{b}$ | 20.19 ± 0.85$^{b}$ | 23.11 ± 2.18$^{b}$ | 12.12 ± 0.36$^{a}$ |
| $\overline{Mz}$ ($\times 10^5$ Da) | 28.49 ± 1.40$^{b}$ | 27.39 ± 1.08$^{b}$ | 31.08 ± 1.77$^{b}$ | 18.78 ± 0.29$^{a}$ |
| Đ | 2.11 ± 0.34$^{bc}$ | 1.57 ± 0.11$^{a}$ | 1.85 ± 0.19$^{b}$ | 2.20 ± 0.12$^{c}$ |
| $\overline{DP}_n$ | 5667 ± 416$^{b}$ | 7138 ± 544$^{c}$ | 7140 ± 833$^{c}$ | 3053 ± 305$^{a}$ |
| [η] (dL.g$^{-1}$) | 9.33 ± 0.3$^{b}$ | 9.04 ± 0.3$^{b}$ | 12.87 ± 0.3$^{c}$ | 7.86 ± 0.1$^{a}$ |
| $R_g$ (nm) | 40.7 ± 0.22$^{b}$ | 40.5 ± 0.18$^{b}$ | 47.6 ± 0.31$^{c}$ | 32.6 ± 0.17$^{a}$ |
| z-diameter (nm) | 97.6 ± 4.2$^{b}$ | 65.5 ± 3.9$^{a}$ | 75.1 ± 5.1$^{a}$ | 128.6 ± 9.8$^{c}$ |

$^{a-d}$ *Different letters between the rows indicate significant difference ($p < 0.05$) according to Tukey's post hoc means comparison test. Symbol used: number average molecular weight (Mn), weight average molecular weight (Mw), z-average molecular weight (Mz), polydispersity index (Đ), number-average degree of polymerisation ($DP_n$), intrinsic viscosity ([η]), radius of gyration ($R_g$).*

## Steady state rheological behaviour

The flow behaviour curves for alfalfa gum dispersions in water at concentrations ranging from 0.1 to 2% wt. are illustrated at Figure 17A. Except for the solution containing 0.1% wt. alfalfa gum, the flow curves indicated a predominant shear thinning behaviour (n < 1), which arises from the macromolecular re-orientation of the polymer chains on shear stress imposing. At very low shear rates, a Newtonian plateau was observed due to the ability of the disrupted polymer chain entanglements to be re-established. Fitting the Cross-Williamson model to the apparent viscosity – shear rate data, the zero-shear viscosity ($\eta_0$), the relaxation time ($\tau$) and the critical shear rate at which the gum dispersions commence to behave as shear-thinning fluids ($\dot{\gamma}_{crit}$) were calculated (Table 4). As expected, the zero-shear rate and the critical shear rate values increased proportionally to the alfalfa gum concentration as the disruption predominates over the establishment of new polymer chain entanglements (Nwokocha et al., 2018; Sittikijyothin et al., 2005).

*Table 4: Steady flow characteristics of alfalfa gum dispersions (0.5 to 4% wt.) as calculated according to Ostwald-de Waele, and Williamson models.*

| Gum concentration | Ostwald – de Waele model | | Cross-Williamson model | | |
|---|---|---|---|---|---|
| % wt. | K ($Pa \cdot s^{-n}$) | n - | τ (s) | $\dot{\gamma}_{crit}$ ($s^{-1}$) | m - |
| 0.1 | - | - | - | - | - |
| 0.25 | 0.031 | 0.811 | 0.006 | 150.5 | 0.407 |
| 0.5 | 0.511 | 0.562 | 0.059 | 16.9 | 0.642 |
| 0.75 | 1.85 | 0.445 | 0.302 | 3.32 | 0.642 |
| 1.0 | 5.63 | 0.351 | 0.582 | 1.72 | 0.736 |
| 1.25 | 11.8 | 0.295 | 1.16 | 0.865 | 0.750 |
| 1.5 | 21.4 | 0.253 | 1.79 | 0.558 | 0.779 |
| 1.75 | 32.0 | 0.226 | 2.21 | 0.453 | 0.827 |
| 2.0 | 47.1 | 0.207 | 3.05 | 0.328 | 0.831 |

In Figure 17B the plot of specific zero viscosity ($\eta_{sp} = \frac{\eta_0 - \eta_s}{\eta_s}$, where $\eta_s$ = 0.89 mPa.s) as function of the dimensionless coil overlap parameter (i.e. c[η]), is given. For most polysaccharides, the existence of two critical concentrations c* and c** is known to delimit the dilute, semi-dilute and entangled solution states (Sittikijyothin et al., 2005). For disordered polysaccharides e.g. dextran, alginates, hyaluronan etc., it has been shown that the intersection point of the dilute and semi-dilute solution states occurs at c[η] = 4 (Morris et al., 1981). Contrary to other random coil ordered polysaccharides, galactomannans exert a lower space occupancy i.e. c[η] = 0.8–3.0, which is generally attributed to the occurrence of specific intermolecular polymer interactions, a phenomenon known as hyperentanglement. According to the obtained master curve for the alfalfa gum dispersion (Figure 17), only the incipient overlap concentration c* = 0.306% wt. was possible to be estimated. At c* the overlap coil concentration was ~ 2.9, which is similar to that of fenugreek and *Mimosa scabrella* gums (M/G ~ 1.0) (Doublier & Launay, 1981; Doyle et al., 2009; Ganter et al., 1992). In highly unsubstituted galactomannans (M/G ~ 2.0 or higher), hyperentanglement occurs via the non-specific association (towards the b crystallographic direction) of the galactosyl free regions ("smooth") of the mannan backbone (Morris et al., 1981). For highly substituted galactomannans (i.e. M/G ~ 1.0), the polymer interchain association via the b-axis direction is not sterically favoured. On the contrary, polymer interchain association occurs in the α-axis direction with the galactosyl groups lying above and under the mannan backbone (Doyle et al., 2009). Considering that the coil overlap parameter receives similar values for galactomannans of similar molecular structure conformation, it can be assumed that alfalfa and fenugreek gum share the same hyperentanglement

mechanisms (c[η] at c* = 2.8 and 2.9, respectively).

According to the master curve (Figure 17B), the specific viscosity dependence on alfalfa gum concentration ($\eta_{sp} = f\,(c[\eta]^b)$) was $\propto c^{2.3}$ and $c^{4.4}$ for the dilute and semi-dilute regimes, respectively. The obtained slope for the dilute regime appeared to be higher than the literature found values ($\propto c^{1.2}$ to $c^{1.7}$) for galactomannans (Gillet et al., 2017). However, upward deviations in the slopes for the dilute regime have been also reported for other galactomannans such as mesquite seed gum ($c^{2.2}$) (Yoo et al., 1994). On the other hand, the slopes for the semi-dilute regime are well within the range reported in the literature for galactomannans i.e. $\propto c^{3.3}$ to $c^{5.5}$ (Gillet et al., 2017) and almost identical to that of fenugreek gum i.e. $\propto c^{4.2}$ (Doyle et al., 2009). In Figure 18, the double logarithmic relationship between the viscosity (specific or apparent) and galactomannans concentration in the semi-dilute regime is given. In corroboration with the observations of Gillet et al. (2017), in the case of the $\eta_{sp}$ – c[η] plots no clear relationships with M/G ratio and $M_W$ were observed. On the other hand, the apparent viscosity exerted a reciprocal correlation ($r = 0.91$, $p < 0.001$) to the $M_W$, as expected.

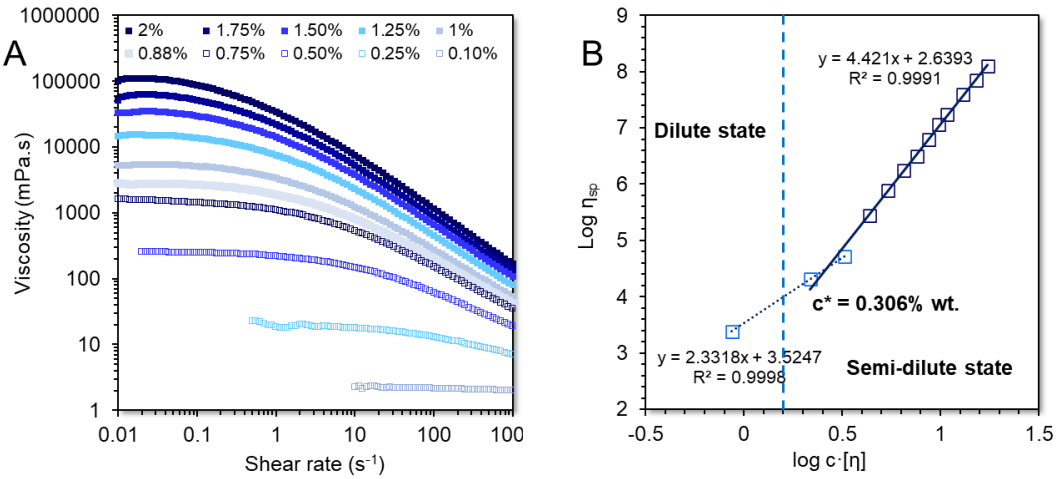


*Figure 17: Flow behaviour curves of alfalfa gum dispersion as influenced by gum concentration (A); double logarithmic plot of specific viscosity at zero shear rate ($\eta_{sp,0}$) as a function of coil overlap parameter c[η] for alfalfa gum dispersions at 25 °C (B).*

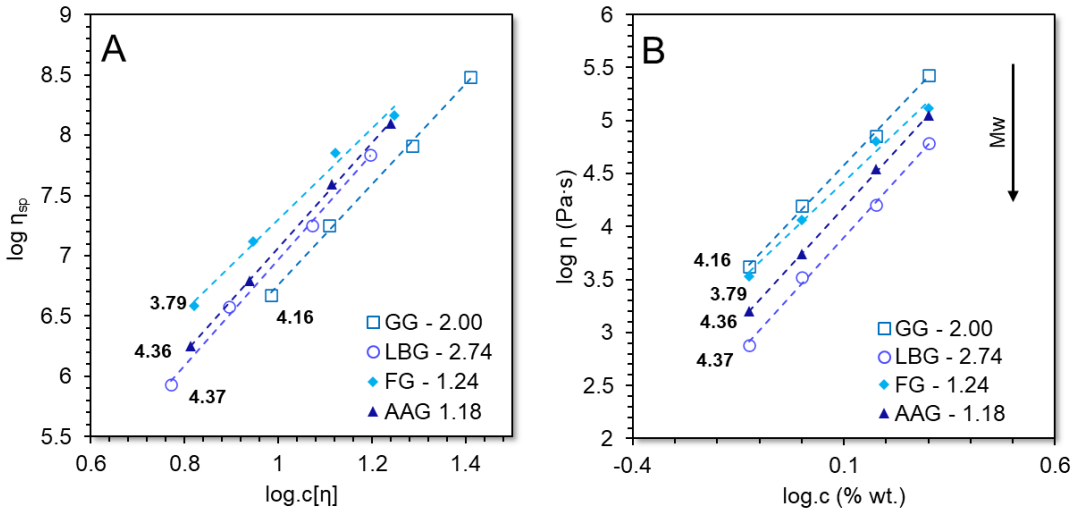


*Figure 18: Double logarithmic viscosity-concentration master curves obtained for different semi-dilute galactomannan dispersions. (A) Specific viscosity – dimensionless concentration, (B) viscosity – concentration. GG: guar gum, LBG: locust bean gum, AAG: alfalfa gum and FG: fenugreek gum*

## Viscoelastic properties

Small amplitude oscillatory shear (SAOS) tests are considered as a standard methodology for assessing the structural and physical state of food colloids as influenced by processing and storage (Gunasekaran & Ak, 2000). To determine the boundary of linear viscoelastic (LVE) region of the alfalfa gum dispersions (1–4% wt.), amplitude sweeps (0.1–1000% of strain) were performed (Figure 19A). As illustrated in Figure 19A, the strain boundary of the LVE regime was rather similar (i.e. 36.3 to 40.4%) for all tested dispersions. However, the yield stress ($\tau_y$) i.e. the minimum stress that is required to be imposed to induce irreversible (plastic) deformation of the systems exhibited a power-raw compliance to alfalfa gum concentration (Table 5).

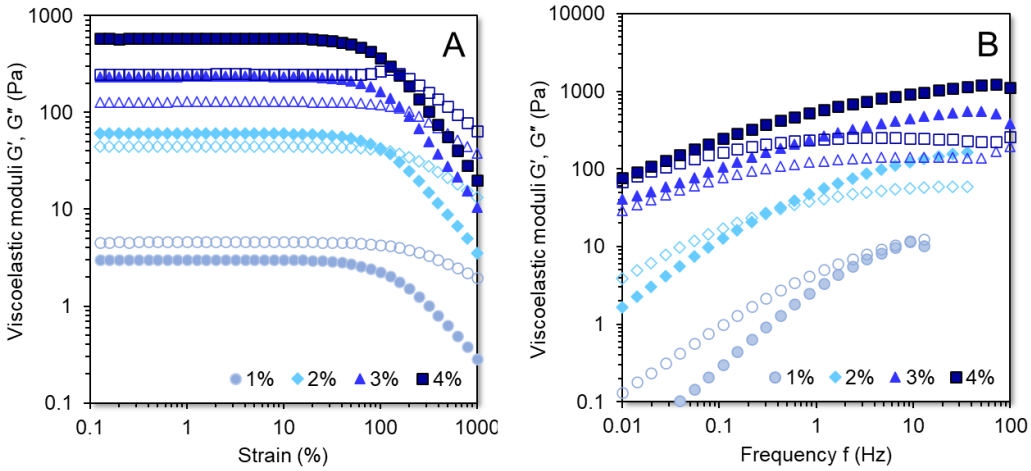


*Figure 19: Amplitude sweep (A) and frequency sweep (B) rheological spectra of alfalfa gum aqueous dispersions as a function of alfalfa gum concentration measured at 25 °C. The closed symbols denote*

*the storage modulus (G') whereas the open ones the loss modulus (G").*

The frequency sweep tests (Figure 19B) were conducted within the LVR regime (strain 0.5%) at 25 °C. As illustrated in Figure 19B, the systems at ≤ 1% wt. of alfalfa gum exhibited a predominant viscous behaviour as G″ < G′ for the entire range of frequencies. At intermediate concentrations of alfalfa gum (i.e. 1 < c < 3% wt.) a distinct viscoelastic behaviour with crossover points in the frequency range from 0.017 to 9.6 Hz was observed.

The crossover frequencies were reciprocally associated to the alfalfa gum concentration due to the increasing relaxation time as the polymer interchain associations becomes more evident (Sittikijyothin et al., 2005). At concentrations ≥ 3% wt., the aqueous alfalfa gum systems exhibited a dominant weak gel-like behaviour as G′ > G″ and 0.6 < tanδ < 0.2 for the entire range of frequencies. The slope of the double logarithmic G′ - ω curves (Table 6), were reduced reciprocally to alfalfa gum confirming the formation of a gel-like polymer network. However, even at the highest gum concentration herein tested, the hydrogels did not achieve a true-gel conformational state (G′ - ω slopes >> 0.1) (Rao, 2014).

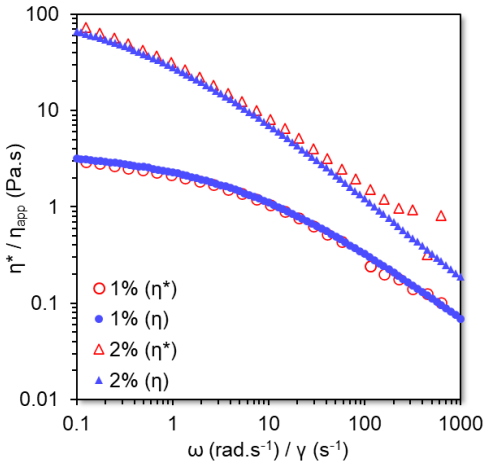


*Figure 20: Cox-Merz plot for assessing the superimposition of steady shear viscosity (η, γ) and dynamic viscosity (η*, ω) measured at 25 °C for different concentrations of alfalfa galactomannan.*

The double logarithmic plot between the steady-state and dynamic rheological properties of alfalfa gum dispersions (1 and 2% wt.) was constructed in order to assess their compliance to the Cox-Merz superimposition rule. As displayed in Figure 20, the Cox-Merz empirical rule was closely obeyed at 1% wt. but a significant departure from superimposition was found at 2% wt. In general, disordered polysaccharides comply to the Cox-Merz rule when the entanglement of the polymer chains takes place via topological (non-specific) physical interactions. Corroborating with our previous

findings, it was shown in previous studies that semi-dilute galactomannan solutions (> 1 to 1.5% wt.) may deviate significantly from the superimposition particularly at low shear rates/frequencies (Nwokocha et al., 2018; Rincón et al., 2014; Sittikijyothin et al., 2005). It has been demonstrated that the weak interchain association of galactomannans (or their aggregates) may exhibit diverse relaxation times under small deformation (η*) and steady state flow (η) conditions and therefore, the Cox-Merz rule is not satisfied (Gillet et al., 2017).

*Table 5: Viscoelastic properties: strain sweeps with controlled shear deformation at 1 Hz and frequency sweeps (within the LVE regime) of the alfalfa gum dispersions (1 to 4% wt., pH = 7) at 25 °C.*

| Alfalfa gum concentration (% wt.) | Strain sweeps | | | | |
|---|---|---|---|---|---|
| | $G'_{LVE}$ (Pa) | $G''_{LVE}$ (Pa) | Yield stress, $\tau_y$ (Pa) | Flow point, $\tau_f$ (Pa) | $G'_f$ (Pa) |
| 1 | 2.84 ± 0.2$^{a}$ | 4.82 ± 0.2a | 1.95 ± 0.1$^{a}$ | nd | nd |
| 2 | 56.6 ± 1.9$^{b}$ | 44.9 ± 2.4$^{b}$ | 27.5 ± 2.1$^{b}$ | 58.5 ± 2.7$^{a}$ | 40.3 ± 3.1$^{a}$ |
| 3 | 220.5 ± 9.4$^{c}$ | 130.6 ± 5.2$^{c}$ | 102.4 ± 4.6$^{c}$ | 257.5 ± 11.3$^{b}$ | 108.4 ± 4.0$^{b}$ |
| 4 | 547.9 ± 25.2$^{d}$ | 256.8 ± 4.3$^{d}$ | 216.8 ± 12.8$^{d}$ | 541.4 ± 12.7$^{c}$ | 208.3 ± 10.1$^{c}$ |

$^{a-d}$ *Different letters between the rows indicate significant difference ($p < 0.05$) according to Tukey's post hoc means comparison test; nd = not detected.*

*Table 6: Viscoelastic properties: frequency sweeps (within the LVE regime) of the alfalfa gum dispersions (1 to 4% wt., pH = 7) at 25 °C.*

| Alfalfa gum concentration (% wt.) | Frequency sweeps | | |
|---|---|---|---|
| | Complex viscosity η* (Pa.s) | Crossover frequency $f_c$ (Hz) | Slope G'- $\omega$ - |
| 1 | 0.515 ± 0.02$^{a}$ | nd | 0.921 ± 0.007$^{d}$ |
| 2 | 7.47 ± 0.19$^{b}$ | 0.41 | 0.671 ± 0.002$^{c}$ |
| 3 | 35.3 ± 1.8$^{c}$ | nd | 0.377 ± 0.002$^{b}$ |
| 4 | 77.3 ± 2.7$^{d}$ | nd | 0.356 ± 0.003$^{a}$ |

As illustrated in Figure 21B, no sol-gel transitions were detected for the aqueous systems containing at least 3% wt. of alfalfa gum, as the loss factor (tanδ) was lower than unity over the entire temperature range. However, both 3 and 4% wt. alfalfa gum dispersions retained their weak gel-like character (tanδ > 0.2), even at very high temperature conditions. At lower gum concentrations, sol-gel transitions were observed to occur at $T_{sol\text{-}gel}$ = 5.2–9.5 and 49.6–54.5 °C for 1 and 2% wt. alfalfa gum dispersions, respectively. It should be noted that in both cases the upward temperature sweeps were associated with a shift of the sol-gel point to the right indicating that heating favoured (proportionally to

the solvent availability) the hydrophobic interchain bonding.

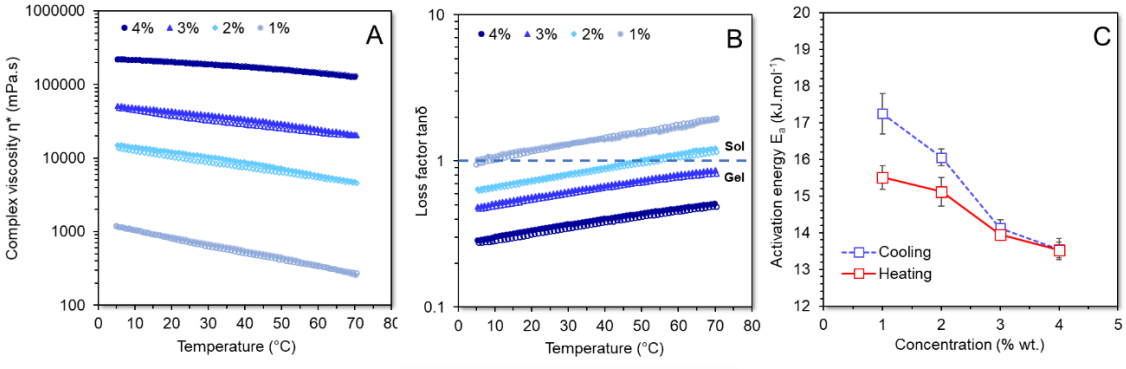


*Figure 21: Oscillatory thermo-rheological spectra of alfalfa gum dispersions measured in the LVE regime (1 Hz, 0.5% strain). complex viscosity (A), loss factor (stiffness) (B) and activation energies (C) for cooling (closed symbols) and heating (open symbols) ramps as a function of alfalfa gum concentration.*

In the present study, non-isothermal kinetic modelling of complex viscosity as function of temperature was conducted. This allows getting a more pragmatic overview of the responsiveness of η* to dynamic temperature conditions e.g. throughout thermal food processing or dynamic food storage conditions. Due to the deviation from superimposition, the activation energy ($E_a$) values for η* were calculated for both cooling and heating steps. Parameters such as the $M_W$, the botanical origin, the ionic strength and the applied shear stress are known to impact the energy barrier to be overcome for initiating the flow of polysaccharide solutions. As seen in Figure 21C, for alfalfa gum concentrations up to 3% wt., the $E_a$ values were higher during the cooling step ($E_a$ = 15.2 vs 14.5 kJ.mol$^{-1}$), whereas the average $E_a$ values (on increasing order of alfalfa gum content) were estimated at 13.5, 14.0, 15.1 and 15.5 kJ.mol$^{-1}$. In general, the herein obtained Ea values are within the literature reported range for semi-dilute galactomannan dispersions i.e. 12–25 kJ.mol$^{-1}$ (Launay et al., 1997; Nwokocha et al., 2017). The elevated $E_a$ values during the cooling process are primarily ascribed to the ability of the polymer hyperentangled networks to store the deformation energy (Razavi et al., 2018). Nevertheless, the reciprocal response of $E_a$ values to gum concentration suggests that above a critical concentration (e.g. > 3% wt.) the dissipated or absorbed thermal energy cannot significantly modify the molecular mobility of the polymer chains.

# CONCLUSIONS

A highly galactosyl substituted galactomannan of low protein residue (< 1.3% wt. on dry basis) was wet extracted from the endosperm of alfalfa seeds. Sugar analysis revealed that

the 99.2% of the total carbohydrate content was composed of mannose and galactose at a ratio of 1.18:1. The alfalfa gum had an average molecular weight of $2 \times 10^6$ Da, an intrinsic viscosity of 9.33 $dL.g^{-1}$ and a $\langle Rg \rangle_z$ of 48.4 nm. Despite its high degree of galactosyl substitution, alfalfa gum exhibited a low solvent (deionised water) affinity favouring the polymer – polymer chain interactions leading to the formation of larger polymer aggregates than other galactomannans of the similar M/G ratio, such as fenugreek gum. The critical dimensionless coil overlap concentration of alfalfa gum was 2.9 corresponding to a $c^* = 0.306\%$ wt. In line with other galactomannans, a steep slope ($\propto c^{4.2}$) of the $\eta_{sp} - c[\eta]$ master curve branch corresponding to the semi-dilute regime was identified, most probably due to hyperentanglement i.e. occurrence of non-specific (–H bonding) polymer chain interactions. The latter also explains the departure of the semi-dilute alfalfa gum dispersions from the Cox-Merz superimposition rule. In the semi-dilute state, alfalfa gum dispersions exhibited a predominant viscous ($c^* < c \leq 1\%$ wt.) to viscoelastic character ($1 \leq c \leq 3\%$ wt.). Aqueous systems containing at least 3% wt. of alfalfa gum exerted a clear weak gel-like behaviour but without attaining a true gel state. Isothermal kinetic modelling of the viscoelastic properties in the LVE regime demonstrated that the temperature responsiveness of complex viscosity is reciprocally increased to alfalfa gum concentration. Alfalfa gum is a novel galactomannan of tremendous potential for the food industry due to its excellent thickening and gelling properties and the sustainable, ecologically versatile, and economically resilient character of alfalfa plant.

# STRUCTURE CONFORMATION, PHYSICOCHEMICAL AND RHEOLOGICAL PROPERTIES OF FLAXSEED GUMS EXTRACTED UNDER ALKALINE AND ACIDIC CONDITIONS

Thierry HELLEBOIS[1,2], Jennyfer FORTUIN[1,3], Xuan XU[1], Alexander S. SHAPLOV[4], Claire GAIANI[2,5] and Christos SOUKOULIS[1]*

[1]Environmental Research and Innovation (ERIN) Department, Luxembourg Institute of Science and Technology (LIST), Esch-sur-Alzette, Luxembourg
[2]Université de Lorraine, LIBio, Nancy, France
[3]Trier University of Applied Sciences, Department of Food Technology, Trier, Germany
[4]Materials Research and Technology (MRT) Department, Luxembourg Institute of Science and Technology (LIST), Esch-sur-Alzette, Luxembourg
[5]Institut Universitaire de France (IUF), France

International Journal of Biological Macromolecules
Volume 192, 1 December 2021, Pages 1217-1230
doi.org/10.1016/j.ijbiomac.2021.10.087

# ABSTRACT

The present work aimed at investigating an extraction protocol based on consecutive steps of isoelectric point (pH ~ 4.25) mediated gum swelling and deproteinisation as an alternative method to produce flaxseed gum extracts of enhanced techno-functional characteristics. The osidic and proximate composition, structure conformation, flow behaviour, dynamic rheological and thermal properties of gums isolated from brown and golden flaxseeds were assessed. Gum extraction under near-to-isoelectric point conditions did not impair the extraction yield, residual protein and ash content, whilst it resulted in minor changes in the sugar composition of the flaxseed gum extracts. The deconvolution of the GPC/SEC chromatographs revealed the presence of four major polysaccharidic populations corresponding to arabinoxylans, rhamnogalacturonan–I and two AX-RG-I composite fractions. The latter appeared to minimise the intra- and interchain polymer non-covalent interactions (hydrogen bonding) leading to a better solvation affinity in water and lyotropic solvents. Golden flaxseed gums exerted higher molecular weight ($M_w$ = 1.34–1.15 × $10^6$ Da) and intrinsic viscosities (6.63–5.13 dL.$g^{-1}$) as well as better thickening and viscoelastic performance than the brown flaxseed gum exemplars. Golden flaxseed gums exhibited a better thermal stability compared to the brown flaxseed counterparts and therefore, they are suitable for product applications involving severe heat treatments.

# INTRODUCTION

Flax (*Linum usitatissimum L.*) is one of the most important industrial crops globally, cultivated for its fibres (used extensively in the textile and bio-composite industry) and seeds (Baley et al., 2020). Owing to its macronutrient-rich profile, i.e. essential lipids, proteins, bioactive peptides (orbitides), and soluble and insoluble dietary fibre, flaxseed has shown promising potential for food and nutraceutical industry applications (Shim et al., 2015). The dietary fibre content of flaxseed accounts for 22–28% of its overall weight, with the outermost (epidermal) seed layer containing about 8% wt. of mucilaginous gum (Liu et al., 2018). Flaxseed mucilage and its derivatives (deproteinised or fractionated) have been extensively investigated over the last decade, mainly due to their food industry relevant inherent techno-functional (thickening, gelling, interface-stabilising and film-forming) properties (Soukoulis et al., 2018). In addition, flaxseed hull polysaccharides and their hydrolysates (FGOS) have antioxidant (Yang et al., 2020), immune-stimulatory (Biao et al., 2020), body fat mass and weight controlling aspects (Luo et al., 2018), as well as other significant health benefits, including the suppression of acute postprandial glycaemic response and glucose diffusion (Fabek et al., 2014; Fabek & Goff, 2015; Kay et al., 2017) and the regulation of gut microbiota (Ying et al., 2013; Zhou et al., 2020). In the latter case, flaxseed gum exhibited a modulatory role in gut microbial ecosystem diversity, as dictated by the alteration of the *Firmicutes* to *Bacteroidetes* ratio and the increase in the relative abundancies of *Prevotella*, *Phascolarctobacterium*, *Clostridrium*, *Megamonas*, *Lactobacilli* and *Bifidobacteria* (Ying et al., 2013; Zhou et al., 2020).

The structural elucidation of crude (non-fractionated) flaxseed mucilage demonstrated the *co*-existence of two major polysaccharide fractions: an acidic arabinan rich rhamnogalacturonan-I (RG-I) fraction and an arabinoxylan with a β-D-(1 → 4)-xylan backbone neutral fraction (Ding et al., 2018; Qian et al., 2012). The chemical structure and molecular properties of flaxseed hull polysaccharides are inextricably associated with the flaxseed genotype and origin. Cui et al., (1996) found that yellow flaxseed cultivars exhibited a lower content in rhamnose and galacturonic acid and a higher arabinoxylan content than brown flaxseed, which was associated with a more pronounced shear-thinning and weak gel-forming capacity of the extracted gums. In two successive studies (Kaewmanee et al., 2014; Liu, Shen, et al., 2016), the techno-functionality (thickening and swelling power, emulsifying and foaming capacity) of the gum extracts, provided by the flaxseed cultivar and origin endowed was clearly dictated. Interestingly, the umami, bitter and sweet sensory modalities, strongly driven by cultivar type, were identified as

the primary determinants of flaxseed gum acceptability (Kaewmanee et al., 2014).

The practices implemented for extracting, isolating, purifying and fractionating the polysaccharide matter from the flaxseed hulls are essential drivers of the chemical structure molecular characteristics and techno-functionality of flaxseed gum (Liu et al., 2018; Ziolkovska, 2012). Water extraction-associated parameters, such as the temperature, pH, ionic strength of the aqueous medium, and seed-to-water ratio are known as the major factors affecting the extraction yield and the chemical composition of the final gum (Soukoulis et al., 2018). As a common rule, flaxseed mucilage is extracted under neutral or mildly alkaline conditions (pH = 6–8) at a temperature of 20 to 90 °C for 1 to 24 h, maintaining a flaxseed-to-water ratio of 1:5–1:40 (Safdar et al., 2020). Increasing the extraction temperature results in higher extraction yields (up to 16–20% of the defatted flaxseed weight) but compromises the purity i.e. protein and ash residual content of the final gum (Kaushik et al., 2017; Roulard et al., 2016). On the other hand, the impact of the seed-to-water ratio on the gum extraction yield appears to be less important than temperature, whereas it becomes negligible when it exceeds the ratio of 1:20 to 1:25 (Ziolkovska, 2012). The protein residual matter of flaxseed gum can be substantially reduced by acidic precipitation (e.g. acetic, trichloroacetic, etc.), salts (e.g. calcium chloride, sodium chloride etc.), proteolytic enzymes, ultrafiltration, or ion exchange chromatography (Elboutachfaiti et al., 2017; Qian et al., 2012; Rashid et al., 2019; Safdar et al., 2020). Moreover, enzymatic – ultrasound-assisted extraction can reduce not only the amount of residual protein but may also enhance the techno-functional properties of the gum extracts (Moczkowska et al., 2019).

In a recent study (Hellebois, Soukoulis, Xu, Hausman, et al., 2021), a procedure based on isoelectric point (4–4.5) gum swelling and extraction followed by an alkaline protein solubilisation (at pH = 10) and isoelectric precipitation allowed the preparation of highly pure (≈ 1% wt. protein residual) galactomannan extracts. The present work explores the aforementioned extraction protocol in conjunction with the flaxseed phenotype (brown vs. golden), based on the compositional, structure conformational, physicochemical and rheological properties of the gum extracts obtained.

# MATERIALS & METHODS

## Extraction and isolation of flaxseed polysaccharides

Brown (Delhaize, Molenbeek, Belgium) and golden (Priméal, Peaugres, France)

flaxseeds were purchased from the local branches of the abovementioned supermarkets. The non-adherent mucilage was extracted from the flaxseed coat layer, as previously described in Soukoulis et al., (2019) with minor modifications (Figure 22). In particular, flaxseeds were soaked in deionised water (18.2 mΩ, Millipore Inc., Burlington, MA, United States) at 50 °C for 2 h under gentle magnetic stirring (IKA GmbH, Staufen, Germany). The pH of the seed suspension was adjusted at either pH = 8 or pH = 4 with 1 M NaOH or 1 M HCl, respectively. To facilitate the hydration of the seed coat layer, the flaxseed-to-water ratio was adjusted to 1:10. The flaxseed suspension was vacuum filtered using a nylon mesh (100 μm, VWR, Leuven, Belgium) and the crude mucilage solution obtained was centrifuged at 18,500*g* for 15 min (Multifuge X3R, Fiberlite F14–6, ThermoFisher, Waltham, MA, United States) to remove the insoluble impurities. Then, the supernatant was mixed 1:2 with absolute ethanol (VWR, Leuven, Belgium) and kept under mechanical stirring for 1 h to allow sufficient aggregation of the polysaccharide fraction. The ethanolic suspension was centrifuged at 18,500*g* for 10 min, and the polysaccharide pellets collected were reconstituted into Milli-Q water adjusted to pH = 10 with 1 M NaOH solution. Following the complete dissolution of the gum pellet, the pH of the gum solution was adjusted at the isoelectric point of the flaxseed proteins (pI ~4.25), kept under stirring for 1 h and finally centrifuged at 18,500*g* for 30 min. The supernatants were neutralised with 1 M NaOH and dialysed against Milli-Q water for 72 h until no remarkable changes in the conductivity of the intermittently renewed (every 12 h) dialysate were recorded. Following lyophilisation at −80 °C for 96 h (Christ, Alpha 1-2LD Plus, Haan, Germany), flaxseed gums were finely powdered using a knife mill (IKA, Staufen, Germany) and stored under controlled temperature and relative humidity conditions ($a_w$ = 0.11, 25 °C) until further use.

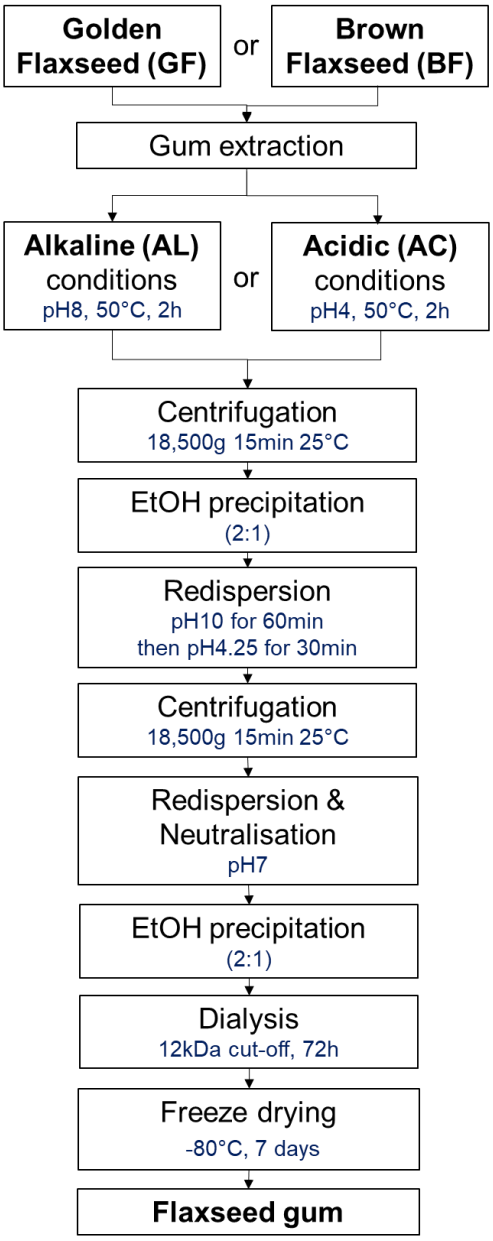


*Figure 22: Extraction flowchart illustrating the implemented procedure to extract, isolate and purify the flaxseed gums.*

## Proximate, sugar monomers and uronic acid composition analyses

The moisture and ash content of the flaxseed gum extracts were gravimetrically determined according to the standard AOAC methods. The protein content was determined according to the Dumas method (protein converting factor = 5.41 (Oomah et al., 1995) using a CHNS analyser (Elementar Vario Cube, Langensenbold, Germany). The total carbohydrate content was measured using an enzymatic assay kit (Megazyme, K-ACHDF 08/16), whilst the total lipid content was measured via gravimetric determination of the n-hexane extracted (3-fold) liposoluble residue.

The sugar monomer composition of the flaxseed gum extracts was determined as detailed

in (Hellebois, Soukoulis, Xu, Hausman, et al., 2021).

## Gel permeation size-exclusion chromatography (GPC/SEC)

A 1200 Infinity gel permeation chromatography (GPC, Agilent Technologies, Santa Clara, CA, United States) was used to determine the number-average ($M_n$), weight-average ($M_w$) and Z-average ($M_z$) molecular weight and dispersity (Đ) of the flaxseed gum extracts. The chromatograph was equipped with an integrated IR detector, two columns (PL aquagel-OH MIXED-H and PL aquagel-OH MIXED-M) and a PL aquagel-OH guard column (Agilent Technologies, Santa Clara, CA, United States). 0.1 M NaNO3 aqueous solution containing 0.02% wt. of NaN3 was used as an eluent, the flow rate was maintained at 1.0 mL $min^{-1}$ and the measurements were performed at 50 °C. Pullulan standards (ReadyCal-Kit Pullulan high, PSS Polymer Standards Service GmbH, $M_p$ = 180–1530 × $10^3$ Da) were used to perform calibration. All the samples were filtered through a 0.2 µm Teflon filter before injection.

Peak deconvolution of the GPC chromatograms was conducted with Origin software (OriginPro v.2019b, OriginLab, Northampton, MA, United States) using the quadratic Savitzky-Golay method.

## Intrinsic viscosity measurements

The intrinsic viscosity [η] of flaxseed gum solutions (0.02–0.1% wt.) in 0.1 M NaNO3 aqueous solution containing 0.02% wt. NaN3 was measured using a 0C Ubbelohde capillary viscometer (Paragon Scientific, United Kingdom) at 25 ± 0.1 °C. The intrinsic viscosity was determined as the intercepts of the Huggins (Equation 16) and Kraemer (Equation 17) equations after extrapolating them to an infinite dilute system:

Equation 16 $$\frac{\eta_{sp}}{c} = [\eta] + k_H[\eta]^2 c$$

Equation 17 $$\frac{\ln \eta_{rel}}{c} = [\eta] + k_K[\eta]^2 c$$

where: $\eta_{sp}$ and $\eta_{rel}$ denote the specific and relative viscosity, respectively, c is the flaxseed gum concentration, and $k_H$ and $k_K$ are the Huggins and Kraemer coefficients.

## Dynamic light scattering and zeta-potential determination

The hydrodynamic diameter and zeta potential of flaxseed gums was recorded using dynamic light scattering (Zetasizer Nano, Malvern Instruments, Worcestershire, United Kingdom). To determine the hydrodynamic diameter of the gum particle, 10 mg of gum was dissolved in 10 mL of 0.1 M $NaNO_3$ aqueous solution and filtered through a cellulose acetate filter (cut-off 0.2 µm) prior analysis.

The zeta-potential of the gums was determined by dissolving flaxseed gum in Milli-Q water to obtain a final concentration of 0.25% wt. The pH of the solutions obtained was adjusted from 7 to 2 using 0.1 M HCl and NaOH solution and filtered through a 0.2 µm cellulose acetate filter (VWR, Leuven, Belgium).

## Steady-state and dynamic rheological measurements

Aqueous solutions (0.1, 0.2, 0.25, 0.375, 0.5, 0.625, 0.75, 0.875, 1, 1.25, 1.5, 2, 2.5, 3, 4 and 5% wt.) of flaxseed gum in either Milli-Q water (adjusted at pH = 7 using 0.1 M NaOH) or $NaNO_3$ 0.1 M were prepared for carrying out the rheological measurements. All rheological analyses were performed using an Anton-Paar oscillatory rheometer (MCR 302, Graz, Austria) equipped with either a concentric cylinder (steady-state rheological measurements: 0.1–2.5% wt.) or cone plate geometry (dynamic rheological measurements: 1–5% wt.).

### i. Flow behaviour

Aliquots of the flaxseed gum solutions (ca. 15 mL) were transferred to the measuring geometry and tempered at ambient temperature (25 ± 0.05 °C) for 10 min before the analyses. Due to the time-dependent flow behaviour of the solutions, the gum solutions were pre-sheared at 200 $s^{-1}$ for 5 min and left to settle for 5 min before measurement. Upward shear rate sweeps in the range of 0.01 to 1000 $s^{-1}$ were performed. The shear stress $\tau$ (Pa) – shear rate $\dot{\gamma}$ ($s^{-1}$) data obtained were fitted into the Ostwald-de Waele (power) model (Equation 18) as follows:

Equation 18 $$\tau = K\,\dot{\gamma}^{n}$$

where K (Pa $s^{-n}$) and n (dimensionless) denote the consistency coefficient and rheological behaviour index, respectively.

### ii. Zero shear viscosity measurements

To define the concentration where the biopolymer chain entanglement takes place, the limiting viscosity of flaxseed gum aqueous solutions at zero shear rate ($\eta_0$) in the concentration range of 0.1 to 2.5% wt. was measured. For this purpose, the Williamson-Cross model (Equation 19), was fitted to the viscosity – shear rate (0.01 to 1000 $s^{-1}$) data obtained:

Equation 19 $$\eta = \eta_\infty + \frac{\eta_0 - \eta_\infty}{1 + C\cdot\dot{\gamma}^{m}}$$

where $\eta_0$ and $\eta_\infty$ represent the zero and infinite shear viscosity, and C, m are the Cross time and rate constants, respectively.

iii. Amplitude and frequency sweep measurements

For the dynamic rheological measurements, the flaxseed gum extracts were dispersed in Milli-Q in the concentration range of 1 to 5% wt. Amplitude sweeps were conducted to determine the linear viscoelastic (LVE) region under controlled shear stress conditions (1 Hz and 25 °C). From the amplitude sweep rheological spectra obtained, the viscoelastic moduli ($G'_{LVE}$ and $G''_{LVE}$) in the LVE region, the yield stress at the limit of LVE region ($\tau_y$) and the stress and elastic modulus ($G'$) at the flow-point ($G' = G''$) were calculated using the RheoCompass analysis software (Anton-Paar, Graz, Austria).

Frequency sweeps (0.1 to 100 Hz) within the LVE region (strain = 0.5%) were performed at 25 °C to evaluate the viscoelastic profile of the flaxseed gum solution profile. The slope of the double logarithmic storage modulus ($G'$) –frequency (f) curves and the complex viscosity $\eta^*$ at f = 1 Hz was calculated using the Rheocompass software (Anton Paar, Graz, Austria). Furthermore, the frequency (f) at which the crossover of the viscoelastic moduli ($G' = G''$) takes place was calculated using Solver (Excel, Microsoft Inc, Redmond, WA, United States).

## Thermal analyses

Thermal gravimetric analysis (TGA) was carried out in air on a TGA2 STARe System (Mettler Toledo, Zurich, Switzerland), applying a heating rate of 5 °C.min$^{-1}$. The onset weight loss temperature ($T_{onset}$) was determined as the point in the TGA curve at which a significant deviation from the horizontal was observed.

Differential scanning calorimetry (DSC) analysis was performed on a DSC3+ STARe System (Mettler Toledo, Zurich, Switzerland). Approximately 5 mg of flaxseed gum extract were placed in aluminium pans and hermetically sealed inside the argon-filled glove-box (MBRAUN MB-Labstar, $H_2O$ and $O_2$ content < 0.5 ppm). To determine the thermal behaviour of the flaxseed gum extracts the following thermal scanning protocol was applied: 1) isothermal hold at 25 °C for 5 min, 2) cooling to −80 °C at 5 °C.min$^{-1}$, 3) isothermal hold at −80 °C for 5 min, 4) heating to 65 °C at 5 °C.min$^{-1}$ and annealing at the same temperature for 10 min, 5) cooling to −80 °C as previously mentioned, 6) heating to 180 °C at 5 °C.min$^{-1}$. A second cooling – heating scan between −80 and 200 °C was repeated for measuring the glass transition temperature of the gum extracts.

## Statistical analyses

The normal distribution of the data was verified employing the Shapiro-Wilk test and Q-Q plot representation. Also, the equality of variance among the variables was verified

using Levene's test. To determine the significance of the gum concentration on the physicochemical and rheological properties, multifactorial (two or three-way) ANOVA was performed. Tukey's multiple range test was used to separate means of data when significant differences ($p < 0.05$) were detected. Hierarchical cluster analysis was carried out using Ward's agglomeration method to cluster, based on rows (flaxseed gum extract) and columns (physico-chemical, rheological and structure conformational main properties). All statistical analyses were conducted using Origin software (OriginPro v.2019b, OriginLab, Northampton, MA, United States).

# RESULTS & DISCUSSION

## Proximate and sugar monomer composition

The flaxseed gum extraction yields were estimated at 2.51, 2.47, 2.02 and 2.57% wt. for alkaline (GFAL) and acidic (GFAC) extracted gum from golden flaxseed and alkaline (BFAL) and acidic (BFAC) extracted gum from brown flaxseed, respectively. These data are in keeping with the findings of Kaewmanee et al., (2014) and Moczkowska et al., (2019), yet are lower than the gum extraction yields achieved in other studies e.g. 4 to 8% wt. (Cui et al., 1996; Oomah et al., 1995; Qian et al., 2012). The variations in gum extraction yields have been ascribed to several parameters, including flaxseed genotype, extraction temperature and pH, seed-to-water ratio, use of intact seeds or seed meal, etc. (Cui et al., 1996; Kaewmanee et al., 2014; Kaushik et al., 2017; Oomah et al., 1995; Qian et al., 2012).

In Table 7, the proximate (on dry basis) composition of the flaxseed gum extracts is given. The protein and ash residual in the gum obtained ranged from 6.5 to 9.5 g.100 $g^{-1}$ and 5.7 to 7.4 g.100 $g^{-1}$, respectively. The residual protein and inorganic matter (ash) content in flaxseed gum is inextricably associated with the extraction conditions i.e. temperature, extraction duration, pH, and ionic strength (Cui et al., 1994; Kaushik et al., 2017). Enzymatic (protease) hydrolysis, acid or salt-induced protein precipitation, ultracentrifugation and ion exchange chromatography may result in a significant reduction in the proteinaceous residue of flaxseed gum (Cui et al., 1994; Qian et al., 2012; Safdar et al., 2020). In our study, an alternative route based on acidic mucilage extraction (at conditions close to the pI of flaxseed proteins i.e. 4–4.5) followed by a pH shifting deproteinisation step, was investigated. The approach was previously proven to be a very effective deproteinisation strategy for non-ionic polysaccharide isolates i.e.

galactomannans (Hellebois, Soukoulis, Xu, Hausman, et al., 2021). As for flaxseed gum, the protein depletion effectiveness of the extraction method was dependent ($p < 0.05$) on the flaxseed type (6.85 and 8.9 g $100.g^{-1}$, for golden and brown flaxseed, respectively), whilst no significant impact of the pH of the aqueous extracting medium on protein was detected. According to literature findings, the protein content in flaxseed gums varies from 6 to 22 g.100 $g^{-1}$ (Elboutachfaiti et al., 2017; Kaushik et al., 2017; Liu, Shim, et al., 2016; Moczkowska et al., 2019; Roulard et al., 2016), which is comparably higher than that reported for other industrially relevant gums such as galactomannans (3–10%), xanthan gum (0.8–4.7%), gellan gum (0–3%), and seaweed polysaccharides (0–1.5%) (Mathur, 2016; Mortensen et al., 2017; Younes, Aggett, Aguilar, Crebelli, Filipic, et al., 2018; Younes, Aggett, Aguilar, Crebelli, Filipič, et al., 2018). A substantial reduction in the proteinaceous matter can be achieved when additional purification steps (e.g. proteolytic attack, ultracentrifugation, membrane or chromatographic separation etc.) are implemented (Kaewmanee et al., 2014; Qian et al., 2012). Moreover, chemical processing aids (acids and salts) may be employed in gum purification, yet undesirable losses in the carbohydrate matter, due to the partial hydrolytic depolymerisation of the gum, may be induced under highly acidic conditions (Safdar et al., 2020).

*Table 7: Proximate and sugar monomer composition of gums extracted from brown and golden flaxseed under acidic and alkaline conditions.*

| | Golden alkaline | Golden acid | Brown alkaline | Brown acid |
|---|---|---|---|---|
| Proximate composition[1] ($g.100g^{-1}$ of dry matter) | | | | |
| Total carbohydrates | $87.1 \pm 2.5^{a}$ | $87.7 \pm 1.9^{a}$ | $84.0 \pm 1.1^{a}$ | $84.4 \pm 0.8^{a}$ |
| Protein | $7.2 \pm 2.3^{a}$ | $6.5 \pm 1.1^{a}$ | $8.6 \pm 0.2^{a}$ | $9.2 \pm 0.1^{a}$ |
| Ash | $5.7 \pm 0.2^{a}$ | $5.8 \pm 0.8^{a}$ | $7.4 \pm 0.6^{b}$ | $6.4 \pm 1.0^{a}$ |
| Sugar monomer composition ($g.100g^{-1}$ of total carbohydrate matter) | | | | |
| Fucose | $4.2 \pm 0.2^{bc}$ | $4.4 \pm 0.4^{c}$ | $3.2 \pm 0.4^{ab}$ | $3.0 \pm 0.5^{a}$ |
| Rhamnose | $24.2 \pm 0.8^{b}$ | $22.3 \pm 1.2^{b}$ | $18.0 \pm 1.1^{a}$ | $18.8 \pm 0.5^{a}$ |
| Arabinose | $8.4 \pm 0.8^{a}$ | $8.5 \pm 0.6^{a}$ | $11.1 \pm 0.9^{b}$ | $10.6 \pm 0.5^{b}$ |
| Galactose | $14.3 \pm 0.7^{a}$ | $14.0 \pm 0.9^{a}$ | $13.5 \pm 0.8^{a}$ | $14.3 \pm 0.4^{a}$ |
| Glucose | $1.4 \pm 1.2^{a}$ | $3.7 \pm 0.9^{b}$ | $5.8 \pm 0.4^{c}$ | $7.9 \pm 0.1^{d}$ |
| Xylose | $25.3 \pm 2.2^{a}$ | $25.0 \pm 2.1^{a}$ | $31.8 \pm 1.4^{c}$ | $29.0 \pm 2.4^{bc}$ |
| Galacturonic acid | $22.3 \pm 1.1^{b}$ | $22.1 \pm 1.6^{b}$ | $16.7 \pm 1.3^{a}$ | $16.4 \pm 0.6^{a}$ |
| Rhamnose/xylose | $0.96^{b}$ | $0.89^{b}$ | $0.57^{a}$ | $0.65^{a}$ |
| Arabinose/xylose | $0.33^{a}$ | $0.34^{ab}$ | $0.35^{bc}$ | $0.37^{c}$ |

*[1] Lipid matter was detected in traces. [a-d] Different letters between the rows indicate a significant difference ($p < 0.05$) according to Tukey's post hoc*

Corroborating the literature data (Liu et al., 2018; Oomah et al., 1995), the osidic composition of the flaxseed gum (Table 7) confirmed the presence of neutral and acidic polysaccharide fractions. The flaxseed gums were composed of xylose (25–31.8%),

rhamnose (18–24.2%), galactose (13.5–14.3%), arabinose (8.4–11.1%), glucose (1.4–7.9%), fucose (3.0–4.4%) and galacturonic acid (16.4–22.3%). The mean rhamnose/xylose ratio was estimated at 0.9 and 0.6 for golden and brown flaxseed gums, respectively. In their studies, Cui et al., (1996) and Oomah et al., (1995) demonstrated that the rhamnose/xylose mass fraction may vary significantly among brown and golden flaxseed cultivars i.e. 0.3–2.2. The rhamnose/xylose ratio is considered an indicator of the proportion of the pectic-like to hemicellulose matter (Oomah et al., 1995) and therefore, it can be deduced that only the flaxseed phenotype affected the major polysaccharide fraction composition of the gum extracts. The average arabinose/xylose ratio, indicative of the branching degree of the polymer chains (Oomah et al., 1995; Wannerberger et al., 1991), was estimated at 0.33, 0.34, 0.35 and 0.37 for GFAL, GFAC, BFAL and BFAC, respectively. Both flaxseed phenotype and extraction conditions were significant ($p < 0.05$). Although the quantification of most of the sugar monomers was in keeping with the existing literature data (Oomah et al., 1995), glucose quantity was remarkably ($p < 0.001$) low. Wannerberger et al., (1991) and Fedeniuk & Biliaderis, (1994) demonstrated that the presence of buffer salt in the aqueous extraction medium leads to the preferential isolation of glucose. The absence of buffer salts in the extracting medium (Milli-Q water) may explain the remarkably low glucose levels. Interestingly, the acidic gum extracts had higher glucose levels (5.8 g.100 $g^{-1}$) than their alkaline extracted counterparts (3.6 g.100 $g^{-1}$). This may be ascribed to the buffering effect of sodium chloride formed during the neutralisation process prior to the pH shifting deproteinisation step.

## Structure conformation and physicochemical properties

To determine the molecular properties of the flaxseed gum extracts, GPC/SEC analysis using 0.1 M $NaNO_3$ as the eluent, was used. The use of nitrate solution instead of water as the mobile phase aimed at preventing the aggregation of the polysaccharide molecules due to intermolecular non-covalent interactions such as electrostatic, van der Waals attraction or hydrogen bonding (Ding et al., 2018; Roulard et al., 2016). The molecular weight distribution profiles of the flaxseed gum extracts are illustrated in Figure 23. Regardless of the extraction method or the botanical origin of the flaxseed, the molecular weight distribution of the gum extracts was broad with the dispersity index (Đ) ranging from 2.11 to 3.82 (Table 8). In general, the average $M_W$ and $DP_n$ values of the golden flaxseed extracts were higher than the brown flaxseed ones but the direct impact of the extraction method remained unclear. The deconvolution of the GPC/SEC chromatograms

allowed a satisfactory separation of the peaks corresponding to the different polysaccharide fractions (Figure 23B). In all flaxseed gum systems, four polysaccharide populations were identified, corresponding to 4513 (less than 3%), 1627 (31–48%), 701 (22–43%) and 231 (19–35%) kDa, which is in keeping with the findings of Qian et al., (2012) and Elboutachfaiti et al., (2017). Studies on fractionated flaxseed gum using ion exchange chromatography have demonstrated its polysaccharidic complexity, as due to neutral (arabinoxylan-rich – $M_W$ up to 5500 kDa), acidic (rhamnogalacturonan–I rich – $M_W$ < 500 kDa) and composite AX-RG-I fractions (1700 < $M_W$ < 700 kDa) *co*-existing (Elboutachfaiti et al., 2017; Goh et al., 2006; Naran et al., 2008; Qian et al., 2012). It is generally accepted that high molar mass arabinoxylans contribute mostly to the inherent viscosity of flaxseed gum, whilst the pectic fractions are considered rather small to significantly alter its thickening potential (Goh et al., 2006; Qian et al., 2012). On the other hand, Naran et al., (2008) and Qian et al., (2012) reported that the thickening capacity of flaxseed gum did not comply with the ideal mixture law (i.e. viscosity does not develop proportionally to the AX and RG-I mass fractions). Conversely, the composite AX-RG-I fractions may result in a significant contribution to the overall viscosity of flaxseed gum solutions, which is ascribed most probably to non-covalent intermolecular interactions between the two polysaccharide species (Naran et al., 2008).

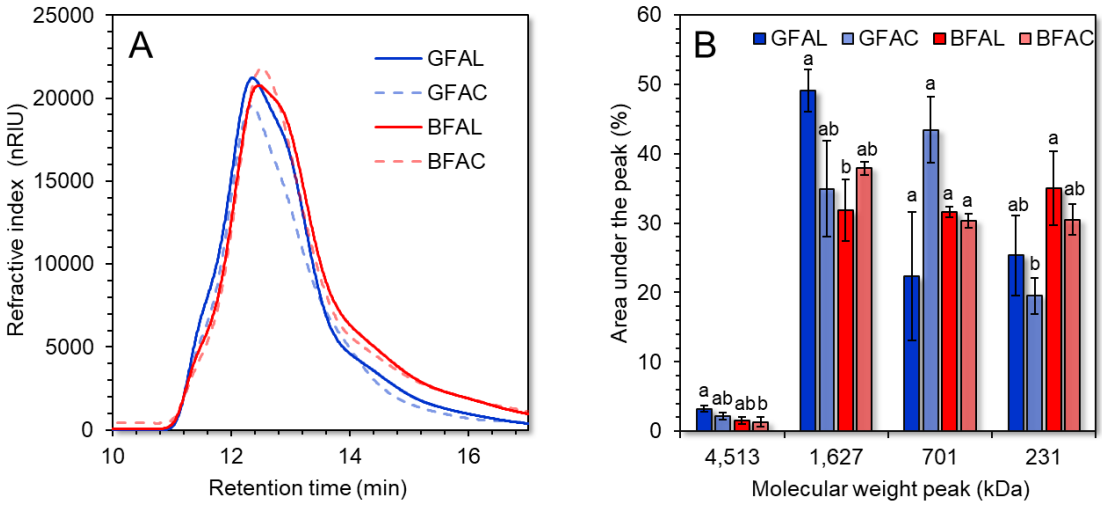


*Figure 23: Gel permeation size-exclusion chromatograms (GPC/SEC, A) and occurrence of the four polysaccharidic populations as detected by peak deconvolution of the GPC/SEC chromatograms of the gums extracted from golden (GF–) and brown (BF–) flaxseed under acidic (–AC) or alkaline (–AL) conditions (B).*

*Table 8: Comparison of structure conformational characteristics of the four flaxseed gum extracts.*

| | Golden alkaline | Golden acid | Brown alkaline | Brown acid |
|---|---|---|---|---|
| $\overline{Mn}$ ($\times 10^5$ Da) | 5.65 ± 0.64$^{ab}$ | 6.50 ± 0.99$^{a}$ | 3.34 ± 0.86$^{c}$ | 4.26 ± 0.40$^{bc}$ |
| $\overline{Mw}$ ($\times 10^5$ Da) | 13.33 ± 0.10$^{a}$ | 13.50 ± 1.16$^{a}$ | 11.48 ± 0.49$^{b}$ | 11.45 ± 0.42$^{b}$ |
| $\overline{Mz}$ ($\times 10^5$ Da) | 21.90 ± 0.18$^{a}$ | 21.69 ± 1.34$^{a}$ | 21.57 ± 1.56$^{a}$ | 19.68 ± 0.55$^{a}$ |
| Đ | 2.40 ± 0.26$^{ab}$ | 2.11 ± 0.14$^{a}$ | 3.82 ± 1.17$^{b}$ | 2.71 ± 0.16$^{ab}$ |
| $\overline{DP_n}$ | 2959 ± 337$^{ab}$ | 3406 ± 517$^{a}$ | 1741 ± 446$^{c}$ | 2220 ± 208$^{bc}$ |
| [η] (dL.g$^{-1}$) | 6.52 ± 0.11$^{a}$ | 6.74 ± 0.08$^{a}$ | 5.01 ± 0.40$^{b}$ | 5.24 ± 0.35$^{b}$ |
| $k_H$ | 0.62 ± 0.02$^{b}$ | 0.55 ± 0.01$^{a}$ | 0.62 ± 0.07$^{ab}$ | 0.56 ± 0.03$^{a}$ |
| c* (g.100 g$^{-1}$) | 0.55 ± 0.02$^{b}$ | 0.50 ± 0.01$^{a}$ | 0.72 ± 0.06$^{c}$ | 0.79 ± 0.04$^{c}$ |
| z-diameter (nm) | 97.8 ± 5.9$^{a}$ | 93.7 ± 4.2$^{a}$ | 109.7 ± 4.3$^{a}$ | 101.2 ± 10.5$^{a}$ |

$^{a-d}$ *Different letters between the rows indicate significant differences ($p < 0.05$) according to Tukey's post hoc means comparison test. Symbols and abbreviations used: number-average molecular weight (Mn), weight-average molecular weight (Mw), z-average molecular weight (Mz), dispersity (Đ), number-average degree of polymerisation ($DP_n$), intrinsic viscosity calculated based on average of Huggins and Kraemer intercepts ([η]), critical coil overlap concentration (c*).*

Dynamic light scattering measurements (Table 8) confirmed that golden flaxseed gum solutions were less prone ($p < 0.05$) to polymer-polymer chain aggregation than brown flaxseed gum. The acidic extracts were characterised by smaller hydrodynamic diameters compared to their alkaline extract counterparts; nevertheless, the differences were not significant. In agreement with the GPC-SEC measurements, the polymer-polymer aggregative phenomena were substantially stronger in Milli-Q water than lyotropic solvents (0.1 M $NaNO_3$) i.e. $d_H$ = 216–262 and 94–110 nm, respectively.

To diminish the polyelectrolyte effects observed in Milli-Q water, the intrinsic viscosities [η] of the flaxseed gum were measured in 0.1 M $NaNO_3$. As a general trend, the golden flaxseed gum extracts exhibited significantly ($p < 0.001$) higher intrinsic viscosities than their brown flaxseed analogues i.e. 6.52–6.74 vs 5.01–5.24 dL.g$^{-1}$ (Figure 24, Table 8). Similar to the $M_w$ observations, the pH of the aqueous extraction media did not significantly modify the intrinsic viscosities of the gums. The intrinsic viscosity is considered an inherent characteristic of biopolymers, which is directly associated with the molecular weight and the rigidity of the polymer chains as well as the solvent affinity (Yousefi & Razavi, 2019). The average Huggins constants ($k_H$) were 0.55 and 0.62 ($p < 0.05$) for the acidic and alkaline extracted gums, respectively, but no differences were identified concerning the flaxseed phenotype. The $k_H$ is a measure of the polymer – polymer and polymer – solvent interactions as influenced by the molecular conformation of the polymer. In general, the $k_H$ received values of around 0.35 for flexible biopolymers with extended coil conformation in good solvents, whereas higher values ranging from 0.5 to 0.8 were observed in theta solvents (Harding, 1997). Based on our findings, it can

be deduced that the solvent did not have a net effect on the polymer conformational state, with the acidic fraction showing a higher degree of polymer chain flexibility than its alkaline counterparts.

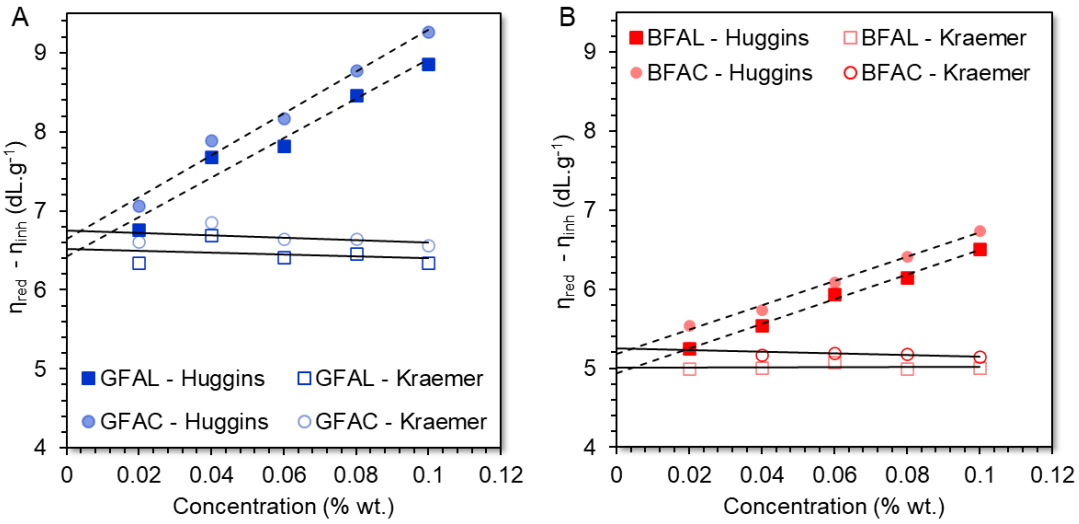


*Figure 24: Inherent (Kraemer) and relative (Huggins) viscosity as a function of golden flaxseed (A) and brown flaxseed (B) gum concentration at 25 °C.*

The surface charge density of the flaxseed gum solutions as a function of pH is illustrated in Figure 25. The reduction of the pH resulted in a progressive decrease ($p < 0.05$) in the net (negative) charge of the gum solutions due to the partial protonation of the carboxylate groups of the RG-I fraction (Ström et al., 2014), whereas the isoionic points ($pK_a$) were estimated at pH = 1.8–2. The surface charge of the polymers was rapidly depleted for pH < 4, which may be attributed to the increase in the positive charge density of the residual proteins (Kaushik et al., 2015).

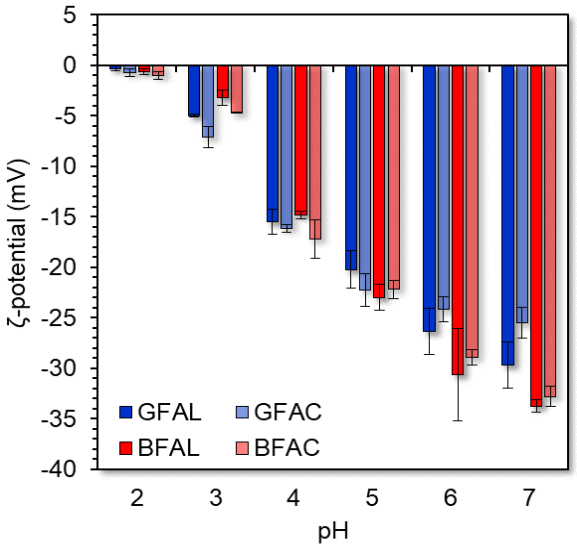


*Figure 25: Surface charge density of golden (GF–) and brown (BF–) flaxseed gums extracted under alkaline (–AL) and acid (–AC) conditions measured in Milli-Q water at 25 °C.*

Thermal gravimetric analysis was performed to study the thermal stability and decomposition pattern of the flaxseed gum extracts. As seen in Figure 26, a weight loss accounting for approx. 16% of the total gum weight was observed in the temperature range from 29.9 to 134.6 °C, which was ascribed to the evaporation of the monolayer (hydrogen bond bound) moisture content. A second thermal event related with the thermal decomposition of the gum extracts (i.e. degradation of the saccharide rings and disintegration of the polymer chains) was detected in the temperature range from 202.2 to 380.0 °C. Similar thermal decomposition patterns have been also reported for other flaxseed gum extracts (Dubois et al., 2020; Rashid et al., 2019). It should be noted that neither the extraction conditions nor the flaxseed phenotype impacted the onset, midpoint and endpoint temperatures of the recorded thermal events. To gain a better insight into the thermal stability of the flaxseed gum extracts the integral procedure decomposition temperature (IPDT) was determined as detailed in Doyle, (1961). The calculated IPDT values were 304.2, 416.7, 368.2 and 276.9 °C, for GFAL, GFAC, BFAL and BFAC, respectively. This implies that golden flaxseed gum extracts exert higher thermal stability compared to the brown flaxseed exemplars, and therefore, they are more suitable in product applications involving severe heat treatments such as baking, sterilisation etc.

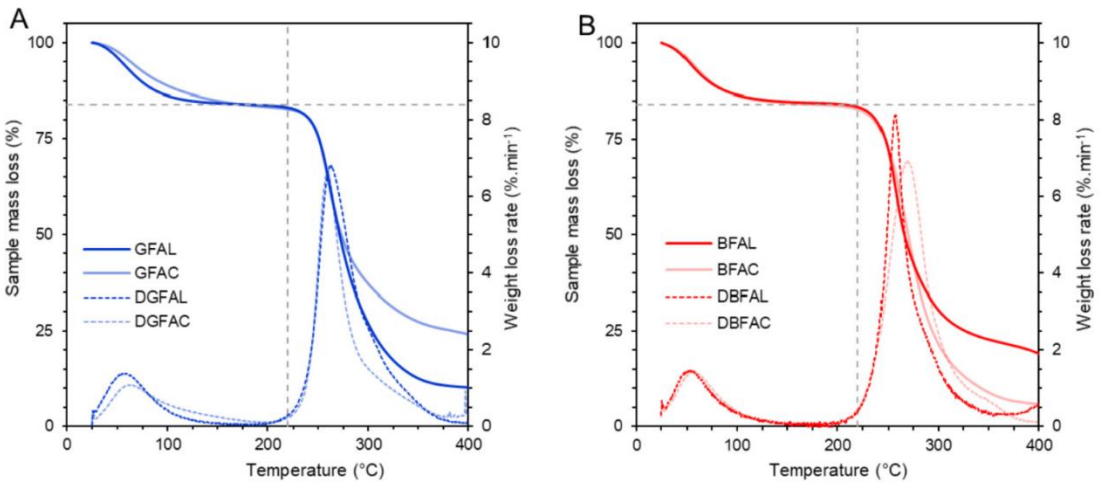


*Figure 26: TGA (continuous lines) and DTG (dashed lines) thermographs of golden (A) and brown (B) flaxseed gum extracts.*

According to the acquired DSC thermographs (data not shown), dinstict temperature regions where changes in the heat capacity took place were detected only during the first heating step (at temperatures well below the water evaporation peak). In order to confirm the $T_g$ values obtained from the first heating step, the samples underwent Thermal Mechanical Anaylsis under inert atmosphere (He) using a DIL 402 select Expedis dilatometer (NETZSCH, Selb, Germany) at a heating rate of 5 °C.min$^{-1}$ and a constant

load of 0.3 N in the range from −140 to 200 °C (data not shown). The thermomechanical spectra confirmed the presence of a physical state change event ($T_{g,onset}$ ~ 42.4 °C, $T_{g,midpoint}$ ~ 56.5 °C), which were generally in accordance with the DSC findings. However, it should be noted that no measurable changes in the heat capacity were observed in the DSC thermographs obtained during the second and third heating step. Instead, the presence of a broad endothermic midpoint peak ranging from 101.1 to 112 °C, which is comparable to the values reported for other mucilages such as tamarind (Alpizar-Reyes et al., 2017), cactus (Manhivi et al., 2018), chia seed (Punia & Dhull, 2019), *Albizia stipulata* gum exudate (Thanzami et al., 2015), and nettle galactomannan (Kutlu et al., 2020), was observed. Although the endothermic thermal event was not recorded during the third step, the acquired thermograph did not allow to evidence any glassy to rubbery state phase transition event. Such a behaviour has been previously reported for several polysaccharides including dextran, pullulan, xanthan, pectin, alginate and galactomannans (Blanshard & Lillford, 1993). Appelqvist et al., (1993) attributed such a phenomenon (observed in low moisture content polysaccharides) to a type of structural melting or phase transition phenomena involving water molecules and the relatively immobilised biopolymer. On this occasion, intermolecular associations between water and polymer residues can be still energetically formed or disrupted instead of achieving a purely glassy state (entropically driven), where the molecular mobility of the polymer backbone is hindered.

## Steady state rheological behaviour

The steady state flow curves of the flaxseed solutions can be seen in Figure 27A-D. To diminish the impact of polyelectrolyte effects, the flaxseed gum extracts were dispersed into a 0.1 M $NaNO_3$ solution. The steady flow rheological data (viscosity vs. shear rate) were fitted into the Cross-Williamson model (Equation 19). Table 9 reports the Cross-Williamson parameters i.e. the time constant τ, the rate constant m and the critical shear $\dot{\gamma}_{crit}$ at which $\eta = \frac{\eta_0 - \eta_\infty}{2}$. For the entire range of concentrations, the flaxseed gum solutions exhibited a shear-thinning flow behaviour, with the intensity of the pseudoplasticity (as expressed by m value) increasing proportionally to flaxseed gum concentration. In addition, the golden flaxseed gum solutions were more pseudoplastic than their brown flaxseed counterparts, which is attributed to their structure conformational and AX to RG-I fraction proportional differences. On the other hand, the impact of extraction conditions on the pseudoplasticity of the gum solutions was governed by the type of the flaxseed

phenotype i.e. acidic gum extraction favoured the shear-thinning character of golden flaxseed gum solutions but reduced the pseudoplasticity of the brown flaxseed gum analogues. A similar pattern concerning the impact of extraction conditions was observed also for the $\tau$ and $\dot{\gamma}_{crit}$ parameters.

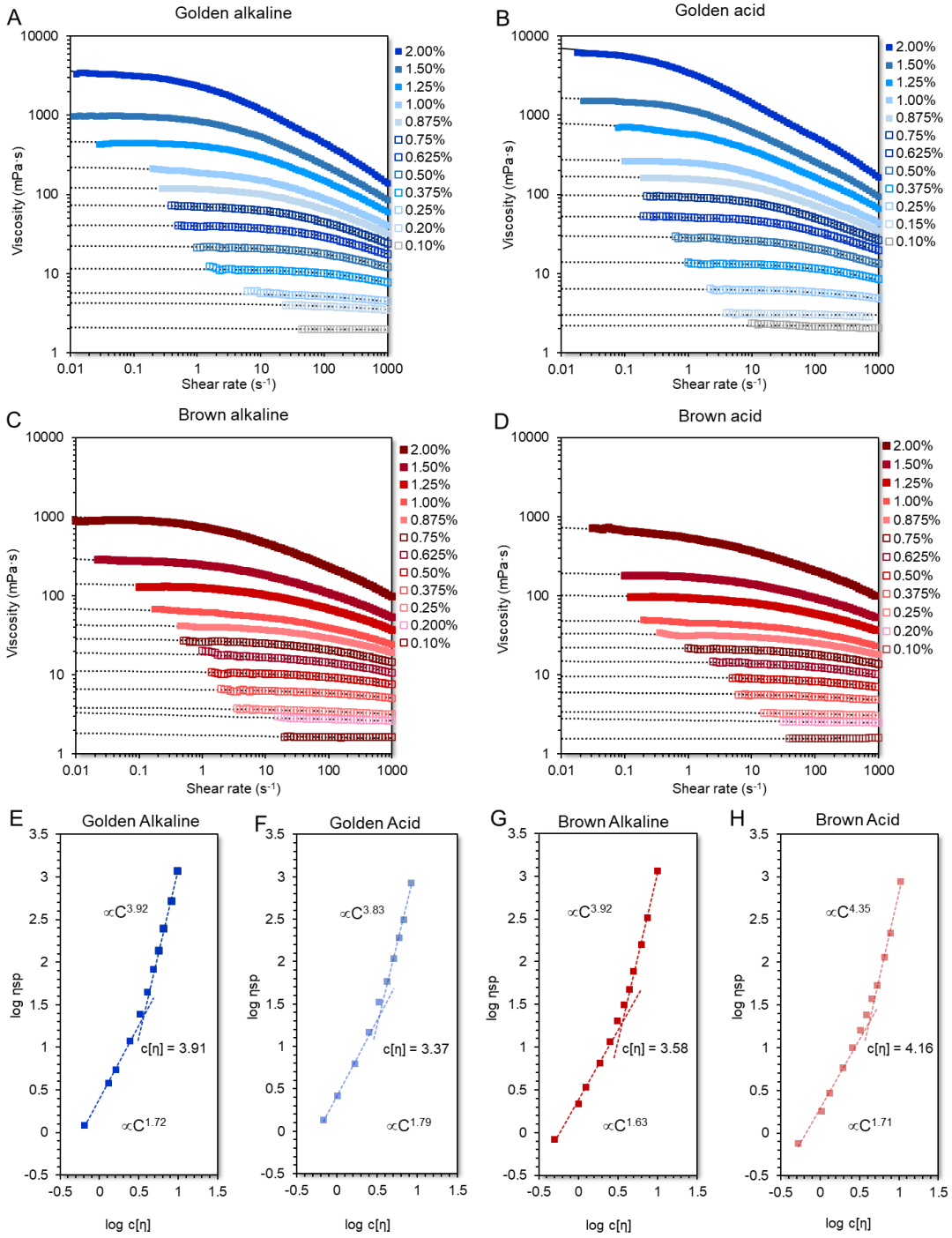


*Figure 27: Flow behaviour curves of flaxseed gum solutions as influenced by gum concentration (A-D); double logarithmic plot of specific viscosity at zero shear rate ($\eta_{sp,0}$) as a function of coil overlap parameter c[η] at 25 °C (E-H).*

*Table 9: Steady flow characteristics of golden and brown flaxseed acid and alkaline-extracted gum solutions for c > c* (0.625 to 2% wt. in 0.1 M $NaNO_3$), calculated according to the Cross-Williamson model.*

| Gum concentration | τ | | $\dot{\gamma}_{crit}$ | | m | |
|---|---|---|---|---|---|---|
| (g 100.g$^{-1}$) | (s) | | (s$^{-1}$) | | - | |
| | GFAL | GFAC | GFAL | GFAC | GFAL | GFAC |
| 0.625 | 0.004 | 0.008 | 246.71 | 119.09 | 0.027 | 0.038 |
| 0.75 | 0.007 | 0.015 | 148.47 | 67.47 | 0.052 | 0.067 |
| 0.875 | 0.012 | 0.026 | 81.87 | 37.86 | 0.057 | 0.104 |
| 1 | 0.023 | 0.042 | 42.79 | 23.8 | 0.163 | 0.138 |
| 1.25 | 0.048 | 0.178 | 20.75 | 5.62 | 0.169 | 0.414 |
| 1.5 | 0.099 | 0.263 | 10.05 | 3.8 | 0.251 | 0.464 |
| 2 | 0.381 | 1.451 | 2.62 | 0.69 | 0.583 | 1.220 |
| | BFAL | BFAC | BFAL | BFAC | BFAL | BFAC |
| 0.625 | - | - | - | - | - | - |
| 0.75 | - | - | - | - | - | - |
| 0.875 | 0.003 | 0.0007 | 291.46 | 1368.19 | 0.063 | 0.047 |
| 1 | 0.005 | 0.001 | 203.42 | 840.46 | 0.127 | 0.067 |
| 1.25 | 0.016 | 0.009 | 60.79 | 116.87 | 0.157 | 0.104 |
| 1.5 | 0.051 | 0.017 | 19.55 | 57.34 | 0.222 | 0.150 |
| 2 | 0.156 | 0.145 | 6.4 | 6.92 | 0.412 | 0.453 |

*Symbols and abbreviations used: Gum extracted from golden flaxseed (GF –) or brown flaxseed (BF –) under alkaline (–AL) or acidic (–AC) conditions; τ: relaxation time; $\dot{\gamma}_{crit}$: critical shear rate; m: Cross constant.*

Employing Milli-Q water as the biopolymer solvation medium did not modify the rheological behaviour of the gum solutions regarding the impact of the gum extraction and flaxseed phenotype conditions. Thus, the consistency coefficient and pseudoplasticity of the aqueous gum solutions was reduced proportionally to the gum concentration. The extraction conditions were impactful on the consistency coefficient only in the case of the brown flaxseed gum extracts (Table 10). Previous studies have demonstrated that the flow behaviour of flaxseed gum may be highly diversified based on its genotype and phenotype, as well as on the extraction, fractionation and purification conditions (Cui et al., 1996; Kaur et al., 2018; Liu, Shim, et al., 2016; Moczkowska et al., 2019; Qian et al., 2012; Repin et al., 2018).

*Table 10: Steady flow characteristics of golden and brown flaxseed acid and alkaline extracted gum aqueous solutions (0.25 to 2.5% wt.), calculated according to the Ostwald-de Waele model.*

| Gum concentration | K | | n | |
|---|---|---|---|---|
| (g 100.g$^{-1}$) | (Pa·s$^{n}$) | | - | |
| | GFAL | GFAC | GFAL | GFAC |
| 0.25 | 0.02$^{A,a}$ | 0.04$^{A,a}$ | 0.881$^{A,a}$ | 0.839$^{A,a}$ |
| 0.5 | 0.07$^{A,a}$ | 0.10$^{B,a}$ | 0.789$^{A,a}$ | 0.766$^{A,ab}$ |
| 0.75 | 0.12$^{A,a}$ | 0.13$^{A,a}$ | 0.771$^{A,ab}$ | 0.753$^{A,abc}$ |
| 1 | 0.28$^{A,a}$ | 0.58$^{B,a}$ | 0.700$^{A,abc}$ | 0.651$^{A,bcd}$ |
| 1.5 | 1.55$^{B,b}$ | 1.74$^{B,b}$ | 0.584$^{A,bcd}$ | 0.582$^{A,bcd}$ |
| 2 | 4.11$^{B,c}$ | 4.32$^{B,c}$ | 0.519$^{A,cd}$ | 0.517$^{A,d}$ |
| 2.5 | 8.80$^{B,d}$ | 9.70$^{B,d}$ | 0.467$^{A,d}$ | 0.466$^{A,d}$ |
| | BFAL | BFAC | BFAL | BFAC |
| 0.25 | 0.04$^{A,a}$ | 0.02$^{A,a}$ | 0.857$^{A,a}$ | 0.903$^{A,a}$ |
| 0.5 | 0.12$^{B,a}$ | 0.05$^{A,ab}$ | 0.784$^{A,ab}$ | 0.851$^{A,ab}$ |
| 0.75 | 0.33$^{B,ab}$ | 0.12$^{A,abc}$ | 0.720$^{A,abc}$ | 0.796$^{A,abc}$ |
| 1 | 0.64$^{B,b}$ | 0.25$^{A,c}$ | 0.678$^{A,abc}$ | 0.751$^{A,abcd}$ |
| 1.5 | 1.80$^{B,c}$ | 0.70$^{A,d}$ | 0.608$^{A,bc}$ | 0.685$^{A,bcd}$ |
| 2 | 2.30$^{B,d}$ | 1.52$^{A,e}$ | 0.634$^{B,bc}$ | 0.624$^{B,cd}$ |
| 2.5 | 3.03$^{A,e}$ | 2.65$^{A,f}$ | 0.573$^{B,c}$ | 0.600$^{B,d}$ |

$^{A-B,a-e}$*Different letters between the flaxseed gum extracts (uppercase) or concentrations (lowercase) for each rheological property indicate a significant difference ($p < 0.05$) according to Tukey's post hoc means comparison test. Abbreviations used: gum extracted from golden flaxseed (GF–) or brown flaxseed (BF–) under alkaline (–AL) or acidic (–AC) conditions; K: consistency coefficient; n: flow behaviour index.*

Morris et al., (1981) demonstrated that for random coil polysaccharides, the specific zero-shear viscosity ($\eta_{sp} = (\eta_0 - \eta_s)/\eta_s$, where $\eta_s$ = 0.885 mPa.s) as a function of the coil overlap parameter c[η] can be described by a power law relationship as follows (Equation 20):

Equation 20 $$\eta_{sp} = f(c.[\eta])^b$$

According to the constructed double logarithmic plots of $\eta_{sp}$ and c[η] (master curves) (Figure 27E-H), the critical coil overlap parameter $c[\eta]_{crit}$ values varied from 3.37, 3.91, 3.58 and 4.16 for GFAL, GFAC, BFAL and BFAC solutions, respectively. The $c[\eta]_{crit}$ is considered as the boundary between the dilute and semi-dilute solution state. This implies that at $c[\eta]_{crit}$ or c* (c* = $c_{crit}$), mark the onset of the transition from the dilute solution state where the polymer coils are isolated to a more concentrated (semi-dilute) state in which the hydrodynamic volume occupied by the polymer chains is higher than the solvent-free volume. Morris et al., (1981) reported that the $c[\eta]_{crit}$ = 4 for polysaccharides exerting a random coil structure conformation, whilst lower values of $c[\eta]_{crit}$ (~ 2.5 to 3.3) have been reported for polysaccharides undergoing specific intermolecular associations (known as hyperentanglement), such as galactomannans (Doyle et al., 2009; Hellebois, Soukoulis, Xu, Hausman, et al., 2021; Morris et al., 1981). The $c[\eta]_{crit}$ values calculated

here are generally in keeping with the previous findings of Qian et al., (2012) and Repin et al., (2018) i.e. $c \cdot [\eta]_{crit} \sim 2.16$ to 4.12. However, it should be noted that the degree of space occupancy appears to be highly dependent not only on the flaxseed cultivar but also on the adopted gum extraction, fractionation and purification practices (Qian et al., 2012; Repin et al., 2018). As seen in Table 8, the c* values of the gum extracts were estimated at 0.50, 0.55, 0.72 and 0.79 for GFAL, GFAC, BFAL and BFAC, respectively. As an inherent polysaccharide property, c* is inextricably associated with the structure conformational and compositional characteristics of flaxseed gum, such as the molar mass, degree of polymer branching, the mass fraction of AX, AX-RG-I and RG-I components etc. (Qian et al., 2012). Indeed, our data showed significant correlations between the c* and molar mass ($r = -0.75$, $p < 0.01$), degree of branching ($r = 0.85$, $p < 0.001$), the hydrodynamic diameter values ($r = 0.66$, $p < 0.05$) as well as the total mass fraction of the AX-RG-I composite ($r = -0.66$, $p < 0.05$).

## Dynamic rheological behaviour

*Small amplitude oscillatory shear tests were performed on flaxseed gum solutions using Milli-Q water (instead of $NaNO_3$) as the solvent, in order to achieve a better understanding of the physical state and the maximal structuring performance of the gums in conditions relevant to food colloids. Amplitude sweep tests (Figure 28A-D) were carried out to define the boundary of the linear viscoelastic regime (LVE) of the flaxseed gum solutions (1 –5% wt.). As seen in*

Table 11, the increase of the flaxseed gum concentration was accompanied by a progressive ($p < 0.001$) increase of the viscoelastic moduli at the offset of the LVE region ($G'_{LVE}$ and $G''_{LVE}$) and the yield stress ($\tau_y$). Based on the responsiveness of the $\tau_y$ to flaxseed gum type and concentration, it can be deduced that golden flaxseed gum systems required an at least two-fold higher energy input to induce the irreversible (plastic) deformation of the polymeric structures of the semi-dilute (1% wt.) or concentrated ($c >$ 2.5% wt.; non-obeying to the Cox-Merz rule) aqueous systems. On the other hand, the impact of the extraction conditions on the dynamic rheological behaviour of the flaxseed gum aqueous solutions remained unclear. In general, no remarkable differences between GFAL and GFAC solutions were observed, whereas in the case of brown flaxseed, the acidic counterparts were characterised by significantly lower viscoelastic moduli and yield stress values.

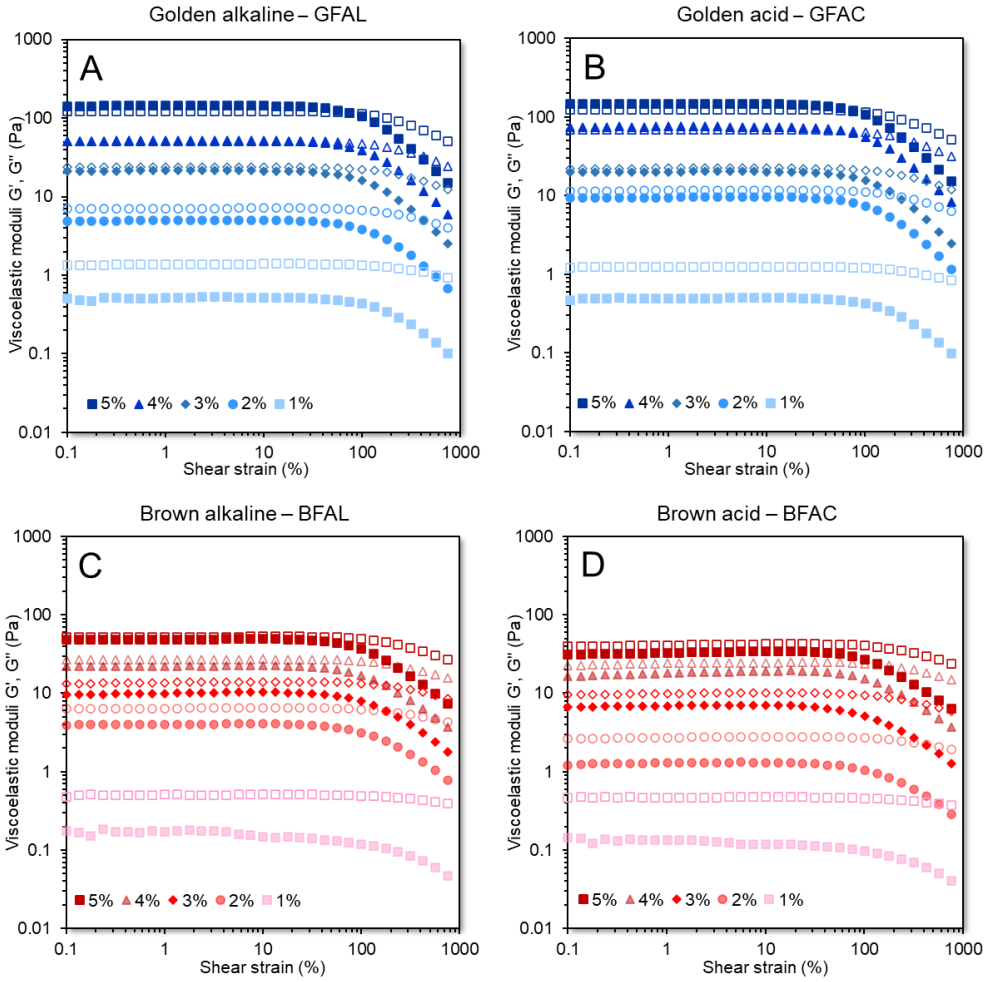


*Figure 28: Amplitude sweep rheological spectra of flaxseed gum aqueous solutions as a function of concentration measured at 25 °C. The closed symbols denote the storage modulus (G') and the open symbols the loss modulus (G").*

The frequency sweep tests (Figure 29A–D) were carried out within the LVE region (strain 0.5%) at 25 °C. For all systems, the increase in the flaxseed gum concentration was followed by a progressive transition from the pronouncedly viscous behaviour to the viscoelastic ($G' \approx G''$) or weak gel-like ($G' > G''$) behaviour. In general, the aqueous solutions of golden flaxseed gum exerted significantly higher ($p < 0.05$) complex viscosities than the brown flaxseed gum analogues for the entire range of concentration, which is in keeping with the observations of Cui et al., (1996). It should be noted that $G'$ - f slope values (Table 12) for all viscoelastic gum solutions remained quite high i.e. $0.95 < G'$ - f slope $< 0.45$, which indicates that contrary to other types of random coil polysaccharides, e.g. galactomannans, carrageenans etc., the gel forming ability of flaxseed gum remains very weak even at concentrations as high as 5% wt. The insufficient capacity of flaxseed gum to undergo true gel formation ($\tan\delta << 0.1$) was observed even in super-concentrated systems containing up to 8% wt. of gum solids (data not shown).

*Table 11: Viscoelastic properties (strain sweeps with controlled shear deformation at 1 Hz) of the flaxseed gum dispersions (1 to 5% wt., pH = 7) at 25 °C.*

| Gum | $G'_{LVE}$ | | $G''_{LVE}$ | | Yield stress, $\tau_y$ | | Flow point, $\tau_f$ | | $G'_f$ | |
|---|---|---|---|---|---|---|---|---|---|---|
| (g 100 g$^{-1}$) | (Pa) | | (Pa) | | (Pa) | | (Pa) | | (Pa) | |
| | GFAL | GFAC | GFAL | GFAC | GFAL | GFAC | GFAL | GFAC | GFAL | GFAC |
| 1 | $0.36^{B,a}$ | $0.40^{B,a}$ | $1.04^{B,a}$ | $0.91^{B,a}$ | $0.79^{B,a}$ | $0.69^{B,a}$ | nd | nd | nd | nd |
| 2 | $4.7^{B,b}$ | $5.1^{B,b}$ | $6.5^{B,b}$ | $6.4^{B,b}$ | $3.8^{B,b}$ | $3.4^{B,b}$ | nd | nd | nd | nd |
| 3 | $19.5^{B,c}$ | $21.1^{B,c}$ | $21.4^{B,c}$ | $21.3^{B,c}$ | $13.5^{B,c}$ | $12.5^{B,c}$ | nd | nd | nd | nd |
| 4 | $52.4^{B,d}$ | $59.4^{B,d}$ | $50.6^{B,d}$ | $51.8^{B,d}$ | $30.6^{B,d}$ | $31.8^{B,d}$ | $42.5^{A,a}$ | $56.9^{B,a}$ | $45.6^{A,a}$ | $40.70^{A,a}$ |
| 5 | $138.2^{C,e}$ | $147.1^{C,e}$ | $118.2^{C,e}$ | $116.2^{C,e}$ | $76.5^{C,e}$ | $74.7^{C,e}$ | $116.2^{A,b}$ | $128.0^{A,b}$ | $111.9^{A,b}$ | $108.35^{A,b}$ |
| | BFAL | BFAC | BFAL | BFAC | BFAL | BFAC | BFAL | BFAC | BFAL | BFAC |
| 1 | $0.15^{A,a}$ | $0.10^{A,a}$ | $0.5^{A,a}$ | $0.4^{A,a}$ | $0.3^{A,a}$ | $0.8^{B,a}$ | nd | nd | nd | nd |
| 2 | $4.10^{B,ab}$ | $1.3^{A,a}$ | $6.6^{B,ab}$ | $2.8^{A,a}$ | $3.4^{B,a}$ | $1.3^{A,a}$ | nd | nd | nd | nd |
| 3 | $10.2^{B,b}$ | $6.9^{A,b}$ | $14.0^{B,b}$ | $10.3^{A,b}$ | $7.9^{A,b}$ | $5.5^{A,b}$ | nd | nd | nd | nd |
| 4 | $22.9^{A,c}$ | $18.6^{A,c}$ | $27.5^{A,c}$ | $24.7^{A,c}$ | $16.1^{A,c}$ | $14.5^{A,c}$ | nd | nd | nd | nd |
| 5 | $49.7^{B,d}$ | $33.4^{A,d}$ | $53.2^{B,d}$ | $41.7^{A,d}$ | $32.4^{B,d}$ | $25.0^{A,d}$ | nd | nd | nd | nd |

$^{A-C,a-e}$*Different letters between the flaxseed gum extracts (uppercase) or concentrations (lowercase) for each rheological property indicate a significant difference ($p < 0.05$) according to Tukey's post hoc means comparison test. Abbreviations used: gum extracted from golden flaxseed (GF--) or brown flaxseed (BF--) under alkaline (--AL) or acidic (--AC) conditions.* $^{*}$*nd = not detected*

*Table 12: Viscoelastic properties ( frequency sweeps within the LVE region) of the flaxseed gum dispersions (1 to 5% wt., pH = 7) at 25 °C.*

| Gum | Complex viscosity η* | | Crossover frequency $f_c$ | | Slope G'- f | |
|---|---|---|---|---|---|---|
| (g 100 g$^{-1}$) | (Pa·s) | | (Hz) | | - | |
| | GFAL | GFAC | GFAL | GFAC | GFAL | GFAC |
| 1 | $0.17^{B,a}$ | $0.15^{B,a}$ | nd | nd | $1.26^{B,c}$ | $1.00^{A,d}$ |
| 2 | $1.3^{B,b}$ | $1.3^{B,b}$ | nd | nd | $0.91^{A,b}$ | $0.90^{A,cd}$ |
| 3 | $4.8^{C,c}$ | $4.8^{C,c}$ | 28.3a | nd | $0.76^{A,ab}$ | $0.72^{A,bc}$ |
| 4 | $11.7^{B,d}$ | $12.1^{B,d}$ | $2.26^{A,b}$ | $8.15^{B,a}$ | $0.67^{A,a}$ | $0.58^{A,ab}$ |
| 5 | $29.3^{C,e}$ | $37.5^{C,e}$ | $0.42^{A,c}$ | $0.59^{A,b}$ | $0.56^{A,a}$ | $0.50^{A,a}$ |
| | BFAL | BFAC | BFAL | BFAC | BFAL | BFAC |
| 1 | $0.24^{C,a}$ | $0.07^{A,a}$ | nd | nd | $1.27^{B,c}$ | $1.28^{B,c}$ |
| 2 | $1.38^{B,ab}$ | $0.53^{A,ab}$ | nd | nd | $0.79^{A,b}$ | $0.74^{A,a}$ |
| 3 | $2.78^{B,b}$ | $2.01^{A,b}$ | nd | nd | $0.70^{A,ab}$ | $0.59^{A,a}$ |
| 4 | $5.75^{A,c}$ | $5.09^{A,c}$ | nd | nd | $0.60^{A,ab}$ | $0.58^{A,a}$ |
| 5 | $11.90^{B,d}$ | $8.65^{A,d}$ | $6.06^{B}$ | $17.0^{C}$ | $0.52^{A,a}$ | $0.58^{A,a}$ |

$^{A-C,a-e}$*Different letters between the flaxseed gum extracts (uppercase) or concentrations (lowercase) for each rheological property indicate a significant difference ($p < 0.05$) according to Tukey's post hoc means comparison test. Abbreviations used: gum extracted from golden flaxseed (GF--) or brown flaxseed (BF--) under alkaline (--AL) or acidic (--AC) conditions.* $^{*}$*nd = not detected*

Using the Time – Concentration – Superimposition (TCS) principle, the data illustrated in Figure 29A–D, were collapsed against the arbitrarily chosen aqueous solutions containing 2% wt. of flaxseed gum extract (Figure 29E–H). According to the obtained master curves, the viscoelastic spectra were satisfactorily reduced to single curves for G′ ($\omega_r$) and G″ ($\omega_r$). As a general trend, all the extracts had a viscous-like behaviour for low frequency range whereas only golden flaxseed extract exhibited a clear viscoelastic moduli crossover point (G′ = G″) at higher frequencies. The horizontal ($a_c$) and vertical ($b_c$) superimposition shift parameters, respectively, were calculated. The changes in the $b_c$ shift factor remained under one order magnitude (0.2–0.3 and 0.3–0.9 for golden and brown flaxseed gum, respectively), which is in agreement with the literature However, a remarkably higher variation in the frequency shift factor $a_c$ values was observed, ranging from 3.2–3.4 to 3.9–4.3 orders for golden and brown flaxseed, respectively (Figure 29I–L). The shift factor - power law dependency, calculated as $a_c \propto c^n$, was estimated at $\propto c^{4.5}$, $c^{4.7}$, $c^{5.6}$ and $c^{5.8}$ for GFAC, GFAL, BFAC and BFAL, respectively. These values were lower than those reported for xanthan gum ($\propto c^{6.9} – c^{7.4}$) (Choppe et al., 2010; Cuvelier & Launay, 1986) but higher than the *Sphingomonas* exopolysaccharide ($\propto c^{3.3}$) (Carmen García et al., 2019) and welan gum ($\propto c^{4.0}$) (Carmona et al., 2019) exemplars.

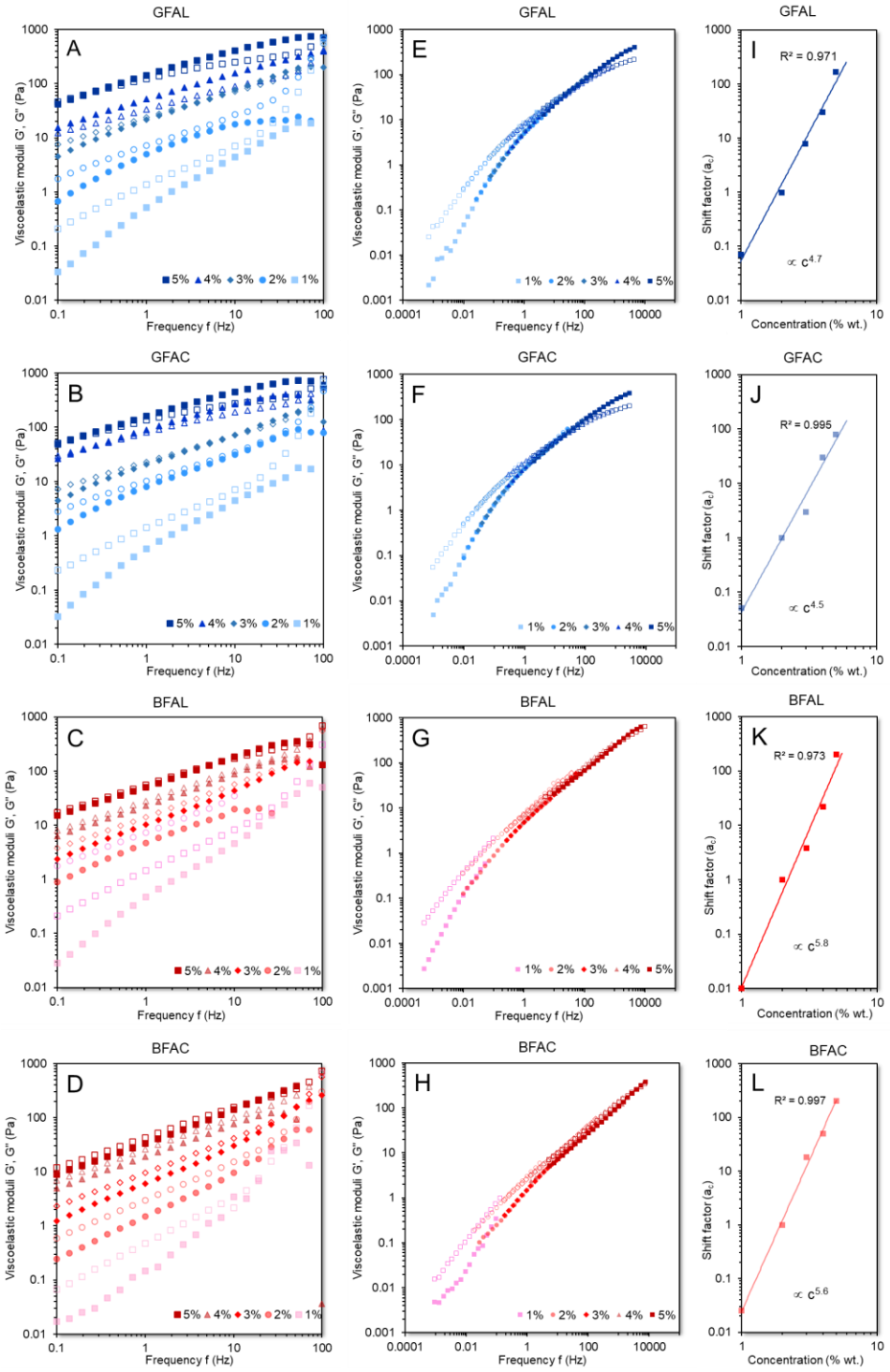


*Figure 29: Frequency sweeps rheological spectra (A–D), frequency – concentration master curves (E–H) and frequency shift factor values ($a_c$; I–L) as influenced by the concentration of the flaxseed gum extracts.*

## Hierarchical cluster analysis

To gain a deeper insight into the techno-functional affinities of the flaxseed gum extracts, the generated data were subjected to a hierarchical cluster analysis based on rows (flaxseed gum extracts) and columns (molecular, physicochemical and rheological

properties) using Ward's agglomeration and the Euclidean distance criteria (Figure 30). As illustrated in Figure 30, gum extracts of the same botanical origin were clustered together without exerting any clear individualisation. Three major clusters i.e. I, III, IV identified the disparities between the gum extracts associated with phenotypes. According to the agglomeration pattern of the variables (columns), it can be deduced that the steady and dynamic rheological properties (cluster I and IV), as well as the inherent molecular characteristics (molecular weight, intrinsic viscosity, degree of polymerisation, critical concentration) and physicochemical aspects (surface charge density and hydrodynamic diameter), were the discriminating factors of the gums based on their phenotype origin. On the other hand, the classification of the gum extracts based on the pH conditions deployed was primarily achieved using the variables found in cluster III. Specifically, seed hydration and gum extraction at pH ≈ pI favoured the isolation of intermediate molar mass polysaccharides (significant reduction of the polysaccharide fractions at 231 and 4513 kDa) leading to a lower surface charge density and hydrodynamic diameter of the polymeric chains. On the other hand, the pI-mediated extraction led to gum isolates with a higher water solvation affinity, which implies that the AX-RG-I composite polymer has a better ability to interact with water via hydrogen bonding, leading to less pronounced polymer-polymer aggregative phenomena. Concerning the variable population comprising cluster II, a mixed effect was observed compared to the extraction conditions and flaxseed phenotype. Therefore, it appears that gum extraction yield, residual protein content and the partition of the AX-RG-I polymer composites in the total polysaccharidic fraction are concomitantly influenced by both the flaxseed phenotype and the pH of the aqueous extraction medium.

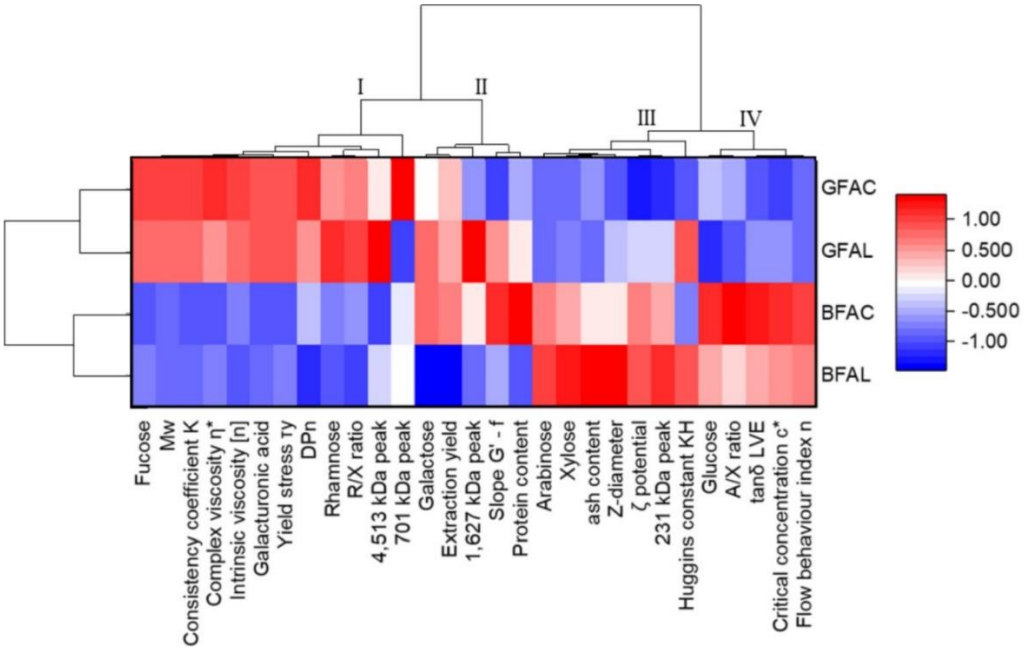


*Figure 30: Heat-map of flaxseed gum extracts as a function of their main physico-chemical, molecular, conformational and rheological properties. Flaxseed gum extracts are clustered by rows and properties by columns.*

# CONCLUSIONS

An alternative approach was studied for the extraction of water-soluble gum from flaxseed husk at pH conditions close to the isoelectric point of flaxseed proteins. Gum extraction at pH ≈ pI did not enable the significant deproteinisation of the gum extracts, most probably due to the intermolecular association of the residual proteins with the polysaccharides. The flaxseed phenotype (golden vs brown) was the most influential parameter of the osidic composition and structure conformational properties of the gum extracts. Four major polysaccharide fractions attributed to arabinoxylans (4513 kDa), rhamnogalacturonan-I (231 kDa) and two AX-RG-I composites (1627 and 701 kDa) were identified. Despite the compositional complexity of the gum extracts, it was observed that the acidic-extracted gums were characterised by lower amounts of AX and RG-I polysaccharide fractions compared to their alkaline counterparts. That explained the better solvation affinity and lower surface charge density of the acidic flaxseed gum extracts. Nevertheless, the polymer – polymer interchain associative phenomena (in both water and lyotropic media) were influenced only by the flaxseed phenotype. The steady state flow behaviour and viscoelasticity of the obtained flaxseed gum solutions (1–5% wt.) was cross-dependent on the flaxseed phenotype and pH of the extraction media. All gum extracts exhibited good thermal and mild-acidic pH stability indicating their technological tangibility for food product applications.

# CHAPTER II: INTERACTIONS OF PLANT SEED GUMS WITH MILK PROTEINS UNDER STATIC *IN VITRO* DIGESTION

## PREAMBLE

This chapter explores the interactions under static *in vitro* digestion between plant seed gums, namely alfalfa and flaxseed gum, and milk proteins, specifically whey protein and sodium caseinate. Understanding the interplay between these biopolymers can provide insight into the design of new food products with improved texture, nutritional quality, and digestibility. The standardise INFOGEST protocol for static *in vitro* digestion was applied to liquid food models containing a binary mixture of milk protein (10% wt.) and gums (0−1% wt.) to assess the impact of gums on protein digestibility. Microscopic and light scattering techniques were employed to monitor colloidal changes, such as biopolymer phase separation, protein aggregation, and particle erosion encountered throughout digestion. The protein digestibility was scrutinised by monitoring the release of amino acids and the cleavage of the intact proteins. The obtained protein hydrolysis degree and the cleavage of intact proteins were then fitted to exponential models to determine their kinetics. The flow behaviour was analysed to evaluate the rheological aspects of these interactions. These key characteristics were monitored across the stages: the initial food model matrix, the oral bolus, and subsequently within the gastric and intestinal chymes. By comprehensively mapping these interactions, the mechanistic pathways of the influence of the gums on protein digestibility were highlighted.

# IMPACT OF ALFALFA (*MEDICAGO SATIVA* L.) GALACTOMANNAN ON THE MICROSTRUCTURAL AND PHYSICOCHEMICAL CHANGES OF MILK PROTEINS UNDER STATIC *IN VITRO* DIGESTION CONDITIONS

Thierry HELLEBOIS[1,2], Claire GAIANI[2,3] and Christos SOUKOULIS[1]*

[1]Environmental Research and Innovation (ERIN) Department, Luxembourg Institute of Science and Technology (LIST), Esch-sur-Alzette, Luxembourg
[2]Université de Lorraine, LIBio, Nancy, France
[3]Institut Universitaire de France (IUF), France

Food Chemistry: X
Volume 14, 30 June 2022, 100330
doi.org/10.1016/j.fochx.2022.100330

# ABSTRACT

This paper reports on the impact of alfalfa galactomannan (AAG, 0.1, 0.5 or 1% wt.) on the colloidal changes and digestibility of sodium caseinate (NaCN) and whey protein isolate (WPI) dispersions (10% wt.) under simulated static *in vitro* digestion conditions. Static laser light scattering and confocal laser scanning microscopy-assisted assessment of the NaCN-based gastric chymes confirmed the ability of AAG to control the acid-induced protein coagulation phenomena. Contrarily, the presence of AAG in the WPI-based gastric chymes was associated with the formation of larger aggregates due to the occurrence of segregative microphase separation. The kinetic modelling of the SDS-PAGE densitometric data showed that the intragastric peptic cleavage rates were higher for caseins than whey proteins (β-lactoglobulin, α-lactalbumin). However, free amino acid (FAA) release rates did not exceed 12% under intragastric conditions, whilst notably higher release rates were achieved in the intestinal digesta (36–52%). In all cases, the FAA release rates significantly increased in the presence of AAG.

# INTRODUCTION

Milk proteins constitute food ingredients with high nutritional value and biological activity, while also having a multifaceted techno-functional role such as thickening, gelling, foaming and emulsifying properties, among others. Milk proteins are classified as caseins, i.e. αs-, β- and κ-caseins, and whey proteins, i.e. β-lactoglobulin, α-lactalbumin, lactoferrin, immunoglobulins and proteose peptones (Walstra et al., 2005). The technological and functional properties of milk proteins can be substantially diversified, due to the conformational dissimilarity of their inherent structure, in which whey proteins exhibit a globular well-defined three-dimensional structure while the casein micelles have a rather loose and more flexible structure (Goulding et al., 2020).

The exposure of milk protein aqueous dispersions to intragastric ambient conditions (i.e. gastric fluids containing acids, digestive enzymes and counterions) induces remarkable microstructural changes in the proteinaceous food bolus (Ye, 2021). Parameters such as the composition (casein to whey ratio, presence of minerals or lipids) and the structure conformational aspects of milk proteins (native vs denatured, micellar vs colloidal calcium phosphate (CCP) depleted etc.) are inextricably associated with their acid and/or pepsin-induced coagulation, as well as with their proteolytic breakdown throughout gastrointestinal transit (Ye, 2021; Ye et al., 2020). Micellar caseins can undergo extensive coagulation in the presence of milk-clotting enzymes (i.e. pepsin and chymosin) due to the peptic cleavage of the κ-casein eliminating the micelle-stabilising role of para-κ-casein, which eventually leads to the formation of protein aggregates (Ye et al., 2016). Contrary to micellar casein, the intragastric coagulation of Na- or Ca-caseinate is exclusively mediated via the formation of acid aggregates when intermolecular electrostatic forces repulsion between the CCP depleted casein molecules occurs (Horne, 2020). Whey proteins, i.e. β-lactoglobulin and α-lactalbumin are generally less responsive to intragastric peptic cleavage than caseins, and this is ascribed mainly to the pepsin selectivity for the looser structure of the latter (Dupont & Tomé, 2020). Nevertheless, caseins are classified as “slow proteins”, a term that is used to denote their ability to induce the sustained release of amino acids into the blood plasma as opposed to the acute postprandial amino-acidemic response of whey proteins (Boirie et al., 1997).

In general, common food processing practices such as thermal processing (e.g. pasteurisation, sterilisation, drying etc.) and homogenisation enhance the *in vitro* digestibility of milk proteins (Barbé et al., 2013; Böttger et al., 2019; Dupont & Tomé, 2020; van Lieshout et al., 2020). In addition, the chemical modification of milk proteins

by means of glycation, oxidation, racemisation, dephosphorylation and enzymatic crosslinking can greatly impact their gastric and intestinal-induced peptic cleavage (van Lieshout et al., 2020). Besides, the heat, acid, rennet or salt mediated sol-gel physical state transitions that occurs are known for modifying the degree of the proteolytic breakdown of milk proteins during digestion (Barbé et al., 2013, 2014; Ye et al., 2020). Macierzanka et al., (2012) demonstrated that the pepsinolytic resistance of heat-treated β-lactoglobulin solutions in various pH conditions was significantly lower in the case of fine-stranded protein aggregates formed in either neutral (pH = 6.5) or highly acidic (pH = 2.5) conditions compared to the firm protein coagulates formed at pH ≈ pI (pH = 5.2). Böttger et al., (2019) reported that the gastro-duodenal digestion resistance of the individual casein epitopes (αs1-, αs2-, β- and κ-) increased when sodium caseinate was crosslinked by means of transglutaminase.

Polysaccharides do not only possess a vital nutritional role as dietary fibres but also confer significant techno-functionalities to food matrices such as structuring, thickening and interface stabilising agents. In general, mixing polysaccharides with milk proteins may result in: a) the *co*-solubility of the biopolymers, b) associative interactions leading to complex coacervation, and c) a non-associative segregative phase separation due to either thermodynamic incompatibility or depletion flocculation phenomena (Turgeon et al., 2003). Although limitedly studied to date, the types of milk protein – polysaccharide interactions are closely related to the resistance of the milk proteins to the peptic cleavage enzymes (Borreani et al., 2016; David et al., 2020; Koutina et al., 2018; Liu & Kong, 2019; Ma et al., 2021; Markussen et al., 2021). Investigating the impact of neutral (konjac gum) and anionic (sodium alginate) polysaccharides on the *in vitro* digestibility of unheated milk proteins Borreani et al., (2016) found that the milk protein pepsinolysis was mainly suppressed by sodium alginate, which was ascribed to the occurrence of electrostatic complexation between sodium alginate and milk proteins. In a consecutive study, Koutina et al., (2018) reported that the molar mass of sodium alginate was adversely related to the *in vitro* digestibility of nanoparticulated whey protein, with peptides derived from β-lactoglobulin in the 55–66 and 109–123 regions being the most resistant to peptic cleavage Markussen et al., (2021) demonstrated that the intragastric release of free amino acids was adversely related to the size of the milk protein concentrate (MPC) – polysaccharide formed coacervates.

In our previous works (Hellebois, Gaiani, Fortuin, et al., 2021; Hellebois, Gaiani, & Soukoulis, 2022a; Hellebois, Soukoulis, Xu, Hausman, et al., 2021), the promising techno-functional aspects of alfalfa (*Medigaco sativa* L.) seed galactomannan were

unveiled. The present work reports on the role of alfalfa galactomannan in modulating the *in vitro* digestibility of milk protein-based (whey protein isolate and sodium caseinate) liquid food models. In this context, it is hypothesised that alfalfa galactomannan may sustain the peptic cleavage of milk proteins through its ability to control the acid-induced protein aggregation phenomena and hinder sterically the proteases diffusivity at the solid – liquid interface boundaries.

# MATERIALS & METHODS

## Materials

Whey protein isolate powder (PRODIET 90S) with a protein content of 85.8% wt. was kindly donated by Ingredia (Arras, France) whereas the sodium caseinate containing 89.4% wt. of protein (N% × 6.25) was purchased from Sigma-Aldrich (Leuven, Belgium). The alfalfa galactomannan (AAG), with a molecular weight of $2.0 \times 10^6$ Da, an intrinsic viscosity of 9.33 $dL.g^{-1}$ and a mannose to galactose ratio of 1.18, was isolated and purified following the procedure detailed in (Hellebois, Soukoulis, Xu, Hausman, et al., 2021). All the other chemicals used were of analytical grade.

## Sample preparation

The appropriate amount of whey protein isolate (WPI) or sodium caseinate (NaCN) was dispersed in Milli-Q to obtain a 10% wt. protein dispersion. The amount of protein content was verified by the Dumas method using an organic elemental analyser (Vario Cube, Elementar GmbH, Langenselbold, Germany). The protein dispersions were kept under magnetic stirring at ambient temperature overnight (IKA GmbH, Staufen, Germany) to allow sufficient hydration followed by centrifugation at 10,000*g* for 5 min to remove any insoluble residual. Then, the milk protein solutions were heat treated at 80 ± 1 °C for 20 min in a shaking water bath (Julabo SW22, Seelbach, Germany) before being three times homogenised at 500 bar (Panda plus 2000, Gea, Düsseldorf, Germany) to break down any protein agglomerates and rapidly cooled down at ambient temperature. The absence of protein agglomerates was confirmed by means of a static laser light scattering particle size analysis (Mastersizer 3000, Malvern Instruments, Worcestershire, United Kingdom). To avoid any bacterial growth, 0.02% wt. of sodium azide was added to the heat-treated protein solutions. The milk protein-AAG binary blend solutions were prepared by dispersing the appropriate amount of gum (i.e. 0.1, 0.5 or 1% wt.) into the milk protein

solution and allowing the biopolymer to dissolve and fully hydrate under magnetic stirring overnight at ambient temperature. All protein – AAG aqueous systems were degassed by centrifugation (3,000*g* for 5 min) prior to their physicochemical and *in vitro* digestibility assessment.

## Static simulated *in vitro* digestion

In order to conduct the static simulated *in vitro* digestion experiments, the INFOGEST v.2.0 protocol was adopted (Brodkorb et al., 2019). Briefly, 10 g of the initial food models (WPI-AAG; NaCN-AAG) were transferred into an Erlenmeyer flask, diluted 1:1 with simulated saliva fluids (SSF) containing α-amylase (150 $U.mL^{-1}$), closed with a glass stopper and incubated for 3 min in a shaking water bath at 37 ± 0.1 °C, 100 Hz. Then, the oral bolus was diluted with an equal amount of pre-warmed (to 37 °C) simulated gastric fluids (SGF) containing pepsin (activity in the final chyme of 2000 $U.mL^{-1}$) adjusted to pH = 2.5 by adding HCl 1 M (at a rate of 60 $\mu L.min^{-1}$) and incubated for 2 h at 37 °C under constant agitation. The intestine phase was initiated by adding an equal amount of pre-warmed simulated intestine fluids (SIF), containing the bile salts and pancreatin enzyme blend (trypsin activity of 200 $U.mL^{-1}$) and adjusted to pH = 7 using NaOH 1 M (at a rate of 60 $\mu L.min^{-1}$) to the gastric chyme. Solution or suspension aliquots were taken from the initial food matrix (FM) both at the end of the oral phase and at pre-selected time intervals (i.e. t = 0, 5, 10, 20, 30, 60, 90 and 120 min) throughout the simulated gastric and intestinal processing steps (120 min total duration for each step). The proteinases activity was stopped by diluting the sample ten-fold in PBS buffer (pH = 7.4) and consecutively adding 10 $\mu L.mL^{-1}$ of protease inhibitor mix (Cytiva, Marlborough, MA, United States). All samples were immediately placed into an ice bath and were analysed.

## *In vitro* digestibility assessment

i. Protein digestibility

The protein proteolytic hydrolysis occurring during the *in vitro* simulated gastrointestinal transit was tracked by SDS-PAGE analysis as follows: all systems were diluted to 5, 5, 10 and 20 µg per well of proteinaceous matter load for the food matrix, oral bolus, and gastric and intestine chymes, respectively. The samples (7.0 µL) were mixed with 2.5 µL of XT sample buffer (Bio-Rad, Hercules, CA, United States) and 0.5 XT reducing agent (Bio-Rad), heated at 95 °C for 5 min followed by rapid cooling in an ice bath. Aliquots of 10 µL were then transferred into the polyacrylamide (12%) gel wells.

SDS-PAGE electrophoresis was run in XT MES (Bio-Rad) buffer solution at 200 V for approx. 45 min until the protein migration reached the edge of the gel. The proteins were then stained with the Serva Purple fluorescent probe following the manufacturer's instructions. The imaging of the gel was performed using a Typhoon FLA 9500 Imager (GE Healthcare, Chicago, IL, United States) with a pixel resolution set at 10 µm. The densitometric analysis of the protein molecular weight bands was carried out using the ImageJ software

ii. Protein hydrolysis quantification

The hydrolysis progress of the milk proteins was monitored by quantifying the amount of primary amino groups present in the collected food matrix, and gastric and small intestine chymes using the O-phthaldialdehyde (OPA) method of Halabi et al., (2020). The food matrix was diluted 50-fold, whilst the gastric and small intestine phases were diluted 25 times. The gastrointestinal phases were then centrifuged for 5 min at 10,000*g*, 4 °C and 20 µL of the supernatant were mixed with 150 µL of ready-to-use OPA solution in a UV 96-well microplate (UV-Star Greiner, Frickenhausen, Germany) following 2 min of incubation in the dark at room temperature, and the absorbance at 340 nm was measured using a UV/VIS Spark 20 M microplate reader (Tecan, Männedorf, Switzerland).

To calculate the total amino acid content in the food matrix, acid hydrolysis was performed in each system. One hundred microlitres of the food matrix were diluted to 1 mL with HCl 6 M, and the samples were hydrolysed at 110 °C for 24 h in Pyrex tubes (Hach, Loveland, United States). The hydrolysed samples were neutralised using 1 mL of NaOH 6 M and diluted to 10 mL with deionised water. The free amino acid quantification was then determined as described above. The degree of hydrolysis of the proteins was determined as follows:

Equation 21
$$DH\ (\%) = \frac{NH_{2digested} - NH_{2FM}}{NH_{2total} - NH_{2FM}} \times 100$$

where DH is the degree of hydrolysis, $NH_{2FM}$, $NH_{2digested}$ denote the primary amino group content of the food matrix and the obtained digesta (gastric or intestine), and $NH_{2total}$ is the content of primary amino group in the acid hydrolysed food matrix.

## Confocal Laser Scanning Microscopy (CLSM)

The microstructure of the protein – galactomannan biopolymer systems was characterised by means of CLSM imaging mounted with a × 10 objective lens. In brief, 1 mL of the initial food matrix, and oral, initial and end gastric chyme, as well as the initial and end small intestine digesta were rapidly transferred into 1 mL Eppendorf tubes, mixed with

10 µL of protease inhibitor to cease the *in vitro* digestion process and were stored in an ice bath until microscopic evaluation. The proteins were non-covalently stained using 10 $\mu L.mL^{-1}$ of Fast Green 0.05% wt. aqueous solution. To assess the protein microstructure, aliquots of 300 µL were transferred into eight-well Nunc Lab-Tek II chamber microscope slides. The excitation and signal emission wavelengths used were 633 and 635–735 nm, respectively.

## Rheological analysis

The steady-state flow behaviour of the individual proteins and protein-AAG solution was measured using an oscillatory rheometer (MCR 302, Anton Paar, Graz, Austria). A double-gap (DG 26.7) geometry of 27.1 mm diameter was used to characterise the flow behaviour of the food matrix, buccal, gastric and intestinal samples (at 37 °C) at shear rates ranging from 1 to 100 $s^{-1}$. For comparison reasons, the consistency coefficient values (K, in $Pa.s^n$) of the orogastrointestinal phases were determined by fitting the shear stress – shear rate data to either pseudoplastic (Ostwald – de Waele) or Newtonian flow behaviour models. To assess the contributory effect of the insoluble acid/pepsin induced protein aggregates to the viscosity, the gastric chymes were centrifuged for 5 min at 4,500*g* and the obtained supernatants were also characterised rheologically as aforementioned.

## Particle size distribution measurements

The volume-weighted particle size distributions and the volume-weighted mean particle diameters ($D_{[4,3]}$) of aliquots obtained from the initial food matrix and the oral, gastric, and intestinal phases obtained were determined using static laser light scattering (Mastersizer 3000, Malvern, Worcestershire, United Kingdom). The refractive indexes of whey protein, sodium caseinate, and water were set at 1.45, 1.34, and 1.33, respectively.

## Statistical analyses

The Shapiro-Wilk test and Q – Q plot representation normality tests were used to verify the normal distribution of the data. To determine the significance of AAG addition on the *in vitro* digestibility of the protein, one-way ANOVA was performed using Origin 2019b software (OriginLab Inc, Northampton, MA, United States). Tukey's multiple range test was used to separate mean values when significant differences ($p < 0.05$) were detected.

# RESULTS & DISCUSSION

## Characterisation of the model food matrices and boluses

In the absence of AAG, both milk protein solutions exhibited a Newtonian flow behaviour with the NaCN, exhibiting generally higher apparent viscosities than the WPI exemplars (Figure 31A and B). As expected, the presence of AAG in the milk protein solutions resulted in a well-defined shear thinning flow behaviour (Hellebois, Gaiani, & Soukoulis, 2022a) with their apparent viscosities increasing proportionally to the AAG concentration ($c_{AAG}$). In general, at $c_{AAG} \geq 0.5\%$ wt., the changes in the apparent viscosities and consistency coefficient of the milk protein solutions became more pronounced (Figure 31, Figure 32). It is well-documented that the rheological behaviour of galactomannan solutions is directly related to their structure conformational properties such as the mannose to galactose (M/G) ratio, the sequence of the galactose depleted (smooth) to galactose substituted (hairy) regions, the molar mass and hydrodynamic radius (Doyle et al., 2009; Hellebois, Soukoulis, Xu, Hausman, et al., 2021; Sittikijyothin et al., 2005). As for alfalfa galactomannan, we have previously shown that at $c_{AAG} = c^* \approx 0.3\%$ wt. the interchain polymer-polymer interactions became significant, resulting in a tangible increase in their apparent viscosity values (Hellebois, Soukoulis, Xu, Hausman, et al., 2021). Besides the direct contribution of the AAG to the flow behaviour characteristics of the WPI solutions, the occurrence of segregative microphase separation phenomena in biopolymer binary blends are also known to induce synergistic or antagonistic effects on viscosity owing to the mutual exclusion of each polymeric component in the microdomain of the other one (Schorsch, Jones, et al., 2000; Sittikijyothin et al., 2010). In the case of WPI-AAG binary blends, a segregative microphase separation at $c_{AAG} \geq 0.1\%$ wt. driven by a depletion-flocculation mechanism was reported (Hellebois, Gaiani, & Soukoulis, 2022a).

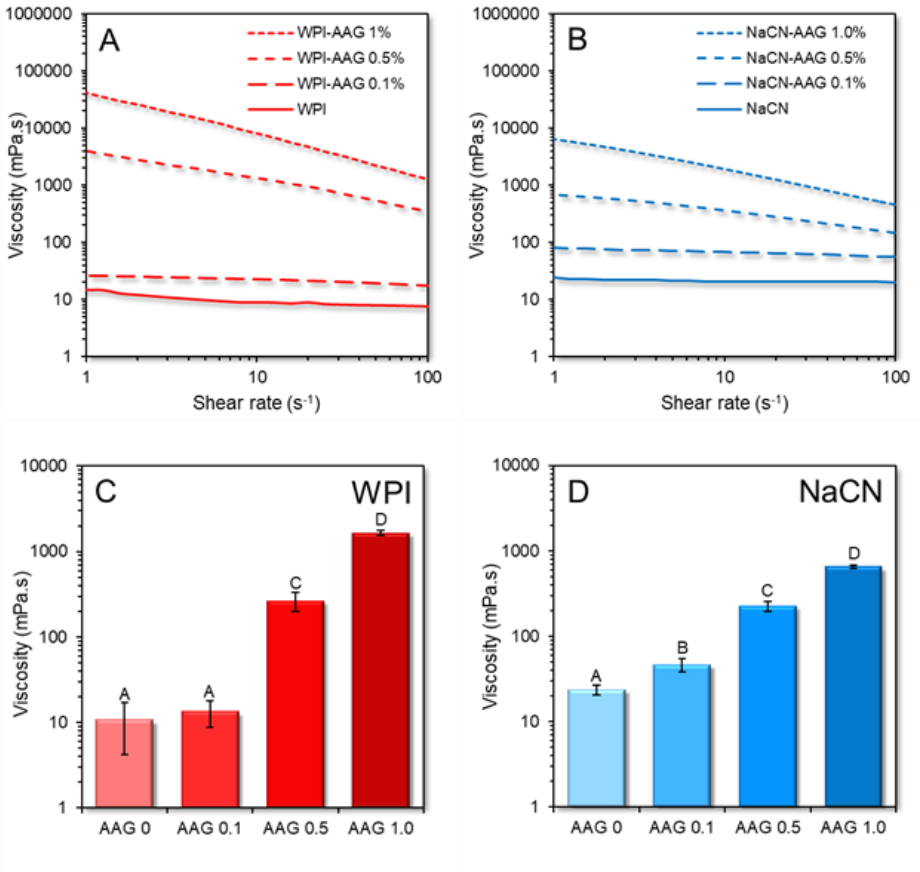


*Figure 31: Flow behaviour curves of WPI (A) and NaCN (B) solutions and their respective viscosity recorded at 50 $s^{-1}$ (C,D) as influenced by the presence of AAG (0.1-1% wt.). $^{A-D}$Different letters between the bars denote a significant difference among samples differing in the amount of AAG*

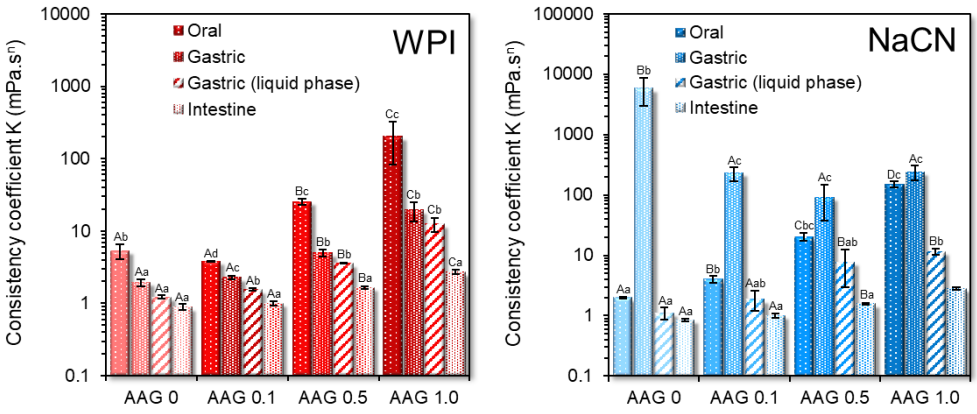


*Figure 32: Consistency coefficient K of the buccal, gastric, and intestinal phases obtained as influenced by the presence of alfalfa galactomannan. All systems were measured at 37 °C from 1 to 100 $s^{-1}$. For comparison purposes, the consistency coefficient of the gastric chymes with or without protein aggregates (centrifuged at 4,500g for 5 min) are reported. $^{A-D, a-e}$Different letters between the bars denote a significant difference among samples differing in the amount of AAG (uppercase) or in the in vitro digestion step (lowercase).*

According to the CLSM micrographs acquired (Figure 33), all binary WPI-AAG systems were microphase-separated, exhibiting diversified structure conformational aspects, i.e. AAG-rich microdroplets constrained into the continuous WPI-rich aqueous phase ($c_{AAG}$ = 0.1% wt.), bicontinuous ($c_{AAG}$ = 0.5% wt.) or protein aggregated-like ($c_{AAG}$ = 1% wt.) microstructures. Contrary to WPI-AAG solutions in which macroscopically (visually detected) separated phases could be detected for all tested protein – galactomannan concentrations, in the case of NaCN-AAG exemplars, it was very difficult to visually detect the occurrence of phase separation. The CLSM-assisted assessment of the microstructural features of the NaCN-AAG confirmed the demixing of the biopolymers at the microscopic scale, which agrees with the observations of López et al., (2017) on NaCN – *Gleditsia amorphoides* galactomannan systems. Although the proteins in NaCN exert a dissociated non-micellar structure conformation, dynamic light scattering studies have evidenced the ability of sodium caseinate to undergo self-assembly, resulting in the formation of rod-like polymer associations that are in accordance with the adhesive hard sphere model (Farrer & Lips, 1999). Also, taking into account the negligible surface charge density of AAG (Figure 34), which renders the electrostatic (repulsive) interactions between AAG and NaCN rather insignificant, it can be postulated that the demixing phenomena in the NaCN-AAG systems are due to depletion – flocculation.

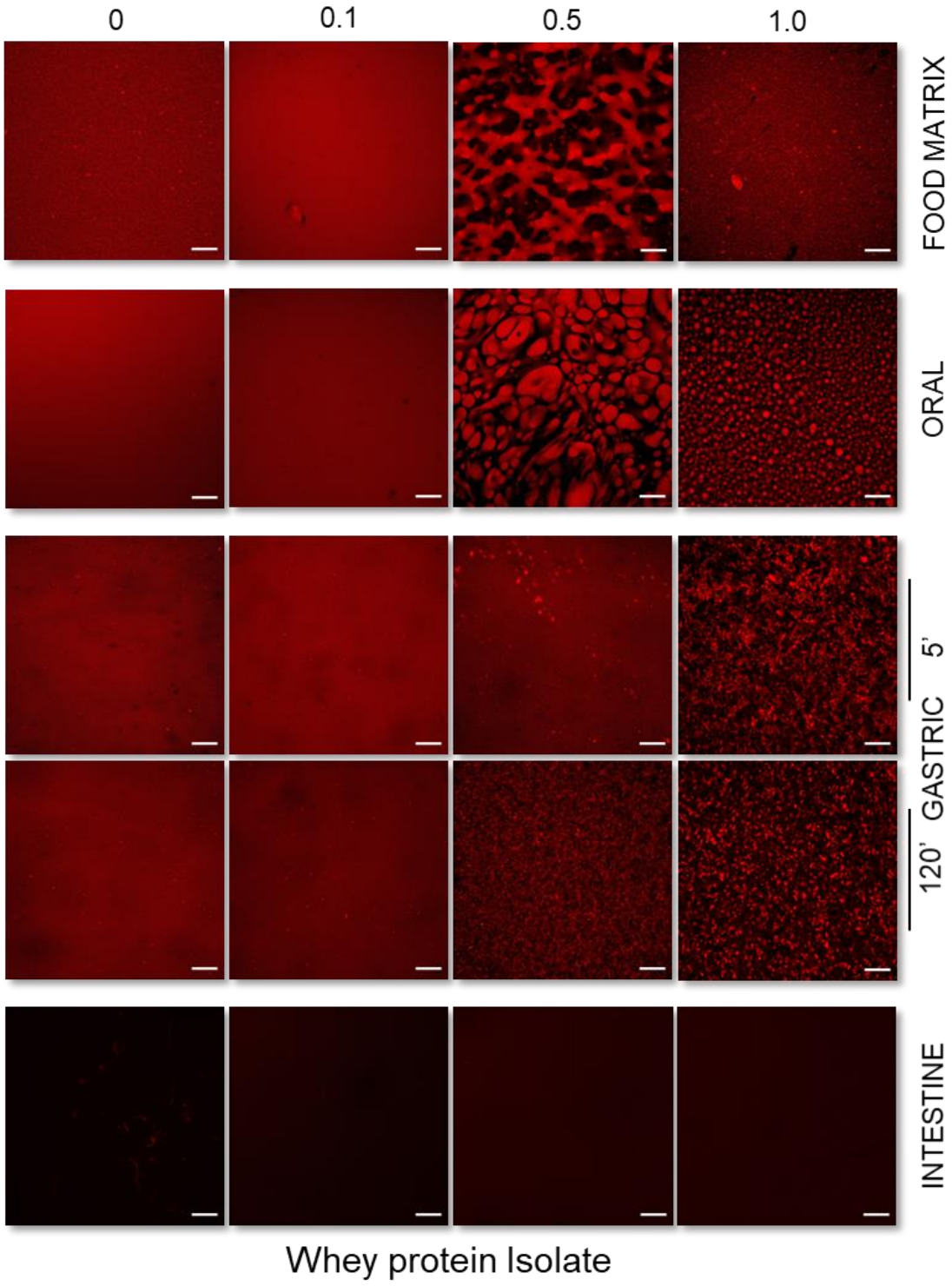


*Figure 33: Confocal laser scanning microscopy acquired micrographs of the initial protein-based models and the buccal, gastric, and intestinal phases obtained as influenced by the milk protein type (WPI vs NaCN) and the amount of alfalfa galactomannan (0.1, 0.5 or 1% wt.). Scale bar = 100 µm.*

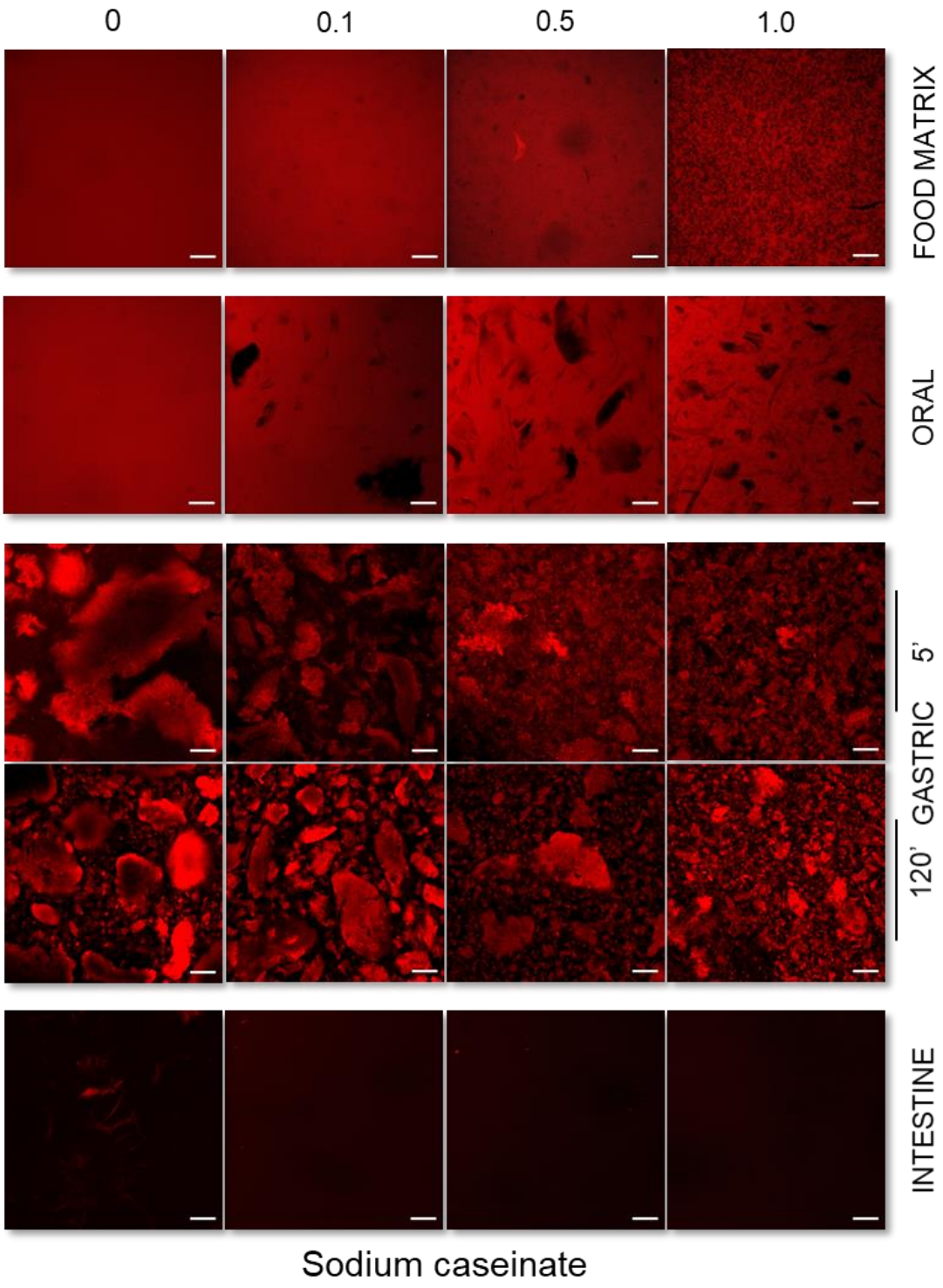


*Figure 33: (continued)*

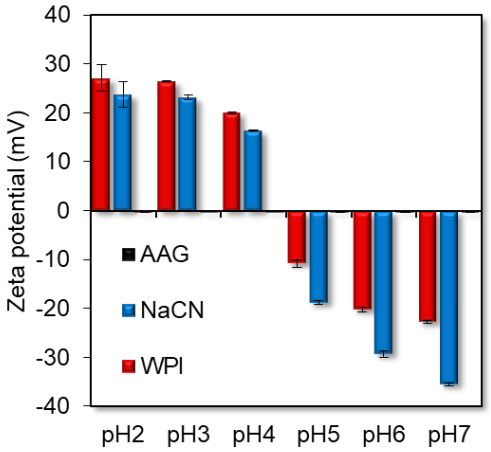


*Figure 34: Surface charge density (ζ-potential) of individual biopolymer systems i.e. NaCN, WPI or AAG as influenced by the pH. The surface charge density of individual WPI, NaCN and AAG solutions (0.1% wt.) was assessed using dynamic light scattering (Zetasizer Nano ZS, Malvern Instruments Ltd, Worcestershire, United Kingdom). Refractive indices of 1.450, 1.341 and 1.334 for WPI, NaCN and AAG, respectively, were adopted.*

On admixing the milk protein food models with the SSF, an abrupt decrease in the consistency coefficient values of the obtained food boluses was observed, as expected (data not shown). Significant microstructural changes may come about in the formation of the bolus in liquid protein – polysaccharide systems, which are primarily associated with the modification of the homopolymer and heteropolymer interactions due to the transition from the semi-dilute to the dilute state, as well as the increase in the ionic strength (Soltanahmadi et al., 2022). According to the CLSM micrographs (Figure 33), evident microstructure conformation changes were observed, i.e. micro-aggregated to water-in-water emulsion-like and interconnected to bicontinuous phase-separated structures. On the other hand, AAG-rich microdomains distributed in the protein-rich bulk (continuous) aqueous phase were detected in the case of the NaCN-based buccal phases.

Static light-scattering measurements of the food matrices and the boluses obtained (Figure 35) confirmed the presence of soluble oligomeric aggregates in WPI (ca. 260 nm) and NaCN (ca. 220 nm) dispersions. The presence of AAG was associated with incremental changes in the mean size of the WPI (0.140 to 29.35 μm) and NaCN (0.285 to 6.830 μm) dispersions. The changes observed can be primarily ascribed to excluded volume effects, i.e. as the opposite polymer-rich microdomains become more concentrated, the alike polymer-polymer interactions are favoured, leading to the formation of loosely associated (via hydrogen bond or hydrophobic interactions) soluble aggregates (Hellebois, Gaiani, & Soukoulis, 2022a).

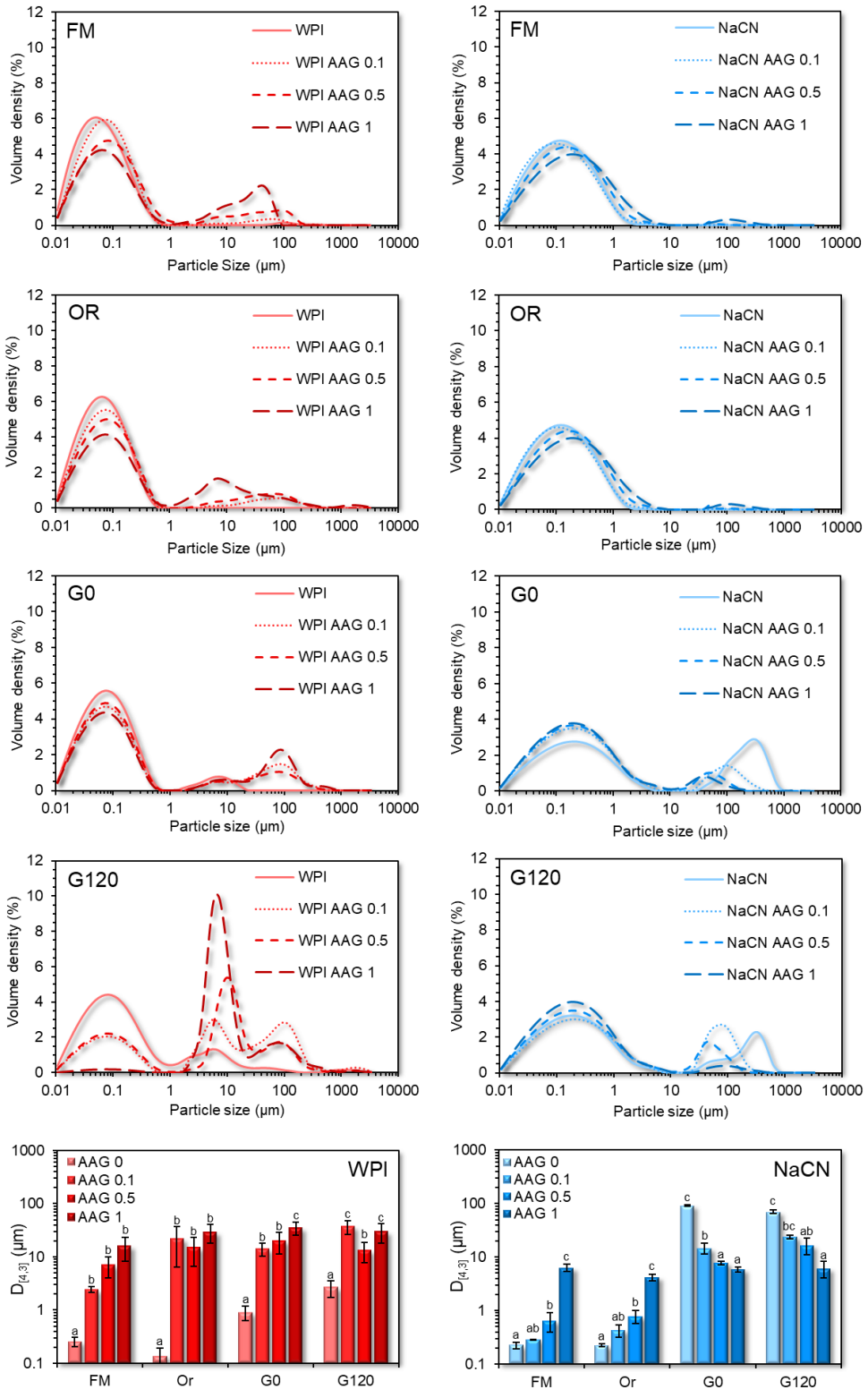


*Figure 35: Particle size distribution curves and $D_{[4,3]}$ values (in µm) of the WPI (red lines) and NaCN (blue lines)-based food models (FM) and the in vitro oral (OR) and gastric phases obtained at t = 0 (G0) and t = 120 min (G120) as influenced by the AAG content (0.1 – 1% wt.). $^{a-c}$Different letters between the bars for the same digestive step denote a significant difference among samples differing in the amount of AAG.*

### *In vitro* gastrointestinal digestion

The oral boluses were sequentially exposed to *in vitro* gastric and small intestine conditions in order to monitor the colloidal changes and digestibility of the proteins influenced by the presence of AAG. The sampling of the gastric and intestinal chymes at pre-determined time intervals aimed to provide a simplistic overview (owing to the per se technical limitations of the static models compared to the semi-dynamic and dynamic models in order to accurately simulate the physiological GI conditions) of the dynamics of the acid-induced aggregation, matrix disintegration and proteolysis. Due to the protein/polysaccharide buffering effects, the amount of HCl added to the gastric chymes was customised for each protein food model. The sampling of the gastric chymes commenced (t = 0 min) when the target pH of 2.5 was achieved, to ensure maximal pepsin activity (Kondjoyan et al., 2015).

i. Microstructural changes

The macroscopic (visual) evaluation of the gastric chymes obtained at t = 5 min (after achieving pH = 2.5) unveiled the formation of large aggregates undergoing fast sedimentation under quiescent conditions (NaCN) or smaller protein clots resulting in a more uniform suspension (WPI). In the case of NaCN, the presence of AAG was related to a reciprocal to galactomannan concentration reduction in the mean size of the protein aggregates, resulting in a thickened, less heterogeneous suspension. The macroscopic observations were also confirmed on a microscopical scale as illustrated in the acquired CLSM micrographs (Figure 33) and the SLS measurements (Figure 35). In the latter case, all systems exhibited a bimodal particle size distribution with the $D_{[4,3]}$ values (ranging from 5.8 to 92 μm) adversely correlated ($p < 0.05$) to the $c_{AAG}$ (Figure 35). The $D_{[4,3]}$ values reported here are generally in the range of those reported in the literature (Borreani et al., 2016; Markussen et al., 2021). Depending on their chemical structure, polysaccharides may affect the colloidal aspects of milk proteins when exposed to gastric fluids via different mechanistic pathways, including electrostatic complexation, microscopic phase separation or the thickening of the continuous phase (Borreani et al., 2016; Koutina et al., 2018; Markussen et al., 2021). To assess the AAG contribution to the macroviscosity of the continuous phase, the consistency coefficient of the gastric chymes before and after centrifugation was determined (Figure 32). As expected, a strong positive correlation between $D_{[4,3]}$ and consistency coefficient values ($r = 0.921$, $p < 0.001$) was found, which is in accordance with the findings of Markussen et al. (2021) for guar gum-milk protein concentrate systems. Following centrifugation, a steep reduction

in the consistency coefficient values of the continuous phase was observed, approaching those of the pure AAG solutions (Hellebois, Soukoulis, Xu, Hausman, et al., 2021). Nevertheless, minor deviations due to the pH, temperature and ionic strength in the hydrodynamic volume of AAG are expected (Repin et al., 2018). In this context, it appears that the SGF-induced colloidal transformation of the NaCN-AAG boluses stems from the thermodynamic incompatibility of the biopolymers (Markussen et al., 2021) and the ability of AAG to slow down the migration of pepsin and acid to the solid-water interface (Borreani et al., 2016).

In the case of the WPI-based gastric chymes, it was not possible to note any distinct visual changes in the size of the acid formed aggregates, with all systems to exhibit a quite homogeneous appearance. On this occasion, CLSM analysis was found to be more assistive in evaluating the morphological differences of the protein aggregates formed (Figure 33). Contrary to NaCN-based gastric chymes, an increase in the size of the protein aggregates (ranging from ca. 0.9 to 35 μm) as a function of $c_{AAG}$ was verified by means of CLSM and SLS measurements (Figure 33 & Figure 35). As pepsin has a negligible effect on whey protein clotting (Dupont & Tomé, 2020), the aggregates were formed mainly due to protein interchain bridging via nonspecific (e.g. electrostatic, hydrogen bond and hydrophobic) interactions. According to the WPI-AAG phase diagram (Hellebois, Gaiani, & Soukoulis, 2022a), and without taking into consideration the possible contributory effects of the electrolytes, it is expected that extensive segregative phase separation will occur at $c_{AAG}$ > 0.5% wt. for the initial food models (0.125% and 2.5% wt. for AAG and WPI, respectively in the gastric chyme). The gastric chymes obtained from the WPI food models containing 0.5% wt. AAG appeared to be very close to the binodal curve (i.e. the boundary between mono- and biphasic protein-polysaccharide systems). Hence, it can be postulated that the gastric-induced aggregation of WPI-AAG is primarily driven by the thermodynamic incompatibility of the two biopolymers (Markussen et al., 2021).

Following 2 h of *in vitro* gastric processing, a re-organisation of the microstructural features of the protein aggregates was generally observed (Figure 33). Nevertheless, the polydisperse character of the particle size distributions was maintained, without any significant reduction in the recurrence of large particle populations being observed for either protein type (Figure 35). This was also reflected in the $D_{[4,3]}$ values measured, which was attributed to the inadequacy of the static *in vitro* digestion model to accurately reproduce the conditions leading to the formation of protein aggregates (the $D_{[4,3]}$ values reported here are the average of at least six independently produced gastric chymes).

Furthermore, a tangible reduction in the $D_{[4,3]}$ values of NaCN gastric chymes from 92 to 70 μm was found. Although CLSM micrographs provided some evidence of particle disintegration, the $D_{[4,3]}$ values for the NaCN containing AAG remained rather unaltered (i.e. ranging from 6.2 to 24.1 μm), most probably due to the enrichment of the above-micron particle populations with fragmented aggregates derived from the very large protein particles ($D_{90}$ = 50 – 160 μm).

With the exception of the WPI-AAG 1% wt. chymes, where to some extent the gastric processing assisted in eroding the particulates formed initially (Figure 33 & Figure 35) as the concomitant result of the proteolytic attack and mechanical forces, the CLSM micrographs of the remaining gastric chymes were comprised of slightly larger particleYet the changes in the $D_{[4,3]}$ values were not significant, accounting for 0.9, 15.4 and 19.9 μm at the beginning of the gastric digestion to 2.1, 27.6 and 13.8 μm at the end for the NaCN control, 0.1% and 0.5% wt. AAG. It is assumed that these changes may be associated with the ripening of the protein particulates during the early stages of the gastric processing. A similar pattern has been reported outlining the evolution of the $D_{[4,3]}$ values in MPC-polysaccharide gastric phases (Markussen et al., 2021).

Admixing the gastric chymes with SIF resulted in an abrupt reduction in the consistency coefficient values (Figure 32), which was attributed to the almost spontaneous disintegration of the protein particles (Figure 33). Due to limitations associated with the very low mean size of the protein particles (< 500 nm) and extensive dilution, it was not possible to get a reliable overview of the microstructural aspects of the intestinal phases by means of CLSM and SLS. Even though the consistency coefficient of the intestinal chymes increased proportionally to the AAG content, no dependence on the protein source i.e. WPI vs NaCN was identified. Similarly to the centrifuged gastric chymes, the luminal viscosities were very close to those previously reported for pure AAG aqueous dilute solutions (Hellebois, Soukoulis, Xu, Hausman, et al., 2021) and thus, it can be assumed that AAG maintains its structure conformational properties and molecular intactness throughout gastrointestinal transit.

ii. Protein digestion

The gastrointestinal fate of the proteins was evaluated by monitoring the release of free amino acids and the amount of residual intact proteins. Since different protein concentrations were used to improve the detection of the intact proteins and their fragments in the buccal, gastric and intestinal phases (i.e. 5, 10 and 20 μg of proteinaceous matter per well), the comparison of the SDS-PAGE images (Figure 36) was made

separately for each *in vitro* digestion stage. Concerning the oral boluses, the proteolytic activity observed was negligible, most probably due to the absence of proteases in the artificial saliva (data not shown). In keeping with the literature, caseins (αs-, β-, and κ-) were more susceptible to peptic cleavage in the gastric phases than WPI (Ye et al., 2020). It is well established that whey proteins, i.e. β-lactoglobulin and α-lactalbumin, possess a high pepsinolytic resistance, which is primarily associated with their native compact structure conformation (Huppertz & Chia, 2021). The SDS-PAGE were image-processed using ImageJ software to obtain a representative semi-quantitative estimation of the residual matter of the principal intact proteins, i.e. total (αs–, β–, and κ–) caseins (at 25–35 kDa) for the NaCN and β-lactoglobulin (at 18.2 kDa) and α-lactalbumin (at 14.4 kDa) found in the NaCN and WPI-based digesta. The SDS-PAGE densitometric data were fitted to an empirical, fractional conversion model that showed the best data fitting (Verkempinck et al., 2022) as follows:

Equation 22 $$c = c_{120} + (c_0 - c_{120})e^{-kt}$$

Equation 23 $$\tau = \frac{\ln 2}{k}$$

where $c_0$, $c_{120}$ denote the % of intact protein content at the beginning and end of the gastric or intestinal step, and k ($h^{-1}$) is the rate of the peptic cleavage of proteins to polypeptides and τ is the time required to achieve a 50% reduction in the amount of intact proteins during the gastric or intestine digestion steps.

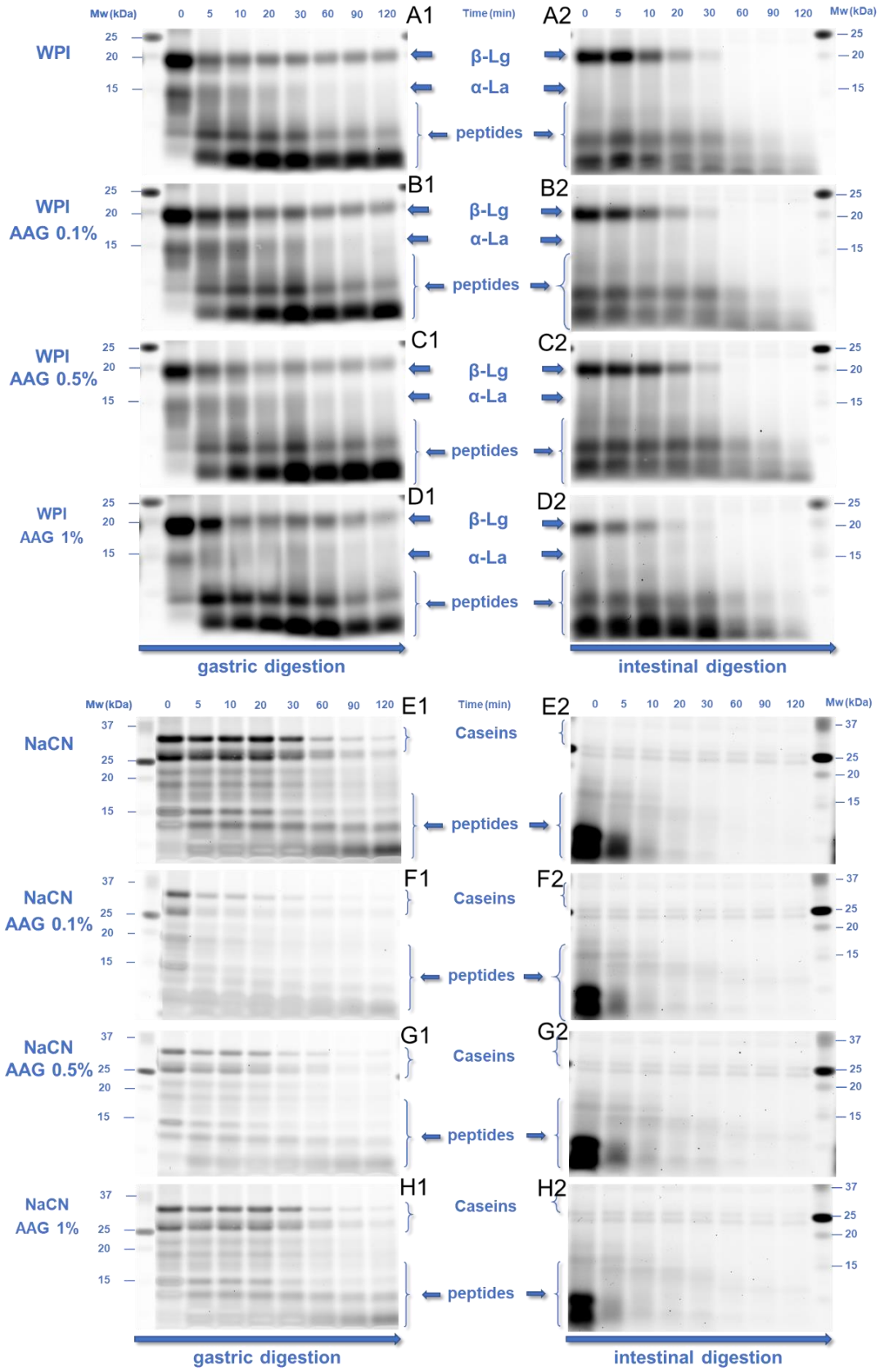


*Figure 36: SDS-PAGE patterns of the gastric (1) and intestinal (2) digesta of the WPI (A-D) and NaCN (E-H)-based food models as a function of gastric and intestinal digestion time (0, 5, 10, 20, 30, 60, 90 and 120 min) as influenced by the AAG content (0.1 – 1% wt.).*

As seen in Figure 37, the peptic cleavage of proteins was more extensive in the gastric chymes than in the intestinal digesta. Under *in vitro* gastric conditions, approximately 72, 2.8 and 15.2 min were required to achieve a 50% reduction in the amount of intact total caseins, β-lactoglobulin and α-lactalbumin, respectively. At the end of the *in vitro* gastric processing, the residual intact protein matter (normalised to t = 0 min) accounted for 10.1, 24.0, and 27.0% in the case of total caseins, β-lactoglobulin and α-lactalbumin, respectively. These values are generally in accordance with previous studies, confirming that caseins are more susceptible to pepsinolysis than whey proteins (Halabi et al., 2020; Phosanam et al., 2021). Even though native whey proteins are generally recognised for their substantially higher intragastric peptic resistance (Borreani et al., 2016), the implementation of thermal processing is known as impacting proportionally to its severity the pepsinolytic breakdown of whey proteins (Barbé et al., 2014; Macierzanka et al., 2012; Peram et al., 2013). The latter explains the relatively low amount of intact whey proteins detected in the gastric chymes. The addition of AAG induced a significant ($p < 0.05$) increase in the pepsin cleavage rates of total caseins ($\tau$ = 72.1 and 6.5 min for control and AAG-containing samples) in the NaCN-based food models. This is most probably associated with the ability of AAG to reduce the average size of the protein aggregates and therefore, to facilitate the access of the pepsin to the cleavage sites on the protein molecules. However, among the AAG containing chymes the severity of pepsinolysis was adversely associated with the $c_{AAG}$ (a reduction in the $k_{gastric}$ values from 0.23 to 0.07 $min^{-1}$ was observed), implying that the thickening effect of AAG may affect the migration rate of pepsin to the solid-water interfaces. In the case of WPI-based food models, only β-lactoglobulin was significantly affected by the presence of AAG ($\tau$ = 4 min, $p < 0.01$); however, no clear correlations between the rate of the peptic cleavage and $c_{AAG}$ were found.

The mixing of the gastric chymes with SIF was accompanied by an abrupt decrease of the total caseins, β-lactoglobulin and α-lactalbumin molecular bands (Figure 36). According to the densitometric data, it was found that $k_{intestinal} < k_{gastric}$, which can be ascribed to the fact that SDS-PAGE dictates only the cleavage of proteins to oligopeptides and not the extent of peptidolysis nor the amount of free amino acids released. Interestingly, no significant differences in the $k_{intestinal}$ values could be detected for any of the protein species, which indicates that the protease- and peptidase-induced cleavage of the proteins is rapid and less selective than the pepsin-induced proteolysis.

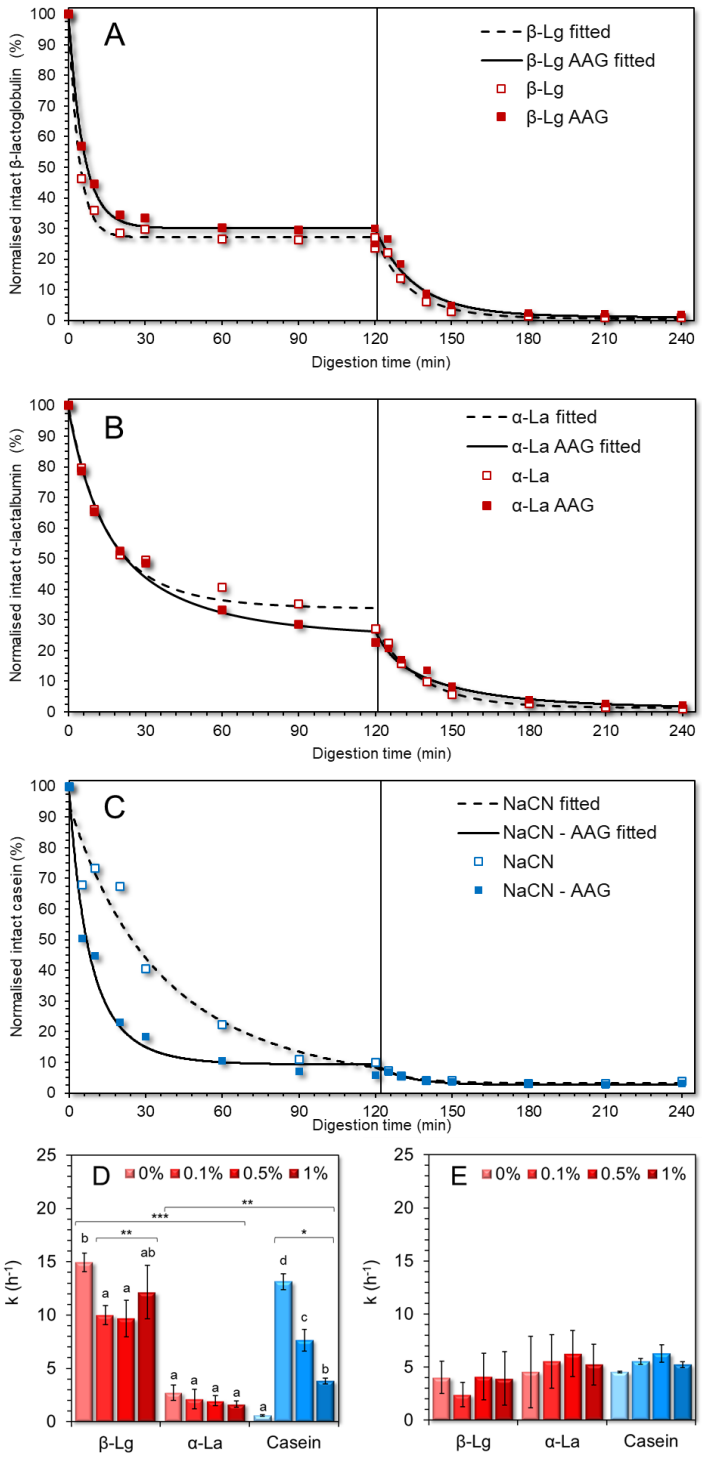


*Figure 37: SDS-PAGE densitometric analysis of the protein fate of β-lactoglobulin (A), α-lactalbumin (B) and total caseins (C) during gastric ($t_0$ - $t_{120}$) and intestinal ($t_{120}$ - $t_{240}$) simulated static in vitro digestion with or without AAG. D and E display the protein cleavage rate in the gastric and intestinal digesta, respectively. $^{a-d}$Different letters between the bars denote a significant difference among samples differing in the amount of AAG.*

To gain a more complete insight into the degree of protein hydrolysis, i.e. the cleavage of peptides and oligopeptides to free amino acids, the gastric and intestine chymes were analysed by means of OPA assay and the data obtained were fitted to the following first-

order kinetics model (Le Feunteun et al., 2021):

Equation 24 $$DH = DH_{\infty}(1 - e^{-kt})$$

where $DH_{\infty}$ denote the degree of hydrolysis (%) at end of the gastric or intestinal digestion step and k ($h^{-1}$) is the rate of peptic cleavage of proteins to polypeptides. In general, the DH of all protein food models (with or without AAG) did not exceed 12% under intragastric conditions (Figure 38A and B), with most of the observed proteolytic changes occurring in the very early stages ($\tau$ = 3 to 8 min) of gastric processing. The limited DH of milk proteins during the gastric processing stage has been also confirmed in other studies (Halabi et al., 2020; Liu & Kong, 2019; Rinaldi et al., 2014). According to the calculated $k_{DH}$ values (Figure 38C,E), the presence of AAG was associated with a significant ($p < 0.05$) increase in the release rates of free amino acids, accounting for 22−47% and 107−152% for NaCN and WPI-based food models, respectively. These findings imply that under the conditions tested here, the release kinetics of free amino acids come mainly from oligomeric protein aggregates and therefore, the ability of AAG to mediate the acid-induced ripening of the protein aggregates in the very early-stage gastric processing.

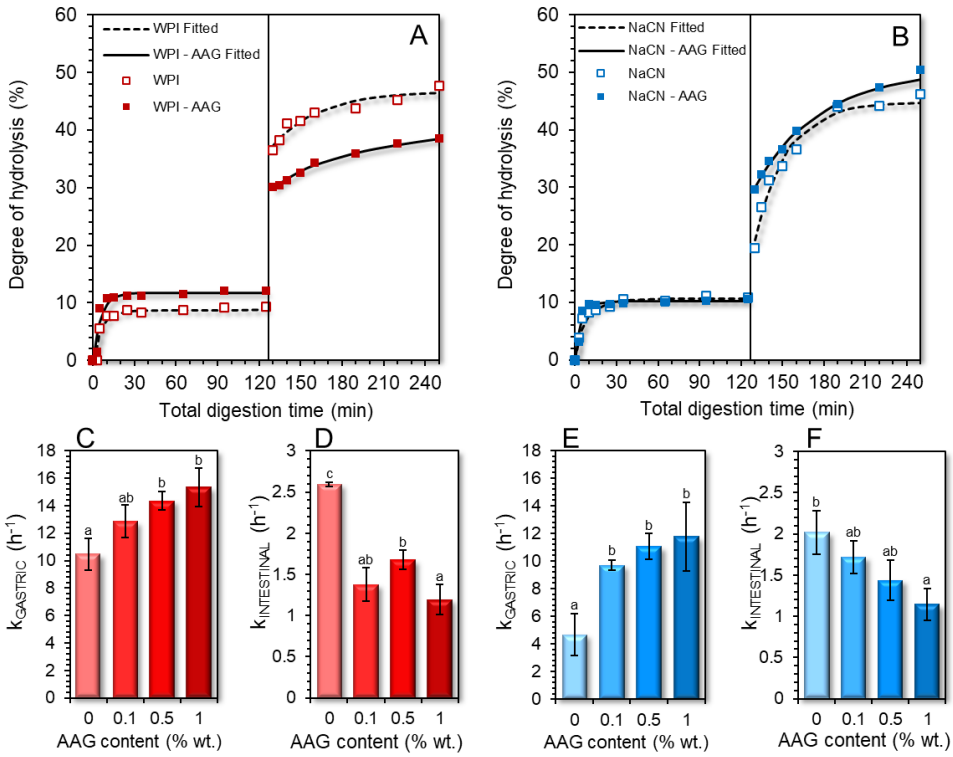


*Figure 38: Degree of protein hydrolysis of whey protein isolate (A) and sodium caseinate (B) during gastric and intestinal in vitro digestion. The protein hydrolysis rates (k) of WPI and NaCN during gastric and intestinal steps are displayed in C-F.* [a-c]*Different letters between the bars denote a significant difference among samples differing in the amount of AAG.*

As regards the intestinal digestion stage, the DH increased rapidly within the first 5 min of exposure to the intestinal proteases and peptidases, followed by a progressive increase in the amount of the free amino acids released until they reached a final DH of 36–52%, which is in line with the values reported for NaCN and WPI. The kinetic modelling of the DH data (Figure 38D and F) revealed that the presence of AAG suppressed the $k_{intestinal}$ values. Nevertheless, a reciprocal interrelationship between $c_{AAG}$ and $k_{intestinal}$ values was only observed in the case of NaCN-based digesta.

# CONCLUSIONS

The aim of the present study was to investigate the effect of an underexplored galactomannan isolated from alfalfa seeds on the *in vitro* digestibility of milk proteins. Although the addition of AAG improved the rheological profile of the initial milk protein-based liquid food models, it also induced extensive segregative phase separation phenomena driven via a depletion flocculation mechanism. The food boluses retained their phase-separated microstructure, but noticeable structure conformational differences were detected depending on the protein type and AAG content. Extensive protein aggregation phenomena in the obtained gastric chymes were confirmed both by CLSM and static light-scattering analysis. The addition of AAG had a modulatory role in controlling the average size of the acid-induced protein particulates and therefore their proteolytic resistance against pepsin-induced cleavage. The increase of the AAG content in NaCN gastric and intestinal chymes favoured the proteolytic attack of the protein aggregates formed. On the other hand, no clear correlations between the AAG concentration and the degree of proteolysis were found; however, the presence of AAG-facilitated pepsin induced the cleavage of β-lactoglobulin. In this context, the present study confirmed that alfalfa galactomannan can be successfully implemented not only as an efficient thickening/structuring agent in dairy based food systems, but it can also be exploited as a non-digestible biopolymer to tailor their post-ingestion colloidal and bio-functional performance. Its role as *co*-structuring biopolymer in milk protein-based delivery carriers will be showcased in a future study.

# IMPACT OF FLAXSEED GUMS ON THE COLLOIDAL CHANGES AND *IN VITRO* DIGESTIBILITY OF MILK PROTEINS

Thierry HELLEBOIS[1,2], Jennyfer Fortuin[1,3], Claire GAIANI[2,4] and Christos SOUKOULIS[1]

[1]Environmental Research and Innovation (ERIN) Department, Luxembourg Institute of Science and Technology (LIST), Esch-sur-Alzette, Luxembourg
[2]Université de Lorraine, LIBio, Nancy, France
[3]Food Quality and Design Group, Wageningen University and Research, Wageningen, The Netherlands
[4]Institut Universitaire de France (IUF), France

Foods
Volume 11(24), 2022, 4096
doi.org/10.3390/foods11244096

# ABSTRACT

Flaxseed (*Linum usitatissimum* L.) mucilage is one of the most studied plant seed gums in terms of its techno-functional and health-promoting properties. Nonetheless, the interplay of flaxseed gum (FG) with other food biopolymers, such as milk proteins, under *in vitro* digestion conditions remains underexplored. The aim of the present work was to investigate the colloidal interplay between flaxseed gum (golden or brown) and milk proteins (sodium caseinate or whey protein isolate) under simulated *in vitro* digestion conditions and its relationship with the attained *in vitro* protein digestibility. The presence of flaxseed gum in the milk protein food models and in the oral food boluses obtained was associated with the occurrence of segregative microphase separation. Flaxseed gum exhibited a prominent role in controlling the acid-mediated protein aggregation phenomena, particularly in the sodium caseinate gastric chymes. The addition of FG in the food models was associated with a higher amount of intact total caseins and β-lactoglobulin at the end of the gastric processing step. Monitoring of the intestinal processing step revealed a very advanced cleavage of the whey proteins (> 98%) and caseins (> 90%). The degree of the milk protein hydrolysis achieved at the end of the intestinal processing was significantly higher in the systems containing flaxseed gum (i.e. 59–62%) than their gum-free protein counterparts (i.e. 46–47%). It was postulated that the electrostatic milk protein complexation capacity and, to a lesser extent, the thickening effect of flaxseed gum influenced the *in vitro* digestibility of the milk proteins.

# INTRODUCTION

Flax (*Linum usitatissimum* L.) is one of the most important industrial crops cultivated for its fibres and seeds. Although flax fibres are prevalently exploited in the manufacturing and composite biomaterials domain (Baley et al., 2020), flaxseed is considered a rapidly emerging food biomass in the production of sustainable dietary relevant ingredients such as soluble dietary fibres (mucilage), proteins, and lipids (Liu et al., 2018). Its mucilaginous matter, located in the outermost seed layer, accounts for 3–9% of the weight of the whole seed. From an osidic composition viewpoint, flaxseed gum (FG) comprised three major polysaccharidic fractions: a low molecular weight rhamnogalacturonan-I (RG-I) rich ($M_w$ ~300–700 kDa), a high molecular weight arabinoxylan (AX) rich ($M_w$ ~ 2000–4000 kDa), and a medium molecular weight ($M_w$ ~700–1500 kDa composite heteropolymeric (RG-I and AX) fraction (Hellebois, Fortuin, Xu, Shaplov, et al., 2021). Other than the phenotypic and genotypic characteristics of flaxseed, the aqueous extraction conditions, i.e. temperature, pH, ionic strength, seed-to-water ratio, the implementation of extraction-aiding physical processing (e.g. ultrasound or microwave), and the gum purification and dehydration methods determine the structure conformation and consequently, the inherent techno-functional properties (e.g. thickening, gelling, stabilising) of flaxseed gums (Soukoulis et al., 2018)

Milk proteins i.e. caseins ($\alpha_s$-, β- and κ-) and whey proteins (primarily β-lactoglobulin, α-lactalbumin, lactoferrin, immunoglobulins, and proteose peptones), possess a substantial techno-functional and dietary role in food product design (Walstra et al., 2005). From a nutritional viewpoint, milk proteins are widely recognised as natural sources of essential amino acids and bioactive peptides (Dupont & Tomé, 2020). Due to their inherent structure conformational dissimilarity, milk proteins exert a diversified colloidal response to intragastric conditions (i.e. acid and pepsin-induced coagulation), which in turn can impact their resistance to the peptic cleavage that takes place during gastrointestinal transit. Due to their loose and more flexible structure, caseins undergo extensive intragastric coagulation compared to the well-defined globular structure conformation of whey proteins (Dupont & Tomé, 2020; Goulding et al., 2020). On the one hand, $\alpha_s$-, β- and κ-caseins are less resistant to peptic cleavage than α-lactalbumin and β-lactoglobulin as a result of the selectivity of pepsin for the looser structure of the former. On the other hand, it is well documented that the ingestion of caseins favours the formation of large aggregates in the stomach, impeding gastric emptying, and thus, caseins exhibit a more sustained postprandial amino-acidemic response than whey proteins (Boirie et al., 1997).

Other parameters associated with food processing, such as homogenisation, and enzymatic or thermal pretreatment, also have been reported to influence the digestibility of milk proteins (Barbé et al., 2013; Böttger et al., 2019; Dupont & Tomé, 2020; van Lieshout et al., 2020).

Polysaccharides play a substantial role in the food industry, serving as natural sources of dietary fibre and as structuring, texturising, thickening, and stabilising agents (Williams & Phillips, 2009). It is well documented that mixing milk proteins with polysaccharides may result in associative (complex coacervation) or non-associative segregative phase separation phenomena (Turgeon et al., 2003). The colloidal interplay between milk proteins and polysaccharides impacts the textural and structural aspects of the food matrix and modulates its colloidal configuration throughout oro-gastrointestinal transit (Ye, 2021). In this context, the presence of polysaccharides in proteinaceous-rich food matrices may sustain their disintegration rate and suppress the susceptibility of milk proteins to peptic cleavage (Borreani et al., 2016; David et al., 2020; Koutina et al., 2018; Liu & Kong, 2019; Ma et al., 2021; Markussen et al., 2021). Borreani et al., (2016) demonstrated that regardless of the protein source (i.e. skim milk powder, whey protein isolate, or sodium caseinate), anionic polysaccharides (sodium alginate) exerted a better ability to hinder the intragastric pepsinolytic activity than the non-ionic exemplars (konjac gum). Studying binary blends of sodium alginate with microparticulated whey protein, Koutina et al., (2018) reported that the degree of the peptic cleavage of whey proteins was adversely associated with the molecular weight of sodium alginate, which was ascribed to the formation of protein-polysaccharide coacervates. Implementing a semi-dynamic *in vitro* digestion model, Markussen et al., (2021) demonstrated that the occurrence of segregative phase separation and complex coacervation phenomena are the major drivers of the intragastric-induced peptic cleavage of milk protein concentrate (MPC). In a recent study, (Hellebois, Gaiani, & Soukoulis, 2022b) demonstrated that alfalfa seed galactomannan modulated the acid-induced aggregation of milk proteins, leading to higher rates of free amino group release in the intestinal digesta.

Notwithstanding the broad techno-functionality of flaxseed gums, their interplay with proteins under *in vitro* digestion-simulating conditions remains unexplored. The present study aimed to understand the impact of two different types of flaxseed gums (brown and golden) on the *in vitro* digestibility of two milk protein (whey protein isolate and sodium caseinate) liquid food models. From a mechanistic standpoint, it is hypothesised that flaxseed gum, due to its anionic character, can modulate the peptic cleavage of milk proteins through its ability to control the acid-induced protein aggregation phenomena

and hinder the proteases diffusivity sterically at the solid–liquid interface boundaries.

# MATERIALS & METHODS

## Materials

Whey protein isolate (WPI) PRODIET 90S, with a protein content of 87.7% wt., was kindly donated by Ingredia (Arras, France). Sodium caseinate (NaCN, protein purity of 89.4% wt.) was obtained from Sigma–Aldrich (Leuven, Belgium). The exact protein content of the milk proteins was determined using the Dumas method (Elementar Vario Cube, Langensenbold, Germany). The gum extraction and isolation from golden and brown flaxseed (GF and BF, respectively) was conducted at pH = 8 following the method explicitly described by Hellebois, Fortuin, Xu, Shaplov, et al., (2021). All the other chemicals used were purchased from Sigma–Aldrich and were of analytical grade.

## Preparation of the milk protein food models

The appropriate amount of protein powder was dissolved in ultrapure water (18.2 mΩ, Merck Millipore, Burlington, MA, United States) to achieve a protein concentration of 10% wt. and was stirred until complete dissolution. Following the complete dissolution of the protein, the solution was heat treated at 80 °C for 20 min in a shaking water bath (SW22, Julabo, Seelbach, Germany). The solution obtained was then homogenised three times using a high-pressure homogeniser (Panda plus 2000, GEA, Düsseldorf, Germany) at 500 bar before being centrifuged at 18,500*g* for 10 min to remove the non-solubilised particles. The homogeneity of the protein suspension was confirmed using laser light scattering particle size analysis (Mastersizer 3000, Malvern Instruments, Worcestershire, United Kingdom). To prevent bacterial growth, 0.02% wt. sodium azide ($NaN_3$) was added. BF or GF was then added to the solution to achieve 0.1, 0.5, and 1.0% wt. and the solution was solubilised overnight. Both WPI and NaCN solutions were prepared using this method.

## *In vitro* gastrointestinal processing of the milk protein food models

The *in vitro* digestion experiment was based on the INFOGEST protocol (Brodkorb et al., 2019), as previously employed in protein-polysaccharide biopolymer systems. Briefly, ten millilitres of the initial matrices (WPI/BF or GF; NaCN/BF or GF) were diluted 1:1 with simulated saliva fluids containing 75 $U.mL^{-1}$ of α-amylase and incubated

for 3 min in a shaking water bath (SW22, Julabo, Seelbach, Germany) at 37 ± 0.1 °C, 100.min$^{-1}$. The oral bolus was then diluted 1:1 with simulated gastric fluids containing 2000 U.mL$^{-1}$ of pepsin, adjusted with HCl 1 M at pH = 2.5 and incubated for 2 h at 37 °C ± 0.1 °C, $f$ = 100 min$^{-1}$. The intestine phase was initiated by diluting 1:1 the gastric chymes with simulated intestine fluids containing the bile salts and 100 U.mL$^{-1}$ of pancreatin and was then adjusted to pH = 7 with NaOH 1 M. Samples were collected in the initial food matrix at the end of the oral phase and at t = 0, 5, 10, 20, 30, 60, 90, and 120 min in the gastric and intestinal phases. The proteases activity was ceased by the addition of a protease inhibitor mix (Cytiva, Marlborough, MA, USA), and the samples were either kept in ice for direct analysis or quench frozen in liquid nitrogen and kept at −80 °C until use.

## Steady state flow rheological measurements

The initial food matrices and the oral, gastric, and intestinal phases were rheologically assessed. The flow behaviour of the systems was measured at a shear rate from 0.1 to 1000 s$^{-1}$ at 37 °C using a double gap (DG 26.7) geometry of 27.1 mm diameter mounted on an oscillatory rheometer (MCR 302, Anton Paar, Graz, Austria). The apparent viscosity of the food matrices and digesta was measured at 50 s$^{-1}$. The contribution of the sedimentable aggregates formed during the gastric phase on the rheological properties was assessed by measuring the soluble fraction after a centrifugation step at 4,500$g$ for 5 min.

## Confocal laser scanning microscopy (CLSM)

The microstructure of the mixed biopolymer systems was characterised using a CLSM microscope (LSM 880 with Airy scan, Zeiss, Jena, Germany) equipped with a × 10 objective. The detailed sample preparation and analysis method is described by Hellebois, Gaiani, & Soukoulis (2022b).

## Particle size distribution measurements

The volume-weighted particle size distributions and the volume-weighted mean particle diameters ($D_{[4,3]}$) of aliquots obtained from the initial food matrix and the oral, gastric, and intestinal phases obtained were determined using static laser light scattering (Mastersizer 3000, Malvern Panalytical, Malvern, United Kingdom). The refractive indexes of whey protein, sodium caseinate, and water were set at 1.45, 1.34, and 1.33, respectively.

### Protein digestibility

The cleavage of the intact milk proteins into peptides during the *in vitro* gastrointestinal processing steps was monitored by SDS-PAGE analysis adopting the protocol described by Hellebois, Gaiani, Paris, et al., (2021). Prior to the analysis, all systems were diluted to 5, 5, 10, and 20 µg of proteinaceous matter per well for the initial food matrix, and oral, gastric, and intestinal chymes, respectively. The samples, XT sample buffer (Bio-Rad, Hercules, CA, United States), and 0.6 XT reducing agent (Bio-Rad) were mixed at a 1:0.25:0.05 ratio, heat treated at 95 °C for 5 min, and then transferred into the SDS-PAGE gel wells.

### Protein hydrolysis quantification

The amino acid release throughout the *in vitro* digestibility was assessed by the O-phthaldialdehyde (OPA) method carefully described by Hellebois, Gaiani, & Soukoulis, (2022b). The degree of hydrolysis of the protein, after considering each dilution step, was determined as follows:

Equation 25 $$DH\ (\%) = \frac{NH_{2_{digested}} - NH_{2_{FM}}}{NH_{2_{total}} - NH_{2_{FM}}} \times 100$$

where DH is the degree of hydrolysis, and $NH_{2_{digested}}$, $NH_{2_{FM}}$, and $NH_{2_{total}}$ denote the primary amino group content of the digested samples, food matrix, and hydrolysed FM aliquots, respectively.

### Statistical analyses

The normal distribution of the experimental data was confirmed by implementing the Shapiro–Wilk test and Q–Q plot representation normality tests. One-way ANOVA coupled with Tukey's post-hoc means comparison test was performed to assess the significance of the tested parameters (milk protein type, FG type and content) on the *in vitro* digestibility data. All analysed were carried out using Origin 2019b software (OriginLab Inc, Northampton, MA, United States).

## RESULTS & DISCUSSION

### Rheological behaviour and colloidal changes during the *in vitro* simulated oral processing.

In keeping with our previous findings (Hellebois, Gaiani, & Soukoulis, 2022b), the milk

protein food models exhibited a Newtonian flow behaviour with the apparent viscosities of 23.8 and 10.8 mPa.s for NaCN and WPI, respectively. Upon FG addition, a proportional increase to the FG concentration increase was observed in the apparent viscosities of the food matrices (Figure 39). No significant differences were found in the average macroviscosity values of the NaCN-based food models as a function of the FG phenotype. On average, the GF-stabilised WPI-based food models exhibited significantly ($p < 0.05$) higher viscosities than their BF counterparts (i.e. 914 and 644 mPa.s, respectively). The rheological behaviour of colloidal dispersions in the presence of polysaccharides is known to be influenced by the molecular properties of the latter, such as the molecular weight, intrinsic viscosity, hydrodynamic radius, and surface charge density (Bai et al., 2017; Ghosh et al., 2012). According to our previous observations (Hellebois, Fortuin, Xu, Shaplov, et al., 2021), GF gum was characterised by a significantly higher molar mass and intrinsic viscosity ($M_w$ = 1340 kDa, [η] = 6.6 $dL.g^{-1}$) than BF gum ($M_w$ = 1147 kDa, [η] = 5.1 $dL.g^{-1}$). Except for the direct contribution of the polysaccharidic fraction to the viscosity of the bulk aqueous phase, the protein–polysaccharide molecular interactions e.g. electrostatic forces (electrostatic complexation or repulsion) and hydrogen bonding can also result in antagonistic or synergistic effects on the bulk rheology (Musampa et al., 2007). Although flaxseed gum is recognised as an anionic biopolymer, differences in the absolute surface charge density have been reported, i.e. |ζ| = 25–30 and 32–34 mV (pH = 7) for GF and BF gum, respectively (Hellebois, Fortuin, Xu, Shaplov, et al., 2021). Close to pH neutrality conditions (i.e. food models and oral boluses) implies that the observed reduction in the macroviscosity of the BF-stabilised milk protein solutions is due to the stronger repulsive forces between the BF and milk protein polymer chains. It should be noted that the macroviscosity dependence on the FG concentration followed a linear trend, with the highest slopes detected in the WPI-based solutions. Contrary to non-ionic polysaccharides, e.g. alfalfa galactomannan (Hellebois, Gaiani, & Soukoulis, 2022b), where the macroviscosity of the milk protein solutions was radically changed at $c > c^*$, in the FG-stabilised protein food models, it was not possible to experimentally justify such a dependence on the critical concentration ($c^*$) i.e. $c^*_{GF}$ = 0.53 and $c^*_{BF}$ = 0.76% (Hellebois, Fortuin, Xu, Shaplov, et al., 2021).

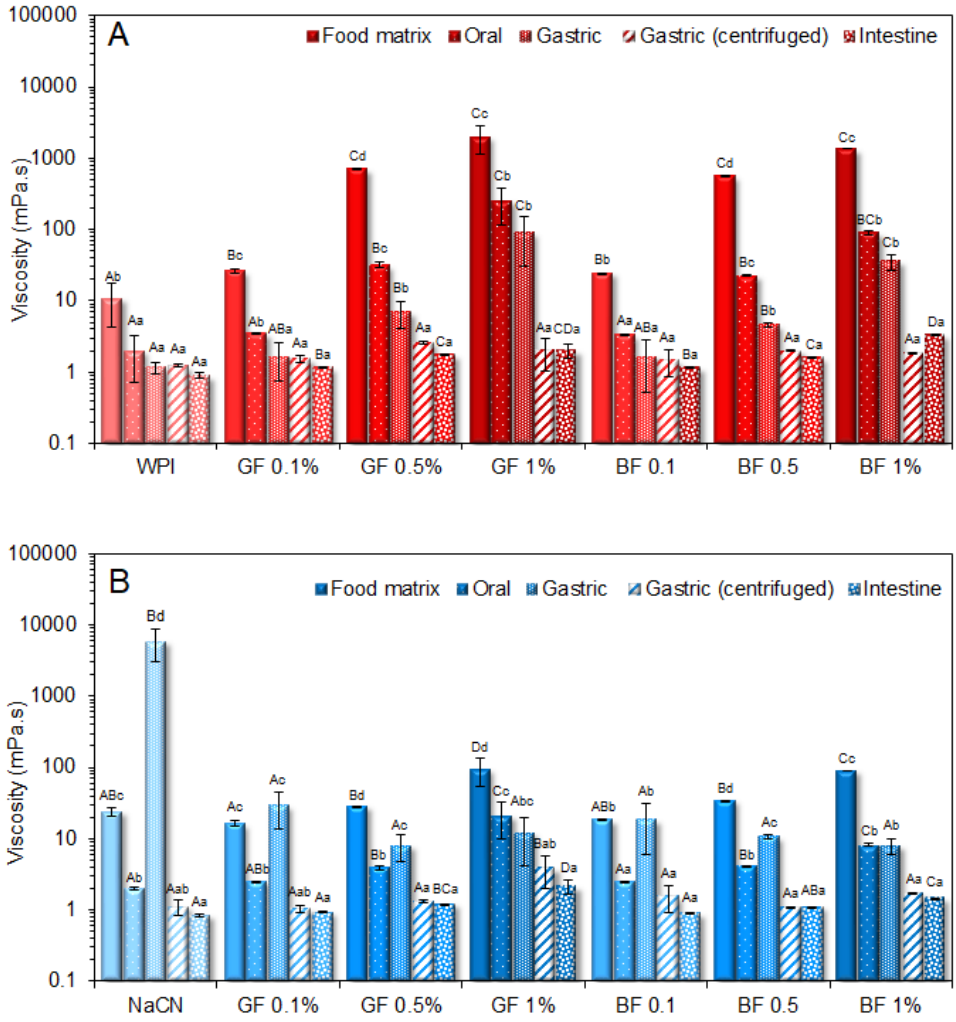


*Figure 39: Impact of the golden (GF) and brown (BF) flaxseed gums (FG) on the apparent viscosities of the whey protein isolate (WPI) (A) and sodium caseinate (NaCN) (B) -based food models and the oral, gastric, and intestine phases obtained. The term "gastric centrifuged" refers to the samples obtained following centrifugation of the gastric chymes at 4,500g for 5 min.* $^{a-d, A-D}$*Different letters between the bars denote a significant difference among the samples differing in FG content and phenotype (uppercase) or in vitro digestion step (lowercase).*

While the solute dilution degree plays a central role in the viscosimetric response of the oral boluses, other parameters, such as the changes in counterion composition and ionic strength upon mixing with the artificial saliva, may be equally influential. As illustrated in Figure 39, admixing the initial protein food models with the artificial saliva was associated with an approximately one-order decrease in the macroviscosity values. The milk protein type and FG phenotype had a significant impact ($p < 0.05$) on the macroviscosity of the oral food boluses obtained. Hence, the WPI systems stabilised by BF experienced the highest decrease in macroviscosity upon oral bolus formation. On the other hand, the impact of the FG concentration on the macroviscosity of the model food boluses was unclear ($p > 0.05$).

To gain insight into the colloidal changes occurring during the oral processing, as influenced by the FG type and concentrations, the initial food models and the oral food boluses obtained were analysed by means of CLSM (Figure 40 and Figure 41) and static laser light scattering (SLS) (Figure 42). FG in the protein food models was associated with a segregative microphase separation phenomena as a cause of the intermolecular repulsive forces between the FG and milk proteins (Hellebois, Gaiani, Cambier, et al., 2022). From a mechanistic point of view, the segregative phase separation in polysaccharide–protein aqueous systems is associated with either the Flory–Huggins or depletion flocculation theories (Doublier et al., 2000). In colloidal dispersions (i.e. biopolymer microspheres dispersed into the semi-dilute polysaccharide-rich aqueous phase), segregative phase separation is driven primarily by the depletion-flocculation mechanism, where the milk proteins behave as colloidal microspheres. Indeed, it has previously been demonstrated that both WPI and NaCN may exhibit a microsphere-like behaviour stemming from either their nano-aggregated (WPI) or rod-like self-assembled (NaCN) structure conformation (Farrer & Lips, 1999; Turgeon et al., 2003).

As illustrated in Figure 40, in the WPI-based food models, a similar segregative phase separation pattern was observed between BF and GF. At $c_{FG}$ = 0.1% wt., the WPI food models exhibited a biphasic w/w emulsion-like conformation where FG-rich water microdroplets were uniformly distributed into the continuous protein-rich aqueous phase. At $c_{FG} \geq 0.5\%$ wt., the FG-stabilised WPI food models had a heterogenous microstructure as evidenced by the presence of protein microaggregates dispersed into the continuous phase. Given that the aggregative phenomena took place at c~c* ($c^*_{GF}$ = 0.53 and $c^*_{BF}$ = 0.76% wt. (Hellebois, Fortuin, Xu, Shaplov, et al., 2021), it is assumed that the transition from the dilute to the semi-dilute regime promotes the noncovalent self-association of the whey proteins (Hellebois, Gaiani, Cambier, et al., 2022). To a lesser extent, electrostatic complexation between FG and WPI proteins may also occur. By adding the artificial saliva, a decisive reduction in the prominence of the demixing phenomena in the systems containing 0.1% wt. was observed (Figure 40B1–2,E1–2), which can be ascribed to the shifting of the thermodynamic equilibrium close to the binodal curve (Hellebois, Gaiani, Cambier, et al., 2022). At $c_{FG} \geq 0.5\%$ wt., the dilution of the initial food matrices with the oral fluids resulted in a sparsely heterogeneous microstructure (Figure 40C1–2, F1–2).

In contrast to the WPI exemplars, the NaCN-based food models exerted a demixed water-in-water emulsion-like microstructure for the whole range of $c_{FG}$, with the BF-stabilised systems being more pronounced (Figure 41A1–G1). Interestingly, the emulsion-like

segregated microstructure was detected in the entity of the NaCN-based oral boluses, but to a lesser extent (Figure 41A2–G2). No clear interrelationship between the FG concentration and the magnitude of the segregative phenomena was noted. According to the SLS measurements (Figure 42), the presence of soluble protein aggregates ($D_{[4,3]}$ = 258 and 225 nm for WPI and NaCN, respectively) was confirmed. The impact of FG on the particle size of the protein aggregates was dependent on the protein type. As for the WPI food models, a proportional increase to the FG concentration increase was observed in the mean size of the soluble protein aggregates. Although the coacervation between FG and WPI at pH > $pH_c$, i.e. ~5.2–5.4 (Liu et al., 2017) is considered unlikely to occur as both biopolymers were negatively charged, the formation of soluble protein aggregates under weakly acidic conditions (pH > 5.5) has been reported, as a result of the intermolecular association between FG and WPI through oppositely charged patch junction zones (Soukoulis et al., 2019).

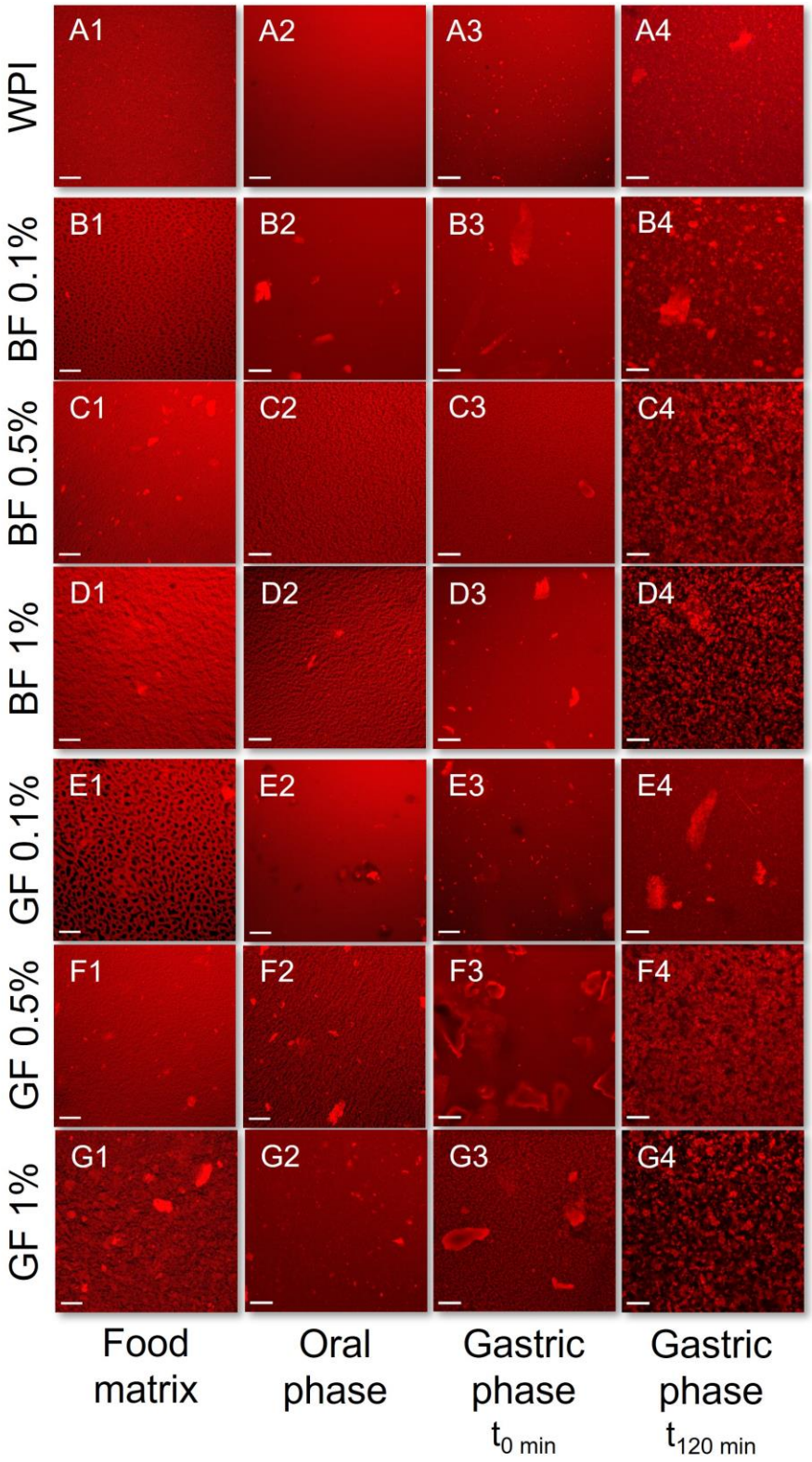


*Figure 40: CLSM assessment of the impact of flaxseed gums on the in vitro oro-gastric induced colloidal changes of the WPI-based food models adopting the INFOGEST 2.0 in vitro digestion model. 1: Food matrix, 2: Oral phase; 3: gastric (start); 4: gastric (end); A: WPI only; B,C,D: WPI + BF; E,F,G: WPI + GF. Scale bar = 100 µm.*

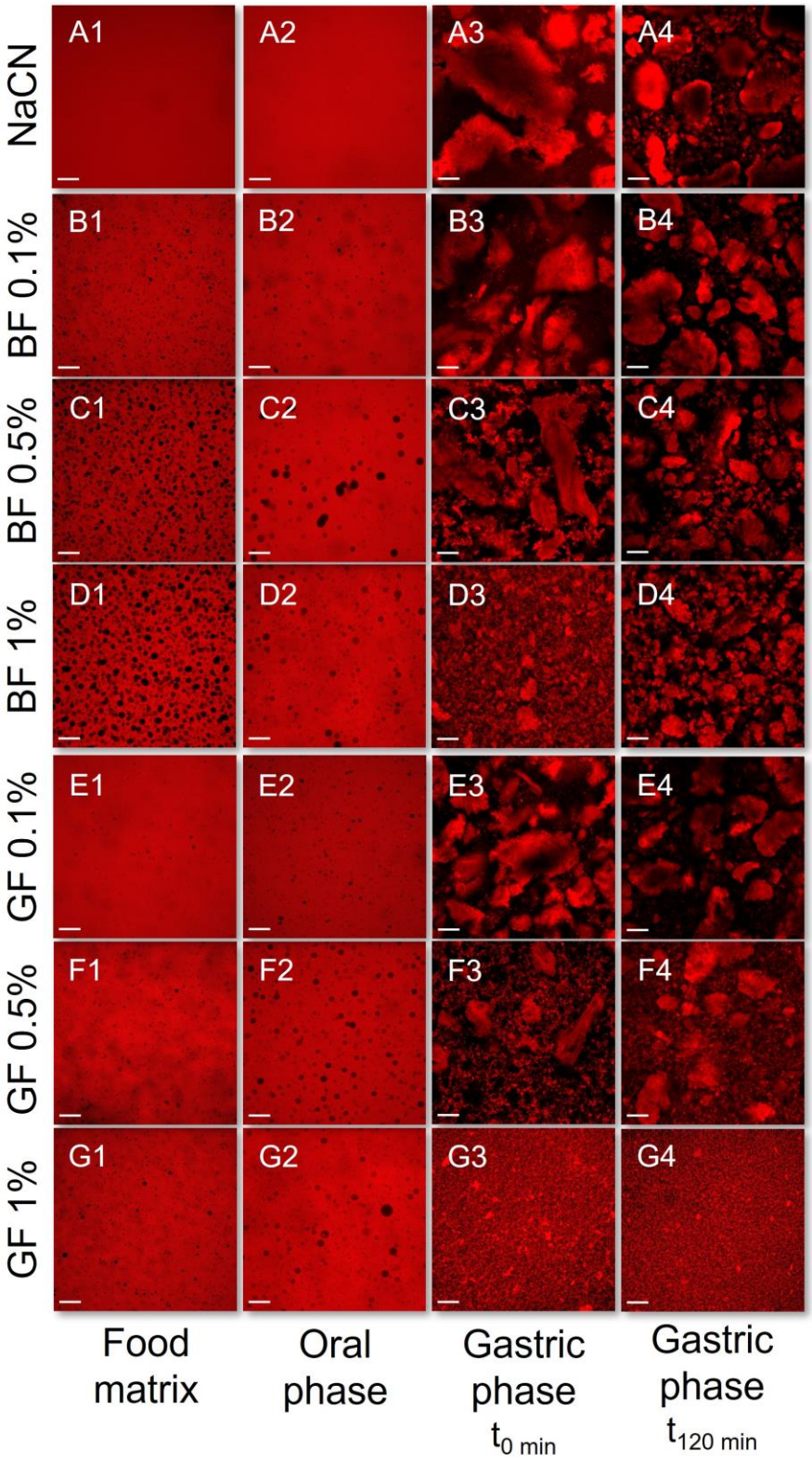


*Figure 41: CLSM assessment of the impact of flaxseed gums on the in vitro oro-gastric induced colloidal changes of the NaCN-based food models adopting the INFOGEST 2.0 in vitro digestion model. 1: Food matrix, 2: Oral phase; 3: gastric (start); 4: gastric (end); A: NaCN only; B,C,D: NaCN + BF; E,F,G: NaCN + GF. Scale bar = 100 µm*

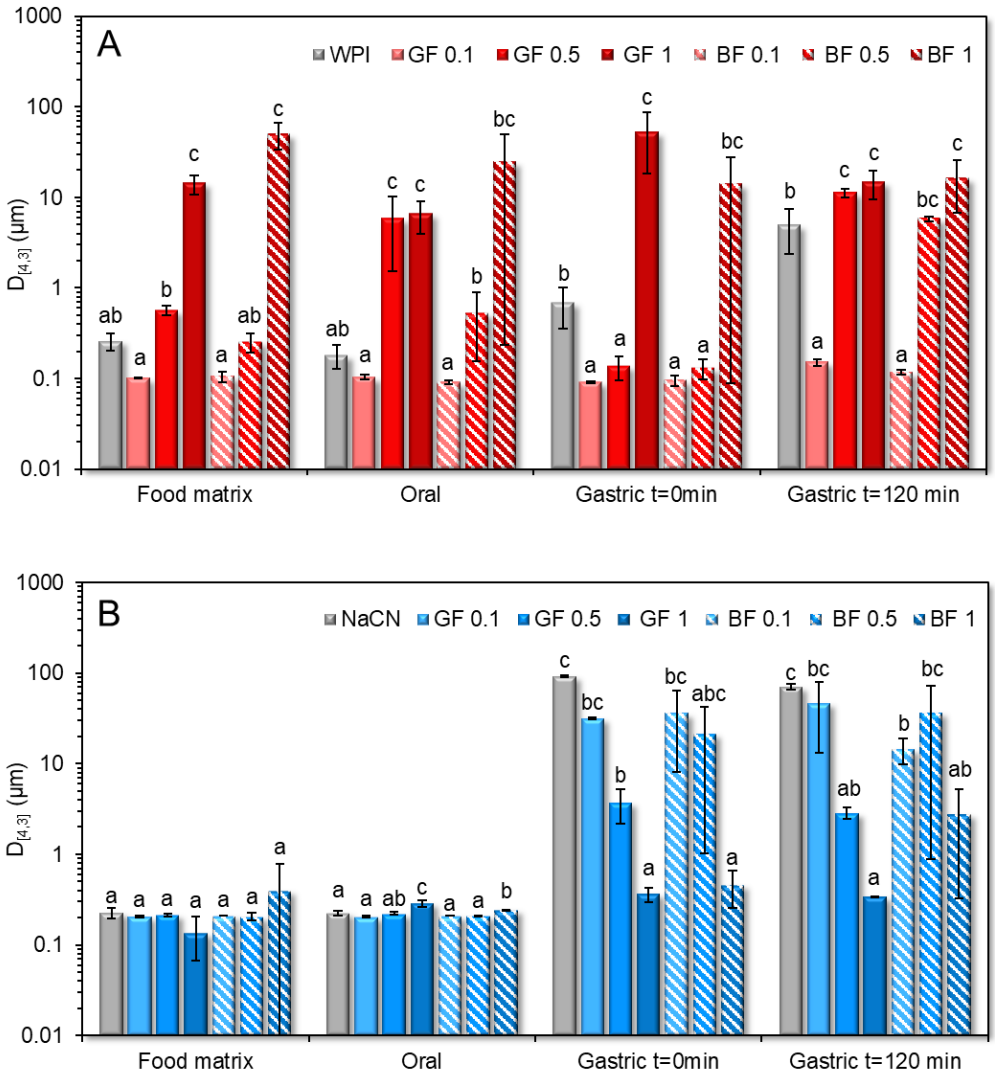


*Figure 42: Changes in the protein aggregate particle size as they occurred throughout the simulated in vitro oro-gastrointestinal processing of the WPI-(A) and NaCN-(B) based food models. [a−c]Different letters between the bar phases denote a significant difference among the samples differing in the amount of gum for the same digestive.*

Nonetheless, the FG phenotype was not influential on the mean size of the soluble protein aggregates. The addition of FG into the NaCN food models did not modify their colloidal properties for the entire range of gum concentration. In mild acidic conditions, NaCN is characterised by a significantly higher negative surface charge density than WPI (Hellebois, Gaiani, & Soukoulis, 2022b), and hence it is assumed that the strong electrostatic repulsion between the FG and NaCN molecules hampered the formation of soluble aggregates. On admixing with the artificial saliva, none of the protein food models tested experienced any significant change in terms of the protein aggregate mean size, which implies that the changes in the ionic strength and counterion composition of the food boluses did not modify the mechanism of the FG–milk protein interactions.

## Rheological behaviour and colloidal changes under *in vitro* gastro-intestinal conditions

To offset the technical limitations of the static *in vitro* digestion models associated with the dynamics of the physiology of digestion (Xavier & Mariutti, 2021), the gastric fluids were added at a constant rate and under constant stirring to achieve the target gastric $pH_{gastric}$ = 2.5 within 5 min (t = 0 min). The enzymatic activity of pepsin was predetermined, and the amount of the HCl required for achieving the $pH_{gastric}$ = 2.5 was customised per food model to minimise the buffering effect of the milk proteins and FG. In addition, the peptic cleavage process was hindered using a protease inhibitor cocktail, whilst a real-time analysis of the samples, stored in an ice bath, was conducted on the same day.

All gastric phases exhibited a suspension-like behaviour owing to the formation of acid-mediated protein aggregates. The viscosimetric characterisation of the gastric phases (before and after centrifugation) revealed that the NaCN-based food models experienced the highest increase in apparent viscosity at 50 $s^{-1}$ compared to the WPI exemplars (Figure 39). Interestingly, centrifugation resulted in an abrupt (almost four-order magnitude) decline in the macroviscosity values of the NaCN-based gastric chymes, which can be attributed to the depletion of their sedimentable protein aggregate matter (Figure 39B). On the other hand, no significant differences in the macroviscosity of the actual and centrifuged WPI gastric phases were observed, indicating the presence of finer and more uniform protein aggregates (Figure 39A).

As well illustrated in the acquired CLSM micrographs (Figure 41) and SLS analysis data (Figure 42), the NaCN-based gastric phases comprised large ($D_{[4,3]}$ = 91 μm) acid-induced protein aggregates. Although caseins may also undergo pepsin-induced clotting, in the case of NaCN, this is considered unlikely owing to its non-micellar structure conformation (Dupont & Tomé, 2020). The bimodal pattern of the particle size distribution curves of the NaCN-based gastric chymes is generally confirmatory of the data in the literature (Borreani et al., 2016; Hellebois, Gaiani, & Soukoulis, 2022b; Markussen et al., 2021). At the end of the gastric processing step, a reduction in the $D_{[4,3]}$ values (i.e. $D_{[4,3]}$ = from 91 to 71 μm) throughout digestion was observed as a result of the peptic cleavage and the *in vitro* simulating mechanical (antral) forces. The presence of increasing FG content was associated with a proportional reduction in the mean size of the NaCN aggregates, as demonstrated by the decay in the intensity of the above-micron particle population peak (Figure 43). Nonetheless, no significant differences in

the $D_{[4,3]}$ values were observed at the start and endpoint of the *in vitro* gastric processing (i.e. 15.7 and 17.3 µm, respectively). Interestingly, the decay in the $D_{[4,3]}$ values followed an exponential trend as follows:

Equation 26 $$D = D_0 + A \cdot e^{-kc \cdot cFG}$$

where D, $D_0$ denote the $D_{[4,3]}$ values (in µm) of the NaCN aggregates in the absence ($D_0$) and presence of FG (D), A is a constant, and $k_c$ is the NaCN aggregate size reduction rate ($\%^{-1}$) as a function of the FG content

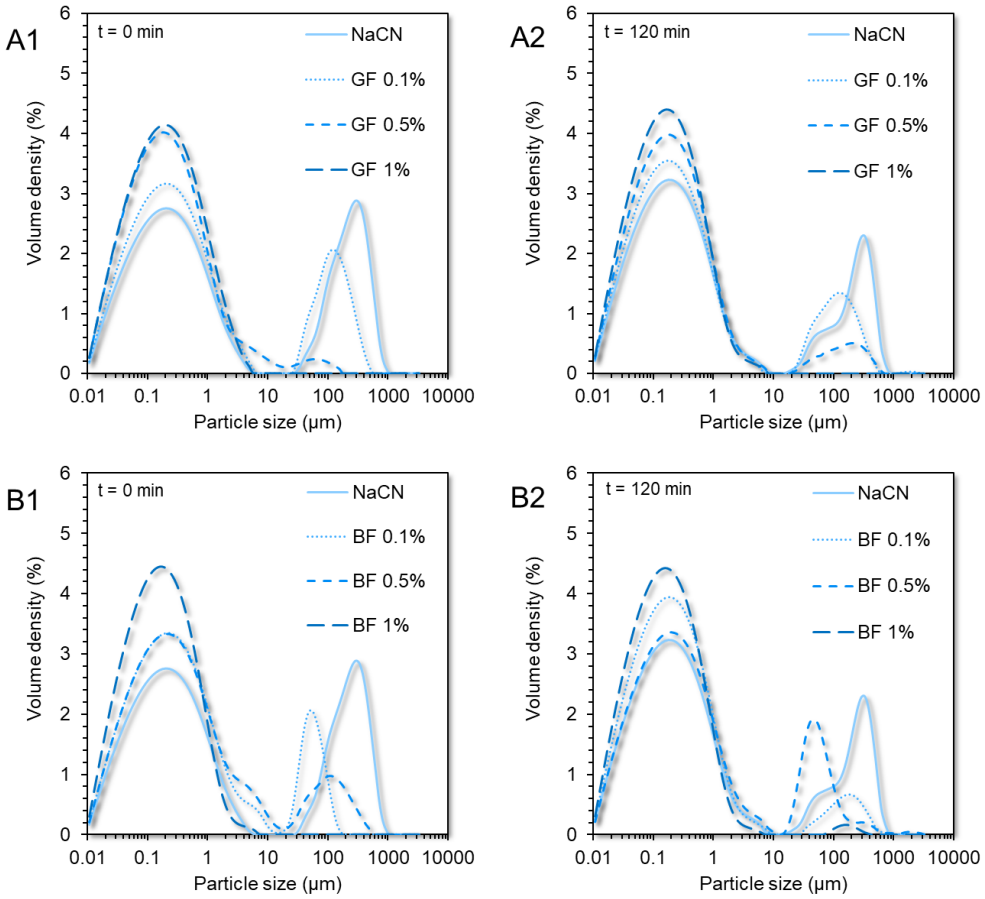


*Figure 43: Particle size distribution profiles of the initial and end NaCN-based gastric phases (1: t = 0 min and 2: t = 120 min) as influenced by the phenotype and concentration of flaxseed gum. (A) = golden flaxseed and (B) = brown flaxseed.*

According to our calculations, the $k_c$ values at t = 0 min were 11.02 ± 0.82 and 11.42 ± 0.99$\%^{-1}$ for GF and BF, respectively, which were significantly higher than the corresponding ones at t = 120 min (i.e. 4.54 ± 0.51 and 4.18 ± 0.73$\%^{-1}$ for GF and BF, respectively). This suggests that the FG impeded the acid-induced aggregation responsiveness of NaCN to the gastric fluids resulting in smaller and more uniform particle size distributions. Indeed, this was confirmed by employing the CLSM (Figure 41) and SLS measurements (Figure 43). Although the mechanism was not evidenced, it can be assumed that the colloidal changes observed were governed by the ability of FG

to adsorb onto the NaCN particles via electrostatic complexation upon acidification, and its direct effect on the continuous aqueous phase macroviscosity of the gastric chymes, which diminished the diffusion rate of pepsin into the solid (protein aggregates)–water interface (Borreani et al., 2016; Hellebois, Gaiani, & Soukoulis, 2022b; Markussen et al., 2021).

In opposition to the beforementioned findings, the initial WPI-based gastric phases exhibited a relatively uniform microstructure ($D_{[4,3]}$ = 0.69 µm), in agreement with our previous observations (Hellebois, Gaiani, & Soukoulis, 2022b). In the absence of FG, a bimodal particle size distribution pattern was confirmed in the WPI exemplars. A significant increase in WPI acid-formed aggregates ($D_{[4,3]}$ = 4.9 µm) was detected at the end of the gastric processing step. Markussen et al., (2021) have reported a similar behaviour in semi-dynamically digested milk protein concentrate (MPC)-based food models. Upon mixing with the gastric fluids, all gastric phases containing FG were characterised by highly polydisperse colloidal suspensions (Figure 44). Despite the positive correlation between the $D_{[4,3]}$ values and the $c_{FG}$, the mean size of the particles was substantially changed only at $c_{FG}$ = 1% wt. (Figure 42). GF addition resulted in the formation of the largest protein aggregates, which may be associated with its higher negative surface charge density in highly acidic conditions (i.e. pH = 2–4) than BF (Hellebois, Fortuin, Xu, Shaplov, et al., 2021), favouring its electrostatic bridging with whey proteins. Throughout gastric processing, a re-organisation of the morphological features of the WPI-FG gastric phases was observed, as illustrated in the CLSM micrographs (Figure 40). As seen in Figure 44, the submicron fraction of the particles (representing the WPI nanoaggregates colloidal dispersion), was decreased at the expense of the fraction larger than a micron, i.e. 1–50 µm, when $c_{FG}$ > 0.5% wt. This implies that the formation of WPI–FG coacervates took place throughout gastric processing leading to the progressive depletion of the colloidal WPI. soluble aggregates and, eventually, to the increase of the sedimentable biopolymer matter. Indeed, the centrifugation of the gastric endpoint phases resulted in a significant decrease in their apparent viscosities (Figure 39). Omitting the discrepancies due to ionic strength, the macroviscosity of the centrifuged gastric phases (i.e. 1.6–2.6 mPa.s) was significantly lower than that of the dilute flaxseed gum solutions (i.e. 9.5–17.6 mPa.s Hellebois, Fortuin, et al., 2021). Hence, the colloidal changes in the WPI-FG gastric phases are driven primarily by an electrostatic complexation mechanism.

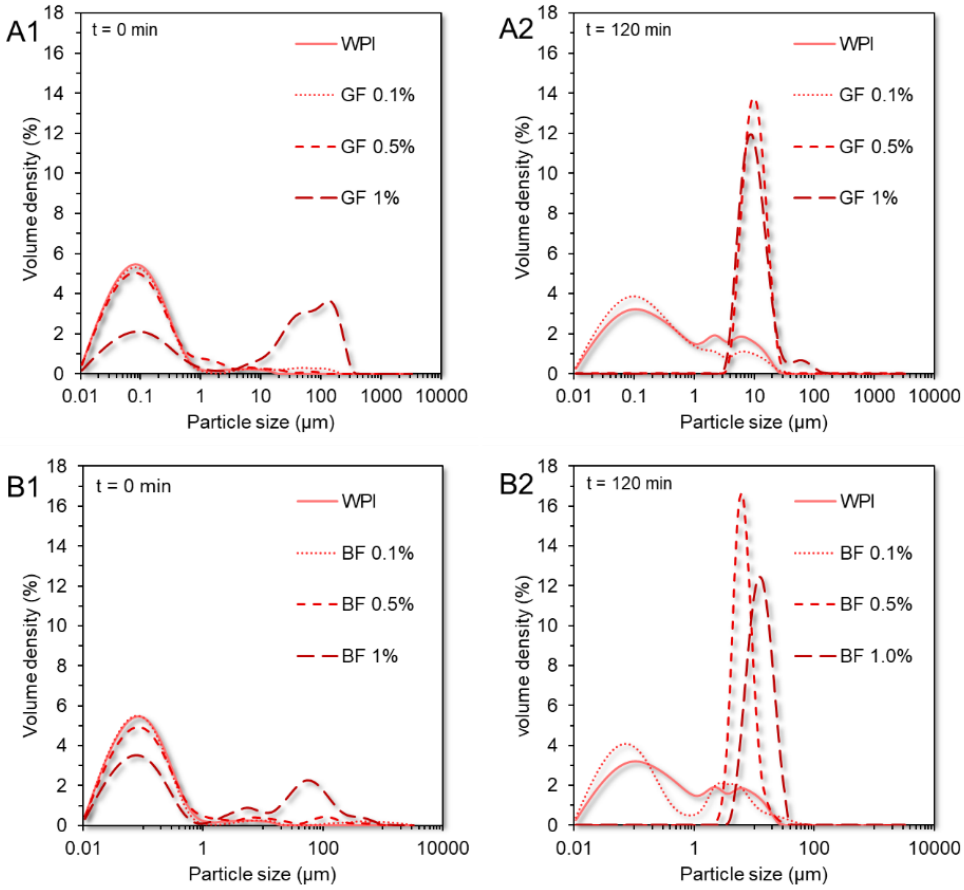


*Figure 44: Particle size distribution profiles of the initial and end WPI-based gastric phases (1: t = 0 min and 2: t = 120 min) as influenced by the phenotype and concentration of flaxseed gum. (A) = Golden flaxseed and (B) = Brown flaxseed*

## *In vitro* digestibility of the milk proteins

The peptic cleavage of milk proteins and the degree of proteolysis were measured employing SDS-PAGE (Figure 45 and Figure 46) and OPA (Figure 47) assay, respectively. To gain insight into the kinetics of the peptic cleavage of the milk proteins, the SDS-PAGE images obtained (Figure 45) were analysed densitometrically using ImageJ software (Figure 46), as previously reported by Hellebois, Gaiani, & Soukoulis, (2022b). Different aliquots of the oral, gastric, and intestinal phases (i.e. 5, 10, and 20 µg of proteinaceous matter per well) were used to improve the detection of the intact and fragmented proteins. Three significant bands identified at 25–35, 18.2, and 14.2 kDa allotted to total caseins ($a_s$–, β–, and κ–casein), β-lactoglobulin (β-Lg), and α-lactalbumin (α-La) were semi-quantified and the densitometric data were fitted to an exponential decay model (Hellebois, Gaiani, & Soukoulis, 2022b; Le Feunteun et al., 2021; Verkempinck et al., 2022), as follows:

Equation 27 $$c = c_{120} + (c_0 - c_{120})e^{-kt}$$

where $c_0$ and $c_{120}$ denote the normalised percentage of the residual intact protein at the beginning or end of the gastric or intestinal processing step, t is the gastric or intestinal processing time (in h), and k ($h^{-1}$) is the peptic cleavage rate of proteins to polypeptides. The time τ (in h) required to cleave the 50% of the initial proteins was calculated according to the half-time (for first-order kinetics) equation:

Equation 28 $$\tau = \frac{\ln 2}{k}$$

In the absence of FG (Figure 45), β-lactoglobulin underwent a faster peptic cleavage during the gastric processing step than α-lactalbumin and total caseins (k = 14.9 ± 0.9, 2.7 ± 0.7 and 1.9 ± 0.8 $min^{-1}$, respectively). Besides the structure conformational aspects of the proteins (Huppertz & Chia, 2021), several processing parameters associated with the implementation and severity of heat treatment, pressure processing, enzymatic pre-treatment, etc., may affect the sensitivity of milk proteins to peptic cleavage (Barbé et al., 2013; Böttger et al., 2019; Halabi et al., 2020; Macierzanka et al., 2012). According to Figure 46A–C, the presence of FG was associated with a higher amount of intact β-lactoglobulin (42–57%) and total caseins (22–27%) and a lower amount of intact α-lactalbumin (16–28%), at the end of the gastric processing step.

It is presumed that the differences in the pepsin-induced cleavage of whey proteins may stem from the differences in their secondary structure conformation and surface charge density. β-Lactoglobulin, due to its higher isoelectric point ($pI_{β\text{-}Lg}$~5.2, $pI_{α\text{-}La}$~4.6), can undergo electrostatic complexation with FG earlier than α-lactalbumin, leading to the steric hampering of the peptic cleavage in the former case. From a kinetic perspective, α-lactalbumin and total caseins underwent pepsin-induced peptic cleavage at a slower pace (τ = 15.2 and 21.4 min, respectively) than β-lactoglobulin (τ = 2.8 min, Figure 46D). In the presence of FG, the time required for cleaving the 50% of the initial intact proteins was shortened (τ = 2.1, 6.1, and 5.7 min for β-lactoglobulin, α-lactalbumin, and total caseins, respectively), although its phenotype did not play any significant role (Figure 46D). The ability of the polysaccharides to modify the kinetics of the pepsin cleavage has been reported in previous studies (Borreani et al., 2016; David et al., 2020; Hellebois, Gaiani, & Soukoulis, 2022b; Koutina et al., 2018; Markussen et al., 2021). For anionic polysaccharides, the major mechanistic pathway associated with the reduced digestibility of milk proteins concerns their direct molecular interactions that sterically impede the access of proteases to the cleaving sites of the protein substrate (Borreani et al., 2016; Markussen et al., 2021). In addition, some anionic polysaccharides i.e. sodium alginate, can selectively inhibit the enzymatic activity of proteases (i.e. pepsin) (Chater et al.,

2015). Although these results could lead us to speculate to some extent on the pepsin-inhibiting capacity of FG, further experiments are required in order to confirm this hypothesis.

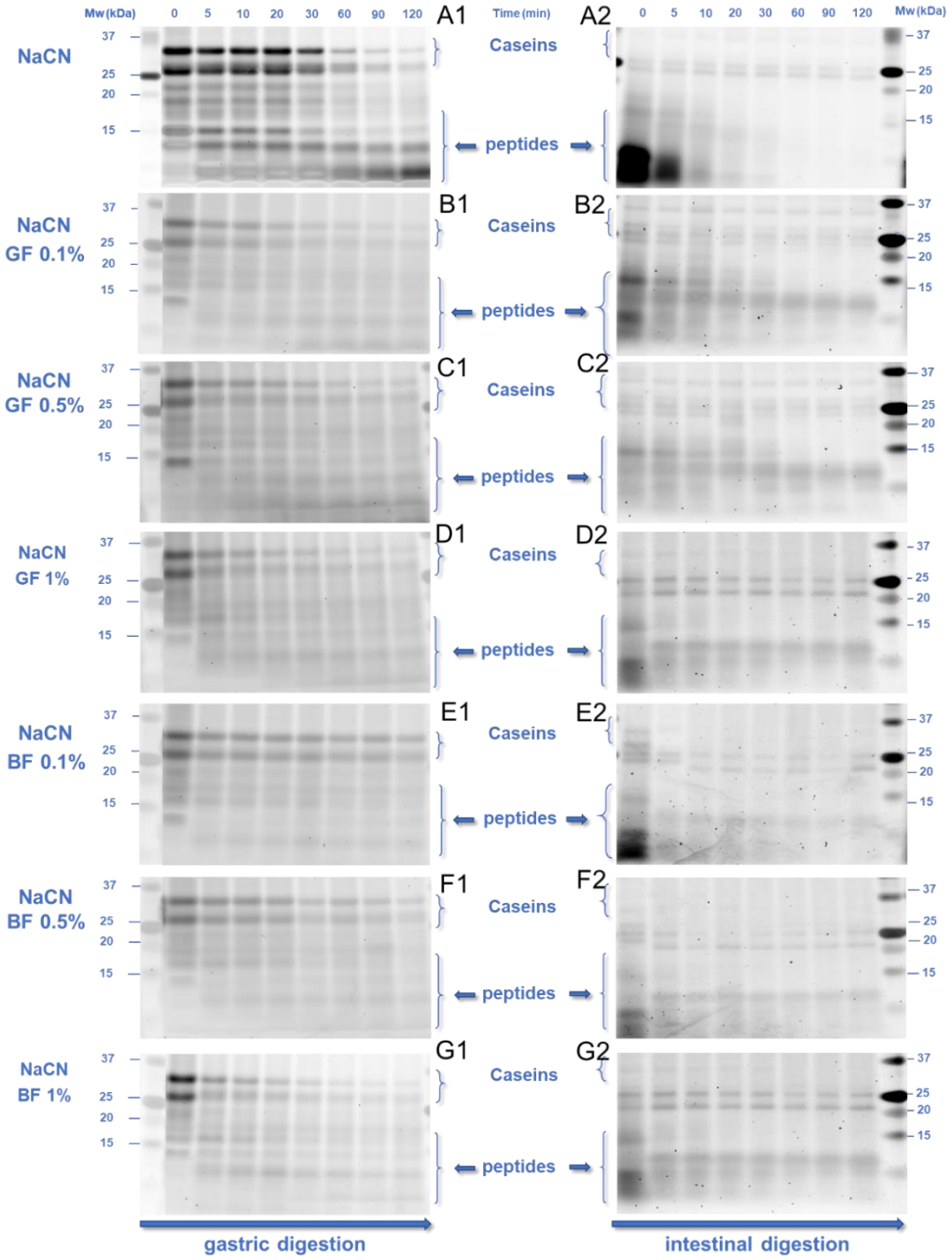


*Figure 45: SDS-PAGE electropherogram of the gastric (left panel, 1) and intestinal (right panel, 2) phases of the NaCN-(A–G) and WPI-(H–N) based food models as influenced by the phenotype and concentration (0.1–1% wt.) of flaxseed gum. An SDS-PAGE analysis was conducted on gastric and intestine aliquots sampled at predetermined time points (0, 5, 10, 20, 30, 60, 90, and 120 min). Abbreviations used: β-Lg: β-lactoglobulin, α-La: α-lactalbumin.*

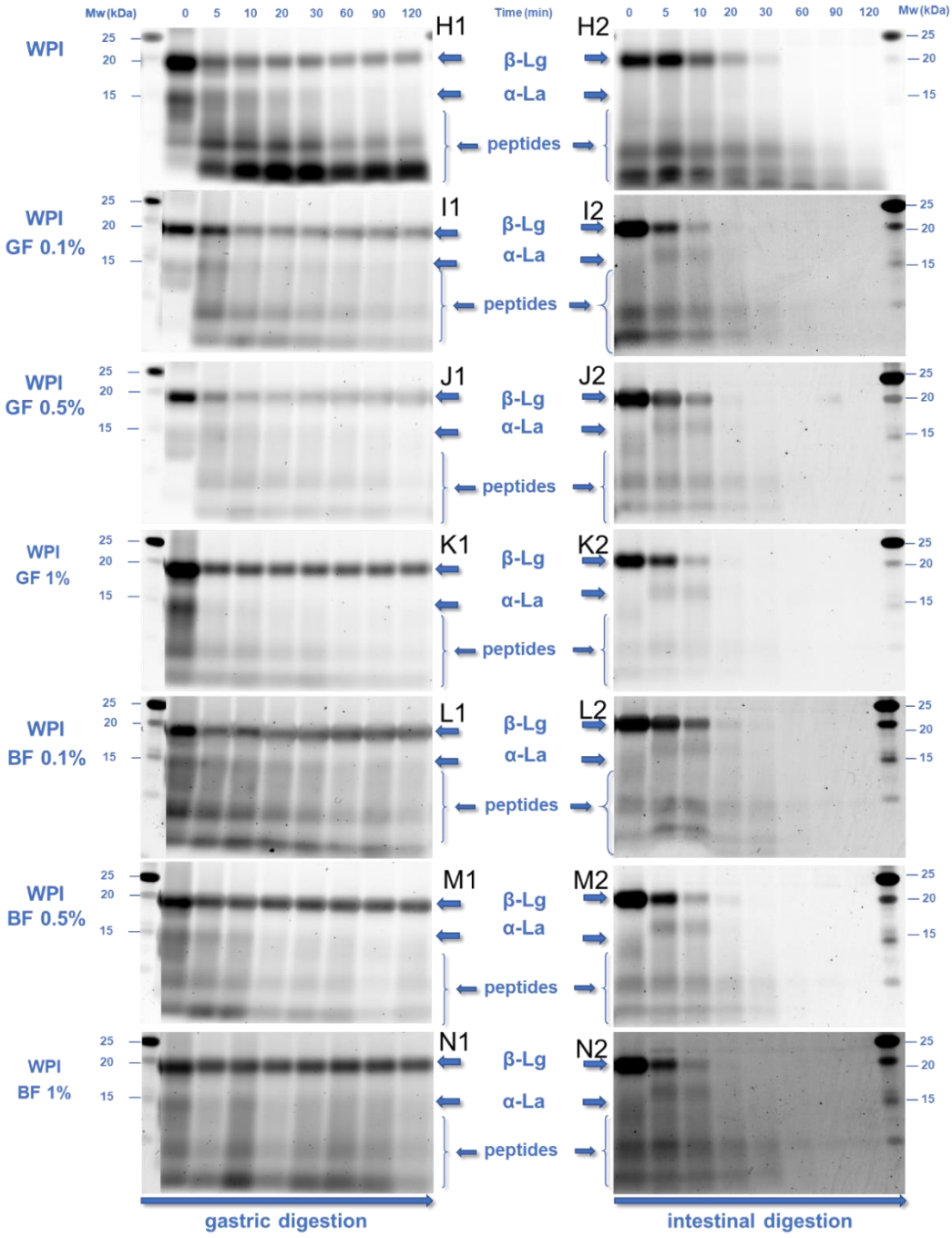


*Figure 45: (continued)*

By monitoring the temporal changes in the intact protein residue in the intestinal phases, an almost complete cleavage of the milk proteins was detected as less than 2–3%, and 10% of intact whey proteins and total caseins remained at the end of the intestinal processing. Based on the calculated kinetic parameters (Figure 46E), no significant differences in the time required for cleaving the 50% of the intragastric residual intact protein matter were found i.e. $\tau$ = 10.3, 9.3, and 13.7 min for β-lactoglobulin, α-lactalbumin and total caseins, respectively. The presence of FG did not modify significantly the peptic cleaving rate of α-lactalbumin (i.e. $\tau$ = 11.3 min). On the other

hand, the pancreas mediated cleaving rates of β-lactoglobulin and total caseins were increased (i.e. $\tau$ = 4.7 and 7 min, respectively); however the differences observed were nonsignificant.

In order to better understand the impact of the FG phenotype and content on the extent of proteolysis throughout the *in vitro* simulated gastric and intestinal processing steps, the data obtained from the OPA assay were fitted to the following mathematical model, as previously reported by Le Feunteun and *co*-workers (Le Feunteun et al., 2021):

Gastric phases:

Equation 29 $$DH_{gastric} = DH_{gastric,\infty} \exp(1 - k_{gastric} t)$$

where the $DH_{gastric,\infty}$ denotes the degree of hydrolysis (%) at the end of the gastric processing and $k_{gastric}$ is the rate of hydrolysis (in $h^{-1}$), and t the digestion time.

Intestinal phases:

Equation 30 $$DH_{int} = DH_{int,120} + \left(DH_{int,0} - DH_{int,120}\right) e^{-k_{int} t}$$

where the $DH_{int,}$ and $DH_{int,120}$ denote the degree of hydrolysis (%) achieved at the beginning and end of the intestine processing step, $k_{int}$ is the rate of hydrolysis (in $h^{-1}$), and t the digestion time.

As displayed in Figure 47A,B, the extent of hydrolysis (% DH) achieved at the end of the gastric processing step was at most 9–11%, regardless of the milk protein type and FG presence. It should be noted that in all gastric chymes, the calculated hydrolysis rates were highly dependent on the changes in the amount of the free amino groups during the very early stages of the gastric processing i.e. within the first 30 min. Similar behaviour in the digestion of food biomacromolecules as influenced by the food matrix characteristics has been reported (Pälchen et al., 2022). In line with previous studies (Halabi et al., 2020; Hellebois, Gaiani, & Soukoulis, 2022b; Rinaldi et al., 2014), the rate of hydrolysis in the WPI only gastric phases was substantially higher than their NaCN only counterparts (Figure 47C,D). This is generally associated with the restricted colloidal responsiveness of WPI to pH and ionic strength changes that sterically favour the peptic cleaving activity of pepsin.

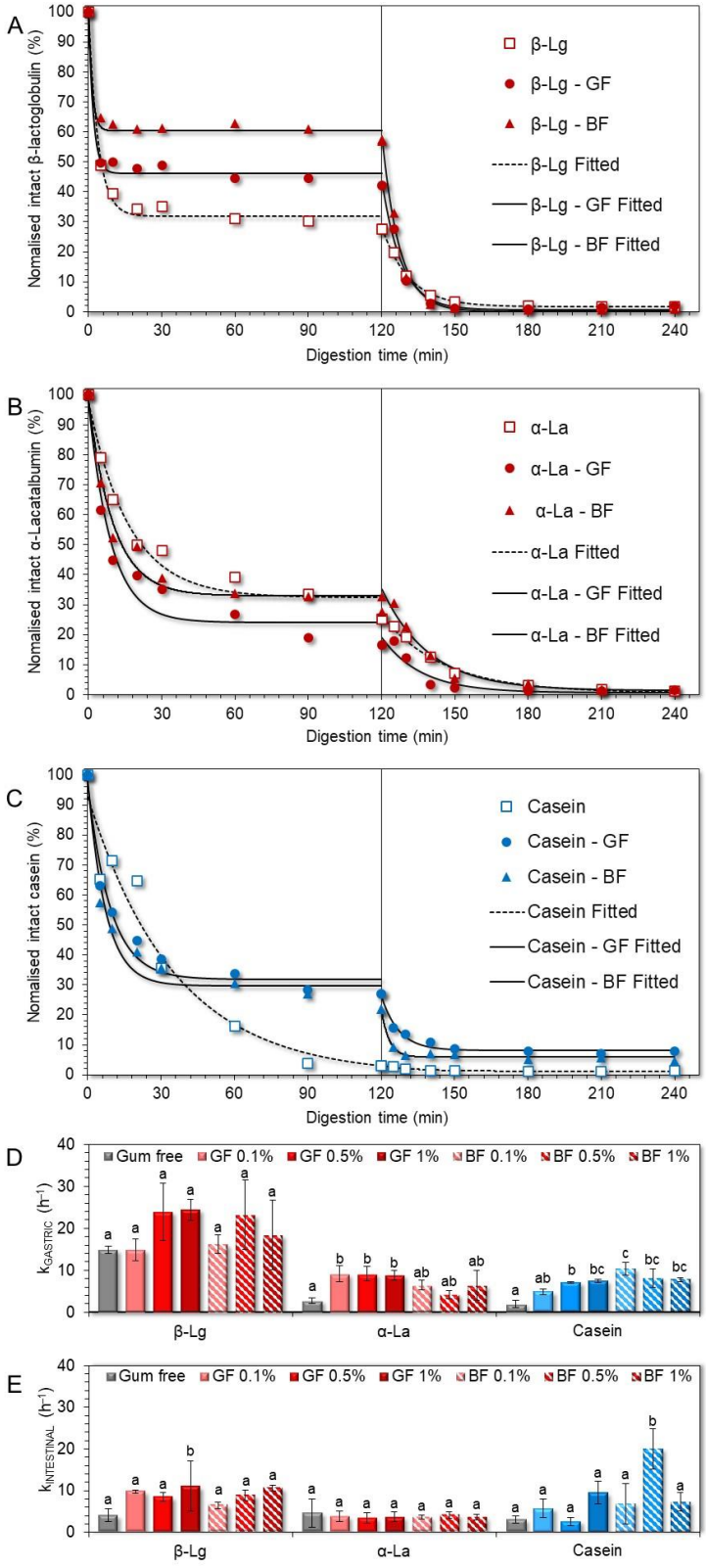


*Figure 46: SDS-PAGE densitometric analysis illustrating the kinetics of β-lactoglobulin (A), α-lactalbumin (B), and total caseins (C) fate in the gastric (t = 0 –120 min) and intestinal (t = 120 –240 min) phases as influenced by the phenotype and concentration of flaxseed gum. The calculated rates for β-Lg, α-La and casein are depicted in (D) (gastric rates) and (E) (intestinal rates).* $^{a-c}$*Different letters for the same protein type denote a significant difference among the samples. Abbreviations used: β-Lg: β-lactoglobulin, α-La: α-lactalbumin.*

Incorporating FG into the initial food models induced a significant increase in the hydrolysis rates achieved during the gastric processing step, i.e. $k_{gastric}$ = 10.5 ± 1.1 and 21.1 ± 3.5 $h^{-1}$ (for WPI-based chymes in the absence and presence of FG, respectively) and 1.5 ± 1.1 and 19.4 ± 6.4 $h^{-1}$ for their NaCN counterparts. This can be ascribed to the ability of FG to control the acid-induced aggregation of the milk proteins and, therefore, the accessibility of pepsin to the protein substrate. The pepsinolysis-modulating role of FG was mainly flaxseed phenotype-driven (Figure 47C,D). In this context, the GF-stabilised food models underwent faster pepsinolysis ($k_{gastric}$ = 22 ± 1.9 and 23.9 ± 5.7 $h^{-1}$ for the WPI and NaCN-based food models, respectively) than their BF exemplars ($k_{gastric}$ = 20.3 ± 3.9 and 15 ± 1.0 $h^{-1}$ for the WPI- and NaCN-based food models, respectively). However, only in the case of NaCN the differences in the rates of hydrolysis were significant ($p < 0.05$). Noteworthily, the $k_{gastric}$ rates obtained hereby were significantly higher than those observed in the case of non-ionic polysaccharides (i.e. alfalfa galactomannan) (Hellebois, Gaiani, & Soukoulis, 2022b). Hence, it appears that the ability of FG to restrict the ripening of the acid-mediated protein aggregates via the formation of electrostatic complexes of controlled mean size is significantly more influential than its direct contribution to the solid–liquid interface mass transfer phenomena. In keeping with the latter, the modulating role of FG concentration in the induced pepsinolysis was unclear as it was only in the case of the GF-stabilised NaCN food models that there was a proportional increase to the gum content increase in hydrolysis rates.

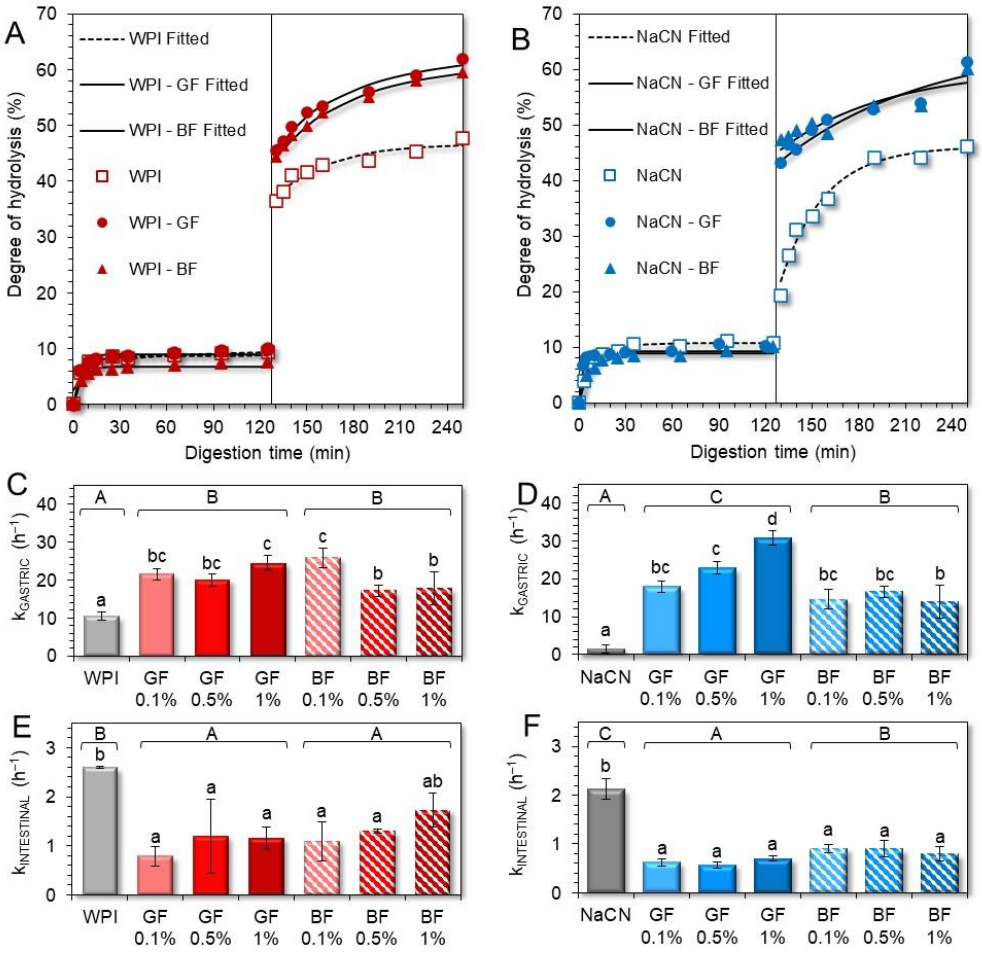


*Figure 47: Degree of protein hydrolysis in the WPI-(A) and NaCN-(B) based gastric and intestinal phases as influenced by the phenotype and concentration (0.1–1% wt.) of flaxseed gum. The protein hydrolysis rates of WPI and NaCN during gastric ($k_{GASTRIC}$) and intestinal ($k_{INTESTINAL}$) steps are displayed in (C–F).* $^{a-d, A-C}$*Different letters between the samples denote a significant difference.*

On the completion of the intestinal digestion, a substantial increase in the DH of the proteins was observed i.e. ca. 47% for individual milk proteins and 59–62% when FG was incorporated in the milk protein-based food models (Figure 47A,B). Nonetheless, the pancreas-mediated hydrolysis rates were significantly ($p < 0.05$) lower in the intestinal digesta containing FG (Figure 47E,F). Although the hydrolysis rates were higher in the intestinal phases containing BF ($k_{intestinal}$ = 1.37 and 0.86 $h^{-1}$ for the WPI- and NaCN-based food models, respectively) than their GF counterparts ($k_{intestinal}$ = 1.05 and 0.63 $h^{-1}$ for the WPI- and NaCN-based food models, respectively), the differences were nonsignificant. Our findings postulate that the equilibrium between the coacervates and precipitates, free proteins, and polyanions had a substantial impact on the extent of pancreas-induced hydrolysis (Chai et al., 2014; Comert et al., 2016). Upon admixing of the gastric chymes with the simulating intestinal fluids, the concomitant increase in the pH (from 2.5 to 7.0), ionic strength, and cationic species ($Na^+$, $K^+$, and $Mg^{2+}$) resulted in

the progressive dissolution of the milk protein-FG electrostatic complexes and the release of free proteins that can be cleaved more easily from the pancreas. At this stage, the solubilisation kinetics of the coacervates, together with the impact of the thickening capacity of the FG on the interphase mass transfer kinetics, became more influential on the rate of the polypeptide peptic cleavage.

# CONCLUSIONS

In the present work, the ability of FG to modulate the colloidal transformation of milk proteins and, consequently, their cleavage throughout *in vitro* digestion was elucidated. Regardless of its phenotype, FG was associated with segregative phase separation in both tested milk protein-based food models. Upon oral processing, only the WPI-based food boluses were colloidally responsive to FG due to the formation of soluble protein-gum complexes. Under intragastric simulating conditions, both milk proteins underwent acid-induced aggregation with the colloidal changes (mean particle size and morphological aspects) in the NaCN-based systems being critically influenced by the presence of FG; however, the FG phenotype played a minor role. On the completion of the gastric processing, the presence of FG was associated with a higher amount of residual intact total caseins and β-lactoglobulin but it did not significantly impact the intact α-lactalbumin residue. No remarkable differences in the amount of the residual intact proteins at the end of the intestinal digestion were observed. Although the FG did not remarkably influence the degree of hydrolysis during the gastric processing step, FG resulted in a significant increase in the degree of hydrolysis in the intestinal digesta obtained. From a mechanistic point of view, the equilibrium between the FG-milk protein coacervates and free polyelectrolytes, as influenced by the physicochemical changes occurring during the gastrointestinal transit, is the principal modulator of the *in vitro* digestibility of the milk proteins. To a lesser extent, the ability of FG to increase the microviscosity in the solid–liquid interphase can also affect the sensitivity of milk proteins to peptic cleavage, particularly in pH conditions where the formation of insoluble protein–polysaccharide complexes is not favoured.

# CHAPTER III: MILK PROTEIN-BASED CRYOGELS AS AN ALTERNATIVE PROBIOTIC DELIVERY SYSTEM

## PREAMBLE

This concluding chapter focuses on developing and characterising an innovative encapsulation technique designed for probiotic delivery in the form of self-standing cryogel monoliths. These cryogels, incorporating *Lacticaseibacillus rhamnosus* GG as a probiotic model, were created by producing hydrogel precursors via the gelation of milk proteins induced by lactic acid, followed by subsequent freeze-drying. For the constitution of the cryogel scaffold, sodium caseinate, whey protein, and a combination of both at 10% wt. were used. Glycerol, trehalose, and glucose were incorporated into the composition as cryoprotective agents, with the latter being also a carbon source for the fermentation process. Furthermore, the influence of alfalfa and flaxseed gum, in varying concentrations ranging from 0.1 to 0.5% wt., was carefully examined. Firstly, the analysis focused on the effect of proteins and gums on the microstructural attributes, physico-chemical, thermal, and mechanical properties of the formed cryogels. Following this, the cryogels' capacity to mitigate the sublethal effects on the probiotics during crucial stages, namely the production process (consisting of fermentation and freeze-drying), controlled-atmosphere storage, and *in vitro* digestion. Lastly, the bioadhesion of probiotics released during the intestinal phase to a *co*-cultured epithelium model, using Caco-2 and HT-29 cells, was evaluated to assess their potential efficacy within the body. The developed cryogel in this chapter demonstrates their versatility, serving not just as carriers for bioactive molecules, but also as a medium for living probiotic cells, suggesting broad potential applications.

# MILK PROTEIN-BASED CRYOGEL MONOLITHS AS NOVEL ENCAPSULANTS OF PROBIOTIC BACTERIA. PART I: MICROSTRUCTURAL, PHYSICOCHEMICAL, AND MECHANICAL CHARACTERISATION

Thierry HELLEBOIS[1,2], Romain CANUEL[1,3], Frédéric ADDIEGO[4], Jean-Nicolas AUDINOT[4], Claire GAIANI[2], Alexander S. SHAPLOV[4] and Christos SOUKOULIS[1]

[1]Environmental Research and Innovation (ERIN) Department, Luxembourg Institute of Science and Technology (LIST), Esch-sur-Alzette, Luxembourg
[2]Université de Lorraine, LIBio, Nancy, France
[3]École Nationale Supérieure de Chimie, de Biologie et de Physique (ENSCBP), Bordeaux INP, Pessac, France
[4]Materials Research and Technology (MRT) Department, Luxembourg Institute of Science and Technology (LIST), Esch-sur-Alzette, Luxembourg

Food Hydrocolloids
Volume 140, July 2023, 108641
doi.org/10.1016/j.foodhyd.2023.108641

# ABSTRACT

The implementation of cryogels as alternative xero-carriers for embedding labile bioactive compounds including probiotic living cells is becoming more popular. In the present work, milk protein-based cryogels were developed by freeze-drying of indirectly acidified protein gels (10% wt. in sodium caseinate or whey protein isolate blended at varying mass ratios i.e. 1:0, 3:1, 1:1, 1:3 and 0:1) comprising *Lacticaseibacillus rhamnosus* GG (LGG) living cells, trehalose (5% wt.), glucose (1% wt.) and glycerol (2.5% wt.). The physicochemical, microstructural, and mechanical characteristics of the cryogels conveying LGG were measured. The acid gel contraction during the fermentation notably influenced the macroscopic (volume contraction) and microscopic aspects (porosity, thickness, and uniformity of the wall material construct) of the cryogels. The amount of monolayer water content (11.5−14.0 g.100 $g^{-1}$), and total surface area (403−488 $m^2.g^{-1}$) as well as the glass transition temperature (Tg = 33−46 °C), of the cryogels increased proportionally to the whey protein content. X-ray microtomography analysis revealed that the mixed protein cryogels were characterised by lower porosities than their individual protein exemplars. However, the uniformity and the structure conformation of the protein network constructs were altered according to the milk protein composition of the cryogels. All the cryogels exhibited a brittle and plastic behaviour when subjected to indentation forces, with the hardest and stiffest cryogels exerting the lowest water reconstituting capacity. The microstructural assessment of the wall material at nanoscale level evidenced a satisfactory intrenching of the LGG cells, which substantiates the feasibility of the cryogels as novel probiotic xero-scaffolds.

# INTRODUCTION

Probiotics are defined as human gut relevant commensals and microbes that have generic or core effects on gut physiology and homeostasis or that support the health of the reproductive tract, oral cavity, lungs, skin and gut-brain axis (Hill et al., 2014). Probiotics encapsulation i.e. the physical engrafting of living cells in a structurally and/or interfacially engineered colloidal micro- or nano-template, is a very efficient technological approach to minimise the loss of the inherent biological activity of probiotics (Gu et al., 2022; Kiepś & Dembczyński, 2022; Yao et al., 2020). To date, anhydrobiotic technology i.e. xero-carriers conveying living cells usually produced via lyophilisation or spray drying, is considered the commonest strategy for probiotic encapsulation (Aschenbrenner, Först, et al., 2015; Burgain et al., 2015). Despite high operational costs and challenging upscalability, the encapsulation of probiotics in freeze-dried scaffolds allows the maximal preservation of the cells, as well as high technological versatility (Koh et al., 2022). A consolidated encapsulation system should provide satisfactory protection against several physicochemical and biological stressors encountered during processing, storage and gastrointestinal transit, such as heat, pH, water vapour, oxygen, osmotic stress, mechanical injuries, bile salts and digestive enzymes (Capozzi et al., 2016; Gu et al., 2022; Yao et al., 2020).

Cryostructuration is an alternative biosynthetic approach for the construction of xero-scaffolds, which is based on: a) the cryogenic processing of a polymeric solution or colloidal dispersion, and b) the removal of the ice via sublimation (Lozinsky, 2018). Macromolecules such as polysaccharides and proteins have been used successfully in the fabrication of cryogels (Bektas et al., 2021; Betz et al., 2012; Groult et al., 2021; Manzocco et al., 2022; Zou & Budtova, 2021, 2021). Food biopolymer-based cryogels are recognised for their tailorable microstructural features, satisfactory mechanical durability and resilience, high biocompatibility and biodegradability, among others (Manzocco et al., 2021). Adhering to the same principles as cryostructuration, the microstructural, physicochemical, and mechanical aspects of cryogels are influenced by several parameters including the type and the concentration of biopolymeric precursors, the colloidal state of the precursor medium, and the cryogenic processing conditions (Lozinsky, 2020).

Like their mesoporous or microporous counterparts (known as aerogels), the assiduous design of the cryogenic processing is inextricably associated with the behaviour of the biopolymer precursor medium under sub-eutectic point conditions and therefore, it

influences the final physicochemical and microstructural aspects (Gun'ko et al., 2013; Shiekh et al., 2021). In addition, the proper design of the cryogel precursor medium (e.g. concentration, pH, type of polymer, degree of cross-linkage etc.) is essential for preventing the risk of structural collapse (e.g. shrinkage, cracking, fissuring etc.) during the freeze-drying process (Betz et al., 2012; Chen et al., 2013; Kleemann et al., 2018). Hitherto, several food biopolymers such as polysaccharides (e.g. starch, galactomannans, alginates, carrageenans, pectins, glucans etc.) and proteins (e.g. whey proteins, caseins, albumin, gelatine etc.) have been deployed individually or as *co*-polymers in the development of cryogels (Fontes-Candia et al., 2022; Kleemann et al., 2018, 2020; Manzocco et al., 2021; Volkova & Berillo, 2021). In contrast with polysaccharides, the development of protein-based cryogels requires their pre-gelation induced via heating, acidification, enzymatic (e.g. rennet, transglutaminase etc.) or cryogenic (freeze-thaw) processing at concentrations close or well above their critical gelation points, which allows the formation of self-standing hydrogels. (Heidebach et al., 2009b; Hellebois, Gaiani, Cambier, et al., 2022; Hellebois, Gaiani, & Soukoulis, 2022a; Kleemann et al., 2020; Schorsch, Carrie, et al., 2000; Selmer et al., 2019).

Recent studies have showcased the feasibility of protein-based cryogels to be deployed as templates for the encapsulation of labile bioactive compounds (Ahmadi et al., 2016; Fontes-Candia et al., 2022; Kleemann et al., 2020; Manzocco et al., 2021). Stemming from their high interfacial activity, protein-based cryogels and aerogels permit satisfactory drug loading yields and encapsulation efficiency (Ahmadi et al., 2016; Kleemann et al., 2020; Manzocco et al., 2022). Protein cryogels are also appealing due to their programmable swelling and release behaviour under simulated *in vitro* gastrointestinal conditions (Fontes-Candia et al., 2022; Kleemann et al., 2020). Swelling trials have evidenced the constrained ability of protein aerogels to undergo disintegration in gastrointestinal fluid media, whilst their resistance to peptic cleavage is strictly dependent on the chemical structure and conformation of the protein (Fontes-Candia et al., 2022; Kleemann et al., 2020). Despite their promising techno-functional properties, there are currently no studies showcasing the suitability of cryogels in the domain of anhydrobiotics.

The aim of the present work was to study the feasibility of milk protein (whey protein and sodium caseinate)-based cryogels as alternative biopolymer scaffolds for embedding living probiotic bacteria (i.e. *Lacticaseibacillus rhamnosus* GG, LGG) cells. Part I investigates the impact of the NaCN to WPI ratios on the macroscopical appearance, microstructural conformation, chemical structure, thermo-physical, and mechanical

properties of probiotic cryogel monoliths. Part II aims to explore the ability of the cryogels to preserve the biological activity of LGG throughout freeze-drying, storage and simulated *in vitro* digestion. In addition, the interplay between the *in vitro* digestion performance (colloidal changes, proteomic profile, and bacteria cell sub-lethality) and storage stability of the probiotic cryogels and their structural and physicochemical characteristics will be elucidated.

# MATERIALS & METHODS

## Materials

Whey protein isolate powder (PRODIET 90S) with a protein content of 85.8% wt. was kindly donated by Ingredia (Arras, France). Sodium caseinate (containing 89.4% wt. of protein), glucose (99.5% wt.) and glycerol (99.9% wt.) were purchased from Sigma-Aldrich (Leuven, Belgium). Trehalose dihydrate (99.4% wt.) was purchased from Louis-François (Croissy-Beaubourg, France). The probiotic strain LGG (ATCC 53103) used was purchased from the VTT Technical Research Centre of Finland Ltd (Espoo, Finland). All other chemicals were analytical grades.

## Preparation of the hydrogels and cryogels

The appropriate amount of whey protein isolate (WPI) or sodium caseinate (NaCN) was dispersed in Milli-Q to obtain a final protein dispersion of 10% wt. The protein dispersions were kept under magnetic stirring at ambient temperature overnight (IKA GmbH, Staufen, Germany) to allow sufficient hydration and were three-times homogenised at 500 bar (Panda plus 2000, Gea, Düsseldorf, Germany) to break down any protein agglomerates. Then, the milk protein solutions were centrifuged at 10,000*g* for 5 min to remove any insoluble residual. The absence of protein agglomerates was confirmed by static laser light scattering particle size analysis (Mastersizer 3000, Malvern Instruments, Worcestershire, United Kingdom). The amount of protein content was verified by the Dumas method using an organic elemental analyser (Vario Cube, Elementar GmbH, Langenselbold, Germany). Then, trehalose, glycerol, and glucose were added to the solution to obtain a final concentration of 5, 2.5 and 1% wt., respectively. The NaCN and WPI solutions were then mixed to obtain five different NaCN:WPI mass ratios ($m_{NaCN/WPI}$) as follows: 1:0, 3:1, 1:1, 1:3 and 0:1. The final protein solutions were heat-treated at 80 ± 1 °C for 20 min in a shaking water bath (SW22, Julabo, Seelbach,

Germany) before being rapidly cooled in an ice bath.

A pre-culture of LGG was prepared by growing aliquots from the cryovials (Microbank 2D, Novolab, Geraardsbergen, Belgium) overnight in a De Man, Rogosa and Sharpe (MRS) broth under anaerobic conditions at 37 ± 1 °C. The next day, the LGG culture was prepared by seeding 100 µL of the pre-culture in 50 mL of fresh MRS broth. At the end of the exponential phase (approximatively 14 h), the bacteria cell suspension was centrifuged (7,000*g*, 2 min) and washed twice with a phosphate-buffered saline (PBS) solution.

To induce the lactic-acid gelation of the milk protein solutions, 4 LGG cell pellets were dispersed within a protein solution of 100 mL. Then, aliquots (1 mL) of the inoculated solutions were rapidly transferred in 24-well plates (Corning, Corning, NY, United States) and incubated for 4 h at 37 ± 1 °C. On completion of the gelation, the samples were frozen at −80 °C for 2 h and underwent a two-stage freeze-drying (18 h at 0.120 mbar followed by 22 h at 0.010 mbar). The resulting cylindrical cryogels (diameter × height = 15 × 10 mm) were stored in hermetically sealed containers filled with $P_2O_5$ to prevent water absorption until further use.

## Monitoring of gelation and characterisation of the acid-induced gels

### i. Dynamic rheological measurements

Dynamic rheological measurements were performed in duplicate with an oscillatory rheometer (MCR 302, Anton Paar, Graz, Austria) using a double gap system (DG 26.7) of diameter 27.1 mm. Eight mL of the LGG-inoculated protein solution were transferred to the measuring cell and covered with a thin layer of silicone oil to prevent water evaporation. The temperature was then raised to 37 ± 0.05 °C to promote the fermentation and the gelation *in situ*. The viscoelastic properties of the systems were measured every 30 s for 4 h at constant shear strain (0.1%) and frequency (1 Hz). In addition, the pH of the systems was recorded using a multi-3430 pH-meter (WTW, Weilheim in Oberbayern, Germany).

### ii. Acid-induced gel stability

The gel colloidal instability due to the spontaneously occurring syneresis was assessed in four independent fermented gels using a LUMiSizer (LUM GmbH, Berlin, Germany). The protein solutions were fermented for 4 h at 37 ± 1 °C in 10 mm polycarbonate LUM cells. The resistance of the final hydrogels to forced serum exudation was assessed by monitoring the light transmittance (λ = 865 nm) over the tube height at 2,300*g* for 10 min

with a 5 s interval between measurements at 25 °C. Data analysis was performed using the SEPView software (LUM GmbH, Berlin, Germany).

iii. Confocal Laser Scanning Microscopy (CLSM)

The microstructural features of the fresh hydrogels (i.e. after 4 h of incubation at 37 °C) were visualised using a CLSM microscope (LSM 880 with Airy scan, Zeiss, Jena, Germany). Freshly inoculated protein solutions were transferred into 1 mL Eppendorf containing 10 µL of protein staining reagent (Fast Green, $\lambda_{Ex}$ = 633 nm, $\lambda_{Em}$ = 635–680 nm), 1.5 µL of stain for living (SYTO9, $\lambda_{Ex}$ = 488 nm, $\lambda_{Em}$ = 498–550 nm) and 1.5 µL of stain for dead (propidium iodide, $\lambda_{Ex}$ = 488 nm, $\lambda_{Em}$ = 585–640 nm) bacteria (LIVE/DEAD BacLight, Thermo Fisher Scientific, Waltham, MA, United States). The samples were homogenised using a benchtop vortex and 300 µL were transferred into eight-chambered microscope slides (Nunc Lab-Tek II, Thermo Fisher Scientific, Waltham, MA, United States). The microstructural assessment was performed using a × 40 objective.

## Characterisation of the cryogels

i. Thermophysical properties

The thermal behaviour of the freshly produced cryogels was assessed in duplicate by differential scanning calorimetry (DSC), thermogravimetric analysis (TGA), and thermo-mechanical analysis (TMA). The DSC analysis was performed on an SC3+ System (Mettler Toledo, Zurich, Switzerland) implementing a heating-cooling protocol as follows: 1) heating from −30 to 150 °C, 2) isothermal hold at 150 °C for 5 min, 3) cooling from 150 to −30 °C, and 4) heating from −30 to 150 °C. All the heating/cooling ramps were performed at a constant rate of 10 °C.min$^{-1}$. The midpoint glass transition ($T_g$) was calculated as the bisector of the angle between the tangents of the curve above and below the glass transition event.

The TGA was carried out in an air atmosphere using a TGA2 STARe System (Mettler Toledo, Zurich, Switzerland), applying a heating rate of 5 °C.min$^{-1}$ from 25 to 600 °C. The onset weight loss temperature ($T_{onset}$) was determined as the point in the TGA curve at which a significant deviation from the horizontal was observed. The midpoints of the mass loss rate changes were determined as the peaks of the first derivative curves (DTG). Finally, the samples underwent TMA under inert atmosphere (He) using a DIL 402 select Expedis dilatometer (NETZSCH, Selb, Germany) at a heating rate of 10 °C.min$^{-1}$ and a

constant load of 0.3 N in the temperature range from −80 to 150 °C. In addition, all the individual components of the cryogels were analysed using TMA and TGA.

ii. Mechanical properties of the cryogels

For the mechanical testing, the desiccated sample was placed sideways on a sand-blasted 25 mm plate geometry and the penetration depth and speed were set at 10 mm and 1 $mm.s^{-1}$, respectively. The normal force (N)-penetration depth curves of at least 12 individual samples were analysed using Origin 2019b software (OriginLab Inc, Northampton, MA, United States) and the following parameters were calculated: a) hardness (in N, normal force maximum) b) stiffness (in $N.mm^{-1}$, the slope of the curve) and the work required to break the cryogel (in mJ, area under the peak until break). An example of peak analysis is shown in Figure 48.

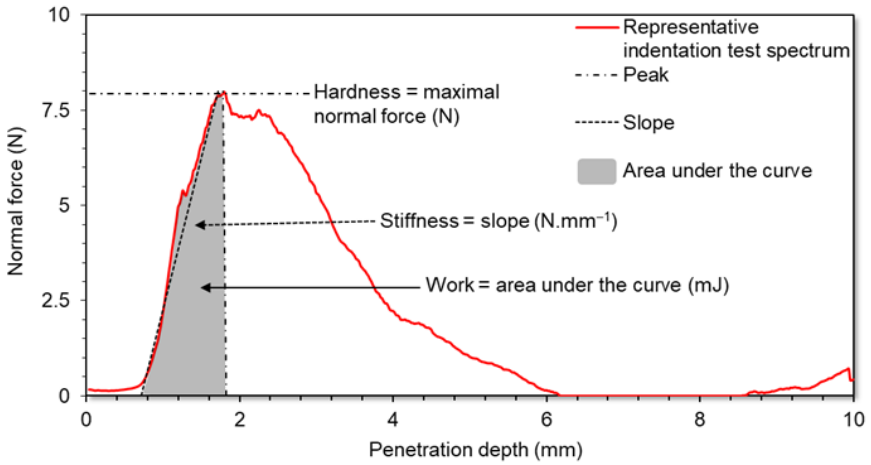


*Figure 48: Representative indentation test spectrum of the cryogels showing how the hardness, stiffness and work were calculated.*

iii. Protein secondary structure

Two different aliquots of the cryogels were ground with KBr (at a 1:100 wt ratio) and compression-moulded into a pellet. Fourier-Transform Infrared spectroscopy (FTIR) spectra were recorded in the range of 4000–500 $cm^{-1}$ using an Optics Vertex spectrometer (Bruker, Billerica, MA, United States) with the Attenuated Total Reflectance (ATR) mode and a resolution of 2 $cm^{-1}$. The ATR crystal is a diamond with an active sampling area of 0.8 mm in diameter and a reflection angle of 45°. Spectra were obtained from 50 scans. The baseline spectra were calculated without samples and subtracted from the obtained cryogel spectra. The deconvolution of the amide I region (i.e. 1700–1600 $cm^{-1}$), corresponding to C=O stretching, was conducted using Origin 2019b software (Jackson & Mantsch, 1995).

iv. Hygroscopicity

The water vapour sorption dynamics of the cryogels (water activity, $a_w$ 0–0.85) from two independent experiments were determined using a dynamic vapour sorption analyser (DVS, Surface Measurement Systems Ltd., London, United Kingdom). A sample of approx. 80 mg was placed into the sealed chamber and dried under a water-free atmosphere until the mass reached an equilibrium (20 ± 0.1 °C). The relative humidity of the chamber was increased stepwise i.e. $a_w$ = 0, 0.11, 0.23, 0.33, 0.44, 0.54, 0.64, 0.75, 0.80 and 0.85, and the respective water mass uptake at the equilibrium was recorded. The points obtained were fitted with the Guggenheim-Anderson-De Boer (GAB, Equation 31, $a_w$ = 0−0.85) (van den Berg & Bruin, 1981) models using the Origin 2019b software. To this end, the following equation was considered:

Equation 31 $$X = \frac{X_m C k a_w}{(1-k a_w)(1-k a_w + C k a_w)}$$

where X denotes the moisture at the equilibrium, $X_m$ the moisture content at the monolayer, C, is a constant that depicts the free enthalpy energy difference between the monolayer and pure liquid water molecules, k is the constant correcting the properties of the multilayer molecules, and $a_w$ the water activity. From Equation 31, the total surface of the monolayer $S_m$, can be obtained (Equation 32) as follows:

Equation 32 $$S_m = X_m \frac{1}{M_{H_2O}} N_A A_{H_2O} = 3.5 \times 10^3 X_m$$

where $X_m$ is analogous with the GAB equation, $M_{H_2O}$ is the molecular weight of water (18 g.mol$^{-1}$), $A_{H_2O}$ is the area of a single water molecule ($1.06 \times 10^{-19}$ m²), and $N_A$ is the Avogadro number ($6 \times 10^{23}$ molecules.mol$^{-1}$) (Mazza & LeMaguer, 1978).

v. Assessment of the morphological aspects

*a.* Degree of shrinkage

The ability of cryogels to retain the dimensional characteristics of the precursor hydrogel system was assessed volumetrically according to Equation 33:

Equation 33 $$\text{Shrinkage (\%)} = 100 \frac{V_p - V_c}{V_p}$$

where $V_p$ and $V_c$ denote the volume (in cm$^3$) of the initial precursor aliquot (prior to fermentation) and the freeze-dried cryogel obtained. The volume of pre-weighted cryogel monoliths was calculated using a silica beads (mean particle size 40–75 µm) displacement method. The bulk density (ρ, in g.cm$^{-3}$) was then calculated as $\rho = m_c/V_c$, where $m_c$ and $V_c$ are the masse and volume of the cryogels, respectively. The density was expressed as the mean value of eight cryogels.

*b.* X-ray microtomography

Micro-computed X-ray tomography (μCT) measurements were performed to visualise and quantify the 3D microstructure of the desiccated cryogels in duplicate. To this end, a laboratory X-ray cone-beam μCT system EasyTom 160 from RX Solutions (Chavanod, France) was used at 60 kV and 120 μA. 1440 projections over 360 ° (step of 0.25 °) were recorded at 0.5 frames $s^{-1}$ by a 16-bit flat panel imager with a total pixel area of 1920 pixels × 1536 pixels. The source-to-object distance (SOD) and the source-to-detector distance (SDD) were set to approx. 2.2 mm and 320 mm, respectively, enabling us to obtain a voxel size of approx. 0.9 μm. Xact software (RX Solutions, Chavanod, France) was used with the projections acquired to reconstruct the volume into stacked slices after applying a sample movement correction (spot deviation module), a system misalignment correction (geometry correction module) and a ring filter (5 pixels). The slices were subsequently analysed by means of the 3D image analysis software Avizo (Konrad-Zuse-Zentrum Berlin/FEI SAS-Thermo Fisher Scientific, Waltham, MA, United States). The following procedure was applied: median filter (3D mode, 6 neighbourhoods) to facilitate the segmentation, grey-level segmentation to isolate the pores and the matrix, quantification of the pore volume fraction and thickness map analysis of the matrix (vessel thickness distribution).

*c.* Scanning Electron Microscopy (SEM) and Helium Ion Microscopy (HIM)

The microstructural aspects of the macroporous protein network were assessed using a field emission scanning electron microscope (SEM, SU-70, Hitachi, Tokyo, Japan). The cryogels were fractured and fixed on aluminium stubs using a carbon tape, coated with 5 nm of platinum (ACE 600, Leica microsystems, Wetzlar, Germany) and analysed using an acceleration of 5 kV, a working distance of 15 mm and a magnification of × 350.

To gain insight into the encapsulation efficiency of the cryogels and the microstructural conformation of the vessels, a Zeiss Orion NanoFab Helium Ion Microscope (HIM, Zeiss Microscopy, Peabody, MA, United States) with the secondary electron detection mode using an Everhardt−Thornley detector was employed. To benefit from the high lateral resolution of the HIM, the primary source was a Helium beam generated in the Gas Field Ion Source, with an acceleration of 25 keV and a current of 0.3 pA. The images were acquired in 1024 pixels × 1024 pixels, with a counting time of 10 μs per pixel and an average of 4 lines. Samples were coated with a thin gold film (5 nm) to prevent a charge effect.

vi. Disintegration profile of the cryogels

The disintegration profile of the cryogels was carried out using static light scattering (Mastersizer 3000, Malvern Instruments, Worcestershire, United Kingdom). The experiment was run by immersing a cryogel in the LV measuring cell filled with Milli-Q water under constant stirring at 3500 rpm for 15 min at 25 ± 1 °C. The particle size distribution was recorded with interval of 10 s during 3 s with blue and red lasers. The refractive index was set at 1.45. The data was then fitted with a first order exponential model (Equation 34) as follows:

Equation 34 $$y = D_{[4,3]_\infty} + \left(D_{[4,3]_0} - D_{[4,3]_\infty}\right) e^{-\frac{\ln 2\, t}{\tau}}$$

where $D_{[4,3]_0}$ and $D_{[4,3]_\infty}$ denote the volume weighted mean particle size (µm) at t = 0 and ∞ min, t the time (s) and τ the time required to reach a 50% $D_{[4,3]_0}$ decrease (Quodbach & Kleinebudde, 2014).

### Statistical analyses

The Shapiro-Wilk test and Q–Q plot representation normality tests were used to verify the normal distribution of the data. To determine the significant differences, one-way ANOVA was performed using Origin 2019b software (OriginLab Inc, Northampton, MA, United States). The Tukey's multiple range test was used to separate mean values when significant differences ($p < 0.05$) were detected. All results were expressed as mean ± standard deviation.

## RESULTS & DISCUSSION

The microstructure conformation and consequently, the physicochemical and mechanical properties of cryogels are influenced by several parameters, including the type and concentration of the polymeric precursors, the presence of kosmotropic small molecules (e.g. sugars) and the cryogenic processing conditions (Lozinsky, 2020). Previous studies have shown that the bestowed physicochemical, structural, and mechanical characteristics of cryogels are inextricably associated with the microstructure and physical state of their hydrogel precursor(s) (Betz et al., 2012; Kleemann et al., 2018; Selmer et al., 2015). In this context, the microstructural, dynamic rheological properties and colloidal stability of the acid-induced hydrogel precursors were studied first.

### Characterisation of the acid-induced hydrogels

The indirect acid-induced gelation curves, as influenced by the protein composition, are

illustrated in Figure 49. As expected, the onset gelation point increased exponentially ($R^2$ = 0.999) to $m_{NaCN/WPI}$ ranging from $t_{gel, onset}$ = 27–170 min. The differences in the gelation kinetics were ascribed primarily to the higher isoelectric point of WPI (~5.2) and the ability of the non-sedimentable whey protein aggregates (ca. 240 nm as determined in this study by DLS analysis) to interact via hydrophobic and hydrogen bridging interactions at the very early stage of gelation i.e. at a pH far from the pI (Donato et al., 2011). As NaCN becomes more prevalent in the milk protein mixture, the intermolecular bridging of the WPI fractals is sterically hindered due to the competing action of NaCN for $Ca^{2+}$, leading to the slowdown of the gel formation (Nguyen et al., 2016). According to the dynamic rheological spectra, the individual protein gels showed minimal colloidal rearrangements throughout gelation, as depicted by the absence of an abrupt decrease in the complex viscosities after the gelation inflection ($t_\theta$) time point (Figure 49). In the case of NaCN-WPI mixtures, an approximative one-order reduction in the $\eta^*$ values were observed at $t \sim t_\theta$, a phenomenon that is most probably associated with the molecular interaction between the WPI fractals and NaCN via covalent thiol-disulphide bonding. In succession, the re-organised protein gel networks commenced slowly restoring their mechanical properties due to the stabilisation of the protein network via supramolecular interactions i.e. hydrogen bonding between the heteroprotein aggregate clusters (Lucey, 2020). Nonetheless, the assiduous investigation of the gelation mechanisms was out of the scope of the present study.

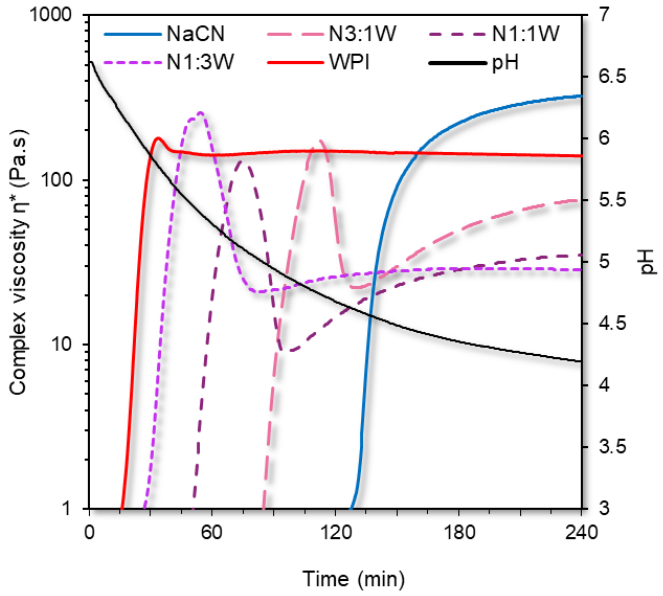


*Figure 49: Representative lactic acid-induced protein gelation profiles of the NaCN and WPI, as well as their blends determined by isothermal oscillatory rheology (f = 1 Hz, γ = 0.1%, 37 °C). The decline of pH throughout the fermentation is represented by the continuous black line.*

In Figure 50, the stability of the gel was assessed when faced with spontaneous serum exudation from the protein gel network. Both NaCN and WPI hydrogels showed insignificant changes in the light transmission measured across the tube height reflecting negligible serum exudation (Figure 50A,E,F). Contrarily in the NaCN-WPI blends (Figure 50B–D,F), a significant increase in the instability index values ($p < 0.001$) was observed. Interestingly, the colloidal stability of the acid-induced gels was positively correlated with change in the complex viscosity $\Delta\eta^*$ at $t \sim t_0$ ($r = 0.777$, $p < 0.01$), implying that the microstructural re-organisation occurring in the binary protein gel systems hampered their capacity to prevent the serum from outflowing through the porous protein network (Lucey, 2002).

From a microstructural point of view (Figure 51), WPI resulted in the formation of homogenous fine-stranded gels (Figure 51, A5) whilst NaCN exhibited a well-defined aggregated-like microstructure (Figure 51, A1). This behaviour is consistent with the results from the literature (Pugnaloni et al., 2005; Soukoulis et al., 2019). In the case of NaCN-WPI hydrogels, composite protein gel networks combining, in a proportional manner, the microstructural features of the individual proteins were detected (Figure 51, 2-4). According to the acquired CLSM micrographs, only the LGG cells located in the voids of the protein network could be clearly identified, without any evidence of acute lethality (as indicated by the presence of red stained bacterial cells) occurring during the fermentation step (Figure 51, B1-5). Finally, the WPI-rich hydrogels enhanced the

embedding of the LGG cells in a continuous protein network compared to their NaCN-rich counterparts, which may be associated with the better cell adhesion capacity of the former (Gomand et al., 2019).

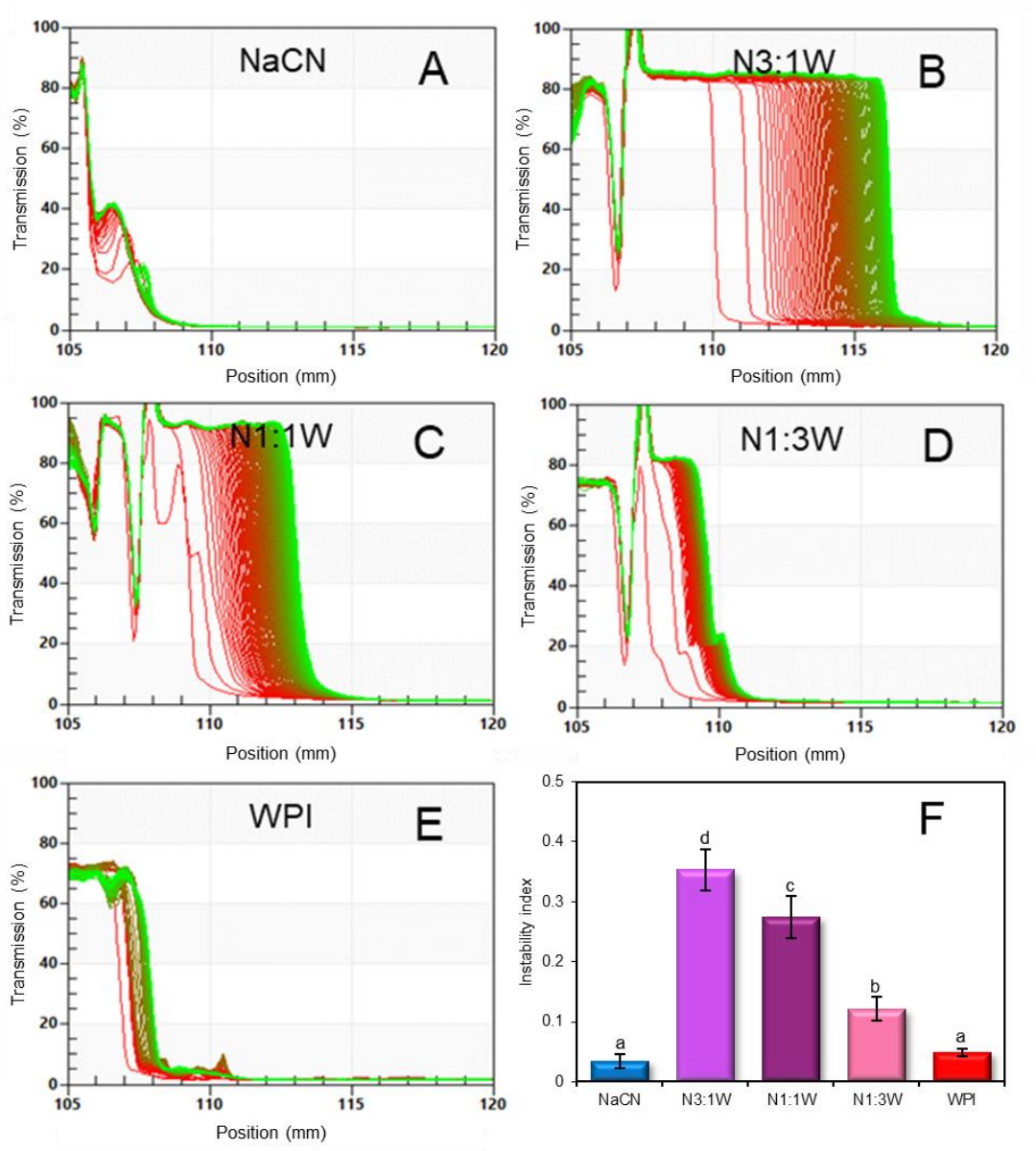


*Figure 50: Dynamic light transmission spectra of NaCN, WPI hydrogels and their blends (A-E) for assessing the temporal evolution of the colloidal stability under accelerated storage conditions (25 °C, 2,300g). Their respective instability indexes (dimensionless) are depicted in F. Red lines and green lines represent the first and last scanning, respectively.* $^{a\text{-}d}$*Different letters between the cryogels (F) denote a significant difference ($p < 0.05$) according to Tukey's post hoc means comparison test. Error bars = standard deviation ($n = 4$).*

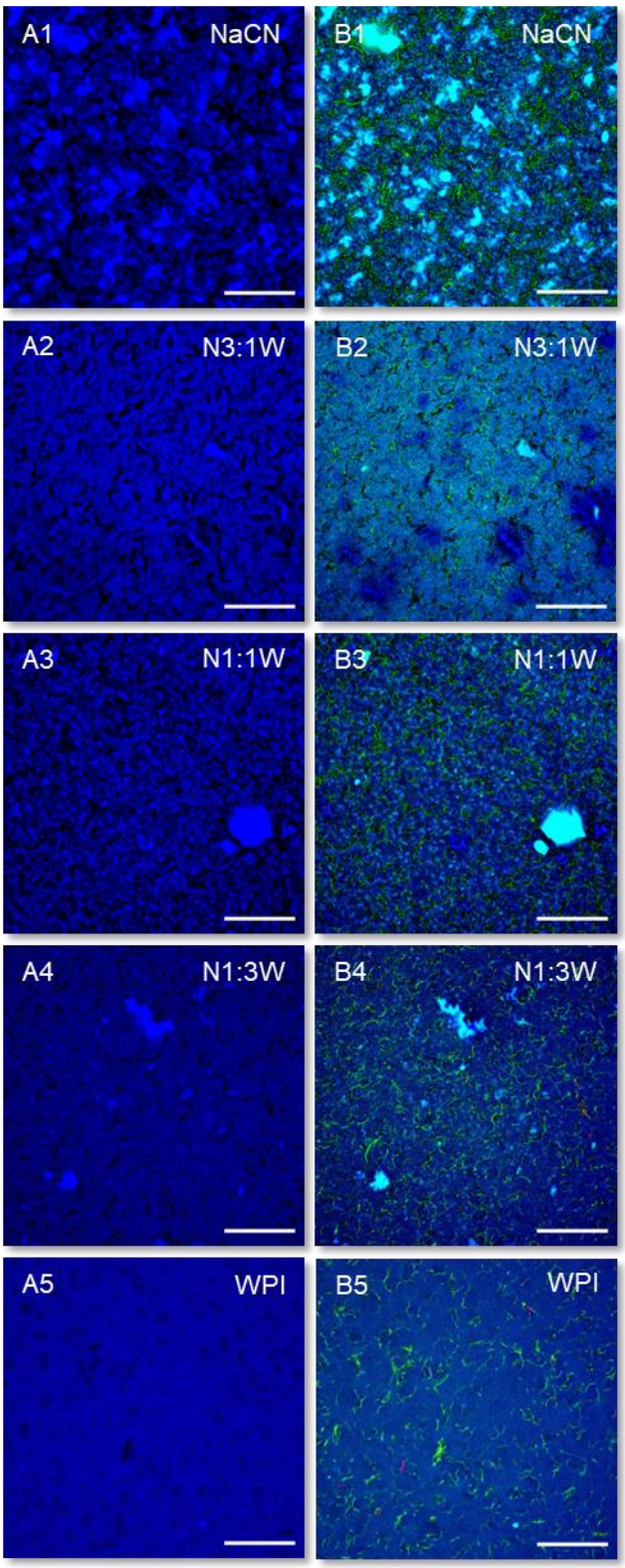


*Figure 51: CLSM micrograph of NaCN, WPI and mixture acid-gels obtained after 4 h of fermentation (37 °C). The protein network (in blue) was stained using Fast Green ($\lambda_{Ex}$ = 633 nm, $\lambda_{Em}$ = 635–680 nm) while living (in green) and dead (in red) LGG cells were stained with SYTO9 and propidium iodide, respectively. All the samples were analysed with a 40 × objective. For improved readability, the microstructure of the protein network is displayed with a single channel staining (A) whereas the LGG distribution is highlighted with green and red staining (B). Scale bar = 50 μm.*

## Characterisation of the cryogels

It is well-accepted that glassy and non-hygroscopic carriers that are less permeable to gases (water vapour and oxygen) are generally associated with the enhanced stability of probiotic cells during storage (Aschenbrenner, Först, et al., 2015). In addition, the microstructural conformation and the mechanical profile of the embedding carrier may play a significant role in controlling its disintegration and tuning the bacterial cell release behaviour, preserving the biological role of probiotics throughout gastrointestinal transit (Jiang et al., 2022). In view of this, the physicochemical, microstructural, mechanical and matrix disintegration aspects of the cryogels were determined.

i. Macroscopic appearance and microstructural characteristics

From a macroscopic viewpoint, the single protein-based cryogels preserved the geometrical (shape and size) aspects of their hydrogel precursors satisfactorily (Figure 52A,E). However, the mixed protein cryogels underwent volume contraction (Figure 52B,C,D, Figure 53) and shape distortion (Figure 52B). A good correlation was found between the cryogel shrinkage percentage and the precursor hydrogel colloidal instability index, which implies that the extent of the contraction of the protein gels during the acidification process defines the macroscopical properties of the cryogels and therefore, the optimisation of the fermentation process parameters e.g. inoculum size, temperature, use of symbiotic cultures, presence of other hydrocolloids, enzymatic crosslinking, etc. (Soukoulis et al., 2007) needs to be thoroughly considered in the cryostructuration of indirectly acid-induced cryogels. In addition, the increase in total milk protein solids (at $c > c_{\text{Least Gelation}}$) may assist to retain the shape and size characteristics of precursor hydrogels, but the inclusion of the living probiotic cells would become challenging, particularly if the impregnation method is implemented as in the case of other bioactives (Betz et al., 2012; Selmer et al., 2015, 2019).

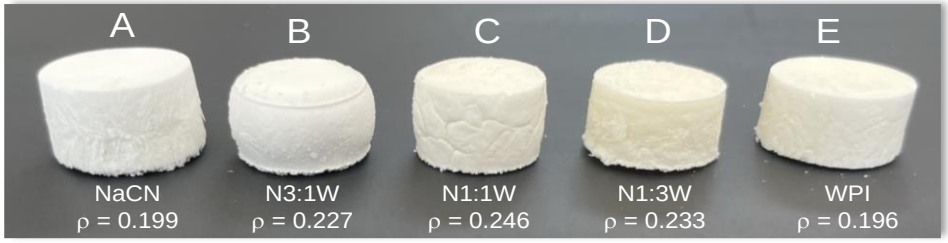


*Figure 52: Macroscopic appearance of the milk protein cryogel monoliths embedding LGG cells. The bulk density of the cryogels (ρ, n = 8) is expressed in g.cm$^{-3}$. Approximative cryogel dimensions: diameter × height = 15 × 10 mm.*

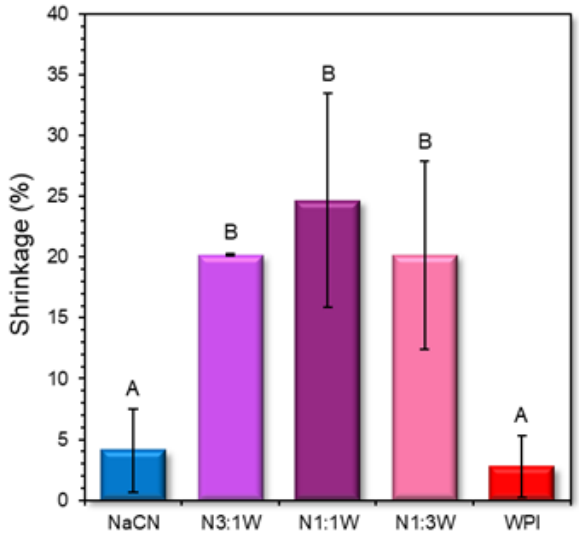


*Figure 53: Degree of shrinkage of the milk protein cryogel monoliths compared to the initial volume of solution.* $^{A\text{-}B}$*Different letters between the cryogels denote a significant difference ($p < 0.05$) according to Tukey's post hoc means comparison test. Error bars = standard deviation ($n = 8$).*

To evaluate the impact of the fermentation step on the microstructural characteristics (e.g. microporosity and microstructure of the wall material), the probiotic cryogels were analysed by µCT (Figure 54 A–C), SEM (Figure 54D) and HIM (Figure 54E). On one hand, as illustrated in µCT volume renderings, the single protein cryogels had the most porous structure, indicated by the macropore volume fraction measured, i.e. $\varphi = 0.78$. On the other hand, the mixed protein hydrogels were significantly ($p < 0.001$) less porous $\varphi = 0.67-0.72$, which is attributed to the compacted microstructure of their acid-induced hydrogel precursors. In agreement with the µCT images, SEM analysis confirmed that the single protein and N1:3W-based cryogels (Figure 54 D1,4–5) were characterised by a honeycomb-like microstructure, with the smallest macropores size observed in the NaCN-based cryogels. On the other hand, the single protein-based cryogels exerted a fairly rough vessel surface compared to the N1:3W. In the latter case, a high degree of lacunarity and the presence of a crystalline-like structure with sharp edges was detected. Finally, the N3:1W and N1:1W (Figure 54 D1–2) samples portrayed a relatively compact structure consisting of globular agglomerated subunits, with the N3:1W former exerting the highest structure-conformational uniformity.

To gain a better insight into the uniformity of the interconnected: vessel network of the cryogels, the cumulative vessel thickness curves were constructed, and a three-parameter sigmoidal model (Equation 35) was fitted as follows:

Equation 35 $$y = 100\frac{a}{1+\left(\frac{x}{b}\right)^n}$$

where: a is an asymptomatic value (100%), b denotes the inflection point that represents

the area at 50% of the cumulative distribution function, and n is a constant associated with the rate of change (slope) of the distribution. In general, the median vessel thickness ($vt_{50}$) ranged from 2.9 to 3.9 µm without showing a clear dependence on the protein composition of the cryogels. However, the vessel thickness distribution width values (i.e. span = $vt_{90}$-$vt_{10}$/$vt_{50}$) increased in this cryogel order: N3:1W < NaCN < N1:1W – WPI < N1:3W, which indicates that a proper consideration of the protein precursor composition is required in order to achieve a fine and uniform filamentous cryogel construct.

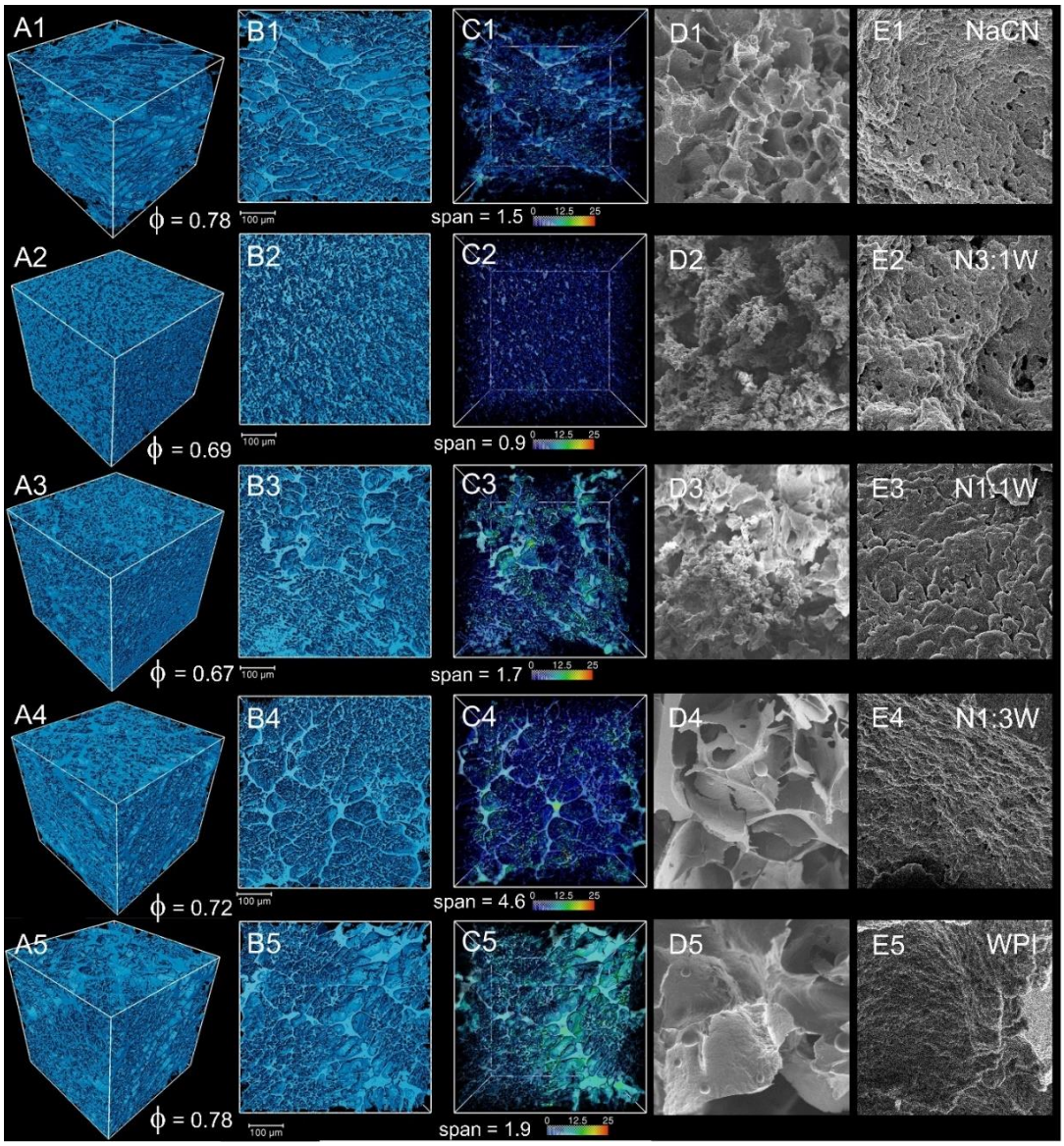


*Figure 54: µCT volume rendering with an angular view (A1–5), front view (B1–5) and front view after vessel thickness analysis (range 0–25 µm, C1–5), SEM (D1–5) and HIM (E1–5) micrographs in the case of NaCN (1), NaCN:WPI blends (2, 3 and 4) and WPI (5) cryogels. Dimensions of: µCT volume rendering = 500 × 500 × 500 voxels (voxel size of about 0.9 µm), SEM micrographs = 240×240 µm$^2$, and HIM micrographs = 8 × 8 µm$^2$. Abbreviations used: ϕ: porosity volume fraction; span: cryogel vessel thickness uniformity defined as $vt_{90}$-$vt_{10}$/$vt_{50}$. (n = 2).*

HIM analysis was carried out to provide insight into the submicron structure of the cryogel monoliths wall material (Figure 54E) as a qualitative assessment of encapsulation efficiency. To a large extent, a satisfactory intrenching of the cells of LGG into the continuous protein networks was observed, which substantiates the feasibility of cryogels as alternative xero-carriers for embedding living probiotic cells (Figure 55).

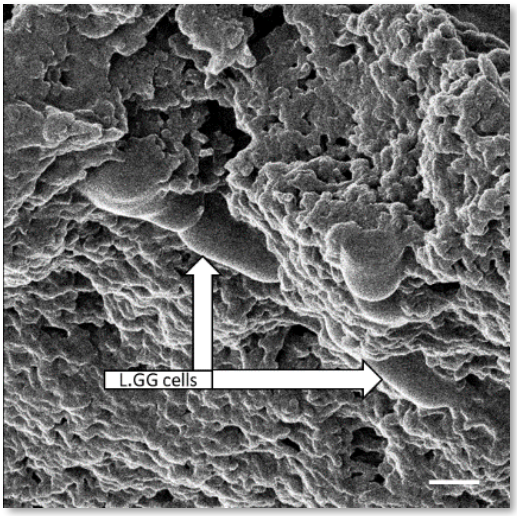


*Figure 55: Representative HIM micrograph of NaCN cryogel illustrating the Lacticaseibacillus rhamnosus GG cell imbrication into the milk protein matrix. Scale bar: 500 nm.*

In regard to the impact of the $m_{NaCN/WPI}$ on the wall material microstructure (Figure 54E), the prevalence of NaCN was associated with a quite coarse microstructure composed of densely packed layers of scale-like, reticular conformations, which is in agreement with the observations of Soukoulis et al., (2016). In contrast, the WPI-rich cryogels were characterised by a more compact and less perforated microstructure of globular-like protein aggregate conformations (Manzocco et al., 2022; Selmer et al., 2019; Soukoulis et al., 2017).

ii. Protein secondary structure conformation

The FTIR spectra of the probiotic cryogels influenced by the $m_{NaCN/WPI}$ are illustrated in Figure 56A. As expected, the amide I, 1700–1600 $cm^{-1}$ (C=O stretching vibrations of peptide bonds), the amide II, 1500–1600 $cm^{-1}$ (N–H bending/C–N stretching modes) and the amide III, 1200–1400 $cm^{-1}$, (N–H in-plane and C–N stretching vibrations) regions, all associated with the secondary structure conformational state of the proteins (Jackson & Mantsch, 1995), were among the most abundant peaks identified in the FTIR spectra. Comparing the FTIR spectra of the cryogels and the individual protein and sugar constituents (data not shown), it was confirmed that the presence of glucose and trehalose does not modify the aspects of the amide I band, which is in agreement with the findings

of Belton & Gil (1994). By deconvoluting the amide I band, four different secondary structure conformations assigned to aggregated β-sheet (1691–1980 $cm^{-1}$), β-turn (1677–1670 $cm^{-1}$), α-helix (1655–1651 $cm^{-1}$) and β-sheet (1630–1623 $cm^{-1}$) were identified (Figure 56B) (Daniloski et al., 2022). As for single protein cryogels, the NaCN exemplars were primarily composed of α-helices (60% α-helix, 31% β-sheet), whilst in the case of WPI the β-sheets were predominant (65% β-sheet, 23% α-helix; Figure 56B). Our findings are in line with the observations of Hussain et al., (2012), who reported that the heat treatment of WPI promotes the establishment of β-sheets at the cost of α-helix and β-turn secondary structures. On the other hand, caseins are known as lacking or having little secondary structure conformation including α-helix, β-sheet, β-turns and 20–25% polyproline II (Markoska et al., 2020). Nonetheless, processing parameters such as heating, cooling and acidification may result in significant changes in the structure conformation of caseins. In a recent study, Markoska et al. (2021) demonstrated that the acidification of β-casein dispersions was accompanied by an abrupt increase in the amount of α-helices at the expense of random coils. It is therefore assumed that the predominance of the α-helix in the NaCN cryogels may stem from changes in the casein structure during the fermentation process. However, the hypothesis needs to be cross validated using additional analytical techniques. In the case of the mixed protein-based cryogels, the predominance of the α-helix and β-sheets was modified proportionally to the $m_{NaCN/WPI}$ (Figure 56B). Nevertheless, no clear tendency was observed concerning the amount of β-turns and aggregated β-sheets. Finally, it should be noted that distinctive glucose and trehalose peaks were identified in all cryogels at 1149, 1107, 1078, 1034 and 989 $cm^{-1}$ (Kačuráková et al., 2000; Márquez et al., 2018) and therefore, only a small amount of the sugars were utilised by LGG for its metabolic activity.

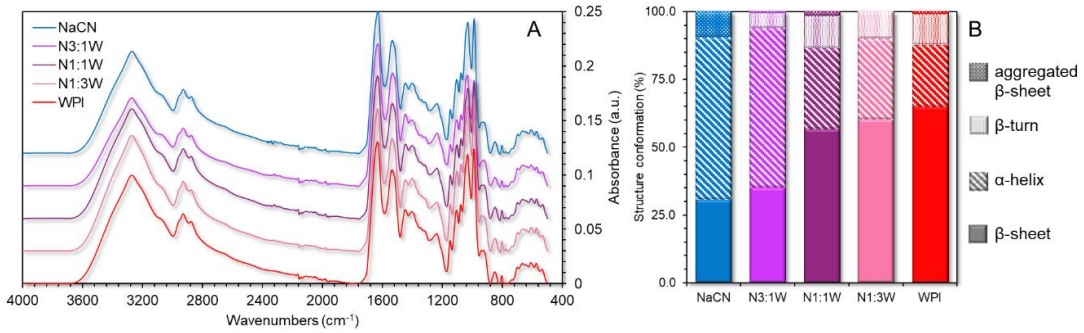


*Figure 56: Fourier transform infrared spectroscopy spectra of the cryogels of NaCN, WPI and their blends (A) and the average protein secondary structure conformation distribution obtained from amide I peak deconvolution (B, n = 2)*

iii. Water vapour sorption isotherms

On the completion of the freeze-drying process, the water content of the cryogels ranged from 4.0 to 4.6 $g_{H_2O}.100\ g^{-1}$ (Table 13). The water vapour sorption isotherms of the cryogels obtained from DVS analysis are illustrated in Figure 57. According to the Brunauer classification, the sorption isotherms obtained from the cryogels were associated to type III i.e. Flory-Huggins, which are characteristic of food matrices rich in soluble components such as sugars and polyols (Rao et al., 2014). Similar water vapour sorption isotherm patterns have also been reported in whey protein-based cryogels and aerogels (Manzocco et al., 2022). At low $a_w$ values ($a_w < 0.23$), no significant differences were found in the moisture content of the cryogels. The progressive increase in the relative water vapour pressure amplified the moisture content discrepancies among the systems. To understand the impact of the $m_{NaCN/WPI}$ on the water vapour adsorption dynamics, the moisture − aw data was satisfactorily fitted ($R^2 > 0.99$) into the GAB model (Equation 31). As shown in Table 13, the monolayer water content ($X_m$) exhibited an increase proportional to the $m_{NaCN/WPI}$ increase, which is associated with highly structured water molecules chemisorbed via hydrogen bond interactions to the binding polar groups (−COO−, −NH+, −OH) of proteins (Kinsella et al., 1986). It is well established that the monolayer water content of proteins may range from 2 to 10 $g.100\ g^{-1}$, with caseins exhibiting a lower water vapour adsorbing ability ($X_m \sim 5.5$) than β-lactoglobulin ($X_m \sim 6.67$) (Kinsella et al., 1986). The discrepancies in the $X_m$ values of the cryogels can be generally ascribed to their high mass fraction in highly hygroscopic constituents such as trehalose, glucose and glycerol, with the latter having a dominant effect (Farahnaky et al., 2009). It should also be noted that the changes in the structure conformational state induced by the treatments (i.e. pasteurisation and acidification) of the wet protein precursor may also affect (to a lesser extent) the water molecule adsorption, as additional binding sites are exposed. As displayed in the PCA biplot (Figure 58), the $X_m$ was closely associated with the secondary structure conformation of the proteins (i.e. the prevalence of α-helix and β-sheet) and $T_{g,1}$. Interestingly, no specific dependence of $X_m$ on the porosity and bulk density was found, which can be attributed to the inadequacy of the X-ray microtomography to provide an accurate estimation of the microporosity, as BET analysis could not be implemented for the determination of the specific surface area.

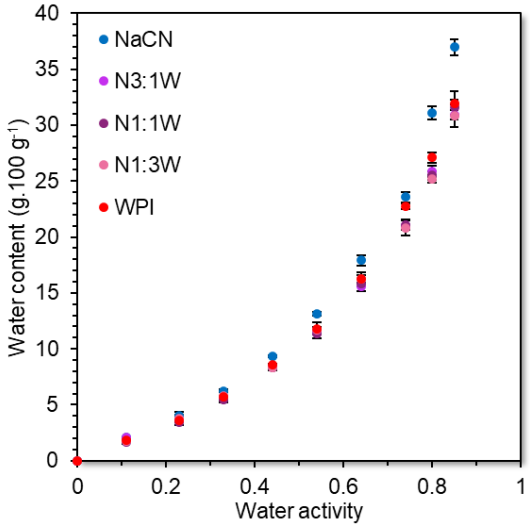


*Figure 57: Water mass fraction changes of cryogels as influenced by increasing water activity ($a_w$) monitored by dynamic vapour sorption.*

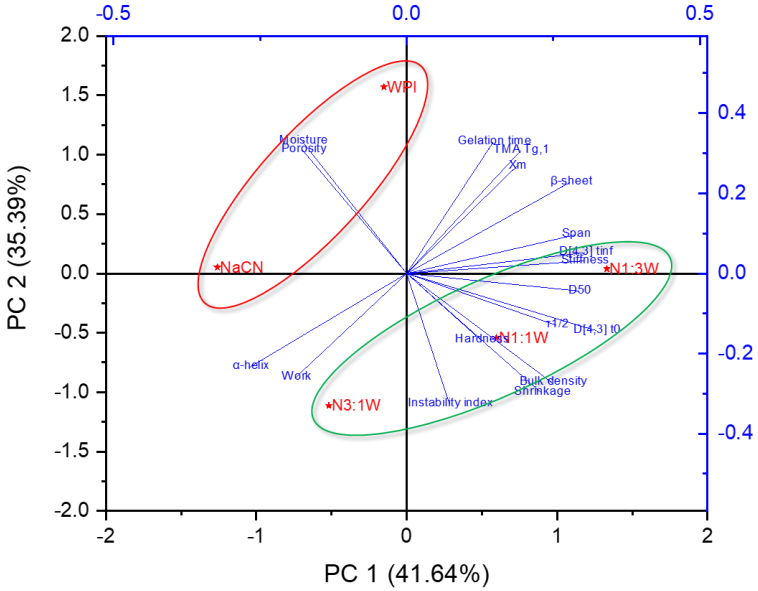


*Figure 58: PCA biplot of the characteristics of milk protein cryogels and their acid-gel precursors.*

Similarly to $X_m$ values, the calculated surface area ($S_m$) was increased reciprocally to the $m_{NaCN/WPI}$ (Table 13). $S_m$ is considered a measure of the number of water molecules binding sites (protein polar groups) and therefore, the extent of hydration at a specific relative water vapour pressure (Kinsella et al., 1986). For milk protein powders, $S_m$ ranges from ca. 140–256 $m^2.g^{-1}$, whilst significantly higher values have been reported in agglomerated or aggregated milk protein fractals, such as cheese curds (800–1200 $m^2.g^{-1}$). It is therefore assumed that the LGG-induced fermentation of the milk-based wet precursor had a contributory role to the increase of the surface area of the cryogels i.e. 403−488 $m^2.g^{-1}$ (Table 13).

*Table 13: Milk protein cryogel moisture and calculated GAB equation parameters fitted with water vapour adsorption data.*

| | Moisture ($g.100g^{-1}$) | $X_m$ ($g.100g^{-1}$) | C - | k - | $S_m$ ($m^2.g^{-1}$) |
|---|---|---|---|---|---|
| NaCN | $4.5 \pm 0.5^{a}$ | $11.53 \pm 0.12^{a}$ | $1.99 \pm 0.03^{c}$ | $0.61 \pm 0.03^{a}$ | $403.4 \pm 4.1^{a}$ |
| N3:1W | $4.1 \pm 0.6^{a}$ | $12.29 \pm 0.11^{ab}$ | $1.78 \pm 0.01^{b}$ | $0.56 \pm 0.00^{a}$ | $430.0 \pm 4.0^{ab}$ |
| N1:1W | $4.0 \pm 0.5^{a}$ | $12.61 \pm 0.04^{ab}$ | $1.73 \pm 0.01^{ab}$ | $0.54 \pm 0.01^{a}$ | $441.5 \pm 1.4^{ab}$ |
| N1:3W | $4.2 \pm 0.7^{a}$ | $13.00 \pm 0.66^{bc}$ | $1.71 \pm 0.01^{a}$ | $0.54 \pm 0.03^{a}$ | $455.0 \pm 23.3^{bc}$ |
| WPI | $4.6 \pm 0.5^{a}$ | $13.95 \pm 0.10^{c}$ | $1.70 \pm 0.01^{a}$ | $0.54 \pm 0.00^{a}$ | $488.2 \pm 3.5^{c}$ |

*Abbreviations used: $X_m$: moisture content at monolayer completion, C: a constant that depicts the free enthalpy energy difference between the monolayer and pure liquid water molecules, k: a constant correcting the properties of the multilayer molecules and $S_m$: the surface of the monolayer. $^{a\text{-}c}$Different letters between the cryogels denote a significant difference ($p < 0.05$) among the cryogels according to Tukey's post hoc means comparison test.*

iv. Thermal properties

For an overview of the thermal stability of the milk protein-based cryogels, the TGA thermographs of the individual ingredients (Figure 59A) and the cryogels obtained shortly after the completion of the freeze-drying process (Figure 59B) were acquired. As seen in Figure 59A, milk proteins experienced two major weight loss events: firstly, an approx. 7.5% mass loss in the range of 30–110 °C ($T_{1,mid}$ = 45 °C), which is ascribed to unbound water evaporation (Talón et al., 2019), and secondly, a 55−62% loss of the initial mass in the range of 250–400 °C ($T_{2,onset}$ = 257 °C and $T_{2,mid}$ = 286 °C), which is indicative of the concomitant thermal decomposition of the protein and residual milkfat matter (Koupantsis et al., 2016; Talón et al., 2019). Moreover, a minor weight loss event at ca. 162 °C was recorded in the TGA spectra of WPI, which is most probably associated with the presence of residual monohydrate lactose, i.e. water of crystallisation loss (Listiohadi et al., 2009). As for sugars, trehalose underwent a low temperature weight loss (about 6% of the initial mass) at 30−110 °C, associated with the water evaporation. Both sugars underwent thermal decomposition at $T_{onset}$ above 200 °C, whilst glycerol experienced an abrupt weight loss at $T_{onset}$ = 187 °C, which is in agreement with the literature data (Talón et al., 2019).

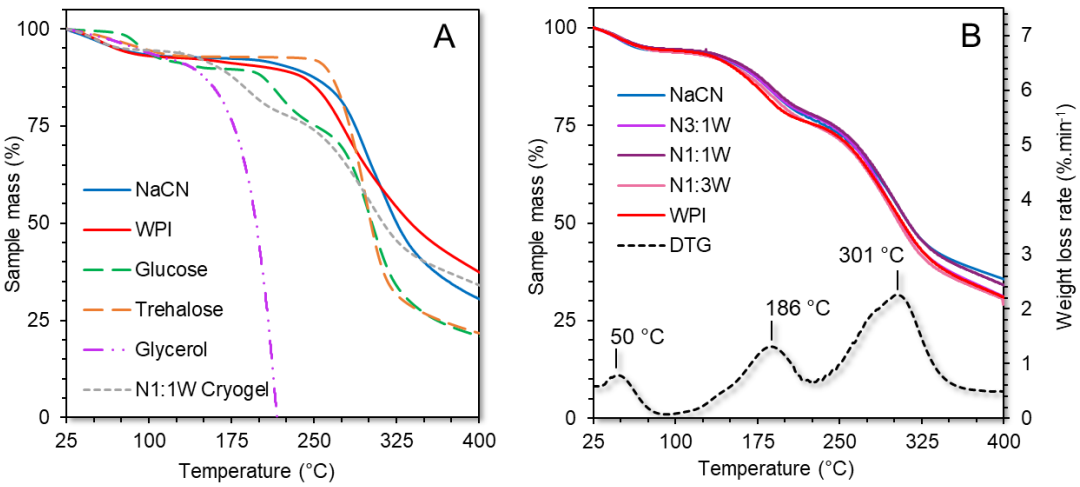


*Figure 59: TGA thermographs of the individual components of the cryogels (A) and TGA (continuous lines) and DTG (dashed line) of the cryogels (B) measured at 5 °C min$^{-1}$.*

Concerning the TGA spectra of the cryogels, three major weight loss events were recorded (Figure 59B). In accordance with the individual milk proteins, a mass loss (approx. 4.5%) was detected at $T_{1,mid}$ = 50 °C associated with the evaporation of the unbound water (Table 14). The intermediate temperature ($T_{2,mid}$ = 186 °C) mass loss event was most probably related to the thermal decomposition of glycerol, and the glycation of the protein molecules i.e. non-enzymatic browning, among others. In the latter case, the weight losses mainly refer to the release of water (Schiff base reaction – early glycation stage) and the volatile products of the Amadori rearrangement and Strecker reactions (van Boekel, 2006). Finally, the thermal decomposition of the cryogels took place at $T_{3,onset}$ = 301 °C. For all the tested cryogel systems, no significant ($p > 0.05$) shift in the onset and midpoints of the TGA steps was observed, which is attributed to their compositional similarities and the minor differences in the thermal stability of the individual milk proteins.

As a successive analytical step, the physical state of the cryogels was measured by means of DSC and TMA. According to the DSC thermographs (data not shown), a transition from the glassy to the rubbery state was identified in the 98–100 °C temperature region, which is in keeping with the findings of (Manzocco et al., 2022) on WPI-based aerogels and cryogels. Nonetheless, the differences in the calculated $T_{g,mid}$ values among the cryogel samples were not significant (Table 14).

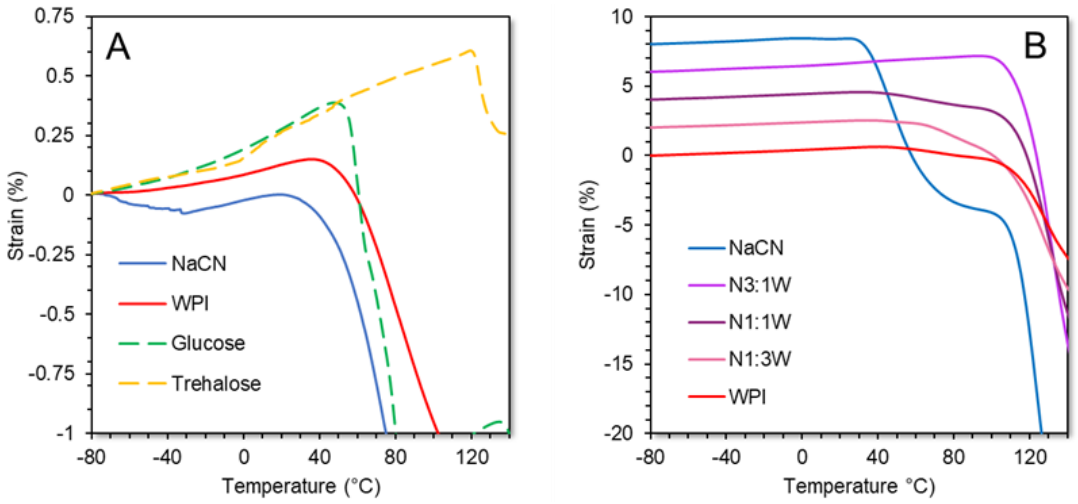


*Figure 60: Thermo-mechanical profile of individual ingredients of the cryogels (A) and milk protein cryogels (B). For improved readability, the TMA spectra of NaCN, N3:1W, N1:1W and N1:3W cryogels were shifted upward by 8, 6, 4 and 2%, respectively.*

To obtain a more accurate overview of their thermophysical contributory role, the components of the cryogels were individually analysed by TMA (Figure 60A). As seen in Table 14, NaCN and WPI protein precursors underwent glass transition at 47.6 and 52.4 °C, respectively. This is in close agreement with the observations of Adhikari et al., (2009) and Boonyai et al., (2006). As for sugars, amorphous (freeze-dried) trehalose and glucose underwent glass transition at 125.6 and 55.0 °C, respectively. The TMA spectra of the cryogels (Figure 60B, Table 14), evidenced the presence of two glass transition regions: $T_{g,1}$ = 33−46 °C and $T_{g,2}$ = 101−126 °C, depending on the $m_{NaCN/WPI}$. Except for the N3:1W system, the $T_{g,1}$ values decreased proportionally to the $m_{NaCN/WPI}$ ($T_{g,1} = -11.9\ m_{NaCN/WPI} + 44.8$, $R^2 = 0.975$). This finding implies that the $T_{g,1}$ denotes the temperature region where the softening of the cryogels occurs as a result of the non-covalent interchain protein interactions (e.g. hydrogen bonding and hydrophobic interactions) weakening. A good correlation was found between the prevalence of the β-sheet or α-helix structure conformational state of the proteins and the $T_{g,1}$ of the cryogels ($r = 0.910$, $p < 0.05$ for β-sheet, and $r = -0.860$, $p < 0.01$ for α-helix), which demonstrates that the glass transition at $T_{g,1}$ is closely associated with the unfolding ability of the proteins upon mechanical compression. Confirming our assumption, DeBenedictis & Keten (2019) reported that the dissipated energy, normalised to the protein characteristics, was significantly higher in β-sheet than in α-helix protein motifs. This was attributed primarily to the ability of the hydrogen bond network of the β-sheet strands to be mechanically loaded in a collective mode that requires larger forces to rupture. Notably, once the required energy for weakening the protein interchain molecular interactions was dissipated, both the WPI

powder and its cryogel exemplars exhibited the lowest deformability upon compression (Figure 60B), which may be indicative of their brittle and friable character (Lefèvre et al., 2005).

*Table 14: Thermophysical properties of the cryogels*

| | DSC $T_g$ (°C) | TMA $T_{g,1}$ (°C) | TMA $T_{g,2}$ (°C) |
|---|---|---|---|
| NaCN | 99.3 | 33.4 | 112.0 |
| N3:1W | 98.9 | Nd | 105.5 |
| N1:1W | 98.7 | 38.1 | 112.8 |
| N1:3W | 99.2 | 41.2 | 101.3 |
| WPI | 99.3 | 45.7 | 110.9 |

*TMA $T_g$ of individual components (°C): NaCN = 47.6, WPI = 52.4, trehalose = 125.6, glucose 55.0. Nd = not detected*

Contrary to $T_{g,1}$, the $T_{g,2}$ values did not show any clear dependence on the $m_{NaCN/WPI}$, suggesting that the $T_{g,2}$ is not associated with changes in the interchain protein interactions. Instead, the $T_{g,2}$ of the cryogels were quite close to those recorded for the amorphous sugars i.e. trehalose ($T_g$ ~ 125 °C) and glucose ($T_g$ ~ 55 °C), and thus, it is assumed that the $T_{g,2}$ depicts the temperature region in which the sugar blend stiffness is being dropped. At $T > T_{g,2}$, a substantial decrease in the deformability of the cryogels was observed, indicating their structural collapse.

v. Mechanical properties

The mechanical characteristics of the cryogel monoliths were probed by indentation testing (Table 15). In general, the hardness (i.e. maximum force at rupture) and stiffness of the cryogels were governed by the thickness and uniformity of the protein filamentous cryogel construct (Figure 54C). In most cases, aerogels and cryogels are characterised as brittle and plastic materials.

In relation to the obtained force – indentation curve profiles (for an example see Figure 48), all protein cryogels exhibited a predominantly brittle character, which was in the agreement with the findings of Chen et al. (2013). Significant differences were detected in the hardness, stiffness and energy dissipated for the cryogel rupture. Nonetheless, it was not possible to identify any proportionality between the mechanical properties and the $m_{NaCN/WPI}$. On the other hand, the energy dissipated (work) for the structural collapse of the cryogels exhibited significant ($p < 0.05$) correlations with the TMA determined $T_{g,1}$ ($r = -0.68$), the protein structure conformational state i.e. α-helix ($r = 0.85$) and β-sheet ($r = -0.81$) prevalence, and $m_{NaCN/WPI}$ ($r = 0.65$). Nonetheless, it was not possible to find

a common mechanistic conjecture regarding the impact of the structure conformational state of the proteins and the mechanical energy, as in the case of the TMA results. This may be attributed to the fact that the work required for the structural collapse of the cryogels is macroscopically driven e.g. creation and propagation of structure imperfections due to the indentation forces. Finally, it should be noted that a good correlation between work and stiffness ($r = -0.55$, $p < 0.05$) was found, which signifies that the lowest amount of energy is dissipated in the most brittle cryogel constructs.

*Table 15: Mechanical properties of the cryogels under penetration stress*

| | Hardness (N) | Stiffness ($N.mm^{-1}$) | Work (mJ) |
|---|---|---|---|
| NaCN | $15.8 \pm 5.5^{ab}$ | $12.2 \pm 3.0^{ab}$ | $9.9 \pm 3.9^{a}$ |
| N3:1W | $15.1 \pm 1.9^{ab}$ | $6.8 \pm 1.3^{a}$ | $17.3 \pm 5.6^{b}$ |
| N1:1W | $12.9 \pm 1.4^{a}$ | $16.9 \pm 2.9^{b}$ | $4.9 \pm 2.4^{a}$ |
| N1:3W | $19.9 \pm 4.2^{b}$ | $30.8 \pm 6.5^{c}$ | $6.1 \pm 1.8^{a}$ |
| WPI | $10.4 \pm 1.1^{a}$ | $11.4 \pm 2.2^{ab}$ | $4.6 \pm 1.3^{a}$ |

*$^{a-c}$Different letters between the cryogels denote a significant difference ($p < 0.05$) among the cryogels according to Tukey's post hoc means comparison test.*

vi. Water reconstitution behaviour

To understand to the reconstitution behaviour of the cryogel monoliths once they come into contact with water, a real-time particle mean size assessment method was implemented (Figure 61, Table 16). In a mechanistic context, the disintegration of dry particulate-based formulations e.g. spray-dried powders and lyophilisates, tablets, aerogels etc. can be described by four kinetically driven physical phenomena including wetting, swelling, dispersion and dissolution (Forny et al., 2011; Markl & Zeitler, 2017).

*Table 16: Disintegration parameters of NaCN, WPI and blends*

| | $D_{[4,3]\ t0}$ (µm) | $D_{[4,3]\ t\infty}$ (µm) | $\tau$ (s) | $\tau_{99\%}$ (s) |
|---|---|---|---|---|
| NaCN | $407.2 \pm 23.7^{a}$ | $75.8 \pm 1.8^{a}$ | $14.2 \pm 1.0^{a}$ | $94.2 \pm 6.5^{a}$ |
| N3:1W | $632.9 \pm 29.5^{b}$ | $68.0 \pm 15.0^{a}$ | $131.9 \pm 11.0^{cd}$ | $876.1 \pm 73.2^{c}$ |
| N1:1W | $685.7 \pm 174.3^{c}$ | $126.1 \pm 19.2^{b}$ | $100.0 \pm 1.3^{bc}$ | $706.2 \pm 65.3^{bc}$ |
| N1:3W | $956.3 \pm 71.9^{d}$ | $406.8 \pm 96.9^{c}$ | $130.3 \pm 33.3^{d}$ | $865.9 \pm 221.0^{c}$ |
| WPI | $449.9 \pm 83.5^{a}$ | $126.6 \pm 35.7^{ab}$ | $84.8 \pm 10.7^{b}$ | $563.1 \pm 65.8^{d}$ |

*Abbreviation used: $D_{[4,3]\ t0}$: particle size (in µm) at $t = 0$ min; $D_{[4,3]\ t\infty}$: particle size (in µm) at $t = \infty$ min; $\tau$: time (in seconds) required to obtain a 50% particle size reduction; $\tau_{99\%}$: time (in second) required to obtain a 99% particle size reduction. $^{a-d}$Different letters between the cryogels denote a significant difference ($p < 0.05$) according to Tukey's post hoc means comparison test ($n = 5$).*

As illustrated in Figure 61, the immersion of the cryogel monoliths into the water tank resulted in their rapid disintegration into large agglomerates ranging from $D_{[4,3]t0}$ = 407–956 µm in size. In the early stages of the disintegration process, the wetting of the outer matrix surface and the progressive capillary diffusion of water are known to result into the omni-directional enlargement of the particles, leading to an increase in internal pressure and pushing apart the adjoining agglomerates (Markl & Zeitler, 2017). Indeed, as displayed in the PCA biplot (Figure 58), the $D_{[4,3]\,t0}$ values were correlated negatively with the porosity (ϕ) of the cryogels and positively with their bulk density and shrinkage. Therefore, due to their more porous and compact microstructure, the mixed protein-based cryogels tended to break down into the larger agglomerates more than their individual protein exemplars. As the reconstitution process progresses, the loose particles start to reduce in size, which is the result of fast-pacing mass transfer phenomena occurring at the solid – solvent interface (Forny et al., 2011). The agglomerate dissolution half-time (τ), $\tau_{99\%}$ and the residual (non-dissolved) cryogel particles $D_{[4,3]\,t\infty}$ were significantly higher ($p < 0.05$) in the case of the mixed protein cryogels (Table 16). A significant correlation ($r > 0.7$, $p < 0.05$) was identified between the dissolution parameters (τ, $\tau_{99\%}$ and $D_{[4,3]\,t\infty}$) and the porosity, filamentous uniformity (span) hardness and stiffness of the cryogels (Figure 58), supporting the diffusion-driven mechanism of the cryogels dissolution behaviour.

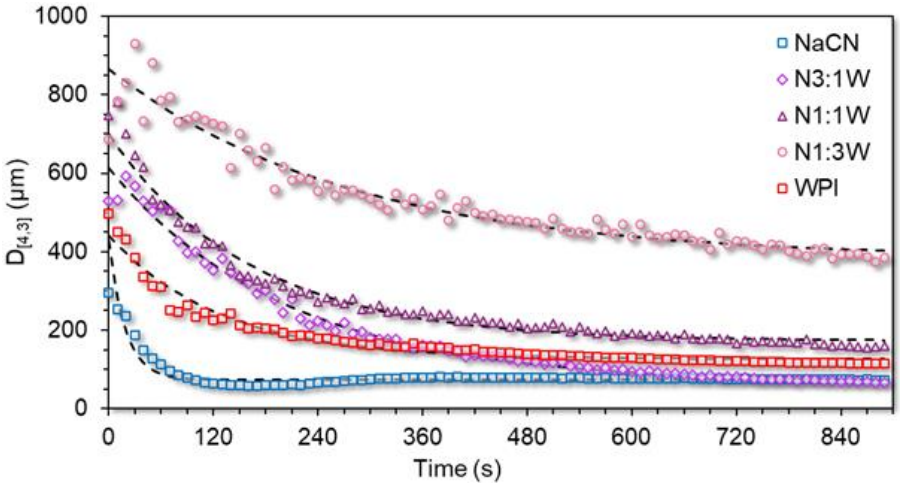


*Figure 61: Disintegration profile of the NaCN, WPI and blend cryogels measured at 20 °C and with a constant shear speed of 3500 rpm. Black lines represent the fitted data using the first-order exponential decay model (Equation 34). The curves and points represent the average of 5 individual disintegration experiments.*

# CONCLUSIONS

A novel xero-scaffold was successfully developed based on freeze-drying-induced cryogels that deployed a pre-fermented milk protein-based hydrogel for embedding living probiotic bacteria cells i.e. *Lacticaseibacillus rhamnosus* GG. The microscopic assessment of the wall material of the cryogels evidenced the satisfactory intrenching of the LGG bacterial cells, an effect that was independent of their compositional profile. The volume contraction and the microstructural conformation of the cryogels were inextricably associated with the behaviour of acid hydrogel precursors during the fermentation step. The mixed protein-based cryogels underwent a higher degree of volume contraction during freeze-drying, resulting in a more compacted, hard and stiff, yet less water-reconstitutable, construct than their individual protein exemplars. From a microstructural viewpoint, the cryogels exhibited a sponge-like microstructure in terms of the macropore volume fraction, as well as the thickness and uniformity of the protein network ligaments, notably dependent on the protein composition of their wet hydrogel precursors. A coarse lamellate wall matter microstructure was observed in the NaCN-rich cryogels as opposed to their WPI-rich exemplars that exerted a compact globular aggregated conformation. The water vapour sorption and the thermo-mechanical properties of the cryogels were the only characteristics showing a consistent dependence on the $m_{NaCN/WPI}$. The second part of this study will assess the feasibility of the cryogels hereby developed to preserve the biological activity of the LGG cells and will report on the inactivation kinetics of LGG under controlled storage conditions, its release and survival throughout *in vitro* digestion, and the peptidomic profile of the gastric and intestinal digesta as influenced by the protein composition and the physicochemical, microstructural and thermo-mechanical properties of the cryogels disclosed in this work.

# MILK PROTEIN-BASED CRYOGEL MONOLITHS AS NOVEL ENCAPSULANTS OF PROBIOTIC BACTERIA. PART II: *LACTICASEIBACILLUS RHAMNOSUS* GG STORAGE STABILITY AND BIOACTIVITY UNDER *IN VITRO* DIGESTION

Thierry HELLEBOIS[1,2], Romain CANUEL[1,3], Céline Leclercq[1], Claire GAIANI[2], and Christos SOUKOULIS[1]

[1]Environmental Research and Innovation (ERIN) Department, Luxembourg Institute of Science and Technology (LIST), Esch-sur-Alzette, Luxembourg
[2]Université de Lorraine, LIBio, Nancy, France
[3]École Nationale Supérieure de Chimie, de Biologie et de Physique (ENSCBP), Bordeaux INP, Pessac, France

Food Hydrocolloids
Volume 146, Part A, January 2024, 109173
doi.org/10.1016/j.foodhyd.2023.109173

# ABSTRACT

The aim of the study was to assess the ability of milk protein-based cryogel monoliths to preserve the biological role of *Lacticaseibacillus rhamnosus* GG (LGG) under cryogenic processing, temperature – $a_w$ controlled storage and under *in vitro* gastrointestinal conditions. The cryogelation process did not result in any significant cellular injuries (losses < 0.5 logCFU.g$^{-1}$) due to the achievement of a vitreous state under the cryogenic conditions implemented. Among the tested storage conditions, temperature was the most impactful parameter on LGG inactivation rates ($k_{LGG}$ = 0.002–0.008 to 0.25–0.56 day$^{-1}$ for 5 and 37 °C, respectively), followed by protein composition (i.e. the presence of sodium caseinate alleviated the lethality of LGG). Glassy cryogels stored at aw ≤ 0.33 enabled good LGG survivability ($k_{LGG}$ 0.033–0.045 day$^{-1}$) compared to their rubbery analogues (i.e. $a_w$ > 0.33). The cryogels exhibited limited disintegration during gastric processing, which aided LGG cells to resist gastric stressors, while complete disintegration occurred during the intestinal step, facilitating the release of LGG cells and promoting the cryogel matrix's digestibility (> 64%). LGG counts in the intestinal phases remained high (> 8.2 logCFU.g$^{-1}$), and the peptidomic profiling confirmed the release of bioactive peptides including angiotensin-converting enzyme and dipeptidyl peptidase-4 inhibitory, antimicrobial, and antioxidant peptides.

# INTRODUCTION

An incrementing number of studies have pinpointed the influential role of gut microbiota on human health, from innate immunity to chronic inflammatory disease (e.g. cardiovascular disease, diabetes, several forms of cancer, etc.) to appetite regulation and energy metabolism (Fan & Pedersen, 2021; Valdes et al., 2018). As part of the human gut microbiota, probiotics pertain to well-defined human gut-relevant commensal microbe consortia, having generic or core effects on gut physiology and homeostasis or supporting the health of the reproductive tract, oral cavity, lungs, skin, and gut-brain axis (Hill et al., 2014). The commonest strategy to deliver probiotics to the human host is via the consumption of fermented foods like yogurt, kefir, cheese, or probiotic-enriched functional foods and supplements. (Şanlier et al., 2019).

The encapsulation of probiotics, i.e. the physically- or chemically-induced engrafting of living cells in biopolymer structure-engineered micro-scaffolds has become popular in the last two decades (Gu et al., 2022; Seifert et al., 2019; Yao et al., 2020). This can be primarily attributed to the ability of the encapsulant to administer sufficiently high amounts of living probiotic cells to the human host (i.e. $> 9-10$ $\log CFU.g^{-1}$) and alleviate the sublethal effects of extrinsic stressors (i.e. mechanical stress, heat, pH, oxygen, water vapour, ionic strength, digestive enzymes, bile salts, etc.) (Garcia-Brand et al., 2022; Gu et al., 2022; Yao et al., 2020). A probiotic-engrafting colloidal reservoir should adequately support cell bioadhesion to the wall material without compromising the cells' ability to adhere to the mucosal tissues Furthermore, the assiduous design of the encapsulation system should allow maximal cell loading and tailored swelling, disintegration, and release properties ensuring a substantial number of live bacterial cells that can successfully reach and colonise the distal intestine and colon (Gomand et al., 2019). To date, starch, soluble dietary fibres (polysaccharides, plant mucilages and prebiotics), and proteins have been the commonest biopolymers employed in the encapsulation of probiotics (Razavi et al., 2021; Rodrigues et al., 2020; Yao et al., 2020). In the case of proteins, they are used in enzyme-responsive and redox-responsive colloidal templates, where the release of the living cells is triggered via their pepsin or pancreases-induced peptic cleavage and biological stimuli generated by the presence of oxidants or reducing agents during the gastrointestinal transit (Garcia-Brand et al., 2022). Besides, secondary physiological effects due to the release of bioavailable bioactive peptides can be also achieved (Amigo & Hernández-Ledesma, 2020).

In industry, anhydrobiotic technology, i.e. the physical entrapment of probiotics in micro-

or macroporous xero-particulates usually produced via spray or freeze-drying, is the most relevant methodology for probiotic encapsulation (Huang et al., 2017; Kiepś & Dembczyński, 2022). This is due to its facile process design and scalability, as well as the prolonged shelf-life of the anhydrobiotic formulations. Stemming from their large specific surface area and open structure, cryogels, i.e. macroporous xero-scaffolds produced via the water sublimation of biopolymer hydrogel precursors, have been successfully deployed as colloidal reservoirs for labile bioactive compounds allowing satisfactory drug-loading yields and encapsulation efficiency (Betz et al., 2012; Kleemann et al., 2020; Manzocco et al., 2021; Selvasekaran & Chidambaram, 2021). For example, a loading efficiency of approximately 70–90% has been reported for vital wheat gluten and whey protein isolate-based cryogels impregnated in labile lipophilic compounds such as limonene and fish oil, respectively (Ahmadi et al., 2016; Blomfeldt et al., 2010). By comparing whey protein isolate cryostructurates produced via freeze (cryogels) or supercritical $CO_2$-assisted (aerogels) drying, Manzocco et al. (2022) found that while the oil loading capacity was not influenced by the cryostructuration process, a controlled oil uptake profile leading to stiffer oleogels was achieved. In a recent study, Fontes-Candia et al. (2022) demonstrated that polysaccharide stabilised casein aerogels could offer tangible bio-functional benefits due to their programmable digestibility, resulting in bioaccessible bioactive peptides.

Despite the deployment of cryogels as colloidal templates for the controlled release of micronutrients and drugs, the engrafting of living cells, such as probiotic bacteria, appears to be a promising encapsulation concept. In a recent study, Sun et al. (2021) showcased a whey protein concentrate–pullulan–trehalose hydrogel template embedding *L. plantarum* cells. According to their findings, trehalose had a modulatory role in preserving the biological activity of the probiotic cells during freeze-drying and storage in chilling conditions. However, more studies exploring the feasibility of cryogels as templates for probiotic encapsulation are needed. In the first part of the study, the microstructural, physicochemical and mechanical aspects of the milk protein-based cryogels containing living *Lacticaseibacillus rhamnosus* GG (LGG) cells were determined (Hellebois et al., 2023). The second part of the study aimed to assess the ability of the cryogels to preserve the biological activity of the LGG cells. In view of this, the viability of LGG throughout freeze-drying, storage and *in vitro* digestion was monitored. In addition, the peptidome of the gastric and intestinal phases, as influenced by the protein composition of the cryogels, was investigated.

# MATERIALS & METHODS

## Materials

Whey protein isolate (WPI) powder (PRODIET 90S) with a protein content of 85.8% wt. was kindly donated by Ingredia (Arras, France). Sodium caseinate (NaCN) protein powder (containing 89.4% wt. of protein, N% × 6.25), glucose (99.5% wt.) and glycerol (99.9% wt.) were purchased from Sigma-Aldrich (Leuven, Belgium). Trehalose (99.4% wt.) was purchased from Louis-François (Croissy-Beaubourg, France). The De Man, Rogosa and Sharpe (MRS) culture media was purchased from Carl Roth (Karlsruhe, Germany). The probiotic strain *Lacticaseibacillus rhamnosus* GG (LGG) ATCC 53103 was purchased from the VTT Technical Research Centre of Finland Ltd (Espoo, Finland). All the other chemicals used were of analytical grade and were purchased from Sigma-Aldrich (Leuven, Belgium).

## Preparation of the *Lacticaseibacillus rhamnosus* GG embedding cryogel monoliths

The LGG embedding milk protein cryogels were prepared according to the procedure detailed in Hellebois et al., (2023). For comparison purposes, LGG-free cryogels were produced via direct acidification using 2.2% wt. of glucono-δ-lactone, mimicking the acidification rate of LGG. All other treatments were identical to the probiotic cryogels.

## Viable *Lacticaseibacillus rhamnosus* GG quantification

The total viable counts (TVC) of the LGG cells were quantified from an aliquot of either 1 mL of solution/dispersion or hydrogel or 1 g of cryogel. The systems were mixed with 9 mL of PBS in a sterile stomacher bag and blended (MiniMix 100 W, Interscience, Roubaix, France) until a homogenous fine dispersion (< 50 µm) was obtained. The dispersions were then sequentially diluted ten-fold in PBS and spread onto MRS agar using the pour-plating method. The plates were then incubated at 37 ± 0.5 °C for 48 h. The colony-forming units (CFU) were determined using a Scan 300 automatic colony-counter (Interscience, Roubaix, France). For comparison purposes, all the bacterial counts are reported on a dry basis.

## *Lacticaseibacillus rhamnosus* GG storage stability

To assess the potential of the milk protein-based cryogel monoliths as probiotic xero-

carriers, the shelf life of LGG cells was assessed under aerobic conditions in diverse temperature and relative humidity conditions. The freshly produced cryogels (i.e. after 40 h of freeze-drying) were stored in hermetically sealed boxes over either P2O5 or different saturated salt solutions of LiCl, $CH_3CO_2K$, $Mg(NO_3)_2$, $MgCl_2$, and NaCl with respective relative humidities of 11%, 23%, 33%, 54%, and 75% at 20 °C, giving a water activity ($a_w$) of 0.01 × %RH (Shrestha et al., 2007). The water activity of cryogels, conditioned under various relative humidity conditions, was measured with a HygroPalm23-aw portable water activity meter (Rotronic, Bassersdorf, Switzerland) at 20 °C. The impact of water activity on LGG TVC was evaluated under an incubation temperature of 20 ± 0.5 °C over a span of 60 days. Additionally, the influence of temperature on LGG viability was examined at 5, 20, and 37 °C, maintaining a consistent water activity of $a_w$ = 0.11. The LGG inactivation data was fitted to a first-order kinetic reaction, as outlined in Soukoulis et al., (2016). To this end, the following equation was considered:

Equation 36 $$\log N_t = \log N_0 - k_T t$$

where: $N_0$, is the number of viable bacteria in the fresh cryogel (t = 0 day), $N_t$ the number of viable bacteria after a specific storage time, t is the storage time, and $k_T$ is the inactivation rate constant ($day^{-1}$) at a temperature T. The shelf-life was calculated using Equation 36 as the time required to reach 6 $logCFU.g^{-1}$.

## *In vitro* digestion

### i. *In vitro* digestion protocol

*In vitro* digestion of the milk protein-based cryogels was carried out following the harmonised INFOGEST v2.0 protocol (Brodkorb et al., 2019). To emphasise the relevance of the cryogels as a potential probiotic delivery system, the digestion was carried out on stored systems (60 days, 5 °C, $a_w$ = 0.11). The food matrix consisted of a cryogel monolith of 400 mg mixed with 4.6 mL of Milli-Q water in an Erlenmeyer flask. The food matrix was subsequently diluted at a ratio of 1:1 with the oral fluids containing α-amylase (75 U $mL^{-1}$ final concentration, Sigma-Aldrich, cat. no. A4551) and incubated in a shaking water bath (37 ± 0.1 °C, 3 min, $f$ = 100 $min^{-1}$, Julabo SW22, Seelbach, Germany). Then, the gastric phase was initiated by diluting the system two-fold with gastric fluids containing pepsin (2000 U $mL^{-1}$ final concentration, Sigma-Aldrich, cat. no. P7000) and gastric lipase (60 U $mL^{-1}$ final concentration, Sigma-Aldrich, cat. no. 80612). The pH was adjusted to 2 using HCl 5 M and the samples were incubated at 37

± 0.1 °C for 120 min. Finally, the gastric chyme was diluted two-fold with pre-warmed intestinal fluids containing pancreatin (100 U $mL^{-1}$ final concentration, Sigma-Aldrich, cat. no. P1750) and the pH was increased to 7 using NaOH 1 M and the solutions were incubated at 37 ± 0.1 °C for 120 min.

The TVC were quantified in the cryogels before the start of the digestion (food matrix) and at the end of the gastric and intestinal phase. To elucidate the effect of the embedment of LGG cells within the cryogel structure, an additional experiment was conducted based on the digestion of a free LGG bacterial suspension (i.e. 4.6 mL to obtain a final LGG concentration equivalent to that of the cryogels approx. 10 log$CFU.g^{-1}$) in the presence and absence of the LGG-free cryogel matrix (approx. 400 mg).

ii. Microscopical assessment of the digesta

The assessment of the microstructural aspects and the viability of LGG cells in the gastric and intestinal phases was carried out using a Confocal Laser Scanning Microscopy (CLSM) microscope (LSM 880, Zeiss, Jena, Germany). One millilitre of the digesta was stained using 10 µL of protein stain (Fast Green, $\lambda_{Ex}$ = 633 nm, $\lambda_{Em}$ = 635–680 nm), 1.5 µL of stain for live (SYTO9, $\lambda_{Ex}$ = 488 nm, $\lambda_{Em}$ = 498–550 nm) and 1.5 µL of stain for dead (propidium iodide, $\lambda_{Ex}$ = 488 nm, $\lambda_{Em}$ = 585–640 nm) bacteria (LIVE/DEAD BacLight, Thermo Fisher Scientific, Waltham, MA, United States). The samples were homogenised using a benchtop vortex and 300 µL were transferred into eight-chambered microscope slides (Nunc Lab-Tek II, Thermo Fisher Scientific, Waltham, MA, United States) and directly analysed. The images were collected using a × 40 objective lens. In addition, semi-quantitative analysis of the protein particle size (maximum Feret's diameter) was conducted using imageJ based on at least 5 images for each system.

iii. Proteolysis analyses

The degree of the protein hydrolysis (DH) was assessed at the end of each digestive phase as described in Hellebois, Gaiani, & Soukoulis, (2022b) using the OPA method (i.e. free $-NH_2$ group quantification).

Capillary SDS-PAGE was used to investigate the peptide cleavage of the protein before and after fermentation, and at the end of the gastric and intestinal phases. The SDS-PAGE was carried out using a Bioanalyzer 2100 and Protein 80 chip kit (Agilent Technologies, Santa Clara, CA, United States) following the manufacturer's instructions. The gel was reconstructed using 2100 Expert software (Agilent Technologies, Santa Clara, CA, United States).

To determine the production of peptides from the milk proteins throughout the digestion, 10 mL aliquots of homogeneous gastric and intestinal chymes prepared in duplicate, were centrifuge-filtered using Amicon tubes (Merck, Darmstadt, Germany) equipped with a filter cut-off of 10 kDa. Then, two technical replicates of 1 mL filtrates obtained from each replicate were vacuum-dried (CentriVap, Labconco, Kansas City, MO, United States) prior to performing the nano-liquid chromatography – mass spectrometry (nano-LC-MS) analyses. All replicates were solubilised and diluted with a 0.1% vol. formic acid (FA) solution. Peptide separation was performed on a NanoLC-425 Eksigent system coupled with a TripleTOF 6600+ mass spectrometer (SCIEX, Darmstadt, Germany) as previously described (Ribeiro et al., 2020). The 30 most intense ions were selected to perform fragmentation in high sensitivity mode using the automatically adjusted system of rolling collision energy. The data acquired were converted and submitted to the Mascot search engine (Matrix science, London, UK) for peptide identification. The searches were restricted to the cow milk protein database in UniprotKB (released on 27 October 2022; 25,681 sequences) using the Mascot Daemon interface (version 2.6.0. Matrix Science, London, UK). For all research, the parameters were as follows: a mass tolerance value of 10 ppm for the precursor, 0.02 Da for the fragment ions; no proteolytic cleavage specificity; no missed cleavages; no static modifications; Met oxidation, pyroglutamic acid at the N-*term* Gln, and Ser/Thr phosphorylation as variable modifications. To eliminate false positives, peptide spectrum matches (PSMs) were filtered using the target decoy database with a false discovery rate (FDR) at a peptide level of 1%, corresponding to a 99% confidence score. In Mascot settings, as matches are usually random to very short peptides, a minimal peptide length was kept to a minimum of 7 amino acids. The MSMS spectra of the two technical replicates were merged into a single search. Data analysis and handling was further computed. Only the proteins identified with a significant Mascot-calculated confidence of 95%, a minimum of two peptides with at least one unique one per protein and a protein and peptide score ≥ 50 were retained.

The Venn diagram representation was constructed using the significant peptide sequences (score ≥ 50) in the gastric and intestinal digesta using OriginLab 2019b. The potential bioactivities of the detected peptide sequences were compared to the Milk Bioactive Peptide Database (Nielsen et al., 2017, http://mbpdb.nws.oregonstate.edu/). The proteomics data were deposited in the ProteomeXchange Consortium via the PRIDE partner (Deutsch et al., 2020; Perez-Riverol et al., 2022) repository. Data are available via ProteomeXchange with identifier PXD040551.

### Statistical analyses

To determine the significance differences among the samples, one-way ANOVA was performed and Tukey's post-hoc means comparison test was used to differentiate the values. In addition, the correlations among the properties were determined using Pearson's correlation coefficient. All statistical analyses were performed using Origin 2019b software (OriginLab Inc, Northampton, MA, United States) and the significant differences were established at $p < 0.05$.

## RESULTS & DISCUSSION

### Viability of the *Lacticaseibacillus rhamnosus* GG during freeze-drying

As detailed in Hellebois et al., (2023), the hydrogel precursor systems were prepared via the indirect acidification (lactic acid fermentation) of milk protein aqueous solutions containing glucose as the primary energy source, trehalose as the cryoprotectant and glycerol as the plasticising cytoprotectant. In most cases, the cryogenic processing parameters should be compromised to allow the vitrification of the freeze-concentrated (serum) phase and prevent the loss of the membrane integrity due to intracellular ice formation (Aschenbrenner, Först, et al., 2015).

On the completion of the freeze-drying process, the obtained cryogels were characterised by a residual water content of 4–4.6% wt. (Hellebois et al., 2023), which is in the range of acceptable limits of bound water in anhydrobiotic formulations (Aschenbrenner, Först, et al., 2015). As illustrated in Figure 62, neither the fermentation nor the freeze-drying had a significant effect on the TVC of LGG. In general, the TVC of LGG were in the ranges of 9.9–10.1, 9.9–10.3, and 9.6–10 $\log CFU.g^{-1}$ for the inoculated milk protein solutions and the hydrogels and cryogels obtained, respectively. The survivability of LGG achieved following freeze-drying (i.e. 42–96%) was similar or higher to that reported in conventional freeze-dried systems containing milk proteins (Pehkonen et al., 2008; D. Y. Ying et al., 2010). It is worth noting that the NaCN to WPI mass fraction ($m_{NaCN/WPI}$) did not play any significant role in regard to the TVC of LGG. In addition to their strain and species' dependency, the viability of the probiotics throughout the dehydration process is governed by the compositional profile of the engrafting medium and the cryogenic processing conditions (Santivarangkna et al., 2008). As seen in the representative freezing curve of the hydrogels (Figure 63), a rapid freezing (ca. 4.2 °C $min^{-1}$) accompanied with a restricted extent of supercooling was achieved. Hence, it is presumed that the

preservation of the LGG cells during freeze-drying is associated with the prevention of intracellular ice formation during the cryogenic processing of the hydrogel precursors.

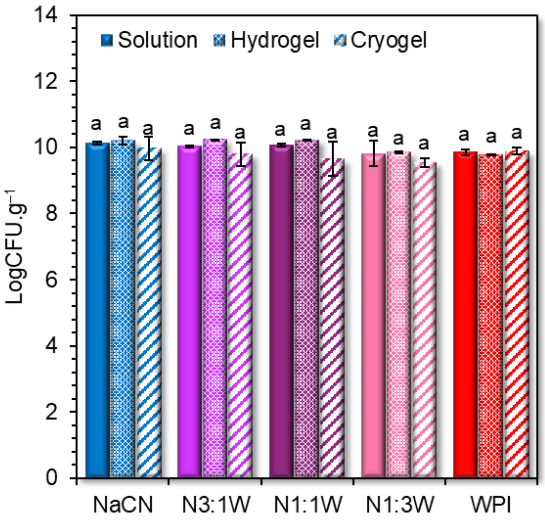


*Figure 62: Total viable counts of LGG (expressed on a dry basis, n = 3) after inoculation of the protein solution (plain bars), following 4 h of fermentation at 37 °C (dotted bars) and 40 h of freeze-drying (dashed bars). [a]No significant differences in the TVC were detected among the samples. NaCN: Sodium Caseinate, WPI: Whey Protein Isolate, N3:1W to N1:3W denote mixed protein systems of varying NaCN:WPI ratio (3:1 to 1:3).*

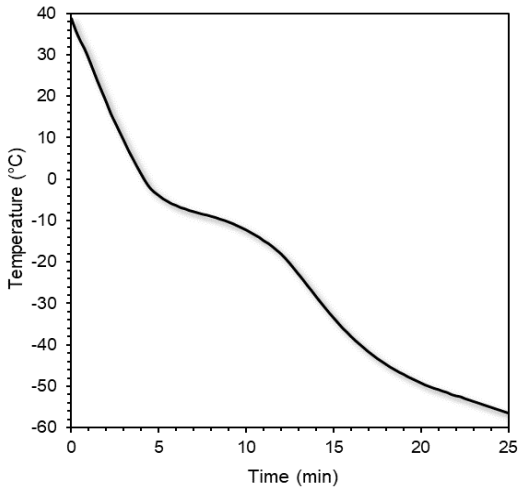


*Figure 63: Representative freezing curve of the milk protein hydrogel precursors. No significant differences in the pattern and the calculated freezing rates were detected among samples.*

To assess their physical state under the cryogenic conditions tested, the hydrogels underwent DSC analysis at a freezing rate of 5 °C $min^{-1}$ and an isothermal hold at −140 °C for 20 min to allow maximal ice formation (data not shown). The glass transition region ($T_g$) of the initial milk protein solutions (non-fermented) and the fermented hydrogel precursor systems was estimated at −36 to −34 °C, which confirms the achievement of a vitreous physical state for the entity of the cryogel precursors during the cryogenic processing. This may partially explain the limited TVC loss during the freeze-drying step (Pehkonen et al., 2008). It should be noted that neither the milk protein composition nor the physical state (i.e. solution vs acid gel) impacted the $T_g$ values of the cryogel precursor systems. On the other hand, the acid-induced milk protein hydrogels exerted significantly lower ice fusion (melting) points (i.e. $T_m$ = −3.2 to −2.8 °C) than their non-fermented counterparts ($T_m$ = −2.3 to −1.8 °C), which may be ascribed to the formation of secondary metabolites, e.g. organic acids such as lactic acid, at the expense of the mono- and disaccharides inducing the suppression of the freezing point of the hydrogel systems.

## Storage stability of *Lacticaseibacillus rhamnosus* GG

The probiotic cryogels obtained were stored for 60 days under diverse temperature (T = 5, 20 and 37 °C) and water activity ($a_w$ = 0, 0.11, 0.23, 0.33, 0.54 and 0.75) conditions (Figure 64 and Figure 65). As expected, the higher the storage temperature, the greater the LGG TVC losses throughout static storage. The LGG inactivation rates ranged from 0.002 to 0.008, 0.032 to 0.061 and 0.25 to 0.56 $day^{-1}$, for 5, 20 and 37 °C, respectively (Figure 64D). The temperature-weighted effect of the $m_{NaCN/WPI}$ on the lethality of LGG during isothermal storage was more pronounced in the systems kept at 37 °C. As a general trend, the WPI-based cryogels exerted the poorest LGG cell protective performance. Nonetheless, the mixed protein-based cryogels hampered the inactivation of the bacterial cells, particularly at 37 °C. The $k_{37°C}$ values were well-correlated ($p < 0.05$) with the cryogel porosity and degree of shrinkage (r = 0.69 and −0.82, respectively) and hence, the mixed protein-based cryogels were able to preserve the biological activity of LGG due to their lower permeability to gases (e.g. water vapour and oxygen).

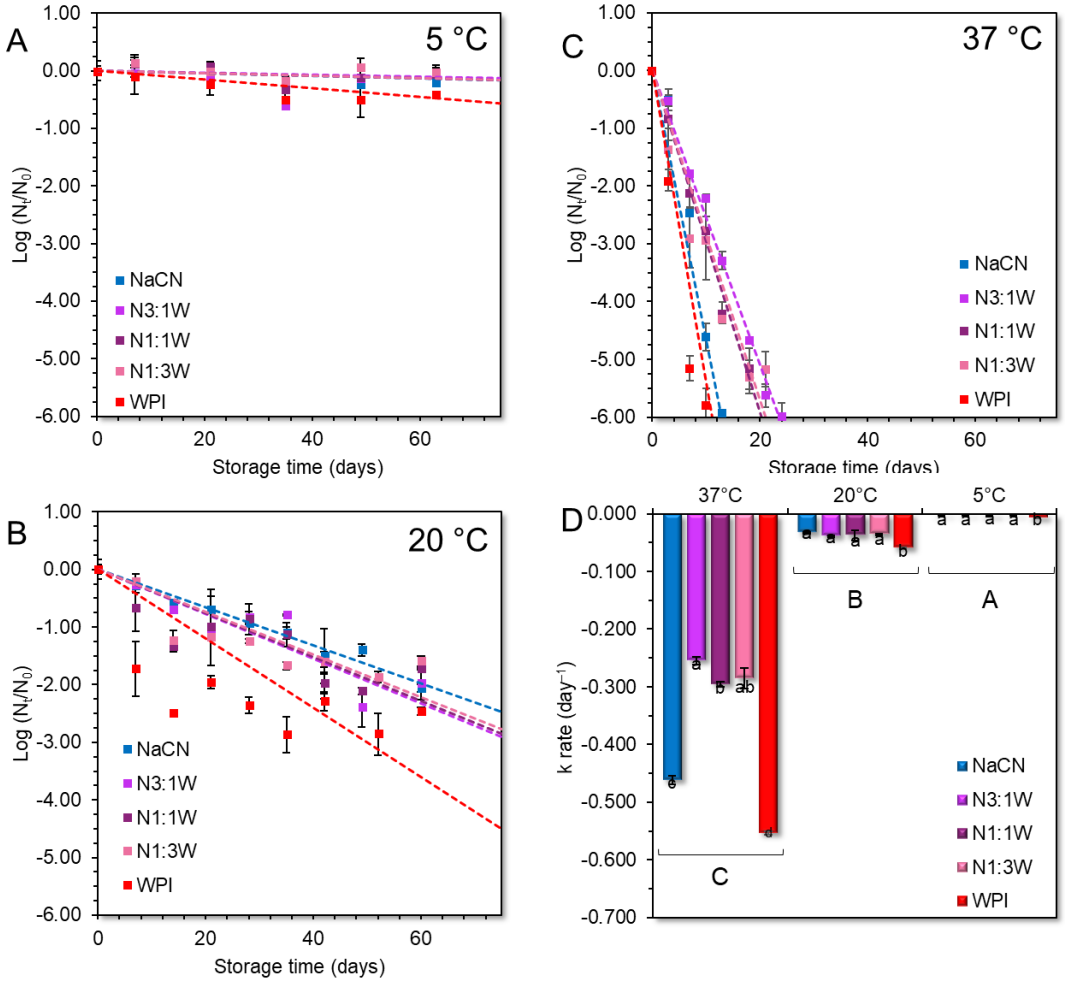


*Figure 64: Inactivation curves of LGG embedded in the milk protein cryogels while being stored at 5 (A), 20 (B) and 37 °C (C) under controlled water activity atmosphere ($a_w$ = 0.11) and their respective inactivation rates (k).* $^{a\text{-}c,A\text{-}C}$ *Different letters between the cryogels (lowercase) and temperature (uppercase) denote a significant difference ($p < 0.05$) according to Tukey's post-hoc means comparison test. Abbreviations used: $N_0$, LGG CFU counts at $t_{storage}$ = 0 day, $N_t$, LGG CFU counts at $t_{storage}$ = t days. NaCN: Sodium Caseinate, WPI: Whey Protein Isolate, N3:1W to N1:3W denote mixed protein systems of varying NaCN:WPI ratio (3:1 to 1:3).*

A satisfactory obedience of the LGG inactivation rate values to the Arrhenius kinetics (Equation 37) was found:

Equation 37 $$\ln k = \ln k_{ref} - \frac{E_a}{R}\left(\frac{1}{T} - \frac{1}{T_{ref}}\right)$$

where k, $k_{ref}$ are the inactivation rates of the LGG at T (in °K) and $T_{ref}$ = 298 K, $E_a$ is the activation energy (in kJ mol$^{-1}$) and R is the universal gas constant (R = 8.314 J mol$^{-1}$ K$^{-1}$). As seen in Table 17, the $E_a$ values ranged from 74 to 121 kJ mol$^{-1}$, which are in line with those reported in the literature. (Adamberg et al., 2003). These values were higher than other *Lactobacillus* strains such as *L. acidophilus* with $E_a$ values of about 32 to 48 kJ mol$^{-1}$ (Adamberg et al., 2003; Soukoulis, Behboudi-Jobbehdar, et al., 2014),

demonstrating the thermal resilience of the LGG cells. It can be noted that an adverse dependence of the $E_a$ values on the $m_{NaCN/WPI}$ ($r = -0.81$, $p < 0.05$) was found. Therefore, the presence of NaCN in the cryogels rendered the inactivation of LGG cells thermodynamically unfavourable under the tested static storage conditions.

As a next step, the impact of the equilibrium relative humidity on the inactivation kinetics of the LGG cells during static storage at 20 °C was assessed. As seen in Figure 65, the inactivation rates of the LGG cells remained almost unaltered at $a_w \leq 0.33$. At higher $a_w$, the inactivation rates of LGG increased proportionally to the equilibrium relative humidity increase. Moreover, the impact of $m_{NaCN/WPI}$ on the inactivation kinetics of LGG became more pronounced in the systems stored at $a_w \geq 0.54$, with the individual protein-based cryogels experiencing the highest cellular lethality, i.e. approx. 3 to 10-fold and 3 to 6-fold for NaCN and WPI, respectively.

*Table 17: Activation energy of Arrhenius-fitted LGG inactivation curves.*

| Sample | $E_a$ ($kJ.mol^{-1}$) | $R^2$ - |
|---|---|---|
| NaCN | $120.0 \pm 4.9^b$ | 0.999 |
| N3:1W | $112.3 \pm 2.6^b$ | 0.981 |
| N1:1W | $98.9 \pm 3.3^a$ | 0.998 |
| N1:3W | $109.9 \pm 4.0^b$ | 0.992 |
| WPI | $96.7 \pm 2.4^a$ | 0.999 |

*[a-b]Different letters between the cryogels denote a significant difference ($p < 0.05$) among the cryogels according to Tukey's post hoc means comparison test. NaCN: Sodium Caseinate, WPI: Whey Protein Isolate, N3:1W to N1:3W denote mixed protein systems of varying NaCN:WPI ratio (3:1 to 1:3).*

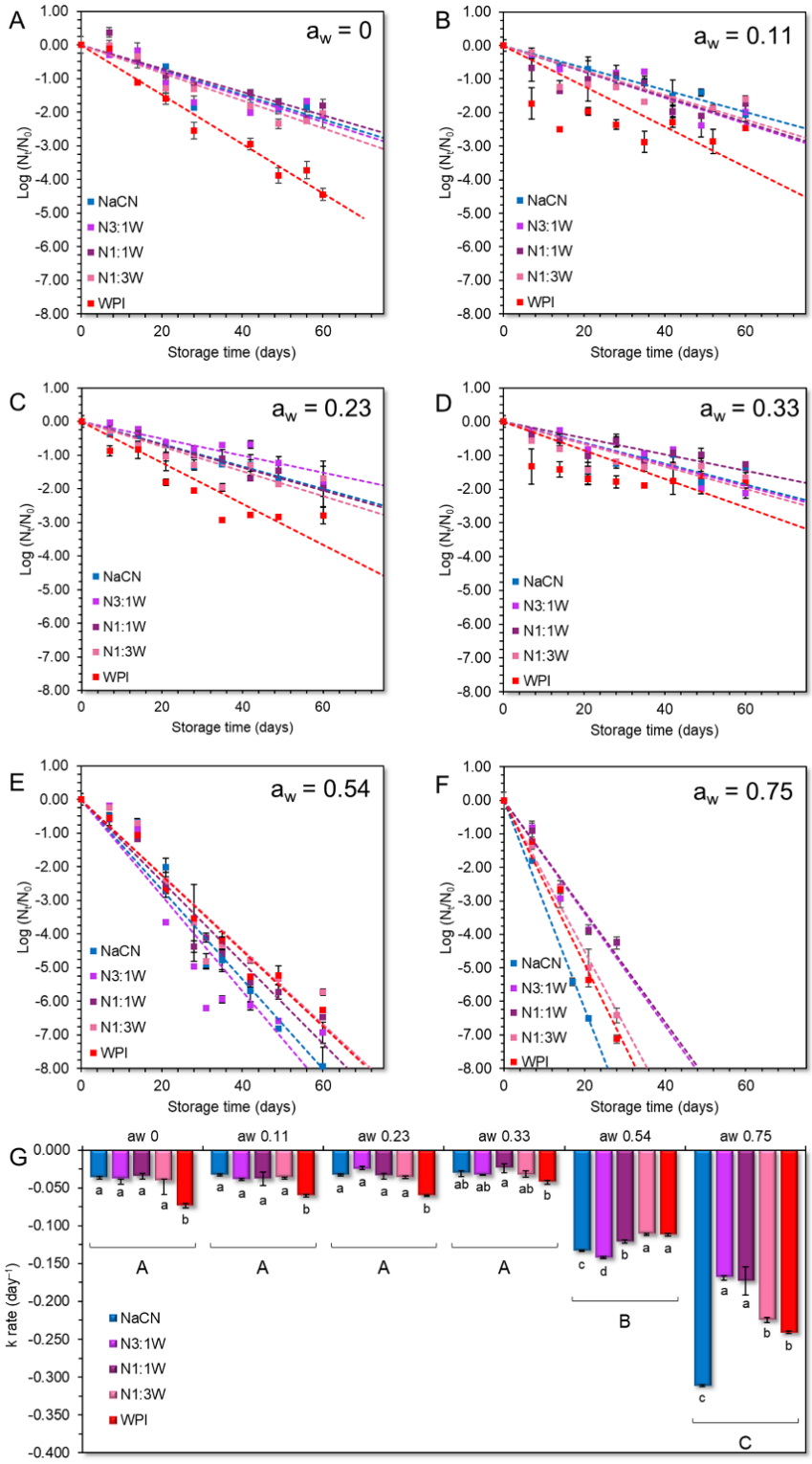


*Figure 65: Inactivation curves of LGG embedded in milk protein cryogels while being stored at 20 °C under different water activity atmospheres 0–0.75 (A–F) and their respective inactivation (k) rates (G).* $^{a\text{-}d,A\text{-}C}$ *Different letters between water activities (uppercase) and the cryogels for the same water activity (lowercase) denote a significant difference ($p < 0.05$) according to Tukey's post hoc means comparison test. Abbreviations used: $N_0$, LGG CFU counts at $t_{storage}$ = 0 day, $N_t$, LGG CFU counts at $t_{storage}$ = t days. NaCN: Sodium Caseinate, WPI: Whey Protein Isolate, N3:1W to N1:3W denote mixed protein systems of varying NaCN:WPI ratio (3:1 to 1:3).*

The preservation of the biological activity of probiotics is inextricably associated with the inherent physicochemical characteristics of the engrafting xero-carrier such as its microstructure, biocompatibility, cell adhesion properties, pH and ionic strength, oxygen content and redox potential (Dos Santos Morais et al., 2022; Rodrigues et al., 2020; Tripathi & Giri, 2014). In addition to these properties, the structural collapse of the engrafting template, due to physical state transitions (i.e. glassy to rubbery) stemming from temperature fluctuations or moisture uptake during storage, may also lead to a substantial reduction of the probiotic cell viability. The theoretical glass transition ($T_g'$) values of the cryogels stored under different relative humidity conditions were calculated according to the Kouchman-Karasz equation (Equation 38) as follows:

Equation 38

$$T_g' = \frac{m_{NaCN}\Delta C_{p,NaCN}T_{g,NaCN}+m_{WPI}\Delta C_{p,WPI}T_{g,WPI}+m_T\Delta C_{p,T}T_{g,T}+m_G\Delta C_{p,G}T_{g,G}+m_{GL}\Delta C_{p,GL}T_{g,GL}+m_W\Delta C_{p,W}T_{g,W}}{m_{NaCN}\Delta C_{p,NaCN}+m_{WPI}\Delta C_{p,WPI}+m_T\Delta C_{p,T}+mw_G\Delta C_{p,G}+m_{GL}\Delta C_{p,GL}+m_W\Delta C_{p,W}}$$

where: $m_i$, $\Delta C_{p,i}$ and $T_{g,i}$ denote the mass fraction, specific heat capacity (in J $g^{-1}$ $K^{-1}$) and glass transition temperature (in K) of the cryogel components (Table 18). The $T_g'$ of amorphous materials is strongly dependent on the presence and amount of plasticising agents (water and glycerol in the present work). As illustrated in Figure 66A, the $T_g'$ values calculated varied from –69 to 50 °C, showing an increase proportional to the $m_{NaCN/WPI}$ increase. Contrary to conventional anhydrobiotics (e.g. spray-dried of freeze-dried powders), which are able to remain in the glassy state at $a_w$ as high as 0.3–0.4 (Pehkonen et al., 2008; Shrestha et al., 2007), the cryogels tested underwent physical state transitions at $a_w \leq 0.23$ depending on their milk protein composition. To evaluate the impact the physical state of the cryogels, the inactivation rates of LGG were plotted against the temperature interval $\Delta T = T - T_g'$ (Figure 66B). The vertical dashed line denotes the boundary between the glassy ($\Delta T < 0$) and rubbery state ($\Delta T > 0$).

*Table 18: Glass transition ($T_g$) and change in heat capacity ($\Delta Cp$) of the pure compounds used to produce the cryogels.*

| compound | $T_g$ (°K) | $\Delta C_p$ (J $g^{-1}$ $K^{-1}$) | Reference |
|---|---|---|---|
| Glucose | 309 | 0.63 | (Roos, 1995, p. 5) |
| Trehalose | 380 | 0.55 | (Roos, 1995, p. 5) |
| WPI | 400 | 0.26 | (Schuck et al., 2005) |
| NaCN | 405 | 0.09 | (Schuck et al., 2005) |
| Glycerol | 190 | 1.25 | (Soukoulis et al., 2017) |
| Water | 134 | 1.94 | (Sugisaki et al., 1968) |

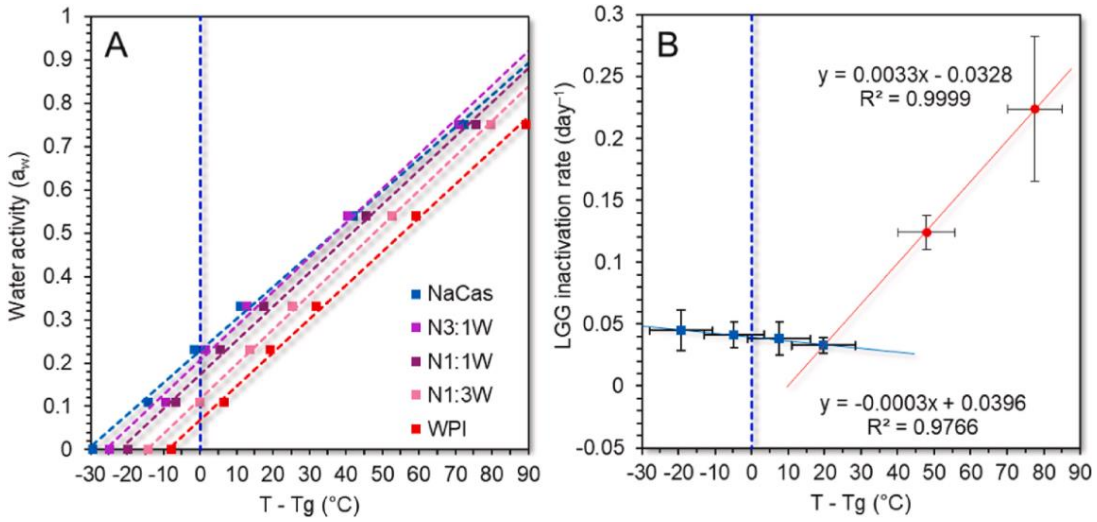


*Figure 66: Effect of the water activity on the glass transition temperature of the milk protein cryogels (A) and LGG inactivation rates as influenced by the vitreous to rubbery phase transition (B) using the $T_g'$ values based on the Kouchman-Karasz equation. NaCN: Sodium Caseinate, WPI: Whey Protein Isolate, N3:1W to N1:3W denote mixed protein systems of varying NaCN:WPI ratio (3:1 to 1:3).*

According to Figure 66B, the inactivation of LGG was described by two linear master curves corresponding to the low (i.e. $a_w \leq 0.33$) and intermediate to high $a_w$ regions (i.e. $a_w \geq 0.33$). Although previous studies have demonstrated the significant increase in the inactivation rates of Lactobacilli at $T > T_g'$ (Aschenbrenner et al., 2012), the xero-scaffolds tested adequately preserved the biological activity of LGG in low relative humidity conditions where the glassy state (Arrhenius) kinetics were not obeyed. Interestingly, at $a_w \leq 0.33$, the inactivation rates of LGG decreased adversely to the water activity, reaching their highest absolute value in zero relative humidity conditions. Nevertheless, these inactivation rates were remarkably lower (almost 10-fold) than those achieved at $a_w > 0.33$. In general, the storage-induced cellular lethality can be substantially restricted in glassy embedding matrices due to the limited translational mobility of small molecules (e.g. sugars or plasticising agents), which can result in detrimental leakage effects stemming from changes in the physical state (i.e. liquid crystalline to gel) and structure conformation of the cell membranes (Aschenbrenner et al., 2012). Nonetheless, the cellular inactivation in glassy matrices cannot be completely hindered, except for processing or storage conditions that achieve an intracellular glassy state (Aschenbrenner et al., 2012). Although it is quite challenging to identify the exact mechanisms involved in the inactivation of LGG in the low-moisture cryogels, it is assumed that the increasing cell lethality and concurrent decrease of $a_w$, is associated with: a) the favouring of the membrane lipid bilayer oxidation at very low $a_w$ (< 0.2), and b) the loss of the cell membrane integrity due to the extensive dehydration of the cytosol

(particularly in extremely dry conditions i.e. $a_w \cong 0$) (Dianawati et al., 2016; Vesterlund et al., 2012). On the other hand, in conditions relatively close to the $T_g'$ ($-30 < \Delta T < 0$), the inactivation rates remained notably low, regardless of the rubbery character of the engrafting matrix. A similar behaviour was reported by Aschenbrenner et al., (2012) in sugar (trehalose and lactose) and polysaccharide (dextran) matrices embedding *L. paracasei*. At higher $a_w$ (> 0.33), the inactivation rates exhibited a steep increase, which implies that in conditions far from the glass transition, the bacterial cell lethality is most probably driven by a diffusional limitation mechanism.

*Table 19: Temperature effect on the cryogel estimated shelf-life (in days).*

| Temperature | 37 °C | 20 °C | 5 °C |
|---|---|---|---|
| NaCN | $9 \pm 0^{a}$ | $120 \pm 5^{b}$ | $1844 \pm 430^{bc}$ |
| N3:1W | $15 \pm 0^{c}$ | $98 \pm 3^{ab}$ | $2233 \pm 195^{c}$ |
| N1:1W | $12 \pm 0^{b}$ | $98 \pm 22^{ab}$ | $1023 \pm 166^{ab}$ |
| N1:3W | $12 \pm 1^{b}$ | $96 \pm 4^{ab}$ | $1697 \pm 402^{bc}$ |
| WPI | $7 \pm 0^{a}$ | $65 \pm 2^{a}$ | $528 \pm 60^{a}$ |

*$^{a-c}$Different letters between the cryogels denote a significant difference ($p < 0.05$) among the cryogels for the same temperature according to Tukey's post hoc means comparison test. The effect of the temperature was significant for all the cryogels tested. The shelf-life was estimated as the maximum storage time with LGG counts of at least 6 log CFU.g$^{-1}$. NaCN: Sodium Caseinate, WPI: Whey Protein Isolate, N3:1W to N1:3W denote mixed protein systems of varying NaCN:WPI ratio (3:1 to 1:3).*

To gain insight into the shelf-life of the probiotic cryogels, the time required for reaching the minimum total viable counts of probiotic bacteria in functional foods according to FAO/WHO, (2002) recommendations (i.e. 6 logCFU.g$^{-1}$) was calculated (Table 19 and Table 20). As expected, the storage temperature was the limiting factor of the shelf-life of the probiotic cryogels (Table 19). The estimated shelf-life of the LGG conveying cryogels stored in chilling conditions was approx. 4 years, steeply declining to 95 and 11 days when stored at 20 and 37 °C, respectively. On the other hand, no significant changes were detected in the shelf-life (i.e. 90 to 119 days) of the probiotic cryogels stored at $a_w \leq 0.33$ and at ambient temperatures. In intermediate $a_w$ (0.55 to 0.74) conditions, the shelf-life was shortened on average to 31 and 18 days, respectively. Our findings support the feasibility of the cryogels as alternative scaffolds for engrafting probiotic cells, particularly when they are stored under controlled temperature and $a_w$ conditions.

*Table 20: Effect of water activity (0–0.75) on the cryogels' estimated shelf-life (in days).*

| Water activity | 0 | 0.11 | 0.23 | 0.33 | 0.54 | 0.75 |
|---|---|---|---|---|---|---|
| NaCN | 108 ± 5$^{b}$ | 120 ± 5$^{b}$ | 119 ± 4$^{bc}$ | 128 ± 15$^{a}$ | 30 ± 0$^{b}$ | 13 ± 0$^{a}$ |
| N3:1W | 99 ± 0$^{b}$ | 98 ± 3$^{ab}$ | 152 ± 26$^{c}$ | 115 ± 2$^{a}$ | 27 ± 0$^{a}$ | 23 ± 0$^{b}$ |
| N1:1W | 105 ± 11$^{b}$ | 98 ± 22$^{ab}$ | 106 ± 12$^{abc}$ | 155 ± 37$^{a}$ | 30± 0$^{b}$ | 21 ± 2$^{b}$ |
| N1:3W | 87 ± 4$^{b}$ | 96 ± 4$^{ab}$ | 96 ± 9$^{ab}$ | 107 ± 19$^{a}$ | 32 ± 0$^{c}$ | 16 ± 0$^{a}$ |
| WPI | 53 ± 2$^{a}$ | 65 ± 2$^{a}$ | 64 ±1$^{a}$ | 92 ± 5$^{a}$ | 35 ± 1$^{d}$ | 16 ± 0$^{a}$ |

*$^{a-d}$Different letters between the cryogels denote a significant difference ($p < 0.05$) among them for the same water activity according to Tukey's post hoc means comparison test. The shelf-life was estimated as the maximum storage time with LGG counts of at least 6 logCFU.g$^{-1}$. NaCN: Sodium Caseinate, WPI: Whey Protein Isolate, N3:1W to N1:3W denote mixed protein systems of varying NaCN:WPI ratio (3:1 to 1:3).*

## Viability of *Lacticaseibacillus rhamnosus* GG throughout *in vitro* digestion

Colloidal templates purposed for the oral administration of probiotics should meet several techno-functional criteria to ensure the maximal viability and controlled release of the living bacterial cells throughout oro-gastrointestinal transit (Jiang et al., 2022). Depending on the targeting release point of the upper gastrointestinal tract, additional parameters must be assiduously considered, such as the oral processability and swallowability of the delivery system as well as its colloidal responsiveness (e.g. matrix disintegration, acid or pepsin-induced gelation) upon exposure to the buccal and gastrointestinal fluid environment (e.g. pH, ionic strength, presence of bile salts and pancreatic enzymes) (Yao et al., 2020). In addition, the release of non-digestible and non-bioaccessible constituents that stimulate the growth of probiotics is also a desirable functional property of the conveying matrix, ensuring satisfactory gut colonisation and balanced microbiota diversity (Yao et al., 2020).

The LGG embedding cryogels underwent static *in vitro* digestion using the INFOGEST 2.0 protocol. For simplicity reasons, the oral phases were prepared by mixing the prewarmed artificial saliva with the cryogel matrices without any mechanical crushing prior to or during oral processing. No significant differences in the TVC values (data not shown) of the initial (dry) cryogels and the obtained oral boluses were found, which is most probably associated with the mild character of the artificial saliva and the short exposure time to the oral fluids, thus restricting the swelling and disintegration of the embedding cryogel matrix. The ability of *L. rhamnosus* strains to survive in artificial and human saliva media for an extended time (> 24 h) has previously been reported (Haukioja

et al., 2006).

The food boluses obtained were successively mixed with the gastric fluids and acidified at pH = 2.5, within the optimum region for peptic cleaving activity (Kondjoyan et al., 2015). At the end of the gastric processing, there was limited disintegration of the mixed protein-based cryogels, whilst a more progressed matrix disintegration was detected macroscopically for NaCN and WPI (Figure 67).

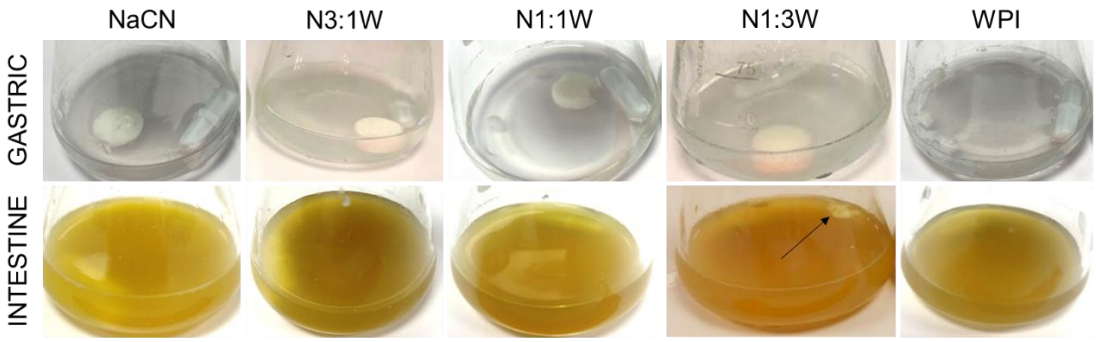


*Figure 67: Macroscopic appearance of the chymes of the digested cryogel at the end of the gastric and intestinal phase.*

Following the removal of the residual intact cryogel matrix, the CLSM-assisted assessment of the end gastric chymes confirmed their highly polydisperse suspension-like character. As illustrated in the CLSM images (Figure 67), the mean size of the cryogel microparticles was influenced by their protein composition (i.e. the maximum Feret's diameters were in the range of 4–37 µm and 9–204 µm for NaCN- and WPI-based cryogels, respectively). This could be associated with the inherent gastric digestibility of the whey proteins and caseins (Dupont & Tomé, 2020), as well as with the structural and mechanical aspects of the hydrogel precursors and cryogels obtained. For example, Guerin et al., (2017) demonstrated that the gastric-induced disintegration of spray-dried particulates produced from elastic and firm milk gels was remarkably reduced compared to their soft and loose structured counterparts. In the present study, it was not possible to identify clear interrelationships between the gastric-induced matrix disintegration and the mechanical and microstructural aspects of the cryogels. However, the prevalence of β-sheet structures was adversely associated with the extent of the cryogel disintegration during gastric step, which is in line with the observations of Zhou et al., (2019).

Admixing the gastric chymes with the simulating intestinal fluids led to a complete disintegration of the residual intact cryogels, except for the N1:3W systems (Figure 67). On the other hand, the CLSM analysis revealed the presence of non-digested cryogel microparticles in the intestinal chymes. It is worth noting that the matrix disintegration degree in the intestinal chymes was more advanced for the single protein cryogels (Figure

68B). A positive correlation between the maximum Feret's diameter of the particles, and the cryogel porosity and bulk density was found. This suggests that the pancreases-induced microparticle disintegration was mechanistically diffusion-driven.

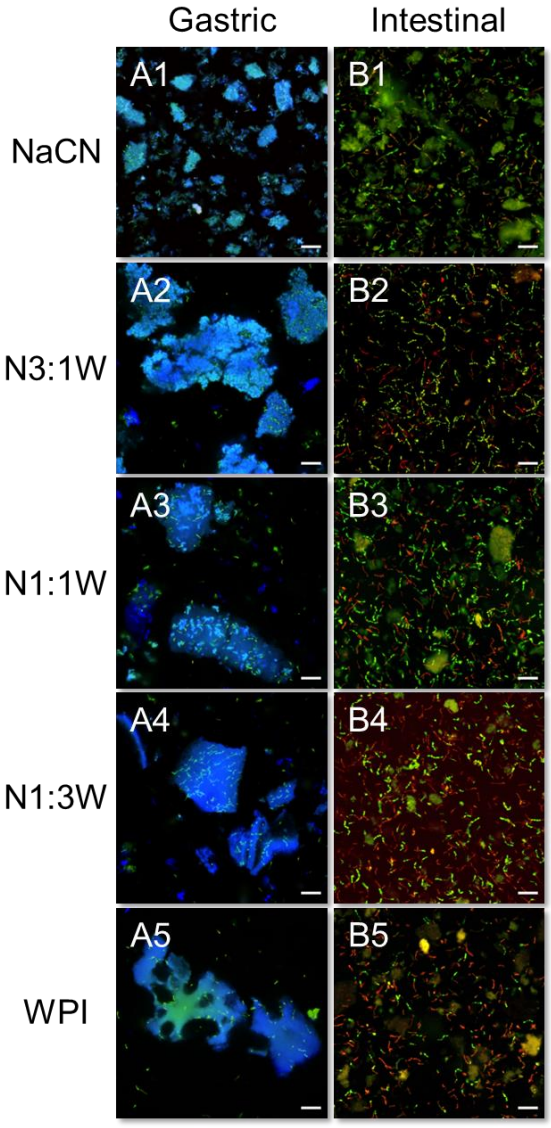


*Figure 68: CLSM micrographs after 120 min of gastric digestion (A) and 120 min of intestinal digestion (B) of the NaCN (1), WPI (5) and hybrid protein (2 –5) cryogels. Proteins are stained in blue (Fast green, $\lambda_{Ex}$ = 633 nm, $\lambda_{Em}$ = 635–680 nm), viable bacteria in green (Syto9, $\lambda_{Ex}$ = 488 nm, $\lambda_{Em}$ = 498–550 nm) and inactivated bacteria in red (propidium iodide, $\lambda_{Ex}$ = 488 nm, $\lambda_{Em}$ = 585–640 nm). NaCN: Sodium Caseinate, WPI: Whey Protein Isolate, N3:1W to N1:3W denote mixed protein systems of varying NaCN:WPI ratio (3:1 to 1:3). Scale bar: 20 µm.*

To gain a satisfactory overview of the protective role of the conveying cryogel matrix, suspensions containing free LGG cells in the absence and presence of a cryogel matrix, obtained from the cryogenic processing and freeze-drying of a direct-acidified (i.e. δ-gluconolactone-induced) hydrogel precursor, were also subjected to *in vitro* digestion. As shown in Figure 69, the free LGG cells experienced an approx. 2.8 $\log CFU.g^{-1}$ loss

throughout gastric processing, which is in conformity with previous literature findings (Soukoulis, Yonekura, et al., 2014). The encapsulation of the LGG cells in the cryogel matrices resulted in a substantial enhancement of their ability to counteract the lethal effects of the harsh gastric conditions with the reduction in TVC values ranging from 0 to 0.5 logCFU.g$^{-1}$. Except for the N1:3W cryogel system, no significant differences were detected in the cytoprotective performance of the cryogels during gastric processing. Interestingly, there was a remarkable loss in the TVC of LGG (i.e. 0.5 to 2.4 logCFU.g$^{-1}$) in the gastric chymes obtained from the free LGG cells + cryogel matrix suspensions, which confirms the cytoprotective role of the natural embedment (via fermentation) of the LGG cells into the cryogel matrix. As illustrated in the CLSM micrographs (Figure 68A), all cryogel systems were partially disintegrated into irregular particles embedding the living LGG cells. Guerin et al., (2017) demonstrated that the presence of whey proteins in milk protein spray-dried microcapsules promoted the internal matrix localisation of LGG cells compared to their micellar casein-based counterparts, where the bacterial cells were primarily located in the outer part of the disintegrated particles. The effect was ascribed to the preferential interaction of the LGG bacterial cells with β-lactoglobulin compared to caseins. In the present study, it was not possible to clearly identify a similar effect, since the majority of the bacterial cells were well-located in the internal structure of the disintegrated cryogel matrices. It is assumed that the formation of exopolysaccharides in the fermented cryogel precursors promoted the matrix – LGG pili interactions via non-covalent short-range molecular interactions e.g. hydrogen bonding, electrostatic bridging etc. (Burgain et al., 2014).

Upon exposure to pancreatic enzymes and bile salts, a significant reduction in viability of free LGG cells was observed (Figure 69). The substantial increase in lethality (3.1 logCFU.g$^{-1}$) can be primarily attributed to the well-known amphipathic nature of bile salts, which allows them to act as detergents, leading to interactions and disruption of the bacterial cell membrane's lipid bilayer (Ventura et al., 2011). Similar observations were found for LGG by Soukoulis et al. (2014). In line with the observations in the gastric phases, the residual amount of viable LGG cells remained significantly higher for the cryogels that embedded LGG (TVC = 8.3 to 9.6 logCFU.g$^{-1}$) than for their free cell + cryogel matrix exemplars (6.6 to 8.1 logCFU.g$^{-1}$) supporting the cytoprotective role of an embedding matrix. However, it should be noted that the average net changes in the LGG viable counts during the intestinal processing were not significant between the embedded cell and free cell + cryogel matrix approaches (0.7 and 0.85 logCFU.g$^{-1}$,

respectively). In practical terms, this implies that the embedment of the LGG cells is only critical for minimising the cellular lethality in harsh gastric conditions. As for the impact of $m_{NaCN/WPI}$, the LGG cell lethality was minimised when $0 \leq m_{NaCN/WPI} < 0.75$ (Figure 69), which highlights the essential role of NaCN in the cryogel formulation.

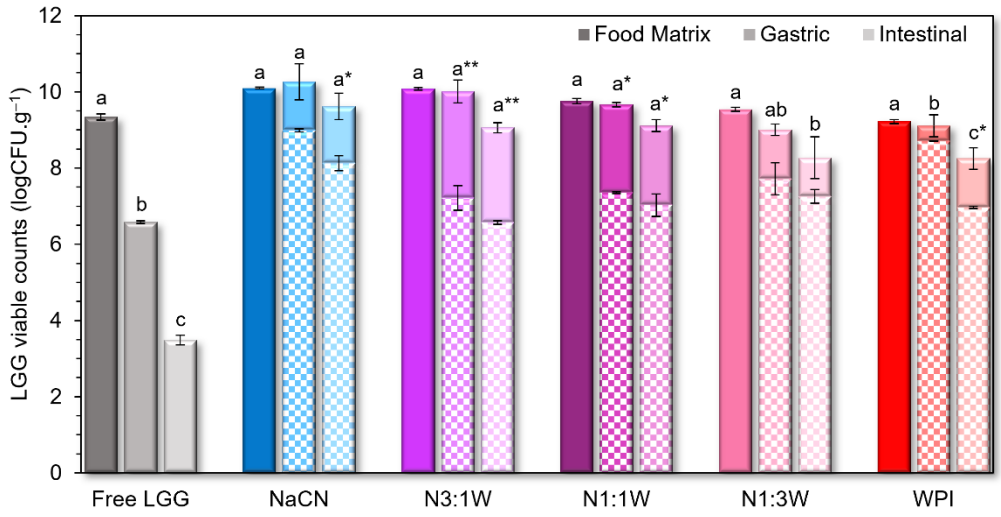


*Figure 69: Total viable counts of LGG throughout the in vitro simulated digestion as influenced by the cryogel matrix and protein composition. The checkered pattern on the bars (in the gastric and intestinal phases) represents the viability of LGG when free cells are digested together with the corresponding bacteria-free protein cryogel. [a-c] Different letters between the digestion step denote a significant decline of the LGG counts ($p < 0.05$) according to Tukey's post hoc means comparison test. **Indicates a significant protection of the bacteria embedded in the cryogel matrix (*$p < 0.05$, **$p < 0.01$). NaCN: Sodium Caseinate, WPI: Whey Protein Isolate, N3:1W to N1:3W denote mixed protein systems of varying NaCN:WPI ratio (3:1 to 1:3).*

## Proteolysis characterisation of the gastric and intestinal phases

Monitoring the changes in the proteomic profile of the gastric and intestinal phases provides useful information regarding the *in vitro* digestibility and fate of the cryogel matrix throughout gastrointestinal transit (Hiolle et al., 2020). In addition, the release of bioactive peptides imparting supplemental bioactivities can be also understood beyond the inherent biological role of the probiotic cells as being influenced by the compositional profile and colloidal transformation of the cryogel (Fontes-Candia et al., 2022). In the present work, the proteomic characterisation of the gastric and intestinal phases involved the determination of the residual intact proteins, free amino groups and peptidome profile (Figure 70 to Figure 72).

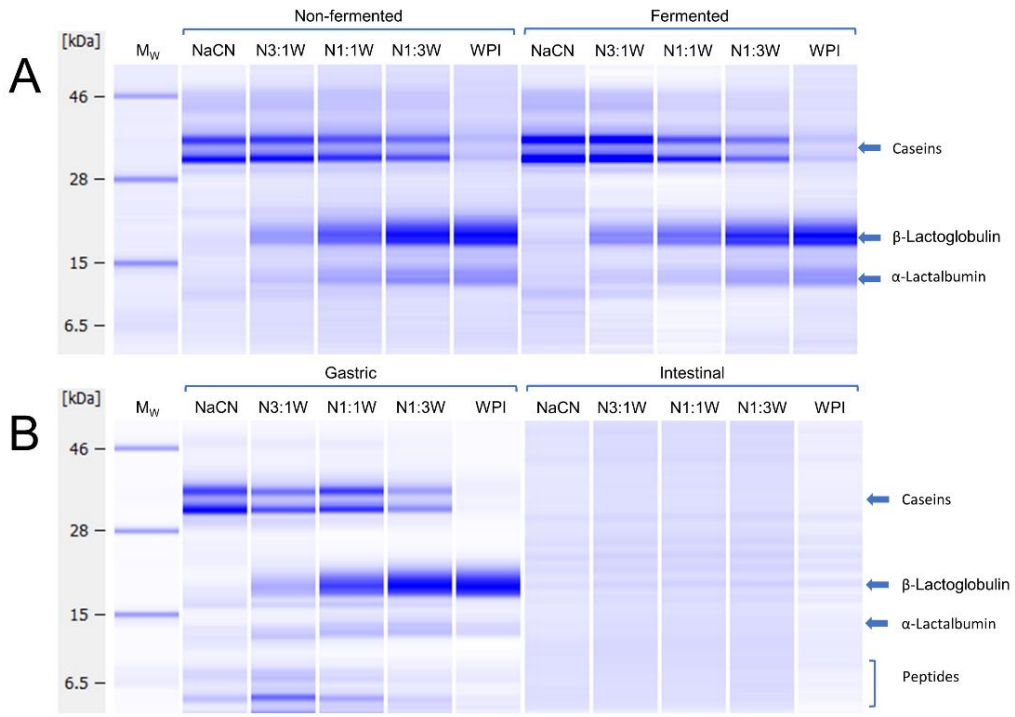


*Figure 70: Capillary SDS-PAGE electropherograms of the non-fermented and fermented (A) and gastric ($t_{gastric}$ = 120 min) and intestinal ($t_{intestinal}$ = 120 min, B) milk protein cryogel digesta as influenced by the $m_{NaCN/WPI}$ ratio. NaCN: Sodium Caseinate, WPI: Whey Protein Isolate, N3:1W to N1:3W denote mixed protein systems of varying NaCN:WPI ratio (3:1 to 1:3).*

As illustrated in the electropherograms obtained by capillary SDS-PAGE (Figure 70), the implementation of the fermentation step to obtain the cryogel precursors (Figure 70A) did not result in any significant modification of the proteomic profile, as no new molecular bands other than those corresponding to total caseins, β-lactoglobulin (β-Lg), and α-lactalbumin (α-La) were detected. This could be ascribed to the relatively short fermentation time (i.e. 4 h) implemented. Similar findings were found in LGG-fermented skimmed milk, where the proteolysis of caseins, β-Lg and α-La after 12 h was limited (Sebastián-Nicolas et al., 2021). As expected, the impact of the $m_{NaCN/WPI}$ ratio on the intensity of the total caseins, β-Lg and α-La bands were well-reflected. Notably, very low amounts (< 5%, according to the densitometric analysis) of caseins and whey proteins were detected as impurities in the individual WPI and NaCN systems, respectively. The gastric processing of the cryogels resulted in the partial pepsin-induced cleavage of the milk proteins as indicated by the generation of new low molecular weight bands (i.e. at $M_w$ < 10 kDa, Figure 70B). Nonetheless, the intensity of the total caseins, β-Lg and α-La molecular bands remained quite high suggesting a rather limited degree of pepsin-induced cleavage of the milk proteins. The susceptibility of milk proteins to peptic cleavage is inextricably associated with their secondary structure conformation, and thus, processing

(e.g. heat, pressure, pH, enzymatic crosslinking etc.) and compositional (e.g. polysaccharides, salts) parameters may affect it (Barbé et al., 2013, 2014; Böttger et al., 2019; Lorieau et al., 2018). On implementing the same static *in vitro* digestion conditions in liquid heat-treated dairy food models (Hellebois, Fortuin, et al., 2022; Hellebois, Gaiani, & Soukoulis, 2022b), it was shown that the amount of residual intact caseins, β-Lg and α-La in the gastric digesta was as low as the 3.1, 46.1 and 32.3% of the initial content, respectively. The very restricted pepsin-induced cleavage of the milk proteins observed in the present work are most probably associated with the low degree of matrix disintegration, which hinders the accessibility of the pepsin onto the liquid-solid interface. Similar results have been reported in other semi-solid or solid dairy matrices such as custards (Borreani et al., 2017), textured model protein gels (Lorieau et al., 2018) and cheese (Fang et al., 2016). This is also well-reflected in the electropherograms of the intestinal digesta (Figure 70B), where the extensive pancreases-induced cleavage of the milk proteins was favoured by the complete matrix disintegration (Figure 67).

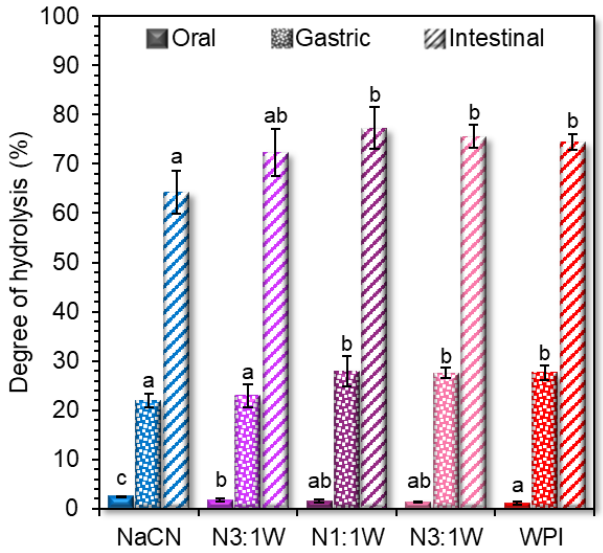


*Figure 71: Degree of protein hydrolysis at the end of each digestive phase (i.e. oral: plain bars, gastric: dotted bars and intestinal: dashed bars).* $^{a\text{-}b}$ *Different letters between the cryogels denote a significant difference ($p < 0.05$) according to Tukey's post hoc means comparison test. A significant difference in the degree of hydrolysis was observed for oral, gastric and intestinal chymes, regardless of the cryogel composition. NaCN: Sodium Caseinate, WPI: Whey Protein Isolate, N3:1W to N1:3W denote mixed protein systems of varying NaCN:WPI ratio (3:1 to 1:3).*

To gain insight into the advancement of the hydrolysis of the milk proteins to oligopeptides and free amino acids, the oral, gastric and intestinal phases were characterised using the OPA assay (Figure 71). As expected, the degree of hydrolysis (DH) in the oral boluses was relatively low (i.e. < 2.5%), which is mainly ascribed to the absence of proteases in the artificial saliva. The free amino groups detected in the oral

phases are most probably associated with the mild proteolytic activity of LGG during the fermentation step (Sebastián-Nicolas et al., 2021). A significant increase in the DH was observed in the gastric phases stemming from the pepsin-cleaving activity. As shown in Figure 71, the DH ranged from 22 to 28% depending on the $m_{NaCN/WPI}$. The DH values achieved are generally significantly higher than those reported for textured model dairy gels i.e. < 1%, (Lorieau et al., (2018)), liquid dairy food models i.e. 9–11% (Hellebois, Gaiani, & Soukoulis, 2022b) and infant food and protein powders i.e. 4–12% (Halabi et al., 2022; Salelles et al., 2021) but within the range for cheese matrices i.e. 13 to 37% (Fang et al., 2016). A good correlation between the secondary structure conformation of the proteins (i.e. β-sheet and α-helix, $r = 0.97$ and $-0.98$, respectively; $p < 0.001$) and the work of fracture ($r = -0.88$; $p < 0.01$) was found. This conforms with the findings of Thévenot et al., (2017) and Lorieau et al., (2018) who demonstrated that casein-rich and friable dairy matrices undergo more significant pepsin-induced hydrolysis than their whey protein-rich and elastic analogues. As the matrix disintegration progressed during duodenal digestion, an eminent increase in the DH values was observed. As illustrated in Figure 71, the DH in the intestinal digesta ranged from 64 to 77%, although the $m_{NaCN/WPI}$ did not play any significant role in this ($r = 0.73$, $p > 0.05$). These DH values conform well with the observations of Mat et al., (2016), who reported that the degree of proteolysis in solid dairy emulsions was significantly lower than their liquid counterparts (80 vs. 52%, respectively). On the other hand, Lorieau et al., (2018) demonstrated that the extent of proteolysis during intestinal digestion was substantially lower in the harder and more cohesive dairy gel matrices compared to their softer and more porous counterparts. Contrary to the gastric-induced DH, it was not possible to identify any significant correlations between the DH, and the mechanical (i.e. hardness, stiffness) and microstructural (porosity, cryogel vessel thickness) properties of the cryogels. It is therefore assumed that the complete disintegration of the residual cryogels during the early stages of the intestinal digestion facilitates the cleavage of the peptide bonds.

To assess any supplementary health-benefitting effects, apart from the biological role of the living LGG cells, the peptide profile (500 to 3000 Da) of the gastric and intestinal phases was determined using nano-LC-MS/MS. The peptidome data were represented in two forms: a) average number of peptides detected on the y-axis versus their amino acids sequence length on the x-axis (Figure 72A), and b) average number of peptides detected on the y-axis versus their protein of origin (Figure 72B). As seen in Figure 72A, peptides composed of 7–20 and 7–24 amino acid units were detected in the gastric and intestinal

digesta, respectively. In both cases, the peptidome data followed a Gaussian distribution with a median of approx. 11 and 10 amino acid units for gastric and intestinal digesta, respectively. Although the prevalence of the intermediate length peptide sequences (i.e. 9–12 units) was similar among gastric and intestinal digesta, in the latter case, the prevalence of short (7–8) and long (> 18) peptide sequences was more pronounced. This behaviour could be attributed on the one hand to the advancement of the proteolysis of the oligopeptides, and on the other hand, to the pancreases-mediated cleavage of the residual intact proteins originating from the intact cryogel matrix. As for the impact of the cryogel protein composition, the presence of NaCN favoured the release of intermediate to long-chain (i.e. > 12) peptides in the gastric phases compared to WPI. Concerning the protein origin of the released peptides (Figure 72B), the majority stemmed from the peptic cleavage of β-caseins and β-Lg, whilst significantly lower amounts originated from $\alpha_{s1}$-casein, κ-casein and α-La, which is in line with previous studies (Halabi et al., 2022). As expected, the number of peptides per protein class was closely associated with the protein composition of their preceding cryogels. Interestingly, the total number of the β-Lg and $\alpha_{s1}$-casein-originating peptides were in line with those reported in fermented non-fat cheese curds (Kopf-Bolanz et al., 2014).

To better assess the peptidome diversity of the gastric and intestinal digesta, the data were represented in the form of Venn diagrams (Figure 72C, D). On average, a total of 139 and 138 sequences were identified in the gastric and intestinal digesta, respectively. According to the Venn diagrams, the digesta of the NaCN-based cryogels were characterised by the highest number of unique peptides compared to the WPI and mixed protein-based exemplars. A total of 254 and 286 different sequences were identified in the entity of the gastric and intestinal digesta, of which only 74 were shared. This implies that the pancreases-mediated cleavage of the proteins increased the peptidome diversity, which could potentially result in diversified bio-functionalities.

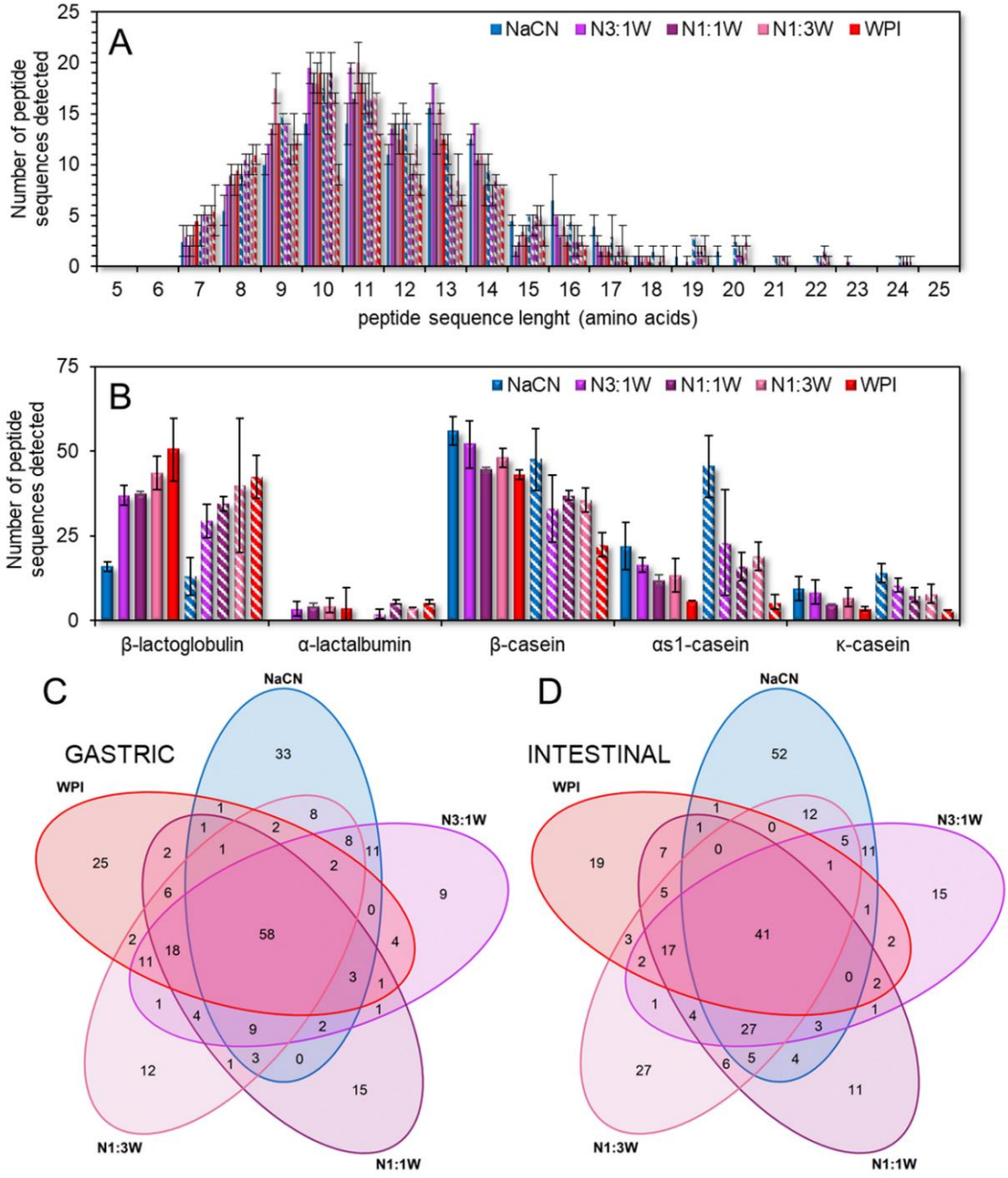


*Figure 72: Peptide sequence length (A) and milk protein origin of the significant peptide diversity (B) from the digestive chymes of the cryogels obtained (plain bars: gastric chymes, dashed bars: intestinal chymes) and Venn diagram of the peptide sequences found in the gastric (C) and intestinal (D) chymes of the digested milk protein cryogels. NaCN: Sodium Caseinate, WPI: Whey Protein Isolate, N3:1W to N1:3W denote mixed protein systems of varying NaCN:WPI ratio (3:1 to 1:3).*

As shown in Table 21, a total of 12 and 6 bioactive peptides were identified in the gastric and intestinal digesta, respectively. The majority of the bioactive peptides originated from β-Lg (six) and β-caseins (four), which is in line with the peptide abundance per protein class (Figure 72B). Although it was not possible to identify a clear relationship between the protein composition of the initial cryogels and the number and type of bioactive peptides identified, only the $^{58}$YVEELKPTPEGDL$^{70}$ and $^{195}$SDIPNPIGSENSEK$^{208}$

regions (associated with antioxidant (Basilicata et al., 2018) and antimicrobial (Hayes et al., 2006) activities, respectively) were persistently detected in the gastric and intestinal digesta. Seven peptide sequences associated with angiotensin-converting enzyme (ACE) inhibitory activity were identified in the gastric digesta, of which the $^{145}$VENLHLPLPLL$^{155}$ ($IC_{50}$ = 175 µM), $^{147}$NLHLPLPLL$^{155}$ ($IC_{50}$ = 15 µM) and $^{148}$LHLPLPL$^{154}$ ($IC_{50}$ = 425 µM) regions exert an enhanced ACE-binding activity deriving from the presence of branched amino acids (leucine) and proline at the N-terminus and third-to-last C-terminus position, respectively (Nielsen et al., 2017). Despite their high proline presence in their sequence, which is known for its resistance to pancreases (Halabi et al., 2022; Nielsen et al., 2017), it was almost impossible to identify the entirety of the ACE-inhibitory peptides in the intestinal digesta. This is most probably associated with the minimum peptide length cut-off fixed at 7 amino acid units during the analysis. It is believed that bioactive sequences produced by porcine pancreases such as $^{150}$LPLP$^{153}$ ($IC_{50}$ = 720 µM) and $^{149}$HLPLP$^{153}$ ($IC_{50}$ = 41 µM) may have been formed during intestinal digestion but not detected (Kohmura et al., 1989; Nielsen et al., 2017; Z. Zou et al., 2022). In opposition, two β-Lg deriving sequences promoting the inhibition of dipeptidyl peptidase-4 (DPP-IV), a glycoprotein that cleaves the N-terminal dipeptides of glucagon-like peptide 1 (GLP-1) and the glucose-dependent insulinotropic polypeptide (GIP) hormones, were detected in the intestinal digesta i.e. $^{62}$LKPTPEGDL$^{70}$ ($IC_{50}$ = 45 µM) and $^{141}$TPEVDDEALEK$^{151}$ ($IC_{50}$ = 579 µM), respectively (Brandelli et al., 2015). Hence, additional benefits associated with the uncompetitively driven control of the blood glucose and insulinotropic responses could potentially be achieved. In this case, the structural engineering of the probiotic cell embedding scaffold using different type of food biopolymers (e.g. proteins, polysaccharides, lipids etc.) could provide tangible solutions in maximising the health-promoting benefits of cryogels.

*Table 21: Milk protein bioactive peptide sequences found at the end of the gastric and intestinal phases of the cryogel in vitro digestion.*

| Bioactive peptide sequence[a] | Protein | Bioactivity | Gastric phase | | | | | Intestinal phase | | | | | References |
|---|---|---|---|---|---|---|---|---|---|---|---|---|---|
| | | | NaCN | N3:1W | N1:1W | N1:3W | WPI | NaCN | N3:1W | N1:1W | N1:3W | WPI | |
| $^{60}$IVQNNDSTEYGLF$^{72}$ | α-lactalbumin | DPP-IV Inhibitory | | | | ✓ | | | | | | | (Lacroix & Li-Chan, 2014) |
| $^{26}$LDIQKVAGTW$^{35}$ | β-lactoglobulin | ACE-inhibitory | ✓ | ✓ | ✓ | ✓ | ✓ | | | ✓ | | | (Lacroix et al., 2016) |
| $^{49}$DAQSAPLRVY$^{58}$ | β-lactoglobulin | ACE-inhibitory | | ✓ | ✓ | | ✓ | | | | | | (Tavares & Xavier Malcata, 2012) |
| $^{58}$YVEELKPTPEGDL$^{70}$ | β-lactoglobulin | Antioxidant | ✓ | ✓ | ✓ | ✓ | ✓ | ✓ | ✓ | ✓ | ✓ | ✓ | (Basilicata et al., 2018) |
| $^{62}$LKPTPEGDL$^{70}$ | β-lactoglobulin | DPP-IV Inhibitory | ✓ | ✓ | ✓ | ✓ | | | ✓ | ✓ | ✓ | ✓ | (Lacroix & Li-Chan, 2014) |
| $^{141}$TPEVDDEALEK$^{151}$ | β-lactoglobulin | DPP-IV Inhibitory | ✓ | | | ✓ | | ✓ | ✓ | ✓ | ✓ | ✓ | (Power et al., 2014) |
| $^{156}$LKALPMH$^{162}$ | β-lactoglobulin | ACE-inhibitory, DPP-IV Inhibitory | | ✓ | | ✓ | ✓ | | | | | | (Lacroix et al., 2016) |
| $^{195}$SDIPNPIGSENSEK$^{208}$ | $\alpha_{S1}$-casein | Antimicrobial | ✓ | ✓ | ✓ | ✓ | | ✓ | ✓ | ✓ | ✓ | ✓ | (Hayes et al., 2006) |
| $^{145}$VENLHLPLPLL$^{155}$ | β-casein | ACE-inhibitory | ✓ | | | ✓ | | | | | | | (Robert et al., 2004) |
| $^{147}$NLHLPLPLL$^{155}$ | β-casein | ACE-inhibitory | ✓ | | ✓ | ✓ | | | | | | | (Robert et al., 2004) |
| $^{148}$LHLPLPL$^{154}$ | β-casein | ACE-inhibitory | | ✓ | | ✓ | | | | | | ✓ | (Quirós et al., 2007; Robert et al., 2004) |
| $^{208}$YQEPVLGPVRGPFPIIV$^{224}$ | β-casein | Antithrombin, antimicrobial, ACE-inhibitory | | | | | ✓ | | | | | | (Coste et al., 1992; Sandré et al., 2001; Yamamoto et al., 1994) |

*✓: Peptide detected; [a]Peptide sequence loci were determined using UniProt protein sequences. NaCN: Sodium Caseinate, WPI: Whey Protein Isolate, N3:1W to N1:3W denote mixed protein systems of varying NaCN:WPI ratio (3:1 to 1:3).*

# CONCLUSIONS

The feasibility of cryogels as alternative xero-scaffolds embedding living *Lacticaseibacillus rhamnosus* GG (ATCC 53103) cells was showcased. The cryogenic processing (i.e. freezing and freeze-drying) of the probiotic hydrogels did not induce any significant reduction in the viable counts of LGG. This was ascribed to the inclusion of cryoprotectants in the hydrogel formulation together with the achievement of a vitreous-like physical state during freezing, which most probably minimised the LGG injuries stemming from intracellular ice formation. The inactivation dynamics of the cryogel-embedded LGG cells were governed primarily by the storage temperature (conforming to Arrhenius kinetics) and the milk protein composition of the cryogel precursors. At $a_w \leq 0.33$, i.e. in the vicinity of or below $T_g$, the inactivation of LGG remained substantially low with the losses observed being primarily ascribed to the oxidation of the cell membrane lipid bilayer and the dehydration of the cytosol. When $a_w > 0.33$, i.e. at the rubbery state, a substantial decline in the ability of the cryogels to preserve the biological activity of LGG was found, stemming from the acceleration of the cellular metabolic activity. All cryogels showed a constrained degree of matrix disintegration during the oral and gastric processing steps, which explains the efficiency of the cryogels in protecting the LGG cells from the harsh gastric conditions. At the end of the intestinal step, an almost complete disintegration of the cryogels was achieved, resulting in the release of free LGG cells and promotion of the proteolytic activity of pancreases. The peptidome profiling of the gastric and intestinal digesta confirmed the presence of different sequences possessing antimicrobial, antioxidant, DPP-IV and/or ACE-inhibitory activities.

# UNRAVELLING THE FUNCTIONALITY OF ANIONIC AND NON-IONIC PLANT SEED GUMS ON MILK PROTEIN CRYOGELS CONVEYING *LACTICASEIBACILLUS RHAMNOSUS* GG

Thierry HELLEBOIS[1,2], Frédéric ADDIEGO[3], Alexander S. SHAPLOV[3], Claire GAIANI[2], and Christos SOUKOULIS[1]

[1]Environmental Research and Innovation (ERIN) Department, Luxembourg Institute of Science and Technology (LIST), Esch-sur-Alzette, Luxembourg
[2]Université de Lorraine, LIBio, Nancy, France
[3]Materials Research and Technology (MRT) Department, Luxembourg Institute of Science and Technology (LIST), Esch-sur-Alzette, Luxembourg

Carbohydrate Polymers
Volume 323, 1 January 2024, 121376
doi.org/10.1016/j.carbpol.2023.121376

# ABSTRACT

Cryogels offer a promising macroporous platform that can be employed as either a functional ingredient in food composites or a colloidal template for incorporating bioactives, including probiotic living cells. The aim of the present work is to explore the functionality of two plant seed polysaccharides, flaxseed gum (FG) and alfalfa galactomannan (AAG), in individual and combined (1:1 ratio) milk protein-based cryogels, namely sodium caseinate (NaCN) and whey protein isolate (WPI). These cryogels were created by freeze-drying hydrogels formed via *L. rhamnosus* GG – a human gut-relevant probiotic strain – fermentation. Our findings showed that including gum in the composition limited volume contraction during lyophilisation, reduced macropore size and thickened cryogel skeleton vessels. Furthermore, gum-containing cryogels displayed improved thermal stability and slower water disintegration rates. The AAG-stabilised cryogels specifically showed a notable reduction in monolayer water content compared to FG. From a mechanistic viewpoint, AAG influenced the physicochemical and microstructural properties of the cryogels, most probably via its self-association during cryogenic processing, promoting the development of intertwined protein-gum networks. FG, on the other hand, enhanced these properties through electrostatic complexation with proteins. Cryogels made from protein-polysaccharide blends exhibited promising techno-functional properties for enhancing and diversifying food product innovation

# INTRODUCTION

Plant seed gums are complex polysaccharides extracted from seeds of various plant families like *Fabaceae, Linaceae, Lamiaceae, Rosaceae, Brassicaceae, and Plantaginaceae* (Goksen et al., 2023; Soukoulis et al., 2018). They have gained attention for their sustainable nature and versatile properties, including thickening, gelling, and interface stabilising. Galactomannans, such as fenugreek, guar, tara, carob, cassia, and others (Prajapati et al., 2013), along with xyloglucans like tamarind gum (Shao et al., 2019) represent the prevalent types of endosperm isolated gums. Recently, a galactomannan isolate with a high degree of galactosyl substitution (M/G ~ 1), obtained from the endosperm of alfalfa seeds was assessed for its molecular, rheological (thickening, gelling) and cryostructuring characteristics as well as its colloidal interplay with milk proteins (Hellebois, Gaiani, Fortuin, et al., 2021; Hellebois, Gaiani, & Soukoulis, 2022a, 2022b; Hellebois, Soukoulis, Xu, Hausman, et al., 2021). The outermost layer of the plant seeds such as chia, flaxseed, psyllium, yellow mustard, quince, etc. contains mucilaginous matter rich in pectic and hemicellulosic carbohydrates (Lin et al., 1994; Soukoulis et al., 2018; Wang et al., 2018). Flaxseed gum is composed of two polysaccharide classes: a complex, low molecular weight acidic polysaccharide fraction (approximately 250 kDa) rich in rhamnogalacturonan-I (RG-I), and a high molecular weight neutral fraction (1500–5500 kDa) rich in neutral arabinoxylan (AX). Additionally, the presence of intermediate molecular weight RG-I/AX composite fractions has also been reported (Hellebois, Fortuin, Xu, Shaplov, et al., 2021; Naran et al., 2008; Qian et al., 2012). Thickening, gelling, emulsifying, and foaming abilities of flaxseed gum as influenced by its botanical origin and the extraction methods have been reported (Liu et al., 2018).

The term "cryogel" refers to highly porous monolithic xero-scaffolds produced through a sequential process comprising the cryogenic processing of a solution, colloidal dispersion, or hydrogel polymeric precursor, and is followed by the removal of frozen water via ice sublimation (Lozinsky, 2018). Despite their highly macroporous structure and low internal surface area, cryogels display structural and techno-functional similarities with their mesoporous counterparts, i.e. aerogels. These similarities encompass tailorable microstructural features, satisfactory mechanical durability and resilience, high biocompatibility and biodegradability (Manzocco et al., 2021). The physicochemical (e.g. residual moisture, glass transition temperature, water vapour sorption, etc.) and structural characteristics (e.g. macroporosity, interconnectivity and

thickness of the wall vessels, etc.) of cryogels are inextricably associated with the cryogenic process conditions (e.g. freezing rate, achievement of vitreous state, etc.) as well as the composition and the colloidal state (liquid, semi-solid or gel-like) of the unfrozen polymeric precursor system (Gun'ko et al., 2013; Okay, 2014; Shiekh et al., 2021). Prior research has shown that factors such as the type and concentration of polymer, pH, and the physical, chemical, or enzymatic crosslinking of the polymers are vital in reducing the risk of structural complications like shrinkage, cracking, or fissuring during the freeze-drying process (Betz et al., 2012; Chen et al., 2013; Kleemann et al., 2018). In the food domain, recent studies have showcased the feasibility of cryogels as microtemplates for the encapsulation and delivery of heat-labile health-promoting compounds (Fontes-Candia et al., 2022; Kleemann et al., 2018, 2020; Manzocco et al., 2021; Volkova & Berillo, 2021) and probiotic cells (Hellebois, Canuel, et al., 2024; Kuo et al., 2022). Furthermore, cryogels can be utilised not only as functional fillers to enhance the texture and structure of food products (Plazzotta et al., 2023), but also as biodegradable and active packaging materials that are compliant with food safety standards (Manzocco et al., 2021). Owing to their ability to undergo interchain polymer entanglement at low concentrations, polysaccharides can enhance the shape retention, structural integrity and mechanical durability of cryogels (Comin et al., 2015; Fontes-Candia et al., 2019; Selvasekaran & Chidambaram, 2021; Zou & Budtova, 2021). Using binary protein – polysaccharide-based hydrogel precursors can also lead to structurally and mechanically enhanced cryogels. In their respective studies, Chen et al., (2013) and Ahmadi et al., (2016) evidenced that the fortification of whey protein hydrogels with sodium alginate and nano-crystalline cellulose significantly improved the mechanical strength and structural aspects of the resultant cryogels. Additionally, the synthesis of hybrid protein-polysaccharide cryogels have demonstrated beneficial characteristics associated with their biological activity e.g., controlled release of bioactive compounds, sustained digestibility and satiety promoting properties (Chen & Zhang, 2020; Fontes-Candia et al., 2022). Recently, the feasibility of cryogels to preserve the biological activity of living probiotic cells throughout freeze-drying, storage and in vitro digestion has been highlighted (Hellebois et al., 2023; Kuo et al., 2022; Sun et al., 2021). In their study, Sun et al., (2021) reported satisfactory survivability of *L. plantarum* cells (losses in total viable counts < 1.1 logCFU.g$^{-1}$) encapsulated in whey protein-pullulan-trehalose freeze-dried hydrogels during 180 days of storage at chilling conditions. Similarly, the encapsulation of *L. rhamnosus* GG cells in whey protein-sodium caseinate-based cryogels restricted cellular lethality during freeze-drying (< 0.2 logCFU.g$^{-1}$) and chilling storage (< 0.22

logCFU.g$^{-1}$ per month) and *in vitro* digestion conditions (< 1.5 logCFU.g$^{-1}$) (Hellebois et al., 2023).

Building on our previous studies (Hellebois et al., 2023), we hypothesised that the colloidal interplay between protein-polysaccharide in the hydrogel precursors dictate the structural and physicochemical attributes of the resultant cryogels. To test this hypothesis, we investigated cryogels fabricated through the freeze-drying of LGG fermented milk protein (whey protein, sodium caseinate) hydrogels fortified with anionic (flaxseed) and non-ionic (alfalfa) seed gums. The microstructural properties of the cryogels were subsequently investigated using Scanning Electron Microscopy (SEM), X-ray micro-computed tomography (μCT), and Confocal Laser Scanning Microscopy (CLSM). Additionally, their physicochemical properties, such as water vapour sorption, thermal properties, and dissolution profiles, were analysed. This research paved the way for producing cryogels with favourable physicochemical and microstructural properties for preserving the biological activity of probiotic bacteria.

# MATERIALS & METHODS

## Materials

Whey protein isolate powder (PRODIET 90S) with a protein content of 85.8% wt. was kindly donated by Ingredia (Arras, France). Sodium caseinate (containing 89.4% wt. of protein), glucose (99.5% wt.) and glycerol (99.9% wt.) were purchased from Sigma-Aldrich (Leuven, Belgium). Trehalose dihydrate, with a purity of 99.4% wt., was procured from Louis-François (Croissy-Beaubourg, France). The alfalfa gum (AAG) was isolated and characterised based on the procedure detailed in Hellebois, Soukoulis, Xu, Hausman, et al., (2021). It primarily consisted of galactomannan with a mannose to galactose ratio of 1.18, a molecular weight of 2 × 10$^6$ Da and an intrinsic viscosity of 9.3 dL.g$^{-1}$. The flaxseed gum (FG) was isolated from golden flaxseed at pH 8, as described in Hellebois, Fortuin, et al. (2021). The flaxseed gum composed of four major polysaccharidic populations corresponding to arabinoxylans (AX), rhamnogalacturonan–I (RG-I) and two AX-RG-I composite fractions. The gum had a molecular weight of 1.4 × 10$^6$ Da, and intrinsic viscosity of 6.7 dL.g$^{-1}$. The probiotic strain *Lacticaseibacillus rhamnosus* GG (ATCC 53103) used for the fermentation was purchased from the VTT Technical Research Centre of Finland Ltd (Espoo, Finland). All the other chemicals used were of analytical grades.

## Preparation of the cryogels

Protein solutions, namely whey protein isolate (WPI) and sodium caseinate (NaCN), as well as their 1:1 binary mixture (N1:1W), were prepared by dispersing the appropriate amount to achieve a protein concentration of 10% wt. The protein solutions were left to hydrate overnight and then threefold homogenised at 500 bar using a Panda Plus 2000 homogeniser (Gea GmbH, Germany). Trehalose (5% wt.), glucose (1% wt.) and glycerol (2.5% wt.) were then added to the protein solutions and subsequently, heat treated at 80 ± 1 °C for 20 min in a shaking water bath (SW22, Julabo, Seelbach, Germany). On completion of the heat treatment, the gums (AAG or FG) were added into the hot protein solutions at two different concentrations, 0.1% and 0.5% wt., cooled down on ice and left to hydrate overnight fully. The procedure detailed in (Hellebois et al., 2023) was adopted to prepare the hydrogels and the cryogel monoliths. In brief, an inoculum of the LGG cells obtained at the end of the exponential growth phase was added to the protein solution to achieve a cell concentration of approximately 10 $logCFU.g^{-1}_{solids}$ and the indirect acid-induced gelation of the milk proteins was achieved by lactic acid fermentation (4 h at 37 °C). The hydrogels obtained were then frozen at −80 °C for 2 h and freeze-dried for 40 h to form the final cryogels.

## Characterisation of the precursors

The microstructure of the initial protein–gum solutions and the fermented hydrogels was visualised using a CLSM microscope (LSM 880 with Airy scan, Zeiss, Jena, Germany) fitted with a × 20 objective. The gums, prior to microscopic analysis, were covalently stained using 5-(4,6-dichlorotriazinyl) aminofluorescein (5-DTAF), according to the procedure detailed by Khin et al., (2021), then underwent a 72 h dialysis process and were subsequently freeze-dried. Protein – 5-DTAF-stained gum solutions were prepared as aforementionned. Aliquots of 1 mL were mixed with 10 µL of Fast Green (0.05% wt.) and transferred onto eight-well Nunc Lab-Tek II microscope slides. To allow the stabilisation of the phase separation phenomenon, it was ensured that the samples remained undisturbed for a duration of 30 min. The excitation and emission wavelengths used were set at $\lambda_{Ex}$ = 633 nm and $\lambda_{Em}$ = 635–690 nm for Fast Green, and $\lambda_{Ex}$ = 488 nm and $\lambda_{Em}$ = 495–550 nm for 5-DTAF.

The colloidal stability of the precursors (both solutions and hydrogels) was evaluated using a LUMiSizer (LUM GmbH, Berlin, Germany). The Instability Index (II) served as a measure for assessing phase separation phenomena, protein precipitation in the solution, and resistance to serum exudation in hydrogel precursors. Measurements were taken at

2300g for 10 min with 5 s intervals between each. The experiment was conducted at a temperature of 25 °C, and light transmittance was measured at λ = 865 nm. Data analysis was carried out using the SEPView software (LUM GmbH, Berlin, Germany).

## Characterisation of the cryogels

### *i.* Thermal stability

The fresh cryogels monoliths obtained on the completion of the freeze-drying step underwent thermogravimetric (TGA) analyses using a TGA2 STAR$^e$ System (Mettler Toledo, Zurich, Switzerland). The same protocol as described in (Hellebois et al., 2023) was applied.

### *ii.* Water vapour sorption properties

To assess the water vapour sorption of the cryogels, a first desiccation step of approx. 3 weeks in dried atmosphere using $P_2O_5$ (i.e. $a_w$ = 0.003) was applied. Then, the weighted cryogels (200 mg) were incubated for 3 weeks at various saturated salt solution-controlled water activity atmospheres in hermetically sealed Nalgene acrylic desiccator cabinets (Thermo Fisher Scientific, Waltham, MA, United States) until the water intake reach an equilibrium at T = 20 ± 1 °C. To this ends, the following salts were considered: LiCl ($a_w$ = 0.11), $CH_3CO_2K$ ($a_w$ = 0.23), $MgCl_2$ ($a_w$ = 0.33), $K_2CO_3$ ($a_w$ = 0.43), $Mg(NO_3)_2$, ($a_w$ = 0.54), NaCl ($a_w$ = 0.75), $NH_4Cl$, ($a_w$ = 0.79), and KCl ($a_w$ = 0.85). The relative water intake was then calculated gravimetrically. The water intake – $a_w$ data obtained were fitted to the Brunauer-Emmett-Teller (BET) equation (Brunauer et al., 1938) as follows (Equation 39):

Equation 39
$$X = \frac{a_w X_m C}{(1-a_w)\,(a_w(C-1)+1)}$$

where X is the water content at the equilibrium ($g.100g^{-1}_{cryogel}$), $X_m$ the water content ($g.100g^{-1}_{cryogel}$) monolayer moisture content, C is a constant related to the net heat of sorption, respectively and $a_w$ the water activity. From Equation 39, the total surface of the monolayer $S_m$, can be obtained as follows (Equation 40):

Equation 40
$$S_m = X_m \frac{1}{M_{H_2O}} N_A A_{H_2O} = 3.5\times10^3 X_m$$

where $X_m$ is analogous with the BET equation, $M_{H_2O}$ is the molecular weight of water (18 $g.mol^{-1}$), $A_{H_2O}$ is the area of a single water molecule ($1.06\times10^{-19}$ $m^2$), and $N_A$ is the Avogadro number ($6\times10^{23}$ $molecules.mol^{-1}$) (Mazza & LeMaguer, 1978).

### *iii.* Assessment of the morphological aspects

The microstructure of the cryogels was investigated by means of micro-computed X-ray tomography (µCT) and scanning electron microscopy (SEM) using a laboratory X-ray cone-beam µCT system EasyTom 160 from RX Solutions (Chavanod, France) and a field emission scanning electron microscope (SEM, SU-70, Hitachi, Tokyo, Japan), respectively. The conditions previously described in (Hellebois et al., 2023) were applied.

*iv.* Shrinkage and density

The dimensions of freshly made cryogels were measured using a precision calliper (Carl Roth, Karlsruhe, Germany) with a resolution of ± 0,03 mm. The volume of the cryogels were estimated based on their cylindrical shapes and the shrinkage percentage ($\Delta V$) was calculated using the formula $\Delta V = \frac{V_0 - V_f}{V_0} \times 100$ where $V_0$ and and $V_f$ are the volume of solution and the volume of the cryogel, respectively. Furthermore, the bulk density of the cryogels ($\rho$, in $g.cm^{-3}$) was then calculated as $\rho = \frac{mc}{Vc}$ where $m_c$ and $V_c$ refer to the mass and volume of the cryogels, respectively.

v. Disintegration profile of the cryogels

The in-water disintegration profiles of the cryogels were measured using static light scattering (hydro LV measuring cell, Mastersizer 3000, Malvern Instruments, Worcestershire, United Kingdom) as described in (Hellebois et al., 2023). In brief, the volume-average mean particle size ($D_{[4,3]}$) was recorded every 10 s for 15 min (3500 rpm, 25 °C) and the data points were fitted to the following fist order exponential decay model:

Equation 41 $$y = D_{[4,3]_\infty} + \left(D_{[4,3]_0} - D_{[4,3]_\infty}\right) e^{-\frac{\ln 2\, t}{\tau}}$$

where $D_{[4,3]_0}$ and $D_{[4,3]_\infty}$ denote the volume-weighted mean particle size (µm) at t = 0 and t = ∞ min, t the time (s) and $\tau$ the half-life (Quodbach & Kleinebudde, 2014).

## Statistical analyses

The Shapiro-Wilk test and Q–Q plot representation normality tests were used to verify the normal distribution of the data. To determine the significant differences, one-way ANOVA was performed using Origin 2019b software (OriginLab Inc, Northampton, MA, United States). The Duncan's post-hoc test was used to separate mean values when significant differences ($p < 0.05$) were detected.

# RESULTS & DISCUSSIONS

## Characterisation of the solution and acid-induced hydrogel precursors

In our previous work, we demonstrated that the colloidal aspects of the cryogel polymeric precursors are directly associated with the structural and mechanical properties of the resultant xero-structurates (Hellebois et al., 2023). Figure 73 illustrates the colloidal conformation of the cryogel precursors (solutions and acid-hydrogels) as influenced by the biopolymer composition. The individual protein solutions formed a homogeneous colloidal dispersion in the absence of gum (Figure 73A-F1). On the other hand, a weak aggregative microphase separation was evident in the mixed protein solutions (Figure 73 C1). This was further confirmed by the higher instability indices values (0.13 vs 0.02–0.05 for mixed and individual protein systems, respectively) and the pattern of the acquired LUMiSizer spectra, implying sedimentation (an increase in light transmittance in the cuvette's upper region) (Figure 74).

Looking at the microstructure of the lactic acid-mediated hydrogels, the inclusion of WPI led to the creation of uniform acid gels. At the same time, NaCN displayed a distinct aggregated microstructure, corroborating our previous findings (Hellebois et al., 2023). The NaCN-WPI hydrogels, on the other hand, exhibited a composite protein gel network form where microstructural characteristics of the individual proteins were proportionally combined. As seen in the Figure 73, the mixed protein-based hydrogels were more susceptible to forced serum exudation than their individual protein counterparts (instability index = 0.27 vs. 0.03–0.05, respectively). This may be ascribed to the occurrence of aggregative microphase separation due to electrostatic interactions between oppositely charged patches on the backbone of the biopolymers favouring the protein-protein interactions at the expense of solvent-protein interactions, resulting in water syneresis (Corredig et al., 2011).

With the exception of the NaCN-based systems, the addition of the AAG (Figure 73A–F2&3) in the WPI and NaCN-WPI systems induced a viscoelastic phase separation resulting in a clearly defined bicontinuous microstructure in some cases (Figure 73E2) and a milk protein continuous including AAG microstructure in others (Figure 73C2–C3&E3), which is in agreement with the findings of Liu & Foster (2022). In contrast, the inclusion of FG in all the protein colloidal dispersions studied led to the formation of FG-rich microdroplets dispersed within the continuous protein-rich aqueous phase, indicating the occurrence of droplet-spinodal decomposition-driven microphase separation (Tanaka,

2000). The mechanistic pathway of the segregative fluid-fluid phase separation depends on various parameters, including molecular properties such as colloidal conformation, surface charge density, and surface tension, as well as the viscoelasticity of the volume-excluded biopolymer-rich phases (Doublier et al., 2000; Tanaka, 2000).

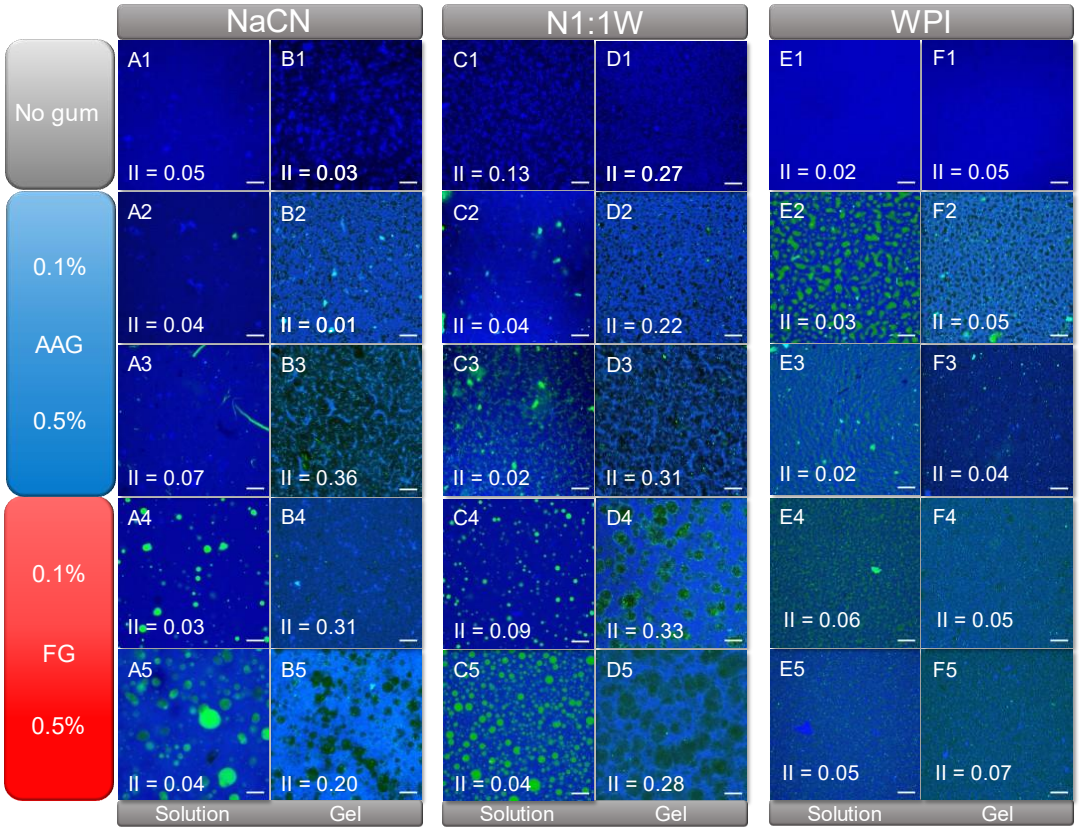


*Figure 73: CLSM micrographs of NaCN (A–B), N1:1W (C–D) and WPI (E–F) solutions (A, C and E) and fermented hydrogels (B, D and F) without the presence of gum (1) or containing 0.1 and 0.5% wt. of alfalfa gum (2–3) and 0.1 and 0.5% wt. of flaxseed gum (4–5). Proteins are stained in blue (using Fast Green), while both AAG and FG are shown in green (using 5-DTAF). Scale bar: 50 µm. Abbreviations used: II: Instability Index, NaCN: Sodium Caseinate, WPI: Whey Protein Isolate, N1:1W: mixed proteins NaCN:WPI at a ratio of 1:1, AAG: alfalfa gum, FG: flaxseed gum.*

As previously reported (Hellebois, Gaiani, Cambier, et al., 2022; Hellebois, Gaiani, & Soukoulis, 2022b), both AAG and FG tend to undergo depletion-flocculation-driven phase separation in milk protein colloidal dispersions. Nonetheless, the differences observed in the morphology of the AAG- and FG-stabilised protein dispersions appear to be closely associated with certain key factors such as viscosity ($c^*$ = 0.31and 0.55% wt. for FG and AAG, respectively), surface charge (ζ-potential = −29.7 and − 0.2 mV for FG and AAG, respectively), and surface tension (σ = 55.7 and 65.3 dyn.cm$^{-1}$ for FG and AAG, respectively). In agreement with the findings of Liu & Foster (2022). Our results also suggested that the formation of microdroplet morphologies was predominantly

favoured under low viscosity and low interfacial tension conditions, especially in the case of FG-stabilised systems. This phenomenon could be attributed to the slow relaxation rate of the droplets.

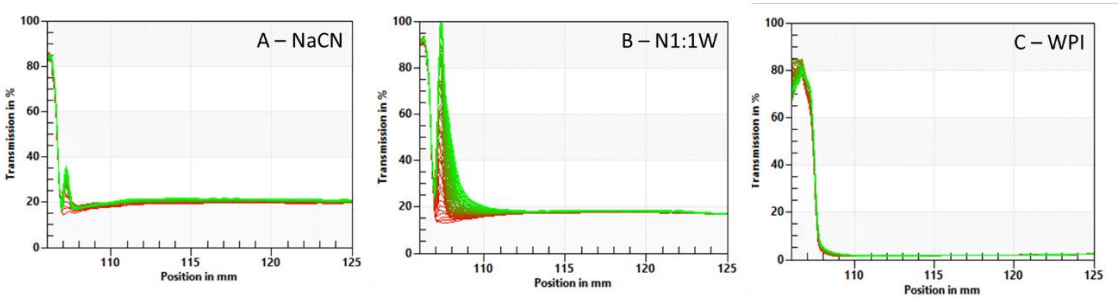


*Figure 74: Dynamic light transmission changes of sodium caseinate (A), whey protein isolate (C) and binary mixture of both proteins at ratio of 1:1 N1:1W (B) under accelerated storage conditions (25 °C, 2300g).*

Upon lactic acid fermentation, sol-gel transitions taking place at $pI < pH < pH_{gel,\ onset}$ were responsible for the partial arrestment of the microstructural elements of the precursor gum-protein solutions. The resulting composite acid-hydrogels merged the structural elements derived from both the protein (i.e. fractal aggregates or fine strands) and gum constituents (i.e. network-like or microdroplet-like morphologies). In most cases, the presence of sodium caseinate was associated with greater colloidal instability throughout the acid gelation process, with II values ranging from 0.20 to 0.36. This effect was not observed in the case of WPI hydrogels, where the II values were between 0.04 and 0.07. It is important to note that no evidence of macroscopic (spontaneous) phase separation was found, akin to the gum-free N1:1W systems. For AAG-NaCN-containing hydrogels, a higher gum content resulted in a significant increase in the colloidal instability, as demonstrated by the formation of a bicontinuous-like gel structure (Figure 73 B3,D3). This can be attributed to the low surface charge density of the AAG polymer chains allowing the demixing phenomena to evolve until the gelation time point is reached ($t_{gel}$). On the other hand, the presence of flaxseed gum promoted the arrestment of the w/w emulsion-like microstructure (due to its electrostatic complexation with proteins at $pH \leq pI$), with the systems containing 0.5% being the most stable. Similar behaviour has been previously observed in polysaccharide (anionic/non-ionic) – protein acid gels (Çakır & Foegeding, 2011; Soukoulis et al., 2019).

## Characterisation of the cryogels

i. Macroscopic appearance and microstructural characteristics

The macroscopic appearance of the cryogel monoliths is presented in Figure 75. Overall,

the observed systems displayed shades ranging from white to yellowish, with the WPI cryogels exhibiting the most pronounced yellowish hue (Figure 75). This aligns with the findings of (Betz et al., 2012) on WPI cryogels and (Schiraldi, 2015) on milk protein aerogels. All cryogel monoliths maintained their dimensional and morphological characteristics satisfactorily, without any apparent macroscopic structure imperfections such as fissures or crevices, as reported in the study of Manzocco et al., (2022). It was previously shown that the type and concentration of the cryogel skeleton polymer material are critical for preserving the dimensional characteristics of the hydrogel precursors (Fontes-Candia et al., 2022).

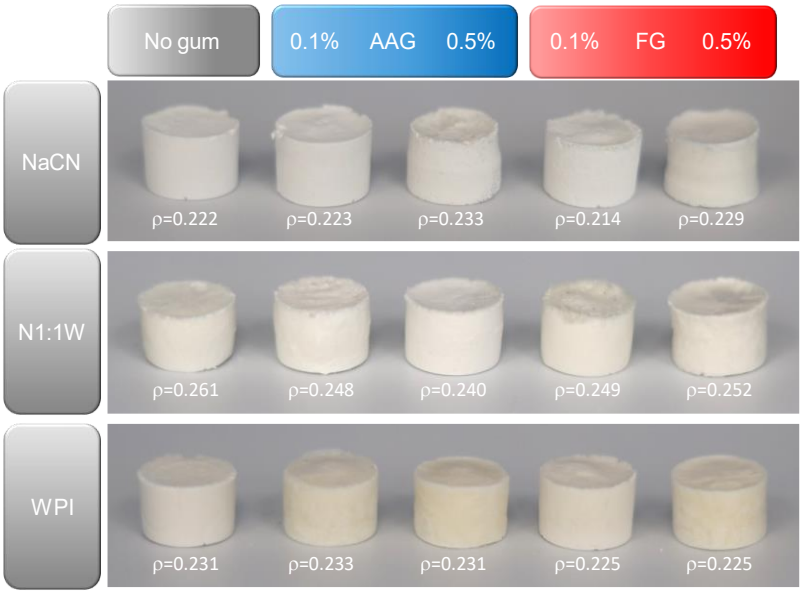


*Figure 75: Macroscopic appearance of the milk protein cryogel monoliths without gum or containing 0.1 and 0.5% wt. of alfalfa and flaxseed gum. The bulk density of the cryogels (ρ) is expressed in g.cm$^{-3}$. Approximative dimensions: diameter × height = 15 × 10 mm. Abbreviations used: NaCN: Sodium Caseinate, WPI: Whey Protein Isolate, N1:1W: mixed proteins NaCN:WPI at a ratio of 1:1, AAG: alfalfa gum, FG: flaxseed gum.*

The bulk densities observed ranged from 0.214 to 0.261 g.cm$^{-3}$ and were higher in mixed protein-based cryogels. These densities were similar to the 0.245–0.295 g.cm$^{-3}$ range reported for whey protein-based cryogel (Betz et al., 2012; Manzocco et al., 2022) and were significantly higher than those of their aerogel counterparts (≤ 0.2 g.cm$^{-3}$) (Jung et al., 2023; Selmer et al., 2015). As shown in Figure 76, the hybrid protein-based systems demonstrated a volume contraction of 24.1 ± 2.8%, which was notably higher than the NaCN (16.1 ± 1.1%) and NaCN-WPI systems (13.7 ± 1.7%), corroborating our previous findings (Hellebois et al., 2023). It is worth noting that incorporating gums improved the resilience of the cryogels to volume contraction during the lyophilisation process. More specifically, the percentages of contractions for no-gum, AAG- and FG-stabilised

cryogels were 29.5, 22.3 and 23.1%, respectively. These values are in range with aerogels made of WPI (Manzocco et al., 2022) and corn and pea starch (García-González & Smirnova, 2013). Nevertheless, it was not possible to detect any significant impact of the gum type and content on the measured shrinkage values.

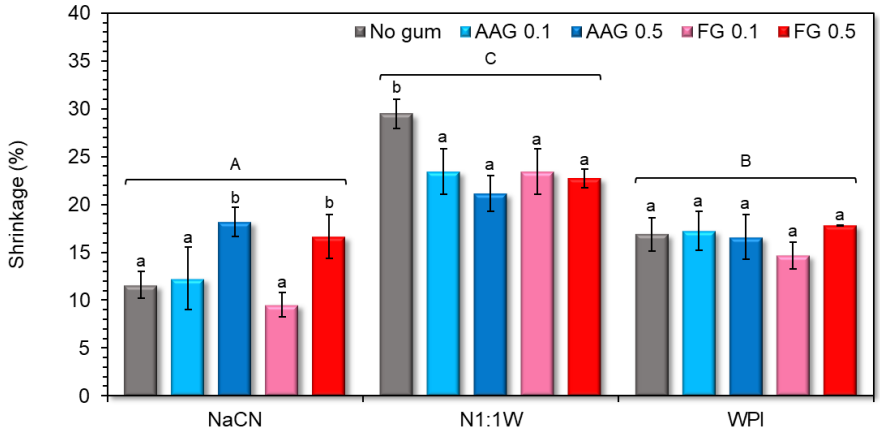


*Figure 76: Degree of shrinkage of the cryogel influenced by the protein and gum types.* $^{A–C,a–b}$ *Different letters denotes significant differences for the same protein type (lowercase) or among the type of proteins (uppercase). Abbreviations used: NaCN: Sodium Caseinate, WPI: Whey Protein Isolate, N1:1W: mixed proteins NaCN:WPI at a ratio of 1:1, AAG: alfalfa gum, FG: flaxseed gum.*

To better understand the microstructural build-up of the macroporous monoliths influenced by the composition of the hydrogel precursors, the cryogels were analysed by means of X-ray micro-computed tomography (Figure 77) and SEM (Figure 78). The µCT tomographs revealed that the cryogel monoliths showed a predominantly macroporous microstructure with an air occupancy fraction (φ) ranging from 0.67 to 0.81, depending on the biopolymer composition of the hydrogel precursors. In line with our previous observations (Hellebois et al., 2023), the mixed protein-based cryogels exhibited the most compact microstructure in the absence of gum. The gum inclusion was associated with a measurable increase in the porosity of the cryogels (i.e. φ = 0.74 and 0.78 for gum-free and gum-containing cryogels, respectively). However, the gum type and concentration did not significantly impact the φ values. According to the SEM micrographs (Figure 78), most cryogels exhibited a highly lacunar, honeycomb-like morphology with sharp edges, which is in agreement with the observations of Betz et al., (2012) and Manzocco et al., (2022). In the absence of gum, remarkable differences in the lacunarity of the monoliths were observed, with the size of the macropores being reduced in the following sequence: N1:1W < NaCN < WPI.

Although the structuration of the polymer precursors through physical or chemical crosslinking is essential to prevent the structural collapse of the cryostructurates during

lyophilisation, the lacunarity of the cryogels is also highly dependent on the ability of the polymer precursors to either affect the ice crystallisation phenomena (i.e. ice nucleation and ice crystals ripening) during cryogenic processing or to undergo self- or intermolecular association (cryogelation) as result of the freeze-concentration (Lozinsky, 2018). As illustrated in Figure 78, the inclusion of AAG induced a notable reduction in the size of the macropores, indicating its active role in the cryostructuration process. According to previous studies, the impact of polysaccharides on the microstructural features of protein-based cryogels and aerogels is highly dependent on the content and type of the biopolymers. In this context, (Kuo et al., 2022) reported that the presence of sodium alginate resulted in a homogeneous microstructure composed of small-sized macropores. On the other hand, (Fontes-Candia et al., 2022) observed a significant increase in the lacunarity of micellar casein cryogels *co*-structured with agar or κ-carrageenan. In addition, solutes (i.e. cryoprotectants and plasticisers) such as trehalose may hamper the protein-polysaccharide molecular interactions, resulting in highly heterogeneous and less lacunar microstructures (Sun et al., 2021). Concerning AAG, we previously demonstrated its inherent ability to undergo freeze-thaw gelation through polymer-polymer hydrogen bond bridging (Hellebois, Gaiani, Fortuin, et al., 2021). In addition, AAG exerted synergistic cryogelation with whey proteins under these conditions, marked by a reduction in serum exudation and lacunarity of the formed cryo-hydrogels (Hellebois, Gaiani, & Soukoulis, 2022a).

The WPI – AAG synergism in the cryogelation process was related to creating of two interpenetrating polymeric networks. The first network, a protein-based structure, was primarily formed by establishing disulphide bonds. In contrast, the second, a galactomannan-based network, was predominantly formed via hydrogen bonding (Figure 79). Therefore, it is assumed that the cryogelation ability of AAG plays a significant role in the control of the porogen growth, thereby resulting in less lacunar cryogels. On the other hand, FG does not possess any cryogel-forming capacity (Hellebois, Gaiani, Cambier, et al., 2022), leading to the hypothesis that the process of porogenesis is predominantly governed by the protein *co*-polymer.

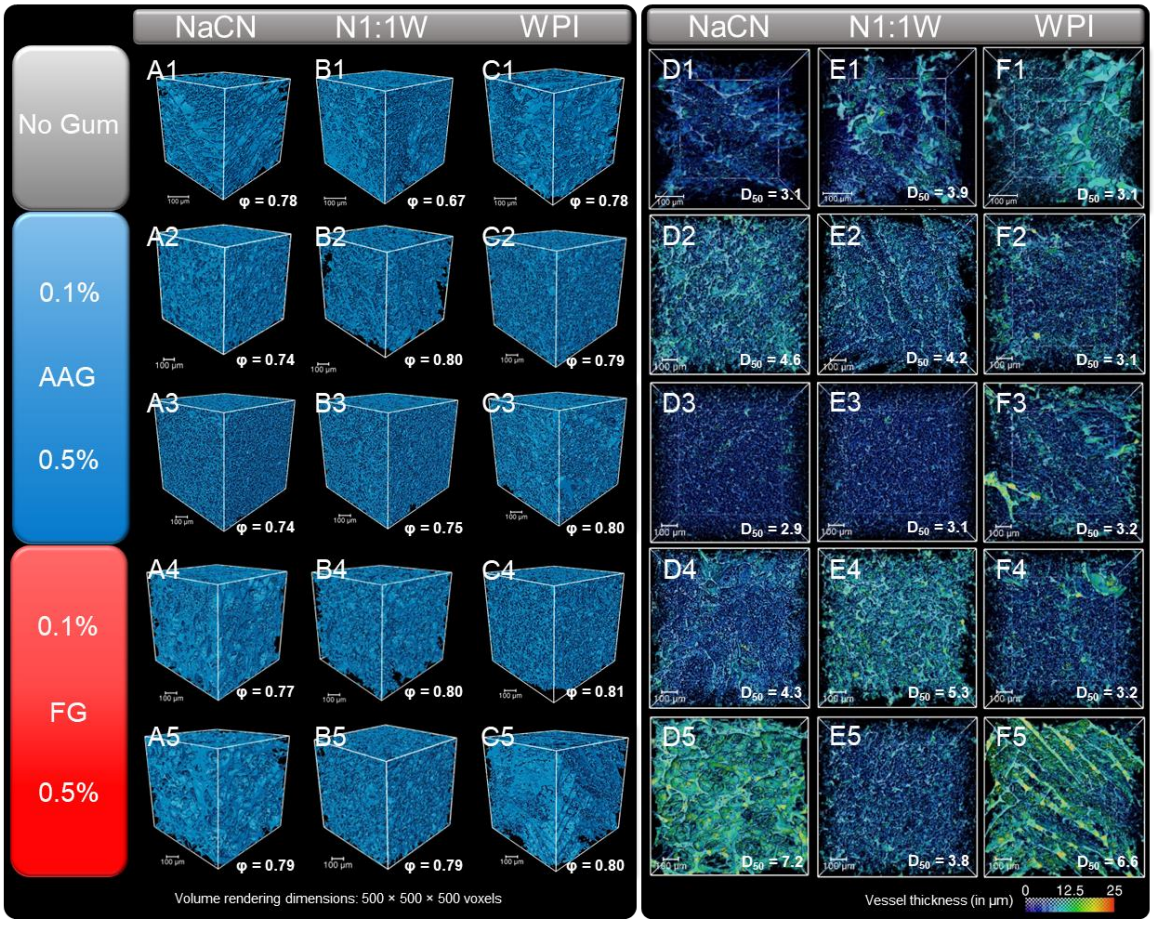


*Figure 77: µCT volume rendering with an angular view (A–C) and front view after vessel thickness analysis (range 0–25 µm, D–F) of the milk protein-based cryogels. The scale may slightly differ from one case to another case because a similar box size in voxels (500 x 500 x 500 voxels) was considered for all the cases, but since the resolution was not rigorously identical between the different cases a different scale resulted. Abbreviations used: φ: porosity volume fraction; $D_{50}$: vessel thickness below which 50% of all vessels are found.*

To gain an insight into the features of the interconnected polymeric network, we generated cumulative vessel thickness curves of the cryogels and then fitted the three-parameter sigmoidal model to them (Equation 42), as described below:

Equation 42 $$y = 100\frac{a}{1+(\frac{x}{b})^n}$$

In this equation, "a" represents the asymptotic value (100%), "b" denotes the inflexion point of the cumulative distribution function, and "n" is a constant associated with the rate of change (slope) of the distribution. In addition, the uniformity of the vessel thickness ($\text{Span} = \frac{D_{90}-D_{10}}{D_{50}}$) was calculated.

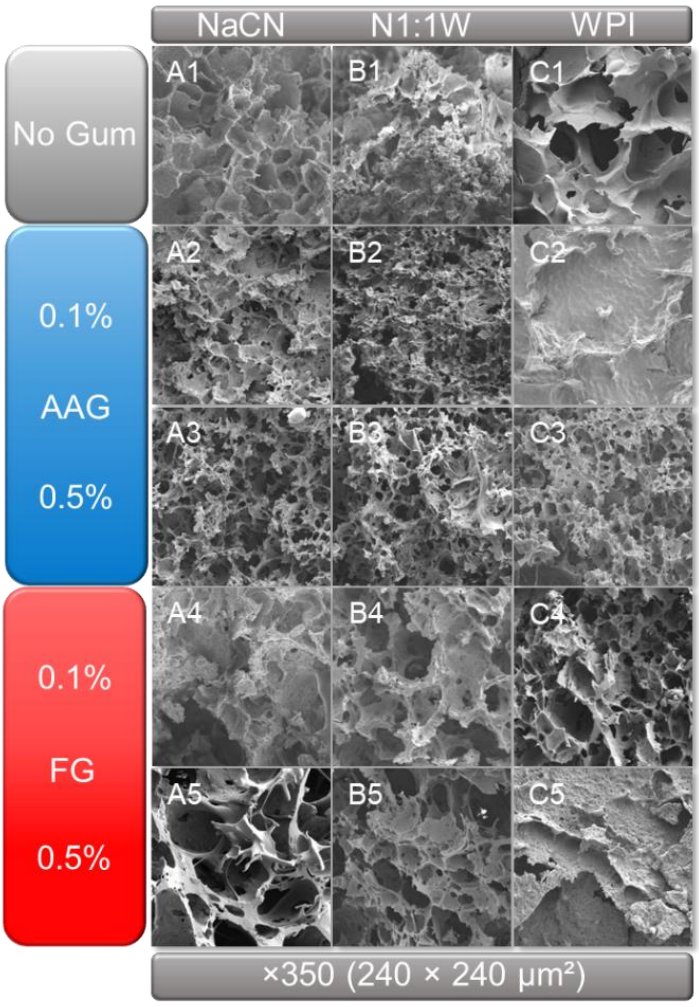


*Figure 78: Scanning electron micrographs of NaCN (A), WPI (C), and their binary mixture (N1:1W, B), either pure (1) or containing 0.1% and 0.5% wt. of alfalfa gum (2−3) and flaxseed gum (4−5). Magnification = ×350. Abbreviations used: NaCN: Sodium Caseinate, WPI: Whey Protein Isolate, N1:1W: mixed proteins NaCN:WPI at a ratio of 1:1, AAG: alfalfa gum, FG: flaxseed gum*

The median vessel thickness ($D_{50}$) generally exhibited proportional reduction correlated to the NaCN:WPI ratio. This trend appears to be associated with the differences identified in the microstructure conformation of the acid-hydrogel precursors, i.e. aggregated fractals vs fine-stranded based morphologies. In contrast, the incorporation of gum significantly ($p < 0.05$) increased the $D_{50}$ values from 3.37 µm for gum-free to 3.62 µm and 5.06 µm for AAG-stabilised and FG-stabilised cryogels, respectively. In the case of AAG, the increase in the $D_{50}$ values can likely be attributed to the formation of interpenetrating protein-AAG networks, as previously discussed. For the FG-stabilised cryogel, it is assumed that the increase in thickness of the vessels can be attributed to the electrostatic molecular interactions between the polymers possessing opposite charges (ζ-potential = −15.5, 16.4, and 20.0 mV for FG, NaCN and WPI, respectively). Ultimately, by analysing the uniformity of the vessels thickness, or span, it was determined that the

WPI cryogels exhibited a higher degree of skeletal heterogeneity compared to their NaCN and NaCN-WPI analogues.

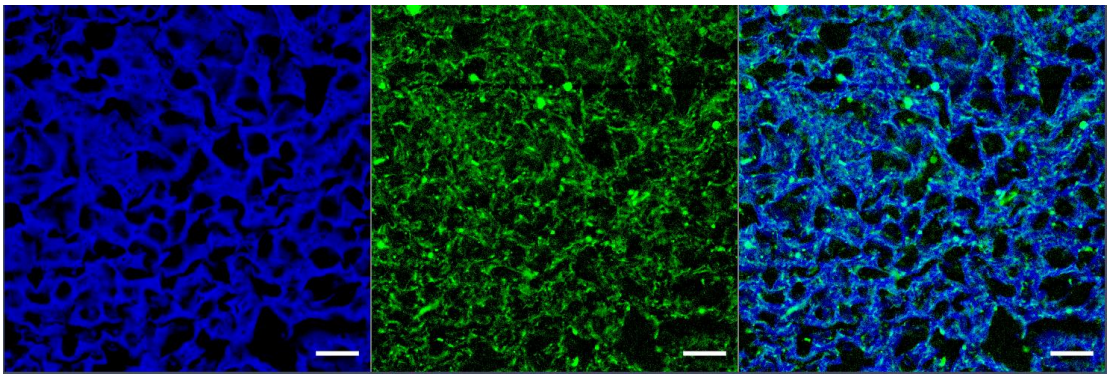

*Figure 79: Confocal Laser Scanning Microscopy (CLSM) micrographs illustrating the cryotropic gelation occurring between WPI (blue, Fast Green dye) and AAG (green, 5-DTAF dye). Individual WPI and AAG networks are on the left and middle, with a merged image on the right. Scale bar: 50 µm.*

ii. Water vapour sorption isotherms

To understand how the composition of the cryogels affects their interaction with water, shortly after the completion of the lyophilisation process, the cryogels were transferred into RH-controlled cabinets. Depending on their composition, microstructural and thermophysical properties, cryogels were reported to exhibit either a type II (Ciuffarin et al., 2023) or type III (Hellebois et al., 2023; Manzocco et al., 2022) water vapour sorption isotherms. As illustrated in Figure 80, the water vapour sorption isotherms displayed a predominantly type III curve pattern. However, a knee point similar to the isotherm type II was identified at low $a_w$ (i.e. 0.14–0.24) in all cases. The hybrid shape observed in the sorption isotherms can be ascribed to the complex composition and structural aspects of the cryogels. Type II isotherms are commonly observed in protein-based macroporous food xero-matrices (Lowell & Shields, 1984) whereas type III isotherms describe accurately xero-particulates rich in amorphous sugars (Al-Muhtaseb et al., 2002). In addition, an inflexion point was identified, indicating a shift in the curvature of the isotherm from convex to concave at $a_w = 0.35 \pm 0.03$, depending on the exact composition of the cryogel. Therefore, at $a_w > a_{w,infl}$ the rate of water vapour absorption increases, promoting physicochemical alterations. In keeping with this, we have recently demonstrated that the inactivation of *L. rhamnosus* GG protein milk protein cryostructurates was increased steeply at $a_w > 0.33$, leading to detrimental losses of their biological activity (Hellebois, Canuel, et al., 2024).

The moisture – $a_w$ data were fitted to the BET model (Equation 39) and the inflection (or

knee) point associated with the monolayer water content ($X_m$) was calculated for the cryogels (Table 22). Contrary to FG, the inclusion of AAG induced a significant ($p < 0.01$) decrease in the $X_m$ of the cryogels irrespective of the protein composition of the cryogels. By comparing the $X_m$ values of the AAG and FG stabilised cryogels, it was shown that AAG resulted in significantly lower values (i.e. $X_m$ = 7.30, 6.83 and 6.69 $gH_2O.100g_{db}^{-1}$ for NaCN, N1:1W, and WPI, respectively) compared to the FG-stabilised exemplars (i.e. $X_m$ = 7.73, 7.04 and 6.74 $g_{H_2O}.100g_{db}^{-1}$ for NaCN, N1:1W, and WPI, respectively). On the other hand, in the FG stabilised cryogels, a significant reduction in the $X_m$ was observed only at 0.1% wt. It is generally accepted that the presence of polysaccharides in protein-based lyophilisates is associated with higher $X_m$ values due to the increasing number of polar sites (i.e. −COOH, −OH) that promote the chemisorption of water molecules via hydrogen bonding (Kinsella et al., 1986). Nevertheless, other parameters such as the surface chemistry, the specific area, and the morphology of the cryogels may also be influential on the water adsorption dynamics (Iglesias & Chirife, 1982; Labuza, 1975). In their study, Manzocco et al., (2022) reported a water content of approximately 22 $g.100\ g_{db}^{-1}$ in cryogels comprising 20% WPI when the systems were incubated at a water activity of 0.85. Contrarily, in the present study, we recorded values ranging from 34 to 42 $g\ 100\ g_{db}^{-1}$ for an identical water activity. Such discrepancies are attributable to the presence of highly hygroscopic solutes, namely glycerol, trehalose, and glucose. The adverse impact of the AAG on the water vapour adsorption capacity of cryogels appeared to be associated with the reduction in the size of the macropores (as evidenced in the SEM micrographs). This renders accessing the water molecules to the hydrophilic binding sites more difficult. In addition, as we have reported previously (Hellebois, Gaiani, Fortuin, et al., 2021; Hellebois, Soukoulis, Xu, Hausman, et al., 2021). AAG exhibits a significantly lower solvent (water) affinity to FG ($k_H$ = 0.85 and 0.67 for AAG and FG, respectively) that could impede the saturation of the hydrophilic binding sites. Ultimately, due to its ability to form its own interpenetrating polymeric networks on cryogenic processing (Hellebois, Gaiani, & Soukoulis, 2022a). AAG may sterically hinder the binding of water to the polar sites of the proteins, i.e. −COO−, −NH+, −OH much more effectively than FG.

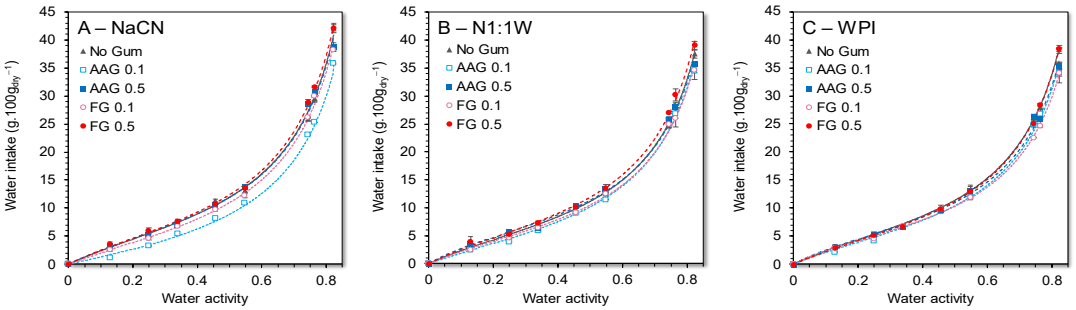


*Figure 80: Water vapour sorption curves of NaCN- (A), N1:1W- (B) and WPI- (C) based cryogels influenced by the presence of 0.1 and 0.5% wt. of AAG and FG. The lines (continuous: no gum, short dash: 0.1%, long dash: 0.5% wt.) represent the fitted BET equation (Equation 39) for each sample. Abbreviations used: NaCN: Sodium Caseinate, WPI: Whey Protein Isolate, N1:1W: mixed proteins NaCN:WPI at a ratio of 1:1, AAG: alfalfa gum, FG: flaxseed gum*

*Table 22: Milk protein cryogels calculated BET equation parameters fitted to water vapour adsorption data.*

| Protein | Gum | $X_m$ (g.100g$_{dry}^{-1}$) | C - | $S_m$ ($m^2.g^{-1}$) |
|---|---|---|---|---|
| NaCN | No gum | 7.67 ± 0.18$^{f}$ | 3.52 ± 0.73$^{bc}$ | 268.3 ± 6.3$^{f}$ |
| | AAG 0.1 | 7.06 ± 0.09$^{cd}$ | 1.80 ± 0.13$^{a}$ | 247.2 ± 3.1$^{cd}$ |
| | AAG 0.5 | 7.55 ± 0.19$^{f}$ | 3.80 ± 0.88$^{bcd}$ | 264.1 ± 6.7$^{f}$ |
| | FG 0.1 | 7.47 ± 0.16$^{f}$ | 2.78 ± 0.46$^{ab}$ | 261.4 ± 5.6$^{f}$ |
| | FG 0.5 | 7.99 ± 0.10$^{g}$ | 3.46 ± 0.36$^{bc}$ | 279.5 ± 3.4$^{g}$ |
| N1:1W | No gum | 7.04 ± 0.10$^{cd}$ | 3.81 ± 0.51$^{bcd}$ | 246.3 ± 3.6$^{cd}$ |
| | AAG 0.1 | 6.85 ± 0.22$^{bc}$ | 2.90 ± 0.73$^{ab}$ | 239.6 ± 7.7$^{bc}$ |
| | AAG 0.5 | 6.82 ± 0.14$^{bc}$ | 5.00 ± 1.10$^{d}$ | 238.8 ± 4.9$^{bc}$ |
| | FG 0.1 | 6.65 ± 0.12$^{b}$ | 3.74 ± 0.62$^{bcd}$ | 232.7 ± 4.3$^{b}$ |
| | FG 0.5 | 7.43 ± 0.12$^{ef}$ | 4.00 ± 0.63$^{bcd}$ | 260.2 ± 4.4$^{ef}$ |
| WPI | No gum | 7.20 ± 0.05$^{de}$ | 3.80 ± 0.25$^{bcd}$ | 252.0 ± 1.8$^{de}$ |
| | AAG 0.1 | 6.67 ± 0.17$^{b}$ | 3.56 ± 0.80$^{bc}$ | 233.4 ± 6.0$^{b}$ |
| | AAG 0.5 | 6.70 ± 0.16$^{b}$ | 4.62 ± 1.15$^{cd}$ | 234.5 ± 5.7$^{b}$ |
| | FG 0.1 | 6.27 ± 0.07$^{a}$ | 4.70 ± 0.53$^{cd}$ | 219.4 ± 2.4$^{a}$ |
| | FG 0.5 | 7.22 ± 0.06$^{de}$ | 3.47 ± 0.24$^{bc}$ | 252.6 ± 2.0$^{de}$ |

*$^{a-g}$Different letters between the cryogels denote a significant difference ($p < 0.05$) for each parameters according to Duncan's post hoc means comparison test. Values are expressed as mean ± standard error. Abbreviation used: $M_0$: water monolayer content (in g per 100g of dry matter), C: an energetic constant and $S_0$: the surface of the monolayer (in $m^2.g^{-1}$)*

iii. Thermal stability

The thermal stability of the protein – plant seed gum cryogels was tested by means of TGA, as illustrated in Figure 81. According to the TGA thermographs obtained, three major mass loss events were registered in the temperature range of 25–400 °C. As previously reported (Hellebois et al., 2023), the mass loss events detected at 44–72 °C and 177–191 °C are associated with the evaporation of the residual (non-bound) water and the decomposition of glycerol, respectively. As expected, the mass losses due to water evaporation were minimal (i.e. $0.7 < \Delta m < 1.7\%$) due to the pre-conditioning of the samples in an inert gas desiccating glove-box system ($a_w = 0.03$). It is worth noting that the total mass losses observed in the 177–191 °C range were well above the total mass of glycerol present in the cryogels (i.e. $16.7 < \Delta m < 20.1\%$) implying the occurrence of a secondary thermal event taking place in the specific temperature range. It is therefore assumed that mass losse resulting from the release of water vapour during the early stages of the protein glycation (Schiff base reaction) and the formation of organic volatile compounds associated with the Amadori rearrangement and Strecker reactions could also occur at temperatures of 171–191 °C (Van Boekel, 2006).

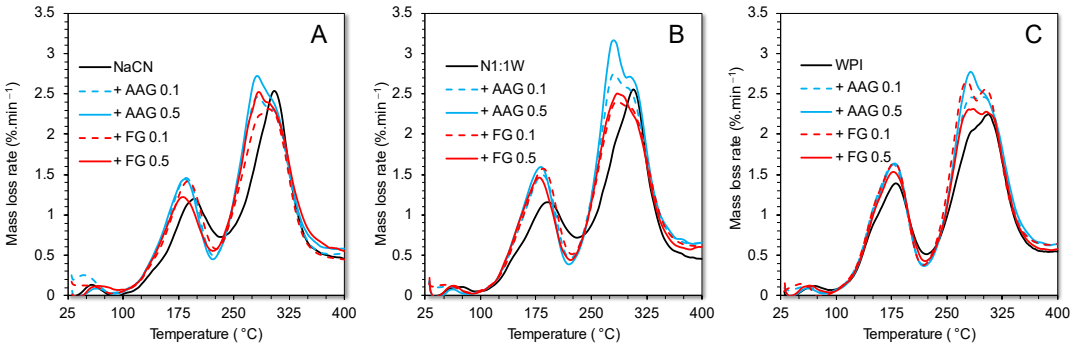


*Figure 81: First derivative (DTG) of TGA curves of NaCN (A) N1:1W (B) and WPI (C) solutions (continuous black lines) as influenced by the presence of alfalfa and flaxseed gum at 0.1 (dashed lines) and 0.5% wt. (continuous coloured lines).*

Four successive thermal decomposition events were detected at 281–288, 299–305, 448–492 and 558–638 °C, amounting to an average mass loss of 23.4 ± 4.5, 24.9 ± 4.5, 18.0 ± 5.5 and 15.7 ± 7.5% (Table 23). The peak detected at 281–288 °C appears to be associated with the decomposition of the polysaccharidic components, as confirmed by the analysis of the pure gums (Figure 82). On the other hand, the intensity of the thermal event observed at 299–305 °C showed a clear dependence ($p < 0.001$) on the protein-to-gum ratio, with the highest mass losses recorded for the gum-absent cryogels. Barreto et al., (2003) reported that the onset decomposition temperature of sodium caseinate and whey protein isolate under inert gas conditions (also applicable for our study) was 300 and 295

°C, respectively. In addition, (Adsare & Annapure, 2021) showed that the presence of arabic gum in coconut protein-based powders resulted in a significant decrease in the residual matter following thermal decomposition.

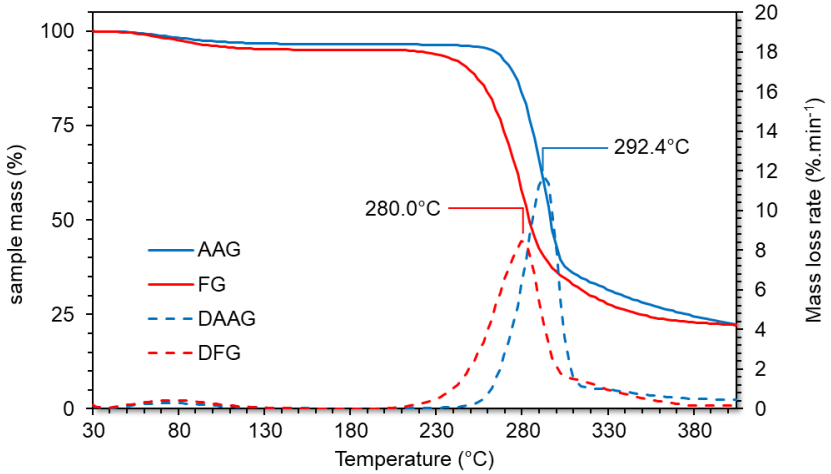


*Figure 82: Thermal gravimetric analyses (TGA, continuous lines) and TGA curve first derivative (DTGA, dashed lines) of alfalfa gum (in blue) and flaxseed gum (in red).*

*Table 23: Relative mass loss of the cryogels obtained from the peak areas of the DTG curves.*

| Protein | Gum | Mass loss (%) | | | | | |
|---|---|---|---|---|---|---|---|
| | | 59 °C | 182 °C | 284 °C | 302 °C | 473 °C | 598 °C |
| NaCN | No gum | 1.0$^{a}$ | 18.0$^{bcd}$ | 13.9$^{a}$ | 38.3$^{e}$ | 9.0$^{a}$ | 26.6$^{f}$ |
| | AAG 0.1 | 2.2$^{a}$ | 18.3$^{bcde}$ | 25.2$^{cd}$ | 20.9$^{ab}$ | 10.3$^{a}$ | 25.2$^{f}$ |
| | AAG 0.5 | 0.7$^{a}$ | 17.7$^{bc}$ | 26.1$^{cd}$ | 20.8$^{ab}$ | 13.7$^{bc}$ | 20.0$^{e}$ |
| | FG 0.1 | 1.6$^{a}$ | 18.5$^{cdef}$ | 30.4$^{d}$ | 23.9$^{bcd}$ | 12.5$^{ab}$ | 24.6$^{f}$ |
| | FG 0.5 | 1.7$^{a}$ | 16.4$^{a}$ | 23.8$^{cd}$ | 22.7$^{abc}$ | 14.9$^{bc}$ | 20.9$^{e}$ |
| N1:1W | No gum | 1.0$^{a}$ | 17.4$^{b}$ | 16.0$^{ab}$ | 28.2$^{d}$ | 12.3$^{ab}$ | 24.8$^{f}$ |
| | AAG 0.1 | 1.0$^{a}$ | 18.8$^{def}$ | 24.3$^{cd}$ | 24.5$^{bc}$ | 20.3$^{e}$ | 10.6$^{bc}$ |
| | AAG 0.5 | 0.6$^{a}$ | 18.9$^{def}$ | 27.4$^{cd}$ | 23.9$^{bc}$ | 20.8$^{e}$ | 8.0$^{ab}$ |
| | FG 0.1 | 1.3$^{a}$ | 20.1$^{g}$ | 23.0$^{abc}$ | 23.0$^{abc}$ | 18.3$^{de}$ | 14.3$^{cd}$ |
| | FG 0.5 | 1.0$^{a}$ | 18.2$^{bcde}$ | 24.9$^{cd}$ | 18.8$^{a}$ | 20.3$^{e}$ | 16.5$^{cd}$ |
| WPI | No gum | 1.0$^{a}$ | 18.7$^{cdef}$ | 16.0$^{ab}$ | 28.3$^{d}$ | 25.6$^{f}$ | 10.7$^{bc}$ |
| | AAG 0.1 | 1.2$^{a}$ | 20.0$^{g}$ | 22.2$^{bc}$ | 24.9$^{bc}$ | 24.4$^{f}$ | 7.0$^{ab}$ |
| | AAG 0.5 | 0.7$^{a}$ | 19.5$^{fg}$ | 24.2$^{cd}$ | 24.1$^{bc}$ | 24.6$^{f}$ | 6.1$^{a}$ |
| | FG 0.1 | 1.2$^{a}$ | 20.1$^{g}$ | 22.0$^{bc}$ | 27.3$^{cd}$ | 23.0$^{ef}$ | 6.1$^{a}$ |
| | FG 0.5 | 0.9$^{a}$ | 19.2$^{efg}$ | 21.4$^{bc}$ | 24.2$^{bcd}$ | 19.5$^{de}$ | 14.2$^{cd}$ |

$^{a-g}$*Different letters between the cryogels denote a significant difference ($p < 0.05$) for each parameters according to Duncan's post hoc means comparison test*

iv. Water reconstitution behaviour

In general, the reconstitution of xero-particulates in water is a dynamic process that involves four major consecutive kinetically driven physical processes: a) wetting, b)

swelling, c) dispersing and d) dissolution (Markl & Zeitler, 2017). The *in situ* monitoring of the particle size aspects (i.e. $D_{[4,3]}$) of the cryogel monoliths under rigorous mixing conditions revealed different disintegration profiles, which were primarily ($p < 0.001$) driven by the protein composition (Figure 83, Table 24). However, gum inclusion was the primary driver of the disintegration kinetic parameters, i.e. $\tau$ and $\tau_{99\%}$. In the absence of gum, the mixed protein-based cryogels exhibited the slowest disintegration profile ($\tau$ = 100 s) compared to the NaCN ($\tau$ = 14 s) and WPI ($\tau$ = 85 s) exemplars, which is in keeping with our previous observations (Hellebois et al., 2023). The inclusion of the gums (at the level of 0.5% wt.) resulted in a significant ($p < 0.05$) increase in the disintegration kinetic parameters ($\tau$ = 66, 66 and 154 s, $\tau_{99\%}$ = 455, 437 and 1025 s for 0, 0.1 and 0.5% wt. of gum, respectively). A positive correlation between the median thickness of the cryogel vessels ($D_{50}$) and the dissolution kinetic parameters, i.e. $\tau$ and $\tau_{99\%}$ was found ($r = 0.62$, $p < 0.05$).

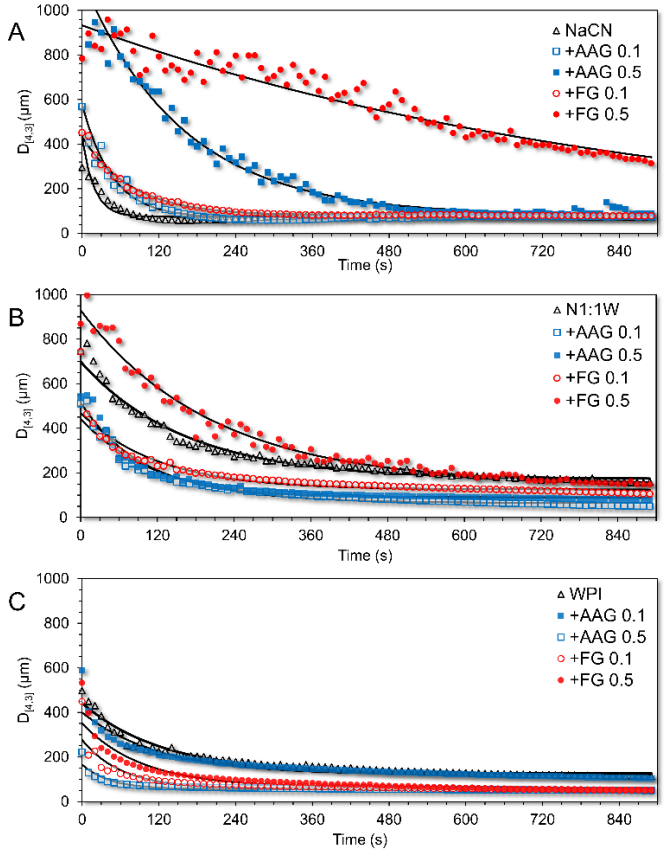


*Figure 83: Matrix disintegration profile of the NaCN (A), N1:1W (B) and WPI (C) cryogels as influence by the presence of alfalfa and flaxseed gums at 0.1 and 0.5% wt. The solid lines represent the Equation 41 fitted to the disintegration data. Abbreviations used: NaCN: Sodium Caseinate, WPI: Whey Protein Isolate, N1:1W: mixed proteins NaCN:WPI at a ratio of 1:1, AAG: alfalfa gum, FG: flaxseed gum.*

In addition, the bulk density ($\rho_{bulk}$) and the mean size of the insoluble residual matter at t

= t∞ also increased proportionally ($r = 0.60$, $p < 0.05$). Therefore, the water reconstitution time increased dramatically in cryogels with a compacted structure composed of thick *co*-polymer vessels, confirming the diffusion-driven dissolution mechanism of protein-based cryogels (Hellebois et al., 2023). It is worth noting that of the two gums tested, only FG resulted in a significant slowdown of the reconstitution kinetics of the cryogels, which can be attributed to their ability to undergo electrostatic complexation with milk proteins, diminishing the diffusivity of the water molecules through the vessel capillaries. A similar behaviour was previously reported in the study of Karrar et al., (2021) where adding acacia gum into WPI spray-dried particulates reduced their solubility and consequently prolonged their wetting time from 9.5 to 12.8 min.

*Table 24: Disintegration parameters of the milk protein-based cryogels according to Equation 41.*

| Protein | Gum | $D_{[4,3]}$ $t_0$ (µm) | $D_{[4,3]}$ $t_\infty$ (µm) | $\tau$ (s) | $\tau_{99\%}$ (s) |
|---|---|---|---|---|---|
| NaCN | No gum | 407 ± 24$^{cd}$ | 76 ± 2$^{ab}$ | 14 ± 1$^{a}$ | 94 ± 7$^{a}$ |
| | AAG 0.1 | 583 ± 76$^{de}$ | 70 ± 2$^{a}$ | 32 ± 1$^{a}$ | 214 ± 9$^{a}$ |
| | AAG 0.5 | 1189 ± 10$^{4g}$ | 81 ± 11$^{abc}$ | 105 ± 18$^{d}$ | 695 ± 121$^{d}$ |
| | FG 0.1 | 433 ± 30$^{cd}$ | 80 ± 2$^{abc}$ | 53 ± 8$^{b}$ | 353 ± 53$^{b}$ |
| | FG 0.5 | 930 ± 79$^{f}$ | 94 ± 52$^{abcd}$ | 521 ± 11$^{f}$ | 3463 ± 74$^{f}$ |
| N1:1W | No gum | 686 ± 174$^{e}$ | 126 ± 19$^{de}$ | 100 ± 1$^{d}$ | 706 ± 65$^{d}$ |
| | AAG 0.1 | 443 ± 26$^{cd}$ | 65 ± 6$^{a}$ | 86 ± 8$^{cd}$ | 569 ± 52$^{cd}$ |
| | AAG 0.5 | 518 ± 47$^{cde}$ | 90 ± 0$^{abcd}$ | 66 ± 3$^{bc}$ | 439 ± 18$^{bc}$ |
| | FG 0.1 | 470 ± 11$^{cd}$ | 125 ± 5$^{cde}$ | 84 ± 1$^{cd}$ | 557 ± 6$^{cd}$ |
| | FG 0.5 | 952 ± 59$^{f}$ | 150 ± 5$^{e}$ | 138 ± 16$^{e}$ | 915 ± 108$^{e}$ |
| WPI | No gum | 450 ± 84$^{cd}$ | 127 ± 36$^{de}$ | 85 ± 11$^{cd}$ | 563 ± 66$^{cd}$ |
| | AAG 0.1 | 399 ± 14$^{bcd}$ | 120 ± 1$^{bcde}$ | 85 ± 8$^{cd}$ | 567 ± 55$^{cd}$ |
| | AAG 0.5 | 165 ± 34$^{a}$ | 56 ± 7$^{a}$ | 31 ± 5$^{a}$ | 205 ± 353$^{a}$ |
| | FG 0.1 | 230 ± 36$^{ab}$ | 59 ± 8$^{a}$ | 55 ± 7$^{b}$ | 362 ± 44$^{b}$ |
| | FG 0.5 | 352 ± 28$^{bc}$ | 63 ± 1$^{a}$ | 65 ± 16$^{bc}$ | 435 ± 104$^{bc}$ |

*Abbreviation used: $D_{[4,3]\ t0}$: particle size (in µm) at t = 0 min; $D_{[4,3]\ t\infty}$: particle size (in µm) at t = ∞ min; $\tau_{1/2}$: time (in seconds) required to obtain a 50% particle size reduction; $\tau_{99\%}$: time (in seconds) required to obtain a 99% particle size reduction. $^{a-g}$Different letters between the cryogels denote a significant difference ($p < 0.05$) for each property according to Duncan's post hoc means comparison test. Lowercase letters indicate differences within the same protein-based cryogels whereas uppercase denotes differences for the same amount of gum in the different protein-based cryogels.*

# CONCLUSIONS

In the present study, we assessed the impact of two plant seed mucilages on the microstructural and physicochemical properties of milk protein-based cryogels. The results revealed that inclusion of both alfalfa and flaxseed gum in milk protein solutions induced a segregative phase separation. Upon fermentation, the microstructural elements of the protein-gum solution were, to a certain degree, arrested. In general, the presence of plant seed gums minimised the volume contraction and lacunarity of the cryogels during freeze-drying and increased the median thickness of their vessels. In the case of alfalfa gum, it was postulated that the observed differences stemmed from its capacity to form an intertwined network with milk proteins during cryogenic processing. In contrast, the role of the flaxseed gum in the modulation of the structural properties of the cryogels primarily arose from its electrostatic complexation with milk proteins. In addition, gums enhanced the thermal stability of the cryogels and prolonged their water disintegration times. Nonetheless, the average size of the residual insoluble particles was influenced exclusively by the protein type. Concerning the water vapour sorption dynamics, only alfalfa gum was able to suppress the monolayer water uptake. This phenomenon was associated with its lower water affinity and the formation of its interpenetration network sterically hindering the binding of water. Although the findings support our hypothesis that the hydrogel precursors' compositional profile substantially impacts the microstructure and physicochemical properties of the cryogels, the colloidal state of the solution and hydrogel precursors was not directly associated. The cryogels that contained alfalfa and flaxseed gum exhibited significant variability in their morphology, microstructure, and dissolution properties. These variations could influence the biological activity of the probiotics during storage and *in vitro* digestion. These aspects will be discussed in our subsequent article.

# STABILITY AND ADHESION PROPERTIES OF *LACTICASEIBACILLUS RHAMNOSUS* GG EMBEDDED IN MILK PROTEIN CRYOGELS: INFLUENCE OF PLANT SEED GUM INCLUSION

Thierry HELLEBOIS[1,2], Jennyfer FORTUIN[1,3], Sébastien CAMBIER[1], Servane CONTAL[1], Céline C. LECLERCQ[1], Claire GAIANI[2], and Christos SOUKOULIS[1]

[1]Environmental Research and Innovation (ERIN) Department, Luxembourg Institute of Science and Technology (LIST), Esch-sur-Alzette, Luxembourg

[2]Université de Lorraine, LIBio, Nancy, France

[3]Food Quality and Design Group, Wageningen University and Research, Wageningen, The Netherlands

Food Hydrocolloids

Volume 151, June 2024, 109867

doi.org/10.1016/j.foodhyd.2024.109867

# ABSTRACT

This work reports on the influence of plant seed gum (PSG) from alfalfa (*Medicago sativa* L.) and flaxseed (*Linum usitatissimum* L.), on cryogels based on sodium caseinate (NaCN), whey protein isolate (WPI), and their combined mixture in embedding the probiotic *Lacticaseibacillus rhamnosus* GG (LGG). A significant preservation of LGG cell viability was achieved during the xero-structuration process. Among the materials tested, sodium caseinate was the standout, most effectively preserving LGG's biological activity across varying temperature and humidity conditions. Elevated storage temperature and relative humidity conditions accelerated LGG inactivation rates, especially in the case of WPI (in the presence or absence of PSG), which was primarily attributed to increased metabolic activity due to the changes in the xero-scaffolds' physical state. Moreover, the specific protein type used played a pivotal role in determining LGG's survival rates during simulated gastrointestinal digestion processes. In adhesion tests using a Caco-2/HT-29 *co*-culture model, LGG showed the highest adhesion found in NaCN. Interestingly, except for NaCN, adding PSG augmented LGG's bioadhesion capabilities, with flaxseed gum showing the highest enhancement in adhesin-mucin interactions. The research also underscored the release of bioactive peptides, which displayed a range of health benefits including antimicrobial and antioxidant properties.

# INTRODUCTION

Galactomannans and mucilages are the most prevalent gums found in the endosperm and outermost seed coat layer of plant seeds, respectively (Cakmak et al., 2023; Kontogiorgos, 2019; Lira et al., 2023; Prajapati et al., 2013; Qian et al., 2012; Soukoulis et al., 2018; Wu et al., 2009a). It was previously demonstrated that the endosperm of alfalfa seeds (*Medicago sativa* L.) is rich in a galactomannan (mannose-to-galactose ratio ~ 1.18), which exhibits satisfactory thickening, gelling and cryogel-forming properties (Hellebois, Gaiani, Cambier, et al., 2022; Hellebois, Soukoulis, Xu, Hausman, et al., 2021). On the other hand, flaxseed (*Linum usitatissimum* L.) is one of the most studied plant seed mucilage composed of a high molecular weight (>1500−2000 kDa) arabinoxylan (AX) fraction, a low molecular weight (<500 kDa) rhamnogalacturonan-I based fraction and two intermediate molecular weight (500−2000 kDa) AX−RG-I composite fractions (Hellebois, Fortuin, Xu, Shaplov, et al., 2021). Heretofore, flaxseed gum has been successfully employed as food thickener, gelling and stabilising agent (Liu et al., 2018), whereas its immunoregulatory, anti-glycaemic, anti-lipidemic and anti-obesity functions have been well documented (Luo et al., 2018; Mueed et al., 2022).

Numerous studies have highlighted that imbalances in the gut microbiome are tied to a range of health issues, including chronic inflammation, obesity, type-II diabetes, various cancers, and irritable bowel syndrome (IBS) (Torres-Fuentes et al., 2017; Venema & Carmo, 2015). A common treatment is the use of probiotics, sometimes combined with soluble dietary fibres. The International Scientific Association for Probiotics and Prebiotics (ISAPP) defines “probiotics” as specific microbial species that, when administered in adequate amounts confer a health benefit on the host (Hill et al., 2014).

Encapsulation, i.e., the physicochemical entrapment of bioactive compounds and/or living cells (such as probiotics) in bespoke soft matter templates, is widely employed for the oral delivery of probiotics. Dry particulates, hydrogels, bigels, and cryogels have been designed to protect the cells against physical and chemical stressors (Cook et al., 2012; Garcia-Brand et al., 2022; Gu et al., 2022; Haji et al., 2022). A range of biopolymers, including proteins, starch and its derivatives and various gums as will, have been deployed for crafting the wall material of probiotic formulations (Burgain et al., 2013; sekhavatizadeh et al., 2023; Zhu et al., 2023). The use of binary protein − polysaccharide wall materials is known to enhance the mechanical and barrier (i.e. oxygen and water vapour permeation) properties of the carrier matrix, thereby enhancing the survivability of the probiotic cells during storage, allowing their targeted release and mediating their

adhesion to the gut mucosa layer (de Melo Pereira et al., 2018; Sanders & Marco, 2010). Cryogels are macroporous carriers of customisable microstructure, mechanical strength, and high biocompatibility and biodegradability crafted through the freeze-drying a polymeric precursor specifically physically or chemically cross-linked to form hydrogels (Lozinsky, 2018; Manzocco et al., 2021). Cryogels offer multifaceted applications in the food industry such as the encapsulation and targeted delivery of bioactive compounds and living probiotic cells (Fontes-Candia et al., 2022; Hellebois, Canuel, et al., 2024; Kleemann et al., 2018, 2020; Manzocco et al., 2021; Volkova & Berillo, 2021). It was recently demonstrated that milk protein based cryogels are excellent carriers to promote the biological activity of *Lacticaseibacillus rhamnosus* GG cells during the cryostructuration process and against diverse physicochemical stressors associated with storage and *in vitro* digestion (Hellebois, Canuel, et al., 2024). The incorporation of soluble dietary fibres such as pullulan (Sun et al., 2021) and sodium alginate (Kuo et al., 2022) in freeze-dried hydrogels was associated with enhanced survivability of the embedded probiotic cells (*L. plantarum* or *L. acidophilus* and *B. lactis*, respectively) during processing, storage, and *in vitro* digestion.

In the present work, we aimed to provide insights into the functional role of plant seed derived gums as *co*-structuring wall material in milk protein cryogel templates for the oral delivery of probiotic cells. In view of this, alfalfa and flaxseed gums were assessed for their ability to preserve the survivability of *Lacticaseibacillus rhamnosus* GG living cells, under controlled storage and in vitro digestion simulated conditions and mediating their bioadhesion into a Caco-2/HT-29 mucin producing *co*-culture cell model of the intestinal epithelium. In addition, the potential of the probiotic cryogels in providing supplementary health benefits associated with the release of bioactive peptides was assessed by means of omics tools.

# MATERIALS & METHODS

## Materials

Whey protein isolate (WPI) powder (PRODIET 90S) with a protein content of 85.8% wt. (wet basis) was kindly donated by Ingredia (Arras, France). Sodium caseinate (NaCN) containing 89.4% wt. of protein (N% × 6.25, wet basis), glucose (99.5% wt.) and glycerol (99.9% wt.) was purchased from Sigma-Aldrich (Leuven, Belgium). Trehalose (99.4% wt.) was obtained from Louis-François (Croissy-Beaubourg, France). The De Man,

Rogosa and Sharpe (MRS) culture media was purchased from Carl Roth (Karlsruhe, Germany). The probiotic stain *Lacticaseibacillus rhamnosus* GG (LGG) ATCC 53103 used was purchased from VTT Technical Research Centre of Finland Ltd (Espoo, Finland). All the other chemicals used were of analytical grade.

### Preparation of the *Lacticaseibacillus rhamnosus* GG embedding cryogel monoliths

The procedure for preparing the milk protein-based cryogels is detailed in Hellebois, Addiego, et al., (2024). Briefly, a solution was formulated with 10% wt. of protein, consisting of sodium caseinate (NaCN), whey protein isolate (WPI), or a balanced binary mixture of NaCN and WPI, in addition to 5% wt. trehalose, 2.5% wt. glycerol, and 1% wt. glucose. After undergoing heat treatment at 80 °C for 20 minutes, either alfalfa gum (AAG) or flaxseed gum (FG) was incorporated into the hot protein solution at concentrations of 0.1% or 0.5% wt., before being left to solubilise overnight. Subsequently, the protein solutions were gelled via indirect acidification by LGG (end of the exponential phase) fermentation at approximately 9.3 $logCFU.mL^{-1}$ for a period of 4 h at 37 °C. Finally, the solutions were frozen at −80 °C for 2 h and then freeze-dried for 40 h (Hellebois, Addiego, et al., 2024).

### Viable *Lacticaseibacillus rhamnosus* GG quantification

The total viable counts (TVC) of LGG were determined utilising the method delineated by Hellebois, Canuel, et al., (2024). Concisely, aliquots, each constituting either 1 mL of the inoculated protein solution at t = 0 min, 1 mL of the fermented hydrogel at t = 240 min, 1 g of freeze-dried cryogels, or 1 mL of digestive chymes, were serially diluted by a factor of ten in phosphate-buffered saline (PBS). These diluted solutions were subsequently cultured on MRS agar plates. To simulate microaerophilic conditions, the plated sample was overlaid with a fine layer of MRS agar, followed by incubation at 37 °C for 48 h.

### *Lacticaseibacillus rhamnosus* GG storage stability

To assess the storage stability of LGG cells, freshly produced cryogel monoliths were transferred into hermetically sealed Nalgene acrylic desiccator cabinets (Thermo Fisher Scientific, Waltham, MA, United States). The effect of the physical state of the cryogels (glassy vs. rubbery) was tested using saturated salt solution – LiCl ($a_w$ = 0.11) and NaCl ($a_w$ = 0.75) – at a constant temperature of 20 °C. The effect of the temperature was

assessed in the glassy state using LiCl saturated salt solution at 5, 20 and 37 °C. The resulting LGG inactivation data was then fitted to the Weibull's model (van Boekel, 2002) as follows:

Equation 43 $$\log S_t = -\frac{1}{2.303}\left(\frac{t}{\alpha}\right)^{\beta}$$

where t is the corresponding time (d), $S_t$ the LGG survival ratio ($N_t/N_{initial}$) at t days, α constant describing the time (in days) required to observe a reduction of 0.434 logCFU.g$^{-1}$ of the initial counts ($N_{initial}$) and β a constant describing the model's curvature. From the Equation 43, can be obtained the following equation:

Equation 44 $$t_{shelf\text{-}life} = \alpha(-\ln(10^{-((N_{initial})-6)})^{\frac{1}{\beta}})$$

Where α and β are analogous with Equation 43, $t_{shelf\text{-}life}$ is the shelf-life (i.e. reduction to 6 logCFU.g$^{-1}$) time (in days) and $N_{initial}$ the LGG counts at t = 0 day. Due to the limited amount of bacteria losses during the storage, a first-order kinetic model (Equation 45) was applied in the case of cryogels stored at 5 °C $a_w$ 0.11 as follows:

Equation 45 $$\log N_t = \log N_{initial} - kt$$

Where $N_0$ and $N_t$ are the number of living LGG cells at t = 0 day and t = t day, respectively and k the inactivation rate constant (day$^{-1}$). From Equation 45 the shelf-life (in days) was calculated as follows:

Equation 46 $$t_{shelf\text{-}life} = \frac{(\log N_{intial})-6}{|k|}$$

Where $t_{shelf\text{-}life}$ and $N_{initial}$ are analogous to Equation 44 and k is analogous to Equation 45.

## *In vitro* digestion

### i. *In vitro* digestion protocol

The INFOGEST v2.0 *in vitro* simulated digestion protocol (Brodkorb et al., 2019) was implemented to access the protein hydrolysis and microstructure as well as the bacteria viability. Minor modification to the protocol were applied and are specifically described in our previous study (Hellebois, Canuel, et al., 2024).

### ii. Microscopical assessment of the digesta

To monitor the colloidal changes of the proteins as well as qualitatively visualise the bacteria lethality during the *in vitro* digestion, aliquots (1 mL) of gastric (t = 120 min) and intestinal (t = 120 min) chyme suspension were non-covalently stained and the following fluorophore were used: 10 µL of 0.05% Fast Green for proteins, 1.5 µL of 3 mM Syto9 for living cells, and 1.5 µL of 20 mM propidium iodide for inactivated cells.

Three hundred microliters were then transferred onto eight-well Nunc Lab-Tek II microscope slides and were microscopically assessed using a ×40 objective lens mounted on a confocal laser scanning microscope (LSM 880 with Airy scan, Zeiss, Jena, Germany).

iii. Proteomic and peptidomic analyses

The cleavage of the proteins in the intestinal (t = 120 min) chymes was monitored by capillary sodium dodecyl sulfate–polyacrylamide gel electrophoresis (SDS-PAGE). The electrophoresis was ran using a Bioanalyzer 2100 with the protein 80 chip kit following the manufacturer instructions (Agilent Technologies, Santa Clara, CA, United States). The gels were reconstructed using 2100 Expert software (Agilent Technologies, Santa Clara, CA, United States).

To determine the production of peptides from the milk proteins at the end of the *in vitro* digestion, 10 mL aliquots of homogeneous intestinal chymes were centrifuge-filtered. Amicon tubes (Merck, Darmstadt, Germany) equipped with a filter cut-off of 10 kDa were used to remove uncleaved proteins. Then, 1 mL of the filtrates obtained were vacuum-dried (CentriVap, Labconco, Kansas City, MO, United States) and analysed using nano-liquid chromatography – mass spectrometry (nano-LC-MS) analyses following the method described in (Hellebois, Canuel, et al., 2024). The significant peptide sequences (score ≥ 50) obtained were then compared to the bioactive peptide database BIOPEP-UWM (Minkiewicz et al., 2019).

## Mucoadhesion behaviour of *Lacticaseibacillus rhamnosus* GG cells

i. Preparation of the intestinal epithelium *co*-culture model

The human colon cancer Caco-2 cell line sub-clone TC7 (Caco-2/TC7) and HT29-MTX cells lines were maintained in Dulbecco's Modified Eagle Medium-Glutamax (DMEM-Glutamax, Invitrogen, Merelbeke, Belgium) supplemented with 10% fetal bovine serum (Invitrogen, Merelbeke, Belgium) at 37 ± 0.5 °C in 10% $CO_2$ atmosphere in a humidified incubator. Their *co*-culture was initiated by seeding the cells at a 90:10 ratio (Caco-2/TC7 and HT29-MTX respectively) and were grown for 14 days at 37 ± 0.5 °C in a 10% $CO_2$ humidified incubator (Georgantzopoulou et al., 2016). The medium was replaced every two days. At the end of the 14 days of differentiation the medium was discarded, and the differentiated *co*-culture was washed with PBS. To prevent the digestion of the Caco2/HT29 epithelium model in the presence of the intestinal enzymes (trypsin), the

cells were fixated using 2.5% vol. glutaraldehyde in PBS for 30 min at 25 ± 1 °C. The glutaraldehyde was washed-out by sequential PBS washings.

ii. Assessment of adhered *Lacticaseibacillus rhamnosus* GG cells

To investigate the adhesion potential of the LGG cells on the intestinal epithelium, PBS was replaced by intestinal chymes (t = 120 min) of the cryogels i.e. 300 µL in eight-chambered microscope slides (Nunc Lab-Tek II, Thermo Fisher Scientific, Waltham, MA, United States) or 2500 µL in six-well microplates (Corning, Corning, NY, United States) for the microscopic assessment and TVC, respectively. After 120 min of incubation at 37 ± 1 °C in an orbital shaker (100 rpm) (Świątecka et al., 2010), the systems were washed twice with PBS. The microscopic evaluation of the adhesion of the bacteria onto the mucosa was assessed in wet conditions using a × 40 objective mounted on a CLSM microscope (LSM 880 with Airy scan, Zeiss, Jena, Germany). Fast Green, SYTO9, and propidium iodide were added as staining agents for protein, viable and inactivated LGG cells, respectively. Simultaneously, a twin system was immobilised using a 2.5% volume of glutaraldehyde in PBS for a duration of 30 min at a temperature of 25 ± 1 °C. The solvent was replaced through a sequential washing process, transitioning from water to ethanol, with concentrations of 10, 30, 50, 70, and 90% employed once, and 100% ethanol three-fold. To preserve the tissue integrity, an ethanol–hexamethyldisilazane (HMDS) solvent exchange was performed. The system was washed once with 10, 30, 50, and 70% HMDS, followed by three washes with 90 and 100% HMDS. The solvent was evaporated overnight at room temperature, and the systems were then affixed to a carbon tape, coated with a 5 nm layer of platinum using an ACE 600 coating system from Leica Microsystems (Wetzlar, Germany) and stored in a desiccator to prevent water absorption until further use. Scanning electron microscopy (SEM) was conducted using a field emission scanning electron microscope (SU-70, Hitachi, Tokyo, Japan). The acceleration was set to 5 kV, with a working distance of 15 mm and a magnification of ×5000.

To enumerate the cultivable adhered LGG cells, the epithelium model was mechanically disrupted in PBS, allowing the bacteria to be released. Subsequently, the bacteria suspensions were plated onto MRS agar medium, which was then overlaid with a second layer of MRS agar. The plated samples were incubated at a temperature of 37 °C for a duration of 2 days.

### Statistical analyses

The normal distribution of the data was assessed using the Shapiro-Wilk test and Q–Q plot visual representations. To identify significant variances, a one-way ANOVA was conducted employing the Origin 2019b software (OriginLab Inc., Northampton, MA, United States). Upon detecting significant discrepancies ($p < 0.05$), Tukey's post-hoc test was employed to differentiate between mean values.

## RESULTS & DISCUSSION

### Viability of the *Lacticaseibacillus rhamnosus* GG during freeze-drying

The impact of the biopolymer composition on the viability of LGG throughout the cryostructuration process (i.e. hydrogel formation and freeze-drying) is illustrated in the Figure 84. According to the ANOVA findings, only the protein type was significantly influential on the total viable counts of LGG, with the survivability rates being proportionally increasing to the increase in the NaCN to WPI mass fraction ($m_{NaCN/WPI}$). As expected, the fermentation of the precursor solutions was associated with a significant – yet minor – increase in the TVCs of LGG, i.e. from 10.16 to 10.31 $logCFU.g^{-1}$. On the other hand, the freeze-drying of the hydrogel precursors was accompanied by a significant ($p < 0.001$) reduction in the TVCs of LGG ranging from 9.79 to 10.36 $logCFU.g^{-1}$ with the highest cellular sublethality being observed in the cryogels exerting the lowest $m_{NaCN/WPI}$. The survival rates of LGG during the freeze-drying step ranged from 41.7 to 83.2%, which is in keeping with the reported survival rates in protein – polysaccharides freeze-dried microtemplates (Oluwatosin et al., 2022).

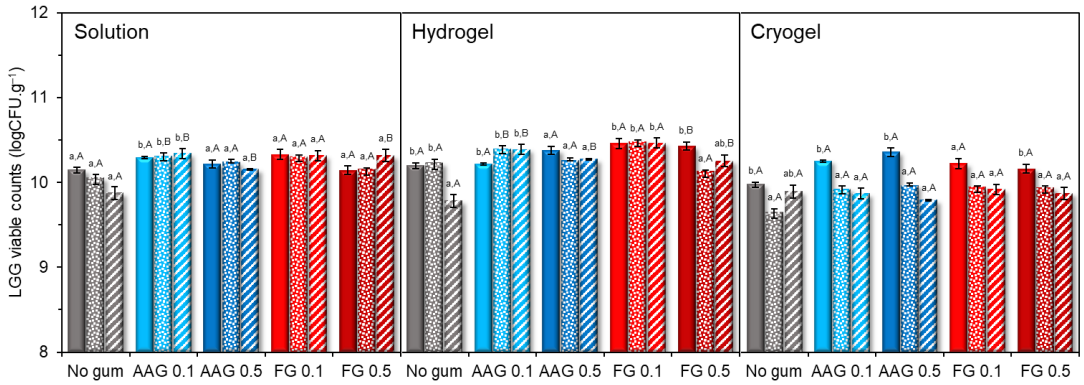


*Figure 84: Lacticaseibacillus rhamnosus GG viably counts ($logCFU.g^{-1}$, expressed on dry basis) after inoculation of the protein solution (Solution), following 4 h of fermentation at 37 °C (Hydrogel) and after 40 h of freeze-drying (Cryogel). Plain bars: sodium caseinate (NaCN)-based cryogels, dashed*

*bars: whey protein isolate (WPI)-based cryogels, dotted bars: Mixed protein cryogel with NaCN:WPI ratio of 1:1 (N1:1W). AAG 0.1 and AAG 0.5: alfalfa gum at 0.1 and 0.5% wt., respectively. FG 0.1 and FG 0.5: flaxseed gum at 0.1 and 0.5% wt., respectively.* $^{a\text{-}c}$*Different letters denote a significant ($p < 0.05$) difference between the protein type at the same state (lowercase) and for the different states for the same sample (uppercase) according to Tukey's post hoc means comparison test.*

As illustrated in the SEM micrographs (Figure 85) in the absence of the PSGs, the probiotic cells were well embedded into the protein-based skeleton of the cryogels with only few LGG chains residing on the outer surface. Interestingly, the inclusion of the PSGs in the cryogel precursors (hydrogels) resulted in an increase in the number of bacterial cells being deposited on the air – matrix interface (Figure 85). The CLSM assisted visualisation of the microstructure of the probiotic solutions (Figure 86) revealed that although the LGG cells show a preferential localisation in the protein-rich microdomains, the occurrence of segregative phase separation pushes some of the bacterial chains to the protein – PSG interface (most probably due to their differences in the osmotic pressure), which are ultimately immobilised during the indirect gelation process. These protein – PSG interface located bacteria appear to be the most sensitive to cellular damage taking place during the cryogenic processing (ice crystallisation of the PSG-rich aqueous pockets) and ice sublimation (dehydration is faster in the porogen microdomains). This may explain why the inclusion of the PSGs resulted in a higher (yet non-significant) reduction in the TVCs of LGG during the freeze-drying.

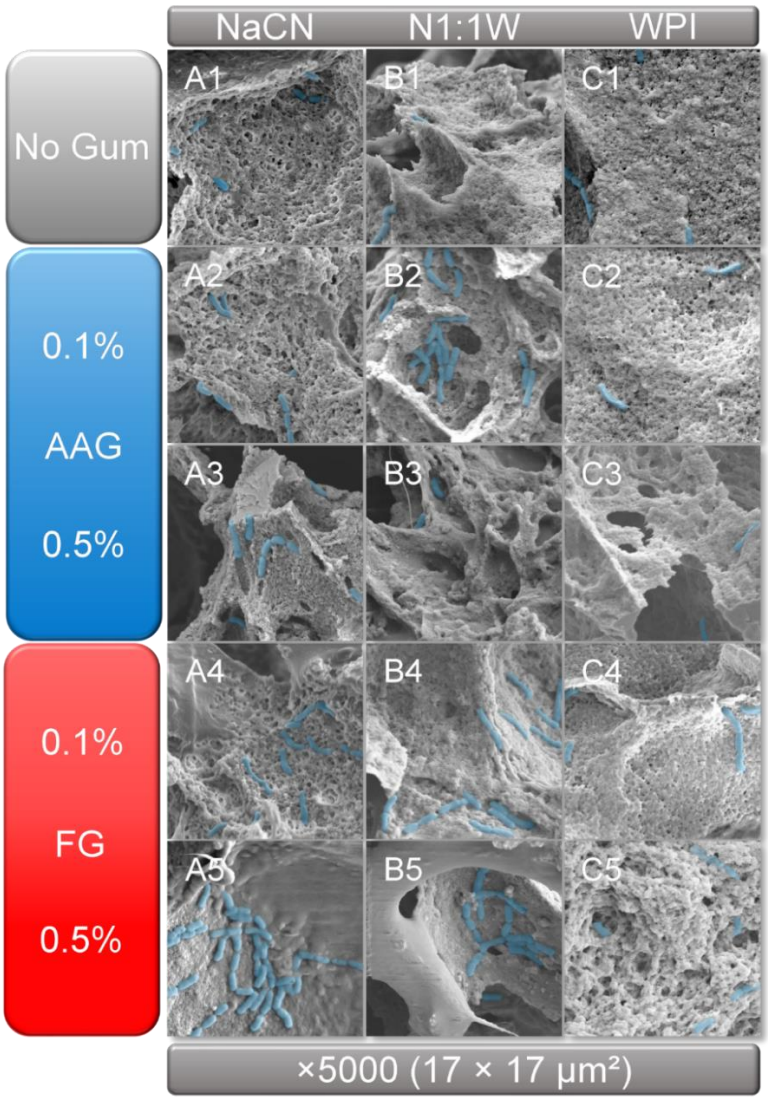


*Figure 85: Scaning electron microscopy images of sodium caseinate (A), mixed sodium caseinate – whey protein isolate at 1:1 ratio (B) and whey protein isolate (C)-based cryogels. Gum free systems are represented in "1", cryogels containing alfalfa gum (AAG) at 0.1 and 0.5% in 2 and 3 and flaxseed gum (FG) at 0.1 and 0.5% in 4 and 5, respectively. For illustration purposes, the LGG cells were coloured in blue.*

It is well demonstrated that the ability of the solutes to affect the colligative properties of the polymeric precursors as well as the ice crystal nucleation and ripening during the cryogenic processing step are inextricably associated with the achieved lyoprotective effects. In general, the frozen storage – glass transition temperature interval, i.e. $\Delta T = T_f - T_g$, is a significant determinant of the probiotics lethality due to the disruption of the cell membrane stemming from the uncontrolled growth of the ice crystals and the osmolytic stress (Guerrero Sanchez et al., 2022; Kuo et al., 2022). As we observed in our previous work (Hellebois, Addiego, et al., 2024), the measured $T_g$ values for the gum-free systems was in the range of −34 to −36 °C, implying their complete vitrification

under the implemented freezing conditions. In addition, the presence of the gums did not induce any remarkable change in the $T_g$ values, due to their high effective molecular weight, which may also explain their non-significant impact on the attained lyoprotective effectiveness.

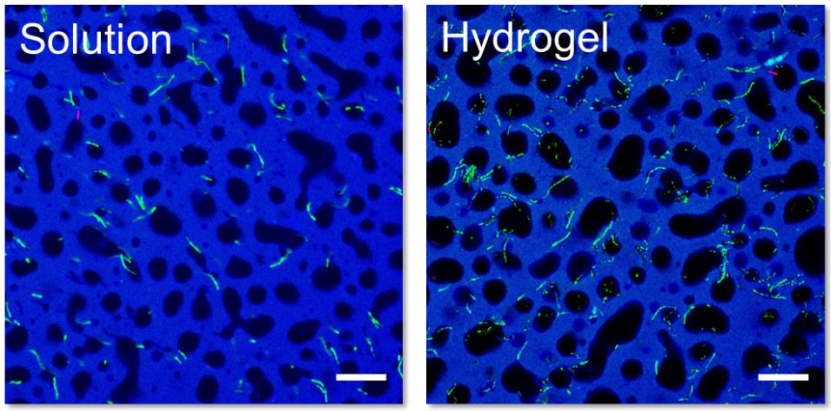


*Figure 86: Representative CLSM micrographs – WPI containing 0.1% of FG – of LGG cells localisation in milk protein-gum systems before and after lactic acid-induced gelation. Scale bar: 20 µm. Protein are stained in blue (fast green), living and dead bacteria in green and red, respectively. The gum microdomains are represented in black (unstained).*

The presence of macromolecular lyoprotectants, i.e. compounds able to preserve the cells membrane fluidity during the dehydration process by binding water via hydrogen bonding in the vicinity of the polar interface of the phospholipid bilayer is another factor associated with the preservation of the biological activity of probiotics during lyophilisation (Aschenbrenner, Foerst, et al., 2015). In general, polysaccharides exert higher solvent (water) affinity compared to proteins due to the higher prevalence of polar side groups able to bind water via hydrogen bonding i.e. –OH and –COOH. Although, some differences in the water affinity of the FG and AAG have been previously reported, i.e. $k_{Huggins}$ = 0.63 and 0.85, respectively (Hellebois, Fortuin, Xu, Shaplov, et al., 2021; Hellebois, Soukoulis, Xu, Hausman, et al., 2021), it was not possible to identify any clear association with the survivability of LGG, which could be ascribed to their quite low mass fraction ($m_{PSG}$ = 0.5–2.6 g.100g$^{-1}$ dry solids). On the contrary, a good correlation between the surface hydrophobicity (i.e. 2.65 and 3.65 µg SDS.500 µg$^{-1}$ for NaCN and WPI, respectively) (Hiller & Lorenzen, 2008) and the solvent affinity (i.e. $k_{Huggins}$ = –1.33 and –0.04 for NaCN and WPI, respectively) (O'Sullivan et al., 2014) of the milk proteins and the survivability of LGG was found, suggesting that NaCN is more effective in binding water molecules than WPI. In keeping with this it was previously demonstrated that the

NaCN based cryogels exhibited a higher water vapour sorption capacity compared to their WPI counterparts (Hellebois, Addiego, et al., 2024).

## Storage stability of *Lacticaseibacillus rhamnosus* GG

To assess the ability of the engrafting xero-scaffolds to preserve the biological activity of the LGG cells under diversified static storage conditions, the probiotic cryogels were transferred into temperature (5, 20 and 37 °C) – relative humidity (11 and 75%) controlled cabinets and stored for 100 days. The LGG cell inactivation dynamics are illustrated in Figure 87 and Table 25. As expected, both storage temperature and relative humidity were highly influential on the survivability of LGG. To gain insight into the LGG cell inactivation kinetics, the TVC – storage time data were analysed using Weibull (Equation 43) and first-order (Equation 45) regression models. As shown in Table 25, only in the case of the cryogels stored at chilling conditions the LGG inactivation were described by first order kinetics. A similar behaviour was also reported by (Fortuin et al., 2023) in protein (pea, whey, or Spirulina) – maltodextrin lyophilisates embedding LGG cells. In the context of microbial inactivation, the Weibull distribution is used to model the probability that a microorganism will be inactivated by a certain treatment or environmental condition at a given time (van Boekel, 2002). The determined kinetic parameters, $\alpha$ and $\beta$ denote the time required for observing a log (1/e) decline in the viable microbial load and the responsiveness of the cells to the imposed stressor (i.e. adaptation or cellular damage accumulation), respectively. At chilling conditions, the LGG cells response to the physicochemical stressors was negligible, with the NaCN cryogels allowing the best cell stabilising effect ($k = 1.43 \times 10^{-3}$, $4.67 \times 10^{-3}$, $4.99 \times 10^{-3}$ $day^{-1}$, for NaCN, N1:1W and WPI, respectively) which is in agreement with our previous study (Hellebois, Canuel, et al., 2024). The elevation of the storage temperature resulted in a significant ($p < 0.001$) shortening of the cell inactivation lag phase as indicated by the $\alpha_T$ parameter ($\alpha_T$ = 14.5 vs. 0.68 days, at 20 and 37 °C, respectively) due to acceleration of the LGG metabolic activity. The $\alpha_T$ parameter was highly dependent on the protein composition of the cryogels with the NaCN-based exemplars showing the best LGG cell stabilising effect ($\alpha_T$ = 1.33, 0.41 and 0.20 vs. 35.7, 4.53 and 3.59 days, for NaCN, N1:1W and WPI cryogels stored at 37 and 20 °C, respectively). As for the $\beta_T$ values, the impact of storage temperature was dependent on the composition of the cryogels. In general, the convexity ($\beta_T < 1$) of the LGG curves was significantly higher in the N1:1W and WPI cryogels, compared to NaCN LGG inactivation curves, which represented a linear to concave behaviour ($\beta_T$ = 0.993 vs. 1.548 at 37 and 20 °C, respectively). As well depicted

in Figure 87, the inclusion of PSGs in the cryogel formulation enhanced the storage stability of LGG embedded in the NaCN based systems but it impaired the LGG sublethality in the mixed protein and WPI exemplars. This illustrates the ability of NaCN to prolong the LGG cell damage accumulation before lethality is being established.

*Table 25: LGG inactivation kinetic parameters influenced by the gum type and concentration, protein type and storage conditions.*

| Protein | Gum | [1]$a_w$ 0.11 5 °C | [2]$a_w$ 0.11 20 °C | | [2]$a_w$ 0.11 37 °C | | [2]$a_w$ 0.75 20 °C | |
|---|---|---|---|---|---|---|---|---|
| | | Slope | α | β | α | β | α | β |
| | | $day^{-1}$ | days | - | days | - | days | - |
| NaCN | No gum | $-0.002^{bc}$ | $12.07^{cd}$ | $0.93^{abc}$ | $1.77^{ab}$ | $1.31^{a}$ | $1.97^{cd}$ | $1.16^{ab}$ |
| | AAG 0.1 | $-0.001^{ab}$ | $43.27^{ab}$ | $1.72^{a}$ | $1.11^{cd}$ | $0.88^{bcd}$ | $0.24^{f}$ | $0.62^{e}$ |
| | AAG 0.5 | $-0.003^{bc}$ | $27.84^{bc}$ | $0.98^{ab}$ | $0.77^{d}$ | $0.77^{cd}$ | $2.41^{c}$ | $1.08^{bc}$ |
| | FG 0.1 | $-0.000^{a}$ | $41.77^{ab}$ | $1.52^{ab}$ | $0.97^{d}$ | $0.82^{bcd}$ | $0.20^{f}$ | $0.61^{e}$ |
| | FG 0.5 | $-0.001^{abc}$ | $50.72^{a}$ | $1.42^{ab}$ | $2.01^{a}$ | $0.89^{bc}$ | $3.55^{a}$ | $1.19^{ab}$ |
| N1:1W | No gum | $-0.002^{c}$ | $2.85^{d}$ | $0.49^{bc}$ | $1.45^{bc}$ | $0.99^{b}$ | $2.18^{bc}$ | $0.93^{bc}$ |
| | AAG 0.1 | $-0.004^{bc}$ | $6.26^{d}$ | $0.85^{abc}$ | $0.02^{e}$ | $0.40^{g}$ | $0.48^{f}$ | $0.61^{e}$ |
| | AAG 0.5 | $-0.003^{bc}$ | $4.60^{d}$ | $0.79^{abc}$ | $0.05^{e}$ | $0.46^{fg}$ | $1.44^{de}$ | $0.89^{cd}$ |
| | FG 0.1 | $-0.004^{c}$ | $2.70^{d}$ | $0.75^{abc}$ | $0.00^{e}$ | $0.05^{h}$ | $0.54^{f}$ | $0.71^{de}$ |
| | FG 0.5 | $-0.008^{c}$ | $3.27^{d}$ | $0.65^{abc}$ | $0.10^{e}$ | $0.51^{efg}$ | $0.91^{ef}$ | $0.76^{de}$ |
| WPI | No gum | $-0.007^{c}$ | $0.00^{d}$ | $0.19^{c}$ | $0.29^{e}$ | $0.73^{cde}$ | $3.35^{ab}$ | $1.32^{a}$ |
| | AAG 0.1 | $-0.008^{c}$ | $3.00^{d}$ | $0.87^{abc}$ | Nd | Nd | $0.21^{f}$ | $0.60^{e}$ |
| | AAG 0.5 | $-0.003^{bc}$ | $7.53^{d}$ | $1.21^{abc}$ | $0.10^{e}$ | $0.65^{def}$ | $2.04^{cd}$ | $1.19^{ab}$ |
| | FG 0.1 | $-0.005^{c}$ | $2.30^{d}$ | $0.83^{abc}$ | Nd | Nd | $0.28^{f}$ | $0.62^{e}$ |
| | FG 0.5 | $-0.003^{bc}$ | $4.91^{d}$ | $1.14^{abc}$ | $0.00^{e}$ | $0.08^{h}$ | $0.51^{f}$ | $0.72^{de}$ |

*[a-h]Different letters between the cryogels denote a significant difference ($p < 0.05$) among the cryogels for the same column to Tukey's post hoc means comparison test. [1]first-order kinetics. [2]Weibull' model parameters. Nd: not detected.*

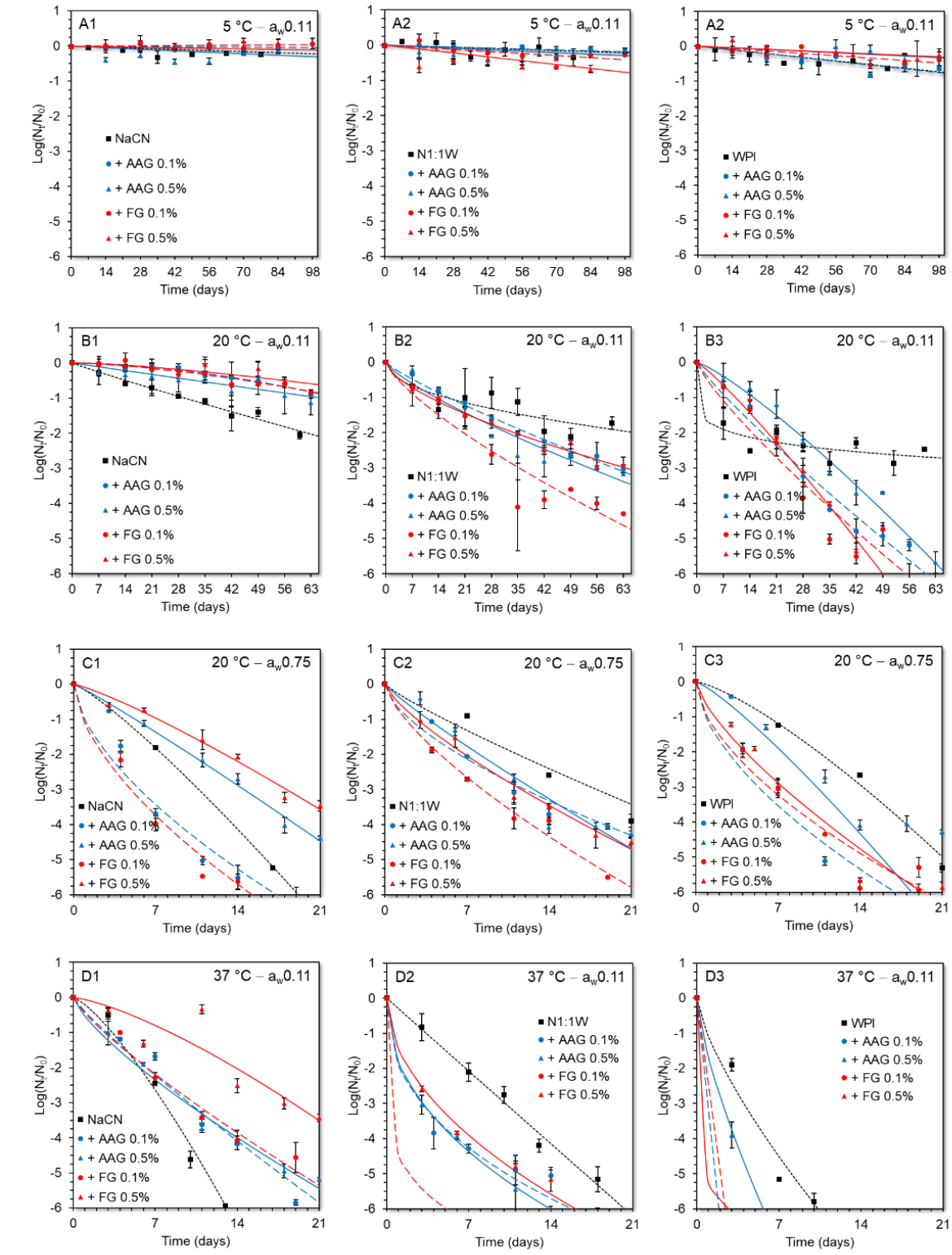


*Figure 87: LGG embeeded in milk protein-based cryogels inactivation curves during storage at 5 °C, $a_w$ 0.11 (A), 20 °C, $a_w$ 0.11 (B), 20 °C, $a_w$ 0.75 (C), 37 °C, $a_w$ 0.11 (D). Sodium caseinate (NaCN)-based cryogels are found in "1", mixed sodium caseinate – whey protein isolate at 1:1 ratio (N1:1W) in "2" and whey protein isolate (WPI) in "3". First order (A) and Weibull's model (B–D) fitted data are represented in black dotted lines for gum free cryogels, in dashed lines for 0.1% and continuous lines for 0.5%. Red: flaxseed gum, blue: alfalfa gum.*

In a manner akin to storage temperature, the increase in the storage relative humidity resulted in a significant ($p < 0.001$) decrease in the calculated kinetic parameters ($\alpha_{RH}$ = 14.5 vs. 1.4 day and $\beta_{RH}$ = 1.01 vs. 0.87, at 11 and 75% RH, respectively), with the $m_{NaCN/WPI}$ being the only influential compositional factor ($\alpha_{RH}$ = 18.6, 2.8 and 2.4, and $\beta_{RH}$ = for NaCN, N1:1W and WPI, respectively, $p < 0.001$). On the other hand, the presence of PSG was rather of minor importance, with the PSG concentration influencing only the $\beta_{RH}$ ($\beta_{RH}$ = 0.86, 0.86 and 1.07, respectively, for 0, 0.1 and 0.5% wt., respectively, $p < 0.05$). Based on the aforementioned, the NaCN-based cryogels containing 0.5% of PSG appeared to be the most adaptable xero-scaffolds to diverse RH conditions. In addition, despite their substantial differences in their molecular and chemical structure configuration, both tested PSGs provided similar shielding capacity against temperature and water vapour stressors throughout storage.

It is well documented that the sublethality of probiotic cells throughout storage is species- and strain-dependent (Wendel, 2022). In addition, extrinsic parameters such as composition, microstructure and physical state of the conveying soft-matter template are of paramount importance for maximising the bacterial cells stabilisation during storage (Gbassi & Vandamme, 2012; Iravani et al., 2015; Sanders & Marco, 2010). Concerning the scaffold composition, previous studies have underlined the importance of proteins in preserving probiotics due to their ability to promote the cell – matrix adhesion (Gomand et al., 2019) allowing a satisfactory embedment of the living cells into the wall material (Hellebois, Canuel, et al., 2024) and thus, suppressing the diffusivity of oxygen and water vapour; both being powerful physicochemical stressors leading to irreversible changes in the cell membrane integrity. Although previous studies have shown that WPI possess a good cell stabilising role (Burgain et al., 2015; Yin et al., 2024), the inferior storage stability of LGG embedded in the WPI cryogels can be primarily attributed to their lower lyostabilising performance compared to the NaCN exemplars. This is in keeping with the observations of (Guerrero Sanchez et al., 2022) who documented that the changes in the integrity of the cell membrane lipid bilayer occurring during the freeze-drying process have a predominant role on the stability of probiotics during storage.

The storage conditions were selected in a fashion that allowed the achievement two distinct physical states, i.e. rubbery (at 75% RH) and glassy (at 11% RH). It is well established that the achievement of a glassy state is an essential factor for maximising the probiotic cells preservation throughout storage due to the suppression of their metabolic activity (Aschenbrenner, Foerst, et al., 2015). In our previous study, we have demonstrated that the inactivation rate of LGG embedded in milk protein cryogels

commenced to progressively accelerate at $a_w > 0.33$ due to the transition from the glassy to the rubbery state (Hellebois, Canuel, et al., 2024). According the calculated $\alpha_{RH}$ and $\beta_{RH}$ parameters, the physical state transition shortened the LGG inactivation lag phase due to alleviation of the steric inhibitors of the metabolic activity and biochemical reactions (e.g. lipid oxidation) taking place during storage. The superior LGG stabilising effects of NaCN compared to WPI, could be attributed into two major factors: a) its richness in peptides with high free radical scavenging performance (Ries et al., 2010; Yin et al., 2022) and b) the finer and more uniform macroporous structure of the NaCN cryogels compared to their WPI counterparts (Hellebois, Addiego, et al., 2024) reducing the water vapour and oxygen permeability.

In most of the cases, the incorporation of soluble dietary fibre aims at the creation of physicochemical barriers against to commonly encountered physicochemical stressors. Except for NaCN–PSG systems, the inclusion of the gums did not offer any tangible cell preservation benefits. Previous studies have shown that preservation performance of polysaccharides is species and strain dependent. In view of this, (Peredo et al., 2016) demonstrated that the inclusion of biopolymers such as psyllium, potato starch or inulin were more efficient in protecting *L. plantarum* than *L. casei Shirota* over 30 days of storage at 4 and 22 °C. On the other hand, the inclusion of rice bran fibres in freeze-dried ionotropically crosslinked pectin capsules preserved better the biological activity of *L. acidophilus* than Hi-maize starch and inulin (Raddatz et al., 2020).

To estimate the shelf-life of the probiotic cryogels, the minimum total load in viable probiotic cells according to the recommendation of FAO/WHO, (2002), i.e. 6 logCFU $g^{-1}$ was used a boundary. As shown in Table 26, the shelf-life of the probiotic cryogels at chilling storage conditions ranged from 1.4 to more than 3 years, which is compliant to the requirement of anhydrobiotics. As expected, the shelf-life of the probiotic cryogels was steeply declined when extrinsic physicochemical stressors were imposed, i.e. $t_{shelf\text{-}life}$ = 2–388 days.

*Table 26: Estimated cryogels shelf-life (in days) cryogels influenced by gum type and content and storage conditions.*

| Protein | Gum | [1] $a_w$ 0.11 5 °C | [2] $a_w$ 0.11 20 °C | [2] $a_w$ 0.11 37 °C | [2] $a_w$ 0.75 20 °C |
|---|---|---|---|---|---|
| NaCN | No gum | > 3 years$^{bc}$ | 141$^{defg}$ | 10$^{c}$ | 13$^{e}$ |
| | AAG 0.1 | > 3 years$^{ab}$ | 162$^{cdefg}$ | 15$^{b}$ | 10$^{gh}$ |
| | AAG 0.5 | > 3 years$^{bc}$ | 213$^{bcde}$ | 16$^{b}$ | 21$^{b}$ |
| | FG 0.1 | > 3 years$^{a}$ | 195$^{bcdef}$ | 16$^{b}$ | 9$^{gh}$ |
| | FG 0.5 | > 3 years$^{abc}$ | 252$^{bcd}$ | 26$^{a}$ | 24$^{a}$ |
| N1:1W | No gum | > 3 years$^{c}$ | 302$^{ab}$ | 14$^{b}$ | 18$^{cd}$ |
| | AAG 0.1 | > 3 years$^{bc}$ | 271$^{bc}$ | 6$^{d}$ | 18$^{cd}$ |
| | AAG 0.5 | > 3 years$^{bc}$ | 77$^{fg}$ | 6$^{d}$ | 17$^{d}$ |
| | FG 0.1 | 942$^{c}$ | 51$^{g}$ | < 2$^{f}$ | 12$^{ef}$ |
| | FG 0.5 | 512$^{c}$ | 97$^{efg}$ | 7$^{d}$ | 17$^{d}$ |
| WPI | No gum | 516$^{c}$ | 388$^{a}$ | 6$^{d}$ | 20$^{bc}$ |
| | AAG 0.1 | 506$^{c}$ | 37$^{g}$ | < 2$^{f}$ | 8$^{h}$ |
| | AAG 0.5 | > 3 years$^{bc}$ | 45$^{g}$ | 3$^{e}$ | 13$^{ef}$ |
| | FG 0.1 | 904$^{c}$ | 33$^{g}$ | < 2$^{f}$ | 9$^{gh}$ |
| | FG 0.5 | > 3 years$^{bc}$ | 33$^{g}$ | < 2$^{f}$ | 11$^{fg}$ |

*[a-g]Different letters between the cryogels denote a significant difference ($p < 0.05$) among the cryogels for the same column to Tukey's post hoc means comparison test. The effect of the temperature and physical state was significant for all the tested cryogels. The shelf-life was estimated as the maximum storage time with LGG counts of at least 6 logCFU.g$^{-1}$. [1]Shelf life estimated by first order kinetics. [2]shelf life estimated by Weibull' model.*

## Colloidal changes of the cryogels and viability of *Lacticaseibacillus rhamnosus* GG throughout *in vitro* digestion

Ensuring the maximal survivability of probiotic cells during processing and storage is an essential parameter for confirming the compliance of the embedded colloidal templates with the standards of probiotic formulations. However, the assessment of the colloidal responsiveness of the cell-conveying matrix to the gastrointestinal environment is crucial for understanding their bioactive potential (de Melo Pereira et al., 2018; Sanders & Marco, 2010). The cryogel boluses were prepared by mixing one cryogel monolith with the appropriate amount of artificial saliva at 50 $s^{-1}$ without any mechanical crushing (e.g. processing in an artificial mouth or Stomacher) of the matrix throughout the simulating oral processing. Therefore, the amount of the released free LGG cells was extremely restricted. Then, the partially swollen cryogel boluses were mixed with the simulating gastric fluids and allowed to incubate for 2 h. As shown in the Figure 88, at the end of *in*

*vitro* gastric processing, the cryogel matrices, particularly those based on NaCN, underwent limited disintegration. Furthermore, the presence of PSGs, especially at 0.5% wt., was found to restrict the disintegration of the swollen cryogels, with AAG being more effective than FG.

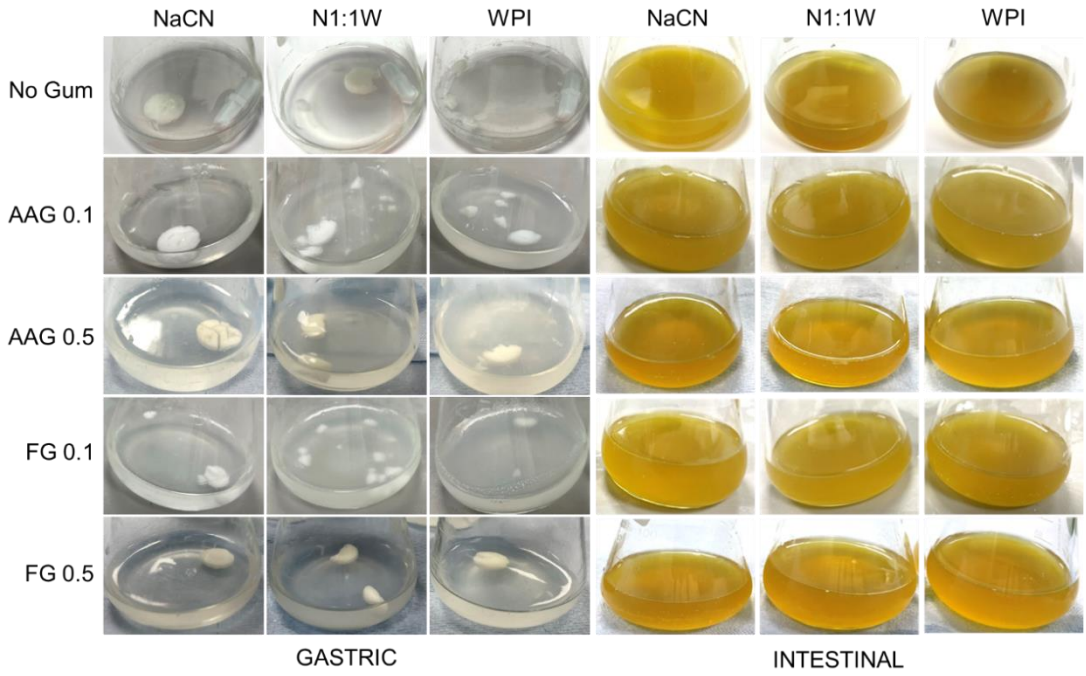


*Figure 88: Pictures of the digested cryogels at the end of the gastric (t = 120 min) and intestinal (t = 120 min) in vitro digestion.*

To gain insight into the mean size of the residual particles in the gastric chymes, after the removal of the intact swollen cryogels, at least five CLSM micrographs were analysed by using ImageJ software and the Feret's diameters ($D_f$) were calculated. As shown in Figure 89, the gastric chymes of the WPI-based cryogels comprised the largest particles (i.e. $D_f$ = 9−204 µm), compared to the mixed protein and NaCN-based exemplars (i.e. $D_f$ = 9−133 µm and 4−37 µm, respectively). This finding corroborates our previous research on the water disintegration behaviour of milk protein-based cryogels (Hellebois et al., 2023). The inclusion of PSGs in the NaCN-based cryogels resulted in an increase in the particles' mean size proportionally to the gum content. In a recent study, we have demonstrated that the presence of AAG and FG prolonged the water disintegration time of NaCN cryogels due to the ability of the gums to reinforce the skeleton of the cryogels (Hellebois, Addiego, et al., 2024). On the other hand, the presence of the PSGs in the mixed protein and WPI based cryogels reduced the mean size of the residual particles in a reciprocal to the gum content fashion. Nonetheless, no clear association of the $D_f$ values with the microstructural (e.g. porosity, vessels thickness) and physicochemical (e.g. bulk density, shrinkage, disintegration time, etc.) aspects of the cryogels was found.

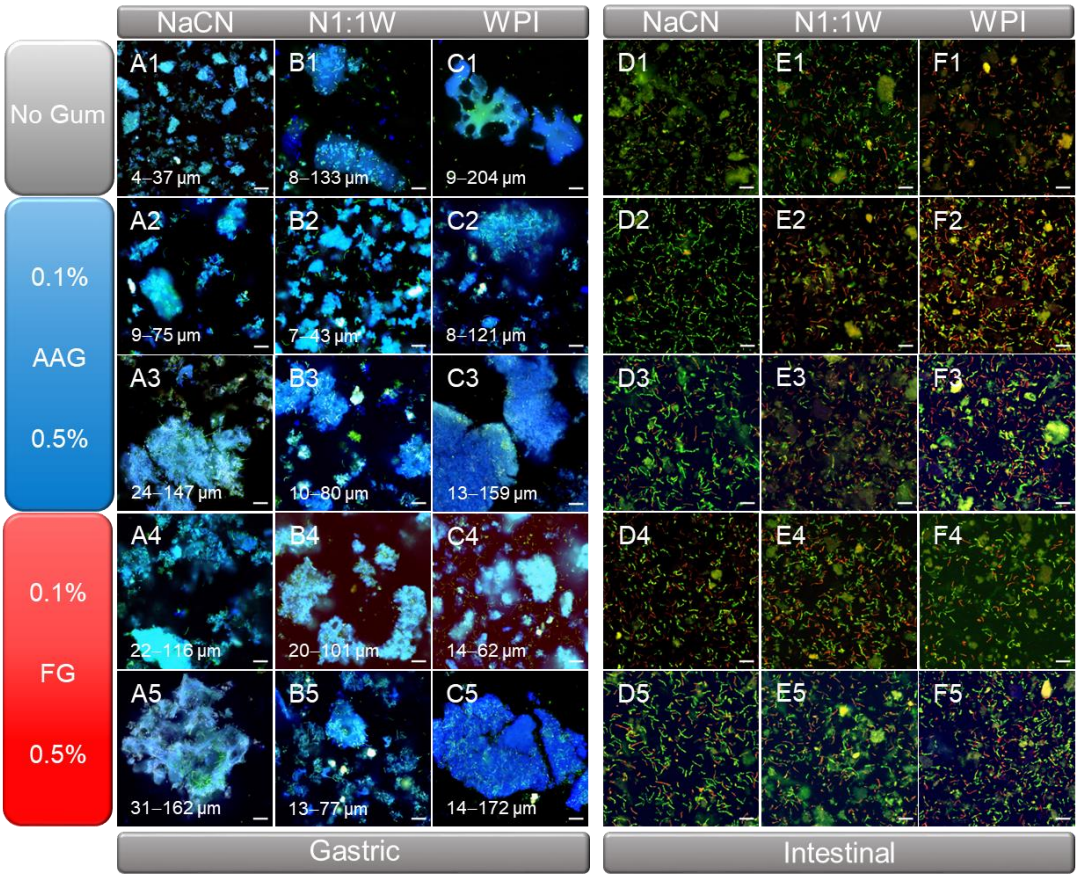


*Figure 89: CLSM acquired micrographs of gastric (A–C) and intestinal (E–F) chymes of the milk protein-based cryogels in the presence of alfalfa and flaxseed gum at 0 (1), 0.1 (2 & 4) and 0.5% wt. (3 & 5). Scale bar: 20 µm. Proteins are stained in blue (Fast Green, $\lambda_{Ex}$ = 633 nm, $\lambda_{Em}$ = 635–680 nm), live bacteria in green (Syto9, $\lambda_{Ex}$ = 488 nm, $\lambda_{Em}$ = 498–550 nm) and inactivated bacteria in red (propidium iodide, $\lambda_{Ex}$ = 488 nm, $\lambda_{Em}$ = 585–640 nm). NaCN: Sodium Caseinate, WPI: Whey Protein, N1:1W: binary mixture of NaCN and WPI protein at 1:1 ratio*

It should be noted that in all cases the CLSM micrographs confirmed the cryogels' ability to prevent the uncontrolled release of free LGG cells in the continuous gastric fluid phase (as indicated by the Syto9 fluorophore-stained living cells), and thus, diminishing the lethal effects of the harsh gastric environment conditions. Indeed, as illustrated in Figure 90 an excellent protection of the viability of the LGG cells in the gastric chymes was observed, i.e. 9.80 vs. 9.45 $\log CFU.g^{-1}$, for initial matrix (cryogels stored at 5 °C for 60 days) and gastric chymes, respectively. In all cases, the embedment of LGG cells into the cryogel scaffold offered a substantial protection against gastric fluids compared to the free (non-encapsulated) LGG cells (Figure 90) Nevertheless, the survivability of LGG under *in vitro* gastric conditions was predominantly influenced by the protein composition ($p < 0.001$) rather than the PSG type and content ($p > 0.05$).

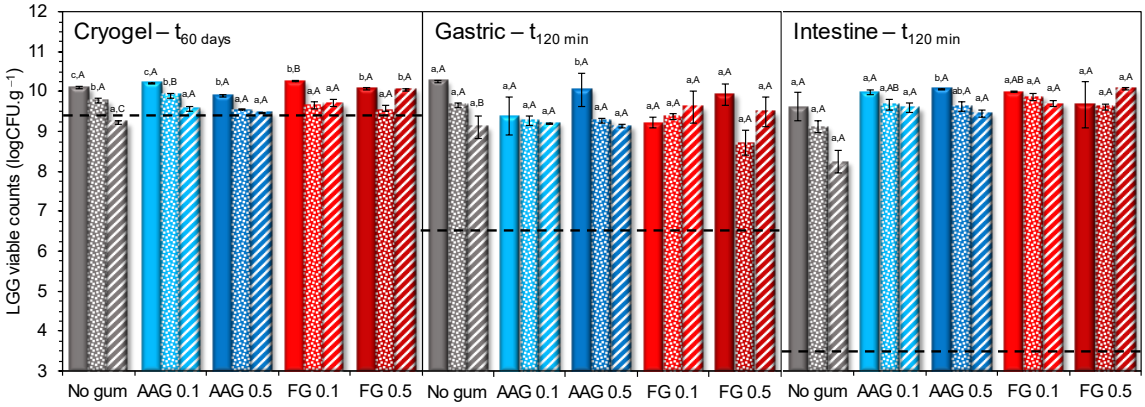


*Figure 90: LGG cells viability throughout the static in vitro simulated digestion following the INFOGEST protocol embeded in sodium caseinate (NaCN, plain bars), mixed sodium caseinate – whey protein isolate at 1:1 ratio (N1:1W, dotted bars) and whey protein isolate (WPI, dashed bars) protein-based cryogels influenced by the presence of alfalfa (AAG) or flaxseed (FG) gums at either 0.1 or 0.5% wt. Dashed lines represents the LGG viable counts in non-encapsulated bacteria systems for each digestive step.* $^{A\text{-}B,a\text{-}c}$*Different letters among the digestive steps for the same cryogel (uppercase) and at each digestive steps among the three protein composition (lowercase) denotes significant ($p < 0.05$) differences.*

In agreement with our previous findings (Hellebois, Canuel, et al., 2024) LGG cell preserving capacity throughout gastric processing was proportional to the increase in the NaCN content. The significance of soluble dietary fibres lies in their capability to protect the viability of probiotics in protein-rich freeze-dried or spray-dried particulates arising from their ability to reduce the rate of gastric fluids diffusion into the protein scaffold, thus enhancing the acid resistance of the encapsulated cells (Desmond et al., 2002; Yao et al., 2023). Moreover, the dense structure of the pre-coagulated milk proteins, coupled with their buffering capacity, has been previously demonstrated to improve the survivability of probiotics by maintaining a higher pH within the core material (Heidebach et al., 2009b). The presence of residual glucose may enhance the viability of LGG under gastric conditions. Prior research has indicated that the presence of metabolisable sugars, such as glucose, enables LGG to produce sufficient quantities of adenosine triphosphate (ATP), necessary for the extrusion of $H^+$ protons from their cytosol via the $F_0F_1$-ATPase, which improves LGG survivability in acidic conditions (Corcoran et al., 2005). The observed minor effects of the polysaccharides on the gastric survivability of LGG are likely due to their relatively low concentration compared to the milk proteins and sugars.

On admixing with the intestinal fluids, a complete disintegration of the cryogel matrices concomitantly with the full release of LGG cells was observed (Figure 89), confirming their feasibility as alternative scaffolds for targeted release of probiotics. As illustrated in

the CLSM micrographs (Figure 89) and TVCs (Figure 90), the bile salt and pancreases induced cellular stress was reduced proportionally to the NaCN to WPI mass ratio (9.87, 9.58, 9.41 for NaCN, N1:1W, and WPI, respectively). Nonetheless, the TVCs in the intestinal digesta were slightly higher than those determined in the gastric chymes (ranging from 0.1 to 0.26 $logCFU.g^{-1}$), implying that in all cases the stressed LGG cells were still cultivable. On the other hand, the free (non-encapsulated) LGG cells experienced an approx. 3 $logCFU.g^{-1}$ reduction in the TVCs suggesting the bile salt sensitivity of LGG at physiologically relevant concentrations. Stemming from their surface-active and amphipathic properties, bile salts can disrupt the bacterial cell membrane's lipid bilayer causing cytoplasmic leakage and damage the intracellular proteins and DNA (Mendonça et al., 2023; Ventura et al., 2011). In accordance with the findings of (Giulio et al., 2005), the presence of trehalose and glucose was associated with a significant improvement of the bile salt tolerance of LGG. In addition, the presence of proteins in the wall material may suppress the bile salt induced cellular injuries due to their capacity to serve as a protective barrier between the bile salts and the phospholipid bilayer (Vargas et al., 2015).

## Adhesion of LGG to an *in vitro* gut epithelium model

Although the preservation of the biological activity of probiotics throughout gastrointestinal transit is an essential aspect of an effective encapsulation strategy, promoting the ability of the living cells to adhere to the mucus layer of the intestinal epithelium should be rigorously evaluated (de Melo Pereira et al., 2018; Sanders & Marco, 2010). To assess the ability of the cryogels to promote the LGG cells adhesion a mucin producing *co*-culture model (Caco-2/HT-29) of the gut epithelium was employed. As clearly depicted in the representative SEM and CLSM micrographs, a satisfactory amount of predominantly living LGG cells was adhered to the mucus-rich microdomains of the *co*-culture model (Figure 91).

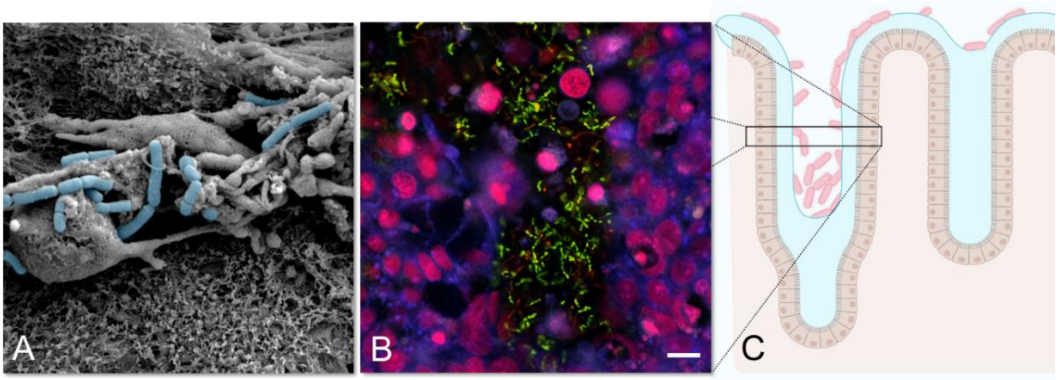

*Figure 91: representative SEM (A) and CLSM (B) micrographs of Caco2/HT29 co-culture model after 120 min of incubation in the presence of intestine chymes of digested and the proposed adhesion mechanism (C). Scale of the micrographs: SEM 17 × 17 µm², CLSM 140 × 140 µm². SEM micrograph blue colour: LGG cells. CLSM micrograph stains: green (Syto9): living LGG cells, red (propidium iodide): inactivated LGG and epithelial cells, blue (fast green): glycoprotein of the mucosa.*

According to the microbial enumeration of the mechanically disrupted epithelial tissues (Figure 92), the LGG bacterial densities ranged from 2.24 to 4.71 logCFU.cm$^{-2}$, with the highest amount of cultivable LGG cells being detected in the NaCN-based digesta (4.56 vs. 4.18 and 4.01 logCFU.cm$^{-2}$, for NaCN, N1:1W and WPI, respectively). Worth to note that in the case of the N1:1W and WPI systems, the presence of PSG significantly enhanced the LGG adhesion properties. Overall, FG exhibited a better LGG adhesion promoting ability compared to AAG i.e. 4.55 vs 4.26 logCFU.cm$^{-2}$, respectively. On the other hand, the presence of AAG in the NaCN based digesta did not significantly modify the LGG adhesion properties. In all cases, the inclusion of PSG at a concentration as low as 0.1% wt. was sufficient to enhance the LGG mucoadhesion. It is established that the adhesion of probiotic cells to the gut mucosa is initiated by weak and reversible hydrophobic binding interactions and in a later stage through specific adhesins – mucins interactions (Bron et al., 2012; Han et al., 2021) represented as follows:

$$B + R \rightleftarrows B{-}R^* \rightarrow BR$$

Where B is the bacterial concentration, R is the constant number of monolayer cell receptor sites, B–R* represents the instable intermediate complex (formed via weak physical interactions) and BR is the stable adhesin – mucin complex. As illustrated in Figure 92 the number of LGG cells adhered onto the mucus layer of the *co*-culture model was highly dependent on the LGG TVCs in the intestinal digesta ($r = 0.88$, $p < 0.001$), indicating the probabilistic character of the cell adhesion phenomena. To get a deeper insight these data were fitted to the Hill's model (Equation 47):

Equation 47
$$BR = R_{max} \frac{B^n}{k^n + B^n}$$

where B and BR denote the viable cells present in the intestinal digesta and adhered onto the mucosa layer, respectively, n is the cooperativity constant, $R_{max}$ is the maximum number of viable LGG cell that can be adhered to the mucosa layer and k denotes the amount LGG cells required to achieve $\frac{R_{max}}{2}$ (Mays et al., 2020). The cooperativity constant was estimated at n = 14.9, suggesting that once a bacterial cell is specifically adhered to the mucins its affinity to intercellular homophilic interactions, i.e. pili – pili hydrophobic bonding, is increased (Tripathi et al., 2013). The maximum adherence capacity was

estimated at $R_{max}$ = 5.1 logCFU.cm$^{-2}$ confirming that the presence of PSGs was crucial for maximising the LGG adhesion capacity.

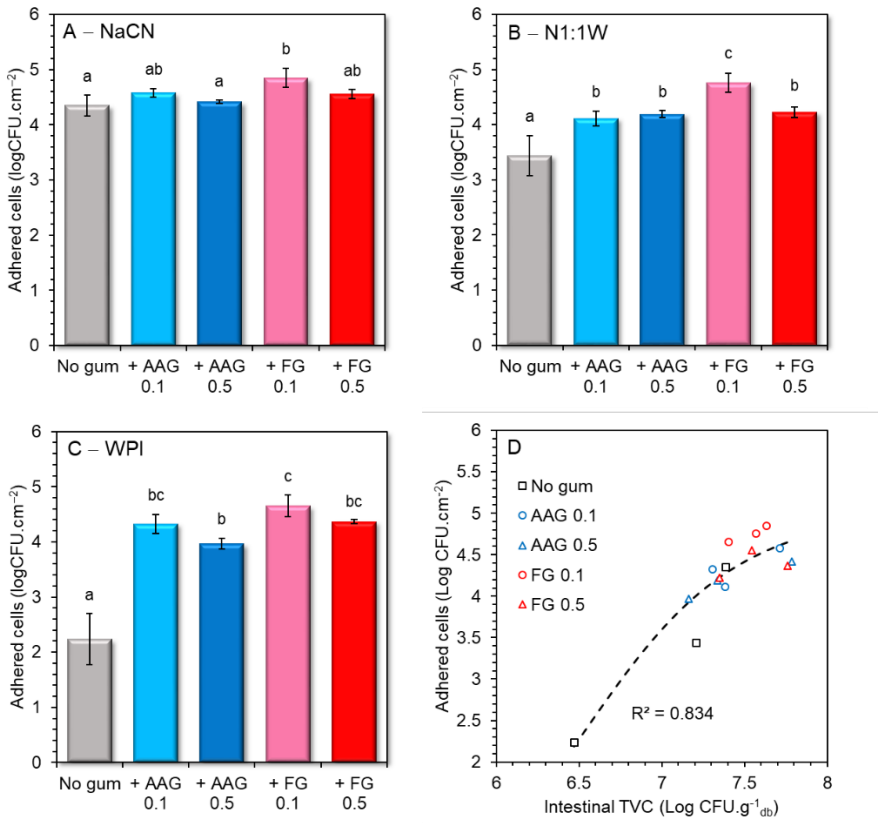


*Figure 92: Number of adhered cultivable LGG cells to the Caco2/HT29 co-culture model (expressed in logCFU.cm$^{-2}$) from digested sodium caseinate (NaCN, A), mixed protein with NaCN:WPI ratio of 1:1 (N1:1W, B) and whey protein isolate (WPI, C)-based cryogels. The relationship between the number of adhered cells and the TVC in the intestinal fluids (t = 120 min) is displayed in D. The dashed line (D) represent the Hill model fitted to the data. AAG 0.1 and AAG 0.5, alfalfa gum at 0.1 and 0.5% wt., respectively. FG 0.1 and FG 0.5, flaxseed gum at 0.1 and 0.5% wt., respectively. $^{a\text{-}c}$Different letters between the samples denote a significant difference ($p < 0.05$) according to Tukey's post hoc means comparison test.*

Although the exact mechanism of action of the PSGs needs to be further investigated, we assume that their presence at the microbe – mucus interface mediates the non-specific microbe – mucin interactions. It is also hypothesised that the presence of carboxyl groups in FG (contrary to AAG) explain the higher adherence capacity of the former. In line with these hypotheses, Liu et al., (2020) demonstrated that the grafting of side functional groups e.g., –COOH or –SH (via TEMPO oxidation and amide reaction) to konjac glucomannan enhanced the adhesin – mucin interactions via non-specific (e.g. hydrogen bonds, van der Waals forces) and disulphide bonding, respectively.

## Proteomic characterisation of the gastric and intestinal phases

As clearly illustrated in the capillary SDS-PAGE electropherograms of the cryogel gastric phases (Figure 93), the intensity of the characteristic bands associated with the presence of total ($\alpha_{s1}$–, β–, and κ–) caseins, β-lactoglobulin and α-lactalbumin was increased proportionally to the increase in the $m_{NaCN/WPI}$. Although native β-lactoglobulin is highly resistant to pepsinolysis, the presence of broad peptide band 10 kDa indicated the partial cleavage of the whey protein during gastric processing. This is mainly attributed to the denaturation of whey proteins during the heat treatment of the cryogel precursors (Barbé et al., 2013). The addition of the PSGs promoted the pepsin induced cleavage of the proteins though only in the case of the FG stabilised cryogels it was possible to detect a dose dependent effect. In this context, the NaCN containing systems showed a higher resistance to pepsinolysis at 0.5% wt. FG, whilst an adverse effect was observed in the WPI-based exemplars. Our findings align with the observations of Markussen et al., (2021) who reported that contrary to galactomannans (guar gum), anionic polysaccharides (sodium alginate and pectin) delayed the *in vitro* gastric peptic cleavage of the caseins fraction of milk protein concentrate. A good correlation between the pepsin induced cleavage of the proteins and the disintegration profile of the cryogels was found. As we have previously demonstrated (Hellebois, Canuel, et al., 2024), the presence of 0.5% FG in the NaCN and N1:1W cryogels resulted in slower disintegration rates ($\tau$ = 521, 138, 65 s, for NaCN, N1:1W and WPI, respectively) and larger residual particles ($D_{[4,3]}$ = 94, 150, 63 μm for NaCN, N1:1W and WPI, respectively) than WPI, inhibiting sterically the progress of pepsinolysis. The opposite effect was observed in the case of WPI cryogels containing 0.1% FG. In accordance with our previous work (Hellebois, Canuel, et al., 2024), the exposure of the gastric phases to the pancreases induced a complete cleavage of the proteins and polypeptides (> 6500 Da).

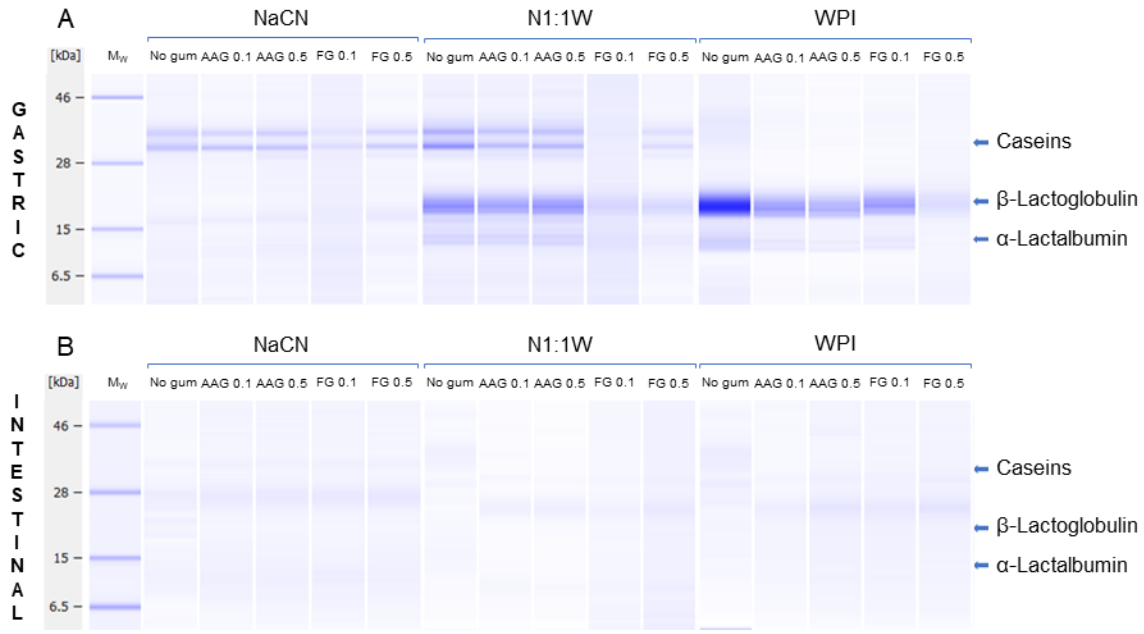


*Figure 93: Capillary SDS-PAGE electropherograms of the gastric (A) ($t_{gastric}$ = 120 min) and intestinal (B) ($t_{intestinal}$ = 120 min) milk protein cryogel digesta as influenced by the protein type (sodium caseinate, NaCN; whey protein, WPI; mixed NaCN:WPI at a ratio of 1:1, N1:1W), gum type (alfalfa gum, AAG; flaxseed gum, FG) at 0.1 and 0.5% wt.*

To gain insight into any potential secondary health benefit conferring effects, the peptidome (500–3000 Da) of the intestinal digesta was analysed using nano-LC-MS/MS. As shown in Figure 94, the intestinal digesta contained peptides composed of 6–24 amino acids, following a Gaussian distribution with a median of 9–11 depending on the cryogel composition, in agreement with our previous study (Hellebois, Canuel, et al., 2024). The prevalence of long-chain (i.e. > 17) peptides was adversely correlated to the NaCN:WPI mass fraction. Interestingly, the presence of PSGs in the intestinal digesta was associated with release of low to intermediate chain peptides, i.e. < 11 (Figure 94A). On the contrary the presence of PSGs in the mixed protein and WPI digesta did not affect in a straightforward fashion the peptides length distribution pattern.

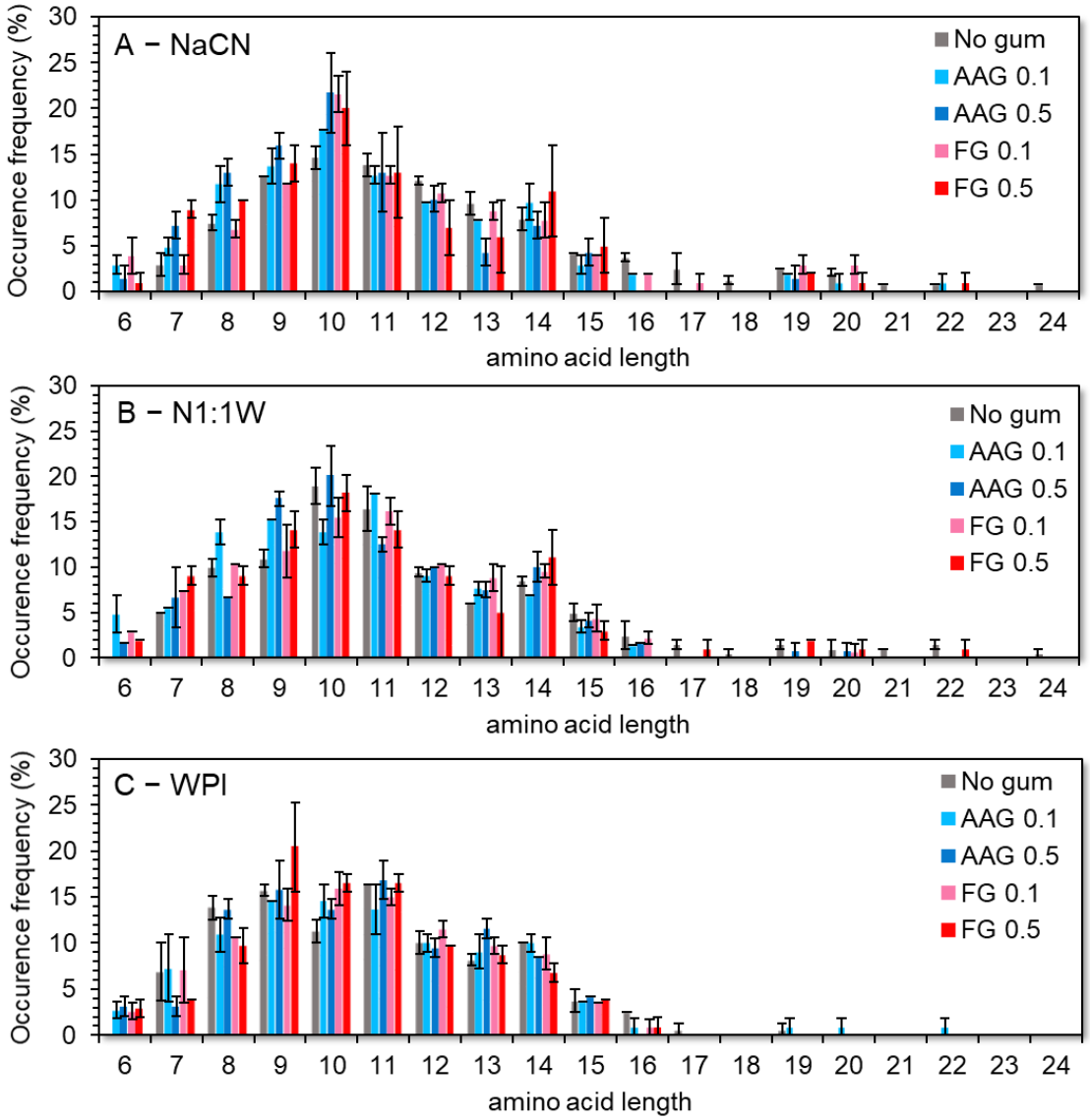


*Figure 94: Milk protein originating peptide sequences length from NaCN (A), N1:1W (B) and WPI (C) cryogels in the intestinal chymes influenced by the protein type (sodium caseinate, NaCN; whey protein, WPI; mixed NaCN:WPI at a ratio of 1:1, N1:1W), and the presence of PSGs (alfalfa gum, AAG; flaxseed gum, FG) at 0.1 and 0.5% wt.*

As regards the protein origin of the release peptides (Figure 95), the prevalence of peptides per protein class was not only associated with the protein composition of the cryogels but also with the PSG type and content. As well depicted in Figure 95, the PSGs did not remarkably modified the peptidome composition, with the majority of the identified peptides being originated from β-Lg and α-La. On the contrary, the peptidomes of the intestinal digesta of the NaCN cryogels containing 0.1% wt. PSG, showed higher affinity to their non-stabilised NaCN counterparts. The increase of the PSG content in the intestinal digesta of the NaCN cryogels resulted in a significant reduction in number of the peptides originating from β-, $\alpha_{s1}$- and κ-caseins yet without impacting those stemming from whey proteins. In a similar fashion, the presence of PSGs in the mixed protein

cryogel intestinal digesta resulted in a proportional to their content decrease in the abundance of β-Lg and α-La derived peptides.

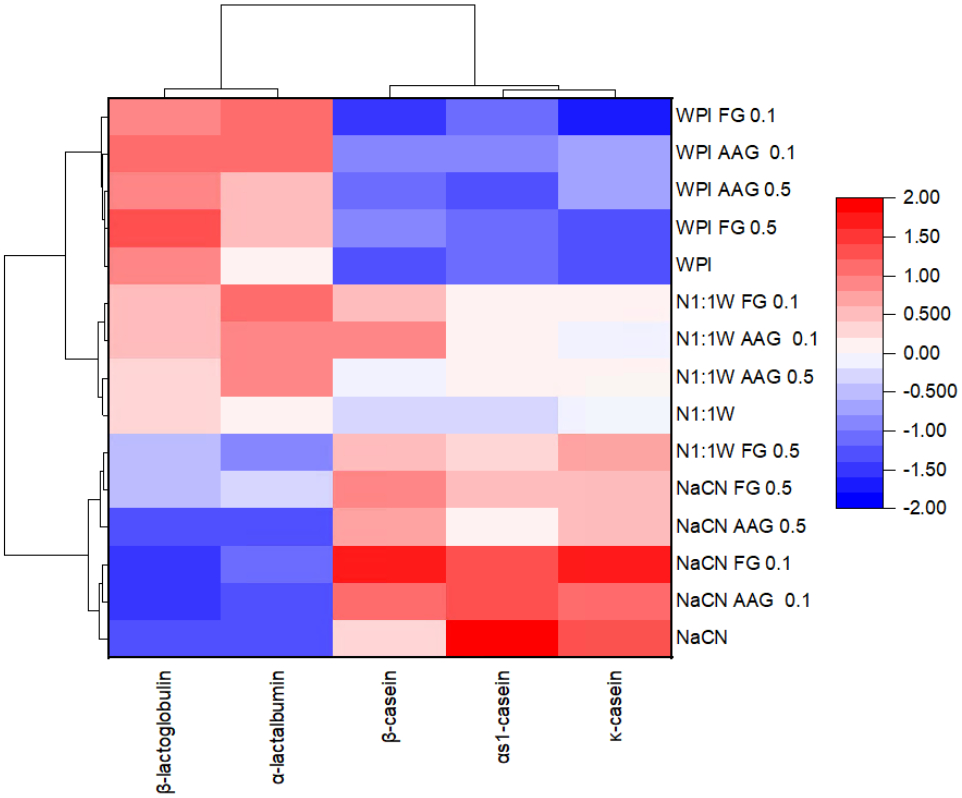


*Figure 95: Heat-map with dendrogram analysis of the effect of the addition of alfalfa (AAG) or flaxseed (FG) gums at either 0.1 or 0.5% on the prevalence of milk protein to produced detectable peptides sequences in the intestinal chymes of the cryogels. NaCN: Sodium Caseinate (A), WPI: Whey Protein Isolate (C), N1:1W denote mixed protein system of NaCN:WPI ratio of 1:1 (B).*

As shown in Table 27, a total of 14 bioactive peptides were at least one aliquot of intestinal digesta. Two bioactive peptides originating from β-Lg, i.e. $^{59}$VEELKPTPEGDLEIL$^{73}$ and $^{141}$TPEVDDEALEK$^{151}$ associated with zinc binding (Udechukwu et al., 2021) and dipeptidyl peptidase-4 (DPP-IV) inhibitory (Power et al., 2014) activities were detected in all intestinal digesta indicating their high resistance to pancreases. Noteworthy, the $^{141}$TPEVDDEALEK$^{151}$ ($IC_{50}$ = 320 μM) was the most abundant bioactive amino acid sequence amounting to 10−15% of the total peptides detected. Three bioactive peptides, i.e. $^{138}$VRTPEVDDE$^{14}$, $^{58}$YVEELKPTPEGDL$^{70}$, $^{195}$SDIPNPIGSENSEK$^{208}$ and $^{62}$LKPTPEGDL$^{70}$ ($IC_{50}$ = 45 μM), associated with zinc binding (Udechukwu et al., 2021), antioxidant (Basilicata et al., 2018), and antimicrobial (Hayes et al., 2006) properties, respectively were persistently detected in the mixed protein and WPI based intestinal phases. On the other hand, the $^{99}$EDVPSER$^{105}$ and $^{195}$SDIPNPIGSE$^{204}$ amino acid sequences, documented for their osteoanabolic (Reddi et al., 2018) and antidiabetic (Gong et al., 2020) potential, were primarily identified in the

NaCN-based cryogel derived intestinal phases. Interestingly, the $^{148}$LHLPLPL$^{154}$ ($IC_{50}$ = 425 µM) amino acid sequence exerting an angiotensin-converting enzyme binding activity – known for its high resistance to pancreases due to the presence of branched amino acids (leucine) and proline at the N-terminus and third-to-last C-terminus position (Nielsen et al., 2017) – was the less prevalent in the intestinal digesta. It is hypothesised that the $^{148}$LHLPLPL$^{154}$ was further cleaved to more pancreases-resistant amino acid sequences, i.e. $^{150}$LPLP$^{153}$ ($IC_{50}$ = 720 µM) and $^{149}$HLPLP$^{153}$ ($IC_{50}$ = 41 µM), which could not be detected according due to the minimum peptide length cut-off of the implemented analytical protocol. Ultimately, it should be highlighted that the PSG type and concentration did not create any clear peptidome patterns and hence, the protein composition of the cryogels is the major driver of the secondary bioactive potential.

*Table 27: Bioactive peptide sequences derived from milk protein after in vitro intestinal digestion of cryogels: Influence of gum type and content.*

| [1]Bioactive peptide sequence | Protein | [2]Bioactivity ($IC_{50}$ µM) | NaCas | | | | | N1:1W | | | | | WPI | | | | |
|---|---|---|---|---|---|---|---|---|---|---|---|---|---|---|---|---|---|
| | | | No gum | AAG 0.1 | AAG 0.5 | FG 0.1 | FG 0.5 | No gum | AAG 0.1 | AAG 0.5 | FG 0.1 | FG 0.5 | No gum | AAG 0.1 | AAG 0.5 | FG 0.1 | FG 0.5 |
| 99EDVPSER105 | αs1-cn | [a]Osteoanabolic | ✓ | ✓ | ✓ | ✓ | ✓ | | ✓ | | ✓ | ✓ | | ✓ | | | |
| 50EKVNELSK56 | αs1-cn | [b]ACE-inhibitory (5998) | ✓ | | | | | | | | | | | | | | |
| 38FFVAPFPEVFGK49 | αs1-cn | [c]ACE-inhibitory (18) | ✓ | | | | | | | | | | | | | | |
| 195SDIPNPIGSENSEK208 | αs1-cn | [d]Antimicrobial | ✓ | | | | ✓ | ✓ | | ✓ | ✓ | ✓ | ✓ | ✓ | | ✓ | |
| 195SDIPNPIGSE204 | αs1-cn | [e]Antidiabetic | ✓ | ✓ | ✓ | ✓ | | ✓ | ✓ | | | | | | | | |
| 160HQPHQPLPPTVMFPPQ175 | β-cn | [f]Zinc binding | ✓ | | | | | | | | | | | | | | |
| 148LHLPLPL154 | β-cn | [g]ACE-inhibitory (433) | | | | | | ✓ | | | | | ✓ | | | | |
| 62LKPTPEGDL70 | β-Lg | [h]DPP-IV Inhibitory (45) | | | | | | ✓ | ✓ | ✓ | | | ✓ | | ✓ | | ✓ |
| 59VEELKPTPEGDLEIL73 | β-Lg | [f]Zinc binding | ✓ | ✓ | ✓ | ✓ | ✓ | ✓ | ✓ | ✓ | ✓ | ✓ | ✓ | ✓ | ✓ | ✓ | ✓ |
| 58YVEELKPTPEGDL70 | β-Lg | [i]Antioxidant | ✓ | | | ✓ | ✓ | ✓ | ✓ | ✓ | ✓ | ✓ | ✓ | ✓ | ✓ | ✓ | ✓ |
| 26LDIQKVAGTW35 | β-Lg | [j]ACE-inhibitory (21) | | | | | | ✓ | | | | | | | | | |
| 141TPEVDDEALEK151 | β-Lg | [k]DPP-IV Inhibitory (320) | ✓ | ✓ | ✓ | ✓ | ✓ | ✓ | ✓ | ✓ | ✓ | ✓ | ✓ | ✓ | ✓ | ✓ | ✓ |
| 138VRTPEVDDE147 | β-Lg | [f]Zinc binding | | | | | ✓ | | ✓ | ✓ | ✓ | ✓ | ✓ | ✓ | ✓ | ✓ | ✓ |
| 108VLVLDTDYK116 | β-Lg | [l]DPP-IV Inhibitory (424) | ✓ | | | | ✓ | ✓ | | ✓ | | ✓ | ✓ | | | | ✓ |

*[1]Peptide sequence loci were determined using UniProt protein sequences. [2]References for the peptides bioactivities: [a](Reddi et al., 2018); [b](Tu et al., 2018); [c](Tauzin et al., 2002); [d](Hayes et al., 2006); [e](Gong et al., 2020); [f](Udechukwu et al., 2021); [g](Quirós et al., 2007; Robert et al., 2004); [h](Lacroix & Li-Chan, 2014); [i](Basilicata et al., 2018); [j](Lacroix et al., 2016); [k](Power et al., 2014); [l](Silveira et al., 2013).*

# CONCLUSIONS

In the present work, the feasibility of protein–plant seed gum cryogels as alternative xero-scaffolds embedding living probiotic cells was assessed. The protein type was found to be the most critical parameter for achieving maximal LGG survivability during the xero-structuration, storage, and *in vitro* gastrointestinal digestion. Sodium caseinate was clearly associated with enhanced lyoprotective ability compared to WPI, due to its efficacy to retain water in the vicinity of the polar phospholipid bilayer interface during the desiccation process. In a similar fashion, NaCN was able to preserve maximally the biological activity of LGG throughout controlled storage by preventing the undesirable changes in the structural integrity of the LGG cell membranes due to physical state and biochemical alterations. As expected, the LGG inactivation rates were significantly higher at elevated temperature (37 °C) and relative humidity conditions (75% RH). The presence of PSG had minor effects on the LGG survival during the desiccation process but mixed effects on the inactivation rates of LGG were observed depending on the protein composition of the cryogels. In most cases, the cryogels exhibited a low degree of disintegration and *in vitro* digestibility in the gastric fluids allowing a high LGG cell protection in the highly acid gastric environment. On the other hand, the exposure of the gastric chymes into the pancreases resulted in a burst release of living LGG cells and bioactive peptides behaviour. Although the LGG bioadhesion properties were ameliorated in the NaCN based intestinal digesta, the presence of PSG and particularly flaxseed gum was identified as a key factor in achieving a maximal load of viable LGG cells adhered to the mucus layer of the gut epithelium model. Our study confirmed that cryogels are promising and easily tuneable xero-templates for targeted delivery of probiotics.

# CONCLUSIONS & PERSPECTIVES

## Thesis highlights

In recent decades, food supplements have gained popularity due to their high nutritional density, consumer awareness, and demand for health-promoting functional food ingredients. These specially formulated products strengthen our dietary intake, can contribute to the human homeostasis, and help to reduce the risk digestive and cardiovascular diseases and cancers. However, developing food supplements that incorporate living probiotic cells faces several challenges. The primary challenge in designing a probiotic food supplement is ensuring the stability of the cells during production, storage, and digestion. Moreover, the delivered probiotics should be able to adhere to the intestines to maximise their health benefits.

In addressing the above-mentioned challenges, the current PhD project aimed to isolate and refine soluble dietary fibres from alfalfa and flax seeds for enhancing the nutritional value of dairy food supplements containing probiotic *Lacticaseibacillus rhamnosus* GG (LGG) bacterial cells. The project endeavoured to unveil how these emerging gums extracted from plant seeds modulate probiotic bacteria' survivability and biological activity against environmental stressors encountered through production to delivery into the gastrointestinal tract.

To meet these objectives, we have employed a new gum extraction method based on the isoelectric precipitation of protein combined with a solvent-induced precipitation of the gum. The refined extracts were then characterised for their compositional, structure-conformational and rheological properties. In a later stage, the gum–protein interplay was assessed using sodium caseinate and whey proteins under *in vitro* simulated digestion. Finally, cryogels composed of LGG pre-fermented sodium caseinate, whey proteins and a blend of the two comprising either alfalfa or flaxseed gum were developed. To evaluate the crafted cryogels as potential food supplements for probiotic delivery, the effect of the colloidal conformation of the solution and hydrogel precursors on the final cryogels were assessed. After freeze-drying, the physicochemical and microstructural attributes of the cryogels were characterised. All these properties were then used to describe the probiotic stability throughout the production process, storage and *in vitro* digestion, and their

mucoadhesion to a *co*-culture model of the human gut epithelium.

# Gum refining & characterisation

Since alfalfa and flaxseed gums were extracted in-house, a complete understanding of their molecular and techno-functional properties was required to describe the mechanisms involved in the final food supplement systems. Indeed, parameters such as surface charge density, solvent affinity, and structure conformational properties can significantly influence the techno-functional properties of gums and their interactions with co-solutes (salts, sugars) or macromolecules (proteins, polysaccharides). Thus, the first part of the PhD project was devoted to demonstrate the potential of plant seed gums as a novel food supplement ingredient by their comprehensive characterisation (Chapter I).

A new galactomannan isolated from alfalfa seed was investigated for the first time for its compositional, structure-conformational and rheological properties. Seeking highly refined gums, we successfully developed and patented a method based on the isoelectric precipitation of proteins during the extraction process using food-grade chemicals. Through this process, we could produce not only a gum extract with a purity of about 95% wt. but also side-products with desirable nutritional and techno-functional properties (i.e. protein flour and protein isolate). However, in the case of flaxseed, the extraction method did not significantly improve the purity of the gum (approx. 85% wt.), most probably due to the intricate intermolecular association of the residual proteins with the polysaccharides. The results also confirmed the assumption that the botanical origin of the seed – not only the species but also the cultivar dependence – significantly influences the gum extract properties. The molecular composition of the two gums was then validated with alfalfa gum comprising a non-ionic polysaccharide ($M_w$ = 2.0 × $10^6$ Da) composed of a mannose backbone with an almost complete galactosyl-substitution, and flaxseed gum revealed an anionic gum characterised by four polysaccharidic populations corresponding to arabinoxylans (AX), rhamnogalacturonan–I (RG-I) and two AX-RG-I composite fractions ($M_w$ = 1.2 × $10^6$ Da). Regarding their techno-functional properties, alfalfa gum had superior thickening ability for most of the tested conditions compared to flaxseed gum. The better solvation affinity of flaxseed gum and the hyperentanglement via polymer–polymer nonspecific association (i.e. hydrogen bonding) occurring in the case of alfalfa gum was the explanation for the discrepancies observed. At high concentrations, alfalfa was more prone to form weak physical gels ($c \geq 2\%$ wt.) compared to flaxseed gum ($c \geq 5\%$ wt.). Interestingly, the molecular characteristics, rheological,

and cryogelling properties of alfalfa gum are similar to those observed for fenugreek gum, the most common fully galactose-substituted galactomannan, suggesting that alfalfa gum could be used interchangeably with fenugreek gum.

# Gum – protein interplay

The first hypothesis of this PhD project postulated that adding gum could reduce the digestion rate of protein thanks to the indigestible character of the gums combined with the increased viscosity of the food matrix. To test this hypothesis, binary mixtures of milk protein – either whey protein or sodium caseinate – at 10% wt. with either alfalfa or flaxseed gum at 0–1% wt. were tested using the standardised static *in vitro* digestion model INFOGEST 2.0. From a colloidal perspective, both gums induced a phase separation phenomenon with varying colloidal conformations (i.e. water-in-water emulsion-like, aggregated and bicontinuous) driven by a depletion-flocculation mechanism. Flaxseed gum generally had the most pronounced phase separation attributed to its more pronounced negative surface charge density in the tested conditions. Unexpectedly, mixing the binary protein-gum food models with gastric fluids was associated with an increased rate of protein hydrolysis. Although adding the gum significantly increased the viscosity of the digestive chymes, it was found that it impeded the acid-induced protein aggregation. This effect was particularly critical in the case of sodium caseinate, which underwent spontaneous and uncontrolled gelation when mixed with gastric chymes (i.e. acidic conditions). During intestinal digestion, the gums had a minor effect in alfalfa-containing systems but reduced the hydrolysis rates in the presence of flaxseed gum. We hypothesised that the phenomenon originated from the flaxseed gum – milk protein coacervates and precipitates, free proteins, and polyanions, substantially impacting the extent of pancreases-induced hydrolysis. In all cases, adding gum increased the degree of protein hydrolysis achieved at the end of the *in vitro* digestion. The results demonstrated the crucial role of the colloidal interplay between protein and plant seed gums during *in vitro* digestion, underscoring the importance of ingredient selection, particularly in the design of liquid-based novel food matrices.

# Cryogels as an alternative delivery method

Cryogels represent an intriguing advancement in biomaterial scaffolds, recently gaining attention for the encapsulation of bioactive molecules. Despite their emerging application

in this domain, limited data exists regarding their potential for probiotic delivery. Cryogels offer notable advantages such as facile structural tailoring, potential for controlled release, and ease of dosing. It is reasonable to assume that the qualities that make cryogels effective for encapsulating bioactive molecules could also be applicable to the field of probiotics. This study assessed the influence of flaxseed and alfalfa seed gums on the physicochemical and microstructural features of the cryogels as well as their impact on the stability (during fermentation and freeze-drying, storage and *in vitro* digestion) and gut mucus adhesion of LGG cells.

The inclusion of plant seed gums in the cryogel precursors (lactic acid-induced hydrogels) led to distinct colloidal states due to phase separation. The bacteria cells were located either in the protein-rich continuous phase or at the protein–polysaccharide interface, probably due to differences in the osmotic pressure between the gum and protein-rich microdomains. Upon fermentation, the microstructural features observed in the solutions were arrested during the *sol–gel* transition. It was suggested that upon freeze-drying, the bacteria present at the protein–polysaccharide interface were exposed at the cryogel wall – air interface, leading to a slight – yet non-significant – reduction of the LGG cell counts. Besides, the production process allowed an optimal preservation of the cells (i.e. 44–77%) thanks to the inclusion of cryoprotectants and the achievement of a vitreous physical state during freezing, minimising the LGG cell injuries.

During storage, we confirmed the hypothesis that higher temperatures and water activities were associated with an increased bacterial loss rate. Interestingly, in these unfavourable storage conditions (i.e. 37 °C and RH = 75%), mixed protein systems (regardless of the NaCN:WPI ratio tested) slowed down the inactivation rates, most probably to their more compact structures. Although some literature reported the glass transition as a boundary above which the loss rates significantly increase, in this work, we obtained relatively fair stability up to $T_g$ + 20 °C, most probably due to the relatively low water activity ($a_w$ = 0.33) limiting the metabolic activity. In dry storage conditions at room temperatures, the cryogels (with or without gums) had a relatively reduced estimated shelf-life estimated at 3 months up to 1 year. As expected, when preserved at chilling conditions under a dry atmosphere (5 °C RH = 0.11%) the cryogels demonstrated an extended shelf-life of > 2 years. Nonetheless, contrarily to our hypothesis, it was not possible to correlate the precursors' colloidal state with their storage stability. It was suggested that the protein composition was the main parameter affecting the storage stability, with sodium caseinate-based cryogels showing the best performance. This was primarily ascribed to the high content of sodium caseinate in free radical scavenging

peptides.

When we exposed the probiotic cryogels to the gastric digestive fluids, they remained mainly intact, with the LGG cells being entrapped within the cryogel wall material. The low degree of particle disintegration and, thus, the slow diffusion of acid within the cryogel particles were found to be the principal mechanisms involved in bacterial stabilisation regardless of the type and gum concentration. Following the intestinal digestion, a complete bacteria release was observed stemming from the advanced protein hydrolysis. Similarly to the storage LGG survivability results, the best cell preservation depended on the protein type rather than the gum type and concentration, with sodium caseinate being the most effective.

The probiotic delivery requires a specific threshold (i.e 6 $\log CFU.g^{-1}$) to ensure sufficient health benefits. In parallel, their mucoadhesion and colonisation of the gastrointestinal tract are critical parameters for prolonged effects. Using an *in vitro* model, we demonstrated that the inclusion of gum, particularly in the case of flaxseed gum, promoted adhesion. We hypothesised that their presence at the microbe – mucus interface mediates the non-specific microbe – mucin interactions, yet more research is still required to highlight the exact mechanisms.

In addition to the health benefits of the probiotics, we identified 14 bioactive peptides in the intestinal fluid with a broad range of bioactivity such as antioxidant, zinc binding, antimicrobial, antihypertensive and osteoanabolic. Notably, the sequence $^{141}$TPEVDDEALEK$^{151}$ inhibiting the dipeptidyl peptidase-IV (i.e. regulation of the glycaemic response) was the most abundant sequence detected. We hypothesised that additional bioactive peptides may have been produced during the digestion but were not detected due to their short amino acid length.

# Limitations & perspectives

The successful integration of emerging gums into the market requires a comprehensive analysis, encompassing not only their techno-functional properties but also other parameters, such as the availability of the raw material and the cost of production. A complete market analysis should show the relevance of these gums compared to the commercially available gums.

Although we addressed several molecular, physicochemical and rheological properties, structural elucidation using nuclear magnetic resonance (NMR) is still required to confirm their molecular structure conformations. In addition, the techno-functional

properties of the gums were affected by the presence of *co*-solutes and proteins (Chapter I and II), and thus, a broader characterisation of their interactions with other *co*-solutes must be investigated to predict their behaviour in other formulations.

Another challenge of novel gums lies in the current purification methods, which often involve organic solvents like ethanol. Such methods do not align with the evolving standards of food ingredient production, which emphasise eco-friendly practices, minimising the use of solvent and chemicals at the profit of reduced processing treatments. More industrially relevant purification techniques could be explored, such as dry fractionation for galactomannans or membrane filtration for mucilages since these require a swelling strep in water to be extracted. Additionally, our research has highlighted that different cultivars and methods can dramatically change the physicochemical and techno-functional properties of the gums. This variability offers a broad spectrum of opportunities for the industries to broaden their portfolio yet at the cost of a more challenging standardisation.

The integration of novel gums into the food market holds significant potential, but regulatory limitations must be considered. From a legislative standpoint, before any new gum can be launched into the market, it must undergo rigorous testing and validation to ensure its safety. The regulatory landscape mandates that any novel ingredient must be thoroughly evaluated for its potential health impacts and environmental effects before being approved for human consumption. The assessment of alfalfa and flaxseed gums as novel food must comply with the maximum levels of chemical and microbiological contamination, the presence of metabolites and anti-nutrients, and the tolerable upper intake levels should be clearly defined. Considering the broad use of alfalfa and flaxseed in human nutrition (grounded, germinated, or whole seed), introducing purified dietary fibres from these seeds may be easier to be approved as novel food. Therefore, the main concern expected for the extraction method used in this project is the presence of residual solvent (ethanol) from the extraction. Furthermore, for these novel plant seed gums to become more attractive to the industry, more in-depth research and studies are required. Demonstrating these gums' potential benefits and functionalities will be crucial for the industry to undertake the validation process at the legislative level. As the industry moves forward, it will be imperative to explore innovative strategies to address these limitations, ensuring the sustainable and safe production of gum-based ingredients.

*In vitro* digestion models, while invaluable for initial screenings, have limitations. They present a simplified overview of complex gastrointestinal processes and might only

capture some intricate interactions and variables in a live system. The INFOGEST *in vitro* digestive model used in this project offers a standardised, cost-effective, and ethical way to quickly assess various aspects of food digestion in a controlled environment. However, it is a simplified system that does not capture the complexity of human digestion, including factors like the rate of gastric emptying, enteral mechanical forces, acidification rates, nutrient absorption, immunological responses, and inter-individual variations, among others. Moving forward, given that the INFOGEST protocol concludes in the jejunum, it might be beneficial to incorporate a step that simulates the colonic environment and assess its interaction with the colonic microbiota. This addition would enhance the validity of the results under the tested conditions.

Concerning the mucoadhesion of LGG to the intestinal epithelium, the data obtained suggested that the cryogels could be deployed to improve gut colonisation by probiotic bacteria. However, this study did not account for several critical variables that could influence the outcome. The first unexamined variable is the competitive interaction between the introduced LGG and the existing host microbiota for mucosal adhesion sites. The second overlooked factor is the composition of the digestive chyme. Under physiological conditions, digested foodstuffs are concurrently present with the probiotic supplement, altering the tripartite interactions among the matrix, the probiotics, and the intestinal mucosa.

Despite the enhanced realism of dynamic models simulating the sequential events and environmental changes of the digestive system without raising ethical issues, the validation of the results of this work necessitates in vivo nutritional studies using animals and humans. Such trials would offer an exhaustive exploration of actual biological interactions, metabolism, and health benefits in the target organism. While *in vitro* models served as a foundation for understanding fundamental interactions cost-effectively, comprehensive validation of the health-promoting properties of the probiotic cryogels would only be achieved through nutritional studies.

Factors related to the design of the matrix, such as processing techniques and material composition, are known to influence the properties of the resultant cryogels substantially. This study carefully selected the composition through a series of preliminary assays, aiming to produce a cryogel with specific characteristics. Specifically, the goal was to develop self-supporting, foam-like scaffolds that exhibited neither brittleness nor stickiness while simultaneously naturally embedding the bacterial cell within the wall material.

A fermentation step was incorporated to achieve these objectives, using *Lacticaseibacillus rhamnosus* GG to establish the required structural network to withstand subsequent freeze-drying processes. This fermentation step is likely responsible for the observed stability of LGG during gastric digestion due to pre-adaptation to an acidic environment (i.e. pH = 4). However, the bactericidal effect of the un-dissociated organic acids may also have negatively affected bacterial viability during long-term storage. Future investigations should better explore cryogels generated through alternative gelation mechanisms of the precursors − such as ionotropic, rennet-induced, or transglutaminase-induced methods − to better understand the influence of acidification on LGG survivability.

Of the milk proteins examined in this study − including sodium caseinate, whey proteins, and their mixtures − sodium caseinate was found to be most effective in preserving bacterial viability during production, storage, and *in vitro* digestion while also enhancing the mucoadhesion of the released LGG cells. Although various potential mechanisms have been postulated, such as enhanced free radical scavenging activity and a more uniform macroporous structure, further research is required to elucidate the precise cellular mechanisms at play.

The study also observed moderate benefits from the incorporation of gum. The protein content was set at 10% wt. to ensure sufficient structural integrity post-freeze-drying. Notably, spontaneous gelation of whey protein isolate occurred when gum concentrations exceeded 0.5% wt. Studies suggest that higher polysaccharide-to-protein ratios may further optimise cryogel performance. To modify the polysaccharide-to-protein ratio in future studies, different potential strategies could be considered: 1) reducing the amount of protein to accommodate an increased level of polysaccharide, 2) opting for alternative proteins and/or polysaccharides, allowing greater flexibility in manipulating the ratio, 3) produce precursors above the least gelation concentration of the protein followed by a disruption upon bacteria addition and 4) reducing the protein content at the profit of bulking material such as prebiotic fibres, maltodextrins, among others. As such, future research should explore variations in the polysaccharide-to-gum ratio to improve the cryogel properties evaluated in the current study.

For this work, LGG was selected as a probiotic model thanks to the broad knowledge garnered in the last decades. However, as discussed in the introductive section, significant variability in metabolism and structural characteristics are observed among the probiotics. This, in turn, affects the sensitivity of the probiotic against stressors, e.g. the high sensitivity of *Bifidobacterium* to oxygen. The evaluation of a broader spectrum of

probiotic microorganisms is required to expand the knowledge of the feasibility of cryogels for probiotic delivery.

# PRESENTATION SYNTHETIQUE DE LA THESE

Dans la société moderne, l'importance d'une alimentation saine est primordiale, surtout compte tenu des avancées médicales qui ont prolongé la durée de vie humaine. Parallèlement à la longévité, il est urgent d'améliorer la qualité de vie. Ainsi, une alimentation équilibrée, combinée à d'autres mesures préventives telles que l'exercice physique régulier et les pratiques de bien-être mental, participent à une qualité de vie élevée pour une période prolongée. Adopter ces mesures de santé holistiques garantit aux individus un bien-être optimal tout au long de leur vie.

Une des voies pour atteindre cet équilibre passe par la régulation de notre microbiote intestinal, c'est à dire la communauté de micro-organismes vivant dans notre tube digestif. Les recherches actuelles montrent le rôle crucial d'un microbiote équilibré dans la promotion de la santé globale. Les fibres alimentaires et les probiotiques, soit des bactéries bénéfiques qui aident à la digestion, se sont révélés être d'excellents candidats pour maintenir cet équilibre. Ils favorisent un environnement intestinal sain, influençant ainsi indirectement divers aspects de notre santé, y compris l'immunité, le bien-être mental ainsi que la santé cardiovasculaire.

Cependant, compte tenu de notre mode de vie effréné, maintenir un apport constant de ces nutriments bénéfiques pour la santé peut s'avérer difficile. Pour surmonter ce besoin, la consommation de compléments alimentaires connaît une tendance croissante. Ces suppléments de probiotiques et de fibres, souvent conçus avec des niveaux concentrés de nutriments essentiels, visent à améliorer l'apport quotidien de ces éléments bénéfiques, comblant ainsi les lacunes laissées par notre alimentation habituelle. En l'état actuel des choses, les compléments alimentaires ont été instrumentalisés pour soutenir un mode de vie plus sain, mais des améliorations sont encore nécessaires pour garantir des résultats de santé optimisés.

Les principaux objectifs de cette thèse sont multidimensionnels, centrés sur l'exploration et la compréhension de gommes (c'est-à-dire des fibres alimentaires solubles) extraites de biomasses végétales présentant un intérêt industriel et leur utilisation dans le développement de compléments alimentaires combinant des cellules probiotiques et des protéines de lait. Le concept fondamental de ce projet repose sur l'hypothèse que les fibres alimentaires pourraient atténuer l'exposition des probiotiques aux différents stress

environnementaux pendant le stockage et de limiter la digestibilité des protéines pendant les phases gastriques en ralentissant la diffusion des enzymes au travers de la matrice. Simultanément les gommes fourniraient une protection aux bactéries contre les conditions défavorables du tractus gastro-intestinal. De plus, notre hypothèse suggère que l'inclusion de fibres alimentaires pourrait également renforcer l'adhésion des bactéries à la muqueuse intestinale, favorisant la colonisation du tractus gastro-intestinal. Pour évaluer cette hypothèse, les objectifs ont été stratégiquement divisés en cinq points clés :

i. Développer une méthode d'extraction optimisée de gommes à partir de graines de plantes sous-exploitées − luzerne et lin − garantissant une grande pureté.

ii. Caractériser la composition et profiler les propriétés techno-fonctionnelles des gommes purifiées.

iii. Comprendre les interactions entre ces gommes et les protéines du lait dans des systèmes aqueux, explorant ainsi comment les gommes peuvent moduler les changements colloïdaux des protéines ainsi que leur digestibilité.

iv. Formuler des matrices déshydratées innovantes contenant *Lacticaseibacillus rhamnosus* GG sous forme de cryogels autoportants utilisant la protéine de lait comme squelette.

v. Améliorer la viabilité des bactéries dans diverses conditions, telles que le stockage et la digestion, et améliorer l'adhésion à l'épithélium intestinal par l'incorporation des gommes dans les cryogels.

En abordant les défis mentionnés ci-dessus, ce projet doctoral visait à isoler et à raffiner les fibres alimentaires solubles (gommes) de la luzerne et des graines de lin afin d'améliorer la valeur nutritionnelle des compléments alimentaires à base protéine de lait (protéines du lactosérum et caséinate de sodium) contenant des cellules bactériennes de la souche probiotique *Lacticaseibacillus rhamnosus* GG (LGG). Le projet s'est efforcé de comprendre les mécanismes par lesquels ces gommes sont impliquées dans la modulation de la capacité de survie et l'activité biologique de LGG face aux stress environnementaux rencontrés de la production à leur relargage dans le tractus gastro-intestinal.
Pour atteindre ces objectifs, nous avons employé une nouvelle méthode d'extraction de gomme basée sur la précipitation isoélectrique des protéines combinée à une précipitation

induite par solvant organique de la gomme. Les extraits raffinés ont ensuite été caractérisés pour leurs compositions et propriétés structurales et rhéologiques. À un stade ultérieur, l'interaction gomme–protéine a été évaluée en utilisant le caséinate de sodium et les protéines de lactosérum lors d'une digestion simulée *in vitro*. Enfin, des cryogels composés de caséinate de sodium, de protéines de lactosérum et d'un mélange des deux préfermentés par LGG contenant soit de la gomme de luzerne, soit de la gomme de graines de lin ont été développés. Pour évaluer les cryogels conçus comme éventuels compléments alimentaires pour l'encapsulation de probiotiques, l'effet de la conformation colloïdale de la solution et des hydrogels précurseurs sur les cryogels finaux a été évaluée. Après lyophilisation, les attributs physicochimiques et microstructuraux des cryogels ont été caractérisés. Toutes ces propriétés ont ensuite été utilisées pour décrire la stabilité du probiotique tout au long du processus de production, du stockage et de la digestion *in vitro*, ainsi que leur mucoadhésion à un modèle *in vitro* de l'épithélium intestinal humain.

Considérant que les gommes de luzerne et de lin ont été extraites et non achetées, une compréhension complète de leurs propriétés moléculaires et techno-fonctionnelles était nécessaire pour décrire les mécanismes impliqués dans les cryogels finaux. En effet, des paramètres tels que la charge de surface, l'affinité avec l'eau et les propriétés conformationnelles peuvent influencer significativement les propriétés techno-fonctionnelles des gommes ainsi que leurs interactions avec les solutés (sels et sucres) ou macromolécules (protéines, polysaccharides). Ainsi, la première partie du projet de doctorat a été consacrée à démontrer le potentiel des gommes de luzerne et de lin comme nouvel ingrédient (Chapitre I).

Un nouveau galactomannane isolé de la graine de luzerne a été étudié pour la première fois pour ses propriétés compositionnelles, conformationnelles et rhéologiques. Cherchant à obtenir des gommes hautement raffinées, nous avons réussi à développer et breveter une méthode basée sur la précipitation isoélectrique des protéines pendant le processus d'extraction en utilisant des produits chimiques de qualité alimentaire. Grâce à ce processus, nous avons pu produire non seulement un extrait de gomme avec une pureté d'environ 95% en poids, mais aussi obtenir des sous-produits aux propriétés nutritionnelles et techno-fonctionnelles intéressantes (soit une farine protéique et isolat protéique). Cependant, dans le cas du lin, la méthode d'extraction n'a pas significativement amélioré la pureté de la gomme (environ 85%), probablement à cause de l'association intermoléculaire complexe entre les protéines résiduelles et les polysaccharides. Les résultats ont également confirmé l'hypothèse selon laquelle l'origine

botanique de la graine – non seulement l'espèce mais aussi la dépendance de la variété – influence significativement les propriétés de la gomme. La composition moléculaire des deux gommes a ensuite été validée. La gomme de luzerne était principalement composée de polysaccharides non-ioniques ($M_w$ = 2,0 × $10^6$ Da) composés d'une chaine principale de mannose avec une substitution en galactose quasi complète. La gomme de lin quant à elle révéla une gomme anionique ($M_w$ = 1,2 × $10^6$ Da) caractérisée par quatre populations polysaccharidiques correspondant à des arabinoxylanes (AX), rhamnogalacturonanes–I (RG-I) et deux fractions composites AX-RG-I. En ce qui concerne leurs propriétés techno-fonctionnelles, la gomme de luzerne a montré une meilleure capacité épaississante pour la plupart des conditions testées par rapport à la gomme de lin. D'une part la meilleure affinité de solvatation de la gomme de lin et d'autre part l'hyper-enchevêtrement via l'association polymère-polymère non spécifique par liaison hydrogène se produisant dans le cas de la gomme de luzerne a été proposé pour expliquer les divergences observées. À des concentrations élevées, la luzerne était plus prédisposée à former des gels physiques faibles ($c \geq 2\%$) par rapport à la gomme de lin ($c \geq 5\%$). Faits intéressants, les caractéristiques moléculaires, rhéologiques et cryogélifiantes de la gomme de luzerne sont similaires à celles observées pour la gomme de fenugrec, le galactomannane entièrement substitué le plus courant, suggérant que la gomme de luzerne pourrait être utilisée de manière interchangeable avec la gomme de fenugrec.

La première hypothèse de ce projet doctoral postulait que l'ajout de gomme pourrait diminuer le taux de digestion des protéines en raison du caractère indigestible des gommes combinées à une augmentation de la viscosité de la matrice alimentaire. Pour tester cette hypothèse, des mélanges binaires constitués de protéines laitières à 10%, (soit de protéines de lactosérum ou de caséinate de sodium), associés soit à de la gomme de luzerne soit à de la gomme de lin à 0–1%. Ces exemples de matrice alimentaires ont ensuite été soumis à une digestion *in vitro* suivant le protocole standardisé INFOGEST 2.0. D'un point de vue colloïdal, les gommes ont induit un phénomène de séparation de phase avec des conformations colloïdales distinctes (par exemple, émulsion eau-dans-eau, agrégation et structure bicontinue) régies par un mécanisme de floculation par déplétion. La gomme de lin présentait généralement une séparation de phase plus marquée, attribuée à sa charge négative plus prononcée dans les conditions expérimentales testées. Contre toute attente, la mise en contact avec les fluides gastriques des formulations protéine-gomme s'est traduit par une augmentation de la vitesse d'hydrolyse protéique. Bien que l'ajout de gomme ait considérablement augmenté la

viscosité des chymes digestifs, il a été observé qu'il entravait l'agrégation protéique induite par l'acidité. Cet effet était particulièrement prononcé pour le caséinate de sodium, qui subissait une gélification spontanée et non maîtrisée en présence des fluides gastriques (c'est-à-dire dans un environnement acide). Au cours de la digestion intestinale, les gommes ont eu un effet limité dans les systèmes contenant de la gomme de luzerne, mais ont réduit les taux d'hydrolyse en présence de gomme de lin. Nous avons postulé que ce phénomène découlait des coacervats et précipités formés par l'interaction de la gomme de lin et de la protéine laitière, influençant significativement l'hydrolyse induite par les enzymes pancréatiques. Dans tous les scénarios, l'incorporation de gomme augmentait le taux d'hydrolyse protéique à la fin de la digestion *in vitro*. Les résultats ont mis en lumière le rôle primordial des interactions colloïdales entre protéines et gommes de la digestion *in vitro*, soulignant l'importance cruciale du choix des ingrédients, notamment dans la conception de matrices alimentaires liquides.

Les cryogels représentent une avancée fascinante dans le domaine des biomatériaux, attirant récemment l'attention pour l'encapsulation de molécules bioactives. Malgré leur application naissante dans ce domaine, peu de données existent sur leur potentiel pour l'encapsulation de probiotiques. Les cryogels offrent des avantages notables tels que la facilité de structuration, le potentiel de libération contrôlée et la simplicité du dosage. Il est raisonnable de supposer que les qualités qui rendent les cryogels efficaces pour encapsuler des molécules bioactives pourraient également s'appliquer au domaine des probiotiques. Cette étude a évalué l'influence des gommes de graines de lin et de luzerne sur les caractéristiques physicochimiques et microstructurales des cryogels ainsi que leur impact sur la stabilité (durant la fermentation et la lyophilisation, le stockage et la digestion *in vitro*) et l'adhésion de LGG au mucus intestinal.

L'inclusion de gommes dans les précurseurs des cryogels (hydrogels induits par l'acide lactique lors de la fermentation) a conduit à des conformations colloïdales distinctes dues à la séparation de phase entre protéines et polysaccharides. Les cellules bactériennes étaient situées soit dans la phase continue riche en protéines soit à l'interface protéine–polysaccharide, probablement en raison des différences de pression osmotique entre les phases riches en gomme et celles riches en protéines. Lors de la fermentation, les caractéristiques microstructurales observées dans les solutions ont été figées lors de la transition *sol–gel*. Il a été suggéré que lors de la lyophilisation, les bactéries présentes à l'interface protéine–polysaccharide étaient exposées à l'interface cryogel–air, entraînant une légère – bien que non significative – réduction du nombre de cellules LGG

cultivables. De plus, le processus de production a permis une préservation optimale des cellules (c'est-à-dire 44–77%) grâce à l'inclusion de lyoprotecteurs et à l'achèvement d'un état physique vitreux lors de la congélation, minimisant les lésions cellulaires.

Durant le stockage, nous avons confirmé l'hypothèse selon laquelle des activités d'eau et des températures plus élevées étaient associées à des taux d'inactivation bactérienne accrue. Bien que la transition vitreuse soit utilisée dans la littérature comme une limite au-delà de laquelle les vitesses d'inactivation augmentent significativement, dans cette étude, nous avons obtenu une stabilité satisfaisante jusqu'à $T_g$ + 20 °C, très probablement en raison de l'activité d'eau basse ($a_w$ = 0,33) limitant l'activité métabolique. Dans les conditions de stockage optimales à température ambiante, les cryogels ont démontré une durée de vie estimée relativement réduite (de 3 mois à 1 an). Comme anticipé, conservés dans des conditions de réfrigération et sous une atmosphère sèche (5 °C RH = 11%), les cryogels présentaient une durée de vie prolongée de plus de 2 ans. Néanmoins, il était impossible de corréler l'état colloïdal des précurseurs avec la stabilité bactérienne observée durant le stockage. Il a été suggéré que la composition en protéines était le principal paramètre affectant la stabilité de stockage, les cryogels à base de caséinate de sodium montrant les meilleures performances. Ceci était principalement attribué à la capacité supérieure du caséinate de sodium à piéger les radicaux libres par rapport aux protéines du lactosérum.

Lorsque nous avons exposé les cryogels aux fluides digestifs gastriques, ceux-ci sont généralement restés intacts, les probiotiques LGG étant piégées à l'intérieur du matériau constituant la paroi des cryogels. Le faible degré de désintégration des particules, et par conséquent, la diffusion lente de l'acide à l'intérieur des particules de cryogel a été identifiés comme le mécanisme principal impliqué dans la stabilisation bactérienne, indépendamment du type et de la concentration de gomme. À la suite de la digestion intestinale, une libération complète des bactéries a été observée, résultant de l'hydrolyse avancée des protéines. De manière similaire aux résultats d'inactivation cellulaire lors de la conservation, la meilleure préservation cellulaire dépendait du type de protéine plutôt que du type et de la concentration de gomme, le caséinate de sodium étant le plus efficace. L'encapsulation de probiotiques nécessite un seuil spécifique (soit 6 $\log CFU.g^{-1}$) pour garantir des bienfaits pour la santé. En parallèle, leur mucoadhésion et leur colonisation du tractus gastro-intestinal sont des paramètres essentiels pour des effets prolongés. En utilisant un modèle *in vitro*, nous avons démontré que l'inclusion de gomme, particulièrement dans le cas de la gomme de lin, favorisait l'adhésion. Nous avons émis l'hypothèse que leur présence à l'interface microbe–mucus médiatise les interactions non

spécifiques entre microbe et mucine, cependant, des recherches supplémentaires sont encore nécessaires pour mettre en lumière les mécanismes exacts.

En plus des bénéfices sanitaire associés aux, nous avons identifié 14 peptides bioactifs dans le chyme intestinal ayant une large gamme de bioactivités telles qu'un pouvoir antioxydant, de fixation du zinc, antimicrobiennes, antihypertensives et ostéoanaboliques. Notamment, la séquence $^{141}$TPEVDDEALEK$^{151}$ inhibant la dipeptidyl peptidase-IV (régulant la réponse glycémique) était la séquence la plus abondamment détectée. Nous avons émis l'hypothèse que d'autres peptides bioactifs auraient pu être produits pendant la digestion mais n'ont pas été détectés en raison de leur courte longueur en acides aminés.

De manière plus générale, ce projet a permis d'approfondir les connaissances sur les gommes extraites de luzerne, leur impact sur la digestion de protéines de lait en phase liquide. De plus cette étude a été l'une des premières à démontrer le potentiel de l'utilisation de cryogel pour l'encapsulation de probiotiques vivants. Cette étude ouvre la voie à de nouveaux usages non seulement de gommes pour un usage alimentaire en tant que texturant mais également à celle des cryogels en tant que compléments alimentaires probiotiques.

# SCIENTIFIC CONTRIBUTIONS & RECOGNITIONS

## Publications

Hellebois, T., Fortuin, J., Cambier, S., Contal, S., Leclercq, C. C., Gaiani, C., & Soukoulis, C. (2024). Stability and adhesion properties of Lacticaseibacillus rhamnosus GG embedded in milk protein cryogels: Influence of plant seed gum inclusion. *Food Hydrocolloids*, 151, 109867.

Hellebois, T., Addiego, F., Gaiani, C., Shaplov, A. S., & Soukoulis, C. (2024). Unravelling the functionality of anionic and non-ionic plant seed gums on milk protein cryogels conveying Lacticaseibacillus rhamnosus GG. *Carbohydrate Polymers*, 323, 121376.

Hellebois, T., Canuel, R., Leclercq, C. C., Gaiani, C., & Soukoulis, C. (2024). Milk protein-based cryogel monoliths as novel encapsulants of probiotic bacteria. Part II: Lacticaseibacillus rhamnosus GG storage stability and bioactivity under *in vitro* digestion. *Food Hydrocolloids*, 146, 109173.

Hellebois, T., Canuel, R., Addiego, F., Audinot, J.-N., Gaiani, C., Shaplov, A. S., & Soukoulis, C. (2023). Milk protein-based cryogel monoliths as novel encapsulants of probiotic bacteria. Part I: Microstructural, physicochemical, and mechanical characterisation. *Food Hydrocolloids*, *140*, 108641.

Hellebois, T., Fortuin, J., Gaiani, C., & Soukoulis, C. (2022). Impact of Flaxseed Gums on the Colloidal Changes and *In Vitro* Digestibility of Milk Proteins. *Foods*, *11*(24), 4096.

Hellebois, T., Gaiani, C., Cambier, S., Noo, A., & Soukoulis, C. (2022). Exploration of the *co*-structuring and stabilising role of flaxseed gum in whey protein isolate based cryo-hydrogels. *Carbohydrate Polymers*, *289*, 119424.

Hellebois, T., Gaiani, C., & Soukoulis, C. (2022). Freeze − thaw induced structuration of

whey protein − alfalfa (Medicago sativa L.) galactomannan binary systems. *Food Hydrocolloids*, *125*, 107389.

Hellebois, T., Gaiani, C., & Soukoulis, C. (2022). Impact of alfalfa (Medicago sativa L.) galactomannan on the microstructural and physicochemical changes of milk proteins under static *in vitro* digestion conditions. *Food Chemistry: X*, *14*, 100330.

Hellebois, T., Fortuin, J., Xu, X., Shaplov, A. S., Gaiani, C., & Soukoulis, C. (2021). Structure conformation, physicochemical and rheological properties of flaxseed gums extracted under alkaline and acidic conditions. *International Journal of Biological Macromolecules*, *192*, 1217–1230.

Hellebois, T., Gaiani, C., Fortuin, J., Shaplov, A., & Soukoulis, C. (2021). Cryotropic gel-forming capacity of alfalfa (Medicago sativa L.) and fenugreek (Trigonella foenum graecum) seed galactomannans. *Carbohydrate Polymers*, *267*, 118190.

Hellebois, T., Soukoulis, C., Xu, X., Hausman, J.-F., Shaplov, A., Taoukis, P. S., & Gaiani, C. (2021). Structure conformational and rheological characterisation of alfalfa seed (Medicago sativa L.) galactomannan. *Carbohydrate Polymers*, *256*, 117394.

Hellebois, T., Tsevdou, M., & Soukoulis, C. (2020). Chapter Five - Functionalizing and bio-preserving processed food products via probiotic and synbiotic edible films and coatings. In A. G. da Cruz, E. S. Prudencio, E. A. Esmerino, & M. C. da Silva (Eds.), *Advances in Food and Nutrition Research* (Vol. 94, pp. 161–221). Academic Press.

# Patent

Hellebois, T., & Soukoulis, C. (2022). *Method of extraction of a galactomannan gum from alfalfa seeds* (World Intellectual Property Organization Patent No. WO2022029103A1).

# Oral communications

7th EPNOE International Polysaccharides Conference 2021, October 11th-15th 2021, Nantes, France. Cryotropic gel-forming capacity of alfalfa and fenugreek seed galactomannans. Hellebois T., Gaiani C. & Soukoulis C.

6th LSfM Luxembourg Microbiology Day, May 11th 2023, Dudelange, Luxembourg. Biopolymer-based cryogels as a novel xero-carrier for probiotics delivery. Hellebois T., Gaiani C. & Soukoulis C.

# Posters

Biomolecules: Research & Development, Markets and Acceptability conference, October 23rd- 25th 2019, Plama de Mallorca (Spain). Study of the *in vitro* gastrointestinal fate of milk proteins as influenced by the presence of brown and yellow flaxseed gum, Hellebois T. et al.

LIST Annual PhD Day, November 26th 2019, Luxembourg Institute of Science and Technology, Belval, Luxembourg. Study of plant seed mucilage as a novel *co*-biopolymer protectant of probiotic cells embedded in milk protein xero-carriers. Hellebois T. et al.,

35th Conference of the European colloid & interface society (ECIS), September 5th-10th, 2021, Athens, Greece. *In vitro* gastrointestinal fate of milk proteins as influenced by a novel galactomannan isolated from alfalfa (*Medicago sativa* L.) seeds. Hellebois T. et al.

35th European Federation of Food Science and Technology (EFFoST) conference, November 1st-4th 2021, Lausanne, Switzerland. Study of the storage stability and *in vitro* digestion viability of *L. Rhamnosus* probiotic cells embedded in milk protein based cryostructurates containing alfalfa or flaxseed gums. Hellebois T., Gaiani C. & Soukoulis C.

36th Conference of the European colloid & interface society (ECIS), September 4th-9th 2022, Chania, Greece. Assessment of the muco-adhesion potential of green extracted

gums from plant seeds Hellebois T., Gaiani C. & Soukoulis C.

21st Gums & stabilisers for the food industry conference, Thessaloniki, Greece, June 6th-9th 2023, Alfalfa gum. Part I: insights into the rheological and structure conformation properties of a novel galactomannan. Hellebois T., Gaiani C. & Soukoulis C.

21st Gums & stabilisers for the food industry conference, Thessaloniki, Greece, June 6th-9th 2023, Alfalfa gum. Part II: Impact on the colloidal aspects and digestibility of milk proteins during *in vitro* digestion. Hellebois T., Gaiani C. & Soukoulis C.

# Distinctions

Best oral presentation award, PhD category, 6th LSfM Luxembourg Microbiology Day, May 11th 2023, Dudelange, Luxembourg. Biopolymer-based cryogels as a novel xero-carrier for probiotics delivery. Hellebois T., Gaiani C. & Soukoulis C.

Third best poster presentation, 21st Gums & stabilisers for the food industry conference, Thessaloniki, Greece, June 6th–9th 2023, Alfalfa gum. Part I: insights into the rheological and structure conformation properties of a novel galactomannan. Hellebois T., Gaiani C. & Soukoulis C.

# REFERENCES


Adamberg, K., Kask, S., Laht, T.-M., & Paalme, T. (2003). The effect of temperature and pH on the growth of lactic acid bacteria: A pH-auxostat study. *International Journal of Food Microbiology*, *85*(1), 171–183. https://doi.org/10.1016/S0168-1605(02)00537-8

Adhikari, B., Howes, T., Bhandari, B. R., & Langrish, T. A. G. (2009). Effect of addition of proteins on the production of amorphous sucrose powder through spray drying. *Journal of Food Engineering*, *94*(2), 144–153. https://doi.org/10.1016/j.jfoodeng.2009.01.029

Adsare, S. R., & Annapure, U. S. (2021). Microencapsulation of curcumin using coconut milk whey and Gum Arabic. *Journal of Food Engineering*, *298*, 110502. https://doi.org/10.1016/j.jfoodeng.2021.110502

Agudelo, J., Cano, A., González-Martínez, C., & Chiralt, A. (2017). Disaccharide incorporation to improve survival during storage of spray dried Lactobacillus rhamnosus in whey protein-maltodextrin carriers. *Journal of Functional Foods*, *37*, 416–423. https://doi.org/10.1016/j.jff.2017.08.014

Ahlawat, A., Basak, S., & Ananthanarayan, L. (2023). Formulation of a probiotic buttermilk powder using cell protectants by spray drying and estimation of its shelf-stability. *International Dairy Journal*, *141*, 105616. https://doi.org/10.1016/j.idairyj.2023.105616

Ahmadi, M., Madadlou, A., & Saboury, A. A. (2016). Whey protein aerogel as blended with cellulose crystalline particles or loaded with fish oil. *Food Chemistry*, *196*, 1016–1022. https://doi.org/10.1016/j.foodchem.2015.10.031

Alam, M. T., Parvez, N., & Sharma, P. K. (2014). FDA-Approved Natural Polymers for Fast Dissolving Tablets. *Journal of Pharmaceutics*, *2014*, 952970. https://doi.org/10.1155/2014/952970

Alander, M., Satokari, R., Korpela, R., Saxelin, M., Vilpponen-Salmela, T., Mattila-Sandholm, T., & von Wright, A. (1999). Persistence of Colonization of Human Colonic Mucosa by a Probiotic Strain, Lactobacillus rhamnosusGG, after Oral Consumption. *Applied and Environmental Microbiology*, *65*(1), 351–354. https://doi.org/10.1128/AEM.65.1.351-354.1999

Ali, M., Cybulska, J., Frąc, M., & Zdunek, A. (2023). Application of polysaccharides for the encapsulation of beneficial microorganisms for agricultural purposes: A review. *International Journal of Biological Macromolecules*, *244*, 125366. https://doi.org/10.1016/j.ijbiomac.2023.125366

Al-Muhtaseb, A. H., McMinn, W. A. M., & Magee, T. R. A. (2002). Moisture Sorption Isotherm Characteristics of Food Products: A Review. *Food and Bioproducts Processing*, *80*(2), 118–128. https://doi.org/10.1205/09603080252938753

Alpizar-Reyes, E., Carrillo-Navas, H., Gallardo-Rivera, R., Varela-Guerrero, V., Alvarez-Ramirez, J., & Pérez-Alonso, C. (2017). Functional properties and physicochemical characteristics of tamarind (Tamarindus indica L.) seed mucilage powder as a novel hydrocolloid. *Journal of Food Engineering*, *209*(Supplement C), 68–75. https://doi.org/10.1016/j.jfoodeng.2017.04.021

Alves, P., Coimbra, P., Ghibaudo, F., Gomez-Zavaglia, A., & Simões, P. N. (2021). Nanostructures for the Stabilization and Delivery of Lactic Acid Bacteria. In A. Gomez-Zavaglia (Ed.), *Basic Protocols in Encapsulation of Food Ingredients* (pp. 111–120). Springer US. https://doi.org/10.1007/978-1-0716-1649-9_11

Amigo, L., & Hernández-Ledesma, B. (2020). Current Evidence on the Bioavailability of Food Bioactive Peptides. *Molecules*, *25*(19), 4479. https://doi.org/10.3390/molecules25194479

Andrade, C. T., Azero, E. G., Luciano, L., & Gonçalves, M. P. (1999). Solution properties of the galactomannans extracted from the seeds of Caesalpinia pulcherrima and Cassia javanica: Comparison with locust bean gum. *International Journal of Biological Macromolecules*, *26*(2), 181–185. https://doi.org/10.1016/S0141-8130(99)00075-6

Appelqvist, I. A. M., Cooke, D., Gidley, M. J., & Lane, S. J. (1993). Thermal properties of polysaccharides at low moisture: 1—An endothermic melting process and water-carbohydrate interactions. *Carbohydrate Polymers*, *20*(4), 291–299. https://doi.org/10.1016/0144-8617(93)90102-A

Aragón-Rojas, S., Quintanilla-Carvajal, M. X., Hernández-Sánchez, H., Hernández-Álvarez, A. J., & Moreno, F. L. (2019). Encapsulation of Lactobacillus fermentum K73 by Refractance Window drying. *Scientific Reports*, *9*(1), 5625. https://doi.org/10.1038/s41598-019-42016-0

Aschenbrenner, M., Foerst, P., & Kulozik, U. (2015). Freeze-drying of Probiotics. In *Advances in*

*Probiotic Technology*. CRC Press.

Aschenbrenner, M., Först, P., & Kulozik, U. (2015). *Freeze-drying of Probiotics* (pp. 213–241). https://doi.org/10.1201/b18807-15

Aschenbrenner, M., Kulozik, U., & Foerst, P. (2012). Evaluation of the relevance of the glassy state as stability criterion for freeze-dried bacteria by application of the Arrhenius and WLF model. *Cryobiology*, *65*(3), 308–318. https://doi.org/10.1016/j.cryobiol.2012.08.005

Aspinall, G. O. (1983). 1—Classification of Polysaccharides. In G. O. Aspinall (Ed.), *The Polysaccharides* (pp. 1–9). Academic Press. https://doi.org/10.1016/B978-0-12-065602-8.50006-6

Avila-de la Rosa, G., Alvarez-Ramirez, J., Vernon-Carter, E. J., Carrillo-Navas, H., & Pérez-Alonso, C. (2015). Viscoelasticity of chia (Salvia hispanica L.) seed mucilage dispersion in the vicinity of an oil-water interface. *Food Hydrocolloids*, *49*, 200–207. https://doi.org/10.1016/j.foodhyd.2015.03.017

Baccigalupi, L., Ricca, E., & Ghelardi, E. (2015). Non-LAB Probiotics: Spore Formers. In *Probiotics and Prebiotics: Current Research and Future Trends* (pp. 93–104). Caister Academic Press. https://doi.org/10.21775/9781910190098.06

Bacenetti, J., Lovarelli, D., Tedesco, D., Pretolani, R., & Ferrante, V. (2018). Environmental impact assessment of alfalfa (Medicago sativa L.) hay production. *Science of The Total Environment*, *635*, 551–558. https://doi.org/10.1016/j.scitotenv.2018.04.161

Bai, L., Liu, F., Xu, X., Huan, S., Gu, J., & McClements, D. J. (2017). Impact of polysaccharide molecular characteristics on viscosity enhancement and depletion flocculation. *Journal of Food Engineering*, *207*, 35–45. https://doi.org/10.1016/j.jfoodeng.2017.03.021

Baley, C., Gomina, M., Breard, J., Bourmaud, A., & Davies, P. (2020). Variability of mechanical properties of flax fibres for composite reinforcement. A review. *Industrial Crops and Products*, *145*, 111984. https://doi.org/10.1016/j.indcrop.2019.111984

Barbé, F., Ménard, O., Gouar, Y. L., Buffière, C., Famelart, M.-H., Laroche, B., Feunteun, S. L., Rémond, D., & Dupont, D. (2014). Acid and rennet gels exhibit strong differences in the kinetics of milk protein digestion and amino acid bioavailability. *Food Chemistry*, *143*, 1–8. https://doi.org/10.1016/j.foodchem.2013.07.100

Barbé, F., Ménard, O., Le Gouar, Y., Buffière, C., Famelart, M.-H., Laroche, B., Le Feunteun, S., Dupont, D., & Rémond, D. (2013). The heat treatment and the gelation are strong determinants of the kinetics of milk proteins digestion and of the peripheral availability of amino acids. *Food Chemistry*, *136*(3), 1203–1212. https://doi.org/10.1016/j.foodchem.2012.09.022

Barreto, P. L. M., Pires, A. T. N., & Soldi, V. (2003). Thermal degradation of edible films based on milk proteins and gelatin in inert atmosphere. *Polymer Degradation and Stability*, *79*(1), 147–152. https://doi.org/10.1016/S0141-3910(02)00267-7

Basilicata, M. G., Pepe, G., Adesso, S., Ostacolo, C., Sala, M., Sommella, E., Scala, M. C., Messore, A., Autore, G., Marzocco, S., & Campiglia, P. (2018). Antioxidant Properties of Buffalo-Milk Dairy Products: A β-Lg Peptide Released after Gastrointestinal Digestion of Buffalo Ricotta Cheese Reduces Oxidative Stress in Intestinal Epithelial Cells. *International Journal of Molecular Sciences*, *19*(7), 1955. https://doi.org/10.3390/ijms19071955

Behrouzian, F., Razavi, S. M. A., & Karazhiyan, H. (2013). The effect of pH, salts and sugars on the rheological properties of cress seed (Lepidium sativum) gum. *International Journal of Food Science & Technology*, *48*(12), 2506–2513. https://doi.org/10.1111/ijfs.12242

Behrouzian, F., Razavi, S. M. A., & Phillips, G. O. (2014). Cress seed (Lepidium sativum) mucilage, an overview. *Bioactive Carbohydrates and Dietary Fibre*, *3*(1), 17–28. https://doi.org/10.1016/j.bcdf.2014.01.001

Beikzadeh, S., Khezerlou, A., Jafari, S. M., Pilevar, Z., & Mortazavian, A. M. (2020). Seed mucilages as the functional ingredients for biodegradable films and edible coatings in the food industry. *Advances in Colloid and Interface Science*, 102164. https://doi.org/10.1016/j.cis.2020.102164

Bektas, E. I., Gurel Pekozer, G., Kök, F. N., & Torun Kose, G. (2021). Evaluation of natural gum-based cryogels for soft tissue engineering. *Carbohydrate Polymers*, *271*, 118407. https://doi.org/10.1016/j.carbpol.2021.118407

Belton, P. S., & Gil, A. M. (1994). IR and Raman spectroscopic studies of the interaction of trehalose with hen egg white lysozyme. *Biopolymers*, *34*(7), 957–961. https://doi.org/10.1002/bip.360340713

Ben-Othman, S., Jõudu, I., & Bhat, R. (2020). Bioactives from Agri-Food Wastes: Present Insights and Future Challenges. *Molecules*, *25*(3), 510. https://doi.org/10.3390/molecules25030510

Bergmann, K. R., Liu, S. X. L., Tian, R., Kushnir, A., Turner, J. R., Li, H.-L., Chou, P. M., Weber, C. R., & Plaen, I. G. D. (2013). Bifidobacteria Stabilize Claudins at Tight Junctions and Prevent Intestinal Barrier Dysfunction in Mouse Necrotizing Enterocolitis. *The American Journal of Pathology*, *182*(5), 1595–1606. https://doi.org/10.1016/j.ajpath.2013.01.013

Bernstein, A. M., Titgemeier, B., Kirkpatrick, K., Golubic, M., & Roizen, M. F. (2013). Major Cereal Grain Fibers and Psyllium in Relation to Cardiovascular Health. *Nutrients*, *5*(5), Article 5. https://doi.org/10.3390/nu5051471

Betz, M., García-González, C. A., Subrahmanyam, R. P., Smirnova, I., & Kulozik, U. (2012). Preparation of novel whey protein-based aerogels as drug carriers for life science applications. *The Journal of Supercritical Fluids*, *72*, 111–119. https://doi.org/10.1016/j.supflu.2012.08.019

Biao, Y., Jiannan, H., Yaolan, C., Shujie, C., Dechun, H., Julian Mcclements, D., & Chongjiang, C. (2020). Identification and characterization of antioxidant and immune-stimulatory polysaccharides in flaxseed hull. *Food Chemistry*, *315*, 126266. https://doi.org/10.1016/j.foodchem.2020.126266

Blanshard, J. M. V., & Lillford, P. (1993). *The Glassy State in Foods*. Nottingham University Press. https://books.google.fr/books?id=3rJzQgAACAAJ

Blomfeldt, T. O. J., Olsson, R. T., Menon, M., Plackett, D., Johansson, E., & Hedenqvist, M. S. (2010). Novel Foams Based on Freeze-Dried Renewable Vital Wheat Gluten. *Macromolecular Materials and Engineering*, *295*(9), 796–801. https://doi.org/10.1002/mame.201000049

Boelt, B., Julier, B., Karagić, Đ., & Hampton, J. (2015). Legume Seed Production Meeting Market Requirements and Economic Impacts. *Critical Reviews in Plant Sciences*, *34*(1–3), 412–427. https://doi.org/10.1080/07352689.2014.898477

Boirie, Y., Dangin, M., Gachon, P., Vasson, M.-P., Maubois, J.-L., & Beaufrère, B. (1997). Slow and fast dietary proteins differently modulate postprandial protein accretion. *Proceedings of the National Academy of Sciences of the United States of America*, *94*(26), 14930–14935.

Boonyai, P., Bhandari, B., & Howes, T. (2006). Applications of Thermal Mechanical Compression Tests in Food Powder Analysis. *International Journal of Food Properties*, *9*(1), 127–134. https://doi.org/10.1080/10942910500473988

Bora, A. F. M., Kouame, K. J. E.-P., Li, X., Liu, L., Sun, Y., Ma, Q., & Liu, Y. (2023). Development, characterization and probiotic encapsulating ability of novel Momordica charantia bioactive polysaccharides/whey protein isolate composite gels. *International Journal of Biological Macromolecules*, *225*, 454–466. https://doi.org/10.1016/j.ijbiomac.2022.11.097

Borreani, J., Llorca, E., Larrea, V., & Hernando, I. (2016). Adding neutral or anionic hydrocolloids to dairy proteins under in vitro gastric digestion conditions. *Food Hydrocolloids*, *57*, 169–177. https://doi.org/10.1016/j.foodhyd.2016.01.030

Borreani, J., Llorca, E., Quiles, A., & Hernando, I. (2017). Designing dairy desserts for weight management: Structure, physical properties and in vitro gastric digestion. *Food Chemistry*, *220*, 137–144. https://doi.org/10.1016/j.foodchem.2016.09.202

Böttger, F., Dupont, D., Marcinkowska, D., Bajka, B., Mackie, A., & Macierzanka, A. (2019). Which casein in sodium caseinate is most resistant to in vitro digestion? Effect of emulsification and enzymatic structuring. *Food Hydrocolloids*, *88*, 114–118. https://doi.org/10.1016/j.foodhyd.2018.09.042

Bourbon, A. I., Pinheiro, A. C., Ribeiro, C., Miranda, C., Maia, J. M., Teixeira, J. A., & Vicente, A. A. (2010). Characterization of galactomannans extracted from seeds of Gleditsia triacanthos and Sophora japonica through shear and extensional rheology: Comparison with guar gum and locust bean gum. *Food Hydrocolloids*, *24*(2), 184–192. https://doi.org/10.1016/j.foodhyd.2009.09.004

Brandelli, A., Daroit, D. J., & Corrêa, A. P. F. (2015). Whey as a source of peptides with remarkable biological activities. *Food Research International*, *73*, 149–161. https://doi.org/10.1016/j.foodres.2015.01.016

Brennan, C. S., Suter, M., Matia-Merino, L., Luethi, T., Ravindran, G., Goh, K., & Ovortrup, J. (2006). Gel and Pasting Behaviour of Fenugreek-Wheat Starch and Fenugreek – Wheat Flour Combinations. *Starch - Stärke*, *58*(10), 527–535. https://doi.org/10.1002/star.200600525

Brodkorb, A., Egger, L., Alminger, M., Alvito, P., Assunção, R., Ballance, S., Bohn, T., Bourlieu-Lacanal, C., Boutrou, R., Carrière, F., Clemente, A., Corredig, M., Dupont, D., Dufour, C., Edwards, C., Golding, M., Karakaya, S., Kirkhus, B., Le Feunteun, S., … Recio, I. (2019). INFOGEST static in vitro simulation of gastrointestinal food digestion. *Nature Protocols*, *14*(4), 991–1014. https://doi.org/10.1038/s41596-018-0119-1

Bron, P. A., Van Baarlen, P., & Kleerebezem, M. (2012). Emerging molecular insights into the

interaction between probiotics and the host intestinal mucosa. *Nature Reviews Microbiology*, *10*(1), 66–78. https://doi.org/10.1038/nrmicro2690

Brummer, Y., Cui, W., & Wang, Q. (2003). Extraction, purification and physicochemical characterization of fenugreek gum. *Food Hydrocolloids*, *17*(3), 229–236. https://doi.org/10.1016/S0268-005X(02)00054-1

Brunauer, S., Emmett, P. H., & Teller, E. (1938). Adsorption of Gases in Multimolecular Layers. *Journal of the American Chemical Society*, *60*(2), 309–319. https://doi.org/10.1021/ja01269a023

Bull-Otterson, L., Feng, W., Kirpich, I., Wang, Y., Qin, X., Liu, Y., Gobejishvili, L., Joshi-Barve, S., Ayvaz, T., Petrosino, J., Kong, M., Barker, D., McClain, C., & Barve, S. (2013). Metagenomic analyses of alcohol induced pathogenic alterations in the intestinal microbiome and the effect of Lactobacillus rhamnosus GG treatment. *PloS One*, *8*(1), e53028. https://doi.org/10.1371/journal.pone.0053028

Burgain, J., Corgneau, M., Scher, J., & Gaiani, C. (2015). Chapter 20—Encapsulation of Probiotics in Milk Protein Microcapsules. In L. M. C. Sagis (Ed.), *Microencapsulation and Microspheres for Food Applications* (pp. 391–406). Academic Press. http://www.sciencedirect.com/science/article/pii/B9780128003503000194

Burgain, J., Gaiani, C., Cailliez-Grimal, C., Jeandel, C., & Scher, J. (2013). Encapsulation of Lactobacillus rhamnosus GG in microparticles: Influence of casein to whey protein ratio on bacterial survival during digestion. *Innovative Food Science & Emerging Technologies*, *19*, 233–242. https://doi.org/10.1016/j.ifset.2013.04.012

Burgain, J., Scher, J., Lebeer, S., Vanderleyden, J., Cailliez-Grimal, C., Corgneau, M., Francius, G., & Gaiani, C. (2014). Significance of bacterial surface molecules interactions with milk proteins to enhance microencapsulation of Lactobacillus rhamnosus GG. *Food Hydrocolloids*, *41*, 60–70. https://doi.org/10.1016/j.foodhyd.2014.03.029

Bustamante, M., Oomah, B. D., Rubilar, M., & Shene, C. (2017). Effective Lactobacillus plantarum and Bifidobacterium infantis encapsulation with chia seed (Salvia hispanica L.) and flaxseed (Linum usitatissimum L.) mucilage and soluble protein by spray drying. *Food Chemistry*, *216*, 97–105. https://doi.org/10.1016/j.foodchem.2016.08.019

Bustamante, M., Villarroel, M., Rubilar, M., & Shene, C. (2015). Lactobacillus acidophilus La-05 encapsulated by spray drying: Effect of mucilage and protein from flaxseed (Linum usitatissimum L.). *LWT - Food Science and Technology*, *62*(2), 1162–1168. https://doi.org/10.1016/j.lwt.2015.02.017

Çakır, E., & Foegeding, E. A. (2011). Combining protein micro-phase separation and protein–polysaccharide segregative phase separation to produce gel structures. *Food Hydrocolloids*, *25*(6), 1538–1546. https://doi.org/10.1016/j.foodhyd.2011.02.002

Cakmak, H., Ilyasoglu-Buyukkestelli, H., Sogut, E., Ozyurt, V. H., Gumus-Bonacina, C. E., & Simsek, S. (2023). A review on recent advances of plant mucilages and their applications in food industry: Extraction, functional properties and health benefits. *Food Hydrocolloids for Health*, *3*, 100131. https://doi.org/10.1016/j.fhfh.2023.100131

Câmara, A. K. F. I., Geraldi, M. V., Okuro, P. K., Maróstica, M. R., da Cunha, R. L., & Pollonio, M. A. R. (2020). Satiety and in vitro digestibility of low saturated fat Bologna sausages added of chia mucilage powder and chia mucilage-based emulsion gel. *Journal of Functional Foods*, *65*, 103753. https://doi.org/10.1016/j.jff.2019.103753

Campbell-Platt, G. (1994). Fermented foods—A world perspective. *Food Research International*, *27*(3), 253–257. https://doi.org/10.1016/0963-9969(94)90093-0

Campos, B. E., Dias Ruivo, T., da Silva Scapim, M. R., Madrona, G. S., & de C. Bergamasco, R. (2016). Optimization of the mucilage extraction process from chia seeds and application in ice cream as a stabilizer and emulsifier. *LWT - Food Science and Technology*, *65*, 874–883. https://doi.org/10.1016/j.lwt.2015.09.021

Capitani, M. I., Corzo-Rios, L. J., Chel-Guerrero, L. A., Betancur-Ancona, D. A., Nolasco, S. M., & Tomás, M. C. (2015). Rheological properties of aqueous dispersions of chia (Salvia hispanica L.) mucilage. *Journal of Food Engineering*, *149*, 70–77. https://doi.org/10.1016/j.jfoodeng.2014.09.043

Capozzi, V., Arena, M. P., Russo, P., Spano, G., & Fiocco, D. (2016). Chapter 16 - Stressors and Food Environment: Toward Strategies to Improve Robustness and Stress Tolerance in Probiotics. In R. R. Watson & V. R. Preedy (Eds.), *Probiotics, Prebiotics, and Synbiotics* (pp. 245–256). Academic Press. http://www.sciencedirect.com/science/article/pii/B9780128021897000162

Carmen García, M., Trujillo, L. A., Carmona, J. A., Muñoz, J., & Carmen Alfaro, M. (2019). Flow, dynamic viscoelastic and creep properties of a biological polymer produced by Sphingomonas sp. As

affected by concentration. *International Journal of Biological Macromolecules*, *125*, 1242–1247. https://doi.org/10.1016/j.ijbiomac.2018.09.100

Carmona, J. A., Ramírez, P., García, M. C., Santos, J., & Muñoz, J. (2019). Linear and non-linear flow behavior of welan gum solutions. *Rheologica Acta*, *58*(1–2), 1–8. https://doi.org/10.1007/s00397-018-1120-x

Carpenter, J. F., Crowe, L. M., & Crowe, J. H. (1987). Stabilization of phosphofructokinase with sugars during freeze-drying: Characterization of enhanced protection in the presence of divalent cations. *Biochimica et Biophysica Acta (BBA) - General Subjects*, *923*(1), 109–115. https://doi.org/10.1016/0304-4165(87)90133-4

Cerqueira, M. A., Bourbon, A. I., Pinheiro, A. C., Martins, J. T., Souza, B. W. S., Teixeira, J. A., & Vicente, A. A. (2011). Galactomannans use in the development of edible films/coatings for food applications. *Trends in Food Science & Technology*, *22*(12), 662–671. https://doi.org/10.1016/j.tifs.2011.07.002

Chai, C., Lee, J., & Huang, Q. (2014). The effect of ionic strength on the rheology of pH-induced bovine serum albumin/κ-carrageenan coacervates. *LWT - Food Science and Technology*, *59*(1), 356–360. https://doi.org/10.1016/j.lwt.2014.05.024

Chang, X., Obianwuna, U. E., Wang, J., Zhang, H., Qi, G., Qiu, K., & Wu, S. (2023). Glycosylated proteins with abnormal glycosylation changes are potential biomarkers for early diagnosis of breast cancer. *International Journal of Biological Macromolecules*, *236*, 123855. https://doi.org/10.1016/j.ijbiomac.2023.123855

Chater, P. I., Wilcox, M. D., Brownlee, I. A., & Pearson, J. P. (2015). Alginate as a protease inhibitor in vitro and in a model gut system; selective inhibition of pepsin but not trypsin. *Carbohydrate Polymers*, *131*, 142–151. https://doi.org/10.1016/j.carbpol.2015.05.062

Chen, H.-B., Wang, Y.-Z., & Schiraldi, D. A. (2013). Foam-like materials based on whey protein isolate. *European Polymer Journal*, *49*(10), 3387–3391. https://doi.org/10.1016/j.eurpolymj.2013.07.019

Chen, H.-H., Xu, S.-Y., & Wang, Z. (2006). Gelation properties of flaxseed gum. *Journal of Food Engineering*, *77*(2), 295–303. https://doi.org/10.1016/j.jfoodeng.2005.06.033

Chen, K., & Zhang, H. (2020). Fabrication of Oleogels via a Facile Method by Oil Absorption in the Aerogel Templates of Protein–Polysaccharide Conjugates. *ACS Applied Materials & Interfaces*, *12*(6), 7795–7804. https://doi.org/10.1021/acsami.9b21435

Chen, L., Liu, J., Zhang, Y., Dai, B., An, Y., & Yu, L. (Lucy). (2015). Structural, Thermal, and Anti-inflammatory Properties of a Novel Pectic Polysaccharide from Alfalfa (Medicago sativa L.) Stem. *Journal of Agricultural and Food Chemistry*, *63*(12), 3219–3228. https://doi.org/10.1021/acs.jafc.5b00494

Chen, L., Liu, J., Zhang, Y., Niu, Y., Dai, B., & Yu, L. (Lucy). (2015). A Novel Alkaline Hemicellulosic Heteroxylan Isolated from Alfalfa (Medicago sativa L.) Stem and Its Thermal and Anti-inflammatory Properties. *Journal of Agricultural and Food Chemistry*, *63*(11), 2970–2978. https://doi.org/10.1021/acs.jafc.5b00063

Cheng, Y., Brown, K. M., & Prud'homme, R. K. (2002). Preparation and characterization of molecular weight fractions of guar galactomannans using acid and enzymatic hydrolysis. *International Journal of Biological Macromolecules*, *31*(1), 29–35. https://doi.org/10.1016/S0141-8130(02)00046-6

Choppe, E., Puaud, F., Nicolai, T., & Benyahia, L. (2010). Rheology of xanthan solutions as a function of temperature, concentration and ionic strength. *Carbohydrate Polymers*, *82*(4), 1228–1235. https://doi.org/10.1016/j.carbpol.2010.06.056

Ciuffarin, F., Négrier, M., Plazzotta, S., Libralato, M., Calligaris, S., Budtova, T., & Manzocco, L. (2023). Interactions of cellulose cryogels and aerogels with water and oil: Structure-function relationships. *Food Hydrocolloids*, *140*, 108631. https://doi.org/10.1016/j.foodhyd.2023.108631

Comert, F., Malanowski, A. J., Azarikia, F., & Dubin, P. L. (2016). Coacervation and precipitation in polysaccharide–protein systems. *Soft Matter*, *12*(18), 4154–4161. https://doi.org/10.1039/C6SM00044D

Comin, L. M., Temelli, F., & Saldaña, M. D. A. (2015). Flax mucilage and barley beta-glucan aerogels obtained using supercritical carbon dioxide: Application as flax lignan carriers. *Innovative Food Science & Emerging Technologies*, *28*(Supplement C), 40–46. https://doi.org/10.1016/j.ifset.2015.01.008

Cook, M. T., Tzortzis, G., Charalampopoulos, D., & Khutoryanskiy, V. V. (2012). Microencapsulation of probiotics for gastrointestinal delivery. *Journal of Controlled Release*, *162*(1), 56–67. https://doi.org/10.1016/j.jconrel.2012.06.003

Corcoran, B. M., Stanton, C., Fitzgerald, G. F., & Ross, R. P. (2005). Survival of Probiotic Lactobacilli in Acidic Environments Is Enhanced in the Presence of Metabolizable Sugars. *Applied and*

*Environmental Microbiology*, *71*(6), 3060–3067. https://doi.org/10.1128/AEM.71.6.3060-3067.2005

Cornara, L., Xiao, J., & Burlando, B. (2016). Therapeutic Potential of Temperate Forage Legumes: A Review. *Critical Reviews in Food Science and Nutrition*, *56*(sup1), S149–S161. https://doi.org/10.1080/10408398.2015.1038378

Corredig, M., Sharafbafi, N., & Kristo, E. (2011). Polysaccharide–protein interactions in dairy matrices, control and design of structures. *Food Hydrocolloids*, *25*(8), 1833–1841. https://doi.org/10.1016/j.foodhyd.2011.05.014

Coste, M., Rochet, V., Léonil, J., Mollé, D., Bouhallab, S., & Tomé, D. (1992). Identification of C-terminal peptides of bovine β-casein that enhance proliferation of rat lymphocytes. *Immunology Letters*, *33*(1), 41–46. https://doi.org/10.1016/0165-2478(92)90091-2

Cryan, J. F., O'Riordan, K. J., Cowan, C. S. M., Sandhu, K. V., Bastiaanssen, T. F. S., Boehme, M., Codagnone, M. G., Cussotto, S., Fulling, C., Golubeva, A. V., Guzzetta, K. E., Jaggar, M., Long-Smith, C. M., Lyte, J. M., Martin, J. A., Molinero-Perez, A., Moloney, G., Morelli, E., Morillas, E., … Dinan, T. G. (2019). The Microbiota-Gut-Brain Axis. *Physiological Reviews*, *99*(4), 1877–2013. https://doi.org/10.1152/physrev.00018.2018

Cui, W., Kenaschuk, E., & Mazza, G. (1996). Influence of genotype on chemical composition and rheological properties of flaxseed gums. *Food Hydrocolloids*, *10*(2), 221–227. https://doi.org/10.1016/S0268-005X(96)80038-5

Cui, W., Mazza, G., Oomah, B. D., & Biliaderis, C. G. (1994). Optimization of an Aqueous Extraction Process for Flaxseed Gum by Response Surface Methodology. *LWT - Food Science and Technology*, *27*(4), 363–369. https://doi.org/10.1006/fstl.1994.1074

Cutting, S. M. (2011). Bacillus probiotics. *Food Microbiology*, *28*(2), 214–220. https://doi.org/10.1016/j.fm.2010.03.007

Cuvelier, G., & Launay, B. (1986). Concentration regimes in xanthan gum solutions deduced from flow and viscoelastic properties. *Carbohydrate Polymers*, *6*(5), 321–333. https://doi.org/10.1016/0144-8617(86)90023-8

Daniloski, D., McCarthy, N. A., Markoska, T., Auldist, M. J., & Vasiljevic, T. (2022). Conformational and physicochemical characteristics of bovine skim milk obtained from cows with different genetic variants of β-casein. *Food Hydrocolloids*, *124*, 107186. https://doi.org/10.1016/j.foodhyd.2021.107186

David, S., Wojciechowska, A., Portmann, R., Shpigelman, A., & Lesmes, U. (2020). The impact of food-grade carrageenans and consumer age on the in vitro proteolysis of whey proteins. *Food Research International*, *130*, 108964. https://doi.org/10.1016/j.foodres.2019.108964

Dawes, E. A., & Senior, P. J. (1973). The Role and Regulation of Energy Reserve Polymers in Micro-organisms. In A. H. Rose & D. W. Tempest (Eds.), *Advances in Microbial Physiology* (Vol. 10, pp. 135–266). Academic Press. https://doi.org/10.1016/S0065-2911(08)60088-0

de Campo, C., dos Santos, P. P., Costa, T. M. H., Paese, K., Guterres, S. S., Rios, A. de O., & Flôres, S. H. (2017). Nanoencapsulation of chia seed oil with chia mucilage (Salvia hispanica L.) as wall material: Characterization and stability evaluation. *Food Chemistry*, *234*, 1–9. https://doi.org/10.1016/j.foodchem.2017.04.153

de Melo Pereira, G. V., de Oliveira Coelho, B., Magalhães Júnior, A. I., Thomaz-Soccol, V., & Soccol, C. R. (2018). How to select a probiotic? A review and update of methods and criteria. *Biotechnology Advances*, *36*(8), 2060–2076. https://doi.org/10.1016/j.biotechadv.2018.09.003

Dea, I. C. M., Morris, E. R., Rees, D. A., Welsh, E. J., Barnes, H. A., & Price, J. (1977). Associations of like and unlike polysaccharides: Mechanism and specificity in galactomannans, interacting bacterial polysaccharides, and related systems. *Carbohydrate Research*, *57*, 249–272. https://doi.org/10.1016/S0008-6215(00)81935-7

Dea, I. C. M., & Morrison, A. (1975). Chemistry and Interactions of Seed Galactomannans. In R. S. Tipson & D. Horton (Eds.), *Advances in Carbohydrate Chemistry and Biochemistry* (Vol. 31, pp. 241–312). Academic Press. https://doi.org/10.1016/S0065-2318(08)60298-X

DeBenedictis, E. P., & Keten, S. (2019). Mechanical unfolding of alpha - and beta-helical protein motifs. *Soft Matter*, *15*(6), 1243–1252. https://doi.org/10.1039/C8SM02046A

Dennis, J. W., Granovsky, M., & Warren, C. E. (1999). Protein glycosylation in development and disease. *BioEssays*, *21*(5), 412–421. https://doi.org/10.1002/(SICI)1521-1878(199905)21:5<412::AID-BIES8>3.0.CO;2-5

Desmond, C., Ross, R. P., O'Callaghan, E., Fitzgerald, G., & Stanton, C. (2002). Improved survival

of Lactobacillus paracasei NFBC 338 in spray-dried powders containing gum acacia. *Journal of Applied Microbiology*, *93*(6), 1003–1011. https://doi.org/10.1046/j.1365-2672.2002.01782.x

Deutsch, E. W., Bandeira, N., Sharma, V., Perez-Riverol, Y., Carver, J. J., Kundu, D. J., García-Seisdedos, D., Jarnuczak, A. F., Hewapathirana, S., Pullman, B. S., Wertz, J., Sun, Z., Kawano, S., Okuda, S., Watanabe, Y., Hermjakob, H., MacLean, B., MacCoss, M. J., Zhu, Y., … Vizcaíno, J. A. (2020). The ProteomeXchange consortium in 2020: Enabling 'big data' approaches in proteomics. *Nucleic Acids Research*, *48*(D1), D1145–D1152. https://doi.org/10.1093/nar/gkz984

Dhull, S. B., Sandhu, K. S., Punia, S., Kaur, M., Chawla, P., & Malik, A. (2020). Functional, thermal and rheological behavior of fenugreek (Trigonella foenum–graecum L.) gums from different cultivars: A comparative study. *International Journal of Biological Macromolecules*, *159*, 406–414. https://doi.org/10.1016/j.ijbiomac.2020.05.094

Di Giorgio, L., Salgado, P. R., & Mauri, A. N. (2021). Fish Oil Encapsulation Using Soy Proteins as Wall Material: Protocols to Ensure PUFA Protection. In A. Gomez-Zavaglia (Ed.), *Basic Protocols in Encapsulation of Food Ingredients* (pp. 121–137). Springer US. https://doi.org/10.1007/978-1-0716-1649-9_12

Dianawati, D., Mishra, V., & Shah, N. P. (2016). Survival of Microencapsulated Probiotic Bacteria after Processing and during Storage: A Review. *Critical Reviews in Food Science and Nutrition*, *56*(10), 1685–1716. https://doi.org/10.1080/10408398.2013.798779

Ding, H. H., Qian, K., Goff, H. D., Wang, Q., & Cui, S. W. (2018). Structural and conformational characterization of arabinoxylans from flaxseed mucilage. *Food Chemistry*, *254*, 266–271. https://doi.org/10.1016/j.foodchem.2018.01.159

Ding, W. K., & Shah, N. P. (2007). Acid, Bile, and Heat Tolerance of Free and Microencapsulated Probiotic Bacteria. *Journal of Food Science*, *72*(9), M446–M450. https://doi.org/10.1111/j.1750-3841.2007.00565.x

Divyashree, S., Anjali, P. G., Somashekaraiah, R., & Sreenivasa, M. Y. (2021). Probiotic properties of Lactobacillus casei – MYSRD 108 and Lactobacillus plantarum-MYSRD 71 with potential antimicrobial activity against Salmonella paratyphi. *Biotechnology Reports*, *32*, e00672. https://doi.org/10.1016/j.btre.2021.e00672

Dobrenz, A. K., Smith, S. E., Poteet, D., & Miller, W. B. (1993). Carbohydrates in Alfalfa Seed Developed for Salt Tolerance during Germination. *Agronomy Journal*, *85*(4), 834–836. https://doi.org/10.2134/agronj1993.00021962008500040010x

Doherty, S. B., Gee, V. L., Ross, R. P., Stanton, C., Fitzgerald, G. F., & Brodkorb, A. (2010). Efficacy of whey protein gel networks as potential viability-enhancing scaffolds for cell immobilization of Lactobacillus rhamnosus GG. *Journal of Microbiological Methods*, *80*(3), 231–241. https://doi.org/10.1016/j.mimet.2009.12.009

Donato, L., Kolodziejcyk, E., & Rouvet, M. (2011). Mixtures of whey protein microgels and soluble aggregates as building blocks to control rheology and structure of acid induced cold-set gels. *Food Hydrocolloids*, *25*(4), 734–742. https://doi.org/10.1016/j.foodhyd.2010.08.020

Dos Santos Morais, R., Gaiani, C., Borges, F., & Burgain, J. (2022). Interactions Microbe-Matrix in Dairy Products. In P. L. H. McSweeney & J. P. McNamara (Eds.), *Encyclopedia of Dairy Sciences (Third Edition)* (pp. 133–143). Academic Press. https://doi.org/10.1016/B978-0-08-100596-5.23004-7

Doublier, J. L., & Launay, B. (1981). Rheology of Galactomannan Solutions: Comparative Study of Guar Gum and Locust Bean Gum. *Journal of Texture Studies*, *12*(2), 151–172. https://doi.org/10.1111/j.1745-4603.1981.tb01229.x

Doublier, J.-L., Garnier, C., Renard, D., & Sanchez, C. (2000). Protein–polysaccharide interactions. *Current Opinion in Colloid & Interface Science*, *5*(3), 202–214. https://doi.org/10.1016/S1359-0294(00)00054-6

Doyle, C. D. (1961). Estimating Thermal Stability of Experimental Polymers by Empirical Thermogravimetric Analysis. *Analytical Chemistry*, *33*(1), 77–79. https://doi.org/10.1021/ac60169a022

Doyle, J. P., Lyons, G., & Morris, E. R. (2009). New proposals on "hyperentanglement" of galactomannans: Solution viscosity of fenugreek gum under neutral and alkaline conditions. *Food Hydrocolloids*, *23*(6), 1501–1510. https://doi.org/10.1016/j.foodhyd.2008.09.007

Dubois, F., Musa, C., Duponchel, B., Tidahy, L., Sécordel, X., Mallard, I., & Delattre, F. (2020). Nuclear Magnetic Resonance and Calorimetric Investigations of Extraction Mode on Flaxseed Gum Composition. *Polymers*, *12*(11), 2654. https://doi.org/10.3390/polym12112654

Duman, D., & Karadag, A. (2021). Inulin added electrospun composite nanofibres by

electrospinning for the encapsulation of probiotics: Characterisation and assessment of viability during storage and simulated gastrointestinal digestion. *International Journal of Food Science & Technology*, *56*(2), 927–935. https://doi.org/10.1111/ijfs.14744

Dupont, D., & Tomé, D. (2020). Chapter 20 - Milk proteins: Digestion and absorption in the gastrointestinal tract. In M. Boland & H. Singh (Eds.), *Milk Proteins (Third Edition)* (pp. 701–714). Academic Press. https://doi.org/10.1016/B978-0-12-815251-5.00020-7

Eghbaljoo, H., Sani, I. K., Sani, M. A., Rahati, S., Mansouri, E., Molaee-Aghaee, E., Fatourehchi, N., Kadi, A., Arab, A., Sarabandi, K., Samborska, K., & Jafari, S. M. (2022). Advances in plant gum polysaccharides; Sources, techno-functional properties, and applications in the food industry—A review. *International Journal of Biological Macromolecules*, *222*, 2327–2340. https://doi.org/10.1016/j.ijbiomac.2022.10.020

Elboutachfaiti, R., Delattre, C., Quéro, A., Roulard, R., Duchêne, J., Mesnard, F., & Petit, E. (2017). Fractionation and structural characterization of six purified rhamnogalacturonans type I from flaxseed mucilage. *Food Hydrocolloids*, *62*(Supplement C), 273–279. https://doi.org/10.1016/j.foodhyd.2016.08.005

El-Kamel, A., Sokar, M., Naggar, V., & Al Gamal, S. (2002). Chitosan and sodium alginate—Based bioadhesive vaginal tablets. *AAPS PharmSci*, *4*(4), 224–230. https://doi.org/10.1208/ps040444

Fabek, H., & Goff, H. D. (2015). Simulated intestinal hydrolysis of native tapioca starch: Understanding the effect of soluble fibre. *Bioactive Carbohydrates and Dietary Fibre*, *6*(2), 83–98. https://doi.org/10.1016/j.bcdf.2015.09.008

Fabek, H., Messerschmidt, S., Brulport, V., & Goff, H. D. (2014). The effect of in vitro digestive processes on the viscosity of dietary fibres and their influence on glucose diffusion. *Food Hydrocolloids*, *35*, 718–726. https://doi.org/10.1016/j.foodhyd.2013.08.007

Falahati, M. T., & Ghoreishi, S. M. (2019). Preparation of Balangu (Lallemantia royleana) seed mucilage aerogels loaded with paracetamol: Evaluation of drug loading via response surface methodology. *The Journal of Supercritical Fluids*, *150*, 1–10. https://doi.org/10.1016/j.supflu.2019.04.003

Fan, Y., & Pedersen, O. (2021). Gut microbiota in human metabolic health and disease. *Nature Reviews Microbiology*, *19*(1), 55–71. https://doi.org/10.1038/s41579-020-0433-9

Fang, X., Rioux, L.-E., Labrie, S., & Turgeon, S. L. (2016). Commercial cheeses with different texture have different disintegration and protein/peptide release rates during simulated in vitro digestion. *International Dairy Journal*, *56*, 169–178. https://doi.org/10.1016/j.idairyj.2016.01.023

FAO/WHO. (2002). Joint FAO/WHO working group report on drafting guidelines for the evaluation of probiotics in food. http://ftp.fao.org/es/esn/food/wgreport2.pdf

Farahnaky, A., Ansari, S., & Majzoobi, M. (2009). Effect of glycerol on the moisture sorption isotherms of figs. *Journal of Food Engineering*, *93*(4), 468–473. https://doi.org/10.1016/j.jfoodeng.2009.02.014

Farrer, D., & Lips, A. (1999). On the self-assembly of sodium caseinate. *International Dairy Journal*, *9*(3), 281–286. https://doi.org/10.1016/S0958-6946(99)00075-8

Fedeniuk, R. W., & Biliaderis, C. G. (1994). Composition and Physicochemical Properties of Linseed (Linum usitatissimum L.) Mucilage. *Journal of Agricultural and Food Chemistry*, *42*(2), 240–247. https://doi.org/10.1021/jf00038a003

Fernandes, S. S., da Silva Cardoso, P., Egea, M. B., Quintal Martínez, J. P., Segura Campos, M. R., & Otero, D. M. (2023). Chia mucilage carrier systems: A review of emulsion, encapsulation, and coating and film strategies. *Food Research International*, *172*, 113125. https://doi.org/10.1016/j.foodres.2023.113125

*Flaxseed Gum: A Versatile Natural Hydrocolloid - FocusHerb*. (2022, May 10). https://www.focusherb.com/food-and-nutrition-ingredients/flaxseed-gum/

Foerst, P., Kulozik, U., Schmitt, M., Bauer, S., & Santivarangkna, C. (2012). Storage stability of vacuum-dried probiotic bacterium Lactobacillus paracasei F19. *Food and Bioproducts Processing*, *90*(2), 295–300. https://doi.org/10.1016/j.fbp.2011.06.004

Fontes-Candia, C., Erboz, E., Martínez-Abad, A., López-Rubio, A., & Martínez-Sanz, M. (2019). Superabsorbent food packaging bioactive cellulose-based aerogels from Arundo donax waste biomass. *Food Hydrocolloids*, *96*, 151–160. https://doi.org/10.1016/j.foodhyd.2019.05.011

Fontes-Candia, C., Jiménez-Barrios, P., Miralles, B., Recio, I., López-Rubio, A., & Martínez-Sanz, M. (2022). Development of polysaccharide-casein gel-like structures resistant to in vitro gastric digestion. *Food Hydrocolloids*, *127*, 107505. https://doi.org/10.1016/j.foodhyd.2022.107505

Forny, L., Marabi, A., & Palzer, S. (2011). Wetting, disintegration and dissolution of agglomerated water soluble powders. *Powder Technology*, *206*(1), 72–78. https://doi.org/10.1016/j.powtec.2010.07.022

Fortuin, J., Hellebois, T., Iken, M., Shaplov, A. S., Villas-Boas, S., Fogliano, V., & Soukoulis, C. (2023). Study of the lyoprotective and stabilising effects of Spirulina (Arthrospira platensis) protein isolate on Lacticaseibacillus rhamnosus GG. *Submitted to Food Hydrocolloids*.

Frost & Sulivan. (2023). Global Food Emulsifiers and Texturizers Growth Opportunities.

G. Gómez-Mascaraque, L., Martínez-Sanz, M., Hogan, S. A., López-Rubio, A., & Brodkorb, A. (2019). Nano- and microstructural evolution of alginate beads in simulated gastrointestinal fluids. Impact of M/G ratio, molecular weight and pH. *Carbohydrate Polymers*, *223*, 115121. https://doi.org/10.1016/j.carbpol.2019.115121

Gadkari, P. V., Tu, S., Chiyarda, K., Reaney, M. J. T., & Ghosh, S. (2018). Rheological characterization of fenugreek gum and comparison with other galactomannans. *International Journal of Biological Macromolecules*, *119*, 486–495. https://doi.org/10.1016/j.ijbiomac.2018.07.108

Ganter, J. L. M. S., Milas, M., Corrêa, J. B. C., Reicher, F., & Rinaudo, M. (1992). Study of solution properties of galactomannan from the seeds of Mimosa scabrella. *Carbohydrate Polymers*, *17*(3), 171–175. https://doi.org/10.1016/0144-8617(92)90001-7

Garcia-Brand, A. J., Quezada, V., Gonzalez-Melo, C., Bolaños-Barbosa, A. D., Cruz, J. C., & Reyes, L. H. (2022). Novel Developments on Stimuli-Responsive Probiotic Encapsulates: From Smart Hydrogels to Nanostructured Platforms. *Fermentation*, *8*(3), 117. https://doi.org/10.3390/fermentation8030117

García-González, C. A., & Smirnova, I. (2013). Use of supercritical fluid technology for the production of tailor-made aerogel particles for delivery systems. *The Journal of Supercritical Fluids*, *79*, 152–158. https://doi.org/10.1016/j.supflu.2013.03.001

Gareau, M. G. (2014). Microbiota-Gut-Brain Axis and Cognitive Function. In M. Lyte & J. F. Cryan (Eds.), *Microbial Endocrinology: The Microbiota-Gut-Brain Axis in Health and Disease* (pp. 357–371). Springer. https://doi.org/10.1007/978-1-4939-0897-4_16

Gbassi, G. K., & Vandamme, T. (2012). Probiotic Encapsulation Technology: From Microencapsulation to Release into the Gut. *Pharmaceutics*, *4*(1), Article 1. https://doi.org/10.3390/pharmaceutics4010149

Georgantzopoulou, A., Serchi, T., Cambier, S., Leclercq, C. C., Renaut, J., Shao, J., Kruszewski, M., Lentzen, E., Grysan, P., Eswara, S., Audinot, J.-N., Contal, S., Ziebel, J., Guignard, C., Hoffmann, L., Murk, A. J., & Gutleb, A. C. (2016). Effects of silver nanoparticles and ions on a co-culture model for the gastrointestinal epithelium. *Particle and Fibre Toxicology*, *13*(1), 9. https://doi.org/10.1186/s12989-016-0117-9

Ghorbani, E., Avan, A., Ryzhikov, M., Ferns, G., Khazaei, M., & Soleimanpour, S. (2022). Role of lactobacillus strains in the management of colorectal cancer: An overview of recent advances. *Nutrition*, *103–104*, 111828. https://doi.org/10.1016/j.nut.2022.111828

Ghosh, A. K., Bandyopadhyay, P., Ghosh, A. K., & Bandyopadhyay, P. (2012). *Polysaccharide-Protein Interactions and Their Relevance in Food Colloids*. IntechOpen. https://doi.org/10.5772/50561

Gillet, S., Aguedo, M., Petrut, R., Olive, G., Anastas, P., Blecker, C., & Richel, A. (2017). Structure impact of two galactomannan fractions on their viscosity properties in dilute solution, unperturbed state and gel state. *International Journal of Biological Macromolecules*, *96*, 550–559. https://doi.org/10.1016/j.ijbiomac.2016.12.057

Giulio, B. D., Orlando, P., Barba, G., Coppola, R., Rosa, M. D., Sada, A., Prisco, P. P. D., & Nazzaro, F. (2005). Use of alginate and cryo-protective sugars to improve the viability of lactic acid bacteria after freezing and freeze-drying. *World Journal of Microbiology and Biotechnology*, *21*(5), 739–746. https://doi.org/10.1007/s11274-004-4735-2

Goh, K. K. T., Pinder, D. N., Hall, C. E., & Hemar, Y. (2006). Rheological and Light Scattering Properties of Flaxseed Polysaccharide Aqueous Solutions. *Biomacromolecules*, *7*(11), 3098–3103. https://doi.org/10.1021/bm060577u

Goksen, G., Demir, D., Dhama, K., Kumar, M., Shao, P., Xie, F., Echegaray, N., & Lorenzo, J. M. (2023). Mucilage polysaccharide as a plant secretion: Potential trends in food and biomedical applications. *International Journal of Biological Macromolecules*, *230*, 123146. https://doi.org/10.1016/j.ijbiomac.2023.123146

Golbaghi, L., Khamforoush, M., & Hatami, T. (2017). Carboxymethyl cellulose production from sugarcane bagasse with steam explosion pulping: Experimental, modeling, and optimization. *Carbohydrate Polymers*, *174*, 780–788. https://doi.org/10.1016/j.carbpol.2017.06.123

Goldin, B. R., Gorbach, S. L., Saxelin, M., Barakat, S., Gualtieri, L., & Salminen, S. (1992). Survival of Lactobacillus species (strain GG) in human gastrointestinal tract. *Digestive Diseases and Sciences*, *37*(1), 121–128. https://doi.org/10.1007/BF01308354

Gomand, F., Borges, F., Burgain, J., Guerin, J., Revol-Junelles, A.-M., & Gaiani, C. (2019). Food Matrix Design for Effective Lactic Acid Bacteria Delivery. *Annual Review of Food Science and Technology*, *10*(1), 285–310. https://doi.org/10.1146/annurev-food-032818-121140

Gong, H., Gao, J., Wang, Y., Luo, Q. W., Guo, K. R., Ren, F. Z., & Mao, X. Y. (2020). Identification of novel peptides from goat milk casein that ameliorate high-glucose-induced insulin resistance in HepG2 cells. *Journal of Dairy Science*, *103*(6), 4907–4918. https://doi.org/10.3168/jds.2019-17513

Gorbach, S. (2000). Probiotics and gastrointestinal health. *The American Journal of Gastroenterology*, *95*(1), S2–S4. https://doi.org/10.1016/S0002-9270(99)00806-0

Gorbach, S., Doron, S., & Magro, F. (2017). Chapter 7—Lactobacillus rhamnosus GG. In M. H. Floch, Y. Ringel, & W. Allan Walker (Eds.), *The Microbiota in Gastrointestinal Pathophysiology* (pp. 79–88). Academic Press. https://doi.org/10.1016/B978-0-12-804024-9.00007-0

Goulding, D. A., Fox, P. F., & O'Mahony, J. A. (2020). Chapter 2 - Milk proteins: An overview. In M. Boland & H. Singh (Eds.), *Milk Proteins (Third Edition)* (pp. 21–98). Academic Press. https://doi.org/10.1016/B978-0-12-815251-5.00002-5

Grasdalen, H., & Painter, T. (1980). N.M.R. Studies of composition and sequence in legume-seed Galactomannans. *Carbohydrate Research*, *81*(1), 59–66. https://doi.org/10.1016/S0008-6215(00)85677-3

Grisel, M., Aguni, Y., Renou, F., & Malhiac, C. (2015). Impact of fine structure of galactomannans on their interactions with xanthan: Two co-existing mechanisms to explain the synergy. *Food Hydrocolloids*, *51*, 449–458. https://doi.org/10.1016/j.foodhyd.2015.05.041

Groult, S., Buwalda, S., & Budtova, T. (2021). Pectin hydrogels, aerogels, cryogels and xerogels: Influence of drying on structural and release properties. *European Polymer Journal*, *149*, 110386. https://doi.org/10.1016/j.eurpolymj.2021.110386

Gu, Q., Yin, Y., Yan, X., Liu, X., Liu, F., & McClements, D. J. (2022). Encapsulation of multiple probiotics, synbiotics, or nutrabiotics for improved health effects: A review. *Advances in Colloid and Interface Science*, *309*, 102781. https://doi.org/10.1016/j.cis.2022.102781

Guérin, H., Kulakauskas, S., & Chapot-Chartier, M.-P. (2022). Structural variations and roles of rhamnose-rich cell wall polysaccharides in Gram-positive bacteria. *Journal of Biological Chemistry*, *298*(10), 102488. https://doi.org/10.1016/j.jbc.2022.102488

Guerin, J., Burgain, J., Borges, F., Bhandari, B., Desobry, S., Scher, J., & Gaiani, C. (2017). Use of imaging techniques to identify efficient controlled release systems of Lactobacillus rhamnosus GG during in vitro digestion. *Food Funct*. https://doi.org/10.1039/C6FO01737A

Guerin, J., Petit, J., Burgain, J., Borges, F., Bhandari, B., Perroud, C., Desobry, S., Scher, J., & Gaiani, C. (2017). Lactobacillus rhamnosus GG encapsulation by spray-drying: Milk proteins clotting control to produce innovative matrices. *Journal of Food Engineering*, *193*, 10–19. https://doi.org/10.1016/j.jfoodeng.2016.08.008

Guerin, J., Soligot, C., Burgain, J., Huguet, M., Francius, G., El-Kirat-Chatel, S., Gomand, F., Lebeer, S., Le Roux, Y., Borges, F., Scher, J., & Gaiani, C. (2018). Adhesive interactions between milk fat globule membrane and Lactobacillus rhamnosus GG inhibit bacterial attachment to Caco-2 TC7 intestinal cell. *Colloids and Surfaces B: Biointerfaces*, *167*, 44–53. https://doi.org/10.1016/j.colsurfb.2018.03.044

Guerrero Sanchez, M., Passot, S., Campoy, S., Olivares, M., & Fonseca, F. (2022). Effect of protective agents on the storage stability of freeze-dried Ligilactobacillus salivarius CECT5713. *Applied Microbiology and Biotechnology*, *106*(21), 7235–7249. https://doi.org/10.1007/s00253-022-12201-9

Guglielmetti, S., Mora, D., Gschwender, M., & Popp, K. (2011). Randomised clinical trial: Bifidobacterium bifidum MIMBb75 significantly alleviates irritable bowel syndrome and improves quality of life — a double-blind, placebo-controlled study. *Alimentary Pharmacology & Therapeutics*, *33*(10), 1123–1132. https://doi.org/10.1111/j.1365-2036.2011.04633.x

Gunasekaran, S., & Ak, M. M. (2000). Dynamic oscillatory shear testing of foods—Selected applications. *Trends in Food Science & Technology*, *11*(3), 115–127. https://doi.org/10.1016/S0924-2244(00)00058-3

Gun'ko, V. M., Savina, I. N., & Mikhalovsky, S. V. (2013). Cryogels: Morphological, structural and adsorption characterisation. *Advances in Colloid and Interface Science*, *187–188*, 1–46. https://doi.org/10.1016/j.cis.2012.11.001

Haji, F., Cheon, J., Baek, J., Wang, Q., & Tam, K. C. (2022). Application of Pickering emulsions in

probiotic encapsulation- A review. *Current Research in Food Science*, *5*, 1603–1615. https://doi.org/10.1016/j.crfs.2022.09.013

Halabi, A., Croguennec, T., Bouhallab, S., Dupont, D., & Deglaire, A. (2020). Modification of protein structures by altering the whey protein profile and heat treatment affects in vitro static digestion of model infant milk formulas. *Food & Function*, *11*(8), 6933–6945. https://doi.org/10.1039/D0FO01362E

Halabi, A., Croguennec, T., Ménard, O., Briard-Bion, V., Jardin, J., Le Gouar, Y., Hennetier, M., Bouhallab, S., Dupont, D., & Deglaire, A. (2022). Protein structure in model infant milk formulas impacts their kinetics of hydrolysis under in vitro dynamic digestion. *Food Hydrocolloids*, *126*, 107368. https://doi.org/10.1016/j.foodhyd.2021.107368

Haltiwanger, R. S., & Lowe, J. B. (2004). Role of Glycosylation in Development. *Annual Review of Biochemistry*, *73*(1), 491–537. https://doi.org/10.1146/annurev.biochem.73.011303.074043

Han, S., Lu, Y., Xie, J., Fei, Y., Zheng, G., Wang, Z., Liu, J., Lv, L., Ling, Z., Berglund, B., Yao, M., & Li, L. (2021). Probiotic Gastrointestinal Transit and Colonization After Oral Administration: A Long Journey. *Frontiers in Cellular and Infection Microbiology*, *11*. https://www.frontiersin.org/articles/10.3389/fcimb.2021.609722

Harding, S. E. (1997). The intrinsic viscosity of biological macromolecules. Progress in measurement, interpretation and application to structure in dilute solution. *Progress in Biophysics and Molecular Biology*, *68*(2), 207–262. https://doi.org/10.1016/S0079-6107(97)00027-8

Haukioja, A., Yli-Knuuttila, H., Loimaranta, V., Kari, K., Ouwehand, A. C., Meurman, J. H., & Tenovuo, J. (2006). Oral adhesion and survival of probiotic and other lactobacilli and bifidobacteria in vitro. *Oral Microbiology and Immunology*, *21*(5), 326–332. https://doi.org/10.1111/j.1399-302X.2006.00299.x

Hayes, M., Ross, R. P., Fitzgerald, G. F., Hill, C., & Stanton, C. (2006). Casein-Derived Antimicrobial Peptides Generated by Lactobacillus acidophilus DPC6026. *Applied and Environmental Microbiology*, *72*(3), 2260–2264. https://doi.org/10.1128/AEM.72.3.2260-2264.2006

Hazards (BIOHAZ), E. P. on B., Koutsoumanis, K., Allende, A., Álvarez-Ordóñez, A., Bolton, D., Bover-Cid, S., Chemaly, M., de Cesare, A., Hilbert, F., Lindqvist, R., Nauta, M., Peixe, L., Ru, G., Simmons, M., Skandamis, P., Suffredini, E., Cocconcelli, P. S., Fernández Escámez, P. S., Maradona, M. P., … Herman, L. (2023). Update of the list of qualified presumption of safety (QPS) recommended microorganisms intentionally added to food or feed as notified to EFSA. *EFSA Journal*, *21*(1), e07747. https://doi.org/10.2903/j.efsa.2023.7747

Hedayati, S., Niakousari, M., Babajafari, S., & Mazloomi, S. M. (2021). Ultrasound-assisted extraction of mucilaginous seed hydrocolloids: Physicochemical properties and food applications. *Trends in Food Science & Technology*, *118*, 356–361. https://doi.org/10.1016/j.tifs.2021.10.022

Heidebach, T., Först, P., & Kulozik, U. (2009a). Microencapsulation of probiotic cells by means of rennet-gelation of milk proteins. *Food Hydrocolloids*, *23*(7), 1670–1677. https://doi.org/10.1016/j.foodhyd.2009.01.006

Heidebach, T., Först, P., & Kulozik, U. (2009b). Transglutaminase-induced caseinate gelation for the microencapsulation of probiotic cells. *International Dairy Journal*, *19*(2), 77–84. https://doi.org/10.1016/j.idairyj.2008.08.003

Hellebois, T., Addiego, F., Gaiani, C., Shaplov, A. S., & Soukoulis, C. (2024). Unravelling the functionality of anionic and non-ionic plant seed gums on milk protein cryogels conveying Lacticaseibacillus rhamnosus GG. *Carbohydrate Polymers*, *323*, 121376. https://doi.org/10.1016/j.carbpol.2023.121376

Hellebois, T., Canuel, R., Addiego, F., Audinot, J.-N., Gaiani, C., Shaplov, A. S., & Soukoulis, C. (2023). Milk protein-based cryogel monoliths as novel encapsulants of probiotic bacteria. Part I: Microstructural, physicochemical, and mechanical characterisation. *Food Hydrocolloids*, 108641. https://doi.org/10.1016/j.foodhyd.2023.108641

Hellebois, T., Canuel, R., Leclercq, C. C., Gaiani, C., & Soukoulis, C. (2024). Milk protein-based cryogel monoliths as novel encapsulants of probiotic bacteria. Part II: Lacticaseibacillus rhamnosus GG storage stability and bioactivity under in vitro digestion. *Food Hydrocolloids*, *146*, 109173. https://doi.org/10.1016/j.foodhyd.2023.109173

Hellebois, T., Fortuin, J., Gaiani, C., & Soukoulis, C. (2022). Impact of Flaxseed Gums on the Colloidal Changes and In Vitro Digestibility of Milk Proteins. *Foods*, *11*(24), 4096. https://doi.org/10.3390/foods11244096

Hellebois, T., Fortuin, J., Xu, X., Shaplov, A. S., Gaiani, C., & Soukoulis, C. (2021). Structure

conformation, physicochemical and rheological properties of flaxseed gums extracted under alkaline and acidic conditions. *International Journal of Biological Macromolecules*, *192*, 1217–1230. https://doi.org/10.1016/j.ijbiomac.2021.10.087

Hellebois, T., Gaiani, C., Cambier, S., Noo, A., & Soukoulis, C. (2022). Exploration of the co-structuring and stabilising role of flaxseed gum in whey protein isolate based cryo-hydrogels. *Carbohydrate Polymers*, *289*, 119424. https://doi.org/10.1016/j.carbpol.2022.119424

Hellebois, T., Gaiani, C., Fortuin, J., Shaplov, A., & Soukoulis, C. (2021). Cryotropic gel-forming capacity of alfalfa (Medicago sativa L.) and fenugreek (Trigonella foenum graecum) seed galactomannans. *Carbohydrate Polymers*, *267*, 118190. https://doi.org/10.1016/j.carbpol.2021.118190

Hellebois, T., Gaiani, C., Paris, C., Planchon, S., Renaut, J., & Soukoulis, C. (2021). Data on the in-vitro digestibility of acid gels prepared from brewers' spent grain protein isolates. *Data in Brief*, *37*, 107160. https://doi.org/10.1016/j.dib.2021.107160

Hellebois, T., Gaiani, C., & Soukoulis, C. (2022a). Freeze − thaw induced structuration of whey protein − alfalfa (Medicago sativa L.) galactomannan binary systems. *Food Hydrocolloids*, *125*, 107389. https://doi.org/10.1016/j.foodhyd.2021.107389

Hellebois, T., Gaiani, C., & Soukoulis, C. (2022b). Impact of alfalfa (Medicago sativa L.) galactomannan on the microstructural and physicochemical changes of milk proteins under static in-vitro digestion conditions. *Food Chemistry: X*, *14*, 100330. https://doi.org/10.1016/j.fochx.2022.100330

Hellebois, T., Soukoulis, C., Xu, X., Hausman, J.-F., Shaplov, A., Taoukis, P. S., & Gaiani, C. (2021). Structure conformational and rheological characterisation of alfalfa seed (Medicago sativa L.) galactomannan. *Carbohydrate Polymers*, *256*, 117394. https://doi.org/10.1016/j.carbpol.2020.117394

Her, J.-Y., Kim, M. S., & Lee, K.-G. (2015). Preparation of probiotic powder by the spray freeze-drying method. *Journal of Food Engineering*, *150*, 70–74. https://doi.org/10.1016/j.jfoodeng.2014.10.029

Hermiati, E., Sondari, D., & Sunarti, T. C. (2023). Chapter 2 - Extraction and classification of starch from different sources: Structure, properties, and characterization. In M. S. Sreekala, L. Ravindran, K. Goda, & S. Thomas (Eds.), *Handbook of Natural Polymers, Volume 1* (pp. 19–60). Elsevier. https://doi.org/10.1016/B978-0-323-99853-6.00012-7

Hesarinejad, M. A., Sami Jokandan, M., Mohammadifar, M. A., Koocheki, A., Razavi, S. M. A., Ale, M. T., & Attar, F. R. (2018). The effects of concentration and heating-cooling rate on rheological properties of Plantago lanceolata seed mucilage. *International Journal of Biological Macromolecules*, *115*, 1260–1266. https://doi.org/10.1016/j.ijbiomac.2017.10.102

Hill, C., Guarner, F., Reid, G., Gibson, G. R., Merenstein, D. J., Pot, B., Morelli, L., Canani, R. B., Flint, H. J., Salminen, S., Calder, P. C., & Sanders, M. E. (2014). The International Scientific Association for Probiotics and Prebiotics consensus statement on the scope and appropriate use of the term probiotic. *Nature Reviews Gastroenterology & Hepatology*, *11*(8), 506–514. https://doi.org/10.1038/nrgastro.2014.66

Hiller, B., & Lorenzen, P. Chr. (2008). Surface Hydrophobicity of Physicochemically and Enzymatically Treated Milk Proteins in Relation to Techno-functional Properties. *Journal of Agricultural and Food Chemistry*, *56*(2), 461–468. https://doi.org/10.1021/jf072400c

Hiolle, M., Lechevalier, V., Floury, J., Boulier-Monthéan, N., Prioul, C., Dupont, D., & Nau, F. (2020). In vitro digestion of complex foods: How microstructure influences food disintegration and micronutrient bioaccessibility. *Food Research International*, *128*, 108817. https://doi.org/10.1016/j.foodres.2019.108817

Hojilla-Evangelista, M. P., Selling, G. W., Hatfield, R., & Digman, M. (2017). Extraction, composition, and functional properties of dried alfalfa (Medicago sativa L.) leaf protein. *Journal of the Science of Food and Agriculture*, *97*(3), 882–888. https://doi.org/10.1002/jsfa.7810

Horne, D. S. (2020). Chapter 6—Casein micelle structure and stability. In M. Boland & H. Singh (Eds.), *Milk Proteins (Third Edition)* (pp. 213–250). Academic Press. https://doi.org/10.1016/B978-0-12-815251-5.00006-2

Hosseini, P., Hojjatoleslamy, M., & Molavi, H. (2023). Investigation of the mixing ratio of quince seed gum, potato starch and gellan gum on the properties of the resulting film by Mixture Design. *International Journal of Biological Macromolecules*, *237*, 123869. https://doi.org/10.1016/j.ijbiomac.2023.123869

Huamaní-Meléndez, V. J., Mauro, M. A., & Darros-Barbosa, R. (2021). Physicochemical and rheological properties of aqueous Tara gum solutions. *Food Hydrocolloids*, *111*, 106195. https://doi.org/10.1016/j.foodhyd.2020.106195

Huang, S., Vignolles, M.-L., Chen, X. D., Le Loir, Y., Jan, G., Schuck, P., & Jeantet, R. (2017).

Spray drying of probiotics and other food-grade bacteria: A review. *Trends in Food Science & Technology*, *63*, 1–17. https://doi.org/10.1016/j.tifs.2017.02.007

Huppertz, T., & Chia, L. W. (2021). Milk protein coagulation under gastric conditions: A review. *International Dairy Journal*, *113*, 104882. https://doi.org/10.1016/j.idairyj.2020.104882

Hussain, R., Gaiani, C., Jeandel, C., Ghanbaja, J., & Scher, J. (2012). Combined effect of heat treatment and ionic strength on the functionality of whey proteins. *Journal of Dairy Science*, *95*(11), 6260–6273. https://doi.org/10.3168/jds.2012-5416

Iglesias, H. A., & Chirife, J. (1982). INTRODUCTION. In *Handbook of Food Isotherms: Water Sorption Parameters for Food and Food Components* (pp. 1–7). Elsevier. https://doi.org/10.1016/B978-0-12-370380-4.50006-2

Iravani, S., Korbekandi, H., & Mirmohammadi, S. V. (2015). Technology and potential applications of probiotic encapsulation in fermented milk products. *Journal of Food Science and Technology*, *52*(8), 4679–4696. https://doi.org/10.1007/s13197-014-1516-2

Isolauri, E., Arvola, T., SÜtas, Y., Moilanen, E., & Salminen, S. (2000). Probiotics in the management of atopic eczema. *Clinical & Experimental Allergy*, *30*(11), 1605–1610. https://doi.org/10.1046/j.1365-2222.2000.00943.x

Issahaku, I., Tetteh, I. K., & Tetteh, A. Y. (2023). Chitosan and chitosan derivatives: Recent advancements in production and applications in environmental remediation. *Environmental Advances*, *11*, 100351. https://doi.org/10.1016/j.envadv.2023.100351

Jackson, M., & Mantsch, H. H. (1995). The use and misuse of FTIR spectroscopy in the determination of protein structure. *Critical Reviews in Biochemistry and Molecular Biology*, *30*(2), 95–120. https://doi.org/10.3109/10409239509085140

Jamir, K., Badithi, N., Venumadhav, K., & Seshagirirao, K. (2019). Characterization and comparative studies of galactomannans from Bauhinia vahlii, Delonix elata, and Peltophorum pterocarpum. *International Journal of Biological Macromolecules*, *134*, 498–506. https://doi.org/10.1016/j.ijbiomac.2019.05.080

Jayaprakash, P., Gaiani, C., Edorh, J.-M., Borges, F., Beaupeux, E., Maudhuit, A., & Desobry, S. (2023). Comparison of Electrostatic Spray Drying, Spray Drying, and Freeze Drying for Lacticaseibacillus rhamnosus GG Dehydration. *Foods*, *12*(16), 3117. https://doi.org/10.3390/foods12163117

Jayaprakash, P., Maudhuit, A., Gaiani, C., & Desobry, S. (2023). Encapsulation of bioactive compounds using competitive emerging techniques: Electrospraying, nano spray drying, and electrostatic spray drying. *Journal of Food Engineering*, *339*, 111260. https://doi.org/10.1016/j.jfoodeng.2022.111260

Jiang, Z., Li, M., McClements, D. J., Liu, X., & Liu, F. (2022). Recent advances in the design and fabrication of probiotic delivery systems to target intestinal inflammation. *Food Hydrocolloids*, *125*, 107438. https://doi.org/10.1016/j.foodhyd.2021.107438

Jouki, M., Mortazavi, S. A., Yazdi, F. T., & Koocheki, A. (2014). Characterization of antioxidant–antibacterial quince seed mucilage films containing thyme essential oil. *Carbohydrate Polymers*, *99*, 537–546. https://doi.org/10.1016/j.carbpol.2013.08.077

Jouki, M., Yazdi, F. T., Mortazavi, S. A., Koocheki, A., & Khazaei, N. (2014). Effect of quince seed mucilage edible films incorporated with oregano or thyme essential oil on shelf life extension of refrigerated rainbow trout fillets. *International Journal of Food Microbiology*, *174*, 88–97. https://doi.org/10.1016/j.ijfoodmicro.2014.01.001

Juhász, A. E., Greff, D., Teutsch, B., Gede, N., Hegyi, P., Horváth, E. M., Deák, P. Á., Nyirády, P., Ács, N., & Juhász, R. (2023). Galactomannans are the most effective soluble dietary fibers in type 2 diabetes: A systematic review and network meta-analysis. *The American Journal of Clinical Nutrition*, *117*(2), 266–277. https://doi.org/10.1016/j.ajcnut.2022.12.015

Jung, I., Schroeter, B., Plazzotta, S., De Berardinis, L., Smirnova, I., Gurikov, P., & Manzocco, L. (2023). Oleogels from mesoporous whey and potato protein based aerogel microparticles: Influence of microstructural properties on oleogelation ability. *Food Hydrocolloids*, *142*, 108758. https://doi.org/10.1016/j.foodhyd.2023.108758

Kačuráková, M., Capek, P., Sasinková, V., Wellner, N., & Ebringerová, A. (2000). FT-IR study of plant cell wall model compounds: Pectic polysaccharides and hemicelluloses. *Carbohydrate Polymers*, *43*(2), 195–203. https://doi.org/10.1016/S0144-8617(00)00151-X

Kaewmanee, T., Bagnasco, L., Benjakul, S., Lanteri, S., Morelli, C. F., Speranza, G., & Cosulich, M. E. (2014). Characterisation of mucilages extracted from seven Italian cultivars of flax. *Food Chemistry*, *148*, 60–69. https://doi.org/10.1016/j.foodchem.2013.10.022

Kang, J., Yin, S., Liu, J., Li, C., Wang, N., Sun, J., Li, W., He, J., Guo, Q., & Cui, S. W. (2022). Fermentation models of dietary fibre in vitro and in vivo—A review. *Food Hydrocolloids*, *131*, 107685. https://doi.org/10.1016/j.foodhyd.2022.107685

Kang, S., Wang, H., Xia, L., Chen, M., Li, L., Cheng, J., Li, X., & Jiang, S. (2020). Colorimetric film based on polyvinyl alcohol/okra mucilage polysaccharide incorporated with rose anthocyanins for shrimp freshness monitoring. *Carbohydrate Polymers*, *229*, 115402. https://doi.org/10.1016/j.carbpol.2019.115402

Kapoor, M. P., Sugita, M., Fukuzawa, Y., & Okubo, T. (2017). Impact of partially hydrolyzed guar gum (PHGG) on constipation prevention: A systematic review and meta-analysis. *Journal of Functional Foods*, *33*, 52–66. https://doi.org/10.1016/j.jff.2017.03.028

Kapoor, M. P., Yamaguchi, H., Ishida, H., Mizutani, Y., Timm, D., & Abe, A. (2023). The effects of prebiotic partially hydrolyzed guar gum on skin hydration: A randomized, open-label, parallel, controlled study in healthy humans. *Journal of Functional Foods*, *103*, 105494. https://doi.org/10.1016/j.jff.2023.105494

Karrar, E., Mahdi, A. A., Sheth, S., Mohamed Ahmed, I. A., Manzoor, M. F., Wei, W., & Wang, X. (2021). Effect of maltodextrin combination with gum arabic and whey protein isolate on the microencapsulation of gurum seed oil using a spray-drying method. *International Journal of Biological Macromolecules*, *171*, 208–216. https://doi.org/10.1016/j.ijbiomac.2020.12.045

Kassem, I. A. A., Joshua Ashaolu, T., Kamel, R., Elkasabgy, N. A., Afifi, S. M., & Farag, M. A. (2021). Mucilage as a functional food hydrocolloid: Ongoing and potential applications in prebiotics and nutraceuticals. *Food & Function*, *12*(11), 4738–4748. https://doi.org/10.1039/D1FO00438G

Kaur, M., Kaur, R., & Punia, S. (2018). Characterization of mucilages extracted from different flaxseed (Linum usitatissiumum L.) cultivars: A heteropolysaccharide with desirable functional and rheological properties. *International Journal of Biological Macromolecules*, *117*, 919–927. https://doi.org/10.1016/j.ijbiomac.2018.06.010

Kaushik, P., Dowling, K., Adhikari, R., Barrow, C. J., & Adhikari, B. (2017). Effect of extraction temperature on composition, structure and functional properties of flaxseed gum. *Food Chemistry*, *215*(Supplement C), 333–340. https://doi.org/10.1016/j.foodchem.2016.07.137

Kaushik, P., Dowling, K., Barrow, C. J., & Adhikari, B. (2015). Complex coacervation between flaxseed protein isolate and flaxseed gum. *Food Research International*, *72*, 91–97. https://doi.org/10.1016/j.foodres.2015.03.046

Kay, B. A., Trigatti, K., MacNeil, M. B., Klingel, S. L., Repin, N., Douglas Goff, H., Wright, A. J., & Duncan, A. M. (2017). Pudding products enriched with yellow mustard mucilage, fenugreek gum or flaxseed mucilage and matched for simulated intestinal viscosity significantly reduce postprandial peak glucose and insulin in adults at risk for type 2 diabetes. *Journal of Functional Foods*, *37*(Supplement C), 603–611. https://doi.org/10.1016/j.jff.2017.08.017

Kearney, S. M., & Gibbons, S. M. (2018). Designing synbiotics for improved human health. *Microbial Biotechnology*, *11*(1), 141–144. https://doi.org/10.1111/1751-7915.12885

Khin, M. NOE., Ahammed, S., & Zhong, F. (2021). Development of (5-(4,6-dichlorotriazinyl) aminofluorescein) DTAF-labelled polysaccharides for characterization of microstructure and phase distribution of composite hydrogel visualization of hydrogels using CLSM. *Food Bioscience*, *41*, 100909. https://doi.org/10.1016/j.fbio.2021.100909

Kiepś, J., & Dembczyński, R. (2022). Current Trends in the Production of Probiotic Formulations. *Foods*, *11*(15), 2330. https://doi.org/10.3390/foods11152330

Kinsella, J. E., Fox, P. F., & Rockland, L. B. (1986). Water sorption by proteins: Milk and whey proteins. *C R C Critical Reviews in Food Science and Nutrition*, *24*(2), 91–139. https://doi.org/10.1080/10408398609527434

Kleemann, C., Schuster, R., Rosenecker, E., Selmer, I., Smirnova, I., & Kulozik, U. (2020). In-vitro-digestion and swelling kinetics of whey protein, egg white protein and sodium caseinate aerogels. *Food Hydrocolloids*, *101*, 105534. https://doi.org/10.1016/j.foodhyd.2019.105534

Kleemann, C., Selmer, I., Smirnova, I., & Kulozik, U. (2018). Tailor made protein based aerogel particles from egg white protein, whey protein isolate and sodium caseinate: Influence of the preceding hydrogel characteristics. *Food Hydrocolloids*, *83*, 365–374. https://doi.org/10.1016/j.foodhyd.2018.05.021

Koh, W. Y., Lim, X. X., Tan, T.-C., Kobun, R., & Rasti, B. (2022). Encapsulated Probiotics: Potential Techniques and Coating Materials for Non-Dairy Food Applications. *Applied Sciences*, *12*(19), 10005. https://doi.org/10.3390/app121910005

Kohmura, M., Nio, N., Kubo, K., Minoshima, Y., Munekata, E., & Ariyoshi, Y. (1989). Inhibition of Angiotensin-converting Enzyme by Synthetic Peptides of Human β-Casein. *Agricultural and Biological Chemistry*, *53*(8), 2107–2114. https://doi.org/10.1080/00021369.1989.10869621

Kondjoyan, A., Daudin, J.-D., & Santé-Lhoutellier, V. (2015). Modelling of pepsin digestibility of myofibrillar proteins and of variations due to heating. *Food Chemistry*, *172*, 265–271. https://doi.org/10.1016/j.foodchem.2014.08.110

Kontogiorgos, V. (2019). Galactomannans (Guar, Locust Bean, Fenugreek, Tara). In *Encyclopedia of Food Chemistry* (pp. 109–113). Elsevier. https://doi.org/10.1016/B978-0-08-100596-5.21589-8

Kopf-Bolanz, K. A., Schwander, F., Gijs, M., Vergères, G., Portmann, R., & Egger, L. (2014). Impact of milk processing on the generation of peptides during digestion. *International Dairy Journal*, *35*(2), 130–138. https://doi.org/10.1016/j.idairyj.2013.10.012

Korus, J., Witczak, T., Ziobro, R., & Juszczak, L. (2015). Linseed (Linum usitatissimum L.) mucilage as a novel structure forming agent in gluten-free bread. *LWT - Food Science and Technology*, *62*(1, Part 1), 257–264. https://doi.org/10.1016/j.lwt.2015.01.040

Koupantsis, T., Pavlidou, E., & Paraskevopoulou, A. (2016). Glycerol and tannic acid as applied in the preparation of milk proteins – CMC complex coavervates for flavour encapsulation. *Food Hydrocolloids*, *57*, 62–71. https://doi.org/10.1016/j.foodhyd.2016.01.007

Koutina, G., Ray, C. A., Lametsch, R., & Ipsen, R. (2018). The effect of protein-to-alginate ratio on in vitro gastric digestion of nanoparticulated whey protein. *International Dairy Journal*, *77*, 10–18. https://doi.org/10.1016/j.idairyj.2017.09.001

Kuo, C.-C., Clark, S., Qin, H., & Shi, X. (2022). Development of a shelf-stable, gel-based delivery system for probiotics by encapsulation, 3D printing, and freeze-drying. *LWT*, *157*, 113075. https://doi.org/10.1016/j.lwt.2022.113075

Kutlu, G., Bozkurt, F., & Tornuk, F. (2020). Extraction of a novel water-soluble gum from nettle (Urtica dioica) seeds: Optimization and characterization. *International Journal of Biological Macromolecules*, *162*, 480–489. https://doi.org/10.1016/j.ijbiomac.2020.06.179

Labuza, T. P. (1975). Sorption Phenomena in Foods: Theoretical and Practical Aspects. In C. Rha (Ed.), *Theory, Determination and Control of Physical Properties of Food Materials* (pp. 197–219). Springer Netherlands. https://doi.org/10.1007/978-94-010-1731-2_11

Lacroix, I. M. E., & Li-Chan, E. C. Y. (2014). Isolation and characterization of peptides with dipeptidyl peptidase-IV inhibitory activity from pepsin-treated bovine whey proteins. *Peptides*, *54*, 39–48. https://doi.org/10.1016/j.peptides.2014.01.002

Lacroix, I. M. E., Meng, G., Cheung, I. W. Y., & Li-Chan, E. C. Y. (2016). Do whey protein-derived peptides have dual dipeptidyl-peptidase IV and angiotensin I-converting enzyme inhibitory activities? *Journal of Functional Foods*, *21*, 87–96. https://doi.org/10.1016/j.jff.2015.11.038

Lam, E. K. Y., Tai, E. K. K., Koo, M. W. L., Wong, H. P. S., Wu, W. K. K., Yu, L., So, W. H. L., Woo, P. C. Y., & Cho, C. H. (2007). Enhancement of gastric mucosal integrity by Lactobacillus rhamnosus GG. *Life Sciences*, *80*(23), 2128–2136. https://doi.org/10.1016/j.lfs.2007.03.018

Larsen, C. N., Nielsen, S., Kæstel, P., Brockmann, E., Bennedsen, M., Christensen, H. R., Eskesen, D. C., Jacobsen, B. L., & Michaelsen, K. F. (2006). Dose–response study of probiotic bacteria Bifidobacterium animalis subsp lactis BB-12 and Lactobacillus paracasei subsp paracasei CRL-341 in healthy young adults. *European Journal of Clinical Nutrition*, *60*(11), 1284–1293. https://doi.org/10.1038/sj.ejcn.1602450

Launay, B., Cuvelier, G., & Martinez-Reyes, S. (1997). Viscosity of locust bean, guar and xanthan gum solutions in the Newtonian domain: A critical examination of the log (ηsp)o-log c[η]o master curves. *Carbohydrate Polymers*, *34*(4), 385–395. https://doi.org/10.1016/S0144-8617(97)00104-5

Le Feunteun, S., Verkempinck, S., Floury, J., Janssen, A., Kondjoyan, A., Marze, S., Mirade, P.-S., Pluschke, A., Sicard, J., van Aken, G., & Grauwet, T. (2021). Mathematical modelling of food hydrolysis during in vitro digestion: From single nutrient to complex foods in static and dynamic conditions. *Trends in Food Science & Technology*, *116*, 870–883. https://doi.org/10.1016/j.tifs.2021.08.030

Lefèvre, T., Subirade, M., & Pézolet, M. (2005). Molecular Description of the Formation and Structure of Plasticized Globular Protein Films. *Biomacromolecules*, *6*(6), 3209–3219. https://doi.org/10.1021/bm050540u

Leser, T. D., Gottlieb, C. T., & Johansen, E. (2015). Bifidobacteria: Regulators of Intestinal Homeostasis. In *Probiotics and Prebiotics: Current Research and Future Trends* (pp. 43–68). Caister Academic Press. https://doi.org/10.21775/9781910190098.04

Li, J., Liu, M., Qin, G., Wu, X., Li, M., Sun, L., Dang, W., Zhang, S., Liang, Y., Zheng, X., Li, L., & Liu, C. (2023). Classification, gelation mechanism and applications of polysaccharide-based hydrocolloids in pasta products: A review. *International Journal of Biological Macromolecules*, *248*, 125956. https://doi.org/10.1016/j.ijbiomac.2023.125956

Lin, K.-Y., Daniel, J. R., & Whistler, R. L. (1994). Structure of chia seed polysaccharide exudate. *Carbohydrate Polymers*, *23*(1), 13–18. https://doi.org/10.1016/0144-8617(94)90085-X

Lira, M. M., Oliveira Filho, J. G. de, Sousa, T. L. de, Costa, N. M. da, Lemes, A. C., Fernandes, S. S., & Egea, M. B. (2023). Selected plants producing mucilage: Overview, composition, and their potential as functional ingredients in the development of plant-based foods. *Food Research International*, *169*, 112822. https://doi.org/10.1016/j.foodres.2023.112822

Listiohadi, Y., Hourigan, J. A., Sleigh, R. W., & Steele, R. J. (2009). Thermal analysis of amorphous lactose and α-lactose monohydrate. *Dairy Science and Technology*, *89*(1), 43–67. https://doi.org/10.1051/dst:2008027

Liu, J., Shen, J., Shim, Y. Y., & Reaney, M. J. T. (2016). Carboxymethyl derivatives of flaxseed (Linum usitatissimum L.) gum: Characterisation and solution rheology. *International Journal of Food Science & Technology*, *51*(2), 530–541. https://doi.org/10.1111/ijfs.12985

Liu, J., Shim, Y. Y., Shen, J., Wang, Y., Ghosh, S., & Reaney, M. J. T. (2016). Variation of composition and functional properties of gum from six Canadian flaxseed (Linum usitatissimum L.) cultivars. *International Journal of Food Science & Technology*, *51*(10), 2313–2326. https://doi.org/10.1111/ijfs.13200

Liu, J., Shim, Y. Y., Shen, J., Wang, Y., & Reaney, M. J. T. (2017). Whey protein isolate and flaxseed (Linum usitatissimum L.) gum electrostatic coacervates: Turbidity and rheology. *Food Hydrocolloids*, *64*, 18–27. https://doi.org/10.1016/j.foodhyd.2016.10.006

Liu, J., Shim, Y. Y., Tse, T. J., Wang, Y., & Reaney, M. J. T. (2018). Flaxseed gum a versatile natural hydrocolloid for food and non-food applications. *Trends in Food Science & Technology*, *75*, 146–157. https://doi.org/10.1016/j.tifs.2018.01.011

Liu, L., & Kong, F. (2019). Influence of nanocellulose on in vitro digestion of whey protein isolate. *Carbohydrate Polymers*, *210*, 399–411. https://doi.org/10.1016/j.carbpol.2019.01.071

Liu, W., & Foster, T. (2022). Phase separation of a milk protein and guar gum: The effect of guar gum molecular weight and oil addition on the phase diagram. *Food Hydrocolloids for Health*, *2*, 100048. https://doi.org/10.1016/j.fhfh.2021.100048

Liu, Y., Lei, F., He, L., Xu, W., & Jiang, J. (2020). Physicochemical characterization of galactomannans extracted from seeds of Gleditsia sinensis Lam and fenugreek. Comparison with commercial guar gum. *International Journal of Biological Macromolecules*, *158*, 1047–1054. https://doi.org/10.1016/j.ijbiomac.2020.04.208

Liu, Y., Xu, W., Lei, F., Li, P., & Jiang, J. (2019). Comparison and characterization of galactomannan at different developmental stages of Gleditsia sinensis Lam. *Carbohydrate Polymers*, *223*, 115127. https://doi.org/10.1016/j.carbpol.2019.115127

López, D. N., Galante, M., Alvarez, E. M., Risso, P. H., & Boeris, V. (2017). Physicochemical study of mixed systems composed by bovine caseinate and the galactomannan from Gleditsia amorphoides. *Carbohydrate Polymers*, *173*, 1–6. https://doi.org/10.1016/j.carbpol.2017.05.044

López-Franco, Y. L., Cervantes-Montaño, C. I., Martínez-Robinson, K. G., Lizardi-Mendoza, J., & Robles-Ozuna, L. E. (2013). Physicochemical characterization and functional properties of galactomannans from mesquite seeds (Prosopis spp.). *Food Hydrocolloids*, *30*(2), 656–660. https://doi.org/10.1016/j.foodhyd.2012.08.012

Lorieau, L., Halabi, A., Ligneul, A., Hazart, E., Dupont, D., & Floury, J. (2018). Impact of the dairy product structure and protein nature on the proteolysis and amino acid bioaccessiblity during in vitro digestion. *Food Hydrocolloids*, *82*, 399–411. https://doi.org/10.1016/j.foodhyd.2018.04.019

Lowell, S., & Shields, J. E. (1984). Adsorption isotherms. In S. Lowell & J. E. Shields, *Powder Surface Area and Porosity* (pp. 11–13). Springer Netherlands. https://doi.org/10.1007/978-94-009-5562-2_3

Lozinsky, V. I. (2018). Cryostructuring of Polymeric Systems. 50.† Cryogels and Cryotropic Gel-Formation: Terms and Definitions. *Gels*, *4*(3), 77. https://doi.org/10.3390/gels4030077

Lozinsky, V. I. (2020). Cryostructuring of Polymeric Systems. 55. Retrospective View on the More than 40 Years of Studies Performed in the A.N.Nesmeyanov Institute of Organoelement Compounds with Respect of the Cryostructuring Processes in Polymeric Systems. *Gels*, *6*(3), 29.

https://doi.org/10.3390/gels6030029

Lucey, J. A. (2002). Formation and Physical Properties of Milk Protein Gels. *Journal of Dairy Science*, *85*(2), 281–294. https://doi.org/10.3168/jds.S0022-0302(02)74078-2

Lucey, J. A. (2020). Chapter 16—Milk protein gels. In M. Boland & H. Singh (Eds.), *Milk Proteins (Third Edition)* (pp. 599–632). Academic Press. https://doi.org/10.1016/B978-0-12-815251-5.00016-5

Luo, J., Li, Y., Mai, Y., Gao, L., Ou, S., Wang, Y., Liu, L., & Peng, X. (2018). Flaxseed gum reduces body weight by regulating gut microbiota. *Journal of Functional Foods*, *47*, 136–142. https://doi.org/10.1016/j.jff.2018.05.042

Ma, J., Xu, C., Yu, H., Feng, Z., Yu, W., Gu, L., Liu, Z., Chen, L., Jiang, Z., & Hou, J. (2021). Electro-encapsulation of probiotics in gum Arabic-pullulan blend nanofibres using electrospinning technology. *Food Hydrocolloids*, *111*, 106381. https://doi.org/10.1016/j.foodhyd.2020.106381

Ma, R., Lin, Z., Wu, Y., Gao, Z., Hu, B., Xu, L., Fang, Y., & Nishinari, K. (2021). Modulating the in vitro gastric digestion of heat-induced beta-lactoglobulin aggregates: Incorporation with polysaccharide. *Food Chemistry*, *354*, 129506. https://doi.org/10.1016/j.foodchem.2021.129506

Macierzanka, A., Böttger, F., Lansonneur, L., Groizard, R., Jean, A.-S., Rigby, N. M., Cross, K., Wellner, N., & Mackie, A. R. (2012). The effect of gel structure on the kinetics of simulated gastrointestinal digestion of bovine β-lactoglobulin. *Food Chemistry*, *134*(4), 2156–2163. https://doi.org/10.1016/j.foodchem.2012.04.018

Maier, H., Anderson, M., Karl, C., Magnuson, K., & Whistler, R. L. (1993). Guar, locust bean, tara, and fenugreek gums. In *Industrial Gums* (pp. 181–226). Elsevier. https://doi.org/10.1016/B978-0-08-092654-4.50012-7

Manhivi, V. E., Venter, S., Amonsou, E. O., & Kudanga, T. (2018). Composition, thermal and rheological properties of polysaccharides from amadumbe (Colocasia esculenta) and cactus (Opuntia spp.). *Carbohydrate Polymers*, *195*, 163–169. https://doi.org/10.1016/j.carbpol.2018.04.062

Manojlović, V., Nedović, V. A., Kailasapathy, K., & Zuidam, N. J. (2010). Encapsulation of Probiotics for use in Food Products. In N. J. Zuidam & V. Nedovic (Eds.), *Encapsulation Technologies for Active Food Ingredients and Food Processing* (pp. 269–302). Springer New York. https://doi.org/10.1007/978-1-4419-1008-0_10

Manzocco, L., Mikkonen, K. S., & García-González, C. A. (2021). Aerogels as porous structures for food applications: Smart ingredients and novel packaging materials. *Food Structure*, *28*, 100188. https://doi.org/10.1016/j.foostr.2021.100188

Manzocco, L., Plazzotta, S., Powell, J., de Vries, A., Rousseau, D., & Calligaris, S. (2022). Structural characterisation and sorption capability of whey protein aerogels obtained by freeze-drying or supercritical drying. *Food Hydrocolloids*, *122*, 107117. https://doi.org/10.1016/j.foodhyd.2021.107117

Mao, L., Lu, Y., Cui, M., Miao, S., & Gao, Y. (2020). Design of gel structures in water and oil phases for improved delivery of bioactive food ingredients. *Critical Reviews in Food Science and Nutrition*, *60*(10), 1651–1666. https://doi.org/10.1080/10408398.2019.1587737

Marani, D., Hjelm, J., & Wandel, M. (2013). Use of Intrinsic Viscosity for Evaluation of Polymer-Solvent Affinity. *Ann. Trans. Nordic Rheol. Soc.*, *21*, 255–262. Scopus.

Markl, D., & Zeitler, J. A. (2017). A Review of Disintegration Mechanisms and Measurement Techniques. *Pharmaceutical Research*, *34*(5), 890–917. https://doi.org/10.1007/s11095-017-2129-z

Markoska, T., Daniloski, D., Vasiljevic, T., & Huppertz, T. (2021). Structural Changes of β-Casein Induced by Temperature and pH Analysed by Nuclear Magnetic Resonance, Fourier-Transform Infrared Spectroscopy, and Chemometrics. *Molecules*, *26*(24), 7650. https://doi.org/10.3390/molecules26247650

Markoska, T., Vasiljevic, T., & Huppertz, T. (2020). Unravelling Conformational Aspects of Milk Protein Structure—Contributions from Nuclear Magnetic Resonance Studies. *Foods*, *9*(8), 1128. https://doi.org/10.3390/foods9081128

Markussen, J. Ø., Madsen, F., Young, J. F., & Corredig, M. (2021). A semi dynamic in vitro digestion study of milk protein concentrate dispersions structured with different polysaccharides. *Current Research in Food Science*, *4*, 250–261. https://doi.org/10.1016/j.crfs.2021.03.012

Márquez, M. J., Romani, D., Díaz, S. B., & Brandán, S. A. (2018). Structural and vibrational characterization of anhydrous and dihydrated species of trehalose based on the FTIR and FTRaman spectra and DFT calculations. *Journal of King Saud University - Science*, *30*(2), 229–249. https://doi.org/10.1016/j.jksus.2017.01.009

Martín, R., Laval, L., Chain, F., Miquel, S., Natividad, J., Cherbuy, C., Sokol, H., Verdu, E. F., van

Hylckama Vlieg, J., Bermudez-Humaran, L. G., Smokvina, T., & Langella, P. (2016). Bifidobacterium animalis ssp. Lactis CNCM-I2494 Restores Gut Barrier Permeability in Chronically Low-Grade Inflamed Mice. *Frontiers in Microbiology*, *7*. https://www.frontiersin.org/articles/10.3389/fmicb.2016.00608

Martínez, J. P., Falomir, M. P., & Gozalbo, D. (2014). Chitin: A Structural Biopolysaccharide with Multiple Applications. In *Encyclopedia of Life Sciences*. John Wiley & Sons, Ltd. https://doi.org/10.1002/9780470015902.a0000694.pub3

Mary, P. R., & Kapoor, M. (2022). Co-culture fermentations suggest cross-feeding among Bacteroides ovatus DSMZ 1896, Lactiplantibacillus plantarum WCFS1 and Bifidobacterium adolescentis DSMZ 20083 for utilizing dietary galactomannans. *Food Research International*, *162*, 111942. https://doi.org/10.1016/j.foodres.2022.111942

Mat, D. J. L., Le Feunteun, S., Michon, C., & Souchon, I. (2016). In vitro digestion of foods using pH-stat and the INFOGEST protocol: Impact of matrix structure on digestion kinetics of macronutrients, proteins and lipids. *Food Research International*, *88*, 226–233. https://doi.org/10.1016/j.foodres.2015.12.002

Mathur, N. K. (2016). *Industrial Galactomannan Polysaccharides*. CRC Press. https://doi.org/10.1201/b11107

Mays, Z. J. S., Chappell, T. C., & Nair, N. U. (2020). Quantifying and Engineering Mucus Adhesion of Probiotics. *ACS Synthetic Biology*, *9*(2), 356–367. https://doi.org/10.1021/acssynbio.9b00356

Mazza, G., & LeMaguer, M. (1978). Water Sorption Properties of Yellow Globe Onion (Allium cepa L.). *Canadian Institute of Food Science and Technology Journal*, *11*(4), 189–193. https://doi.org/10.1016/S0315-5463(78)73269-4

McCleary, B. V., & Matheson, N. K. (1975). Galactomannan structure and β-mannanase and β-mannosidase activity in germinating legume seeds. *Phytochemistry*, *14*(5), 1187–1194. https://doi.org/10.1016/S0031-9422(00)98592-3

Mei, L., Zhang, D., Shao, H., Hao, Y., Zhang, T., Zheng, W., Ji, Y., Ling, P., Lu, Y., & Zhou, Q. (2022). Injectable and Self-Healing Probiotics-Loaded Hydrogel for Promoting Superbacteria-Infected Wound Healing. *ACS Applied Materials & Interfaces*, *14*(18), 20538–20550. https://doi.org/10.1021/acsami.1c23713

Mendonça, A. A., Pinto-Neto, W. de P., da Paixão, G. A., Santos, D. da S., De Morais, M. A., & De Souza, R. B. (2023). Journey of the Probiotic Bacteria: Survival of the Fittest. *Microorganisms*, *11*(1), Article 1. https://doi.org/10.3390/microorganisms11010095

Meurman, J. H., Antila, H., & Salminen, S. (1994). Recovery of Lactobacillus Strain GG (ATCC 53103) from Saliva of Healthy Volunteers after Consumption of Yoghurt Prepared with the Bacterium. *Microbial Ecology in Health and Disease*, *7*(6), 295–298. https://doi.org/10.3109/08910609409141368

Miao, M., Shi, Y., Li, Y., Jiang, Z., Liu, J., & Yang, S. (2021). Non-digestible galactomannan oligosaccharides from Cassia seed gum modulate microbiota composition and metabolites of human fecal inoculum. *Journal of Functional Foods*, *86*, 104705. https://doi.org/10.1016/j.jff.2021.104705

Miart, F., Fournet, F., Dubrulle, N., Petit, E., Demailly, H., Dupont, L., Zabijak, L., Marcelo, P., Boudaoud, A., Pineau, C., Guénin, S., Van Wuytswinkel, O., Mesnard, F., & Pageau, K. (2019). Cytological Approaches Combined With Chemical Analysis Reveals the Layered Nature of Flax Mucilage. *Frontiers in Plant Science*, *10*. https://www.frontiersin.org/articles/10.3389/fpls.2019.00684

Mielmann, A. (2013). The utilisation of lucerne (Medicago sativa): A review. *British Food Journal*, *115*(4), 590–600. https://doi.org/10.1108/00070701311317865

Minkiewicz, P., Iwaniak, A., & Darewicz, M. (2019). BIOPEP-UWM Database of Bioactive Peptides: Current Opportunities. *International Journal of Molecular Sciences*, *20*(23), Article 23. https://doi.org/10.3390/ijms20235978

Moayyedi, P., Ford, A. C., Talley, N. J., Cremonini, F., Foxx-Orenstein, A. E., Brandt, L. J., & Quigley, E. M. M. (2010). The efficacy of probiotics in the treatment of irritable bowel syndrome: A systematic review. *Gut*, *59*(3), 325–332. https://doi.org/10.1136/gut.2008.167270

Moczkowska, M., Karp, S., Niu, Y., & Kurek, M. A. (2019). Enzymatic, enzymatic-ultrasonic and alkaline extraction of soluble dietary fibre from flaxseed – A physicochemical approach. *Food Hydrocolloids*, *90*, 105–112. https://doi.org/10.1016/j.foodhyd.2018.12.018

Moreira, A. S. P., Nunes, F. M., Domingues, M. R. M., & Coimbra, M. A. (2015). Chapter 19—Galactomannans in Coffee. In V. R. Preedy (Ed.), *Coffee in Health and Disease Prevention* (pp. 173–182). Academic Press. https://doi.org/10.1016/B978-0-12-409517-5.00019-X

Morris, E. R., Cutler, A. N., Ross-Murphy, S. B., Rees, D. A., & Price, J. (1981). Concentration and

shear rate dependence of viscosity in random coil polysaccharide solutions. *Carbohydrate Polymers*, *1*(1), 5–21. https://doi.org/10.1016/0144-8617(81)90011-4

Mortensen, A., Aguilar, F., Crebelli, R., Domenico, A. D., Frutos, M. J., Galtier, P., Gott, D., Gundert-Remy, U., Lambré, C., Leblanc, J.-C., Lindtner, O., Moldeus, P., Mosesso, P., Oskarsson, A., Parent-Massin, D., Stankovic, I., Waalkens-Berendsen, I., Woutersen, R. A., Wright, M., … Dusemund, B. (2017). Re-evaluation of xanthan gum (E 415) as a food additive. *EFSA Journal*, *15*(7), e04909. https://doi.org/10.2903/j.efsa.2017.4909

Moser, S. A., & Savage, D. C. (2001). Bile Salt Hydrolase Activity and Resistance to Toxicity of Conjugated Bile Salts Are Unrelated Properties in Lactobacilli. *Applied and Environmental Microbiology*, *67*(8), 3476–3480. https://doi.org/10.1128/AEM.67.8.3476-3480.2001

Moubareck, C., Gavini, F., Vaugien, L., Butel, M. J., & Doucet-Populaire, F. (2005). Antimicrobial susceptibility of bifidobacteria. *Journal of Antimicrobial Chemotherapy*, *55*(1), 38–44. https://doi.org/10.1093/jac/dkh495

Mueed, A., Shibli, S., Korma, S. A., Madjirebaye, P., Esatbeyoglu, T., & Deng, Z. (2022). Flaxseed Bioactive Compounds: Chemical Composition, Functional Properties, Food Applications and Health Benefits-Related Gut Microbes. *Foods*, *11*(20), Article 20. https://doi.org/10.3390/foods11203307

Musampa, R. M., Alves, M. M., & Maia, J. M. (2007). Phase separation, rheology and microstructure of pea protein–kappa-carrageenan mixtures. *Food Hydrocolloids*, *21*(1), 92–99. https://doi.org/10.1016/j.foodhyd.2006.02.005

Muzzarelli, R. A. A., Greco, F., Busilacchi, A., Sollazzo, V., & Gigante, A. (2012). Chitosan, hyaluronan and chondroitin sulfate in tissue engineering for cartilage regeneration: A review. *Carbohydrate Polymers*, *89*(3), 723–739. https://doi.org/10.1016/j.carbpol.2012.04.057

Najafian, N., Aarabi, A., & Nezamzadeh-Ejhieh, A. (2022). Evaluation of physicomechanical properties of gluten-based film incorporated with Persian gum and Guar gum. *International Journal of Biological Macromolecules*, *223*, 1257–1267. https://doi.org/10.1016/j.ijbiomac.2022.11.056

Naji-Tabasi, S., Razavi, S. M. A., Mohebbi, M., & Malaekeh-Nikouei, B. (2016). New studies on basil (Ocimum bacilicum L.) seed gum: Part I – Fractionation, physicochemical and surface activity characterization. *Food Hydrocolloids*, *52*, 350–358. https://doi.org/10.1016/j.foodhyd.2015.07.011

Naran, R., Chen, G., & Carpita, N. C. (2008). Novel Rhamnogalacturonan I and Arabinoxylan Polysaccharides of Flax Seed Mucilage. *Plant Physiology*, *148*(1), 132–141. https://doi.org/10.1104/pp.108.123513

Nazir, S., & Wani, I. A. (2022). Development and characterization of an antimicrobial edible film from basil seed (Ocimum basilicum L.) mucilage and sodium alginate. *Biocatalysis and Agricultural Biotechnology*, *44*, 102450. https://doi.org/10.1016/j.bcab.2022.102450

Nermes, M., Kantele, J. M., Atosuo, T. J., Salminen, S., & Isolauri, E. (2011). Interaction of orally administered Lactobacillus rhamnosus GG with skin and gut microbiota and humoral immunity in infants with atopic dermatitis: Lactobacillus rhamnosus GG; interaction with human microbiota and immunity. *Clinical & Experimental Allergy*, *41*(3), 370–377. https://doi.org/10.1111/j.1365-2222.2010.03657.x

Nguyen, B. T., Nicolai, T., Chassenieux, C., Schmitt, C., & Bovetto, L. (2016). Heat-induced gelation of mixtures of whey protein isolate and sodium caseinate between pH 5.8 and pH 6.6. *Food Hydrocolloids*, *61*, 433–441. https://doi.org/10.1016/j.foodhyd.2016.05.030

Nielsen, S. D., Beverly, R. L., Qu, Y., & Dallas, D. C. (2017). Milk bioactive peptide database: A comprehensive database of milk protein-derived bioactive peptides and novel visualization. *Food Chemistry*, *232*, 673–682. https://doi.org/10.1016/j.foodchem.2017.04.056

Niknam, R., Mousavi, M., & Kiani, H. (2020). New Studies on the Galactomannan Extracted from Trigonella foenum-graecum (Fenugreek) Seed: Effect of Subsequent Use of Ultrasound and Microwave on the Physicochemical and Rheological Properties. *Food and Bioprocess Technology*, *13*(5), 882–900. https://doi.org/10.1007/s11947-020-02437-6

Nwokocha, L. M. (2021). Galactomannans. In *Handbook of Hydrocolloids* (pp. 273–293). Elsevier. https://doi.org/10.1016/B978-0-12-820104-6.00033-4

Nwokocha, L. M., Senan, C., Williams, P. A., & Yadav, M. P. (2017). Characterisation and solution properties of a galactomannan from Bauhinia monandra seeds. *International Journal of Biological Macromolecules*, *101*, 904–909. https://doi.org/10.1016/j.ijbiomac.2017.03.105

Nwokocha, L. M., Williams, P. A., & Yadav, M. P. (2018). Physicochemical characterisation of the galactomannan from Delonix regia seed. *Food Hydrocolloids*, *78*, 132–139. https://doi.org/10.1016/j.foodhyd.2017.02.016

O'Connell, A., Goycoolea, F. M., Gulotta, A., Holmqvist, P., Schuetz, P., & Mattsson, J. (2023). The structure and dynamics of locust bean gum in aqueous solution. *Food Hydrocolloids*, *138*, 108446. https://doi.org/10.1016/j.foodhyd.2022.108446

Okay, O. (Ed.). (2014). *Polymeric Cryogels: Macroporous Gels with Remarkable Properties* (Vol. 263). Springer International Publishing. https://doi.org/10.1007/978-3-319-05846-7

Oliveira, P. D., Michel, R. C., McBride, A. J. A., Moreira, A. S., Lomba, R. F. T., & Vendruscolo, C. T. (2013). Concentration Regimes of Biopolymers Xanthan, Tara, and Clairana, Comparing Dynamic Light Scattering and Distribution of Relaxation Time. *PLOS ONE*, *8*(5), e62713. https://doi.org/10.1371/journal.pone.0062713

Oluwatosin, S. O., Tai, S. L., & Fagan-Endres, M. A. (2022). Sucrose, maltodextrin and inulin efficacy as cryoprotectant, preservative and prebiotic – towards a freeze dried Lactobacillus plantarum topical probiotic. *Biotechnology Reports*, *33*, e00696. https://doi.org/10.1016/j.btre.2021.e00696

Oomah, B. D., Kenaschuk, E. O., Cui, W., & Mazza, G. (1995). Variation in the composition of water-soluble polysaccharides in flaxseed. *Journal of Agricultural and Food Chemistry*, *43*(6), 1484–1488. https://doi.org/10.1021/jf00054a013

Oriach, C. S., Robertson, R. C., Stanton, C., Cryan, J. F., & Dinan, T. G. (2016). Food for thought: The role of nutrition in the microbiota-gut–brain axis. *Clinical Nutrition Experimental*, *6*, 25–38. https://doi.org/10.1016/j.yclnex.2016.01.003

O'Sullivan, J., Arellano, M., Pichot, R., & Norton, I. (2014). The effect of ultrasound treatment on the structural, physical and emulsifying properties of dairy proteins. *Food Hydrocolloids*, *42*, 386–396. https://doi.org/10.1016/j.foodhyd.2014.05.011

Pajić, N., & Marković, T. (2016). Economic results in alfalfa seed production. *Ratarstvo i Povrtarstvo*, *53*(3), 111–115. https://doi.org/10.5937/ratpov53-10851

Pälchen, K., Bredie, W. L. P., Duijsens, D., Isaac Alfie Castillo, A., Hendrickx, M., Van Loey, A., Raben, A., & Grauwet, T. (2022). Effect of processing and microstructural properties of chickpea-flours on in vitro digestion and appetite sensations. *Food Research International*, *157*, 111245. https://doi.org/10.1016/j.foodres.2022.111245

Patmore, J. V., Goff, H. D., & Fernandes, S. (2003). Cryo-gelation of galactomannans in ice cream model systems. *Food Hydrocolloids*, *17*(2), 161–169. https://doi.org/10.1016/S0268-005X(02)00048-6

Pavli, F., Tassou, C., Nychas, G.-J. E., & Chorianopoulos, N. (2018). Probiotic Incorporation in Edible Films and Coatings: Bioactive Solution for Functional Foods. *International Journal of Molecular Sciences*, *19*(1), 150. https://doi.org/10.3390/ijms19010150

Pehkonen, K. s., Roos, Y. h., Miao, S., Ross, R. p., & Stanton, C. (2008). State transitions and physicochemical aspects of cryoprotection and stabilization in freeze-drying of Lactobacillus rhamnosus GG (LGG). *Journal of Applied Microbiology*, *104*(6), 1732–1743. https://doi.org/10.1111/j.1365-2672.2007.03719.x

Peram, M. R., Loveday, S. M., Ye, A., & Singh, H. (2013). In vitro gastric digestion of heat-induced aggregates of β-lactoglobulin. *Journal of Dairy Science*, *96*(1), 63–74. https://doi.org/10.3168/jds.2012-5896

Peredo, A. G., Beristain, C. I., Pascual, L. A., Azuara, E., & Jimenez, M. (2016). The effect of prebiotics on the viability of encapsulated probiotic bacteria. *LWT*, *73*, 191–196. https://doi.org/10.1016/j.lwt.2016.06.021

Perez-Riverol, Y., Bai, J., Bandla, C., García-Seisdedos, D., Hewapathirana, S., Kamatchinathan, S., Kundu, D. J., Prakash, A., Frericks-Zipper, A., Eisenacher, M., Walzer, M., Wang, S., Brazma, A., & Vizcaíno, J. A. (2022). The PRIDE database resources in 2022: A hub for mass spectrometry-based proteomics evidences. *Nucleic Acids Research*, *50*(D1), D543–D552. https://doi.org/10.1093/nar/gkab1038

Petitjean, M., & Isasi, J. R. (2022). Locust Bean Gum, a Vegetable Hydrocolloid with Industrial and Biopharmaceutical Applications. *Molecules*, *27*(23), Article 23. https://doi.org/10.3390/molecules27238265

Phosanam, A., Chandrapala, J., Huppertz, T., Adhikari, B., & Zisu, B. (2021). In vitro digestion of infant formula model systems: Influence of casein to whey protein ratio. *International Dairy Journal*, *117*, 105008. https://doi.org/10.1016/j.idairyj.2021.105008

Pi, X.-E., Fu, H., Yang, X.-X., Yu, Z.-C., Teng, W.-L., Zhang, Y., Ye, X.-W., Quan, H. H., Lu, L.-Z., & Liu, W. (2024). Bacterial, short-chain fatty acid and gas profiles of partially hydrolyzed guar gum in vitro fermentation by human fecal microbiota. *Food Chemistry*, *430*, 137006. https://doi.org/10.1016/j.foodchem.2023.137006

Plazzotta, S., Calligaris, S., & Manzocco, L. (2023). Feasibility of protein aerogel particles as food ingredient: The case of cocoa spreads. *Journal of Food Engineering*, *351*, 111522. https://doi.org/10.1016/j.jfoodeng.2023.111522

Pollard, M. A., Eder, B., Fischer, P., & Windhab, E. J. (2010). Characterization of galactomannans isolated from legume endosperms of Caesalpinioideae and Faboideae subfamilies by multidetection aqueous SEC. *Carbohydrate Polymers*, *79*(1), 70–84. https://doi.org/10.1016/j.carbpol.2009.07.028

Power, O., Fernández, A., Norris, R., Riera, F. A., & FitzGerald, R. J. (2014). Selective enrichment of bioactive properties during ultrafiltration of a tryptic digest of β-lactoglobulin. *Journal of Functional Foods*, *9*, 38–47. https://doi.org/10.1016/j.jff.2014.04.002

Prado, B. M., Kim, S., Özen, B. F., & Mauer, L. J. (2005). Differentiation of Carbohydrate Gums and Mixtures Using Fourier Transform Infrared Spectroscopy and Chemometrics. *Journal of Agricultural and Food Chemistry*, *53*(8), 2823–2829. https://doi.org/10.1021/jf0485537

Prajapati, V. D., Jani, G. K., Moradiya, N. G., Randeria, N. P., Nagar, B. J., Naikwadi, N. N., & Variya, B. C. (2013). Galactomannan: A versatile biodegradable seed polysaccharide. *International Journal of Biological Macromolecules*, *60*, 83–92. https://doi.org/10.1016/j.ijbiomac.2013.05.017

Pugnaloni, L. A., Matia-Merino, L., & Dickinson, E. (2005). Microstructure of acid-induced caseinate gels containing sucrose: Quantification from confocal microscopy and image analysis. *Colloids and Surfaces B: Biointerfaces*, *42*(3–4), 211–217. https://doi.org/10.1016/j.colsurfb.2005.03.002

Punia, S., & Dhull, S. B. (2019). Chia seed (Salvia hispanica L.) mucilage (a heteropolysaccharide): Functional, thermal, rheological behaviour and its utilization. *International Journal of Biological Macromolecules*, *140*, 1084–1090. https://doi.org/10.1016/j.ijbiomac.2019.08.205

Qi, X., Simsek, S., Ohm, J.-B., Chen, B., & Rao, J. (2020). Viability of Lactobacillus rhamnosus GG microencapsulated in alginate/chitosan hydrogel particles during storage and simulated gastrointestinal digestion: Role of chitosan molecular weight. *Soft Matter*, *16*(7), 1877–1887. https://doi.org/10.1039/C9SM02387A

Qian, K. Y., Cui, S. W., Wu, Y., & Goff, H. D. (2012). Flaxseed gum from flaxseed hulls: Extraction, fractionation, and characterization. *Food Hydrocolloids*, *28*(2), 275–283. https://doi.org/10.1016/j.foodhyd.2011.12.019

Qian, K.-Y., Cui, S. W., Nikiforuk, J., & Goff, H. D. (2012). Structural elucidation of rhamnogalacturonans from flaxseed hulls. *Carbohydrate Research*, *362*, 47–55. https://doi.org/10.1016/j.carres.2012.08.005

Quirós, A., Ramos, M., Muguerza, B., Delgado, M. A., Miguel, M., Aleixandre, A., & Recio, I. (2007). Identification of novel antihypertensive peptides in milk fermented with Enterococcus faecalis. *International Dairy Journal*, *17*(1), 33–41. https://doi.org/10.1016/j.idairyj.2005.12.011

Quodbach, J., & Kleinebudde, P. (2014). A New Apparatus for Real-Time Assessment of the Particle Size Distribution of Disintegrating Tablets. *Journal of Pharmaceutical Sciences*, *103*(11), 3657–3665. https://doi.org/10.1002/jps.24168

Raddatz, G. C., Poletto, G., Deus, C. de, Codevilla, C. F., Cichoski, A. J., Jacob-Lopes, E., Muller, E. I., Flores, E. M. M., Esmerino, E. A., & de Menezes, C. R. (2020). Use of prebiotic sources to increase probiotic viability in pectin microparticles obtained by emulsification/internal gelation followed by freeze-drying. *Food Research International*, *130*, 108902. https://doi.org/10.1016/j.foodres.2019.108902

Rahman, S. (Ed.). (2007). *Handbook of food preservation* (2nd ed). CRC Press.

Rao, M. A. (2014). *Rheology of Fluid, Semisolid, and Solid Foods: Principles and Applications* (3rd ed.). Springer US. https://doi.org/10.1007/978-1-4614-9230-6

Rao, M. A., Rizvi, S. S. H., Datta, A. K., & Ahmed, J. (2014). *Engineering Properties of Foods, Fourth Edition*. CRC Press.

Rashid, F., Ahmed, Z., Hussain, S., Huang, J.-Y., & Ahmad, A. (2019). Linum usitatissimum L. seeds: Flax gum extraction, physicochemical and functional characterization. *Carbohydrate Polymers*, *215*, 29–38. Scopus. https://doi.org/10.1016/j.carbpol.2019.03.054

Rauseo, A. M., Hink, T., Reske, K. A., Seiler, S. M., Bommarito, K. M., Fraser, V. J., Burnham, C.-A. D., Dubberke, E. R., & for the CDC Prevention Epicenter Program. (2022). A randomized controlled trial of Lactobacillus rhamnosus GG on antimicrobial-resistant organism colonization. *Infection Control & Hospital Epidemiology*, *43*(2), 167–173. https://doi.org/10.1017/ice.2021.94

Ray, S., Paynel, F., Morvan, C., Lerouge, P., Driouich, A., & Ray, B. (2013). Characterization of mucilage polysaccharides, arabinogalactanproteins and cell-wall hemicellulosic polysaccharides isolated from flax seed meal: A wealth of structural moieties. *Carbohydrate Polymers*, *93*(2), 651–660.

https://doi.org/10.1016/j.carbpol.2012.12.034

Razavi, S., Janfaza, S., Tasnim, N., Gibson, D. L., & Hoorfar, M. (2021). Microencapsulating polymers for probiotics delivery systems: Preparation, characterization, and applications. *Food Hydrocolloids*, *120*, 106882. https://doi.org/10.1016/j.foodhyd.2021.106882

Razavi, S. M. A., Alghooneh, A., & Behrouzian, F. (2018). Thermo-rheology and thermodynamic analysis of binary biopolymer blend: A case study on sage seed gum-xanthan gum blends. *Food Hydrocolloids*, *77*, 307–321. https://doi.org/10.1016/j.foodhyd.2017.10.007

Razmkhah, S., Razavi, S. M. A., & Mohammadifar, M. A. (2016). Purification of cress seed (Lepidium sativum) gum: A comprehensive rheological study. *Food Hydrocolloids*, *61*, 358–368. https://doi.org/10.1016/j.foodhyd.2016.05.035

Razmkhah, S., Razavi, S. M. A., Mohammadifar, M. A., Ale, M. T., & Gavlighi, H. A. (2016). Protein-free cress seed (Lepidium sativum) gum: Physicochemical characterization and rheological properties. *Carbohydrate Polymers*, *153*, 14–24. https://doi.org/10.1016/j.carbpol.2016.07.086

Reddi, S., Shanmugam, V. P., Tanedjeu, K. S., Kapila, S., & Kapila, R. (2018). Effect of buffalo casein-derived novel bioactive peptides on osteoblast differentiation. *European Journal of Nutrition*, *57*(2), 593–605. https://doi.org/10.1007/s00394-016-1346-2

Repin, N., Cui, S. W., & Goff, H. D. (2018). Rheological behavior of dietary fibre in simulated small intestinal conditions. *Food Hydrocolloids*, *76*(Supplement C), 216–225. https://doi.org/10.1016/j.foodhyd.2016.10.033

Reunanen, J., von Ossowski, I., Hendrickx, A. P. A., Palva, A., & de Vos, W. M. (2012). Characterization of the SpaCBA Pilus Fibers in the Probiotic Lactobacillus rhamnosus GG. *Applied and Environmental Microbiology*, *78*(7), 2337–2344. https://doi.org/10.1128/AEM.07047-11

Ribeiro, D. M., Planchon, S., Leclercq, C. C., Dentinho, M. T. P., Bessa, R. J. B., Santos-Silva, J., Paulos, K., Jerónimo, E., Renaut, J., & Almeida, A. M. (2020). The effects of improving low dietary protein utilization on the proteome of lamb tissues. *Journal of Proteomics*, *223*, 103798. https://doi.org/10.1016/j.jprot.2020.103798

Richardson, P. H., Willmer, J., & Foster, T. J. (1998). Dilute solution properties of guar and locust bean gum in sucrose solutions. *Food Hydrocolloids*, *12*(3), 339–348. https://doi.org/10.1016/S0268-005X(98)00025-3

Ricklefs-Johnson, K., Johnston, C. S., & Sweazea, K. L. (2017). Ground flaxseed increased nitric oxide levels in adults with type 2 diabetes: A randomized comparative effectiveness study of supplemental flaxseed and psyllium fiber. *Obesity Medicine*, *5*, 16–24. https://doi.org/10.1016/j.obmed.2017.01.002

Ries, D., Ye, A., Haisman, D., & Singh, H. (2010). Antioxidant properties of caseins and whey proteins in model oil-in-water emulsions. *International Dairy Journal*, *20*(2), 72–78. https://doi.org/10.1016/j.idairyj.2009.09.001

Rinaldi, L., Gauthier, S. F., Britten, M., & Turgeon, S. L. (2014). In vitro gastrointestinal digestion of liquid and semi-liquid dairy matrixes. *LWT - Food Science and Technology*, *57*(1), 99–105. https://doi.org/10.1016/j.lwt.2014.01.026

Rinaudo, M. (2008). Main properties and current applications of some polysaccharides as biomaterials. *Polymer International*, *57*(3), 397–430. https://doi.org/10.1002/pi.2378

Rincón, F., Muñoz, J., Ramírez, P., Galán, H., & Alfaro, M. C. (2014). Physicochemical and rheological characterization of Prosopis juliflora seed gum aqueous dispersions. *Food Hydrocolloids*, *35*, 348–357. https://doi.org/10.1016/j.foodhyd.2013.06.013

Robert, M.-C., Razaname, A., Mutter, M., & Juillerat, M. A. (2004). Identification of Angiotensin-I-Converting Enzyme Inhibitory Peptides Derived from Sodium Caseinate Hydrolysates Produced by *Lactobacillus helveticus* NCC 2765. *Journal of Agricultural and Food Chemistry*, *52*(23), 6923–6931. https://doi.org/10.1021/jf049510t

Rodrigues, F. J., Cedran, M. F., Bicas, J. L., & Sato, H. H. (2020). Encapsulated probiotic cells: Relevant techniques, natural sources as encapsulating materials and food applications – A narrative review. *Food Research International*, *137*, 109682. https://doi.org/10.1016/j.foodres.2020.109682

Rodrigues, F. J., Cedran, M. F., & Garcia, S. (2018). Influence of Linseed Mucilage Incorporated into an Alginate-Base Edible Coating Containing Probiotic Bacteria on Shelf-Life of Fresh-Cut Yacon (Smallanthus sonchifolius). *Food and Bioprocess Technology*, *11*(8), 1605–1614. https://doi.org/10.1007/s11947-018-2128-z

Rodriguez-Canto, W., Chel-Guerrero, L., Fernandez, V. V. A., & Aguilar-Vega, M. (2019). Delonix regia galactomannan hydrolysates: Rheological behavior and physicochemical characterization.

*Carbohydrate Polymers*, *206*, 573–582. https://doi.org/10.1016/j.carbpol.2018.11.028

Romero-Chapol, O. O., Varela-Pérez, A., Castillo-Olmos, A. G., García, H. S., Singh, J., García-Ramírez, P. J., Viveros-Contreras, R., Figueroa-Hernández, C. Y., & Cano-Sarmiento, C. (2022). Encapsulation of Lacticaseibacillus rhamnosus GG: Probiotic Survival, In Vitro Digestion and Viability in Apple Juice and Yogurt. *Applied Sciences*, *12*(4), 2141. https://doi.org/10.3390/app12042141

Roos, Y. H. (1995). CHAPTER 5—Food Components and Polymers. In Y. H. Roos (Ed.), *Phase Transitions in Foods* (pp. 109–156). Academic Press. https://doi.org/10.1016/B978-012595340-5/50005-5

Roulard, R., Petit, E., Mesnard, F., & Rhazi, L. (2016). Molecular investigations of flaxseed mucilage polysaccharides. *International Journal of Biological Macromolecules*, *86*, 840–847. https://doi.org/10.1016/j.ijbiomac.2016.01.093

Sadeghi, A., Ebrahimi, M., Shahryari, S., Kharazmi, M. S., & Jafari, S. M. (2022). Food applications of probiotic yeasts; focusing on their techno-functional, postbiotic and protective capabilities. *Trends in Food Science & Technology*, *128*, 278–295. https://doi.org/10.1016/j.tifs.2022.08.018

Safdar, B., Pang, Z., Liu, X., Jatoi, M. A., & Rashid, M. T. (2020). Optimising deproteinisation methods and effect of deproteinisation on structural and functional characteristics of flaxseed gum. *International Journal of Food Science & Technology*, *55*(6), 2481–2491. https://doi.org/10.1111/ijfs.14500

Saldanha, L. G. (2008). US Food and Drug Administration Regulations Governing Label Claims for Food Products, Including Probiotics. *Clinical Infectious Diseases*, *46*(s2), S119–S121. https://doi.org/10.1086/523328

Salelles, L., Floury, J., & Feunteun, S. L. (2021). Pepsin activity as a function of pH and digestion time on caseins and egg white proteins under static in vitro conditions. *Food & Function*, *12*(24), 12468–12478. https://doi.org/10.1039/D1FO02453A

Sanders, M. E., & Marco, M. L. (2010). Food Formats for Effective Delivery of Probiotics. *Annual Review of Food Science and Technology*, *1*(1), 65–85. https://doi.org/10.1146/annurev.food.080708.100743

Sandré, C., Gleizes, A., Forestier, F., Gorges-Kergot, R., Chilmonczyk, S., Léonil, J., Moreau, M.-C., & Labarre, C. (2001). A Peptide Derived from Bovine β-Casein Modulates Functional Properties of Bone Marrow-Derived Macrophages from Germfree and Human Flora-Associated Mice. *The Journal of Nutrition*, *131*(11), 2936–2942. https://doi.org/10.1093/jn/131.11.2936

Sangeethapriya, M., & Siddhuraju, P. (2014). Health related functional characteristics and antioxidant potential of mucilage (dietary fiber) from Zizyphus mauritiana fruits. *Food Science and Human Wellness*, *3*(2), 79–88. https://doi.org/10.1016/j.fshw.2014.05.003

Şanlier, N., Gökcen, B. B., & Sezgin, A. C. (2019). Health benefits of fermented foods. *Critical Reviews in Food Science and Nutrition*, *59*(3), 506–527. https://doi.org/10.1080/10408398.2017.1383355

Santivarangkna, C., Kulozik, U., & Foerst, P. (2006). Effect of carbohydrates on the survival of Lactobacillus helveticus during vacuum drying. *Letters in Applied Microbiology*, *42*(3), 271–276. https://doi.org/10.1111/j.1472-765X.2005.01835.x

Santivarangkna, C., Kulozik, U., & Foerst, P. (2008). Inactivation mechanisms of lactic acid starter cultures preserved by drying processes. *Journal of Applied Microbiology*, *105*(1), 1–13. https://doi.org/10.1111/j.1365-2672.2008.03744.x

Schell, D., & Beermann, C. (2014). Fluidized bed microencapsulation of Lactobacillus reuteri with sweet whey and shellac for improved acid resistance and in-vitro gastro-intestinal survival. *Food Research International*, *62*, 308–314. https://doi.org/10.1016/j.foodres.2014.03.016

Schiraldi, D. A. (2015). Green Polymer Aerogels. In *Green Polymer Chemistry: Biobased Materials and Biocatalysis* (Vol. 1192, pp. 471–482). American Chemical Society. https://doi.org/10.1021/bk-2015-1192.ch028

Schneider, W., & Gear, A. R. L. (2008). Significance of Glucose and Glycogen Metabolism for Platelet Function. In K. Elliott & J. Knight (Eds.), *Novartis Foundation Symposia* (pp. 225–238). John Wiley & Sons, Ltd. https://doi.org/10.1002/9780470720172.ch11

Schorsch, C., Carrie, H., & Norton, I. T. (2000). Cross-linking casein micelles by a microbial transglutaminase: In#uence of cross-links in acid-induced gelation. *International Dairy Journal*, 11.

Schorsch, C., Jones, M. G., & Norton, I. T. (1999). Thermodynamic incompatibility and microstructure of milk protein/locust bean gum/sucrose systems. *Food Hydrocolloids*, *13*(2), 89–99. https://doi.org/10.1016/S0268-005X(98)00074-5

Schorsch, C., Jones, M. G., & Norton, I. T. (2000). Phase behaviour of pure micellar casein/κ-

carrageenan systems in milk salt ultrafiltrate. *Food Hydrocolloids*, *14*(4), 347–358. https://doi.org/10.1016/S0268-005X(00)00011-4

Schuck, P., Blanchard, E., Dolivet, A., Méjean, S., Onillon, E., & Jeantet, R. (2005). Water activity and glass transition in dairy ingredients. *Le Lait*, *85*(4–5), 295–304. https://doi.org/10.1051/lait:2005020

Sciarini, L. S., Maldonado, F., Ribotta, P. D., Pérez, G. T., & León, A. E. (2009). Chemical composition and functional properties of Gleditsia triacanthos gum. *Food Hydrocolloids*, *23*(2), 306–313. https://doi.org/10.1016/j.foodhyd.2008.02.011

Sebastián-Nicolas, J. L., Contreras-López, E., Ramírez-Godínez, J., Cruz-Guerrero, A. E., Rodríguez-Serrano, G. M., Añorve-Morga, J., Jaimez-Ordaz, J., Castañeda-Ovando, A., Pérez-Escalante, E., Ayala-Niño, A., & González-Olivares, L. G. (2021). Milk Fermentation by Lacticaseibacillus rhamnosus GG and Streptococcus thermophilus SY-102: Proteolytic Profile and ACE-Inhibitory Activity. *Fermentation*, *7*(4), 215. https://doi.org/10.3390/fermentation7040215

Segers, M. E., & Lebeer, S. (2014). Towards a better understanding of Lactobacillus rhamnosus GG - host interactions. *Microbial Cell Factories*, *13*(1), S7. https://doi.org/10.1186/1475-2859-13-S1-S7

Seifert, A., Kashi, Y., & Livney, Y. D. (2019). Delivery to the gut microbiota: A rapidly proliferating research field. *Advances in Colloid and Interface Science*, *274*, 102038. https://doi.org/10.1016/j.cis.2019.102038

sekhavatizadeh, S. S., Pourakbar, N., Ganje, M., Shekarfroush, S. S., & Hosseinzadeh, S. (2023). Physicochemical and sensory properties of probiotic yogurt containing Lactobacillus plantarum ATCC 10241 microencapsulated with okra (Abelmoschus esculentus) mucilage and sodium alginate. *Bioactive Carbohydrates and Dietary Fibre*, *30*, 100364. https://doi.org/10.1016/j.bcdf.2023.100364

Selmer, I., Karnetzke, J., Kleemann, C., Lehtonen, M., Mikkonen, K. S., Kulozik, U., & Smirnova, I. (2019). Encapsulation of fish oil in protein aerogel micro-particles. *Journal of Food Engineering*, *260*, 1–11. https://doi.org/10.1016/j.jfoodeng.2019.04.016

Selmer, I., Kleemann, C., Kulozik, U., Heinrich, S., & Smirnova, I. (2015). Development of egg white protein aerogels as new matrix material for microencapsulation in food. *The Journal of Supercritical Fluids*, *106*, 42–49. https://doi.org/10.1016/j.supflu.2015.05.023

Selvasekaran, P., & Chidambaram, R. (2021). Food-grade aerogels obtained from polysaccharides, proteins, and seed mucilages: Role as a carrier matrix of functional food ingredients. *Trends in Food Science & Technology*, *112*, 455–470. https://doi.org/10.1016/j.tifs.2021.04.021

Semwal, A., Ambatipudi, K., & Navani, N. K. (2022). Development and characterization of sodium caseinate based probiotic edible film with chia mucilage as a protectant for the safe delivery of probiotics in functional bakery. *Food Hydrocolloids for Health*, *2*, 100065. https://doi.org/10.1016/j.fhfh.2022.100065

Semyonov, D., Ramon, O., Kaplun, Z., Levin-Brener, L., Gurevich, N., & Shimoni, E. (2010). Microencapsulation of Lactobacillus paracasei by spray freeze drying. *Food Research International*, *43*(1), 193–202. https://doi.org/10.1016/j.foodres.2009.09.028

Sengupta, A., & Datta, P. (2021). 2—Chemical modifications of polysaccharides. In K. Pal, I. Banerjee, P. Sarkar, A. Bit, D. Kim, A. Anis, & S. Maji (Eds.), *Food, Medical, and Environmental Applications of Polysaccharides* (pp. 47–77). Elsevier. https://doi.org/10.1016/B978-0-12-819239-9.00008-7

Shah, A., Gani, A., Ahmad, M., Ashwar, B. A., & Masoodi, F. A. (2016). β-Glucan as an encapsulating agent: Effect on probiotic survival in simulated gastrointestinal tract. *International Journal of Biological Macromolecules*, *82*, 217–222. https://doi.org/10.1016/j.ijbiomac.2015.11.017

Shah, B. R., Li, B., Al Sabbah, H., Xu, W., & Mráz, J. (2020). Effects of prebiotic dietary fibers and probiotics on human health: With special focus on recent advancement in their encapsulated formulations. *Trends in Food Science & Technology*, *102*, 178–192. https://doi.org/10.1016/j.tifs.2020.06.010

Shao, H., Zhang, H., Tian, Y., Song, Z., Lai, P. F. H., & Ai, L. (2019). Composition and Rheological Properties of Polysaccharide Extracted from Tamarind (Tamarindus indica L.) Seed. *Molecules*, *24*(7), 1218. https://doi.org/10.3390/molecules24071218

Shiekh, P. A., Andrabi, S. M., Singh, A., Majumder, S., & Kumar, A. (2021). Designing cryogels through cryostructuring of polymeric matrices for biomedical applications. *European Polymer Journal*, *144*, 110234. https://doi.org/10.1016/j.eurpolymj.2020.110234

Shim, Y. Y., Gui, B., Wang, Y., & Reaney, M. J. T. (2015). Flaxseed (Linum usitatissimum L.) oil processing and selected products. *Trends in Food Science & Technology*, *43*(2), 162–177. https://doi.org/10.1016/j.tifs.2015.03.001

Shrestha, A. K., Howes, T., Adhikari, B. P., Wood, B. J., & Bhandari, B. R. (2007). Effect of protein concentration on the surface composition, water sorption and glass transition temperature of spray-dried skim milk powders. *Food Chemistry*, *104*(4), 1436–1444. https://doi.org/10.1016/j.foodchem.2007.02.015

Shruthi, B., Deepa, N., Somashekaraiah, R., Adithi, G., Divyashree, S., & Sreenivasa, M. Y. (2022). Exploring biotechnological and functional characteristics of probiotic yeasts: A review. *Biotechnology Reports*, *34*, e00716. https://doi.org/10.1016/j.btre.2022.e00716

Silva, M., Jacobus, N. V., Deneke, C., & Gorbach, S. L. (1987). Antimicrobial substance from a human Lactobacillus strain. *Antimicrobial Agents and Chemotherapy*, *31*(8), 1231–1233. https://doi.org/10.1128/AAC.31.8.1231

Silveira, S. T., Martínez-Maqueda, D., Recio, I., & Hernández-Ledesma, B. (2013). Dipeptidyl peptidase-IV inhibitory peptides generated by tryptic hydrolysis of a whey protein concentrate rich in β-lactoglobulin. *Food Chemistry*, *141*(2), 1072–1077. https://doi.org/10.1016/j.foodchem.2013.03.056

Singh, R. S., Kaur, N., & Kennedy, J. F. (2019). Pullulan production from agro-industrial waste and its applications in food industry: A review. *Carbohydrate Polymers*, *217*, 46–57. https://doi.org/10.1016/j.carbpol.2019.04.050

Sittikijyothin, W., Sampaio, P., & Gonçalves, M. P. (2010). Microstructure and rheology of β-lactoglobulin–galactomannan aqueous mixtures. *Food Hydrocolloids*, *24*(8), 726–734. https://doi.org/10.1016/j.foodhyd.2010.03.014

Sittikijyothin, W., Torres, D., & Gonçalves, M. P. (2005). Modelling the rheological behaviour of galactomannan aqueous solutions. *Carbohydrate Polymers*, *59*(3), 339–350. https://doi.org/10.1016/j.carbpol.2004.10.005

Sivamaruthi, B. S., Kesika, P., & Chaiyasut, C. (2020). The Role of Probiotics in Colorectal Cancer Management. *Evidence-Based Complementary and Alternative Medicine*, *2020*, e3535982. https://doi.org/10.1155/2020/3535982

Sohail, A., Turner, M. S., Coombes, A., Bostrom, T., & Bhandari, B. (2011). Survivability of probiotics encapsulated in alginate gel microbeads using a novel impinging aerosols method. *International Journal of Food Microbiology*, *145*(1), 162–168. https://doi.org/10.1016/j.ijfoodmicro.2010.12.007

Solanki, H. K., & Shah, D. A. (2016). Formulation Optimization and Evaluation of Probiotic *Lactobacillus sporogenes*-Loaded Sodium Alginate with Carboxymethyl Cellulose Mucoadhesive Beads Using Design Expert Software. *Journal of Food Processing*, *2016*, e6041671. https://doi.org/10.1155/2016/6041671

Soltanahmadi, S., Murray, B. S., & Sarkar, A. (2022). Comparison of oral tribological performance of proteinaceous microgel systems with protein-polysaccharide combinations. *Food Hydrocolloids*, *129*, 107660. https://doi.org/10.1016/j.foodhyd.2022.107660

*Soluble Linseed Gum Powder*. (2021, March 20). https://gumstabilizer.com/products/flaxseed-gum/

Soukoulis, C., Behboudi-Jobbehdar, S., Macnaughtan, W., Parmenter, C., & Fisk, I. D. (2017). Stability of Lactobacillus rhamnosus GG incorporated in edible films: Impact of anionic biopolymers and whey protein concentrate. *Food Hydrocolloids*, *70*, 345–355. https://doi.org/10.1016/j.foodhyd.2017.04.014

Soukoulis, C., Behboudi-Jobbehdar, S., Yonekura, L., Parmenter, C., & Fisk, I. (2014). Impact of Milk Protein Type on the Viability and Storage Stability of Microencapsulated Lactobacillus acidophilus NCIMB 701748 Using Spray Drying. *Food and Bioprocess Technology*, *7*(5), 1255–1268. https://doi.org/10.1007/s11947-013-1120-x

Soukoulis, C., Cambier, S., Serchi, T., Tsevdou, M., Gaiani, C., Ferrer, P., Taoukis, P. S., & Hoffmann, L. (2019). Rheological and structural characterisation of whey protein acid gels co-structured with chia (Salvia hispanica L.) or flax seed (Linum usitatissimum L.) mucilage. *Food Hydrocolloids*, *89*, 542–553. https://doi.org/10.1016/j.foodhyd.2018.11.002

Soukoulis, C., Gaiani, C., & Hoffmann, L. (2018). Plant seed mucilage as emerging biopolymer in food industry applications. *Current Opinion in Food Science*, *22*, 28–42. https://doi.org/10.1016/j.cofs.2018.01.004

Soukoulis, C., Panagiotidis, P., Koureli, R., & Tzia, C. (2007). Industrial Yogurt Manufacture: Monitoring of Fermentation Process and Improvement of Final Product Quality. *Journal of Dairy Science*, *90*(6), 2641–2654. https://doi.org/10.3168/jds.2006-802

Soukoulis, C., Singh, P., Macnaughtan, W., Parmenter, C., & Fisk, I. D. (2016). Compositional and physicochemical factors governing the viability of Lactobacillus rhamnosus GG embedded in starch-protein based edible films. *Food Hydrocolloids*, *52*, 876–887.

https://doi.org/10.1016/j.foodhyd.2015.08.025

Soukoulis, C., Yonekura, L., Gan, H.-H., Behboudi-Jobbehdar, S., Parmenter, C., & Fisk, I. (2014). Probiotic edible films as a new strategy for developing functional bakery products: The case of pan bread. *Food Hydrocolloids*, *39*, 231–242. https://doi.org/10.1016/j.foodhyd.2014.01.023

Ström, A., Schuster, E., & Goh, S. M. (2014). Rheological characterization of acid pectin samples in the absence and presence of monovalent ions. *Carbohydrate Polymers*, *113*, 336–343. https://doi.org/10.1016/j.carbpol.2014.06.090

Stummer, S., Toegel, S., Rabenreither, M.-C., Unger, F. M., Wirth, M., Viernstein, H., & Salar-Behzadi, S. (2012). Fluidized-bed drying as a feasible method for dehydration of Enterococcus faecium M74. *Journal of Food Engineering*, *111*(1), 156–165. https://doi.org/10.1016/j.jfoodeng.2012.01.005

Sturm, A. (1999). Invertases. Primary Structures, Functions, and Roles in Plant Development and Sucrose Partitioning. *Plant Physiology*, *121*(1), 1–8. https://doi.org/10.1104/pp.121.1.1

Sugisaki, M., Suga, H., & Seki, S. (1968). Calorimetric Study of the Glassy State. IV. Heat Capacities of Glassy Water and Cubic Ice. *Bulletin of the Chemical Society of Japan*, *41*(11), 2591–2599. https://doi.org/10.1246/bcsj.41.2591

Sun, H., Zhang, M., Liu, Y., Wang, Y., Chen, Y., Guan, W., Li, X., & Wang, Y. (2021). Improved viability of Lactobacillus Plantarum embedded in whey protein concentrate/pullulan/trehalose hydrogel during freeze drying. *Carbohydrate Polymers*, 117843. https://doi.org/10.1016/j.carbpol.2021.117843

Świątecka, D., Małgorzata, I., Aleksander, Ś., Henryk, K., & Elżbieta, K. (2010). The impact of glycated pea proteins on bacterial adhesion. *Food Research International*, *43*(6), 1566–1576. https://doi.org/10.1016/j.foodres.2010.03.003

Szajewska, H., Skórka, A., Ruszczyński, M., & Gieruszczak-Białek, D. (2007). Meta-analysis: Lactobacillus GG for treating acute diarrhoea in children. *Alimentary Pharmacology & Therapeutics*, *25*(8), 871–881. https://doi.org/10.1111/j.1365-2036.2007.03282.x

Talón, E., Lampi, A.-M., Vargas, M., Chiralt, A., Jouppila, K., & González-Martínez, C. (2019). Encapsulation of eugenol by spray-drying using whey protein isolate or lecithin: Release kinetics, antioxidant and antimicrobial properties. *Food Chemistry*, *295*, 588–598. https://doi.org/10.1016/j.foodchem.2019.05.115

Tanaka, H. (2000). Viscoelastic phase separation. *Journal of Physics: Condensed Matter*, *12*(15), R207. https://doi.org/10.1088/0953-8984/12/15/201

Tanaka, H., Doesburg, K., Iwasaki, T., & Mierau, I. (1999). Screening of Lactic Acid Bacteria for Bile Salt Hydrolase Activity. *Journal of Dairy Science*, *82*(12), 2530–2535. https://doi.org/10.3168/jds.S0022-0302(99)75506-2

Tantiwatcharothai, S., & Prachayawarakorn, J. (2020). Property improvement of antibacterial wound dressing from basil seed (O. basilicum L.) mucilage- ZnO nanocomposite by borax crosslinking. *Carbohydrate Polymers*, *227*, 115360. https://doi.org/10.1016/j.carbpol.2019.115360

Tauzin, J., Miclo, L., & Gaillard, J.-L. (2002). Angiotensin-I-converting enzyme inhibitory peptides from tryptic hydrolysate of bovine αS2-casein. *FEBS Letters*, *531*(2), 369–374. https://doi.org/10.1016/S0014-5793(02)03576-7

Tavares, T. G., & Xavier Malcata, F. (2012). The Portuguese Paradox: Why do some inhabitants of Portugal appear to live so long when their diet is based on whey cheese? *Food Chemistry*, *131*(3), 727–729. https://doi.org/10.1016/j.foodchem.2011.09.052

Thanzami, K., Malsawmtluangi, C., Lalhlenmawia, H., Seelan, T. V., Palanisamy, S., Kandasamy, R., & Pachuau, L. (2015). Characterization and in vitro antioxidant activity of Albizia stipulata Boiv. Gum exudates. *International Journal of Biological Macromolecules*, *80*, 231–239. https://doi.org/10.1016/j.ijbiomac.2015.06.043

Thévenot, J., Cauty, C., Legland, D., Dupont, D., & Floury, J. (2017). Pepsin diffusion in dairy gels depends on casein concentration and microstructure. *Food Chemistry*, *223*, 54–61. https://doi.org/10.1016/j.foodchem.2016.12.014

Torres-Fuentes, C., Schellekens, H., Dinan, T. G., & Cryan, J. F. (2017). The microbiota–gut–brain axis in obesity. *The Lancet Gastroenterology & Hepatology*, *2*(10), 747–756. https://doi.org/10.1016/S2468-1253(17)30147-4

Tosif, M. M., Najda, A., Bains, A., Kaushik, R., Dhull, S. B., Chawla, P., & Walasek-Janusz, M. (2021). A Comprehensive Review on Plant-Derived Mucilage: Characterization, Functional Properties, Applications, and Its Utilization for Nanocarrier Fabrication. *Polymers*, *13*(7), Article 7. https://doi.org/10.3390/polym13071066

Tripathi, M. K., & Giri, S. K. (2014). Probiotic functional foods: Survival of probiotics during processing and storage. *Journal of Functional Foods*, *9*, 225–241. https://doi.org/10.1016/j.jff.2014.04.030

Tripathi, P., Beaussart, A., Alsteens, D., Dupres, V., Claes, I., von Ossowski, I., de Vos, W. M., Palva, A., Lebeer, S., Vanderleyden, J., & Dufrêne, Y. F. (2013). Adhesion and nanomechanics of pili from the probiotic Lactobacillus rhamnosus GG. *ACS Nano*, *7*(4), 3685–3697. https://doi.org/10.1021/nn400705u

Tu, M., Liu, H., Zhang, R., Chen, H., Mao, F., Cheng, S., Lu, W., & Du, M. (2018). Analysis and Evaluation of the Inhibitory Mechanism of a Novel Angiotensin-I-Converting Enzyme Inhibitory Peptide Derived from Casein Hydrolysate. *Journal of Agricultural and Food Chemistry*, *66*(16), 4139–4144. https://doi.org/10.1021/acs.jafc.8b00732

Tudu, M., & Samanta, A. (2023). Natural polysaccharides: Chemical properties and application in pharmaceutical formulations. *European Polymer Journal*, *184*, 111801. https://doi.org/10.1016/j.eurpolymj.2022.111801

Turgeon, S. L., Beaulieu, M., Schmitt, C., & Sanchez, C. (2003). Protein–polysaccharide interactions: Phase-ordering kinetics, thermodynamic and structural aspects. *Current Opinion in Colloid & Interface Science*, *8*(4), 401–414. https://doi.org/10.1016/S1359-0294(03)00093-1

Turnbaugh, P. J., Hamady, M., Yatsunenko, T., Cantarel, B. L., Duncan, A., Ley, R. E., Sogin, M. L., Jones, W. J., Roe, B. A., Affourtit, J. P., Egholm, M., Henrissat, B., Heath, A. C., Knight, R., & Gordon, J. I. (2009). A core gut microbiome in obese and lean twins. *Nature*, *457*(7228), 480–484. https://doi.org/10.1038/nature07540

Tytgat, H. L. P., Rasinkangas, P., Ritari, J., Reunanen, J., Aalvink, S., Lin, C., Palva, A., Douillard, F. P., & de Vos, W. M. (2021). Selection and characterization of a SpaCBA pilus-secreting food-grade derivative of Lacticaseibacillus rhamnosus GG. *Applied Microbiology and Biotechnology*, *105*(3), 1123–1131. https://doi.org/10.1007/s00253-020-11051-7

Ubeyitogullari, A., & Ciftci, O. N. (2020). Fabrication of bioaerogels from camelina seed mucilage for food applications. *Food Hydrocolloids*, *102*, 105597. https://doi.org/10.1016/j.foodhyd.2019.105597

Udechukwu, M. C., Dang, C., & Udenigwe, C. C. (2021). Identification of zinc-binding peptides in ADAM17-inhibiting whey protein hydrolysates using IMAC-Zn2+ coupled with shotgun peptidomics. *Food Production, Processing and Nutrition*, *3*(1), 5. https://doi.org/10.1186/s43014-020-00048-4

Valdes, A. M., Walter, J., Segal, E., & Spector, T. D. (2018). Role of the gut microbiota in nutrition and health. *BMJ*, k2179. https://doi.org/10.1136/bmj.k2179

van Boekel, M. (2002). On the use of the Weibull model to describe thermal inactivation of microbial vegetative cells. *International Journal of Food Microbiology*, *74*(1–2), 139–159. https://doi.org/10.1016/S0168-1605(01)00742-5

van Boekel, M. A. J. S. (2006). Formation of flavour compounds in the Maillard reaction. *Biotechnology Advances*, *24*(2), 230–233. https://doi.org/10.1016/j.biotechadv.2005.11.004

van den Berg, C., & Bruin, S. (1981). Water activity and its estimation in food systems: Theoretical aspects. In L. B. Rockland & G. F. Stewart (Eds.), *Water Activity: Influences on Food Quality* (pp. 1–61). Academic Press. https://doi.org/10.1016/B978-0-12-591350-8.50007-3

van Lieshout, G. A. A., Lambers, T. T., Bragt, M. C. E., & Hettinga, K. A. (2020). How processing may affect milk protein digestion and overall physiological outcomes: A systematic review. *Critical Reviews in Food Science and Nutrition*, *60*(14), 2422–2445. https://doi.org/10.1080/10408398.2019.1646703

Vargas, L. A., Olson, D. W., & Aryana, K. J. (2015). Whey protein isolate improves acid and bile tolerances of Streptococcus thermophilus ST-M5 and Lactobacillus delbrueckii ssp. Bulgaricus LB-12. *Journal of Dairy Science*, *98*(4), 2215–2221. https://doi.org/10.3168/jds.2014-8869

Vasiljevic, T. (2022). Probiotic Cultures in Cheese and Yogurt. In *Encyclopedia of Dairy Sciences* (pp. 472–488). Elsevier. https://doi.org/10.1016/B978-0-12-818766-1.00163-X

Venema, K., & Carmo, A. P. do. (2015). Probiotics and Prebiotics: Current Status and Future Trends. In *Probiotics and Prebiotics: Current Research and Future Trends* (pp. 3–12). Caister Academic Press. https://doi.org/10.21775/9781910190098.01

Venema, K., & Meijerink, M. (2015). Lactobacilli as Probiotics: Discovering New Functional Aspects and Target Sites. In *Probiotics and Prebiotics: Current Research and Future Trends* (pp. 29–42). Caister Academic Press. https://doi.org/10.21775/9781910190098.03

Venter, C., Meyer, R. W., Greenhawt, M., Pali-Schöll, I., Nwaru, B., Roduit, C., Untersmayr, E., Adel-Patient, K., Agache, I., Agostoni, C., Akdis, C. A., Feeney, M., Hoffmann-Sommergruber, K.,

Lunjani, N., Grimshaw, K., Reese, I., Smith, P. K., Sokolowska, M., Vassilopoulou, E., … O'Mahony, L. (2022). Role of dietary fiber in promoting immune health—An EAACI position paper. *Allergy*, *77*(11), 3185–3198. https://doi.org/10.1111/all.15430

Ventura, M., Margolles, A., Turroni, F., Zomer, A., de los Reyes-Gavilán, C. G., & van Sinderen, D. (2011). Stress Responses of Bifidobacteria. In E. Tsakalidou & K. Papadimitriou (Eds.), *Stress Responses of Lactic Acid Bacteria* (pp. 323–347). Springer US. https://doi.org/10.1007/978-0-387-92771-8_14

Vera C., N., Laguna, L., Zura, L., Puente, L., & Muñoz, L. A. (2019). Evaluation of the physical changes of different soluble fibres produced during an in vitro digestion. *Journal of Functional Foods*, *62*, 103518. https://doi.org/10.1016/j.jff.2019.103518

Verkempinck, S. H. E., Guevara-Zambrano, J. M., Infantes-Garcia, M. R., Naranjo, M. C., Soliva-Fortuny, R., Elez-Martínez, P., & Grauwet, T. (2022). Gastric and small intestinal lipid digestion kinetics as affected by the gradual addition of lipases and bile salts. *Food Bioscience*, 101595. https://doi.org/10.1016/j.fbio.2022.101595

Vesterlund, S., Salminen, K., & Salminen, S. (2012). Water activity in dry foods containing live probiotic bacteria should be carefully considered: A case study with Lactobacillus rhamnosus GG in flaxseed. *International Journal of Food Microbiology*, *157*(2), 319–321. https://doi.org/10.1016/j.ijfoodmicro.2012.05.016

Vivek, K., Mishra, S., Pradhan, R. C., Nagarajan, M., Kumar, P. K., Singh, S. S., Manvi, D., & Gowda, N. N. (2023). A comprehensive review on microencapsulation of probiotics: Technology, carriers and current trends. *Applied Food Research*, *3*(1), 100248. https://doi.org/10.1016/j.afres.2022.100248

Volkova, N., & Berillo, D. (2021). Water Uptake as a Crucial Factor on the Properties of Cryogels of Gelatine Cross-Linked by Dextran Dialdehyde. *Gels*, *7*(4), 159. https://doi.org/10.3390/gels7040159

Walstra, P., Walstra, P., Wouters, J. T. M., & Geurts, T. J. (2005). *Dairy Science and Technology* (2nd ed.). CRC Press. https://doi.org/10.1201/9781420028010

Wang, L., Liu, H.-M., Xie, A.-J., Wang, X.-D., Zhu, C.-Y., & Qin, G.-Y. (2018). Chinese quince (Chaenomeles sinensis) seed gum: Structural characterization. *Food Hydrocolloids*, *75*, 237–245. https://doi.org/10.1016/j.foodhyd.2017.08.001

Wang, S., Dong, X., Ma, H., Cui, Y., & Tong, J. (2014). Purification, characterisation and protective effects of polysaccharides from alfalfa on hepatocytes. *Carbohydrate Polymers*, *112*, 608–614. https://doi.org/10.1016/j.carbpol.2014.06.047

Wang, S., Dong, X., & Tong, J. (2013). Optimization of enzyme-assisted extraction of polysaccharides from alfalfa and its antioxidant activity. *International Journal of Biological Macromolecules*, *62*, 387–396. https://doi.org/10.1016/j.ijbiomac.2013.09.029

Wannerberger, K., Nylander, T., & Nyman, M. (1991). Rheological and Chemical Properties of Mucilage in Different Varieties from Linseed (Linum usitatissimum). *Acta Agriculturae Scandinavica*, *41*(3), 311–319. https://doi.org/10.1080/00015129109439914

Wei, Y., Lin, Y., Xie, R., Xu, Y., Yao, J., & Zhang, J. (2015). The flow behavior, thixotropy and dynamical viscoelasticity of fenugreek gum. *Journal of Food Engineering*, *166*, 21–28. https://doi.org/10.1016/j.jfoodeng.2015.05.015

Wendel, U. (2022). Assessing Viability and Stress Tolerance of Probiotics—A Review. *Frontiers in Microbiology*, *12*. https://www.frontiersin.org/articles/10.3389/fmicb.2021.818468

Western, T. L. (2012). The sticky tale of seed coat mucilages: Production, genetics, and role in seed germination and dispersal. *Seed Science Research*, *22*(1), 1–25. https://doi.org/10.1017/S0960258511000249

Western, T. L., Skinner, D. J., & Haughn, G. W. (2000). Differentiation of Mucilage Secretory Cells of the Arabidopsis Seed Coat. *Plant Physiology*, *122*(2), 345–356. https://doi.org/10.1104/pp.122.2.345

Whitney, S. E. C., Gothard, M. G. E., Mitchell, J. T., & Gidley, M. J. (1999). Roles of Cellulose and Xyloglucan in Determining the Mechanical Properties of Primary Plant Cell Walls1. *Plant Physiology*, *121*(2), 657–664. https://doi.org/10.1104/pp.121.2.657

Wientjes, R. H. W., Duits, M. H. G., Jongschaap, R. J. J., & Mellema, J. (2000). Linear Rheology of Guar Gum Solutions. *Macromolecules*, *33*(26), 9594–9605. https://doi.org/10.1021/ma001065p

Williams, P. A., & Phillips, G. O. (2009). 1—Introduction to food hydrocolloids. In G. O. Phillips & P. A. Williams (Eds.), *Handbook of Hydrocolloids (Second Edition)* (pp. 1–22). Woodhead Publishing. https://doi.org/10.1533/9781845695873.1

Williams, P. A., & Phillips, G. O. (2021). Introduction to food hydrocolloids. In *Handbook of Hydrocolloids* (pp. 3–26). Elsevier. https://doi.org/10.1016/B978-0-12-820104-6.00017-6

Wu, Y., Cui, W., Eskin, N. A. M., & Goff, H. D. (2009a). Fractionation and partial characterization of non-pectic polysaccharides from yellow mustard mucilage. *Food Hydrocolloids*, *23*(6), 1535–1541. https://doi.org/10.1016/j.foodhyd.2008.10.010

Wu, Y., Cui, W., Eskin, N. A. M., & Goff, H. D. (2009b). Rheological investigation of synergistic interactions between galactomannans and non-pectic polysaccharide fraction from water soluble yellow mustard mucilage. *Carbohydrate Polymers*, *78*(1), 112–116. https://doi.org/10.1016/j.carbpol.2009.03.024

Wu, Y., Eskin, N. A. M., Cui, W., & Pokharel, B. (2015). Emulsifying properties of water soluble yellow mustard mucilage: A comparative study with gum Arabic and citrus pectin. *Food Hydrocolloids*, *47*, 191–196. https://doi.org/10.1016/j.foodhyd.2015.01.020

Wu, Y., Li, W., Cui, W., Eskin, N. A. M., & Goff, H. D. (2012). A molecular modeling approach to understand conformation–functionality relationships of galactomannans with different mannose/galactose ratios. *Food Hydrocolloids*, *26*(2), 359–364. https://doi.org/10.1016/j.foodhyd.2011.02.029

Xavier, A. A., & Mariutti, L. R. (2021). Static and semi-dynamic in vitro digestion methods: State of the art and recent achievements towards standardization. *Current Opinion in Food Science*, *41*, 260–273. https://doi.org/10.1016/j.cofs.2021.08.002

Xie, A., Zhao, S., Liu, Z., Yue, X., Shao, J., Li, M., & Li, Z. (2023). Polysaccharides, proteins, and their complex as microencapsulation carriers for delivery of probiotics: A review on carrier types and encapsulation techniques. *International Journal of Biological Macromolecules*, *242*, 124784. https://doi.org/10.1016/j.ijbiomac.2023.124784

Xie, H., Ni, F., Cao, M., & Gu, Q. (2022). 2—The encapsulation of probiotics by polysaccharides. In J. Venkatesan, S.-K. Kim, S. Anil, & R. P. d (Eds.), *Polysaccharide Nanoparticles* (pp. 31–64). Elsevier. https://doi.org/10.1016/B978-0-12-822351-2.00013-9

Xu, C., Ban, Q., Wang, W., Hou, J., & Jiang, Z. (2022). Novel nano-encapsulated probiotic agents: Encapsulate materials, delivery, and encapsulation systems. *Journal of Controlled Release*, *349*, 184–205. https://doi.org/10.1016/j.jconrel.2022.06.061

Xu, D., Liu, Z., An, Z., Hu, L., Li, H., Mo, H., & Hati, S. (2023). Incorporation of probiotics into 3D printed Pickering emulsion gel stabilized by tea protein/xanthan gum. *Food Chemistry*, *409*, 135289. https://doi.org/10.1016/j.foodchem.2022.135289

Yamamoto, N., Akino, A., & Takano, T. (1994). Antihypertensive Effect of the Peptides Derived from Casein by an Extracellular Proteinase from Lactobacillus helveticus CP790. *Journal of Dairy Science*, *77*(4), 917–922. https://doi.org/10.3168/jds.S0022-0302(94)77026-0

Yang, C., Hu, C., Zhang, H., Chen, W., Deng, Q., Tang, H., & Huang, F. (2020). Optimation for preparation of oligosaccharides from flaxseed gum and evaluation of antioxidant and antitumor activities in vitro. *International Journal of Biological Macromolecules*, *153*, 1107–1116. https://doi.org/10.1016/j.ijbiomac.2019.10.241

Yang, L., Han, Z., Chen, C., Li, Z., Yu, S., Qu, Y., & Zeng, R. (2020). Novel probiotic-bound oxidized Bletilla striata polysaccharide-chitosan composite hydrogel. *Materials Science and Engineering: C*, *117*, 111265. https://doi.org/10.1016/j.msec.2020.111265

Yang, W., Zhao, P., Li, X., Guo, L., & Gao, W. (2022). The potential roles of natural plant polysaccharides in inflammatory bowel disease: A review. *Carbohydrate Polymers*, *277*, 118821. https://doi.org/10.1016/j.carbpol.2021.118821

Yao, H., Liu, B., He, L., Hu, J., & Liu, H. (2023). The incorporation of peach gum polysaccharide into soy protein based microparticles improves probiotic bacterial survival during simulated gastrointestinal digestion and storage. *Food Chemistry*, *413*, 135596. https://doi.org/10.1016/j.foodchem.2023.135596

Yao, M., Xie, J., Du, H., McClements, D. J., Xiao, H., & Li, L. (2020). Progress in microencapsulation of probiotics: A review. *Comprehensive Reviews in Food Science and Food Safety*, *19*(2), 857–874. https://doi.org/10.1111/1541-4337.12532

Ye, A. (2021). Gastric colloidal behaviour of milk protein as a tool for manipulating nutrient digestion in dairy products and protein emulsions. *Food Hydrocolloids*, *115*, 106599. https://doi.org/10.1016/j.foodhyd.2021.106599

Ye, A., Cui, J., Dalgleish, D., & Singh, H. (2016). Formation of a structured clot during the gastric digestion of milk: Impact on the rate of protein hydrolysis. *Food Hydrocolloids*, *52*, 478–486. https://doi.org/10.1016/j.foodhyd.2015.07.023

Ye, A., Roy, D., & Singh, H. (2020). Chapter 19—Structural changes to milk protein products during

gastrointestinal digestion. In M. Boland & H. Singh (Eds.), *Milk Proteins (Third Edition)* (pp. 671–700). Academic Press. https://doi.org/10.1016/B978-0-12-815251-5.00019-0

Ye, S., Shah, B. R., Li, J., Liang, H., Zhan, F., Geng, F., & Li, B. (2022). A critical review on interplay between dietary fibers and gut microbiota. *Trends in Food Science & Technology*, *124*, 237–249. https://doi.org/10.1016/j.tifs.2022.04.010

Yin, M., Chen, M., Yuan, Y., Liu, F., & Zhong, F. (2024). Encapsulation of Lactobacillus rhamnosus GG in whey protein isolate-shortening oil and gum Arabic by complex coacervation: Enhanced the viability of probiotics during spray drying and storage. *Food Hydrocolloids*, *146*, 109252. https://doi.org/10.1016/j.foodhyd.2023.109252

Yin, X., Cheng, H., Wusigale, Dong, H., Huang, W., & Liang, L. (2022). Resveratrol Stabilization and Loss by Sodium Caseinate, Whey and Soy Protein Isolates: Loading, Antioxidant Activity, Oxidability. *Antioxidants*, *11*(4), 647. https://doi.org/10.3390/antiox11040647

Ying, D. Y., Phoon, M. C., Sanguansri, L., Weerakkody, R., Burgar, I., & Augustin, M. A. (2010). Microencapsulated Lactobacillus rhamnosus GG Powders: Relationship of Powder Physical Properties to Probiotic Survival during Storage. *Journal of Food Science*, *75*(9), E588–E595. https://doi.org/10.1111/j.1750-3841.2010.01838.x

Ying, X., Gong, J., Goff, H. D., Yu, H., Wang, Q., & Cui, S. W. (2013). Effects of pig colonic digesta and dietary fibres on in vitro microbial fermentation profiles. *Bioactive Carbohydrates and Dietary Fibre*, *1*(2), 120–130. https://doi.org/10.1016/j.bcdf.2013.03.002

Yoha, K. S., Moses, J. A., & Anandharamakrishnan, C. (2020). Conductive hydro drying through refractance window drying – An alternative technique for drying of *Lactobacillus plantarum* (NCIM 2083). *Drying Technology*, *38*(5–6), 610–620. https://doi.org/10.1080/07373937.2019.1624972

Yoo, B., Figueiredo, A. A., & Rao, M. A. (1994). Rheological Properties of Mesquite Seed Gum in Steady and Dynamic Shear. *LWT - Food Science and Technology*, *27*(2), 151–157. https://doi.org/10.1006/fstl.1994.1031

Younes, M., Aggett, P., Aguilar, F., Crebelli, R., Filipič, M., Frutos, M. J., Galtier, P., Gott, D., Gundert-Remy, U., Kuhnle, G. G., Lambré, C., Leblanc, J.-C., Lillegaard, I. T., Moldeus, P., Mortensen, A., Oskarsson, A., Stankovic, I., Waalkens-Berendsen, I., Woutersen, R. A., … Dusemund, B. (2018). Re-evaluation of carrageenan (E 407) and processed Eucheuma seaweed (E 407a) as food additives. *EFSA Journal*, *16*(4), e05238. https://doi.org/10.2903/j.efsa.2018.5238

Younes, M., Aggett, P., Aguilar, F., Crebelli, R., Filipic, M., Frutos, M. J., Galtier, P., Gott, D., Gundert-Remy, U., Kuhnle, G. G., Lambré, C., Leblanc, J.-C., Lillegaard, I. T., Moldeus, P., Mortensen, A., Oskarsson, A., Stankovic, I., Waalkens-Berendsen, I., Woutersen, R. A., … Dusemund, B. (2018). Re-evaluation of gellan gum (E 418) as food additive. *EFSA Journal*, *16*(6), e05296. https://doi.org/10.2903/j.efsa.2018.5296

Yousefi, A. R., & Razavi, S. M. A. (2019). Dilute Solution Properties of Emerging Hydrocolloids. In *Emerging Natural Hydrocolloids* (pp. 53–79). John Wiley & Sons, Ltd. https://doi.org/10.1002/9781119418511.ch2

Youssef, M. K., Wang, Q., Cui, S. W., & Barbut, S. (2009). Purification and partial physicochemical characteristics of protein free fenugreek gums. *Food Hydrocolloids*, *23*(8), 2049–2053. https://doi.org/10.1016/j.foodhyd.2009.03.017

Yu, L., Stokes, J. R., & Yakubov, G. E. (2021). Viscoelastic behaviour of rapid and slow self-healing hydrogels formed by densely branched arabinoxylans from Plantago ovata seed mucilage. *Carbohydrate Polymers*, *269*, 118318. https://doi.org/10.1016/j.carbpol.2021.118318

Yu, L., Yakubov, G. E., Zeng, W., Xing, X., Stenson, J., Bulone, V., & Stokes, J. R. (2017). Multi-layer mucilage of Plantago ovata seeds: Rheological differences arise from variations in arabinoxylan side chains. *Carbohydrate Polymers*, *165*, 132–141. https://doi.org/10.1016/j.carbpol.2017.02.038

Yu, M., Hu, S., Tang, B., Yang, H., & Sun, D. (2023). Engineering Escherichia coli Nissle 1917 as a microbial chassis for therapeutic and industrial applications. *Biotechnology Advances*, *67*, 108202. https://doi.org/10.1016/j.biotechadv.2023.108202

Zemzmi, J., Ródenas, L., Blas, E., Najar, T., & Pascual, J. J. (2020). Characterisation and In Vitro Evaluation of Fenugreek (Trigonella foenum-graecum) Seed Gum as a Potential Prebiotic in Growing Rabbit Nutrition. *Animals*, *10*(6), 1041. https://doi.org/10.3390/ani10061041

Zheng, J., Wittouck, S., Salvetti, E., Franz, C. M. A. P., Harris, H. M. B., Mattarelli, P., O'Toole, P. W., Pot, B., Vandamme, P., Walter, J., Watanabe, K., Wuyts, S., Felis, G. E., Gänzle, M. G., & Lebeer, S. (2020). A taxonomic note on the genus Lactobacillus: Description of 23 novel genera, emended description

of the genus Lactobacillus Beijerinck 1901, and union of Lactobacillaceae and Leuconostocaceae. *International Journal of Systematic and Evolutionary Microbiology*, *70*(4), 2782–2858. https://doi.org/10.1099/ijsem.0.004107

Zhou, C.-Y., Cao, J.-X., Zhuang, X.-B., Bai, Y., Li, C.-B., Xu, X.-L., & Zhou, G.-H. (2019). Evaluation of the secondary structure and digestibility of myofibrillar proteins in cooked ham. *CyTA - Journal of Food*, *17*(1), 78–86. https://doi.org/10.1080/19476337.2018.1554704

Zhou, X., Zhang, Z., Huang, F., Yang, C., & Huang, Q. (2020). In Vitro Digestion and Fermentation by Human Fecal Microbiota of Polysaccharides from Flaxseed. *Molecules*, *25*(19), 4354. https://doi.org/10.3390/molecules25194354

Zhu, Q., Tang, J., Yao, S., Feng, J., Mi, B., Zhu, W., Chen, Q., Liu, D., & Xu, E. (2023). Controllable structure of porous starch facilitates bioactive encapsulation by mild gelatinization. *Food Hydrocolloids*, *145*, 109135. https://doi.org/10.1016/j.foodhyd.2023.109135

Zhuang, X., Clark, S., & Acevedo, N. (2021). Bigels—Oleocolloid matrices—As probiotic protective systems in yogurt. *Journal of Food Science*, *86*(11), 4892–4900. https://doi.org/10.1111/1750-3841.15928

Ziolkovska, A. (2012). Laws of flaxseed mucilage extraction. *Food Hydrocolloids*, *26*(1), 197–204. https://doi.org/10.1016/j.foodhyd.2011.04.022

Zong, M., Tong, X., Farid, M. S., Chang, C., Guo, Y., Lian, L., Zeng, X., Pan, D., & Wu, Z. (2023). Enhancement of gum Arabic/casein microencapsulation on the survival of Lactiplantibacillus plantarum in the stimulated gastrointestinal conditions. *International Journal of Biological Macromolecules*, *246*, 125639. https://doi.org/10.1016/j.ijbiomac.2023.125639

Zou, F., & Budtova, T. (2021). Tailoring the morphology and properties of starch aerogels and cryogels via starch source and process parameter. *Carbohydrate Polymers*, *255*, 117344. https://doi.org/10.1016/j.carbpol.2020.117344

Zou, Z., Duley, J. A., Cowley, D. M., Reed, S., Arachchige, B. J., Koorts, P., Shaw, P. N., & Bansal, N. (2022). Digestibility of proteins in camel milk in comparison to bovine and human milk using an in vitro infant gastrointestinal digestion system. *Food Chemistry*, *374*, 131704. https://doi.org/10.1016/j.foodchem.2021.131704